Boundary Element Analysis of Cracks in Shear Deformable Plates and Shells

By

Tatacipta Dirgantara

Thesis submitted for the degree of Doctor of Philosophy

of the University of London

Department of Engineering

Queen Mary and Westfield College

University of London

2000

And if all the trees on the earth were pens and the ocean (were ink),
with seven oceans behind it to add to its (supply),
yet would not the Words of Allah be exhausted (in the writing).
Verily, Allah is All-Mighty, All-Wise.

English translation of the meaning
of the Holy Qur'an
Surah 31: Luqman, verse 27

To my parents

for their love, prayer and encouragement

To my wife

for her love, support and understanding

Acknowledgements

Praise be to Allah Almighty, the Lord of the Universe for the peace, strength and guidance He gives to those whose minds are with Him.

I would like to expresses my sincere appreciation and gratitude to my supervisor, Professor M. H. Aliabadi for his continuous invaluable advice, support, friendship and encouragement throughout the duration of this work.

The financial support from PT Industri Pesawat Terbang Nusantara, Bandung, Indonesia is greatly acknowledge.

I wish to thank Dr. P. H. Wen and Dr. Y. F. Rashed for many fruitful discussions, and also to Prof. S. Kamil and Dr. ir. I. S. Putra for their support, help and advice.

Thanks are due to my colleagues in Computational Mechanics Group: Mr. D. Widagdo, Mr. J. J. Perez-Gavilan and Mr. J. Purbolaksono, colleagues and staff at Department of Engineering, Queen Mary and Westfield College, University of London, colleagues and staff at Department of Aeronautical Engineering, Institut Teknologi Bandung, my cousins Hermawan Judawisastra and Rai Aidasari in Leuven, Belgium, as well as all my friends in London, especially the ones in 'Al-Ikhlas' - Indonesian Muslim Students Study Circle, for their friendship, help and advice.

Thanks are also due to my mother-in-law and my father-in-law, and all of my brothers and sisters in Bandung, Indonesia for the prayers they do, and for their support and encouragement.

Special thanks and gratitude to my wife, Julia Mufidah Ahmad, for her love, support, patience, companionship and understanding throughout the development of this work.

Finally, I would like to express my sincere thanks and gratitude to my mother and father – who have brought me up – for their love, patience, pray, and continuous support and encouragement.

Abstract

This thesis presents new boundary element formulations for solution of bending problems in plates and shells. Also presented are the dual boundary element formulations for analysis of crack problems in plates and shells.

Reissner plate theory is adopted to represent the bending and shear, and two dimensional (2-D) plane stress is used to model the membrane behaviour of the plate. New set of boundary element formulations to solve bending problems of shear deformable shallow shells having quadratic mid-surface is derived based on the modified Reissner plate and two dimensional plane stress governing equations which are now coupled due to the curvature of the shell.

Dual Boundary Element Methods (DBEM) for plates and shells are developed for fracture mechanics analysis of structures loaded in combine bending and tension. Five stress intensity factors, that is, two for membrane and three for bending and shear are computed. The J-Integral technique and Crack Surface Displacements Extrapolation (CSDE) technique are used to compute the stress intensity factors. Special shape functions for crack tip elements are implemented to represent more accurately displacement fields close to the crack tip.

Crack growth processes are simulated with an incremental crack extension analysis. During the simulation, crack growth direction is determined using the maximum principal stress criterion. The crack extension is modelled by adding new boundary elements to the previous crack boundaries. As a consequence remeshing of existing boundaries is not required, and using this method the simulation can be effectively performed.

Finally, a multi-region boundary element formulation is presented for modelling assembled plate-structures. The formulation enforces the compatibility of translations and rotations as well as equilibrium of membrane, bending and shear tractions.

Examples are presented for plate and shell structures with different geometry, loading and boundary conditions to demonstrate the accuracy of the proposed formulations. The results obtained are shown to be in good agreement with analytical and other numerical results. Also presented are crack growth simulations of flat and curved panels loaded in combine bending and tension. The DBEM results are in good agreement with existing numerical and experimental results. Assembled plate-structure and a non-shallow shell bending problems are also analysed using a multi-region formulation developed in this thesis.

Contents

List of Figures

List of Tables

List of Notations

a	half crack length
$A(z), B(z)$	linear combination of the modified Bessel functions
B	$\left(= Eh/\left(1-\nu^2\right)\right)$ tension stiffness
$\mathbf{b}$	domain load vectors
C_p	empirical constant for material, used in fatigue crack growth calculation
C	$\left(= \left[D(1-\nu)\lambda^2\right]/2\right)$ shear stiffness
$\mathbf{C}$	coefficient matrix for crack surface displacements extrapolation
$\mathbf{C}$	matrix for compatibility equations, used in multi-region BEM formulation
c_{ij}	jump terms
D	$\left(= Eh^3/\left[12\left(1-\nu^2\right)\right]\right)$ bending stiffness
E	modulus of elasticity
$\mathbf{E}$	matrix for equilibrium equations, used in multi-region BEM formulation
e_1, e_2, e_3	unit vectors parallel to x_1, x_2, and x_3 – axes
F_1, F_2, F_3	total forces acting on entire surface of the shell
F	$(= 1 + r)$ radial basis function, used in dual reciprocity technique
f_1, f_2, f_3	body forces in the x_1-, x_2- and x_3- directions
G_1, G_2, G_3, G_4, G_5	energy release rate
$\mathbf{G}$	boundary element influence matrix
$\mathbf{H}$	boundary element influence matrix
h	shell thickness

I	moment of inertia
$I_0(z), I_1(z)$	modified Bessel functions of the first kind
J	$J-$integral
$J(\xi)$	Jacobian of transformation
K_I, K_{II}, K_{III}	stress intensity factors for mode I, II and III
K_1, K_2, K_3	stress resultant intensity factors for mode I, II and III
$K_0(z), K_1(z)$	modified Bessel functions of the second kind
k_{11}, k_{22}	$(=1/R_1, 1/R_2)$ principal curvatures of the shell in the x_1- and x_2- directions
L_{ik}	Navier differential operator
m_1, m_2, m_3	tractions in global coordinate system, used in multi-region BEM formulation
m_p	empirical constant for material, used in fatigue crack growth calculation
$M_{\alpha\beta}$	bending stress resultants
$\hat{M}^i_{m\alpha\beta}$	bending stress resultant particular solutions for plate bending problems
N	number of cycles in fatigue crack growth calculation
N_i	special shape functions for crack tip element
$N_{\alpha\beta}$	membrane stress resultants
$\hat{N}^\gamma_{m\alpha\beta}$	membrane stress resultant particular solutions for two-dimensional plane stress problems
n_1, n_2	outward unit normal vectors at the boundary in x_1- and x_2- directions
P^*_{ij}, P^*_{ijk}	plate bending traction fundamental solutions
p_1, p_2, p_3	generalised bending and shear tractions
$\hat{p}^i_{mk}$	traction particular solutions for plate bending problems
$\mathbf{p}$	bending and shear traction vectors
p_0	uniform pressure
Q_α	shear stress resultants
$\hat{Q}^i_{m\beta}$	shear stress resultant particular solutions for plate bending problems

q_i	domain loads
q_i^*	equivalent body forces
R_1, R_2	radius of curvature in the x_1- and x_2- directions
r	absolute distance between the source and the field points
r, θ	polar coordinates
$T^*_{\theta\alpha}, T^*_{\alpha\beta\gamma}$	2-D plane stress traction fundamental solutions
t_1, t_2	generalised membrane tractions
t_1, t_2, t_3	tractions in global coordinate system, used in multi-region BEM formulation
$\hat{t}^\alpha_{m\beta}$	traction particular solutions for two-dimensional plane stress problems
$\mathbf{t}$	membrane traction vectors
$U^*_{\theta\alpha}, U^*_{\alpha\beta\gamma}$	2-D plane stress displacement fundamental solutions
u_1, u_2	generalised in-plane displacements
u_1, u_2, u_3	displacements in global coordinate system, used in multi-region BEM formulation
u, v, w	translational displacements
$\hat{u}^\alpha_{m\beta}$	displacement particular solutions for two-dimensional plane stress problems
$\mathbf{u}$	in-plane displacement vectors
$V^*_{i,\beta}, Q^*_{i\beta}$	kernels for transformation of domain integrals to boundary integral
W^*_{ij}, W^*_{ijk}	plate bending displacement fundamental solutions
W	strain energy density
$\hat{w}^i_{mk}$	displacement particular solutions for plate bending problems
w_1, w_2, w_3	generalised rotations and out-of-plane displacements
$\mathbf{w}$	rotations and out-of-plane displacement vectors
$\mathbf{x}, \mathbf{X}$	field points, where $\mathbf{x} \in \mathbf{\Gamma}$, $\mathbf{X} \in \mathbf{\Omega}$
$\mathbf{x}', \mathbf{X}'$	source points, where $\mathbf{x}' \in \mathbf{\Gamma}$, $\mathbf{X}' \in \mathbf{\Omega}$
x_1, x_2, x_3	Cartesian coordinates

z	$(=\lambda r)$
α	contribution factor in K_{eff} calculation
β	correction angle in incremental crack-extension procedure
γ	Euler constant
Γ	boundary of the plate/shell
δ	Dirac delta function
$\delta_{\alpha\beta}$	Kronecker delta function
$\varepsilon_{ij}, \gamma_{ij}$	normal and shear strains
ϵ_{ijk}	permutation tensor
θ_t	crack extension direction
$\theta_1, \theta_2, \theta_3$	rotations in global coordinate system, used in multi-region BEM formulation
λ	$\left(=\sqrt{10}/h\right)$ shear factor
ν	Poisson's ratio
ξ', ξ	source point and field point in local coordinate
ξ_1, ξ_2, ζ	Curvilinear coordinates
Φ^m	shape functions
Ω	domain of the plate/shell
σ_{ij}	normal and shear stresses
ϕ_{x_1}, ϕ_{x_2}	rotational displacements

Chapter 1

Introduction

1.1 General

There are many aspects that have to be considered during the design stage of aircraft structures. During flight, all parts should be able to sustain loads which may be caused by air pressure and inertia forces, or ground reactions during landing. The structure must be able to endure extreme weather conditions, such as hailstorm and lightning strikes, and also must operate in corrosive environments. The aircraft has to be serviceable for around 15-20 years with minimum maintenance and light enough to be economically competitive. As a consequence, relatively high stresses will occur on the structure during service and components life times become limited.

On the other hand, cracks can be present in all structures either as a result of material and manufacturing defects or localized damage during service. These cracks may grow by processes such as fatigue, stress-corrosion or creep. The growth of cracks will decrease the static structural strength. Thus, when the service loading cannot be sustained by the current residual static strength, fracture will occur leading to the failure of the structure, as shown schematically in Figure 1-1.

In order to deal with the decrease in the structural strength, several design philosophies have been developed for aircraft structures, namely: safe-life, fail-safe and damage tolerance. The essence of safe-life design philosophy is that fatigue failure should not occur during the expected life of components. Safe-life concept is usually used if the crack cannot be detected before it reaches a critical size, therefore

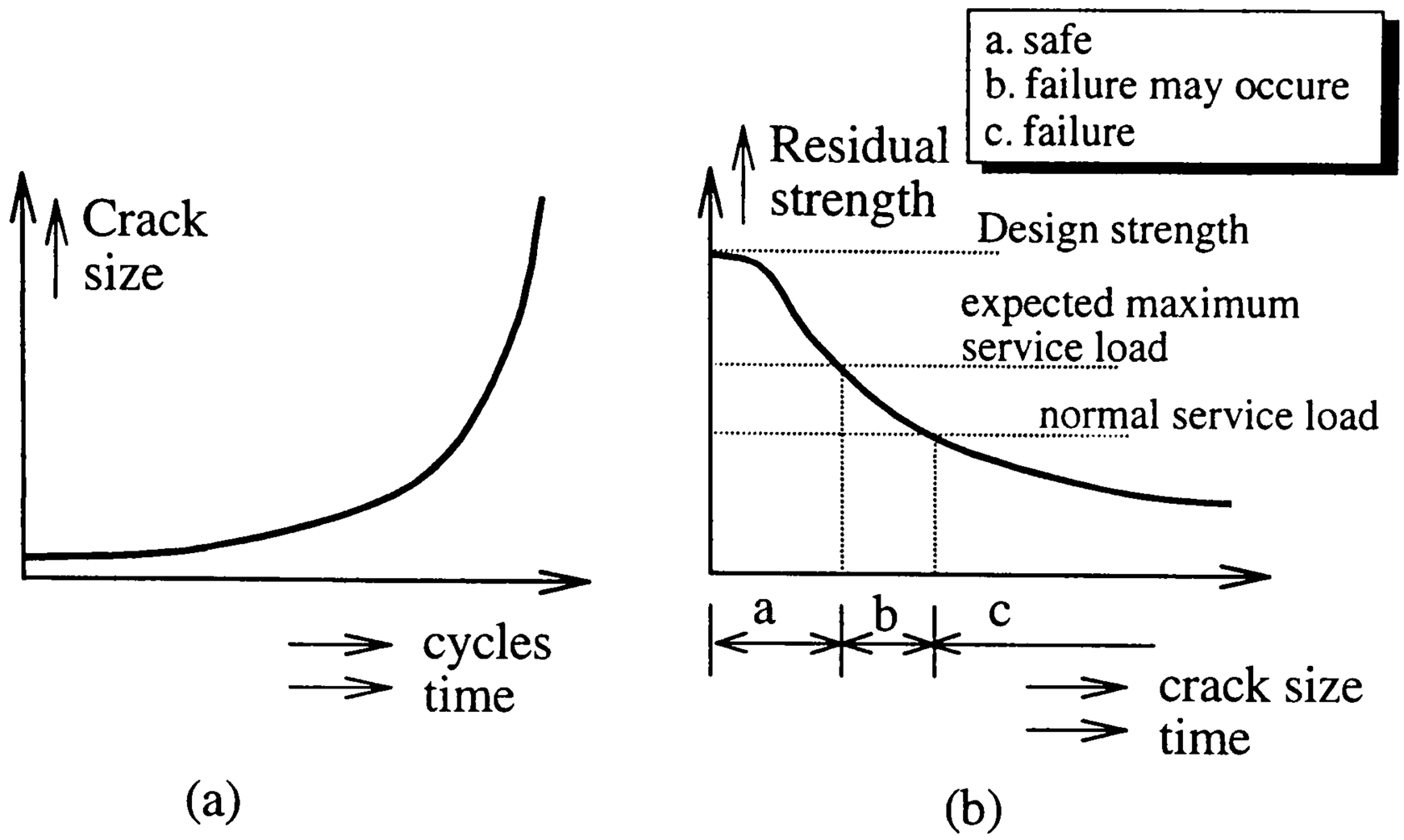

Figure 1-1: (a) Crack growth curve (b) Residual strength curve.

safe-life components must remain crack free during service life. Landing gear is an example of the safe-life component.

The fail-safe philosophy is based on the concept that the failure or obvious partial failure of a single principal structural element should not cause the loss of the aircraft during flight. Based on this concept, the components are designed using statically indeterminate and/or multiple element structure, to provide multiple load paths. Wing-fuselage attachment is an example of aircraft component which is designed using the fail-safe concept.

Another comprehensive design philosophy known as damage tolerance has been developed over the last 30 years. The structure is damage tolerant if it can sustain cracks safely until it is repaired or replaced, or if its economic service life has expired. This concept is usually applied to components in which cracks can be detected before reaching a critical size. Therefore damage tolerance analysis is required to provide information about:

- the effect of cracks on the residual strength of the structure, to evaluate the maximum permissible crack length;
- crack growth as a function of time or number of loading cycles, to evaluate the

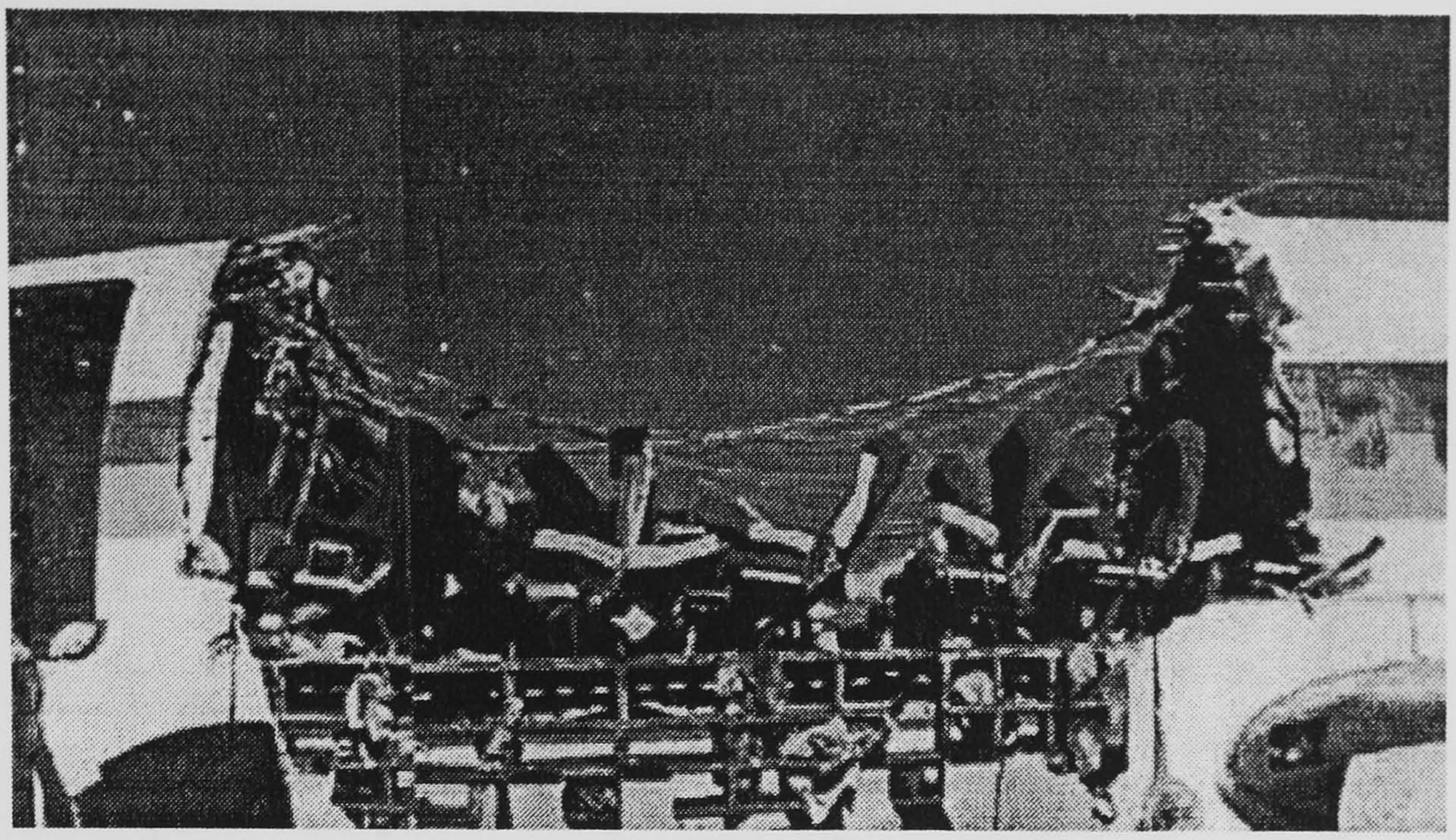

Figure 1-2: Fatigue failure of Boeing 737-200 Aloha Airlines fuselage structure, 28^{th} April 1988 [1].

safe crack growth life, i.e. the time that will be necessary for a crack to grow starting from its detectable size until it reaches its critical length.

Driven by economic pressures, today's commercial transport aircraft are remaining in service longer than their original design life. As consequence of that, to ensure the safety, problems related to aging aircraft have emerged as important research topics. Much of the work on this particular subject was initiated by Boeing 737-200 Aloha Airlines accident on 28th April, 1988 near Maui, Hawaii. The airplane experienced an explosive decompression and structural failure at 24,000 feet. About 18 feet of the upper part of the fuselage was separated from the airplane during flight, as shown in Figure 1-2. The U. S. National Transportation Safety Board stated in its report that *"The failure mechanism was a result of multiple site fatigue cracking of the skin adjacent to rivet holes along the lap joint upper rivet row and tear strap disbond which negated the fail-safe characteristics of the fuselage"*[1]. Since then, a great deal of research has been conducted to gain better understanding of the behaviour of damaged fuselage panels.

A common approach in investigating such a complex structural problem has been by simplifying it into simple structures. There are several simple models which are usually used to represent fuselage structure, i.e. bi-axial tension plate, plate loaded

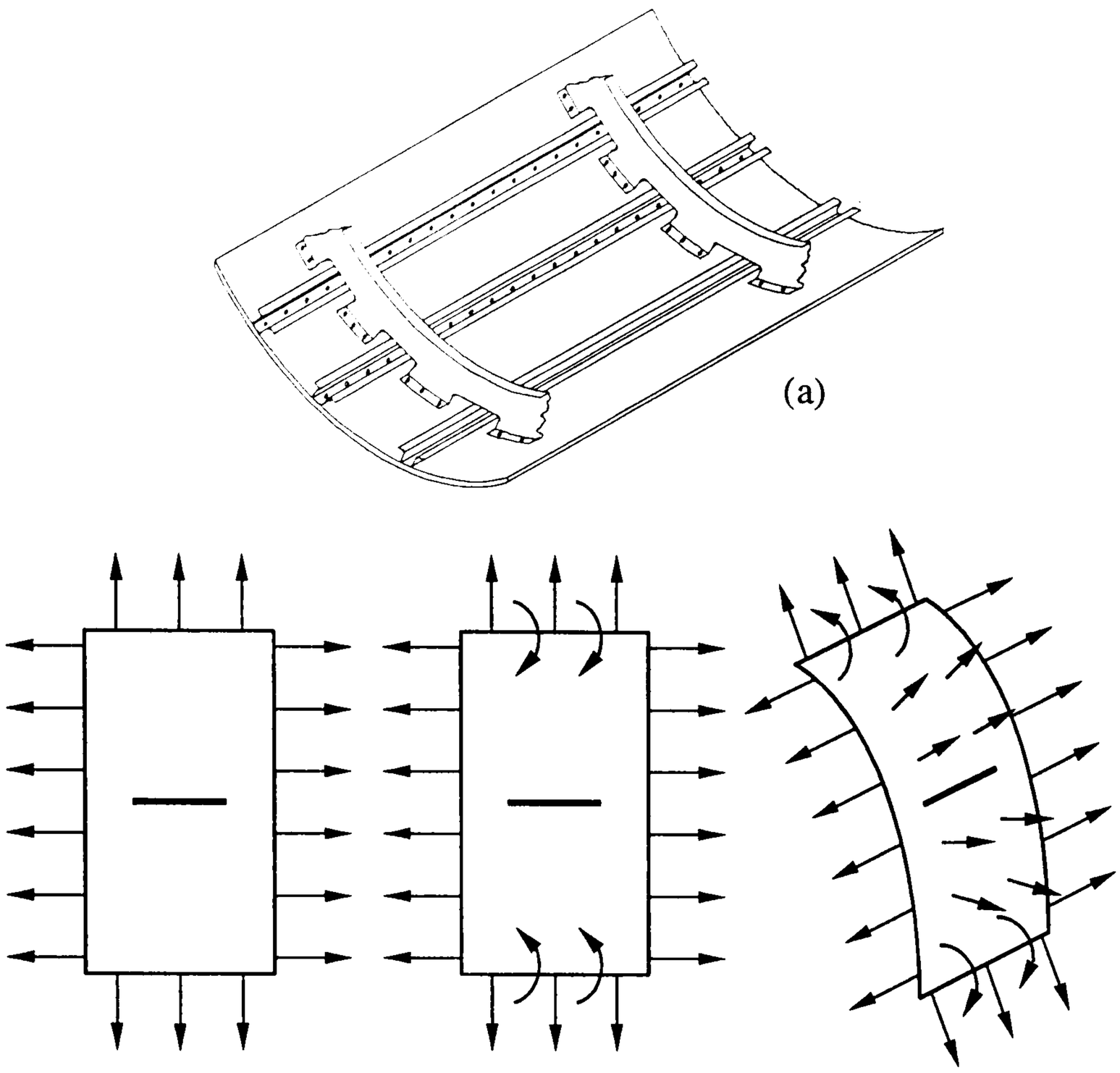

Figure 1-3: (a) Typical aircraft fuselage structure; (b) Simplified model of fuselage panel.

by combine bending and tension and shell loaded by distributed load, as shown in Figure 1-3. The first model is considered as a two-dimensional structure and can be solved using the plane stress theory of elasticity [129], the second problem can be represented by superposition of plate bending [107][130] and two-dimensional plane stress theory [129], while the third one is classified as a shell structure and should be solved using the shell theory [90][87][120][130].

Basically, there are two major theories of plates and shells. The first theory is commonly referred to as the classical or the thin plate and shell theory (as it neglects the shear deformation through the plate thickness). This theory was first proposed

by Kirchhoff [1] [76] in 1850 for plate problems. The other theory is shear deformable plate and shell theory. This theory takes into account the shear deformation and the transverse normal stresses. It was first proposed by Reissner [107] in 1947 for plate problems and extended to shell problems by Naghdi [87]. The Reissner theory is based on modelling the plate structure as two-dimensional structure with assumed stress variation through the plate thickness (the third dimension). In 1951, Mindlin [85] proposed another plate formulation to account for shear deformation based on a prescribed displacement field through the plate thickness.

The classical theory is sufficient for most practical applications. However, it was proved by comparisons to experimental analysis (see for example, References [5,6] in the paper reported by Reissner [107]) that Kirchhoff theory of thin plates is not in accordance with the experimental results for problems with stress concentrations such as, stresses at an edge of a hole when the hole diameter became so small as to be of the order of magnitude of the plate thickness. Moreover, when the Kirchhoff theory is applied to crack problems, the angular distributions of the bending and membrane stress resultants around the crack tip are entirely different. This incompatibility leads to difficulties when combine stress fields due to membrane and bending are required.

On the other hand, the shear deformable theory can overcome problems which appear on the application of classical theory. The other important feature of shear deformable plate and shell theories is that they can be used to analyse both thin and thick plates and shells.

Linear elastic fracture mechanics can provide concepts and mathematical basis for damage tolerance analysis and determination of behaviour of cracks. The most important parameter in fracture mechanics analysis that is used to describe crack behaviour is the stress intensity factors. For structures or components with simple geometries, the normalized stress intensity factors are available in the reference books or database, for example references [9][86]. However, due to the complexity of engineering structures, it is frequently necessary to perform numerical structural analysis to obtain accurate solutions. Therefore, development of numerical tools for

---

[1] In some text, it is referred to as Kirchhoff-Love theory, as Love [78] extended the theory to cope with shells (Love's first approximation).

fracture mechanics analysis in plates and shells is important.

1.2 Numerical Models for Fracture Mechanics Analysis of Plates and Shells

As has been mentioned in the previous section, aircraft fuselage is built using thin plates and shells as its main structural parts. Many other engineering structures such as ships, pressure vessels, pipes, reinforced concrete roof of buildings, and cooling towers are also mainly constructed using plate and shell structures. Plates and shells become widely used in many engineering applications because of the fact that these type of structure combine light weight with high strength.

To ensure the safety and reliability of such structures, the development of numerical tools which can describe bending behaviour of plates and shells with and without the presence of crack, and also predict crack growth and its effect to the overall structure is necessary. In general, several numerical methods are used for practical problems, they include: the Finite Difference Method (FDM), the Finite Element Method (FEM), and the Boundary Element Method (BEM).

The FDM is based on the direct solution of the differential form of the governing differential equation using difference equations. Some applications of the FDM to the classical and shear deformable plate theories can be found in [130, 60]. The integral representation of the differential equation can also be solved using the FEM [146]. In the FEM the structure is discretised into elements and the continuity and equilibrium are ensured at the nodal positions. Zienkiewicz and Taylor [147] presented FEM applications in the classical Kirchhoff plate and also in shear deformable plate theory. FEM has also been successfully applied to fracture mechanics of plate bending based on the classical and shear deformable plate theories. For example, Boduroglu and Erdogan [33], Sosa and Eischen[121], Sosa and Herrmann[122] presented stress intensity factor solutions for several finite width Reissner plate bending problems. More recently, Viz *et al.* [136] computed membrane and bending stress intensity factors for thin plate based on the Kirchhoff plate theory. The application of the FEM to the fracture mechanics analysis of shell can be found in [19][20][45], and more recently in [31][62][63].

All of the above mentioned methods are called domain methods as they require the discretisation of the problem domain. The boundary element method [27], on the other hand, is known as a boundary type method. The most important feature of boundary elements is that it only requires discretisation of the boundary rather than the domain. The BEM provides a continuous modelling of the interior since no discretisation of the interior is required, therefore it can give a high resolution of interior stresses and displacements.

The application of the BEM to the classical theory of plates was first proposed by Jaswon *et al.* [68] using the indirect formulation. The formulation used in [68] was based on biharmonic analysis for two unknown boundary values, deflection and normal slope. The formulation replaced corners with smooth curves and it was also valid only for simply supported and clamped plates. Forbes and Robinson [54] were the first to develop direct BEM to plate theory based on the Kirchhoff theory for plates with smooth boundary. Next, the works of Bézine [23] and Stern [123] were the first papers to consider plate bending problems with corner points and different types of boundary conditions via the direct formulation. They used the integral equation for the out-of-plane deflection and used its derivative to obtain an additional integral equation for the normal slope. Independently, Tottenham [132] also developed the direct formulation for plate bending. In his formulation, corner forces are treated as two concentrated couples. After the above works, other researchers (see for example, Stern [124], Stern and Lin [125], Hartmann and Zormantel [58], Abdel-Akher and Hartley [2][3], Karami *et al.* [71]) have improved and applied the formulation in different aspects.

The derivation of boundary integral equation and the fundamental solution for the Reissner plate theory was reported by Vander Weeën [134]. Karam and Telles [69] confirmed that Reissner plate model can be applied to both thin and thick plates, and the same authors later applied it to elastoplastic analysis [70]. The development of traction integral equation for Reissner plates have been reported independently by Rashed, Aliabadi and Brebbia [103][104] and Ahmadi-Brooghani and Wearing [5]. Later, El-Zafrany, Debbih and Fadhil [47] presented a modified fundamental solution, by separating parts of the kernel representing the effect of transverse shear, to allow analysis of thin and thick plates. Recent developments

in boundary element method for plate bending analysis can be found in the book edited by Aliabadi [12].

Thin walled structures loaded by in-plane and out-of-plane loads are widely used in engineering, therefore it is important to develop accurate methods of analysis of such structures. However, it appears that only Tanaka and Miyazaki [126] have presented the use of direct BEM for analysis of elastic plate-structure based on the Kirchhoff plate and plane stress theory of elasticity. Recently, Dirgantara and Aliabadi [43] presented a BEM formulation for assembled plate-structure based on the Reissner plate and two-dimensional plane stress.

There are not many publications for the application of BEM to shell problems. Newton and Tottenham [91], and Tottenham [132] presented an application of BEM to shallow shell problems, by decomposition of the fourth order governing equation into a second order equation. Antes [14] derived a BEM formulation for circular cylindrical shells, but no numerical examples were reported. Tosaka and Miyake [131] derived the direct BEM formulation for a shallow shell starting from the reduced single complex-valued equation of the coupled $w - \phi$ formulation. More recently Lu and Huang [80] developed a direct BEM formulation for shallow shells involving shear deformation. As stated in the review by Beskos [22], the application of direct BEM for shell problems involve complicated fundamental solutions (see e.g. [74][79][81]).

There is however, another approach that has been developed to deal with shallow shell problems. The formulations derived using this approach are formed by coupling boundary element formulation of classical plate bending and two dimensional plane stress. The work of Forbes and Robinson [54] was the first which developed the application of this approach for the static analysis of shallow shells. Zhang and Atluri [144] have also successfully derived a formulation for static and dynamic analysis of shallow shells base on the weighted residual method. Providakis and Beskos [94] and Beskos [22] extended the method developed by Zhang and Atluri [144] to solve static and vibration analysis of shallow shells. They derived the formulation with the aid of the reciprocal theorem. Later, Jinmu and Shuyao [75] used this method to carry out geometrically nonlinear analysis of shallow shells. There are advantages and disadvantages to this approach. The main advantage is that the fundamental solutions involved are much simpler than the ones in the direct BEM. However, due

to additional curvature terms in equilibrium equations, this method contains domain integrals as well as boundary integrals. Recently, Dirgantara and Aliabadi [36] have extended this approach to analysis of shear deformable shell problems. Wen, Aliabadi and Young [140] used the formulation proposed in [36] and transformed the domain integrals to boundary integrals using the dual reciprocity technique.

During the last decade, BEM has emerged as a robust numerical method for fracture mechanic problems. Several special techniques have been developed to model cracked structures. Among these the most important are: crack Green's function method, the displacement discontinuity method, the sub-region method and the dual boundary element method. The Dual Boundary Element Method (DBEM), which is based on displacement and traction integral equations, has been developed and applied to many fracture mechanics problems such as two dimensional and three dimensional elasticity, thermoelastic, concrete cracking, composite materials, elastoplastic, stiffened panel, and dynamic fracture mechanics, as has been reviewed by Aliabadi [10]. Recently, the application of dual boundary element method has been extended to fracture mechanics analysis of plates loaded by combine bending and tension, and to fracture mechanics analysis of shells. Ahmadi-Brooghani and Wearing [5] developed the application of DBEM for fracture mechanics analysis of Reissner plate bending problems. Dirgantara and Aliabadi [41] have developed application of the DBEM for crack growth analysis of plates loaded in combine bending and tension, and also for crack analysis of shear deformable shell bending problems [42].

1.3 Overview of the Present Work

The aim of this thesis is to investigate and develop boundary element methods for analysis of bending problems and fracture mechanics of shear deformable plates and shear deformable shells.

Chapter 2 describes some basic concepts of the shear deformable theory for elastic plates and shells, two-dimensional plane stress, and review of linear elastic fracture mechanics related to two-dimensional plane stress, plate and shell bending problems.

In **Chapter 3**, the displacement integral representation of the governing equation for shear deformable shells is derived. The fundamental solutions are introduced and the boundary integral equations are derived. The boundary integral equations are discretised using quadratic elements. The method for the evaluation of the singular integrals are described in details. Treatment of domain integrals using cells and transformation of domain integrals to boundary integrals using the dual reciprocity technique are presented. Also presented are boundary integral equations for shear deformable plates and two-dimensional plane stress. Several examples with different geometries, loadings and boundary conditions are analysed to demonstrate the accuracy of the proposed method.

Chapter 4 presents the hypersingular formulation for shear deformable shell bending analysis. Five integral equations, representing the bending, the shear and the membrane stress resultant integral equations are derived in details. The traction boundary integral equations are set up. Transformation of domain integrals to boundary integrals using the dual reciprocity technique are presented. Discussions on the computational aspects of the singular integrals are presented. Also presented are hypersingular integral equations for shear deformable plates and two-dimensional plane stress.

Chapter 5 presents the dual boundary element method for fracture mechanics analysis for shear deformable shallow shells and plates loaded in combine bending and tension. Modelling strategies, stress intensity factors evaluation using crack opening displacement (COD) and $J-$ integral techniques are explained. The decomposition of the $J-$ integral for mixed mode problems is also presented. Some examples are solved to demonstrate the accuracy of the stress intensity factors of shear deformable plate loaded in combine bending and tension.

Chapter 6 presents crack growth simulations for shear deformable shallow shells and plates loaded in combine bending and tension using the dual boundary element method. Modelling strategies, prediction of crack growth direction and fatigue life calculations are explained. Also presented is a simulation strategy for multiple crack growth analysis. Some examples are solved to demonstrate the robustness of the proposed method.

In **Chapter 7**, analysis of assembled plate-structures subjected to arbitrary load-

ings is presented. A multi-region formulation is developed to model such problems. The compatibility of translations and rotations as well as equilibrium of membrane, bending and shear tractions are enforced along the interfaces in this technique. Some examples are presented to demonstrate the accuracy of the method.

Finally, conclusions are presented in **Chapter 8**.

1.4 Author's Published Works

The following section contains the published and the submitted papers pertaining to the present work.

1.4.1 International journals

1. Dirgantara, T. and Aliabadi, M. H., A new boundary element formulation for shear deformable shells analysis, *International Journal for Numerical Methods in Engineering,* **45**, 1257-1275, 1999

2. Dirgantara, T. and Aliabadi, M. H., Crack growth analysis of plates loaded by bending and tension using dual boundary element method, *International Journal of Fracture* (accepted for publication and due to appear), 2000

3. Dirgantara, T. and Aliabadi, M. H., Dual boundary element formulation for fracture mechanics analysis of shear deformable shells, (submitted for publication), 2000

4. Dirgantara, T. and Aliabadi, M. H., Boundary element method analysis of assembled plate-structures, (submitted for publication), 2000

5. Dirgantara, T. and Aliabadi, M. H., Incremental crack growth simulation of shallow shells using dual boundary element method, (submitted for publication), 2000

6. Dirgantara, T. and Aliabadi, M. H., Stress intensity factors of cracks in plates loaded by bending and tension, (submitted for publication), 2000

1.4.2 Conference proceedings

1. Dirgantara, T., Aliabadi, M. H., Boundary element method for analysis of shallow shells, in *Association for Computational Mechanics in Engineering, The 7th. Annual Conference*, P. Bettess, (Ed.), University of Durham, UK, Spring 1999

2. Dirgantara, T., Aliabadi, M. H., Dual boundary element analysis of the crack propagation of plate bending and tension, in *Boundary Element Techniques*, M. H. Aliabadi (Ed.), Queen Mary and Westfield College, University Of London, UK, 87-96, July 1999

3. Dirgantara, T., Aliabadi, M. H., Fatigue crack growth simulation of plate bending and tension, in *Fracture and Damage Mechanics*, M. H. Aliabadi (Ed.), Queen Mary and Westfield College, University Of London, UK, 91-100, July 1999

4. Dirgantara, T., Aliabadi, M. H., Shear deformable shallow shells analysis using boundary element method, in *Second UK Conference on Boundary Integral Methods*, L. C. Wrobel and S. N. Chandler-Wilde (Eds.), Brunell University, UK, 62-72, September 1999

Chapter 2

Basic Concepts

2.1 Introduction

In this chapter, some basic concepts of elasticity theory of shear deformable shallow shells, shear deformable plates and two-dimensional plane stress are reviewed. Also reviewed are the fundamental concepts of fracture mechanics. The main sources of information for the elasticity theory of shallow shells are Novozhilov [90], Naghdi [87][88], and Sih [118], for the elasticity theory of plates and two-dimensional plane stress are Reissner [107], Mindlin [85] and Timoshenko and Goodier [129], and for fracture mechanics of Sih [118], Broek [29], Anderson [13], and Aliabadi and Rooke [8].

Indicial notation is used throughout the thesis. Greek indices will vary from 1 to 2 and Roman indices from 1 to 3. The partial derivative of (...) with respect to the coordinate x_α will be denoted by comma subscript, such as $(...)_{,\alpha} = \partial_\alpha(...) = \frac{\partial}{\partial x_\alpha}(...)$, and $(...)_{,n}$ denotes the derivative of (...) with respect to the outward normal n.

2.2 Basic Definitions of Shallow Shells

The term shell is usually applied to a body bounded by two curved surfaces, and the distance between the surfaces, which is the shell thickness, is small compared to other dimensions. The locus of points which lie at equal distances from these two surfaces defines the middle surface of the shell. Every point in the shell middle

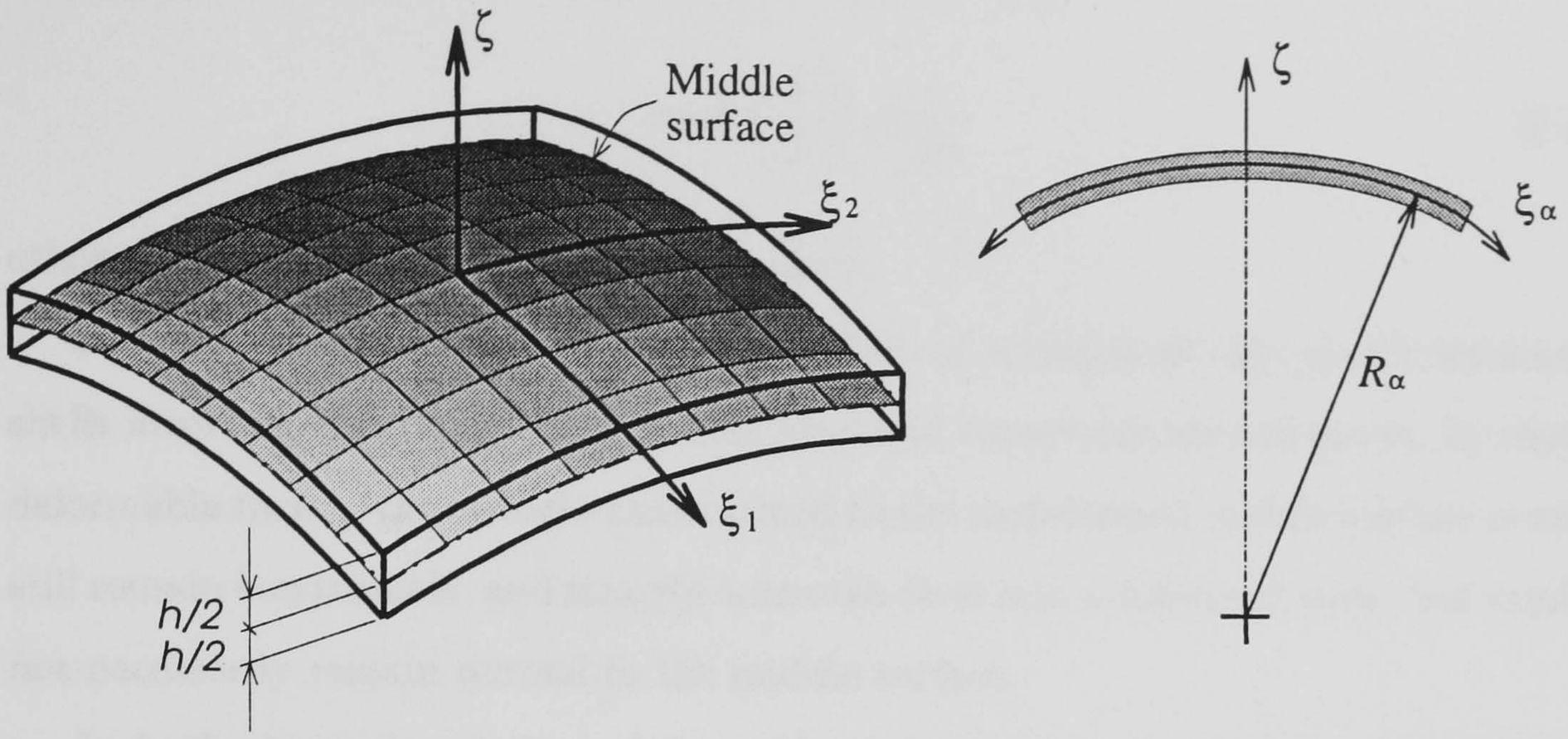

Figure 2-1: Curvilinear coordinates of shell.

surface is defined using curvilinear coordinates ξ_1 and ξ_2, and the third coordinate in the surface is the distance ζ from the middle surface, measured along the normal to the middle surface, as shown in Figure 2-1.

General classical theory of thin elastic shells can be found in the books of Love [78], Novozhilov [90], and Timoshenko [130]. The classical theory of elastic shells is based on the following assumptions:

1. shell thickness h should be at least an order of magnitude smaller than the least radius of curvature R of the middle surface, i.e. $h/R \ll 1$;

2. the strains and displacements are small enough for changes in geometry to be negligible;

3. the component of stress normal to the middle surface is small compared to other components of stress, and it may be neglected in the stress-strain relations;

4. straight lines normal to the undeformed middle surface would remain inextensible, straight and normal to the middle surface when the shell is in a deformed state, which implies the transverse shear strains are neglected.

According to Novozhilov [90], a shell is called thin if

$$max\left(\frac{h}{R}\right) \leqslant \frac{1}{20} \tag{2.1}$$

otherwise it will be considered as thick shell.

Reissner [109], followed by Naghdi [88] derived a theory of thin elastic isotropic shells involving transverse shear deformation and transverse normal stress. In shear deformable theory, the straight lines normal to the undeformed middle surface would still remain inextensible, and straight when the shell is in a deformed state, but would not necessarily remain normal to the middle surface.

In both classical and shear deformable shell theories, the stresses are replaced by a system of stress resultants and stress couples.

Based on the theory derived in [88], Naghdi [87] deduced an elastic theory of shallow shells involving transverse shear deformation. Sih and Hagendorf [120] further developed the theory and applied it for fracture mechanics analysis of shallow shells.

A shell is considered to be shallow (i.e. slightly curved) if the middle surface is sufficiently smooth and all points on this surface are sufficiently close to a plane. According to Vlasov [138], the shell is considered shallow if the ratio of the rise to the shorter side (for a shell of rectangular plan) or to the diameter (for a shell of circular plan) (i.e. H/D) is less than 1/5, see Figure 2-2.

In shallow shell theory, all points on the middle surface are located by the Cartesian coordinates of their projection on the x_1x_2- plane, that is,

$$x_1 = \xi_1; \qquad x_2 = \xi_2; \qquad x_3 = f(\xi_1, \xi_2) \tag{2.2}$$

where $\xi_1; \xi_2$ are the curvilinear coordinates and $f(\xi_1, \xi_2)$ is the equation of the middle surface of the shell. General theory of shallow shell is the simplification of the general theory of shell based on the following assumptions:

1. the squares of the derivatives $\dfrac{\partial f}{\partial x_\alpha}$ and their products are negligible in comparison to unity, i.e. $\left(\dfrac{\partial f}{\partial x_\alpha}\right)^2 \ll 1, \left(\dfrac{\partial f}{\partial x_\alpha}\dfrac{\partial f}{\partial x_\beta}\right) \ll 1;$

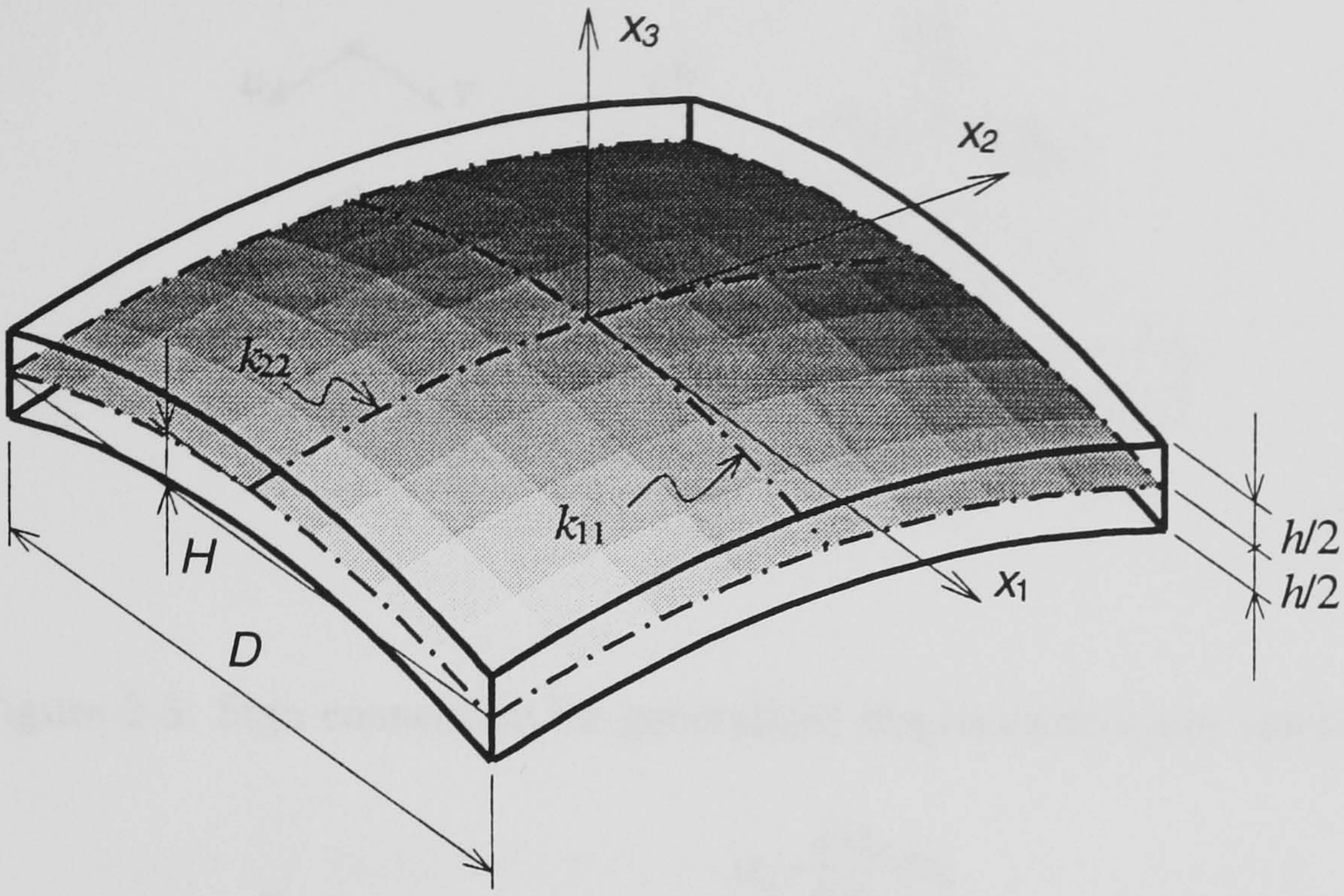

Figure 2-2: Shallow shell geometry.

2. the transverse shear resultants Q_α in the two equilibrium equations of stress resultants in x_1- and x_2- directions are negligible;

3. the tangential displacements u_α in the expression for the transverse shearing strain $\gamma_{\alpha 3}$ are negligible.

Now, consider an arbitrary shell of thickness h, as shown in Figure 2-2 with a quadratic middle surface given by

$$x_3 = -\frac{1}{2}\left(k_{11}\, {x_1}^2 + k_{22}\, {x_2}^2\right) \tag{2.3}$$

Based on this definition, the shell has only $k_{11} = 1/R_1$ and $k_{22} = 1/R_2$ which are principal curvatures of the shell in the x_1- and x_2- directions respectively, while $k_{12} = k_{21} = 0$. The bottom surface of the shell is located at $(x_3 - h/2)$ and the top surface at $(x_3 + h/2)$.

The generalised displacements are defined by Naghdi [87] and are denoted as w_i and u_α, where w_α denotes the change of the slope of the normal to the middle surface (ϕ_{x_1} and ϕ_{x_2}), w_3 denotes the out-of-plane displacement w normal to the middle surface and u_α denotes in-plane displacements of the middle surface (u and v), as shown in Figure 2-3.

Figure 2-3: Sign convention for generalized displacements and tractions.

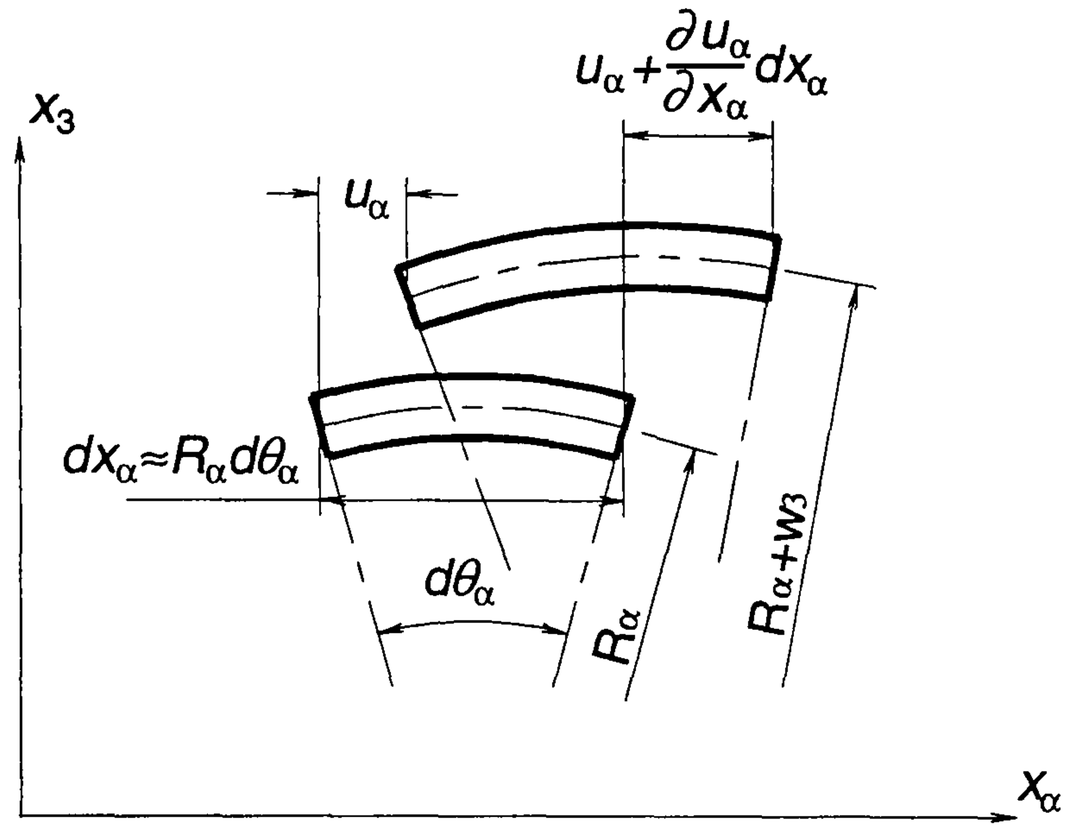

Figure 2-4: Basic definition of displacements and strains (a).

The generalised tractions are denoted as p_i and t_α, where p_α denotes tractions due to the stress couples (m_1 and m_2), p_3 denotes the traction due to shear stress resultant (t_3) and t_α denotes tractions due to membrane stress resultants (t_1 and t_2). Figure 2-3 shows the sign convention for the generalised tractions.

2.3 Governing Equations of Shallow Shells

2.3.1 Strain-displacement relationships

Consider an element of a shallow shell as shown in Figure 2-4. It can be seen that

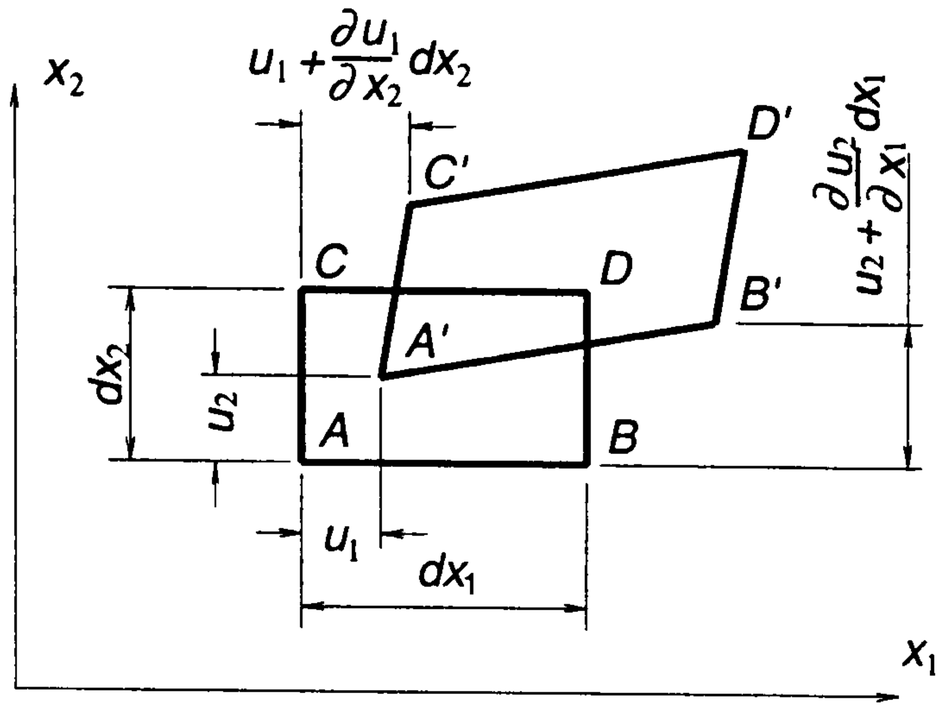

Figure 2-5: Basic definition of displacements and strains (b).

the increase of element length due to displacement along x_α is $\dfrac{\partial u_\alpha}{\partial x_\alpha}\, dx_\alpha$ and because of the radial displacement w_3, the element length increases by $w_3 d\theta_\alpha \approx w_3 \dfrac{dx_\alpha}{R_\alpha}$. Hence the total change of the element length is

$$\frac{\partial u_\alpha}{\partial x_\alpha} dx_\alpha + w_3 \frac{dx_\alpha}{R_\alpha} \tag{2.4}$$

Dividing the above value by the element length dx_α, the in-plane normal strain is obtained as

$$\varepsilon_{\alpha\alpha} = u_{\alpha,\alpha} + \frac{w_3}{R_\alpha} \tag{2.5}$$

Similarly from the elasticity theory of two dimensional bodies, in-plane shear strain can be obtained from the distortion of angle between sides of element as shown in Figure 2-5. From the figure, it can be seen that the initial angle CAB of an undeformed element $ABDC$ is diminished by the angle

$$\begin{aligned} &\frac{\left(u_2 + \dfrac{\partial u_2}{\partial x_1} dx_1\right) - u_2}{dx_1} + \frac{\left(u_1 + \dfrac{\partial u_1}{\partial x_2} dx_2\right) - u_1}{dx_2} \\ &= \frac{\partial u_1}{\partial x_2} + \frac{\partial u_2}{\partial x_1} \end{aligned} \tag{2.6}$$

to become angle $C'A'B'$ of the deformed element $A'B'D'C'$. Therefore the in-plane

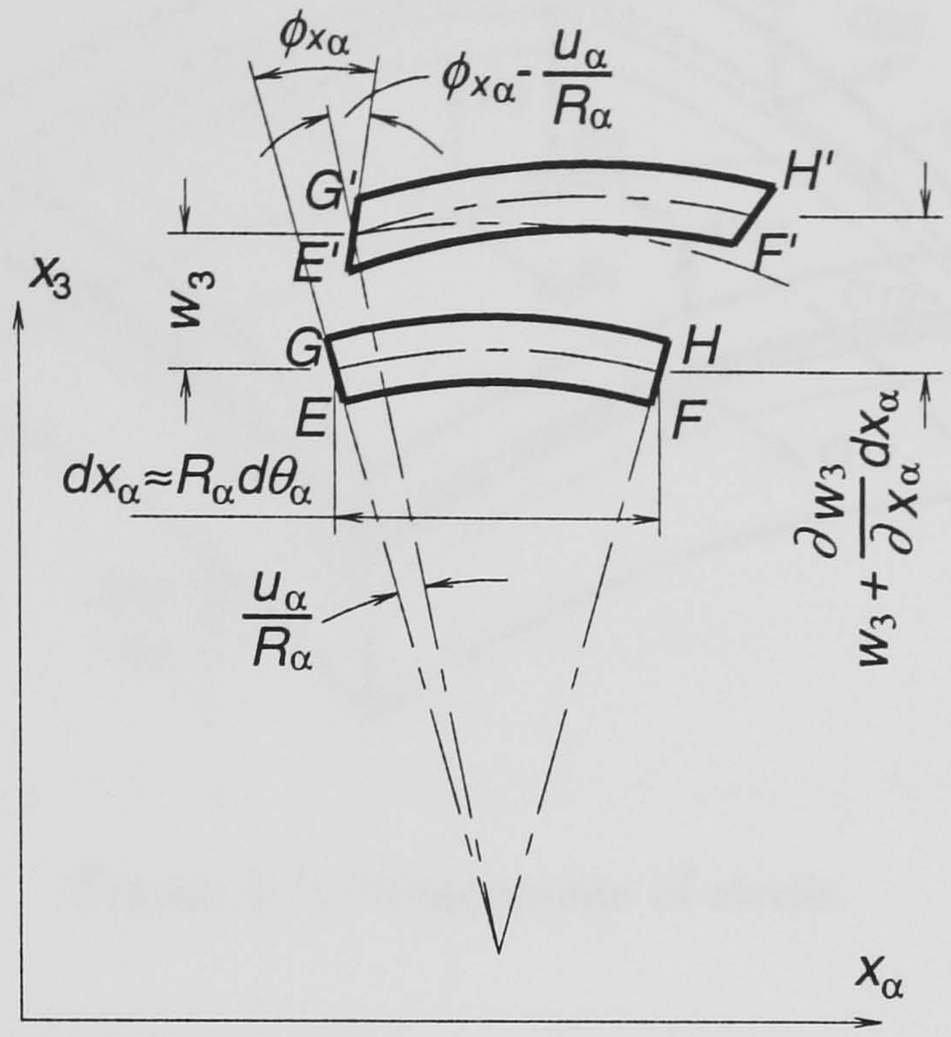

Figure 2-6: Basic definition of displacements and strains (c).

shear strain of the element can be written as

$$\gamma_{\alpha\beta} = 2\varepsilon_{\alpha\beta} = u_{\alpha,\beta} + u_{\beta,\alpha}; \qquad \alpha \neq \beta \tag{2.7}$$

Transverse shear strain is obtained from the distortion of angle of the face of shell element perpendicular to x_1- or x_2- axis, as can be seen in Figure 2-6. An initial angle GEF of an undeformed face of shell element $EFHG$ is distorted by the angle $\phi_{x_\alpha} - \frac{u_\alpha}{R_\alpha} + \frac{dw_3}{dx_\alpha}$ to become the angle $G'E'F'$. Using the third assumption of shallow shells mentioned above, by neglecting the term $\frac{u_\alpha}{R_\alpha}$, the transverse shear strains of the element can be written as

$$\gamma_{\alpha 3} = w_\alpha + w_{3,\alpha} \tag{2.8}$$

The curvature relationships with the derivatives of generalised displacements can be written as

$$\kappa_{\alpha\beta} = 2\chi_{\alpha\beta} = w_{\alpha,\beta} + w_{\beta,\alpha} \tag{2.9}$$

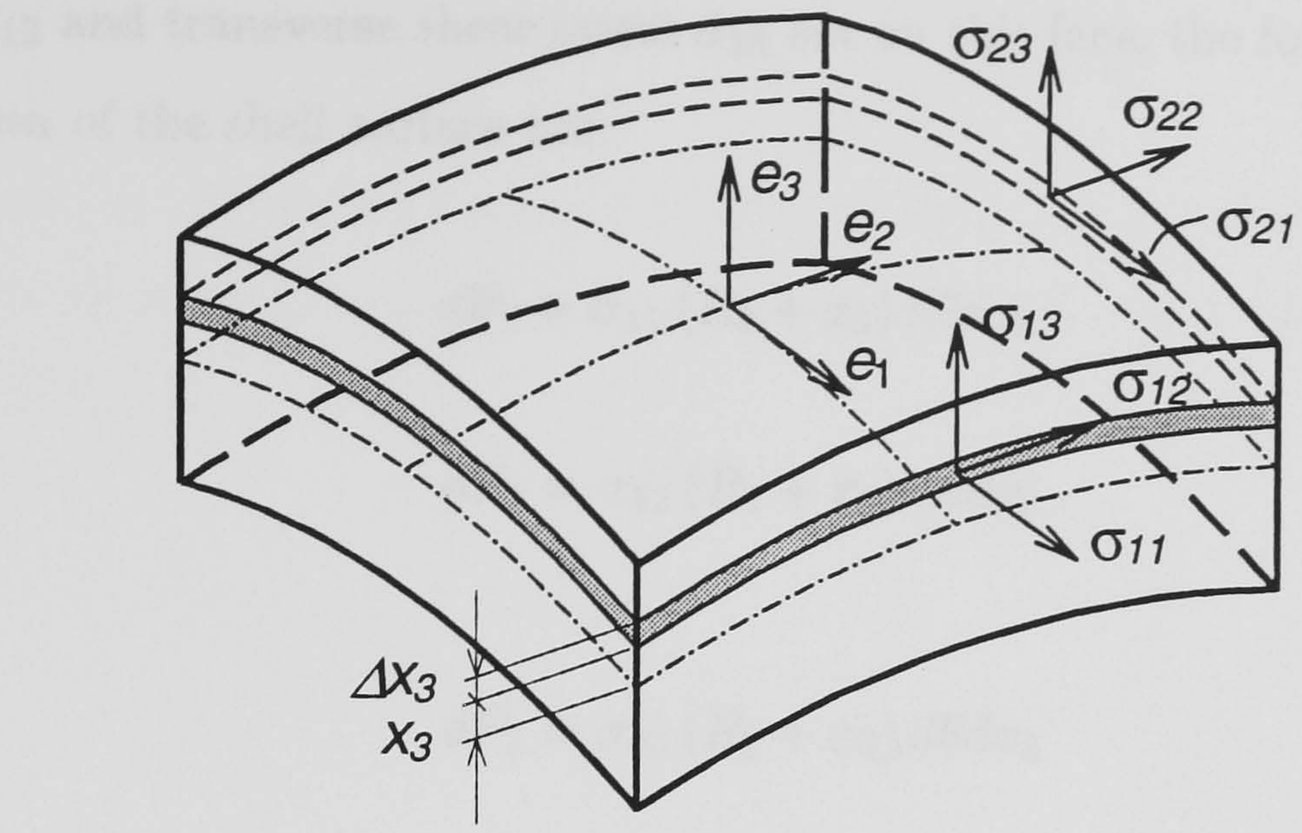

Figure 2-7: Components of stress.

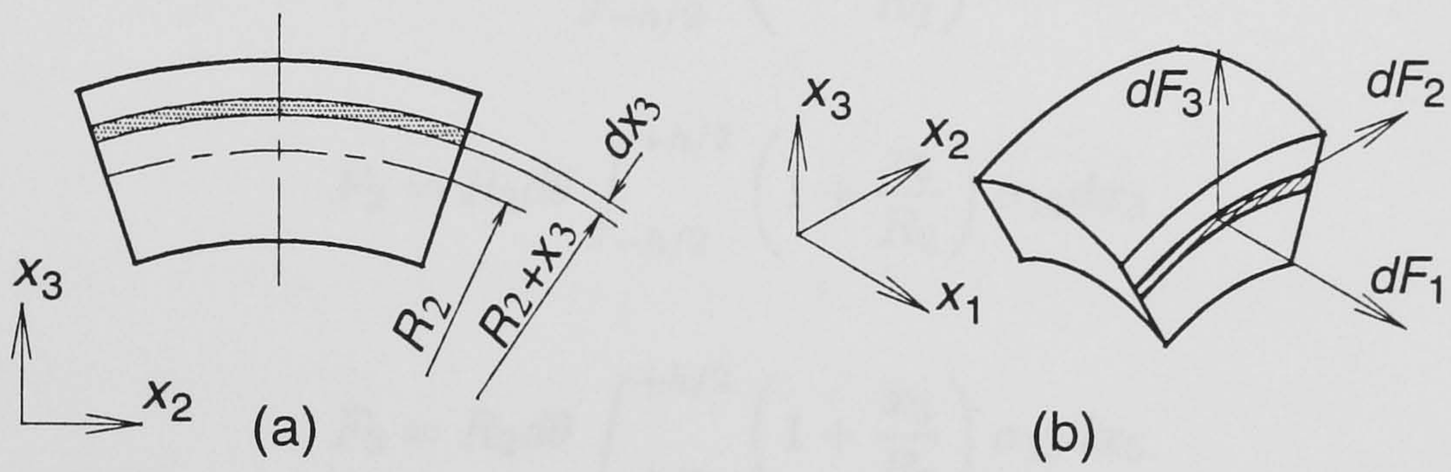

Figure 2-8: (a) A surface of shell element perpendicular to x_1- axis; (b) components of forces acting on a face of the shell element.

2.3.2 Stress resultants and stress couples

Consider an element of a shell, as shown in Figure 2-7. Let σ_{11} and σ_{22} be normal stresses, acting on the faces of the element, σ_{12} and σ_{21} are shear stresses on these faces, acting parallel to the middle surface, and σ_{13} and σ_{23} are transverse shear stresses, acting normal to the middle surface. Positive directions of these stresses are shown in Figure 2-7, where e_1, e_2, and e_3 are unit vectors parallel to x_1, x_2, and x_3- axes respectively.

To define stress resultants and stress couples, now consider a face of the shell element in Figure 2-8(a) which is perpendicular to the x_1- axis. The length of the arc in the middle surface is $dx_2 = R_2 d\theta$ and the length of the arc at a distance x_3 from the middle surface is $(R_2 + x_3)\, d\theta$. Assuming that a normal stress σ_{11}, shear

stresses σ_{12} and transverse shear stress σ_{13} act on this face, the forces acting on the shaded area of the shell surface are:

$$dF_1 = \sigma_{11}\left(R_2 + x_3\right) d\theta dx_3; \tag{2.10}$$

$$dF_2 = \sigma_{12}\left(R_2 + x_3\right) d\theta dx_3 \tag{2.11}$$

and

$$dF_3 = \sigma_{13}\left(R_2 + x_3\right) d\theta dx_3 \tag{2.12}$$

Hence the total forces (as a resultant of the stresses) acting on entire surface of the shell will be equal to:

$$F_1 = R_2 d\theta \int_{-h/2}^{+h/2} \left(1 + \frac{x_3}{R_2}\right) \sigma_{11} dx_3; \tag{2.13}$$

$$F_2 = R_2 d\theta \int_{-h/2}^{+h/2} \left(1 + \frac{x_3}{R_2}\right) \sigma_{12} dx_3 \tag{2.14}$$

and

$$F_3 = R_2 d\theta \int_{-h/2}^{+h/2} \left(1 + \frac{x_3}{R_2}\right) \sigma_{13} dx_3 \tag{2.15}$$

The stress resultants (defined as forces per unit length along dx_2), are the membrane stress resultants $N_{\alpha\beta}$ and the shearing stress resultants Q_α and are given as:

$$N_{11} = \frac{F_1}{R_2 d\theta} = \int_{-h/2}^{+h/2} \left(1 + \frac{x_3}{R_2}\right) \sigma_{11} dx_3; \tag{2.16}$$

$$N_{12} = \frac{F_2}{R_2 d\theta} = \int_{-h/2}^{+h/2} \left(1 + \frac{x_3}{R_2}\right) \sigma_{12} dx_3 \tag{2.17}$$

and

$$Q_1 = \frac{F_3}{R_2 d\theta} = \int_{-h/2}^{+h/2} \left(1 + \frac{x_3}{R_2}\right) \sigma_{13} dx_3 \tag{2.18}$$

and the bending stress couples $M_{\alpha\beta}$, defined as the bending and twisting moments per unit length along dx_2, can be obtained in similar way to give:

$$M_{11} = \int_{-h/2}^{+h/2} \left(1 + \frac{x_3}{R_2}\right) x_3 \sigma_{11} dx_3; \tag{2.19}$$

$$M_{12} = \int_{-h/2}^{+h/2} \left(1 + \frac{x_3}{R_2}\right) x_3 \sigma_{12} dx_3 \tag{2.20}$$

Similarly, by considering the other face of the shell element which is perpendicular to the x_2- axis, other components of stress resultants and stress couples can be obtained as follows:

$$N_{22} = \int_{-h/2}^{+h/2} \left(1 + \frac{x_3}{R_1}\right) \sigma_{22} dx_3; \tag{2.21}$$

$$N_{21} = \int_{-h/2}^{+h/2} \left(1 + \frac{x_3}{R_1}\right) \sigma_{21} dx_3; \tag{2.22}$$

$$Q_2 = \int_{-h/2}^{+h/2} \left(1 + \frac{x_3}{R_1}\right) \sigma_{23} dx_3 \tag{2.23}$$

and

$$M_{22} = \int_{-h/2}^{+h/2} \left(1 + \frac{x_3}{R_1}\right) x_3 \sigma_{22} dx_3; \tag{2.24}$$

$$M_{21} = \int_{-h/2}^{+h/2} \left(1 + \frac{x_3}{R_1}\right) x_3 \sigma_{21} dx_3 \tag{2.25}$$

For the sake of simplicity, throughout this thesis both the stress resultants and stress couples will be referred to as the generalised stress resultants.

Reissner [109] and Naghdi [88] assumed that the stresses due to membrane forces are uniform, the stresses due to bending and twisting moments vary linearly and the transverse shear stresses vary parabolically over the thickness, and proposed expressions for the stress components as follows:

$$\left(1 + \frac{x_3}{R_\gamma}\right) \sigma_{\alpha\beta} = \frac{1}{h} N_{\alpha\beta} + \frac{12 x_3}{h^3} M_{\alpha\beta}; \quad \begin{cases} \gamma = \beta \text{ if } \alpha \neq \beta \\ \gamma \neq \beta \text{ if } \alpha = \beta \end{cases} \tag{2.26}$$

and

$$\left(1 + \frac{x_3}{R_\gamma}\right) \sigma_{\alpha 3} = \frac{3}{2h} \left[1 - \left(\frac{2x_3}{h}\right)^2\right] Q_\alpha; \ \gamma \neq \alpha \tag{2.27}$$

The generalised tractions at a boundary point can be defined as:

$$\begin{aligned} p_\alpha &= M_{\alpha\beta} n_\beta; \\ p_3 &= Q_\alpha n_\alpha; \end{aligned}$$

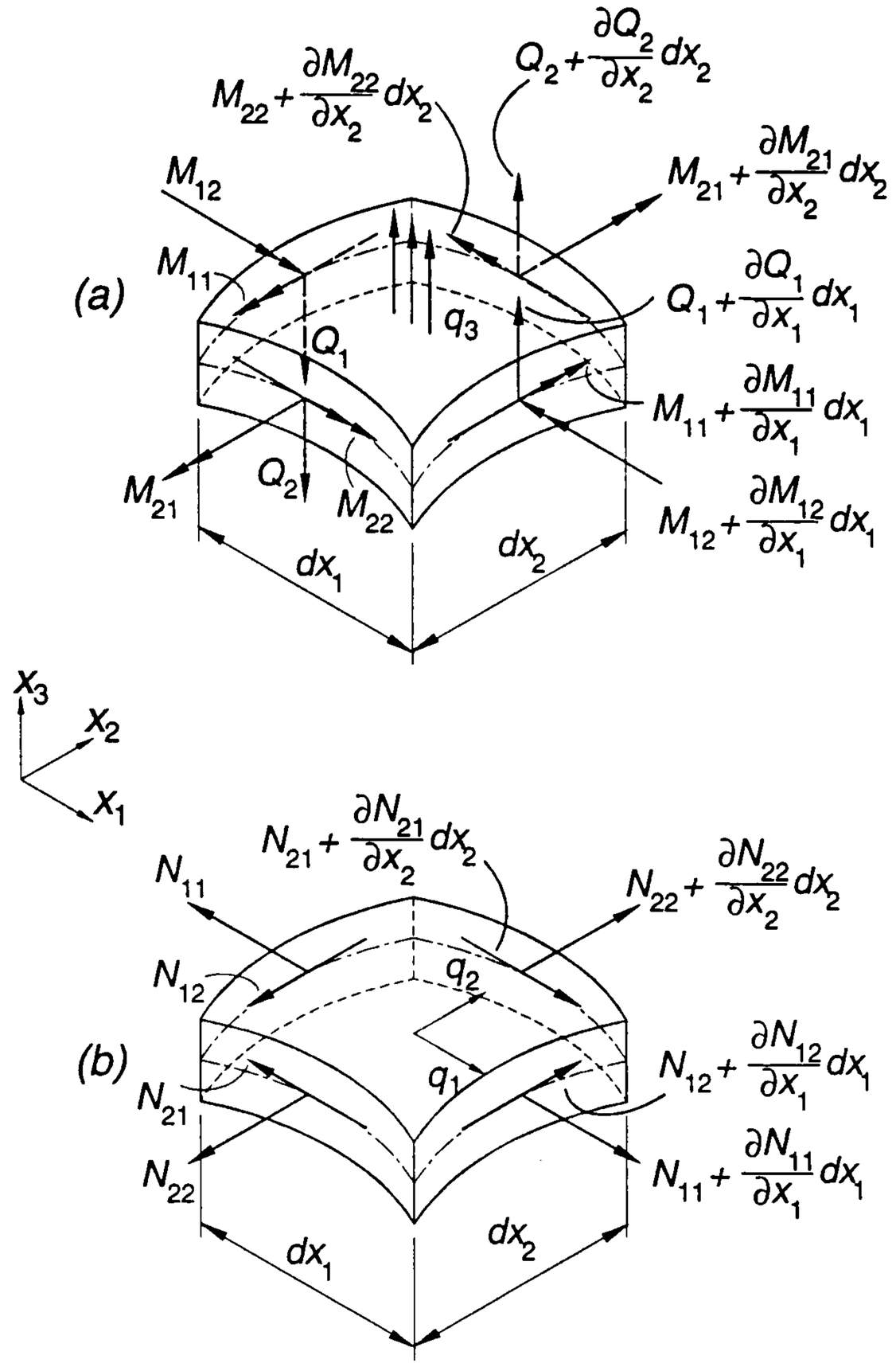

Figure 2-9: Stress resultant equilibrium of a shell element: (a) bending and shear stress resultants; (b) membrane stress resultants.

and

$$t_\alpha = N_{\alpha\beta} n_\beta \tag{2.28}$$

where n_β are the components of the outward normal vector to the shell boundary (see Figure 2-3).

2.3.3 Equilibrium equations

With the aid of Figures 2-9 and 2-10, and taking into consideration the effect of the domain loads q_i acting over the entire of the middle surface area, equilibrium of

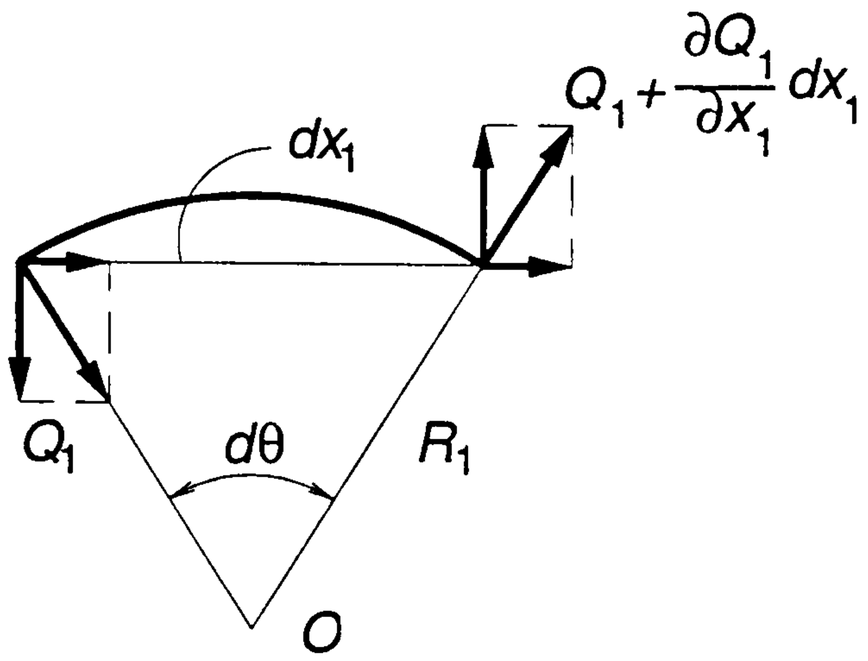

Figure 2-10: Contribution of shear stress resultant Q_1 to equilibrium equation along x_1- axis.

forces along x_1- axis are:

$$N_{11}dx_2 - \left(N_{11} + \frac{\partial N_{11}}{\partial x_1}dx_1\right)dx_2 + N_{21}dx_1 - \left(N_{21} + \frac{\partial N_{21}}{\partial x_2}dx_2\right)dx_1$$
$$+Q_1 dx_2 \sin\left(\frac{d\theta}{2}\right) + \left(Q_1 + \frac{\partial Q_1}{\partial x_1}dx_1\right)dx_2 \sin\left(\frac{d\theta}{2}\right) + q_1 dx_1 dx_2 = 0 \quad (2.29)$$

Because the angle $d\theta$ is infinitely small, $\sin\left(\frac{d\theta}{2}\right) \approx \frac{d\theta}{2}$, and $dx_1 \approx R_1 d\theta$, therefore the term $Q_1 dx_2 \sin\left(\frac{d\theta}{2}\right) + \left(Q_1 + \frac{\partial Q_1}{\partial x_1}dx_1\right)dx_2 \sin\left(\frac{d\theta}{2}\right)$ in equation (2.29) can be represented as follows:

$$Q_1 dx_2 \sin\left(\frac{d\theta}{2}\right) + \left(Q_1 + \frac{\partial Q_1}{\partial x_1}dx_1\right)dx_2 \sin\left(\frac{d\theta}{2}\right) \approx$$

$$Q_1 d\theta dx_2 + \frac{\partial Q_1}{\partial x_1}dx_1 \frac{d\theta}{2}dx_2 \approx$$

$$\frac{Q_1}{R_1}dx_1 dx_2 + \frac{\partial Q_1}{\partial x_1}\frac{1}{2R_1}dx_1 dx_1 dx_2 \quad (2.30)$$

Neglecting the last term in (2.30), substituting equation (2.30) into equation (2.29), and then simplifying and dividing all terms with $dx_1 dx_2$ gives:

$$\frac{\partial N_{11}}{\partial x_1} + \frac{\partial N_{21}}{\partial x_2} + \frac{Q_1}{R_1} + q_1 = 0 \quad (2.31)$$

The equilibrium equations for forces and moments on the other directions can

be derived in a similar manner to give:

$$\frac{\partial N_{12}}{\partial x_1} + \frac{\partial N_{22}}{\partial x_2} + \frac{Q_2}{R_2} + q_2 = 0 \tag{2.32}$$

$$\frac{\partial M_{11}}{\partial x_1} + \frac{\partial M_{21}}{\partial x_2} - Q_1 = 0 \tag{2.33}$$

$$\frac{\partial M_{12}}{\partial x_1} + \frac{\partial M_{22}}{\partial x_2} - Q_2 = 0 \tag{2.34}$$

$$\frac{\partial Q_1}{\partial x_1} + \frac{\partial Q_2}{\partial x_2} - \left(\frac{N_{11}}{R_1} + \frac{N_{22}}{R_2}\right) + q_3 = 0 \tag{2.35}$$

$$N_{12} - N_{21} + \frac{M_{12}}{R_1} - \frac{M_{21}}{R_2} = 0 \tag{2.36}$$

By substituting expressions of the stress resultants and stress couples in equations (2.17), (2.20), (2.22) and (2.25) into equation (2.36), it can be shown that equation (2.36) is identically satisfied.

Utilising the second assumption of general shallow shell theory, the effect of the term $\frac{Q_\alpha}{R_\alpha}$ in equation (2.31 – 2.32) can be neglected.

Hence the equations of equilibrium (2.31 – 2.35) can be rewritten using indicial notation as:

$$M_{\alpha\beta,\beta} - Q_\alpha = 0; \tag{2.37}$$

$$Q_{\alpha,\alpha} - k_{\alpha\beta}N_{\alpha\beta} + q_3 = 0; \tag{2.38}$$

and

$$N_{\alpha\beta,\beta} + q_\alpha = 0 \tag{2.39}$$

where $k_{12} = k_{21} = 0$.

2.3.4 Stress resultant-strain relationships

Using Reissner's variational theorem of elasticity [108], Naghdi [88] derived the relationships between stress resultant and strain as follows:

$$M_{\alpha\beta} = D\frac{1-\nu}{2}\left(2\chi_{\alpha\beta} + \frac{2\nu}{1-\nu}\chi_{\gamma\gamma}\delta_{\alpha\beta}\right); \tag{2.40}$$

$$Q_\alpha = C\gamma_{\alpha 3}; \tag{2.41}$$

and

$$N_{\alpha\beta} = B\frac{1-\nu}{2}\left(\varepsilon_{\alpha\beta} + \varepsilon_{\beta\alpha} + \frac{2\nu}{1-\nu}\varepsilon_{\gamma\gamma}\delta_{\alpha\beta}\right) \tag{2.42}$$

where $B(= Eh/\left(1-\nu^2\right))$ is known as the tension stiffness; $D(= Eh^3/\left[12\left(1-\nu^2\right)\right])$ is the bending stiffness of the shell; $C(=\left[D\left(1-\nu\right)\lambda^2\right]/2)$ is the shear stiffness; $\lambda = \sqrt{10}/h$ is called the shear factor and $\delta_{\alpha\beta}$ is the Kronecker delta function, which has property

$$\delta_{\alpha\beta} = \begin{cases} 1 \text{ if } \alpha = \beta \\ 0 \text{ if} \alpha \neq \beta \end{cases} \tag{2.43}$$

2.3.5 Stress resultant-displacement relationships

By substituting equations $(2.5 - 2.9)$ into $(2.40 - 2.42)$, the stress resultant-displacement relationships are obtained as

$$M_{\alpha\beta} = D\frac{1-\nu}{2}\left(w_{\alpha,\beta} + w_{\beta,\alpha} + \frac{2\nu}{1-\nu}w_{\gamma,\gamma}\delta_{\alpha\beta}\right); \tag{2.44}$$

$$Q_\alpha = C(w_\alpha + w_{3,\alpha}); \tag{2.45}$$

and

$$\begin{aligned} N_{\alpha\beta} &= B\frac{1-\nu}{2}\left(u_{\alpha,\beta} + u_{\beta,\alpha} + \frac{2\nu}{1-\nu}u_{\gamma,\gamma}\delta_{\alpha\beta}\right) + B\left[(1-\nu)k_{\alpha\beta} + \nu\delta_{\alpha\beta}k_{\phi\phi}\right]w_3 \\ &= N^{(i)}_{\alpha\beta} + N^{(ii)}_{\alpha\beta} \end{aligned} \tag{2.46}$$

To make the representation more convenient, the term $N_{\alpha\beta}$ is separated into $N^{(i)}_{\alpha\beta}$ which are due to in-plane displacements and $N^{(ii)}_{\alpha\beta}$ which are due to curvature and out-of-plane displacements.

2.3.6 Equilibrium equations in term of displacements

By substituting $(2.44 - 2.46)$ into $(2.37 - 2.39)$, the equilibrium equations in term of displacements are obtained as follows:

$$D\nabla^2 w_1 + \frac{D}{2}\left(1+\nu\right)\frac{\partial}{\partial x_2}\left(-\frac{\partial w_1}{\partial x_2} + \frac{\partial w_2}{\partial x_1}\right) - Cw_1 - C\frac{\partial w_3}{\partial x_1} = 0 \tag{2.47}$$

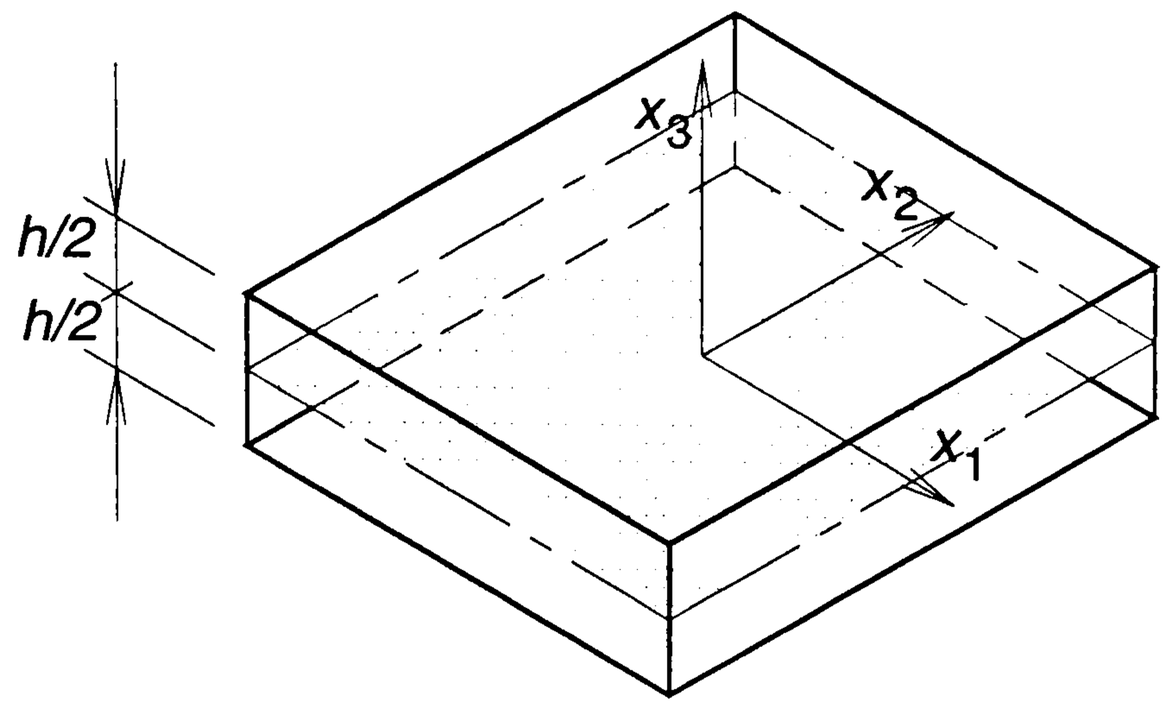

Figure 2-11: Plate geometry.

$$\frac{D}{2}(1+\nu)\frac{\partial}{\partial x_1}\left(\frac{\partial w_1}{\partial x_2}-\frac{\partial w_2}{\partial x_1}\right)+D\nabla^2 w_2-Cw_2-C\frac{\partial w_3}{\partial x_2}=0 \tag{2.48}$$

$$C\nabla^2 w_3+C\frac{\partial w_1}{\partial x_1}+C\frac{\partial w_2}{\partial x_2}+q_3-B(k_{11}+\nu k_{22})\frac{\partial u_1}{\partial x_1}$$

$$-B(\nu k_{11}+k_{22})\frac{\partial u_2}{\partial x_2}-B(k_{11}^2+k_{22}^2+2\nu k_{11}k_{22})w_3=0 \tag{2.49}$$

$$B\nabla^2 u_1+\frac{B}{2}(1+\nu)\frac{\partial}{\partial x_2}\left(-\frac{\partial u_1}{\partial x_2}+\frac{\partial u_2}{\partial x_1}\right)+q_1+B(k_{11}+\nu k_{22})\frac{\partial w_3}{\partial x_1}=0 \tag{2.50}$$

$$\frac{B}{2}(1+\nu)\frac{\partial}{\partial x_1}\left(\frac{\partial u_1}{\partial x_2}-\frac{\partial u_2}{\partial x_1}\right)+B\nabla^2 u_2+q_2+B(\nu k_{11}+k_{22})\frac{\partial w_3}{\partial x_2}=0 \tag{2.51}$$

2.4 Governing Equations of Flat Plates

If the curvatures of a shell are $k_{11}=k_{22}=0$, the surfaces which bound the body become flat, the bending and shear loads will have no effect to the membrane behaviour and vice versa. The body is now called plate and its behaviour can be evaluated separately by using shear deformable plate bending and/or two dimensional plane stress theories depending on external loadings.

Consider an arbitrary plate of thickness h in the x_i space as shown in Figure 2-11. The x_1-x_2 plane is assumed to be located at the middle surface $x_3=0$, where $-h/2 \leqslant x_3 \leqslant +h/2$. As in the previous section, the generalised displacements for bending and shear are denoted as w_i and for in-plane as u_α, with the same sign convention as for the shallow shell (see Figure 2-3). Exact definition of the

generalised displacements can be found in [107].

2.4.1 Stress resultants and stress couples

The bending stress resultants $M_{\alpha\beta}$, and the shearing stress resultants Q_α can be defined as:

$$M_{\alpha\beta} = \int_{-h/2}^{+h/2} x_3 \sigma_{\alpha\beta} dx_3$$

$$Q_\alpha = \int_{-h/2}^{+h/2} \sigma_{\alpha 3} dx_3 \tag{2.52}$$

where $\sigma_{\alpha\beta}$ are the three-dimensional components of the normal stresses through the plate thickness and $\sigma_{\alpha 3}$ are the components of the transverse shear stresses.

The membrane stress resultants $N_{\alpha\beta}$ are defined as:

$$N_{\alpha\beta} = \int_{-h/2}^{+h/2} \sigma_{\alpha\beta} dx_3 \tag{2.53}$$

Based on two-dimensional theory of elasticity, the normal stresses $\sigma_{\alpha\beta}$ due to membrane forces are assumed to be uniformly distributed over the thickness, and as proposed by Reissner [107] for shear deformable plate bending, the normal stresses due to bending and twisting moments $\sigma_{\alpha\beta}$ vary linearly and the transverse shear stresses $\sigma_{\alpha 3}$ vary parabolically over the thickness. Hence, the stress components can be expressed via the following relationships:

$$\sigma_{\alpha\beta} = \frac{1}{h} N_{\alpha\beta} + \frac{12 x_3}{h^3} M_{\alpha\beta} \tag{2.54}$$

and

$$\sigma_{\alpha 3} = \frac{3}{2h} \left[1 - \left(\frac{2x_3}{h} \right)^2 \right] Q_\alpha \tag{2.55}$$

The generalised bending and shear tractions at a boundary point can be defined as:

$$p_\alpha = M_{\alpha\beta} n_\beta \qquad \text{and} \qquad p_3 = Q_\alpha n_\alpha \tag{2.56}$$

and membrane tractions

$$t_\alpha = N_{\alpha\beta} n_\beta \tag{2.57}$$

where n_β are components of the outward normal vector to the plate boundary. The sign convention for the generalised tractions is same as the shallow shell theory (see Figure 2-3).

2.4.2 Strain-displacement relationships

Strain-displacement relationships can be derived in a similar way as in shallow shell theory, but in this case, in-plane strains and displacements are uncoupled with bending strains and displacements. The transverse shear strains of the element can be written as

$$\gamma_{\alpha 3} = \psi_\alpha = w_\alpha + w_{3,\alpha} \tag{2.58}$$

the curvature relationships or the flexural strain as

$$\kappa_{\alpha\beta} = 2\chi_{\alpha\beta} = w_{\alpha,\beta} + w_{\beta,\alpha} \tag{2.59}$$

and the in-plane strains of the element as

$$\varepsilon_{\alpha\beta} = \frac{1}{2}\left(u_{\alpha,\beta} + u_{\beta,\alpha}\right) \tag{2.60}$$

2.4.3 Equilibrium equations

The equilibrium equations can be formed by considering the equilibrium of a typical plate element having dimensions of $dx_1 \times dx_2 \times h$ and under uniform load q_i (per unit area), which is regarded to be positive when it applied in x_i directions (see Figure 2-12). These equations are derived in a similar manner to the section 2.3 and can be written in indicial notation as follows:

$$M_{\alpha\beta,\beta} - Q_\alpha = 0;$$

$$Q_{\alpha,\alpha} + q_3 = 0; \tag{2.61}$$

and

$$N_{\alpha\beta,\beta} + q_\alpha = 0 \tag{2.62}$$

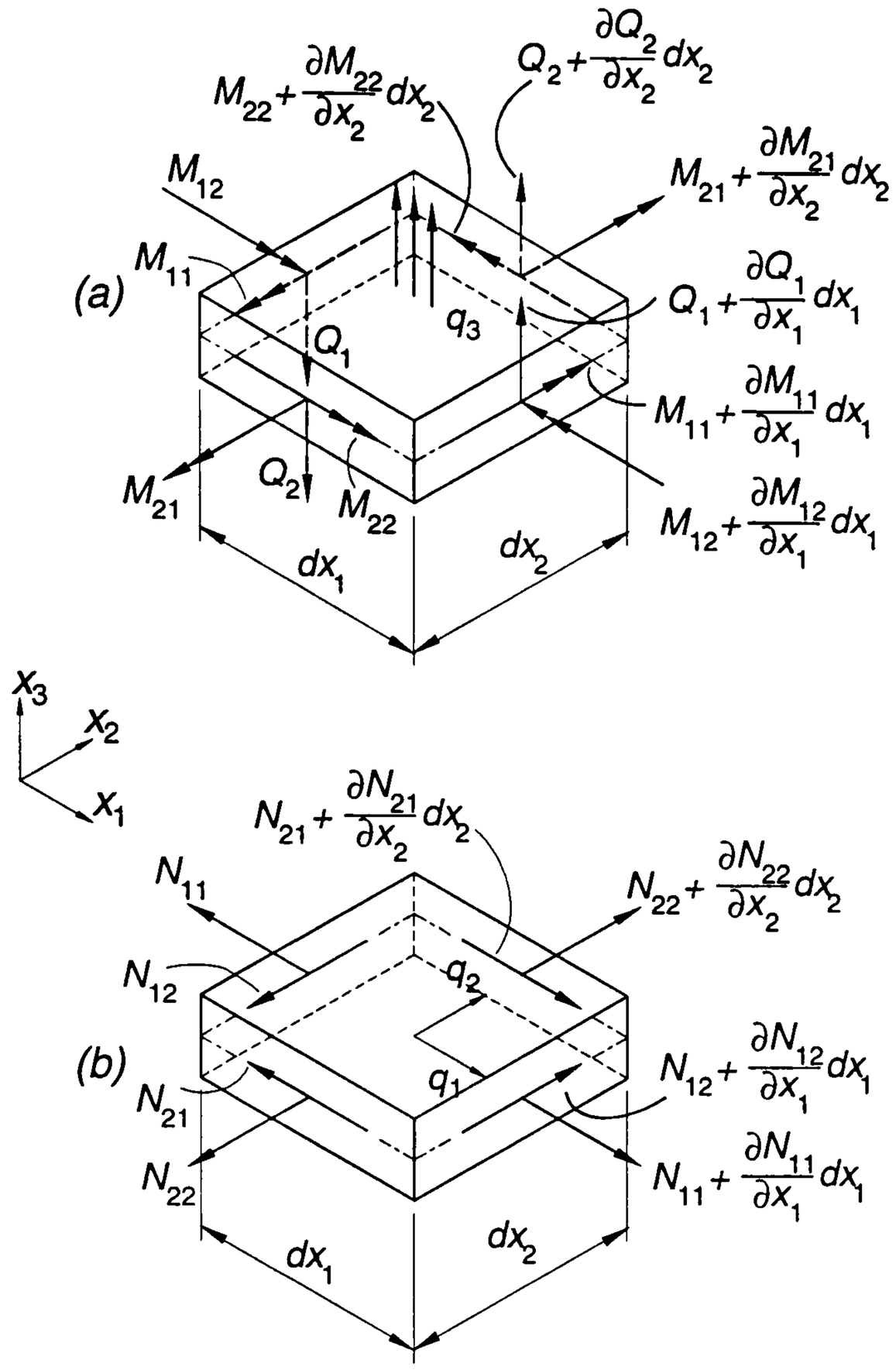

Figure 2-12: Stress resultant equilibrium of a plate element.

2.4.4 Stress resultant-strain relationships

Reissner [107] derived the stress resultant-strain relationships for plate bending using the basic minimum principal for the stresses (Castigliano theorem of least work), to give[1]:

$$M_{\alpha\beta} = D\frac{1-\nu}{2}\left(2\chi_{\alpha\beta} + \frac{2\nu}{1-\nu}\chi_{\gamma\gamma}\delta_{\alpha\beta}\right);$$

$$Q_\alpha = C\psi_\alpha \tag{2.63}$$

[1] In Reissner [107], there is a term relating the effect of the transverse normal stresses on the bending stress resultants, but according to Mindlin [85], this term has a negligible contribution to the results. For the sake of simplicity and to be consistent with the stress resultant-strain relationships for shallow shells, following Mindlin [85], this term will be ignored in this thesis.

and based on Hooke's law for two-dimensional plane stress, membrane stress resultant-strain relationships can be written as follows:

$$N_{\alpha\beta} = B\frac{1-\nu}{2}\left(2\varepsilon_{\alpha\beta} + \frac{2\nu}{1-\nu}\varepsilon_{\gamma\gamma}\delta_{\alpha\beta}\right) \tag{2.64}$$

Equations (2.63 – 2.64) represent the generalised Hooke's law. Equations (2.63 – 2.64) together with equations (2.58 – 2.60) represent the stress resultant-displacement relationships as follows:

$$\begin{aligned} M_{\alpha\beta} &= D\frac{1-\nu}{2}\left(w_{\alpha,\beta} + w_{\beta,\alpha} + \frac{2\nu}{1-\nu}w_{\gamma,\gamma}\delta_{\alpha\beta}\right); \\ Q_{\alpha} &= C(w_{\alpha} + w_{3,\alpha}) \end{aligned} \tag{2.65}$$

and

$$N_{\alpha\beta} = B\frac{1-\nu}{2}\left(u_{\alpha,\beta} + u_{\beta,\alpha} + \frac{2\nu}{1-\nu}u_{\gamma,\gamma}\delta_{\alpha\beta}\right) \tag{2.66}$$

which are the stress resultant-displacement relationships. Tension stiffness B, bending stiffness D of the shell, shear stiffness C and the shear factor λ are same as the ones defined in the section 2.3 for shallow shells.

2.4.5 Equilibrium equations in terms of displacements

By substituting (2.65 – 2.66) into (2.61 – 2.62), the equilibrium equations in terms of displacements are obtained as follows:

$$D\nabla^2 w_1 + \frac{D}{2}(1+\nu)\frac{\partial}{\partial x_2}\left(-\frac{\partial w_1}{\partial x_2} + \frac{\partial w_2}{\partial x_1}\right) - Cw_1 - C\frac{\partial w_3}{\partial x_1} = 0 \tag{2.67}$$

$$\frac{D}{2}(1+\nu)\frac{\partial}{\partial x_1}\left(\frac{\partial w_1}{\partial x_2} - \frac{\partial w_2}{\partial x_1}\right) + D\nabla^2 w_2 - Cw_2 - C\frac{\partial w_3}{\partial x_2} = 0 \tag{2.68}$$

$$C\nabla^2 w_3 + C\frac{\partial w_1}{\partial x_1} + C\frac{\partial w_2}{\partial x_2} + q_3 = 0 \tag{2.69}$$

and

$$B\nabla^2 u_1 + \frac{B}{2}(1+\nu)\frac{\partial}{\partial x_2}\left(-\frac{\partial u_1}{\partial x_2} + \frac{\partial u_2}{\partial x_1}\right) + q_1 = 0 \tag{2.70}$$

$$\frac{B}{2}(1+\nu)\frac{\partial}{\partial x_1}\left(\frac{\partial u_1}{\partial x_2} - \frac{\partial u_2}{\partial x_1}\right) + B\nabla^2 u_2 + q_2 = 0 \tag{2.71}$$

2.5 Basic Concepts of Fracture Mechanics

Although fracture mechanics is a relatively new scientific discipline, its importance to engineering design is no longer in question. Since the pioneering investigation in 1920 by Griffith [55], followed by Irwin [67] in 1948, and through rapid development during 1960s and 1970s, fracture mechanics has become the primary approach for analysing and preventing failures in structures.

Most of the studies on fracture mechanics have been based on situations and materials for which the use of linear elasticity are valid or constitute a good approximation. It is referred to as Linear Elastic Fracture Mechanics (LEFM). One of the most important parameters used in LEFM analysis is the stress intensity factor (SIF). This parameter is used to determine the crack tip stress field in a cracked structure. With a knowledge of the stress intensity factors, crack growth, life expectancy and residual strength of engineering structures can be determined. Therefore, to predict crack behaviour in a structure, a knowledge of stress intensity factors is essential.

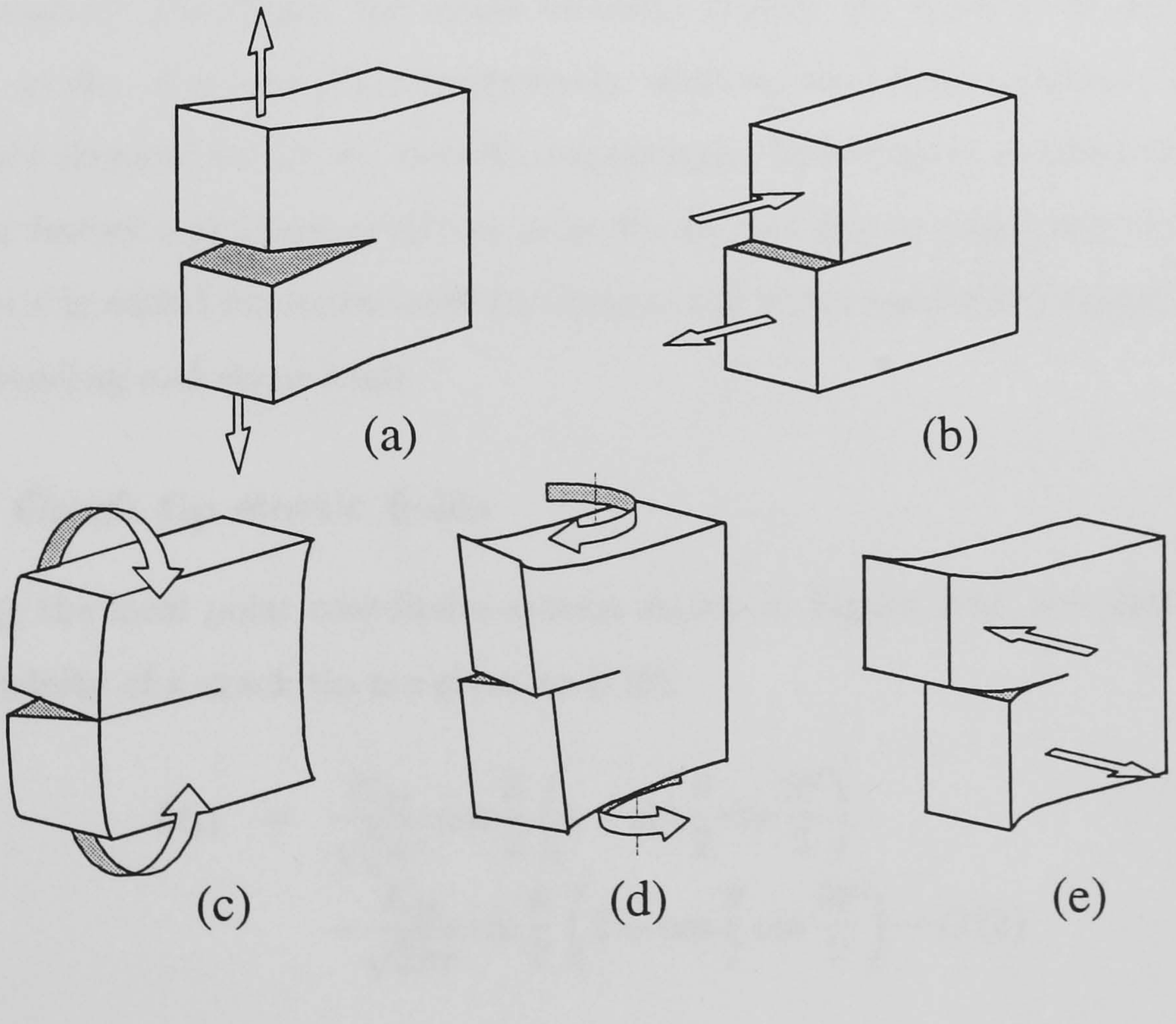

Figure 2-13: Five crack modes.

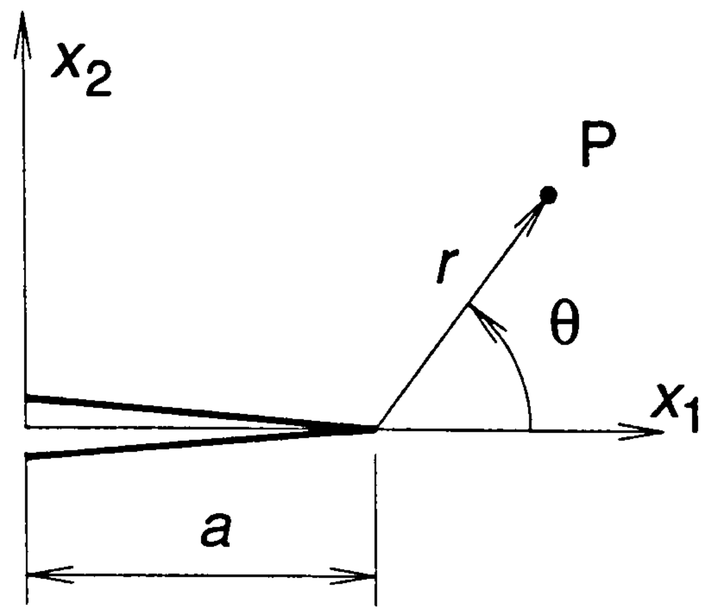

Figure 2-14: Straight crack in an infinite medium.

For plate and shell problems, five stress intensity factors, two SIFs due to membrane loads (as shown in Figure 2-13(a) and (b)) and three SIFs due to bending moments and shear loads (as shown in Figure 2-13(c), (d) and (e)) have to be computed. The stress intensity factors for a flat plate loaded in combine bending and tension can be represented by superposition of SIFs of plate bending and two-dimensional plane stress theory. In shell problems, the SIFs due to bending and membrane loadings are always coupled due to the curvature of the shell.

Throughout the thesis, the stress intensity factors for mode I, II and III are denoted as K_I, K_{II} and K_{III} respectively, whereas the stress resultant intensity factors are denoted as K_1, K_2 and K_3 respectively. Subscript m is added for stress intensity factors and stress resultant intensity factors due to membrane loads, and subscript b is added for stress intensity factors and stress resultant intensity factors due to bending and shear loads.

2.5.1 Crack tip elastic fields

Using the local polar coordinate system shown in Figure 2-14, the elastic fields in the vicinity of a crack tip are given as [118]:

$$\begin{aligned} M_{11} &= \frac{K_{1b}}{\sqrt{2\pi r}} \cos\frac{\theta}{2}\left(1-\sin\frac{\theta}{2}\sin\frac{3\theta}{2}\right) \\ &\quad -\frac{K_{2b}}{\sqrt{2\pi r}} \sin\frac{\theta}{2}\left(2+\cos\frac{\theta}{2}\cos\frac{3\theta}{2}\right)+O(1) \end{aligned} \tag{2.72}$$

$$M_{22} = \frac{K_{1b}}{\sqrt{2\pi r}} \cos\frac{\theta}{2}\left(1+\sin\frac{\theta}{2}\sin\frac{3\theta}{2}\right)+\frac{K_{2b}}{\sqrt{2\pi r}} \sin\frac{\theta}{2}\cos\frac{\theta}{2}\cos\frac{3\theta}{2}+O(1) \tag{2.73}$$

$$M_{12} = \frac{K_{1b}}{\sqrt{2\pi r}} \sin\frac{\theta}{2}\cos\frac{\theta}{2}\cos\frac{3\theta}{2} + \frac{K_{2b}}{\sqrt{2\pi r}}\cos\frac{\theta}{2}\left(1 - \sin\frac{\theta}{2}\sin\frac{3\theta}{2}\right) + O(1) \quad (2.74)$$

$$Q_1 = -\frac{K_{3b}}{\sqrt{2\pi r}}\sin\frac{\theta}{2} + O(1) \quad (2.75)$$

$$Q_2 = \frac{K_{3b}}{\sqrt{2\pi r}}\cos\frac{\theta}{2} + O(1) \quad (2.76)$$

$$\begin{aligned} N_{11} &= \frac{K_{1m}}{\sqrt{2\pi r}}\cos\frac{\theta}{2}\left(1 - \sin\frac{\theta}{2}\sin\frac{3\theta}{2}\right) \\ &\quad -\frac{K_{2m}}{\sqrt{2\pi r}}\sin\frac{\theta}{2}\left(2 + \cos\frac{\theta}{2}\cos\frac{3\theta}{2}\right) + O(1) \end{aligned} \quad (2.77)$$

$$N_{22} = \frac{K_{1m}}{\sqrt{2\pi r}}\cos\frac{\theta}{2}\left(1 + \sin\frac{\theta}{2}\sin\frac{3\theta}{2}\right) + \frac{K_{2m}}{\sqrt{2\pi r}}\sin\frac{\theta}{2}\cos\frac{\theta}{2}\cos\frac{3\theta}{2} + O(1) \quad (2.78)$$

$$N_{12} = \frac{K_{1m}}{\sqrt{2\pi r}}\sin\frac{\theta}{2}\cos\frac{\theta}{2}\cos\frac{3\theta}{2} + \frac{K_{2m}}{\sqrt{2\pi r}}\cos\frac{\theta}{2}\left(1 - \sin\frac{\theta}{2}\sin\frac{3\theta}{2}\right) + O(1) \quad (2.79)$$

for stress resultants, and

$$\begin{aligned} \phi_1 &= \frac{1+\nu}{E}\left(\frac{12}{h^3}\right)\sqrt{\frac{r}{2\pi}}\left[K_{1b}\cos\frac{\theta}{2}\left(\frac{3-\nu}{1+\nu} - \cos\theta\right)\right. \\ &\quad \left. + K_{2b}\sin\frac{\theta}{2}\left(\frac{5+\nu}{1+\nu} - \cos\theta\right)\right] + O(r) \end{aligned} \quad (2.80)$$

$$\begin{aligned} \phi_2 &= \frac{1+\nu}{E}\left(\frac{12}{h^3}\right)\sqrt{\frac{r}{2\pi}}\left[K_{1b}\sin\frac{\theta}{2}\left(\frac{3-\nu}{1+\nu} - \cos\theta\right)\right. \\ &\quad \left. + K_{2b}\cos\frac{\theta}{2}\left(\frac{1-3\nu}{1+\nu} - \cos\theta\right)\right] + O(r) \end{aligned} \quad (2.81)$$

$$w_3 = \frac{24(1+\nu)}{5Eh}\sqrt{\frac{r}{2\pi}}K_{3b}\sin\frac{\theta}{2} + O(r) \quad (2.82)$$

$$\begin{aligned} u_1 &= \frac{2(1+\nu)}{Eh}\sqrt{\frac{r}{2\pi}}\left[K_{1m}\cos\frac{\theta}{2}\left(\frac{1-\nu}{1+\nu} + \sin^2\frac{\theta}{2}\right)\right. \\ &\quad \left. + K_{2m}\sin\frac{\theta}{2}\left(\frac{2}{1+\nu} + \cos^2\frac{\theta}{2}\right)\right] + O(r) \end{aligned} \quad (2.83)$$

$$u_2 = \frac{2(1+\nu)}{Eh}\sqrt{\frac{r}{2\pi}}\left[K_{1m}\sin\frac{\theta}{2}\left(\frac{2}{1+\nu} - \cos^2\frac{\theta}{2}\right)\right.$$

$$+K_{2m}\cos\frac{\theta}{2}\left(\frac{\nu-1}{1+\nu}+\sin^2\frac{\theta}{2}\right)\Bigg]+O(r) \tag{2.84}$$

for displacements[139], where (r,θ) are the polar coordinates measured from the crack tip, K_{1m} and K_{2m} are mode I and mode II membrane stress resultant intensity factors respectively, K_{1b}, K_{2b}, and K_{3b} are two bending and shear stress resultant intensity factors respectively.

It is worth noting that the angular functions of the bending and membrane stress resultants for shear deformable plates and shells around the crack tip are identical. This feature permits the bending and membrane stress fields to be combined. Using the relationships in equations (2.26 – 2.27) and (2.54 – 2.55), the above stress resultant intensity factors can be related to stress intensity factors K_I, K_{II}, and K_{III} through the following relationships

$$\left[1+\frac{x_3}{2}\left(\frac{1}{R_1}+\frac{1}{R_2}\right)\right]K_I=\frac{1}{h}K_{1m}+\frac{12x_3}{h^3}K_{1b}; \tag{2.85}$$

$$\left[1+\frac{x_3}{2}\left(\frac{1}{R_1}+\frac{1}{R_2}\right)\right]K_{II}=\frac{1}{h}K_{2m}+\frac{12x_3}{h^3}K_{2b} \tag{2.86}$$

and

$$\left[1+\frac{x_3}{2}\left(\frac{1}{R_1}+\frac{1}{R_2}\right)\right]K_{III}=\frac{3}{2h}\left[1-\left(\frac{2x_3}{h}\right)^2\right]K_{3b} \tag{2.87}$$

for shallow shells, and

$$K_I=\frac{1}{h}K_{1m}+\frac{12x_3}{h^3}K_{1b}; \tag{2.88}$$

$$K_{II}=\frac{1}{h}K_{2m}+\frac{12x_3}{h^3}K_{2b} \tag{2.89}$$

and

$$K_{III}=\frac{3}{2h}\left[1-\left(\frac{2x_3}{h}\right)^2\right]K_{3b} \tag{2.90}$$

for plates.

2.5.2 Stress intensity factors evaluation

The stress intensity factors can be evaluated in several ways. Stress resultant intensity factors can be explicitly derived from equations (2.72 – 2.79). Substituting $\theta=0$ in equations (2.72 – 2.79), the stress resultant intensity factors can be ex-

pressed as:

$$K_{1b} = \lim_{r \to 0} M_{22} \sqrt{2\pi r}\,(r, 0)\,; \tag{2.91}$$

$$K_{2b} = \lim_{r \to 0} M_{12} \sqrt{2\pi r}\,(r, 0)\,; \tag{2.92}$$

$$K_{3b} = \lim_{r \to 0} Q_2 \sqrt{2\pi r}\,(r, 0)\,; \tag{2.93}$$

$$K_{1m} = \lim_{r \to 0} N_{22} \sqrt{2\pi r}\,(r, 0) \tag{2.94}$$

and

$$K_{2m} = \lim_{r \to 0} N_{12} \sqrt{2\pi r}\,(r, 0) \tag{2.95}$$

By omitting the $O(r)$ terms in equations (2.80 – 2.84) for small r and substituting θ with $\pm\pi$, the displacements on the crack surfaces near the tip are obtained as:

$$\left\{ \begin{array}{c} \Delta\phi_2 \\ \Delta\phi_1 \\ \Delta w_3 \\ \Delta u_2 \\ \Delta u_1 \end{array} \right\} = \left\{ \begin{array}{c} \phi_2 \\ \phi_1 \\ w_3 \\ u_2 \\ u_1 \end{array} \right\}_{\theta=180^0} - \left\{ \begin{array}{c} \phi_2 \\ \phi_1 \\ w_3 \\ u_2 \\ u_1 \end{array} \right\}_{\theta=-180^0} \tag{2.96}$$

$$= \left[\begin{array}{ccccc} \frac{48}{Eh^3}\sqrt{\frac{2r}{\pi}} & 0 & 0 & 0 & 0 \\ 0 & \frac{48}{Eh^3}\sqrt{\frac{2r}{\pi}} & 0 & 0 & 0 \\ 0 & 0 & \frac{24\,(1+\nu)}{5Eh}\sqrt{\frac{2r}{\pi}} & 0 & 0 \\ 0 & 0 & 0 & \frac{8}{Eh}\sqrt{\frac{r}{2\pi}} & 0 \\ 0 & 0 & 0 & 0 & \frac{8}{Eh}\sqrt{\frac{r}{2\pi}} \end{array} \right] \left\{ \begin{array}{c} K_{1b} \\ K_{2b} \\ K_{3b} \\ K_{1m} \\ K_{2m} \end{array} \right\}$$

The stress intensity factors can then be written in terms of displacements on the crack surfaces, as

$$\{K\} = \frac{1}{\sqrt{r}}\,[\mathbf{C}]\,\{w\} \tag{2.97}$$

where

$$\{K\} = \begin{Bmatrix} K_{1b} \\ K_{2b} \\ K_{3b} \\ K_{1m} \\ K_{2m} \end{Bmatrix}, \qquad \{w\} = \begin{Bmatrix} \Delta\phi_2 \\ \Delta\phi_1 \\ \Delta w_3 \\ \Delta u_2 \\ \Delta u_1 \end{Bmatrix} \tag{2.98}$$

and

$$[\mathbf{C}] = \begin{bmatrix} \frac{Eh^3}{48}\sqrt{\frac{\pi}{2}} & 0 & 0 & 0 & 0 \\ 0 & \frac{Eh^3}{48}\sqrt{\frac{\pi}{2}} & 0 & 0 & 0 \\ 0 & 0 & \frac{5Eh}{24\,(1+\nu)}\sqrt{\frac{\pi}{2}} & 0 & 0 \\ 0 & 0 & 0 & \frac{Eh}{8}\sqrt{2\pi} & 0 \\ 0 & 0 & 0 & 0 & \frac{Eh}{8}\sqrt{2\pi} \end{bmatrix} \tag{2.99}$$

2.5.3 $J-$ integral

The stress intensity factors can also be determined by the path independent $J-$ integral. In the absence of body forces, the path independent $J-$ integral; the rate of energy released per unit of crack extension in the x_δ direction is defined for plate bending as [122]

$$J_{\delta b} = \int_\Gamma \left(W_b - qw_3\right) n_\delta d\Gamma - \int_\Gamma p_i w_{i,\delta} d\Gamma + \int_\Omega q_{,\delta} w_3 d\Omega \tag{2.100}$$

and for two-dimensional plane stress as [111]

$$J_{\delta m} = \int_\Gamma \left(W_m n_\delta - t_\beta u_{\beta,\delta}\right) d\Gamma \tag{2.101}$$

where boundary Γ is an arbitrary contour surrounding the crack tip. In the case of uniform domain load, $q_{,\delta}$ is equal to zero, therefore the third integral on the RHS of equation (2.100) will vanish. It is worth mentioning that in this work the strain energy density and the tractions are defined over the thickness of the plate. The strain energy density is defined as the strain energy per unit area, and the tractions have the same unit as the stress resultants.

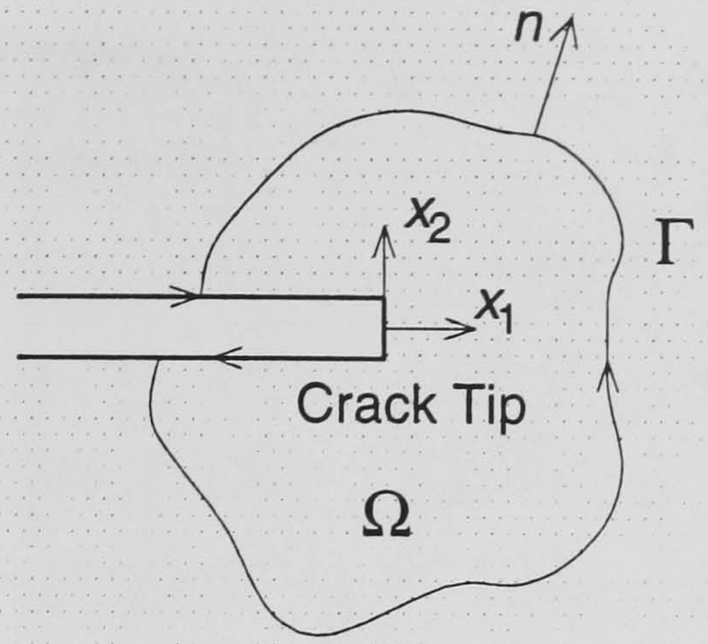

Figure 2-15: Arbitrary contour surrounding a crack tip.

The strain energy density for plate bending , W_b, and for two dimensional plane stress W_m, are defined as

$$W_b = \frac{1}{2}\left[M_{\alpha\beta}\left(\frac{w_{\alpha,\beta}+w_{\beta,\alpha}}{2}\right)+Q_\alpha\left(w_\alpha+w_{3,\alpha}\right)\right] \tag{2.102}$$

and

$$W_m = \frac{1}{2}N_{\alpha\beta}\varepsilon_{\alpha\beta} \tag{2.103}$$

where $w_{i,j}$, $\varepsilon_{\alpha\beta}$ are the strain tensors, and n_α are the components of the unit outward normal to the contour path.

The relationship between the component of $J-$ integral in x_1- direction and the bending and shear stress resultant intensity factors is given as

$$J_{1b} = \frac{12}{Eh^3}\left[{K_{1b}}^2+{K_{2b}}^2+\frac{h^2}{10}\left(1+\nu\right){K_{3b}}^2\right] \tag{2.104}$$

and the relationship between the component of $J-$ integral and the membrane stress resultant intensity factors is given as

$$J_{1m} = \frac{{K_{1m}}^2+{K_{2m}}^2}{E'} \tag{2.105}$$

where the constants E' is the elasticity modulus; E' is equal to E for plane stress

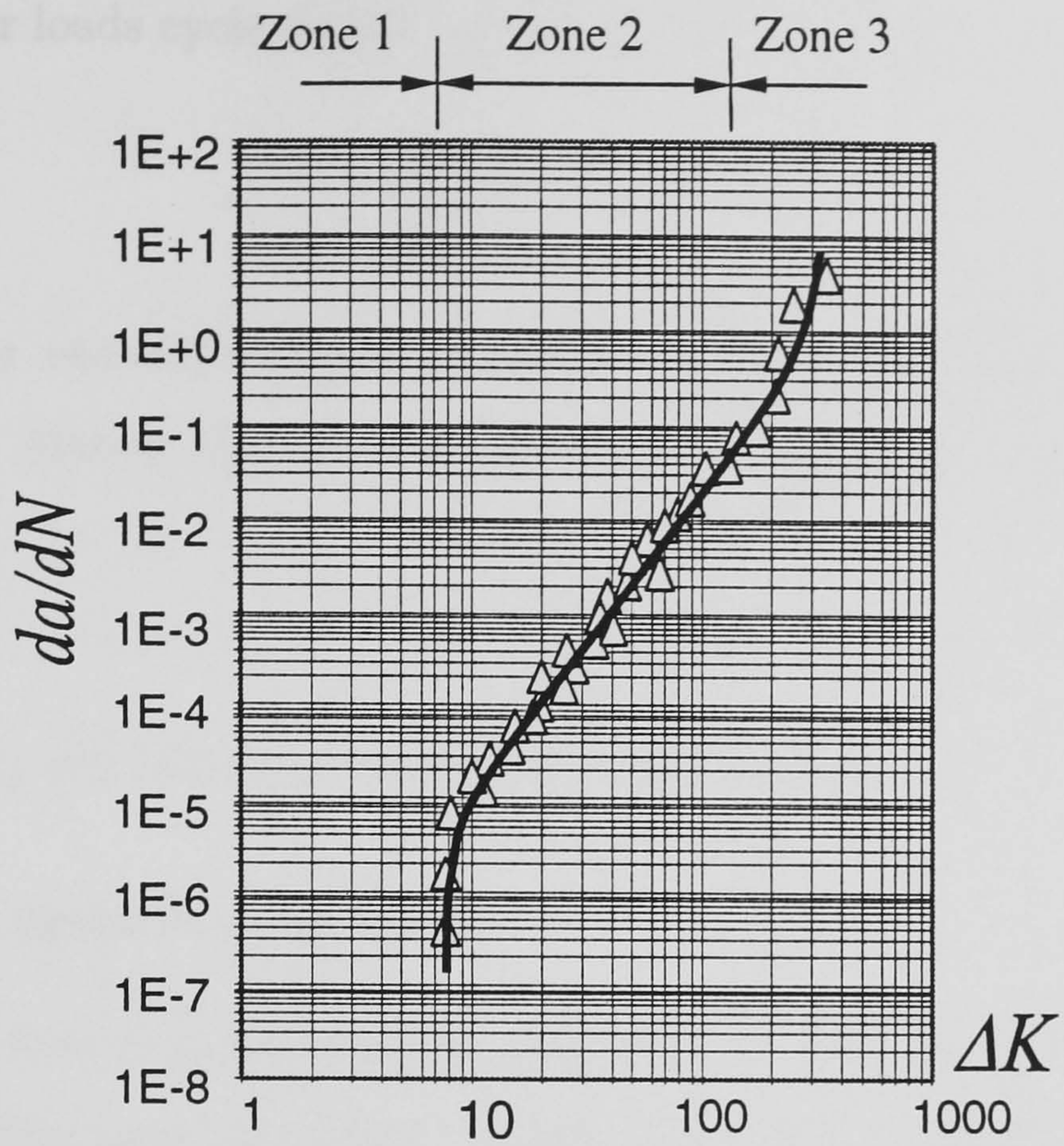

Figure 2-16: Typical fatigue crack growth rate diagram da/dN vs ΔK.

conditions and $E' = E/\left(1-\nu^2\right)$ for plane strain conditions.

2.5.4 Fatigue crack growth

During service, structures are subjected to service loads, usually in the form of cyclic loading. As a consequence of that, crack growth can take place at much lower stress level. Linear elastic fracture mechanics provides a means of predicting crack growth rate under cyclic loading.

Every material has different crack growth characteristic, depending on its alloy contents and manufacturing processes, loading frequency, environment, and the load level. The material properties are usually determined through laboratory test. Figure 2-16 shows a typical fatigue crack growth rate diagram of a material. Zone I is crack initiation phase, Zone II is stable crack growth region, and Zone III is unstable/ rapid crack growth region.

Paris, Gomez and Anderson [95] developed an empirical formula for the rate of

crack growth per loads cycle da/dN as a function of $\Delta K = K_{\max} - K_{\min}$, as

$$\frac{da}{dN} = f(\Delta K) \tag{2.106}$$

Several other researchers have presented different functions of ΔK to fit the empirical data. Among them, the simplest form suggested by Paris and Erdogan [96] was

$$\frac{da}{dN} = C_p (\Delta K)^{m_p} \tag{2.107}$$

where C_p and m_p are empirical constants of the material.

2.5.5 Crack growth direction

Several criteria have been proposed to describe the local direction of mixed-mode crack growth. The most prominent theories are based on minimum strain energy density [117], maximum energy release theory [66] and maximum circumferential stress theory [50]. However, all of these theories are only correlated to the two membrane stress intensity factors and there is no generally accepted criterion for predicting crack growth in plate subjected to bending and membrane stress resultants.

Sih [119] proposed a crack growth criterion based on the strain energy density for plate bending problems, but according to his formulation K_{3b} does not affect the propagation angle, and at the plate mid-surface the bending stress intensity factors K_{1b} and K_{2b} also do not affect the propagation angle. (Since values of stress intensity factors K_I and K_{II} due to bending at the mid-surface are equal to 0 as result of the relationships in equations (2.88 – 2.90)). Potyondy *et al.* [102], based on the maximum principal stress theory, also suggested that as at the plate mid-surface the bending stress intensity factors are equal to 0, they do not affect propagation angle.

The maximum principal stress criterion is adopted in this thesis. This criterion postulates that the growth of crack will occur in a direction perpendicular to the maximum principal stress. Hence, cracks will grow from the tip in the direction θ_t along which the shear stress is zero, that is

$$K_{I(m)} \sin\theta_t + K_{II(m)} (3\cos\theta_t - 1) = 0 \tag{2.108}$$

where θ_t is an angular coordinate centered at the crack tip and measured from the crack axis ahead of the crack tip (see Figure 2-14).

2.6 Note on Classical Plate and Shell Theories

As has been mentioned in the beginning of this chapter, the classical or the thin plate and shell theories are based on the assumptions which neglect the effect of transverse shear strains. Plates and shells analyses based on these theories are sufficient for most practical applications, as large number of engineering structures are built using thin plates and shells.

However, it was proved by comparisons to experimental analysis (see for example, References [5,6] in the paper reported by Reissner [107]) that Kirchhoff theory of thin plates is not in accordance with the experimental results for problems with stress concentrations such as, stresses at an edge of a hole when the hole diameter became so small as to be of the order of magnitude of the plate thickness.

This particular application is very important for aircraft structure, since many aircraft structures are made of thin sheets of metal reinforced by longitudinal and transverse stiffeners. In many cases, the stiffeners are attached to the sheet by means of fasteners. Fasteners are also used in lap joints between two sheets. Consequently, sheets in aircraft structure usually have many fastener holes. Therefore another theories which can give more accurate results are required for analyses of aircraft structures.

Moreover, in the case of composite or anisotropic plates, where the shear moduli ratio are large, the classical plate and shell theories can give inaccurate results [106].

Another shortcomings in classical theory is that the boundary conditions are satisfied approximately in the Kirchhoff sense, that is two boundary conditions on an edge of the plate and four for shell, while physically there are three independent boundary conditions on an edge of the plate and five on an edge of the shell. This approximation leads to several theoretical and numerical difficulties.

If Kirchhoff approximation is applied to a plate or a shell which contains corners, supported along the edges and loaded, there are not only reactions distributed along the boundaries, but also concentrated reactions at the corners (see Timoshenko and

Woinowsky-Krieger [130]) which does not happen physically.

When then Kirchhoff approximation is applied to the case of cracked plates and shells, the angular distributions of the bending and membrane stress resultants around the crack tip are entirely different (see, for example [49][52][53]). This incompatibility lead to difficulties when one wants to combine the stress fields due to membrane and bending.

On the other hand, the shear deformable theory satisfy the physical boundary conditions on the edge of plate and shell and acquired a three dimensional character in the crack front stresses for a through crack in a thick plate [116]. Based on shear deformable theory, the angular functions of the bending and membrane stress resultants around the crack tip are identical. This feature permits the bending and membrane stress fields to be combined in a natural fashion, and finally the relationship between stress intensity factors and stress resultant intensity factors due to bending and membrane can be established. This is very important feature for failure analysis, since fracture toughness of a material – a material property for the maximum allowable stress and crack length before fracture failure occurs – is presented in term of the stress intensity factor.

The application of BEM for plate and shell bending based on the classical theory also has numerical difficulties. Slope integral equation is obtain from the derivative of out-of-plane displacement integral equation. The slope equation contains hypersingular kernels of order $1/r^2$. Traction integral equations, which is required for Dual Boundary Element Method, will have kernels of order $1/r^3$ and $1/r^4$. Such high order of singularities are very difficult to handle. It appears that only Knöpke [77] has tried to derive a hypersingular integral equation for bending moments in the classical plate theory. In his work, the shear force equation was ignored and no numerical results were presented.

Another important feature of shear deformable plates and shells theories is that they can be used to analyse both thin and thick plates.

2.7 Summary

In this chapter, the basic concepts for the elasticity theories of shear deformable shells and shear deformable plates as well as the two-dimensional plane stress were reviewed. Also reviewed were some basic fundamental concepts of fracture mechanics. The next chapter will present a new formulation of the integral representation and the boundary element formulation for the theories presented in this chapter.

Chapter 3

The Boundary Element Method

3.1 Introduction

Although Boundary Element Method (BEM) has been established as an alternative numerical method to the finite element method for the solution of linear elastic problems, its development for plates and shells has not been as rapid as for the two- and three-dimensional problems. These particular applications of BEM is relatively difficult because of a high order differential equation governing the plate bending and even higher order for the shell.

The development of direct BEM to plate theory based on Kirchhoff theory was introduced by Forbes and Robinson [54] for plates with smooth boundary, followed by the works of Bézine [23] and Stern [123] for problems with corner points and different types of boundary conditions. They used the integral equation for out-of-plane deflection and used its derivative to obtain the additional integral equation for the normal slope. Hartmann and Zormantel [58], developed further the method and implemented it for plates with relatively complex geometries, loadings and supports. Following the above works, others (see for example, Stern [124], Stern and Lin [125], Abdel-Akher and Hartley [2][3], Karami *et al.* [71]) have further improved and applied the plate bending formulation.

The application of the direct BEM for analysis of Reissner plate was first presented by Vander Weeën [134, 135] in 1982. In his work, Weeën derived the boundary integral equation from Betti's theorem and derived the fundamental solution using

the Hörmander's method. Following his formulation, Karam and Telles [69] reported that Reissner's plate model is suitable for both thin and thick plates. They also extend the formulation to account for infinite regions. Barcellos and Silva [18] presented a similar formulation to that of Vander Weeën [134] for Mindlin plate model. Their formulation differs from the Reissner formulation in the shear factor constant. Westphal and Barcellos [141] discussed the importance of the neglected terms in the fundamental solution derived by Vander Weeën [134]. They concluded that these terms have no effect on the results. Later, El-Zafrany, Debbih and Fadhil [46] derived fundamental solutions for the Reissner plate based on the Hankel integral transformation. The results were shown to be same as that of Vander Weeën [134]. In [47], a modified form of the fundamental solutions were derived, by separating parts of the kernel representing the effect of transverse shear, to allow analysis of thin and thick plates. Recent advances in the boundary element method for plate bending analysis can be found in the book edited by Aliabadi [12].

There are fewer works on the use of direct BEM for analysis of shallow shells, and only a hand full of publications for shear deformable shallow shells. This particular application of BEM is relatively difficult because of the high order differential equations governing the shell. Newton and Tottenham [91], and Tottenham [132] presented an early applications of BEM to shallow shell problems, by decomposition of the fourth order governing equations into a second order equations. Antes [14] derived a BEM formulation for circular cylindrical shells, but no numerical examples were presented. Tosaka and Miyake [131] derived the direct BEM formulation for a shallow shell starting from the reduced single complex-valued equation of the coupled $w - \phi$ formulation. More recently Lu and Huang [80] developed a direct BEM formulation for shallow shell involving shear deformation.

As stated in the review by Beskos [22], the application of direct BEM for shell problems as reported in the above works involve complicated fundamental solutions (see e.g. [81][79][74]), therefore it will be difficult to extend this method to any other applications such as hypersingular integral equations, elastoplasticity or geometric non-linearity.

There is, however, another approach that has been developed to deal with shallow shell problems. The method is called the domain-boundary element method. The

work of Forbes and Robinson [54] was the first which develop the direct domain-boundary element method for the static analysis of shallow shells. Zhang and Atluri [144] have also successfully derived the formulation for static and dynamic analysis of shallow shells base on weighted residual method. Providakis and Beskos [94] and Beskos [22] extended the method to solve static and vibration analysis of shallow shells. They derived the formulation with the aid of the reciprocal theorem. Recently, Jinmu and Shuyao [75] used this method for geometrically nonlinear analysis of shallow shells. All the formulations derived using this approach are formed by coupling the boundary element formulation of Kirchhoff plate bending and the two dimensional plane stress elasticity. There are advantages and disadvantages in this approach. The main advantage is that the fundamental solutions involved in this method are much simpler than the ones in the direct BEM. However, due to additional curvature terms in the equilibrium equations, this method contains domain integrals as well as boundary integrals.

In this chapter the derivation of boundary integral equations for the analysis of shallow shells involving shear deformation is presented. The formulation is formed by coupling boundary element formulations of shear deformable plate bending and two dimensional plane stress elasticity. The boundary is discretised into quadratic isoparametric elements. The domain integrals which appear in this formulation are treated in two different ways: firstly the integrals are evaluated numerically using constant cell discretisation, and secondly they are transformed to boundary integrals using the dual reciprocity technique. Also presented are the boundary integral equations for the analysis of shear deformable plate bending and two-dimensional plane stress problems. Some examples with different geometry and loading conditions are presented to demonstrate the efficiency of the proposed formulation.

3.2 The Integral Representations

The equilibrium equations of shear deformable shallow shell in equations (2.47 – 2.51) can be rewritten as follows:

$$D\nabla^2 w_1 + \frac{D}{2}(1+\nu)\frac{\partial}{\partial x_2}\left(-\frac{\partial w_1}{\partial x_2} + \frac{\partial w_2}{\partial x_1}\right) - Cw_1 - C\frac{\partial w_3}{\partial x_1} = 0 \qquad (3.1)$$

$$\frac{D}{2}(1+\nu)\frac{\partial}{\partial x_1}\left(\frac{\partial w_1}{\partial x_2}-\frac{\partial w_2}{\partial x_1}\right)+D\nabla^2 w_2-Cw_2-C\frac{\partial w_3}{\partial x_2}=0 \tag{3.2}$$

$$C\nabla^2 w_3+C\frac{\partial w_1}{\partial x_1}+C\frac{\partial w_2}{\partial x_2}+q_3^*=0 \tag{3.3}$$

$$B\nabla^2 u_1+\frac{B}{2}(1+\nu)\frac{\partial}{\partial x_2}\left(-\frac{\partial u_1}{\partial x_2}+\frac{\partial u_2}{\partial x_1}\right)+q_1^*=0 \tag{3.4}$$

$$\frac{B}{2}(1+\nu)\frac{\partial}{\partial x_1}\left(\frac{\partial u_1}{\partial x_2}-\frac{\partial u_2}{\partial x_1}\right)+B\nabla^2 u_2+q_2^*=0 \tag{3.5}$$

where q_1^*, q_2^*, q_3^* are equivalent body forces

$$q_1^*=q_1+B(k_{11}+\nu k_{22})\frac{\partial w_3}{\partial x_1} \tag{3.6}$$

$$q_2^*=q_2+B(\nu k_{11}+k_{22})\frac{\partial w_3}{\partial x_2} \tag{3.7}$$

$$\begin{aligned} q_3^* \;=\; & q_3-B(k_{11}+\nu k_{22})\frac{\partial u_1}{\partial x_1}-B(\nu k_{11}+k_{22})\frac{\partial u_2}{\partial x_2} \\ & -B(k_{11}^2+k_{22}^2+2\nu k_{11}k_{22})w_3 \end{aligned} \tag{3.8}$$

It can be seen that equations (3.1 – 3.5) have the form of equations (2.67 – 2.71) which represent shear deformable plate bending and two dimensional plane stress static deformations respectively for which boundary integral formulation procedures and fundamental solutions have already been developed. Therefore boundary integral representation for the above equations can be achieved by employing similar procedures to shear deformable plate bending and two dimensional plane stress. The force terms q_1^*, q_2^*, q_3^* consist of the coupling terms which should vanish for flat plates, i.e. $k_{11}=k_{22}=0$.

Equations (3.1 – 3.5) can be rewritten as follows:

$$L_{ik}^b w_k+f_i^b=0 \tag{3.9}$$

and

$$L_{\alpha\beta}^m u_\beta+f_\alpha^m=0 \tag{3.10}$$

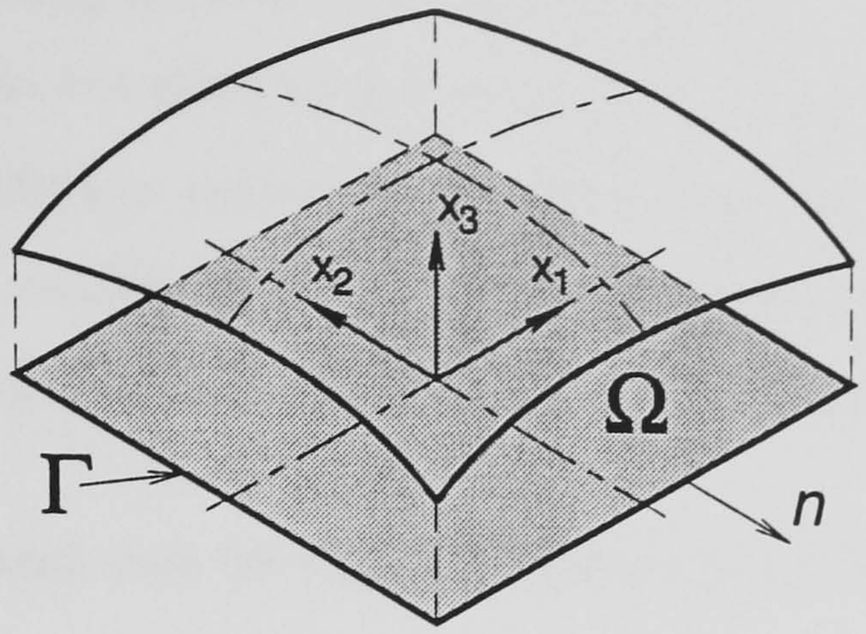

Figure 3-1: Shell geometry and its projection on $x_1 - x_2$ plane.

where L^b_{ik} is the Navier differential operator for shear deformable plate bending problems

$$L^b_{\alpha\beta} = \frac{D\,(1-\nu)}{2}\left[\left(\nabla^2 - \lambda^2\right)\delta_{\alpha\beta} + \frac{(1+\nu)}{(1-\nu)}\frac{\partial}{\partial x_\alpha}\frac{\partial}{\partial x_\beta}\right] \tag{3.11}$$

$$L^b_{\alpha 3} = -\frac{(1-\nu)\,D}{2}\lambda^2\frac{\partial}{\partial x_\alpha} \tag{3.12}$$

$$L^b_{3\alpha} = -L^b_{\alpha 3} \tag{3.13}$$

$$L^b_{33} = \frac{(1-\nu)\,D}{2}\lambda^2\nabla^2 \tag{3.14}$$

with $f^b_\alpha = 0$ and $f^b_3 = q^*_3$, while $L^m_{\alpha\beta}$ is the Navier differential operator for two-dimensional plane stress problems

$$L^m_{\alpha\beta} = B\nabla^2\delta_{\alpha\beta} + \frac{B\,(1+\nu)}{2}\frac{\partial}{\partial x_\alpha}\frac{\partial}{\partial x_\beta}\left(1 - 2\delta_{\alpha\beta}\right) \tag{3.15}$$

with $f^m_\alpha = q^*_\alpha$.

The integral equations for shallow shell problems can be derived by considering the integral representations of the governing equations (2.37 – 2.39) from the following integral identities:

$$\int_\Omega \left[\left(M_{\alpha\beta,\beta} - Q_\alpha\right)W^*_\alpha + \left(Q_{\alpha,\alpha} - k_{\alpha\beta}N_{\alpha\beta} + q_3\right)W^*_3\right]d\Omega = 0 \tag{3.16}$$

and

$$\int_\Omega \left(N_{\alpha\beta,\beta} + q_\alpha\right)U^*_\alpha d\Omega = 0 \tag{3.17}$$

where U^*_α and $W^*_i (i = \alpha, 3)$ are weighting functions and Ω is the projected domain of a shell on $x_1 - x_2$ plane, bounded by boundary Γ (see Figure 3-1). Equation (3.16) is an integral representation related to the governing equations for bending and transverse shear stress resultants, while equation (3.17) is an integral representation related to the governing equations for membrane stress resultants.

3.2.1 Rotations and out-of-plane displacement integral representations

Here, the integral representations related to the governing equations for bending and transverse shear stress resultants are derived by using the weighted residual method. Integrating equation (3.16) by parts (applying the Green's identity[1]), gives:

$$\int_\Gamma M_{\alpha\beta} n_\beta W^*_\alpha d\Gamma - \int_\Omega M_{\alpha\beta} W^*_{\alpha,\beta} d\Omega - \int_\Omega Q_\alpha W^*_\alpha d\Omega$$

$$+ \int_\Gamma Q_\alpha n_\alpha W^*_3 d\Gamma - \int_\Omega Q_\alpha W^*_{3,\alpha} d\Omega - \int_\Omega k_{\alpha\beta} N_{\alpha\beta} W^*_3 d\Omega + \int_\Omega q_3 W^*_3 d\Omega = 0 \quad (3.18)$$

then, by substituting the relationships for p_j in equation (2.28), equation (3.18) can be written as follows:

$$\int_\Gamma p_j W^*_j d\Gamma - \int_\Omega M_{\alpha\beta} W^*_{\alpha,\beta} d\Omega - \int_\Omega Q_\alpha (W^*_\alpha + W^*_{3,\alpha}) d\Omega$$

$$- \int_\Omega k_{\alpha\beta} N_{\alpha\beta} W^*_3 d\Omega + \int_\Omega q_3 W^*_3 d\Omega = 0 \quad (3.19)$$

where $(j = \alpha, 3)$. Replacing the bending and shear stress resultants ($M_{\alpha\beta}$ and Q_α) with the generalised displacements and their derivatives using equations (2.44 – 2.45), equation (3.19) will become

$$\int_\Gamma p_j W^*_j d\Gamma - \int_\Omega W^*_{\alpha,\beta} \left\{ \frac{D(1-\nu)}{2} \left(w_{\alpha,\beta} + w_{\beta,\alpha} + \frac{2\nu}{(1-\nu)} \delta_{\alpha\beta} w_{\gamma,\gamma} \right) \right\} d\Omega$$

[1] The Green's identity between two functions P and $u_{,\alpha}$ can be written as follows[56]:

$$\int_\Omega P u_{,\alpha} d\Omega = \int_\Gamma P u n_\alpha d\Gamma - \int_\Omega P_{,\alpha} u d\Omega$$

$$-\int_\Omega C(w_\alpha + w_{3,\alpha})(W^*_\alpha + W^*_{3,\alpha})d\Omega - \int_\Omega k_{\alpha\beta}N_{\alpha\beta}W^*_3 d\Omega + \int_\Omega q_3 W^*_3 d\Omega = 0 \quad (3.20)$$

then applying Green's identity for the $M_{\alpha\beta}$ integral and rearranging the third integral on the left hand side (LHS) of equation (3.20), gives:

$$\int_\Gamma p_j W^*_j d\Gamma - \int_\Gamma W^*_{\alpha,\beta}\left\{\frac{D(1-\nu)}{2}\left(w_\alpha n_\beta + w_\beta n_\alpha + \frac{2\nu}{(1-\nu)}\delta_{\alpha\beta}w_\gamma n_\gamma\right)\right\}d\Gamma$$

$$+\int_\Omega \frac{D(1-\nu)}{2}\left(w_\alpha W^*_{\alpha,\beta\beta} + w_\beta W^*_{\alpha,\beta\alpha} + \frac{2\nu}{(1-\nu)}w_\gamma W^*_{\alpha,\beta\gamma}\delta_{\alpha\beta}\right)d\Omega$$

$$-\int_\Omega Q^*_\alpha(w_\alpha + w_{3,\alpha})d\Omega - \int_\Omega k_{\alpha\beta}N_{\alpha\beta}W^*_3 d\Omega + \int_\Omega q_3 W^*_3 d\Omega = 0 \quad (3.21)$$

Equation (3.21) can be written in following form:

$$I_1 - I_2 + I_3 - I_4 - I_5 + I_6 = 0 \quad (3.22)$$

In the following some of the integrals in equation (3.22) will be expanded and considered individually.

The integrals I_2 and I_3

Making use of the relationships $w_\beta = w_\alpha\delta_{\alpha\beta}$; $w_\gamma = w_\alpha\delta_{\alpha\gamma}$; $n_\alpha = n_\beta\delta_{\alpha\beta}$ and $n_\gamma = n_\beta\delta_{\beta\gamma}$, and relationship for $M_{\alpha\beta}$ in equations (2.44) the integrals I_2 and I_3 can be rewritten as

$$\begin{aligned}
I_2 &= \int_\Gamma W^*_{\alpha,\beta}\left\{\frac{D(1-\nu)}{2}\left(w_\alpha n_\beta + w_\beta n_\alpha + \frac{2\nu}{(1-\nu)}\delta_{\alpha\beta}w_\gamma n_\gamma\right)\right\}d\Gamma \\
&= \int_\Gamma w_\alpha n_\beta\left\{\frac{D(1-\nu)}{2}\left(W^*_{\alpha,\beta} + W^*_{\alpha,\beta}\delta_{\alpha\beta}\delta_{\alpha\beta} + \frac{2\nu}{(1-\nu)}\delta_{\alpha\beta}W^*_{\alpha,\beta}\delta_{\alpha\gamma}\delta_{\beta\gamma}\right)\right\}d\Gamma \\
&= \int_\Gamma w_\alpha M^*_{\alpha\beta}n_\beta d\Gamma \\
&= \int_\Gamma w_\alpha P^*_\alpha d\Gamma \qquad (3.23)
\end{aligned}$$

and

$$\begin{aligned}
I_3 &= \int_\Omega \frac{D(1-\nu)}{2}\left(w_\alpha W^*_{\alpha,\beta\beta} + w_\beta W^*_{\alpha,\beta\alpha} + \frac{2\nu}{(1-\nu)}w_\gamma W^*_{\alpha,\beta\gamma}\delta_{\alpha\beta}\right)d\Omega \\
&= \int_\Omega w_\alpha\left\{\frac{D(1-\nu)}{2}\left(W^*_{\alpha,\beta\beta} + \delta_{\alpha\beta}W^*_{\alpha,\beta\alpha} + \frac{2\nu}{(1-\nu)}\delta_{\alpha\gamma}W^*_{\alpha,\beta\gamma}\delta_{\alpha\beta}\right)\right\}d\Omega
\end{aligned}$$

$$
\begin{aligned}
&= \int_\Omega w_\alpha \left\{ \frac{D(1-\nu)}{2} \left(W^*_{\alpha,\beta\beta} + W^*_{\beta,\alpha\beta} + \frac{2\nu}{(1-\nu)} \delta_{\alpha\gamma} W^*_{\gamma,\gamma\beta} \delta_{\alpha\beta} \right) \right\} d\Omega \\
&= \int_\Omega w_\alpha M^*_{\alpha\beta,\beta} d\Omega
\end{aligned} \tag{3.24}
$$

The integral I_4

The integral I_4 can be decomposed using the Green's identity and making use of the relationships for p_3 in equation (2.28), as follows:

$$
\begin{aligned}
I_4 &= \int_\Omega Q^*_\alpha (w_\alpha + w_{3,\alpha}) d\Omega \\
&= \int_\Omega Q^*_\alpha w_\alpha d\Omega + \int_\Omega Q^*_\alpha w_{3,\alpha} d\Omega \\
&= \int_\Omega Q^*_\alpha w_\alpha d\Omega + \int_\Gamma Q^*_\alpha w_3 n_\alpha d\Gamma - \int_\Omega Q^*_{\alpha,\alpha} w_3 d\Omega \\
&= \int_\Gamma P^*_3 w_3 d\Gamma + \int_\Omega (Q^*_\alpha w_\alpha - Q^*_{\alpha,\alpha} w_3) d\Omega
\end{aligned} \tag{3.25}
$$

The integral I_5

The integral I_5 can also be decomposed using the Green's identity and making use of the relationships for $N_{\alpha\beta}$ in (2.46), as follows:

$$
\begin{aligned}
I_5 &= \int_\Omega k_{\alpha\beta} N_{\alpha\beta} W^*_3 d\Omega \\
&= \int_\Omega k_{\alpha\beta} W^*_3 \left[B \frac{1-\nu}{2} \left(u_{\alpha,\beta} + u_{\beta,\alpha} + \frac{2\nu}{1-\nu} u_{\gamma,\gamma} \delta_{\alpha\beta} \right) \right] d\Omega \\
&\quad + \int_\Omega k_{\alpha\beta} W^*_3 \left[B \left((1-\nu) k_{\alpha\beta} + \nu \delta_{\alpha\beta} k_{\gamma\gamma} \right) w_3 \right] d\Omega \\
&= \int_\Gamma k_{\alpha\beta} B \frac{1-\nu}{2} \left(u_\alpha n_\beta + u_\beta n_\alpha + \frac{2\nu}{1-\nu} u_\gamma n_\gamma \delta_{\alpha\beta} \right) W^*_3 d\Gamma \\
&\quad - \int_\Omega k_{\alpha\beta} B \frac{1-\nu}{2} \left(u_\alpha W^*_{3,\beta} + u_\beta W^*_{3,\alpha} + \frac{2\nu}{1-\nu} u_\gamma W^*_{3,\gamma} \delta_{\alpha\beta} \right) d\Omega \\
&\quad + \int_\Omega k_{\alpha\beta} B \left((1-\nu) k_{\alpha\beta} + \nu \delta_{\alpha\beta} k_{\gamma\gamma} \right) w_3 W^*_3 d\Omega
\end{aligned} \tag{3.26}
$$

Now, by substituting equations (3.23), (3.24), (3.25) and (3.26) into equation (3.21) and grouping, equation (3.21) will become:

$$
\int_\Gamma (W^*_j p_j - P^*_j w_j) d\Gamma - \int_\Gamma k_{\alpha\beta} B \frac{1-\nu}{2} \left(u_\alpha n_\beta + u_\beta n_\alpha + \frac{2\nu}{1-\nu} u_\gamma n_\gamma \delta_{\alpha\beta} \right) W^*_3 d\Gamma
$$

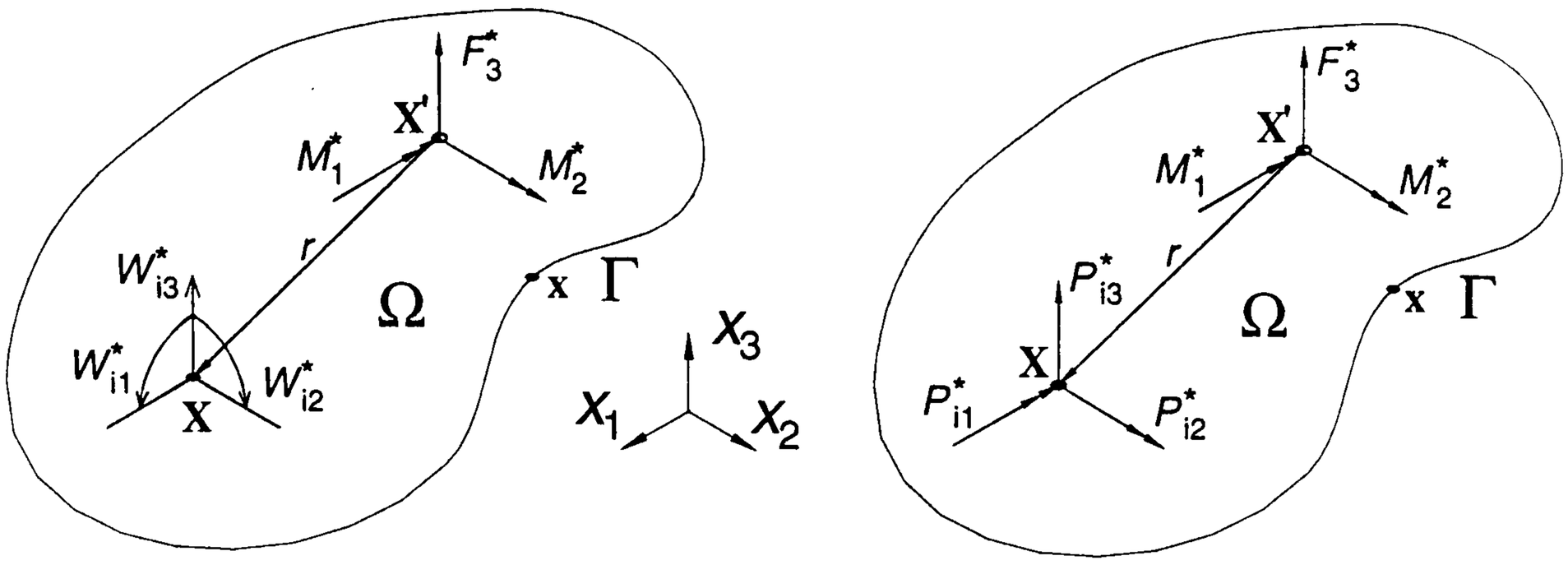

Figure 3-2: Fundamental state of displacements and tractions due to concentrated shear force and bending moments.

$$+\int_\Omega k_{\alpha\beta}B\frac{1-\nu}{2}\left(u_\alpha W^*_{3,\beta}+u_\beta W^*_{3,\alpha}+\frac{2\nu}{1-\nu}u_\gamma W^*_{3,\gamma}\delta_{\alpha\beta}\right)d\Omega$$

$$-\int_\Omega k_{\alpha\beta}B\left[(1-\nu)k_{\alpha\beta}+\nu\delta_{\alpha\beta}k_{\gamma\gamma}\right]w_3W^*_3d\Omega$$

$$+\int_\Omega[(M^*_{\alpha\beta,\beta}-Q^*_\alpha)w_\alpha+Q^*_{\alpha,\alpha}w_3]d\Omega+\int_\Omega W^*_3q_3d\Omega=0 \tag{3.27}$$

It has to be noted that the $(\cdot)^*$ state can be chosen arbitrary. If the state is defined for concentrated generalised loads: two bending moments ($i=\alpha=1,2$) and one concentrated shear force ($i=3$) at an arbitrary source point $\mathbf{X}'\in\Omega$ as shown in Figure 3-2, then equation (3.27) can be rewritten after introducing the direction of the load i as follows:

$$\int_\Gamma\left[W^*_{ij}\left(\mathbf{X}',\mathbf{x}\right)p_j\left(\mathbf{x}\right)-P^*_{ij}\left(\mathbf{X}',\mathbf{x}\right)w_j\left(\mathbf{x}\right)\right]d\Gamma\left(\mathbf{x}\right)+\int_\Omega W^*_{i3}\left(\mathbf{X}',\mathbf{X}\right)q_3d\Omega\left(\mathbf{X}\right)$$

$$-\int_\Gamma k_{\alpha\beta}B\frac{1-\nu}{2}\left[u_\alpha\left(\mathbf{x}\right)n_\beta+u_\beta\left(\mathbf{x}\right)n_\alpha+\frac{2\nu}{1-\nu}u_\gamma\left(\mathbf{x}\right)n_\gamma\delta_{\alpha\beta}\right]W^*_{i3}\left(\mathbf{X}',\mathbf{x}\right)d\Gamma\left(\mathbf{x}\right)$$

$$+\int_\Omega k_{\alpha\beta}B\frac{1-\nu}{2}\left[u_\alpha\left(\mathbf{X}\right)W^*_{i3,\beta}\left(\mathbf{X}',\mathbf{X}\right)+u_\beta\left(\mathbf{X}\right)W^*_{i3,\alpha}\left(\mathbf{X}',\mathbf{X}\right)\right.$$

$$\left.+\frac{2\nu}{1-\nu}u_\gamma\left(\mathbf{X}\right)W^*_{i3,\gamma}\left(\mathbf{X}',\mathbf{X}\right)\delta_{\alpha\beta}\right]d\Omega\left(\mathbf{X}\right)$$

$$-\int_\Omega k_{\alpha\beta}B\left[(1-\nu)k_{\alpha\beta}+\nu\delta_{\alpha\beta}k_{\gamma\gamma}\right]w_3\left(\mathbf{X}\right)W^*_{i3}\left(\mathbf{X}',\mathbf{X}\right)d\Omega\left(\mathbf{X}\right)$$

$$+\int_{\Omega}\left[M^{*}_{i\alpha\beta,\beta}(\mathbf{X}',\mathbf{X})-Q^{*}_{i\alpha}(\mathbf{X}',\mathbf{X})\right]w_{\alpha}(\mathbf{X})d\Omega(\mathbf{X})$$

$$+\int_{\Omega}Q^{*}_{i\alpha,\alpha}(\mathbf{X}',\mathbf{X})w_{3}(\mathbf{X})d\Omega(\mathbf{X})=0 \tag{3.28}$$

where $\mathbf{x}\in\Gamma$ and $\mathbf{X}\in\Omega$ are field points. By choosing the $(\cdot)^{*}$ state to represent the fundamental state such as:

$$M^{*}_{i\alpha\beta,\beta}(\mathbf{X}',\mathbf{X})-Q^{*}_{i\alpha}(\mathbf{X}',\mathbf{X})+\delta(\mathbf{X}',\mathbf{X})\delta_{i\alpha}=0$$

$$Q^{*}_{i\alpha,\alpha}(\mathbf{X}',\mathbf{X})+\delta(\mathbf{X}',\mathbf{X})\delta_{i3}=0 \tag{3.29}$$

where $\delta(\mathbf{X}',\mathbf{X})$ is the Dirac delta, and making use of the following property:

$$\int_{\Omega}\delta(\mathbf{X}',\mathbf{X})w_{i}(\mathbf{X})d\Omega=w_{i}(\mathbf{X}') \tag{3.30}$$

then equation (3.28) can be written for an internal source point $\mathbf{X}'$ as:

$$w_{i}(\mathbf{X}')+\int_{\Gamma}P^{*}_{ij}(\mathbf{X}',\mathbf{x})w_{j}\left(\mathbf{x}\right)d\Gamma\left(\mathbf{x}\right)=\int_{\Gamma}W^{*}_{ij}(\mathbf{X}',\mathbf{x})p_{j}\left(\mathbf{x}\right)d\Gamma\left(\mathbf{x}\right)$$

$$-\int_{\Gamma}k_{\alpha\beta}B\frac{1-\nu}{2}\left(u_{\alpha}\left(\mathbf{x}\right)n_{\beta}+u_{\beta}\left(\mathbf{x}\right)n_{\alpha}+\frac{2\nu}{1-\nu}u_{\gamma}\left(\mathbf{x}\right)n_{\gamma}\delta_{\alpha\beta}\right)W^{*}_{i3}\left(\mathbf{X}',\mathbf{x}\right)d\Gamma\left(\mathbf{x}\right)$$

$$+\int_{\Omega}k_{\alpha\beta}B\frac{1-\nu}{2}\left[u_{\alpha}\left(\mathbf{X}\right)W^{*}_{i3,\beta}\left(\mathbf{X}',\mathbf{X}\right)+u_{\beta}\left(\mathbf{X}\right)W^{*}_{i3,\alpha}\left(\mathbf{X}',\mathbf{X}\right)\right.$$

$$\left.+\frac{2\nu}{1-\nu}u_{\gamma}\left(\mathbf{X}\right)W^{*}_{i3,\gamma}\left(\mathbf{X}',\mathbf{X}\right)\delta_{\alpha\beta}\right]d\Omega\left(\mathbf{X}\right)$$

$$-\int_{\Omega}k_{\alpha\beta}B\left[(1-\nu)k_{\alpha\beta}+\nu\delta_{\alpha\beta}k_{\gamma\gamma}\right]w_{3}\left(\mathbf{X}\right)W^{*}_{i3}\left(\mathbf{X}',\mathbf{X}\right)d\Omega\left(\mathbf{X}\right)$$

$$+\int_{\Omega}W^{*}_{i3}(\mathbf{X}',\mathbf{X})q_{3}(\mathbf{X})d\Omega(\mathbf{X}) \tag{3.31}$$

where $W^{*}_{ij}(\mathbf{X}',\mathbf{x})$ and $P^{*}_{ij}(\mathbf{X}',\mathbf{x})$ are the fundamental solutions for rotations and out-of-plane displacements and bending and shear tractions respectively. It represents the displacement or the tractions at the point $\mathbf{x}$ or $\mathbf{X}$ in the direction j due to unit load applied at $\mathbf{X}'$ at the direction i.

3.2.2 Fundamental solutions

The expressions for the kernels W^*_{ij} and P^*_{ij} are given by Vander Weeën [134] as follows:

$$\begin{aligned}
W^*_{\alpha\beta} &= \frac{1}{8\pi D(1-\nu)}\{[8B(z)-(1-\nu)(2\ln z-1)]\delta_{\alpha\beta} \\
&- [8A(z)+2(1-\nu)]r_{,\alpha}r_{,\beta}\} \\
W^*_{\alpha 3} &= -W^*_{3\alpha} = \frac{1}{8\pi D}(2\ln z-1)rr_{,\alpha} \\
W^*_{33} &= \frac{1}{8\pi D(1-\nu)\lambda^2}[(1-\nu)z^2(\ln z-1)-8\ln z]
\end{aligned} \tag{3.32}$$

and

$$\begin{aligned}
P^*_{\gamma\alpha} &= \frac{-1}{4\pi r}[(4A(z)+2zK_1(z)+1-\nu)(\delta_{\alpha\gamma}r_{,n}+r_{,\alpha}n_\gamma) \\
&+ (4A(z)+1+\nu)r_{,\gamma}n_\alpha - 2(8A(z)+2zK_1(z)+1-\nu)r_{,\alpha}r_{,\gamma}r_{,n}] \\
P^*_{\gamma 3} &= \frac{\lambda^2}{2\pi}[B(z)n_\gamma - A(z)r_{,\gamma}r_{,n}] \\
P^*_{3\alpha} &= \frac{-(1-\nu)}{8\pi}\left[\left(2\frac{(1+\nu)}{(1-\nu)}\ln z-1\right)n_\alpha + 2r_{,\alpha}r_{,n}\right] \\
P^*_{33} &= \frac{-1}{2\pi r}r_{,n}
\end{aligned} \tag{3.33}$$

where

$$\begin{aligned}
A(z) &= K_0(z)+\frac{2}{z}\left[K_1(z)-\frac{1}{z}\right] \\
B(z) &= K_0(z)+\frac{1}{z}\left[K_1(z)-\frac{1}{z}\right]
\end{aligned} \tag{3.34}$$

in which $K_0(z)$ and $K_1(z)$ are modified Bessel functions of the second kind [4], $z=\lambda r$, λ is the shear factor defined in section 2.3.4, r is the absolute distance between the source and the field points, $r_{,\alpha}=r_\alpha/r$, where $r_\alpha = x_\alpha(\mathbf{x})-x_\alpha(\mathbf{x}')$ and $r_{,n}=r_{,\alpha}n_\alpha$.

Expanding the modified Bessel functions for small arguments:

$$\begin{aligned}
K_0(z) &= \left[-\gamma-\ln(\frac{z}{2})\right]+\left[-\gamma+1-\ln(\frac{z}{2})\right]\frac{(z^2/4)}{(1!)^2} \\
&+\left[-\gamma+1+\frac{1}{2}-\ln(\frac{z}{2})\right]\frac{(z^2/4)^2}{(2!)^2}
\end{aligned}$$

$$+\left[-\gamma+1+\frac{1}{2}+\frac{1}{3}-\ln(\frac{z}{2})\right]\frac{(z^2/4)^3}{(3!)^2}+\cdots \tag{3.35}$$

$$\begin{aligned} K_1(z) &= \frac{1}{z}-\left[-\gamma+\frac{1}{2}-\ln(\frac{z}{2})\right]\frac{(z^2/4)^{1/2}}{0!1!} \\ &\quad -\left[-\gamma+1+\frac{1}{4}-\ln(\frac{z}{2})\right]\frac{(z^2/4)^{3/2}}{1!2!} \\ &\quad -\left[-\gamma+1+\frac{1}{2}+\frac{1}{6}-\ln(\frac{z}{2})\right]\frac{(z^2/4)^{5/2}}{2!3!}+\cdots \end{aligned} \tag{3.36}$$

where $\gamma = 0.5772156649$ is the Euler constant. Substitute equations (3.35 – 3.36) into (3.34) and take the limit as $r \to 0$:

$$\begin{aligned} \lim_{r\to 0} A(z) &= \frac{-1}{2}, \\ \lim_{r\to 0} B(z) &= -\frac{1}{2}\left[\lim_{r\to 0}\ln(\frac{z}{2})+\gamma+\frac{1}{2}\right] \end{aligned} \tag{3.37}$$

As it can be seen, $A(z)$ is a smooth function, whereas, $B(z)$ is a weakly singular $O(\ln r)$. Therefore W^*_{ij} is weakly singular and P^*_{ij} has a strong (Cauchy principal value) singularity $O(1/r)$.

In this work, the modified Bessel functions are evaluated using polynomial approximations given by Abramowitz and Stegun [4] (see appendix A).

3.2.3 In-plane displacements integral representations

The integral representations related to governing equations for membrane stress resultants can be solved in a similar way. Separating the terms in the bracket in equation (3.17) then integrating by parts (applying Green's identity), gives:

$$\int_\Gamma N^{(i)}_{\alpha\beta}n_\beta U^*_\alpha d\Gamma - \int_\Omega N^{(i)}_{\alpha\beta}U^*_{\alpha,\beta}d\Omega + \int_\Omega N^{(ii)}_{\alpha\beta,\beta}U^*_\alpha d\Omega + \int_\Omega q_\alpha U^*_\alpha d\Omega = 0 \tag{3.38}$$

Using the relationships for t_α in equation (2.28), defining $t_\alpha = t^{(i)}_\alpha + t^{(ii)}_\alpha$, then

$$t^{(i)}_\alpha = N^{(i)}_{\alpha\beta}n_\beta \qquad \text{and} \qquad t^{(ii)}_\alpha = N^{(ii)}_{\alpha\beta}n_\beta \tag{3.39}$$

Utilising the above definitions and substituting equation (2.46) into (3.38), gives:

$$\int_\Gamma t_\alpha^{(i)} U_\alpha^* d\Gamma - \int_\Omega B \frac{1-\nu}{2} \left(u_{\alpha,\beta} + u_{\beta,\alpha} + \frac{2\nu}{1-\nu} u_{\gamma,\gamma} \delta_{\alpha\beta} \right) U_{\alpha,\beta}^* d\Omega$$

$$+ \int_\Omega B \left[(1-\nu) k_{\alpha\beta} + \nu \delta_{\alpha\beta} k_{\gamma\gamma} \right] w_{3,\beta} U_\alpha^* d\Omega + \int_\Omega q_\alpha U_\alpha^* d\Omega = 0 \qquad (3.40)$$

Integrating by parts the second and the third integrals in LHS of equation (3.40), gives:

$$\int_\Gamma t_\alpha^{(i)} U_\alpha^* d\Gamma - \int_\Gamma B \frac{1-\nu}{2} \left(u_\alpha n_\beta + u_\beta n_\alpha + \frac{2\nu}{1-\nu} u_\gamma n_\gamma \delta_{\alpha\beta} \right) U_{\alpha,\beta}^* d\Gamma$$

$$+ \int_\Omega B \frac{1-\nu}{2} \left(u_\alpha U_{\alpha,\beta\beta}^* + u_\beta U_{\alpha,\beta\alpha}^* + \frac{2\nu}{1-\nu} \delta_{\alpha\beta} u_\gamma U_{\alpha,\beta\gamma}^* \right) d\Omega$$

$$+ \int_\Gamma B \left[(1-\nu) k_{\alpha\beta} + \nu \delta_{\alpha\beta} k_{\gamma\gamma} \right] w_3 n_\beta U_\alpha^* d\Gamma$$

$$- \int_\Omega B \left[(1-\nu) k_{\alpha\beta} + \nu \delta_{\alpha\beta} k_{\gamma\gamma} \right] w_3 U_{\alpha,\beta}^* d\Omega + \int_\Omega q_\alpha U_\alpha^* d\Omega = 0 \qquad (3.41)$$

Equation (3.41) can be written in following form:

$$I_7 - I_8 + I_9 + I_{10} - I_{11} + I_{12} = 0 \qquad (3.42)$$

In the following some of the integrals in equation (3.42) will be expanded and considered individually.

The integrals I_8 and I_9

Making use of the relationships $u_\beta = u_\alpha \delta_{\alpha\beta}$; $u_\gamma = u_\alpha \delta_{\alpha\gamma}$; $n_\alpha = n_\beta \delta_{\alpha\beta}$ and $n_\gamma = n_\beta \delta_{\beta\gamma}$, and for $N_{\alpha\beta}$ in equation (2.46), the integrals I_8 and I_9 can be represented as follows:

$$\begin{aligned} I_8 &= \int_\Gamma B \frac{1-\nu}{2} \left(u_\alpha n_\beta + u_\beta n_\alpha + \frac{2\nu}{1-\nu} u_\gamma n_\gamma \delta_{\alpha\beta} \right) U_{\alpha,\beta}^* d\Gamma \\ &= \int_\Gamma B \frac{1-\nu}{2} u_\alpha \left(U_{\alpha,\beta}^* n_\beta + U_{\alpha,\beta}^* \delta_{\alpha\beta} n_\alpha + \frac{2\nu}{1-\nu} U_{\alpha,\beta}^* n_\gamma \delta_{\alpha\beta} \delta_{\alpha\gamma} \right) d\Gamma \\ &= \int_\Gamma B \frac{1-\nu}{2} u_\alpha n_\beta \left(U_{\alpha,\beta}^* + U_{\beta,\alpha}^* + \frac{2\nu}{1-\nu} \delta_{\alpha\beta} U_{\gamma,\gamma}^* \right) d\Gamma \end{aligned}$$

$$= \int_{\Gamma} u_\alpha T_\alpha^{(i)*} d\Gamma \tag{3.43}$$

$$\begin{aligned} I_9 &= \int_{\Omega} B\frac{1-\nu}{2}\left(u_\alpha U^*_{\alpha,\beta\beta} + u_\beta U^*_{\alpha,\beta\alpha} + \frac{2\nu}{1-\nu}\delta_{\alpha\beta}u_\gamma U^*_{\alpha,\beta\gamma}\right) d\Omega \\ &= \int_{\Omega} B\frac{1-\nu}{2}u_\alpha\left(U^*_{\alpha,\beta\beta} + \delta_{\alpha\beta}U^*_{\alpha,\beta\alpha} + \frac{2\nu}{1-\nu}\delta_{\alpha\beta}\delta_{\alpha\gamma}U^*_{\alpha,\beta\gamma}\right) d\Omega \\ &= \int_{\Omega} B\frac{1-\nu}{2}u_\alpha\left(U^*_{\alpha,\beta\beta} + U^*_{\beta,\alpha\beta} + \frac{2\nu}{1-\nu}\delta_{\alpha\beta}U^*_{\gamma,\gamma\beta}\right) d\Omega \\ &= \int_{\Omega} u_\alpha N^{(i)*}_{\alpha\beta,\beta} d\Omega \end{aligned} \tag{3.44}$$

The integral I_{10}

Using relationships for $N_{\alpha\beta}$ and t_α in equations (2.46) and (3.39), the integrals I_{10} will become:

$$\begin{aligned} I_{10} &= \int_{\Gamma} B\left[(1-\nu)k_{\alpha\beta} + \nu\delta_{\alpha\beta}k_{\gamma\gamma}\right] w_3 n_\beta U^*_\alpha d\Gamma \\ &= \int_{\Gamma} t^{(ii)}_\alpha U^*_\alpha d\Gamma \end{aligned} \tag{3.45}$$

Now, substituting equations (3.43), (3.44) and (3.45) into equation (3.41), gives

$$\begin{aligned} &\int_{\Gamma} t^{(i)}_\alpha U^*_\alpha d\Gamma - \int_{\Gamma} u_\alpha T^{(i)*}_\alpha d\Gamma + \int_{\Omega} u_\alpha N^{(i)*}_{\alpha\beta,\beta} d\Omega + \int_{\Gamma} t^{(ii)}_\alpha U^*_\alpha d\Gamma \\ &- \int_{\Omega} B\left[(1-\nu)k_{\alpha\beta} + \nu\delta_{\alpha\beta}k_{\gamma\gamma}\right] w_3 U^*_{\alpha,\beta} d\Omega + \int_{\Omega} q_\alpha U^*_\alpha d\Omega = 0 \end{aligned} \tag{3.46}$$

Regrouping the first and the fourth integrals using definition for t_α, equation (3.46) will become

$$\begin{aligned} &\int_{\Gamma} t_\alpha U^*_\alpha d\Gamma - \int_{\Gamma} u_\alpha T^{(i)*}_\alpha d\Gamma + \int_{\Omega} u_\alpha N^{(i)*}_{\alpha\beta,\beta} d\Omega \\ &- \int_{\Omega} B\left[(1-\nu)k_{\alpha\beta} + \nu\delta_{\alpha\beta}k_{\gamma\gamma}\right] w_3 U^*_{\alpha,\beta} d\Omega + \int_{\Omega} q_\alpha U^*_\alpha d\Omega = 0 \end{aligned} \tag{3.47}$$

Again, the $(\cdot)^*$ state are defined for concentrated generalised loads: two concentrated membrane forces ($\theta = 1, 2$) at an arbitrary point $\mathbf{X}' \in \Omega$. Thus, equation

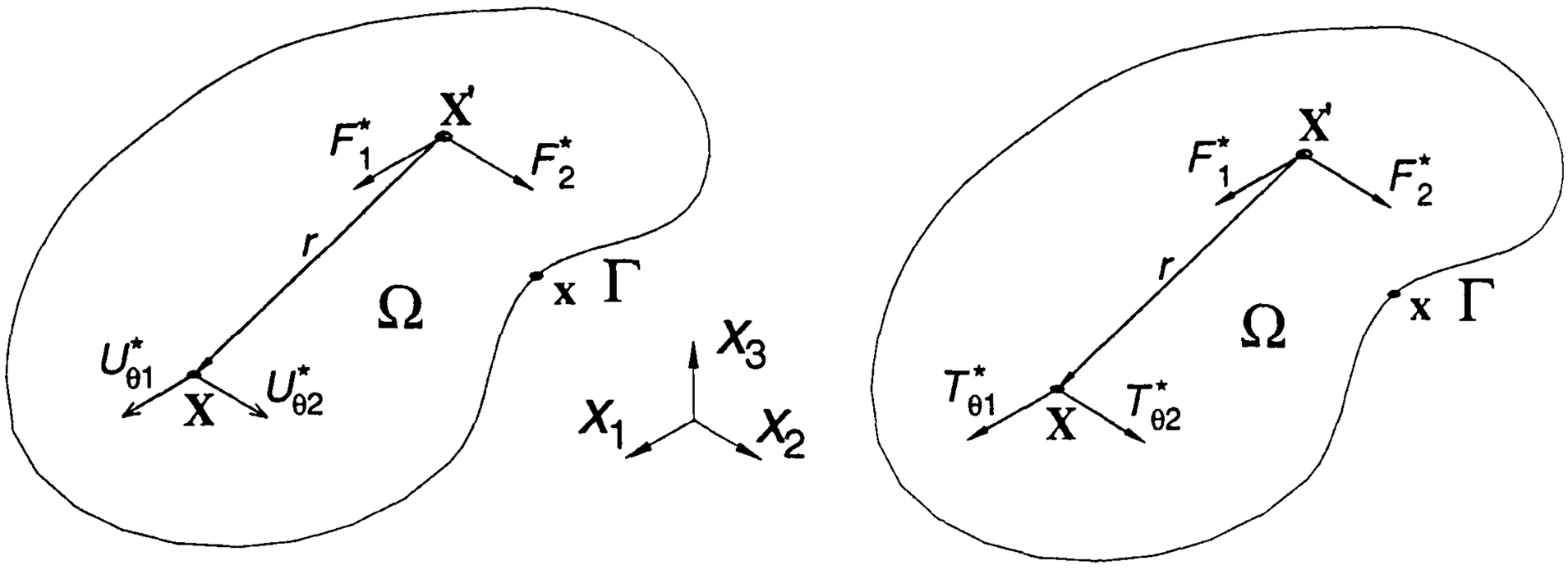

Figure 3-3: Fundamental state of displacements and tractions due to concentrated membrane forces.

(3.47) can be rewritten after introducing the direction of the load θ as follows:

$$\int_\Gamma U_{\theta\alpha}^* \left(\mathbf{X}', \mathbf{x}\right) t_\alpha \left(\mathbf{x}\right) d\Gamma \left(\mathbf{x}\right) - \int_\Gamma T_{\theta\alpha}^{(i)*} \left(\mathbf{X}', \mathbf{x}\right) u_\alpha \left(\mathbf{x}\right) d\Gamma \left(\mathbf{x}\right)$$

$$+ \int_\Omega N_{\theta\alpha\beta,\beta}^{(i)*} \left(\mathbf{X}', \mathbf{X}\right) u_\alpha \left(\mathbf{x}\right) d\Omega \left(\mathbf{X}\right) + \int_\Omega U_{\theta\alpha}^* \left(\mathbf{X}', \mathbf{X}\right) q_\alpha d\Omega \left(\mathbf{X}\right)$$

$$- \int_\Omega U_{\theta\alpha,\beta}^* \left(\mathbf{X}', \mathbf{X}\right) B \left[(1-\nu) k_{\alpha\beta} + \nu \delta_{\alpha\beta} k_{\gamma\gamma}\right] w_3 \left(\mathbf{X}\right) d\Omega \left(\mathbf{X}\right) = 0 \tag{3.48}$$

By choosing the $(\cdot)^*$ state to represent the fundamental state such as:

$$N_{\theta\alpha\beta,\beta}^{(i)*} \left(\mathbf{X}', \mathbf{X}\right) + \delta(\mathbf{X}', \mathbf{X}) \delta_{\theta\alpha} = 0 \tag{3.49}$$

and making use of the Dirac delta property (3.30), equation (3.49) can be written for an internal source point $\mathbf{X}'$ as:

$$u_\theta \left(\mathbf{X}'\right) + \int_\Gamma T_{\theta\alpha}^{(i)*} \left(\mathbf{X}', \mathbf{x}\right) u_\alpha \left(\mathbf{x}\right) d\Gamma \left(\mathbf{x}\right)$$

$$+ \int_\Omega U_{\theta\alpha,\beta}^* \left(\mathbf{X}', \mathbf{X}\right) B \left[(1-\nu) k_{\alpha\beta} + \nu \delta_{\alpha\beta} k_{\gamma\gamma}\right] w_3 \left(\mathbf{X}\right) d\Omega \left(\mathbf{X}\right)$$

$$= \int_\Gamma U_{\theta\alpha}^* \left(\mathbf{X}', \mathbf{x}\right) t_\alpha \left(\mathbf{x}\right) d\Gamma \left(\mathbf{x}\right) + \int_\Omega U_{\theta\alpha}^* \left(\mathbf{X}', \mathbf{X}\right) q_\alpha d\Omega \left(\mathbf{X}\right) \tag{3.50}$$

where $U_{\theta\alpha}^*(\mathbf{X}', \mathbf{x})$ and $T_{\theta\alpha}^{(i)*}(\mathbf{X}', \mathbf{x})$ are the fundamental solutions for in-plane displacements and membrane tractions respectively. It represents displacements or

tractions at the field point $\mathbf{x}$ or $\mathbf{X}$ in the direction α due to unit load applied at the source point $\mathbf{X}'$ in the direction θ.

3.2.4 Fundamental solutions

The expressions for the kernels $U^*_{\theta\alpha}$ and $T^*_{\theta\alpha}$ are well known (Kelvin solution) for two-dimensional plane stress problems, and are given as [144] :

$$U^*_{\theta\alpha} = \frac{1}{4\pi B\,(1-\nu)}\left[(3-\nu)\ln\left(\frac{1}{r}\right)\delta_{\theta\alpha} + (1+\nu)\,r_{,\theta}r_{,\alpha}\right] \tag{3.51}$$

$$\begin{aligned} T^{(i)*}_{\theta\alpha} \;=\; & -\frac{1}{4\pi r}\left\{r_{,n}\left[(1-\nu)\,\delta_{\theta\alpha} + 2\,(1+\nu)\,r_{,\theta}r_{,\alpha}\right]\right. \\ & \left. +(1-\nu)\left[n_\theta r_{,\alpha} - n_\alpha r_{,\theta}\right]\right\} \end{aligned} \tag{3.52}$$

where $U^*_{\theta\alpha}$ are weakly singular kernels of order $O(\ln\frac{1}{r})$ and $T^*_{\theta\alpha}$ are strongly singular in order $O(1/r)$.

3.3 Boundary Integral Equations

The above integrals are regular provided $r \neq 0$. If the point $\mathbf{X}'$ is taken to the boundary, that is $\mathbf{X}' \to \mathbf{x}' \in \Gamma$, the distance r tends to zero and, in the limit, the fundamental solutions exhibit singularities. In analysing the limit, a semi-circular domain with boundary Γ^*_ε and radius ε centered at the source point $\mathbf{x}'$ is introduced, as shown in Figure 3-4.

By taking the point $\mathbf{X}'$ to the boundary, that is $\mathbf{X}' \to \mathbf{x}' \in \Gamma$, and assuming that the displacements w_i and u_θ satisfy Hölder continuity,

$$\left|w_i\,(\mathbf{x}) - w_i(\mathbf{x}')\right| < Ar^\alpha; \qquad A:\ \text{constant} > 1,\ \text{and}\ 0 < \alpha \leqslant 1 \tag{3.53}$$

equation (3.31) can be written as follows :

$$w_i(\mathbf{x}') + \lim_{\varepsilon\to 0}\int_{\Gamma-\Gamma_\varepsilon+\Gamma^*_\varepsilon} P^*_{ij}(\mathbf{x}',\mathbf{x})w_j\,(\mathbf{x})\,d\Gamma\,(\mathbf{x}) = \lim_{\varepsilon\to 0}\int_{\Gamma-\Gamma_\varepsilon+\Gamma^*_\varepsilon} W^*_{ij}(\mathbf{x}',\mathbf{x})p_j\,(\mathbf{x})\,d\Gamma\,(\mathbf{x})$$

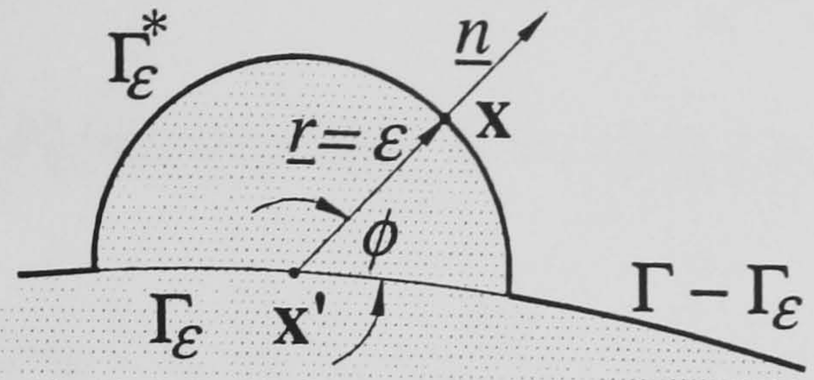

Figure 3-4: Semi-circular region around the source point when it approaches the boundary.

$$
\begin{aligned}
&-\lim_{\varepsilon\to 0}\int_{\Gamma-\Gamma_\epsilon+\Gamma_\varepsilon^*} k_{\alpha\beta}B\frac{1-\nu}{2}\left[u_\alpha(\mathbf{x})\,n_\beta+u_\beta(\mathbf{x})\,n_\alpha\right.\\
&\qquad\left.+\frac{2\nu}{1-\nu}u_\gamma(\mathbf{x})\,n_\gamma\delta_{\alpha\beta}\right]W_{i3}^*(\mathbf{x}',\mathbf{x})\,d\Gamma(\mathbf{x})\\
&+\int_\Omega k_{\alpha\beta}B\frac{1-\nu}{2}\left[u_\alpha(\mathbf{X})\,W_{i3,\beta}^*(\mathbf{X}',\mathbf{X})+u_\beta(\mathbf{X})\,W_{i3,\alpha}^*(\mathbf{X}',\mathbf{X})\right.\\
&\qquad\left.+\frac{2\nu}{1-\nu}u_\gamma(\mathbf{X})\,W_{i3,\gamma}^*(\mathbf{X}',\mathbf{X})\,\delta_{\alpha\beta}\right]d\Omega(\mathbf{X})\\
&-\int_\Omega k_{\alpha\beta}B\left[(1-\nu)k_{\alpha\beta}+\nu\delta_{\alpha\beta}k_{\gamma\gamma}\right]w_3(\mathbf{X})\,W_{i3}^*(\mathbf{X}',\mathbf{X})\,d\Omega(\mathbf{X})\\
&+\int_\Omega W_{i3}^*(\mathbf{X}',\mathbf{X})q_3(\mathbf{X})d\Omega(\mathbf{X})
\end{aligned}
\tag{3.54}
$$

and equation (3.50) can be written as

$$
\begin{aligned}
&u_\theta(\mathbf{x}')+\lim_{\varepsilon\to 0}\int_{\Gamma-\Gamma_\epsilon+\Gamma_\varepsilon^*} T_{\theta\alpha}^{(i)*}(\mathbf{x}',\mathbf{x})\,u_\alpha(\mathbf{x})\,d\Gamma(\mathbf{x})\\
&\quad+\int_\Omega U_{\theta\alpha,\beta}^*(\mathbf{X}',\mathbf{X})\,B\left[(1-\nu)k_{\alpha\beta}+\nu\delta_{\alpha\beta}k_{\gamma\gamma}\right]w_3(\mathbf{X})\,d\Omega(\mathbf{X})\\
&=\lim_{\varepsilon\to 0}\int_{\Gamma-\Gamma_\epsilon+\Gamma_\varepsilon^*} U_{\theta\alpha}^*(\mathbf{x}',\mathbf{x})\,t_\alpha(\mathbf{x})\,d\Gamma(\mathbf{x})+\int_\Omega U_{\theta\alpha}^*(\mathbf{X}',\mathbf{X})\,q_\alpha d\Omega(\mathbf{X})
\end{aligned}
\tag{3.55}
$$

All limiting process can be found in the Appendix B. Taking into account all the

limits and the jump terms, the boundary integral equations are obtained as follows:

$$c_{ij}(\mathbf{x}')w_j(\mathbf{x}') + \oint_\Gamma P^*_{ij}(\mathbf{x}',\mathbf{x})w_j(\mathbf{x})\,d\Gamma(\mathbf{x}) = \int_\Gamma W^*_{ij}(\mathbf{x}',\mathbf{x})p_j(\mathbf{x})\,d\Gamma(\mathbf{x})$$

$$-\int_\Gamma k_{\alpha\beta}B\frac{1-\nu}{2}\left[u_\alpha(\mathbf{x})n_\beta + u_\beta(\mathbf{x})n_\alpha + \frac{2\nu}{1-\nu}u_\gamma(\mathbf{x})n_\gamma\delta_{\alpha\beta}\right]W^*_{i3}(\mathbf{x}',\mathbf{x})\,d\Gamma(\mathbf{x})$$

$$+\int_\Omega k_{\alpha\beta}B\frac{1-\nu}{2}\left[u_\alpha(\mathbf{X})W^*_{i3,\beta}(\mathbf{x}',\mathbf{X}) + u_\beta(\mathbf{X})W^*_{i3,\alpha}(\mathbf{x}',\mathbf{X})\right.$$

$$\left.+\frac{2\nu}{1-\nu}u_\gamma(\mathbf{X})W^*_{i3,\gamma}(\mathbf{x}',\mathbf{X})\delta_{\alpha\beta}\right]d\Omega(\mathbf{X})$$

$$-\int_\Omega k_{\alpha\beta}B\left[(1-\nu)k_{\alpha\beta}+\nu\delta_{\alpha\beta}k_{\gamma\gamma}\right]w_3(\mathbf{X})W^*_{i3}(\mathbf{x}',\mathbf{X})\,d\Omega(\mathbf{X})$$

$$+\int_\Omega W^*_{i3}(\mathbf{x}',\mathbf{X})q_3(\mathbf{X})d\Omega(\mathbf{X}) \tag{3.56}$$

and

$$c_{\theta\alpha}(\mathbf{x}')u_\alpha(\mathbf{x}') + \oint_\Gamma T^{*(i)}_{\theta\alpha}(\mathbf{x}',\mathbf{x})u_\alpha(\mathbf{x})d\Gamma(\mathbf{x})$$

$$+\int_\Omega U^*_{\theta\alpha,\beta}(\mathbf{X}',\mathbf{X})B\left[k_{\alpha\beta}(1-\nu)+\nu\delta_{\alpha\beta}k_{\gamma\gamma}\right]w_3(\mathbf{X})d\Omega(\mathbf{X})$$

$$=\int_\Gamma U^*_{\theta\alpha}(\mathbf{x}',\mathbf{x})t_\alpha(\mathbf{x})d\Gamma(\mathbf{x}) + \int_\Omega U^*_{\theta\alpha}(\mathbf{X}',\mathbf{X})q_\alpha(\mathbf{X})d\Omega(\mathbf{X}) \tag{3.57}$$

where $\oint$ denotes a Cauchy principal value integral, $\mathbf{x}', \mathbf{x} \in \Gamma$ are source and field points respectively, and $c_{ij}(\mathbf{x}')$ are the jump terms. The value of $c_{ij}(\mathbf{x}')$ is equal to $\frac{1}{2}\delta_{ij}$ when $\mathbf{x}'$ is located on a smooth boundary.

Equations (3.56 – 3.57) represent five boundary integral equations, the first two in (3.56) ($i = \alpha = 1, 2$) are for rotations, the third ($i = 3$) is for the out-of-plane displacement and two in (3.57) ($\alpha = 1, 2$) for in-plane displacements, which can be used to solve shear deformable shallow shell bending problems.

By applying the divergence theorem, the last domain integral in (3.56) can be transferred to boundary integral, in the case of a uniform load (q_3 = constant) to give:

$$\int_\Omega W^*_{i3}(\mathbf{x}',\mathbf{X})q_3(\mathbf{X})d\Omega(\mathbf{X}) = q_3\int_\Gamma V^*_{i,\alpha}(\mathbf{x}',\mathbf{x})n_\alpha(\mathbf{x})d\Gamma(\mathbf{x}) \tag{3.58}$$

where V^*_i are the particular solutions of the equation $V^*_{i,\theta\theta} = W^*_{i3}$. The expressions

for $V^*_{i,\beta}$ are:

$$\begin{aligned} V^*_{\alpha,\beta} &= \frac{r^2}{128\pi D}[(4\ln z - 5)\delta_{\alpha\beta} + 2(4\ln z - 3)r_{,\alpha}r_{,\beta}] \\ V^*_{3,\beta} &= \frac{-rr_{,\beta}}{128\pi D(1-\nu)\lambda^2}[32(2\ln z - 1) - z^2(1-v)(4\ln z - 5)] \end{aligned} \tag{3.59}$$

If q_3 is not uniform, then this term cannot be taken out of the integral. The transformation of domain integrals for other distribution cases of q_3 can be carried out by using the dual reciprocity technique, as explained in section 3.5.

3.4 Numerical Implementation

3.4.1 Discretisation

In this thesis, quadratic isoparametric boundary elements are used to describe the geometry and the function along the boundary, while for the domain, quadratic quadrilateral isoparametric elements are used to describe the geometry and constant interpolations for the function. Semi-discontinuous elements are used for corners to avoid difficulties with discontinuity of the tractions at corners.

Assuming that q_3 is uniform, equation (3.31) can be rewritten in a discretised forms as:

$$c_{ij}(\mathbf{x}')w_j(\mathbf{x}') + \sum_{n=1}^{N_e}\sum_{m=1}^{3} w_j^{nm}\int_{\xi=-1}^{\xi=+1} P^*_{ij}(\mathbf{x}',\mathbf{x})\Phi^m(\xi)J_n(\xi)d\xi$$

$$= \sum_{n=1}^{N_e}\sum_{m=1}^{3} p_j^{nm}\int_{\xi=-1}^{\xi=+1} W^*_{ij}(\mathbf{x}',\mathbf{x})\Phi^m(\xi)J_n(\xi)d\xi$$

$$-\sum_{n=1}^{N_e}\sum_{m=1}^{3} k_{\alpha\beta}B\frac{1-\nu}{2}\left(u_\alpha^{nm}n_\beta^{nm} + u_\beta^{nm}n_\alpha^{nm} + \frac{2\nu}{1-\nu}u_\gamma^{nm}n_\gamma^{nm}\delta_{\alpha\beta}\right)$$

$$\times\int_{\xi=-1}^{\xi=+1} W^*_{i3}\left(\mathbf{x}',\mathbf{x}\right)\Phi^m(\xi)J_n(\xi)d\xi +$$

$$+\sum_{k=1}^{N_c} k_{\alpha\beta}B\frac{1-\nu}{2}u_\alpha^k\int_{\eta=-1}^{\eta=+1}\int_{\xi=-1}^{\xi=+1} W^*_{i3,\beta}\left(\mathbf{x}',\mathbf{X}\right)J_k(\xi,\eta)d\xi d\eta$$

$$+\sum_{k=1}^{N_c} k_{\alpha\beta} B \frac{1-\nu}{2} u_\beta^k \int_{\eta=-1}^{\eta=+1} \int_{\xi=-1}^{\xi=+1} W_{i3,\alpha}^* \left(\mathbf{x}', \mathbf{X}\right) J_k(\xi,\eta) d\xi d\eta$$

$$+\sum_{k=1}^{N_c} k_{\alpha\beta} B \nu u_\gamma^k \int_{\eta=-1}^{\eta=+1} \int_{\xi=-1}^{\xi=+1} W_{i3,\gamma}^* \left(\mathbf{x}', \mathbf{X}\right) J_k(\xi,\eta) d\xi d\eta$$

$$-\sum_{k=1}^{N_c} k_{\alpha\beta} B \left[(1-\nu) k_{\alpha\beta} + \nu \delta_{\alpha\beta} k_{\gamma\gamma}\right] w_3^k \int_{\eta=-1}^{\eta=+1} \int_{\xi=-1}^{\xi=+1} W_{i3}^* \left(\mathbf{x}', \mathbf{X}\right) J_k(\xi,\eta) d\xi d\eta$$

$$+q \sum_{n=1}^{N_e} \int_{\xi=-1}^{\xi=+1} V_{i,\alpha}^*(\mathbf{x}', \mathbf{x}) n_\alpha(\xi) J_n(\xi) d\xi \tag{3.60}$$

and assuming $q_\alpha = 0$ equation (3.50) can be written as

$$c_{\theta\alpha}\left(\mathbf{x}'\right) u_\alpha(\mathbf{x}') + \sum_{n=1}^{N_e} \sum_{m=1}^{3} u_\alpha^{nm} \int_{\xi=-1}^{\xi=+1} T_{\theta\alpha}^{*(i)}(\mathbf{x}', \mathbf{x}) \Phi^m(\xi) J_n(\xi) d\xi$$

$$+\sum_{k=1}^{N_c} B \left[k_{\alpha\beta}\left(1-\nu\right) + \nu \delta_{\alpha\beta} k_{\gamma\gamma}\right] w_3^k \int_{\eta=-1}^{\eta=+1} \int_{\xi=-1}^{\xi=+1} U_{\theta\alpha,\beta}^* \left(\mathbf{x}', \mathbf{X}\right) J_k(\xi,\eta) d\xi d\eta$$

$$= \sum_{n=1}^{N_e} \sum_{m=1}^{3} t_\alpha^{nm} \int_{\xi=-1}^{\xi=+1} U_{\theta\alpha}^{*(i)}(\mathbf{x}', \mathbf{x}) \Phi^m(\xi) J_n(\xi) d\xi \tag{3.61}$$

where N_e and N_c are number of boundary elements and internal cells respectively, Φ^m are the quadratic shape functions. For a continuous quadratic element, they are defined as:

$$\begin{aligned} \Phi_C^1(\xi) &= \frac{1}{2}\xi(\xi-1) \\ \Phi_C^2(\xi) &= (1-\xi)(1+\xi) \\ \Phi_C^3(\xi) &= \frac{1}{2}\xi(\xi+1) \end{aligned} \tag{3.62}$$

and for a semi-discontinuous element, with nodes are placed at $\xi = -\frac{2}{3}, 0, +1$, as:

$$\begin{aligned} \Phi_{S1}^1(\xi) &= \frac{9}{10}\xi(\xi-1) \\ \Phi_{S1}^2(\xi) &= -\frac{3}{2}(\xi-1)(\xi+\frac{2}{3}) \\ \Phi_{S1}^3(\xi) &= \frac{6}{10}\xi(\xi+\frac{2}{3}) \end{aligned} \tag{3.63}$$

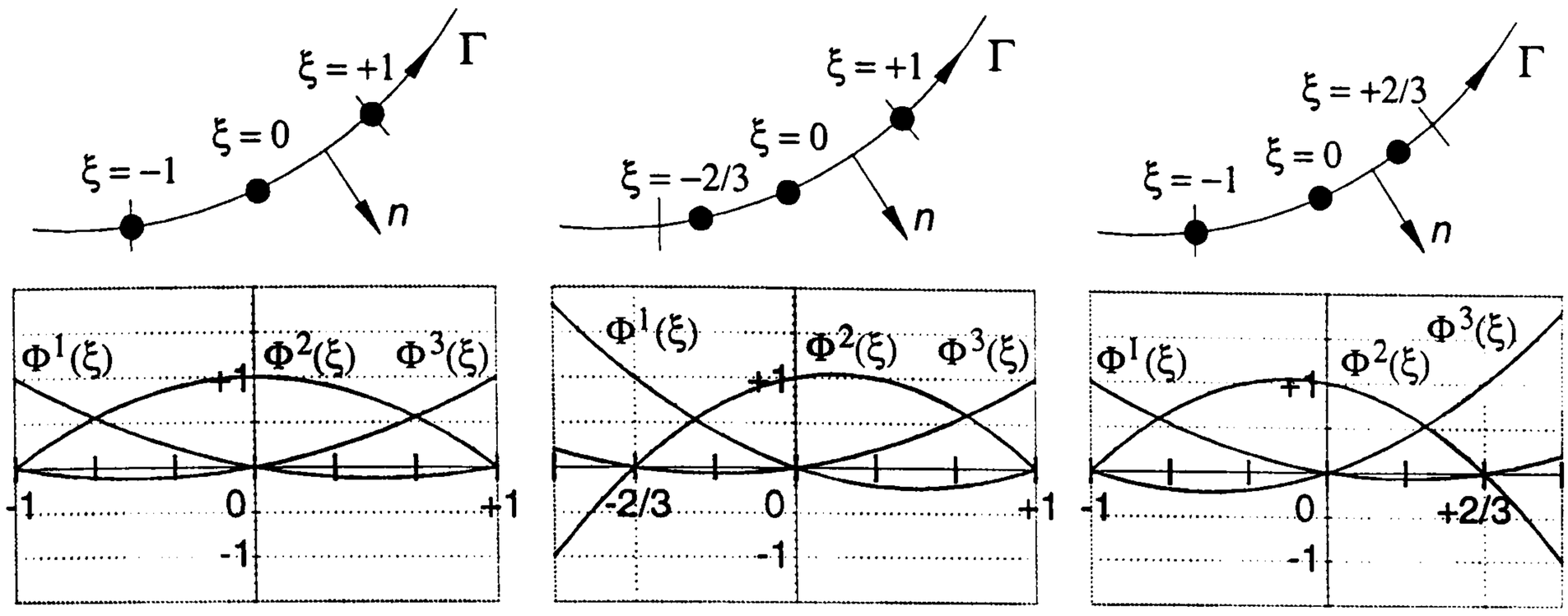

(a) (b) (c)

Figure 3-5: Shape functions for continuous and semi-discontinuous quadratic elements.

and for an element with nodes are placed at $\xi = -1, 0, +\frac{2}{3}$, as:

$$\begin{aligned} \Phi^1_{S3}(\xi) &= \frac{6}{10}\xi(\xi - \frac{2}{3}) \\ \Phi^2_{S3}(\xi) &= -\frac{3}{2}(\xi + 1)(\xi - \frac{2}{3}) \\ \Phi^3_{S3}(\xi) &= \frac{9}{10}\xi(\xi + 1) \end{aligned} \tag{3.64}$$

The position of the internal node in semi-discontinuous element is chosen arbitrarily at $-\frac{2}{3}$ or $+\frac{2}{3}$, not very close to the element end point to avoid near singularity problems.

The Jacobian of transformation for boundary elements is defined as:

$$J_n(\xi) = \sqrt{\frac{\partial x_\theta(\xi)}{\partial \xi}\frac{\partial x_\theta(\xi)}{\partial \xi}} \tag{3.65}$$

where $\frac{\partial x_\theta(\xi)}{\partial \xi}$ is the derivative of the global coordinates x_θ with respect to the local coordinate ξ, and the normal as:

$$n_\alpha(\xi) = \frac{1}{J(\xi)}\frac{\partial x_\beta(\xi)}{\partial \xi}\epsilon_{\alpha\beta 3} \tag{3.66}$$

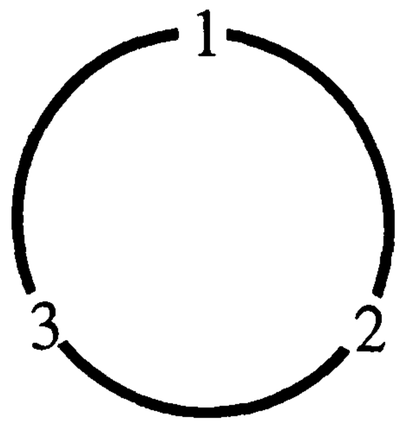

Figure 3-6: Sequence of permutation tensor.

where $\epsilon_{\alpha\beta 3}$ is the permutation tensor and is defined by the following set of rules:

$\epsilon_{\alpha\beta 3} = +1,$ if $\alpha, \beta, 3$ is a clockwise cyclic sequence

$\epsilon_{\alpha\beta 3} = -1,$ if $\alpha, \beta, 3$ is an anti clockwise cyclic sequence

and

$\epsilon_{\alpha\beta 3} = 0,$ if $\alpha, \beta, 3$ is an acyclic sequence

The Jacobian of transformation for cell elements is defined as:

$$J_k(\xi) = \sqrt{\left(N_{31}^2 + N_{32}^2 + N_{33}^2\right)} \tag{3.67}$$

where N_{ij} is a minor of

$$\begin{bmatrix} \dfrac{\partial x_1(\xi,\eta)}{\partial \xi} & \dfrac{\partial x_2(\xi,\eta)}{\partial \xi} & \dfrac{\partial x_3(\xi,\eta)}{\partial \xi} \\ \dfrac{\partial x_1(\eta)}{\partial \eta} & \dfrac{\partial x_2(\xi,\eta)}{\partial \eta} & \dfrac{\partial x_2(\xi,\eta)}{\partial \eta} \\ 1 & 1 & 1 \end{bmatrix} \tag{3.68}$$

For every collocation node, equations (3.60 – 3.61) will give the following linear system of equation in a matrix form:

$$\begin{bmatrix} \mathbf{H}^p & \mathbf{H}^u \\ \mathbf{H}^w & \mathbf{H}^s \end{bmatrix}_{5\times5} \begin{Bmatrix} \mathbf{w} \\ \mathbf{u} \end{Bmatrix}_{5\times1} = \begin{bmatrix} \mathbf{G}^p & 0 \\ 0 & \mathbf{G}^s \end{bmatrix}_{5\times5} \begin{Bmatrix} \mathbf{p} \\ \mathbf{t} \end{Bmatrix}_{5\times1} + \begin{Bmatrix} \mathbf{b} \\ \mathbf{0} \end{Bmatrix}_{5\times1} \tag{3.69}$$

where $\mathbf{w} = \{w_1, w_2, w_3\}^\intercal$, $\mathbf{u} = \{u_1, u_2\}^\intercal$, $\mathbf{p} = \{p_1, p_2, p_3\}^\intercal$, and $\mathbf{t} = \{t_1, t_2\}^\intercal$ are displacement and traction vectors for plate bending and plane stress formulations

respectively, $\mathrm{b} = \{0, 0, q_3\}^{\mathrm{T}}$ is domain load vectors, $\mathbf{H}^p$, $\mathbf{H}^s$, $\mathbf{G}^p$ and $\mathbf{G}^s$ are boundary element influence matrices for plate bending and plane stress formulations respectively, $\mathbf{H}^u$, and $\mathbf{H}^w$ are matrices which contain coupled terms between plate bending and plane stress formulations. The matrices $\mathbf{H}^p$, $\mathbf{H}^s$, $\mathbf{H}^u$, $\mathbf{H}^w$, $\mathbf{G}^p$ and $\mathbf{G}^s$ then form shallow shell influence matrices. After performing all of the collocation process, equations (3.60 – 3.61) can be written as

$$\begin{aligned} & [H]_{5Nbn+3Nin \times 5Nbn+3Nin} \{w\}_{5Nbn+3Nin \times 1} \\ = \; & [G]_{5Nbn+3Nin \times 15Nbe} \{p\}_{15Nbe \times 1} + \{Q\}_{5Nbn+3Nin \times 1} \end{aligned} \tag{3.70}$$

where $[H]$ and $[G]$ are the well-known boundary element influence matrices [28], $\{w\}$ is the boundary and domain displacement vector, $\{p\}$ is the boundary traction vector, and $\{Q\}$ is the domain load vector. Nbn, Nin and Nbe are number of boundary nodes, internal nodes and boundary elements respectively.

After imposing boundary conditions, equation (3.70) can be written as:

$$[A]_{5Nbn+3Nin \times 5Nbn+3Nin} \{x\}_{5Nbn+3Nin \times 1} = \{b\}_{5Nbn+3Nin \times 1} \tag{3.71}$$

where $[A]$ is the system matrix, $\{x\}$ is the unknown vector and $\{b\}$ is the vector of prescribed boundary values. Using the LU decomposition, the system of algebraic equations can be solved for the boundary unknowns.

3.4.2 Treatment of singularities

The boundary integral equations discussed above contain integrands with several different orders of singularities. These singular integrals are treated separately based on their order of singularity. In this thesis, all of the regular integrals are evaluated numerically using the standard Gauss quadrature formulae. The influence matrix $[G]$ and the load vector matrix $\{Q\}$ contain weakly singular integrals, which are treated using a nonlinear coordinate transformation as in Telles [128]. However, for better numerical accuracy, as it was shown by Okada *et al.* [93], a suitable number of element sub divisions must be used with the non-linear transformation. Therefore, in this thesis four element sub divisions are used.

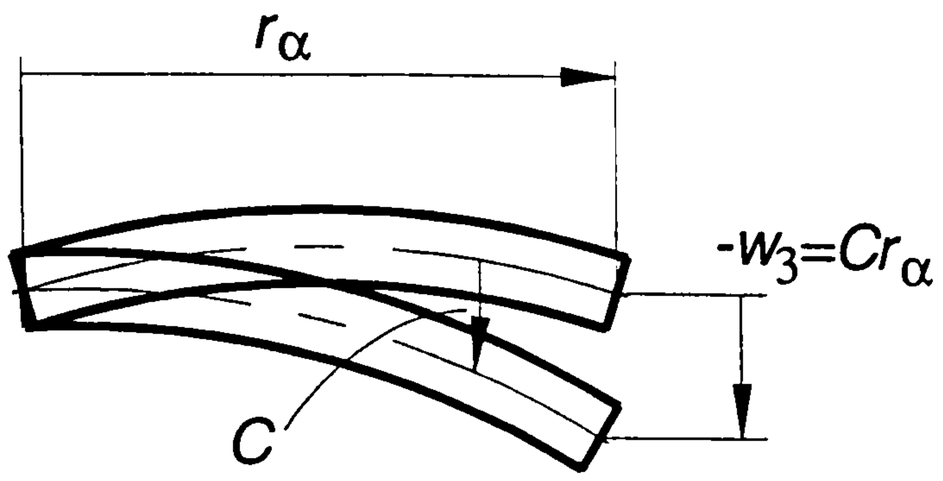

Figure 3-7: Rigid body rotations.

The influence matrix $[H]$ contains strongly singular integrals, and in this work these integrals are computed indirectly by considering the generalised rigid body movements. This can be achieved as follows:

If a traction-free problem is considered, five independent cases may be observed, that is, two rigid body rotations:

- $u_1 = 0$, $u_2 = 0$, $w_1 = C$ and $w_2 = 0$, then $w_3 = -Cr_1$,
- $u_1 = 0$, $u_2 = 0$, $w_2 = C$ and $w_1 = 0$, then $w_3 = -Cr_2$

as shown in Figure 3-7 and a rigid body out-of-plane translation:

- $u_1 = 0$, $u_2 = 0$, $w_3 = C$, $w_1 = 0$, and $w_2 = 0$

for the rotations and out-of-plane displacement integral equations, and two rigid body conditions for in-plane translations

- $u_1 = C$, $u_2 = 0$, $w_1 = 0$, $w_2 = 0$, and $w_3 = 0$
- $u_2 = C$, $u_1 = 0$, $w_1 = 0$, $w_2 = 0$, and $w_3 = 0$

for the in-plane displacements integral equations. The term C is an arbitrary constant, and r_α denotes components of vector r in x_α coordinates.

By applying the above cases to the system of equations in (3.70), the following expressions can be written:

$$H^{i\alpha}(\mathbf{x}') = -\int_\Gamma [P^*_{i\alpha}(\mathbf{x}', \mathbf{x}) + (-r_\alpha) P^*_{i3}(\mathbf{x}', \mathbf{x})] d\Gamma(\mathbf{x})$$

$$
\begin{aligned}
H^{i3}(\mathbf{x}') &= -\int_{\Gamma} P^*_{i3}(\mathbf{x}', \mathbf{x}) d\Gamma(\mathbf{x}) \\
H^{(3+\theta)(3+\alpha)}(\mathbf{x}') &= -\int_{\Gamma} T^*_{\theta\alpha}(\mathbf{x}', \mathbf{x}) d\Gamma(\mathbf{x})
\end{aligned} \tag{3.72}
$$

where $H^{i\alpha}(\mathbf{x}')$, $H^{i3}(\mathbf{x}')$ and $H^{(3+\theta)(3+\alpha)}(\mathbf{x}')$ include the diagonal sub-matrix and the jump term c_{ij} in the influence matrix $[H]$. All terms in the integrals in equation (3.72) were already computed except the second term in the first integral. Fortunately, in the second term of the first integral, the distance r_α cancels the weak singularity in $P^*_{\alpha 3}$ and the strong singularity in P^*_{33} in the singular element under consideration.

There are also weak singular terms in the domain integrals. When these integrals are computed numerically using cell discretisations, the weak singular kernels are treated using a triangle to square transformation technique as explained in Aliabadi and Rooke [8].

Details of the treatment of singularities using a nonlinear coordinate transformation and triangle to square transformation are given in Appendix C.

3.4.3 Boundary conditions

There are three possible boundary conditions considered in this work, i.e. clamped, simply supported and free boundary. These boundary conditions can be summarised as follows:

Clamped boundary condition

$$
w_t = 0, \quad w_n = 0, \quad w_3 = 0, \quad u_t = 0, \quad \text{and} \quad u_n = 0 \tag{3.73}
$$

Simply supported boundary condition

$$
w_t = 0, \quad w_3 = 0, \quad M_n = 0 \quad \text{and} \quad (u_1 = 0 \quad \text{or} \quad u_2 = 0) \tag{3.74}
$$

The above boundary conditions are appropriate for shells and have also been

adopted in [131][80].

Free boundary condition

$$M_t = 0, \quad M_n = 0, \quad p_3 = 0, \quad N_t = 0, \quad \text{and} \quad N_n = 0, \tag{3.75}$$

3.5 Transformation of Domain Integrals

The domain integrals which appear in the boundary integral equations derived in section 3.2 can be transformed to boundary integrals with the use of the dual reciprocity technique [97]. Recently Wen, Aliabadi and Young [140] used the formulations developed by Dirgantara and Aliabadi [36] and transformed the domain integrals into boundary integrals. The shell can be discretised into quadratic isoparametric boundary elements.

With slightly different arrangements as written in section 3.2, to avoid the use of derivatives of the kernels W^*_{i3} and $U^*_{\theta\alpha}$, the integral equations (3.31) and (3.50) can be rewritten as follows :

$$\begin{aligned} & w_i(\mathbf{X}') + \int_\Gamma P^*_{ij}(\mathbf{X}', \mathbf{x}) w_j(\mathbf{x})\, d\Gamma(\mathbf{x}) = \int_\Gamma W^*_{ij}(\mathbf{X}', \mathbf{x}) p_j(\mathbf{x})\, d\Gamma(\mathbf{x}) \\ & - \int_\Omega k_{\alpha\beta} B \frac{1-\nu}{2} \left(u_{\alpha,\beta}(\mathbf{X}) + u_{\beta,\alpha}(\mathbf{X}) + \frac{2\nu}{1-\nu} u_{\phi,\phi}(\mathbf{X})\, \delta_{\alpha\beta} \right) W^*_{i3}(\mathbf{X}', \mathbf{X})\, d\Omega(\mathbf{x}) \\ & - \int_\Omega k_{\alpha\beta} B \left((1-\nu) k_{\alpha\beta} + \nu \delta_{\alpha\beta} k_{\gamma\gamma} \right) w_3(\mathbf{X})\, W^*_{i3}(\mathbf{X}', \mathbf{X})\, d\Omega(\mathbf{X}) \\ & + \int_\Omega W^*_{i3}(\mathbf{X}', \mathbf{X}) q_3(\mathbf{X}) d\Omega(\mathbf{X}) \end{aligned} \tag{3.76}$$

and

$$\begin{aligned} & u_\theta(\mathbf{X}') + \int_\Gamma T^{(i)*}_{\theta\alpha}(\mathbf{X}', \mathbf{x})\, u_\alpha(\mathbf{x})\, d\Gamma(\mathbf{x}) \\ & + \int_\Gamma U^*_{\theta\alpha}(\mathbf{x}', \mathbf{x}) B \left[k_{\alpha\beta}(1-\nu) + \nu \delta_{\alpha\beta} k_{\phi\phi} \right] w_3(\mathbf{x}) n_\beta(\mathbf{x}) d\Gamma(\mathbf{x}) \\ & - \int_\Omega U^*_{\theta\alpha}(\mathbf{X}', \mathbf{X}) B \left[k_{\alpha\beta}(1-\nu) + \nu \delta_{\alpha\beta} k_{\phi\phi} \right] w_{3,\beta}(\mathbf{X}) d\Omega(\mathbf{X}) \\ & = \int_\Gamma U^*_{\theta\alpha}(\mathbf{X}', \mathbf{x})\, t_\alpha(\mathbf{x})\, d\Gamma(\mathbf{x}) + \int_\Omega U^*_{\theta\alpha}(\mathbf{X}', \mathbf{X})\, q_\alpha d\Omega(\mathbf{X}) \end{aligned} \tag{3.77}$$

By taking the point $\mathbf{X}'$ to the boundary, that is $\mathbf{X}' \to \mathbf{x}' \in \Gamma$, and assuming displacements w_j and u_θ satisfy Hölder continuity, equation (3.76) can be written as follows:

$$c_{ij}(\mathbf{x}')w_j(\mathbf{x}') + \int_\Gamma P^*_{ij}(\mathbf{x}',\mathbf{x})w_j(\mathbf{x})\,d\Gamma(\mathbf{x}) = \int_\Gamma W^*_{ij}(\mathbf{x}',\mathbf{x})p_j(\mathbf{x})\,d\Gamma(\mathbf{x})$$

$$- \int_\Omega W^*_{i3}(\mathbf{x}',\mathbf{X})\,k_{\alpha\beta}B\frac{1-\nu}{2}\left[u_{\alpha,\beta}(\mathbf{X}) + u_{\beta,\alpha}(\mathbf{X}) + \frac{2\nu}{1-\nu}u_{\phi,\phi}(\mathbf{X})\,\delta_{\alpha\beta}\right]d\Omega(\mathbf{X})$$

$$- \int_\Omega W^*_{i3}(\mathbf{x}',\mathbf{X})\,k_{\alpha\beta}B\left((1-\nu)k_{\alpha\beta} + \nu\delta_{\alpha\beta}k_{\phi\phi}\right)w_3(\mathbf{X})\,d\Omega(\mathbf{X})$$

$$+ \int_\Omega W^*_{i3}(\mathbf{x}',\mathbf{X})q_3(\mathbf{X})d\Omega(\mathbf{X}) \tag{3.78}$$

and equation (3.77) can be written as

$$c_{\theta\alpha}(\mathbf{x}')\,u_\alpha(\mathbf{x}') + \int_\Gamma T^{*(i)}_{\theta\alpha}(\mathbf{x}',\mathbf{x})u_\alpha(\mathbf{x})d\Gamma(\mathbf{x})$$

$$+ \int_\Gamma U^*_{\theta\alpha}(\mathbf{x}',\mathbf{x})B\left[k_{\alpha\beta}(1-\nu) + \nu\delta_{\alpha\beta}k_{\phi\phi}\right]w_3(\mathbf{x})n_\beta(\mathbf{x})d\Gamma(\mathbf{x})$$

$$- \int_\Omega U^*_{\theta\alpha}(\mathbf{x}',\mathbf{X})B\left[k_{\alpha\beta}(1-\nu) + \nu\delta_{\alpha\beta}k_{\phi\phi}\right]w_{3,\beta}(\mathbf{X})d\Omega(\mathbf{X})$$

$$= \int_\Gamma U^*_{\theta\alpha}(\mathbf{x}',\mathbf{x})t_\alpha(\mathbf{x})d\Gamma(\mathbf{x}) + \int_\Omega U^*_{\theta\alpha}(\mathbf{x}',\mathbf{X})q_\alpha(\mathbf{X})d\Omega(\mathbf{X}) \tag{3.79}$$

If the membrane body forces $q_1 = q_2 = 0$, in the boundary integral equations $(3.78 - 3.79)$ there are six domain integrals as follows:

$$I^D_1 = \int_\Omega W^*_{i3}w_3 d\Omega, \qquad I^D_2 = \int_\Omega W^*_{i3}\frac{\partial u_1}{\partial x_1}d\Omega,$$

$$I^D_3 = \int_\Omega W^*_{i3}\frac{\partial u_2}{\partial x_2}d\Omega, \qquad I^D_4 = \int_\Omega W^*_{i3}q_3 d\Omega,$$

$$I^D_5 = \int_\Omega U^*_{\alpha 1}\frac{\partial w_3}{\partial x_1}d\Omega, \qquad I^D_6 = \int_\Omega U^*_{\alpha 2}\frac{\partial w_3}{\partial x_2}d\Omega \tag{3.80}$$

From the particular solution $\hat{w}^3_{mk}$, which satisfy the differential equation,

$$L^{b,adj}_{\alpha k}\hat{w}^3_{mk} = 0 \qquad \text{and} \qquad L^{b,adj}_{3k}\hat{w}^3_{mk} = F_m(r) \tag{3.81}$$

where $L_{\alpha k}^{b,adj}$ and $L_{3k}^{b,adj}$ are adjoint operator of original differential operator L_{ik}^{b} for plate bending problem in equation (3.9) and the boundary integral equations for plate bending problem becomes

$$c_{ik}(\mathbf{x}')\hat{w}_{mk}^{3}(\mathbf{x}') = \int_{\Gamma} W_{ik}^{*}(\mathbf{x}',\mathbf{x})\hat{p}_{mk}^{3}(\mathbf{x})\,d\Gamma(\mathbf{x}) - \oint_{\Gamma} P_{ik}^{*}(\mathbf{x}',\mathbf{x})\hat{w}_{mk}^{3}(\mathbf{x})\,d\Gamma(\mathbf{x})$$

$$+ \int_{\Omega} W_{i3}^{*}(\mathbf{x}',\mathbf{X})F_{m}(r)\,d\Omega(\mathbf{X}) \tag{3.82}$$

which implies that

$$I_{1}^{D} = \sum_{m=1}^{M}\left[c_{ik}(\mathbf{x}')\hat{w}_{mk}^{3}(\mathbf{x}') - \int_{\Gamma} W_{ik}^{*}(\mathbf{x}',\mathbf{x})\hat{p}_{mk}^{3}(\mathbf{x})\,d\Gamma(\mathbf{x})\right.$$

$$\left. + \oint_{\Gamma} P_{ik}^{*}(\mathbf{x}',\mathbf{x})\hat{w}_{mk}^{3}(\mathbf{x})\,d\Gamma(\mathbf{x})\right]\mathbf{F}^{-1}w_{3} \tag{3.83}$$

The particular solution $\hat{w}_{mk}^{3}$ and $\hat{p}_{mk}^{3}$ for radial basis function $F_{m}(r) = 1 + r$ were derived in [140] and are given in the Appendix D. Similar to the previous procedure, if

$$L_{\alpha k}^{b,adj}\hat{w}_{mk}^{3} = 0 \qquad \text{and} \qquad L_{3k}^{b,adj}\hat{w}_{mk}^{3} = \frac{\partial F_{m}(r)}{\partial x_{\alpha}} = \frac{x_{\alpha}}{r} \tag{3.84}$$

the domain integral

$$I_{2}^{D} = \sum_{m=1}^{M}\left[c_{ik}(\mathbf{x}')\hat{w}_{mk}^{1}(\mathbf{x}') - \int_{\Gamma} W_{ik}^{*}(\mathbf{x}',\mathbf{x})\hat{p}_{mk}^{1}(\mathbf{x})\,d\Gamma(\mathbf{x})\right.$$

$$\left. + \oint_{\Gamma} P_{ik}^{*}(\mathbf{x}',\mathbf{x})\hat{w}_{mk}^{1}(\mathbf{x})\,d\Gamma(\mathbf{x})\right]\mathbf{F}^{-1}u_{1} \tag{3.85}$$

and

$$I_{3}^{D} = \sum_{m=1}^{M}\left[c_{ik}(\mathbf{x}')\hat{w}_{mk}^{2}(\mathbf{x}') - \int_{\Gamma} W_{ik}^{*}(\mathbf{x}',\mathbf{x})\hat{p}_{mk}^{2}(\mathbf{x})\,d\Gamma(\mathbf{x})\right.$$

$$\left. + \oint_{\Gamma} P_{ik}^{*}(\mathbf{x}',\mathbf{x})\hat{w}_{mk}^{2}(\mathbf{x})\,d\Gamma(\mathbf{x})\right]\mathbf{F}^{-1}u_{2} \tag{3.86}$$

The particular solutions $\hat{w}_{mk}^{\alpha}$ and $\hat{p}_{mk}^{\alpha}$ are given in the Appendix D.

Domain integral I_{4}^{D} can be solved like equation (3.83) by replacing w_{3} with q_{3},

to give:

$$I_4^D = \sum_{m=1}^{M} \left[c_{ik}(\mathbf{x}')\hat{w}_{mk}^3(\mathbf{x}') - \int_\Gamma W_{ik}^*(\mathbf{x}', \mathbf{x})\hat{p}_{mk}^3(\mathbf{x})\, d\Gamma(\mathbf{x}) \right.$$

$$\left. + \oint_\Gamma P_{ik}^*(\mathbf{x}', \mathbf{x})\hat{w}_{mk}^3(\mathbf{x})\, d\Gamma(\mathbf{x}) \right] \mathbf{F}^{-1} q_3 \tag{3.87}$$

I_5^D can be evaluated from the particular solution $\hat{u}_{m\alpha}^1$ for two-dimensional plane stress elasticity problem, that satisfy the differential equation

$$L_{1\alpha}^{m,adj}\hat{u}_{m\alpha}^1 = \frac{\partial F_m(r)}{\partial x_1} = \frac{x_1}{r} \qquad \text{and} \qquad L_{2\alpha}^{m,adj}\hat{u}_{m\alpha}^1 = 0 \tag{3.88}$$

to give

$$I_5^D = \sum_{m=1}^{M} \left[c_{\alpha\beta}(\mathbf{x}')\hat{u}_{m\beta}^1(\mathbf{x}') - \int_\Gamma U_{\alpha\beta}^*(\mathbf{x}', \mathbf{x})\hat{t}_{m\beta}^1(\mathbf{x})\, d\Gamma(\mathbf{x}) \right.$$

$$\left. + \oint_\Gamma T_{\alpha\beta}^*(\mathbf{x}', \mathbf{x})\hat{u}_{m\beta}^1(\mathbf{x})\, d\Gamma(\mathbf{x}) \right] \mathbf{F}^{-1} w_3 \tag{3.89}$$

The last domain integral I_6^D can be obtained from the particular solution $\hat{u}_{m\alpha}^2$ for two-dimensional plane stress elasticity problem, that satisfy the differential equation

$$L_{1\alpha}^{m,adj}\hat{u}_{m\alpha}^2 = 0 \qquad \text{and} \qquad L_{2\alpha}^{m,adj}\hat{u}_{m\alpha}^2 = \frac{\partial F_m(r)}{\partial x_2} = \frac{x_2}{r} \tag{3.90}$$

to give

$$I_6^D = \sum_{m=1}^{M} \left[c_{\alpha\beta}(\mathbf{x}')\hat{u}_{m\beta}^2(\mathbf{x}') - \int_\Gamma U_{\alpha\beta}^*(\mathbf{x}', \mathbf{x})\hat{t}_{m\beta}^2(\mathbf{x})\, d\Gamma(\mathbf{x}) \right.$$

$$\left. + \oint_\Gamma T_{\alpha\beta}^*(\mathbf{x}', \mathbf{x})\hat{u}_{m\beta}^2(\mathbf{x})\, d\Gamma(\mathbf{x}) \right] \mathbf{F}^{-1} w_3 \tag{3.91}$$

3.6 Internal Stress Resultants

The stress resultants at domain point $\mathbf{X}'$ can be evaluated from (3.76 – 3.77) by using relationships in equations (2.44 – 2.46), substituting the term q_3^* in equation (3.8) to give:

$$M_{\alpha\beta}(\mathbf{X}') = \int_\Gamma W_{\alpha\beta k}^*(\mathbf{X}', \mathbf{x}) p_k(\mathbf{x}) d\Gamma(\mathbf{x}) - \int_\Gamma P_{\alpha\beta k}^*(\mathbf{X}', \mathbf{x}) w_k(\mathbf{x}) d\Gamma(\mathbf{x})$$

$$+\int_{\Omega} W^*_{\alpha\beta 3}(\mathbf{X}',\mathbf{X})q^*_3 d\Omega(\mathbf{X})\ ; \tag{3.92}$$

$$Q_\beta(\mathbf{X}') = \int_\Gamma W^*_{3\beta k}(\mathbf{X}',\mathbf{x})p_k(\mathbf{x})d\Gamma(\mathbf{x}) - \int_\Gamma P^*_{3\beta k}(\mathbf{X}',\mathbf{x})w_k(\mathbf{x})d\Gamma(\mathbf{x})$$

$$+\int_{\Omega} W^*_{3\beta 3}(\mathbf{X}',\mathbf{X})q^*_3 d\Omega(\mathbf{X}) \tag{3.93}$$

and

$$N_{\alpha\beta}(\mathbf{X}') = \int_\Gamma U^*_{\alpha\beta\gamma}(\mathbf{X}',\mathbf{x})t_\gamma(\mathbf{x})d\Gamma(\mathbf{x}) - \int_\Gamma T^{(i)*}_{\alpha\beta\gamma}(\mathbf{X}',\mathbf{x})u_\gamma(\mathbf{x})d\Gamma(\mathbf{x})$$

$$-\int_\Gamma U^*_{\alpha\beta\gamma}(\mathbf{X}',\mathbf{x})B\left[k_{\alpha\gamma}(1-\nu)+\nu\delta_{\alpha\gamma}k_{\phi\phi}\right]w_3(\mathbf{x})n_\gamma(\mathbf{x})d\Gamma(\mathbf{x})$$

$$+\int_\Omega U^*_{\alpha\beta\gamma}(\mathbf{X}',\mathbf{X})q^*_\gamma d\Omega(\mathbf{X}) + B\left[(1-\nu)k_{\alpha\beta}+\nu\delta_{\alpha\beta}k_{\phi\phi}\right]w_3(\mathbf{X}') \tag{3.94}$$

In the case of a uniform load, the domain integral $\int_\Omega W^*_{i\beta 3}(\mathbf{x}',\mathbf{X})q_3(\mathbf{X})d\Omega(\mathbf{X})$ in (3.92 – 3.93) can be transferred to boundary integral, by applying the divergence theorem, to give:

$$\int_\Omega W^*_{i\beta 3}(\mathbf{x}',\mathbf{X})q_3(\mathbf{X})d\Omega(\mathbf{X}) = q_3\int_\Gamma Q^*_{i\beta}(\mathbf{x}',\mathbf{x})d\Gamma(\mathbf{x}) \tag{3.95}$$

The kernels $W^*_{i\beta k}$, $P^*_{i\beta k}$ and $Q^*_{i\beta}$ are linear combination of the first derivatives of W^*_{ij}, P^*_{ij} and $V^*_{i,\beta}$ where the kernels $U^*_{\alpha\beta\gamma}$ and $T^*_{\alpha\beta\gamma}$ are linear combination of the first derivatives of $U^*_{\alpha\beta}$ and $T^*_{\alpha\beta}$. The expression of W^*_{ijk}, P^*_{ijk} and $Q^*_{i\beta}$ are [134]:

$$\begin{aligned}
W^*_{\alpha\beta\gamma} &= \frac{1}{4\pi r}[(4A(z)+2zK_1(z)+1-\nu)(\delta_{\beta\gamma}r_{,\alpha}+\delta_{\alpha\gamma}r_{,\beta}) \\
&- 2(8A(z)+2zK_1(z)+1-\nu)r_{,\alpha}r_{,\beta}r_{,\gamma}+(4A(z)+1+\nu)\delta_{\alpha\beta}r_{,\gamma}] \\
W^*_{\alpha\beta 3} &= \frac{-(1-\nu)}{8\pi}\left[\left(2\frac{(1+\nu)}{(1-\nu)}\ln z-1\right)\delta_{\alpha\beta}+2r_{,\alpha}r_{,\beta}\right] \\
W^*_{3\beta\gamma} &= \frac{\lambda^2}{2\pi}[B(z)\delta_{\gamma\beta}-A(z)r_{,\gamma}r_{,\beta}] \\
W^*_{3\beta 3} &= \frac{1}{2\pi r}r_{,\beta}
\end{aligned} \tag{3.96}$$

$$\begin{aligned}
P^*_{\alpha\beta\gamma} &= \frac{D(1-\nu)}{4\pi r^2}\{(4A(z)+2zK_1(z)+1-\nu)(\delta_{\gamma\alpha}n_\beta+\delta_{\gamma\beta}n_\alpha) \\
&+ (4A(z)+1+3\nu)\delta_{\alpha\beta}n_\gamma-(16A(z)+6zK_1(z)+z^2K_0(z)+2-2\nu) \\
&\times [(n_\alpha r_{,\beta}+n_\beta r_{,\alpha})r_{,\gamma}+(\delta_{\gamma\alpha}r_{,\beta}+\delta_{\gamma\beta}r_{,\alpha})r_{,n}]
\end{aligned}$$

$$
\begin{aligned}
&- \quad 2(8A(z)+2zK_1(z)+1+\nu)(\delta_{\alpha\beta}r_{,\gamma}r_{,n}+n_\gamma r_{,\alpha}r_{,\beta}) \\
&+ \quad 4(24A(z)+8zK_1(z)+z^2K_0(z)+2-2\nu)r_{,\alpha}r_{,\beta}r_{,\gamma}r_{,n}\} \\
P^*_{\alpha\beta 3} &= \frac{D(1-\nu)\lambda^2}{4\pi r}[(2A(z)+zK_1(z))(r_{,\beta}n_\alpha+r_{,\alpha}n_\beta) \\
&- \quad 2(4A(z)+zK_1(z))r_{,\alpha}r_{,\beta}r_{,n}+2A(z)\delta_{\alpha\beta}r_{,n}] \\
P^*_{3\beta\gamma} &= \frac{-D(1-\nu)\lambda^2}{4\pi r}[(2A(z)+zK_1(z))(\delta_{\gamma\beta}r_{,n}+r_{,\gamma}n_\beta) \\
&+ \quad 2A(z)n_\gamma r_{,\beta}-2(4A(z)+zK_1(z))r_{,\gamma}r_{,\beta}r_{,n}] \\
P^*_{3\beta 3} &= \frac{D(1-\nu)\lambda^2}{4\pi r^2}[(z^2B(z)+1)n_\beta-(z^2A(z)+2)r_{,\beta}r_{,n}]
\end{aligned} \tag{3.97}
$$

$$
\begin{aligned}
Q^*_{\alpha\beta} &= \frac{-r}{64\pi}\{(4\ln z-3)[(1-\nu)(r_{,\beta}n_\alpha+r_{,\alpha}n_\beta)+(1+3\nu)\delta_{\alpha\beta}r_{,n}] \\
&+ \quad 4[(1-\nu)r_{,\alpha}r_{,\beta}+\nu\delta_{\alpha\beta}]r_{,n}\} \\
Q^*_{3\beta} &= \frac{1}{8\pi}[(2\ln z-1)n_\beta+2r_{,\beta}r_{,n}]
\end{aligned} \tag{3.98}
$$

and the expressions for the kernels $U^*_{\alpha\beta\gamma}$, and $T^*_{\alpha\beta\gamma}$ are :

$$
U^*_{\alpha\beta\gamma} = \frac{1}{4\pi r}\left[(1-\nu)\left(\delta_{\gamma\alpha}r_{,\beta}+\delta_{\gamma\beta}r_{,\alpha}-\delta_{\alpha\beta}r_{,\gamma}\right)+2\left(1+\nu\right)r_{,\alpha}r_{,\beta}r_{,\gamma}\right] \tag{3.99}
$$

$$
\begin{aligned}
T^{(i)*}_{\alpha\beta\gamma} &= \frac{B\left(1-\nu\right)}{4\pi r^2}\{2r_{,n}\left[(1-\nu)\,\delta_{\alpha\beta}r_{,\gamma}+\nu\left(\delta_{\gamma\alpha}r_{,\beta}+\delta_{\gamma\beta}r_{,\alpha}\right)-4\left(1+\nu\right)r_{,\alpha}r_{,\beta}r_{,\gamma}\right] \\
&+2\nu\left(n_\alpha r_{,\beta}r_{,\gamma}+n_\beta r_{,\alpha}r_{,\gamma}\right)+\left(1-\nu\right)\left(2n_\gamma r_{,\alpha}r_{,\beta}+n_\beta\delta_{\alpha\gamma}+n_\alpha\delta_{\beta\gamma}\right) \\
&-\left(1-3\nu\right)n_\gamma\delta_{\alpha\beta}\}
\end{aligned} \tag{3.100}
$$

3.7 Evaluation of Boundary Stress Resultants

The boundary stress resultants can be evaluated from the local tractions and by computing the generalised local strains on the boundary using displacement derivatives, and then make use of the stress resultant-strain relationships of shear deformable shell as in two- or three-dimensional elasticity problems [8]. Consider the local coordinate system shown in Figure 3-8. The generalised displacements (w^o_i and u^o_θ) and tractions (p^o_i, t^o_θ) at the point $\mathbf{x}'$ in the local system of coordinate are

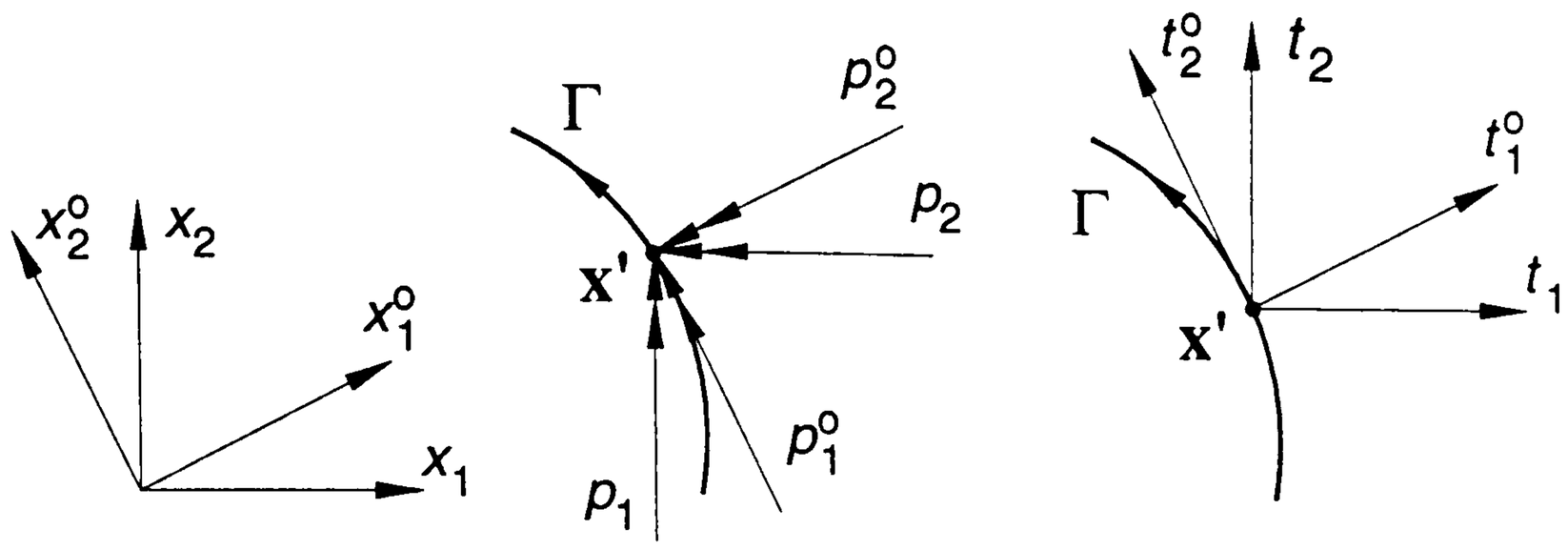

Figure 3-8: Local and global coordinate system at $\mathbf{x}'$.

related to those in global coordinate system, as follows:

$$\begin{aligned} w_i^o &= e_{ij}^o w_j \qquad \text{and} \qquad u_\theta^o = e_{\theta\gamma}^o u_\gamma \\ p_i^o &= e_{ij}^o p_j \qquad \text{and} \qquad t_\theta^o = e_{\theta\gamma}^o t_\gamma \end{aligned} \tag{3.101}$$

and the tensor e_{ij}^o is the rotation matrix and can be written in terms of the known normal components by:

$$e_{ij}^o = \begin{bmatrix} n_1 & n_2 & 0 \\ -n_2 & n_1 & 0 \\ 0 & 0 & 1 \end{bmatrix} \tag{3.102}$$

By considering the equilibrium of stress resultants in the local coordinate system, it can be seen that:

$$\begin{aligned} M_{1\alpha}^o &= p_\alpha^o \\ Q_1^o &= p_3^o \\ N_{1\alpha}^o &= t_\alpha^o \end{aligned} \tag{3.103}$$

Other components of the local stress resultant tensor can be evaluated using relationships in equations (2.44 – 2.46) as follows:

$$M_{22}^o = \nu p_1^o + D\left(1-\nu^2\right) w_{2,2}^o$$

$$Q_2^o = \frac{D(1-\nu)\lambda^2}{2}[w_2^o + w_{3,2}^o]$$

$$N_{22}^o = \nu t_1^o + B\left(1-\nu^2\right) u_{2,2}^o + B\left(1-\nu^2\right) k_{22}^o w_3^o \tag{3.104}$$

By considering Figure 3-8, one can find the following relationships [8]:

$$\frac{\partial \xi}{\partial x_2^o(\mathbf{x}')} = \frac{1}{J(\mathbf{x}')} \tag{3.105}$$

The displacement approximation in terms of the element shape functions Φ^k may be written as:

$$\begin{aligned} w_j^o &= \Phi^k w_j^{ok} \\ u_\theta^o &= \Phi^k u_\theta^{ok} \end{aligned} \tag{3.106}$$

where w_j^{ok} and u_θ^{ok} are the local generalised boundary displacements. The displacement derivatives in equation (3.104) can then be rewritten in the following form:

$$\begin{aligned} w_{j,2}^o &= \Phi_{,2}^k w_j^{ok} = \frac{\partial \Phi^k}{\partial \xi} e_{ji}^o w_i^k \frac{\partial \xi}{\partial x_2^o(\mathbf{x}')} \\ u_{\theta,2}^o &= \Phi_{,2}^k u_\theta^{ok} = \frac{\partial \Phi^k}{\partial \xi} e_{\theta\gamma}^o u_\gamma^k \frac{\partial \xi}{\partial x_2^o(\mathbf{x}')} \end{aligned} \tag{3.107}$$

Using equation (3.107), the displacement derivatives can be computed. The local curvature term k_{22}^o can be obtained from the following transformation:

$$k_{22}^o = {n_2}^2 k_{11} + {n_1}^2 k_{22} \tag{3.108}$$

and hence, the local boundary stress resultant tensor can be evaluated. The global stress resultant tensor can be evaluated via the following transformation:

$$\begin{aligned} M_{\alpha\beta} &= e_{\theta\alpha}^o e_{\gamma\beta}^o M_{\theta\gamma}^o \\ Q_\alpha &= e_{\beta\alpha}^o Q_\beta^o \\ N_{\alpha\beta} &= e_{\theta\alpha}^o e_{\gamma\beta}^o N_{\theta\gamma}^o \end{aligned} \tag{3.109}$$

3.8 Boundary Integrals of Shear Deformable Plate Bending and Two-Dimensional Plane Stress

If the shell under consideration is flat, thus the value of $k_{11} = k_{22} = 0$, all integrals which contain $k_{\alpha\beta}$ in equations (3.31) and (3.50) will be vanish and there are no coupling anymore between the plate bending and the plane stress formulations. The integrals in (3.31) will become integral representations of the shear deformable plate bending problems, and can be written as follows

$$w_i(\mathbf{X}') + \int_\Gamma P^*_{ij}(\mathbf{X}', \mathbf{x}) w_j(\mathbf{x})\, d\Gamma(\mathbf{x}) = \int_\Gamma W^*_{ij}(\mathbf{X}', \mathbf{x}) p_j(\mathbf{x})\, d\Gamma(\mathbf{x})$$

$$+ \int_\Omega W^*_{i3}(\mathbf{X}', \mathbf{X}) q_3(\mathbf{X}) d\Omega(\mathbf{X}) \tag{3.110}$$

and the integrals in (3.50) will become integral representation of the two-dimensional plane stress elasticity problems,

$$u_\theta(\mathbf{X}') + \int_\Gamma T^*_{\theta\alpha}(\mathbf{X}', \mathbf{x})\, u_\alpha(\mathbf{x})\, d\Gamma(\mathbf{x}) = \int_\Gamma U^*_{\theta\alpha}(\mathbf{X}', \mathbf{x})\, t_\alpha(\mathbf{x})\, d\Gamma(\mathbf{x}) \tag{3.111}$$

Similarly as in the previous section, if the point $\mathbf{X}'$ is taken to the boundary, $(\mathbf{X}' \to \mathbf{x}' \in \Gamma)$, and assuming that the displacements w_j and u_α are Hölder continuities, equation (3.110) for the source points on the boundary can be written as follows:

$$c_{ij}(\mathbf{x}') w_j(\mathbf{x}') + \oint_\Gamma P^*_{ij}(\mathbf{x}', \mathbf{x}) w_j(\mathbf{x})\, d\Gamma(\mathbf{x}) = \int_\Gamma W^*_{ij}(\mathbf{x}', \mathbf{x}) p_j(\mathbf{x})\, d\Gamma(\mathbf{x})$$

$$+ \int_\Omega W^*_{i3}(\mathbf{x}', \mathbf{X}) q_3(\mathbf{X}) d\Omega(\mathbf{X}) \tag{3.112}$$

and equation (3.111) can be written as

$$c_{\theta\alpha}(\mathbf{x}')\, u_\alpha(\mathbf{x}') + \oint_\Gamma T^*_{\theta\alpha}(\mathbf{x}', \mathbf{x}) u_\alpha(\mathbf{x}) d\Gamma(\mathbf{x}) = \int_\Gamma U^*_{\theta\alpha}(\mathbf{x}', \mathbf{x}) t_\alpha(\mathbf{x}) d\Gamma(\mathbf{x}) \tag{3.113}$$

The term $c_{ij}(\mathbf{x}')$ is equal to $\frac{1}{2}\delta_{ij}$ when $\mathbf{x}'$ is located on a smooth boundary.

The stress resultant components are obtained by differentiation of equation (3.110) with respect to the coordinate of the source point $\mathbf{X}'$ and then substituting

them into the stress resultant-displacement relations in equations (2.65) to give:

$$M_{\alpha\beta}(\mathbf{X}') = \int_\Gamma W^*_{\alpha\beta k}(\mathbf{X}',\mathbf{x})p_k(\mathbf{x})d\Gamma(\mathbf{x}) - \int_\Gamma P^*_{\alpha\beta k}(\mathbf{X}',\mathbf{x})w_k(\mathbf{x})d\Gamma(\mathbf{x}) + \int_\Omega W^*_{\alpha\beta 3}(\mathbf{X}',\mathbf{X})q_3 d\Omega(\mathbf{X}) \tag{3.114}$$

$$Q_\beta(\mathbf{X}') = \int_\Gamma W^*_{3\beta k}(\mathbf{X}',\mathbf{x})p_k(\mathbf{x})d\Gamma(\mathbf{x}) - \int_\Gamma P^*_{3\beta k}(\mathbf{X}',\mathbf{x})w_k(\mathbf{x})d\Gamma(\mathbf{x}) + \int_\Omega W^*_{3\beta 3}(\mathbf{X}',\mathbf{X})q_3 d\Omega(\mathbf{X}) \tag{3.115}$$

and by differentiation of equation (3.111) with respect to the coordinate of the source point $\mathbf{X}'$ followed by the application of equations (2.66) to obtain:

$$N_{\alpha\beta}(\mathbf{X}') + \int_\Gamma T^*_{\alpha\beta\gamma}(\mathbf{X}',\mathbf{x})u_\gamma(\mathbf{x})d\Gamma(\mathbf{x}) = \int_\Gamma U^*_{\alpha\beta\gamma}(\mathbf{X}',\mathbf{x})t_\gamma(\mathbf{x})d\Gamma(\mathbf{x}) \tag{3.116}$$

In the case of a uniform domain load, the domain integral in (3.112) can be transferred to boundary integral using equation (3.58), and equation (3.95) for the transformation of domain integrals in (3.114 – 3.115). For other distribution cases of q_3, the transformation of domain integrals can be carried out by using the dual reciprocity techniques, as explained in section 3.5.

The kernels W^*_{ij}, P^*_{ij}, $V^*_{i,\beta}$, $U^*_{\theta\alpha}$, $T^*_{\theta\alpha}$, W^*_{ijk}, P^*_{ijk}, $Q^*_{i\beta}$, $U^*_{\alpha\beta\gamma}$ and $T^*_{\alpha\beta\gamma}$ are the same as the kernels for shallow shell formulation and have been listed in the section 3.6.

3.9 Numerical Examples

Several numerical examples are presented to demonstrate the ability of the proposed method to solve shallow shell problems with different geometries, loadings and boundary conditions. All possible boundary conditions i.e. clamped, simply supported and free edge are tested.

3.9.1 Circular shallow spherical shell: uniformly loaded

In this example, a shallow spherical cap as shown in Figure 3-9 is analysed. The geometric and material properties of the cap is as follows: $a = 5$; $h/a = 0.02$;

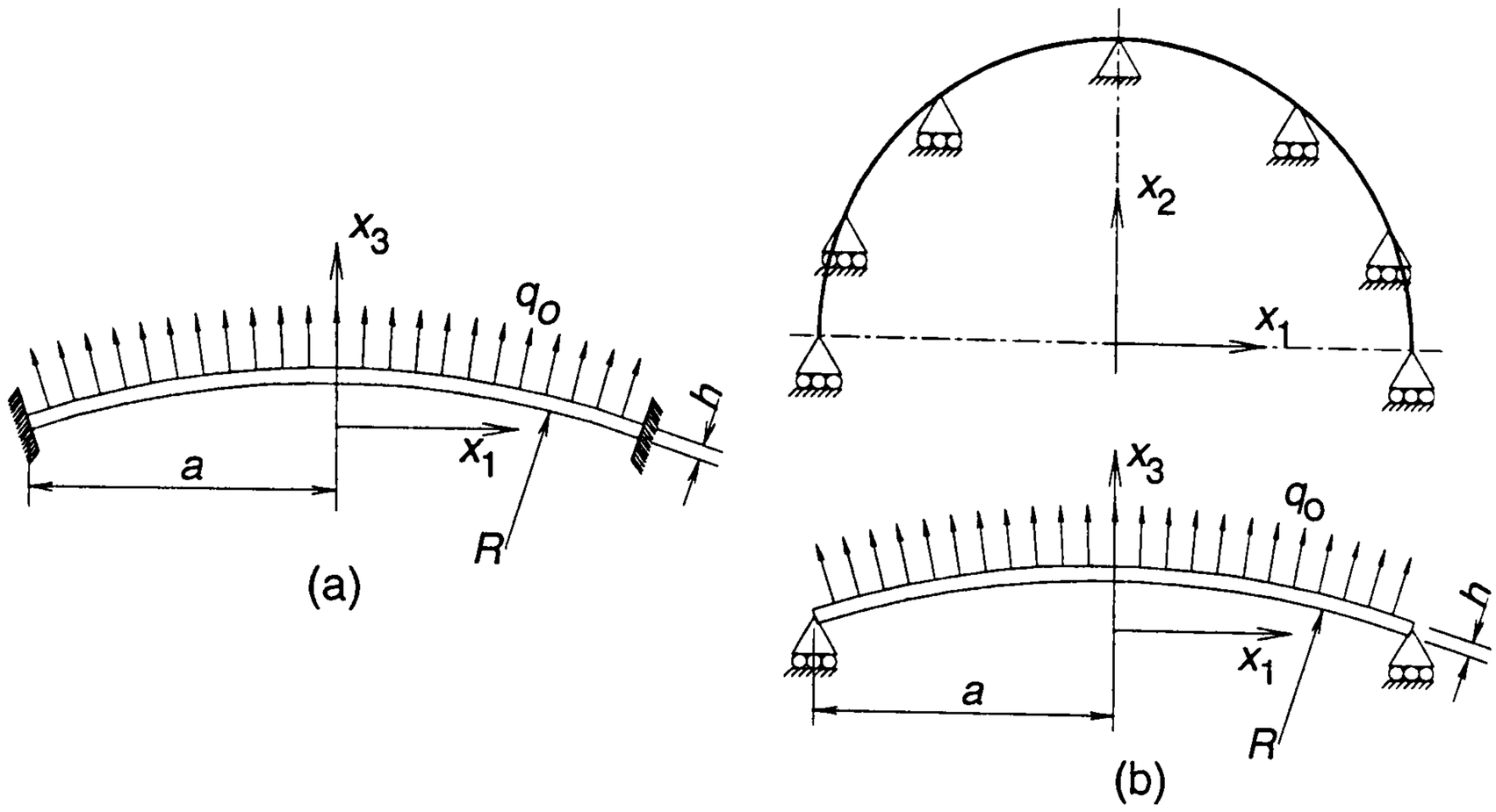

Figure 3-9: Circular shallow spherical shell: uniformly loaded. (a) clamped edge; (b) simply supported edge.

$k_{11} = k_{22} = 1/R$, where $a/R = 0.05$. The cap is loaded with uniform pressure q_0 with the ratio of $E/q_0 = 210000$ and Poisson's ratio $\nu = 0.3$. Two types of boundary conditions are employed here, i.e. clamped and simply supported. For the clamped edge problem, the boundary conditions are $w_i = 0$, and $u_\alpha = 0$ along the boundary, while for the simply supported edge, $M_n = 0$, $w_3 = 0$, and $u_2 = 0$ along the boundary.

Three different BEM meshes are being used. Mesh A has 8 boundary elements and 9 cells, Mesh B has 12 boundary elements and 30 cells, Mesh C has 16 quadratic boundary elements and 81 constant cells.

For comparison, FEM analyses are also being performed. The analysis is carried out using a commercial software package. The shell element formulation used in this software package is a 4-node linear element which is a combination of membrane and plate bending behaviour. The membrane is an isoparametric formulation including translational in-plane stiffness components and a rotational component in the direction normal to the plane of the element [127], and the plate bending behaviour include two out-of-plane rotational stiffness components and a translational in the direction normal to the plane of the element. The analysis does not include any effect of shear deformation [21]. Element forces, in element local coordinate

system, are evaluated at the integration points and extrapolated to the joints of the element. Three FEM meshes are analysed, Mesh D has 120 elements, Mesh E has 240 elements, and Mesh F has 540 elements.

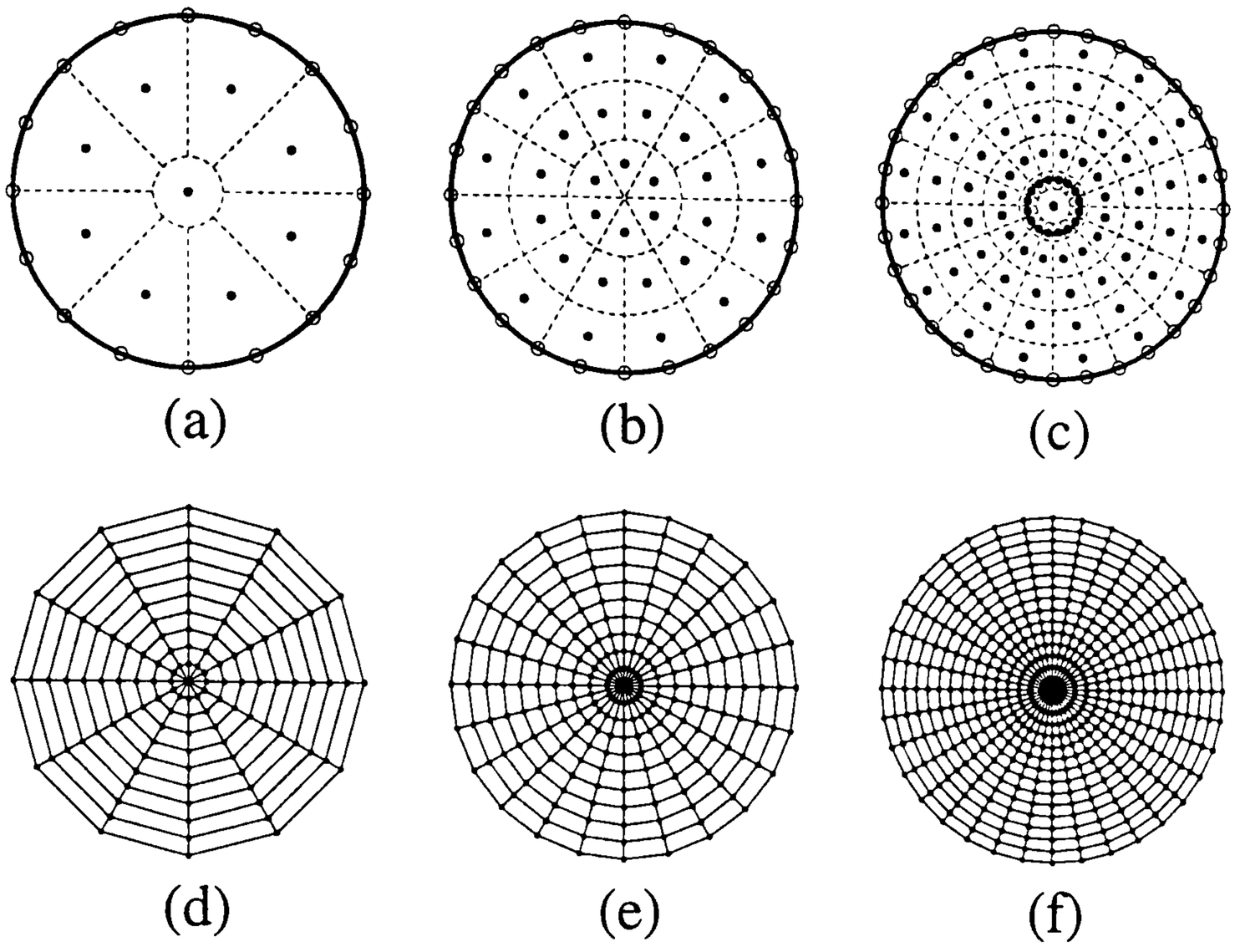

Figure 3-10: BEM and FEM mesh.

Table 3.1: Boundary results of the clamped circular shell.

Clamped	B E M			F E M		
	mesh A	mesh B	mesh C	mesh D	mesh E	mesh F
$M_n/\left(a^2 q_0\right)$	0.05658	0.06186	0.06028	0.05658	0.05911	0.05966
$Q_n/\left(a q_0\right)$	0.22300	0.29331	0.28588	--	--	--
$N_n/\left(a q_0\right)$	6.42208	4.63500	4.54572	4.5880	4.6358	4.5758

Tables 3.1 – 3.2 and Figures 3-11 – 3-12 show the results of this example. All three BEM meshes show good agreement with FEM mesh F for clamped edge and FEM mesh E for simply supported edge. It can be seen that using the present formulation convergence can be achieved with only small number of elements and cells, while in FEM convergence was achieved after comparatively larger number of elements.

Next, comparison are made between the cell BEM formulation and the dual

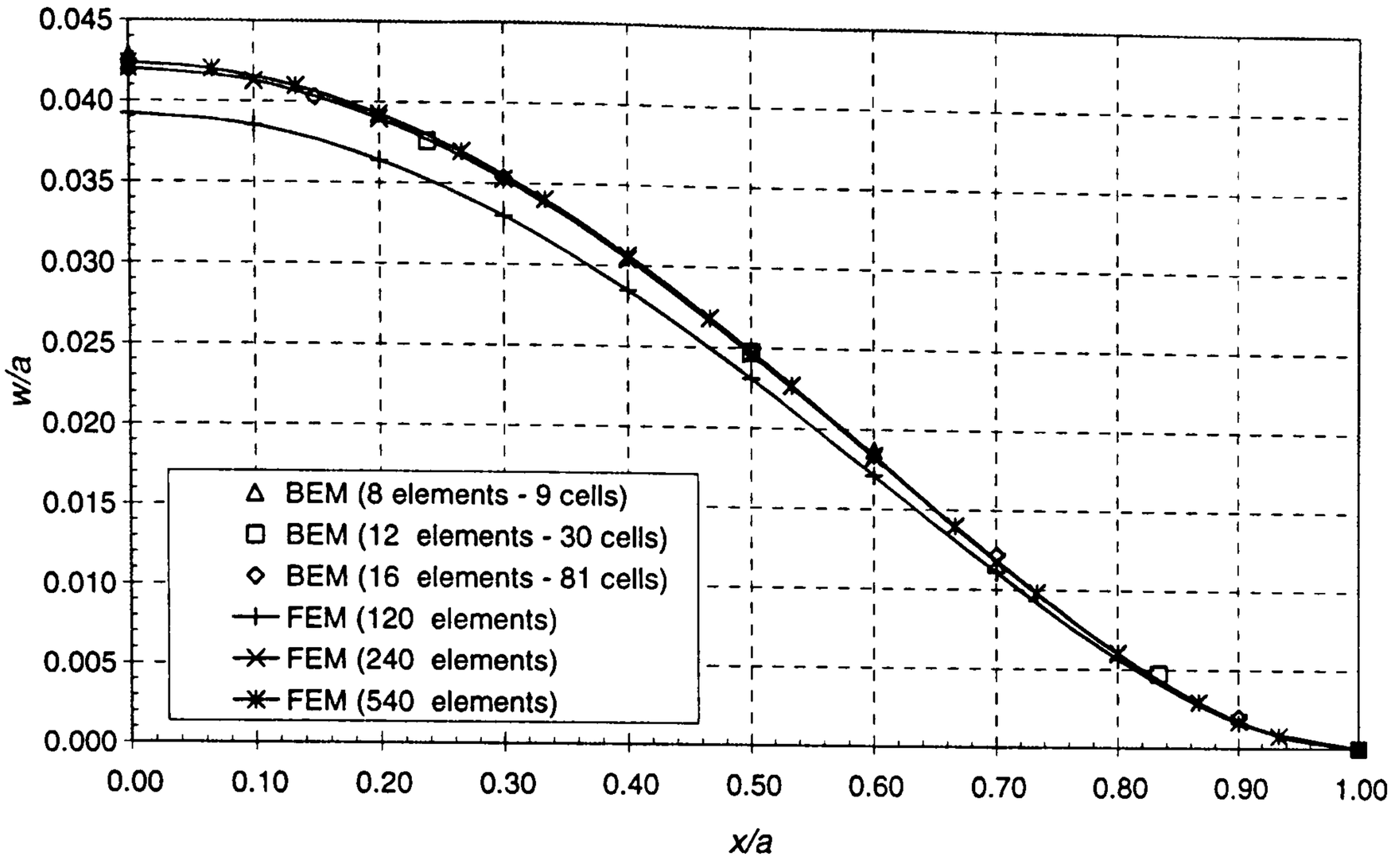

Figure 3-11: Out-of-plane displacement along the centre line of the clamped shallow spherical shell.

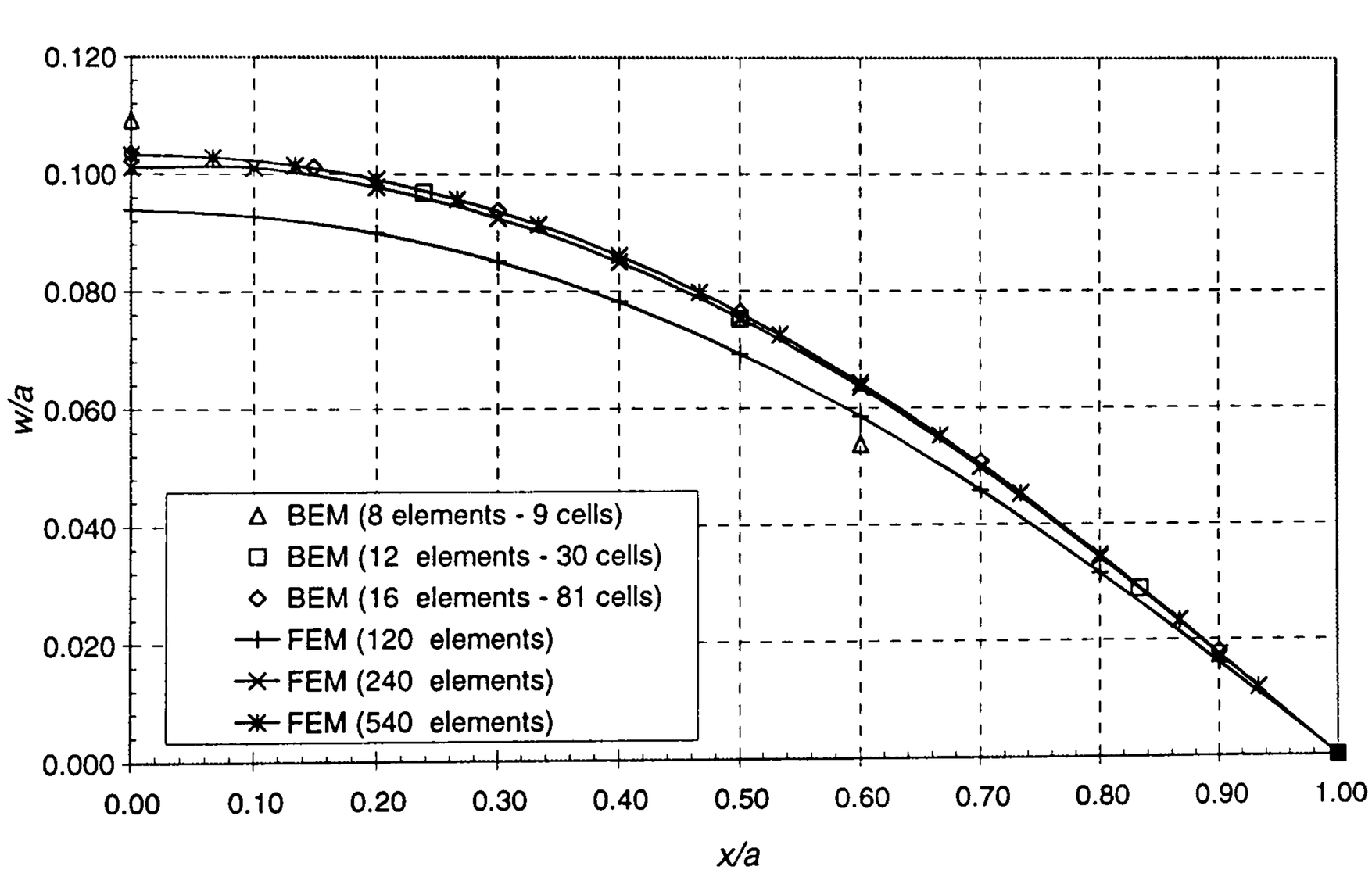

Figure 3-12: Out-of-plane displacement along the centre line of the simply supported shallow spherical shell.

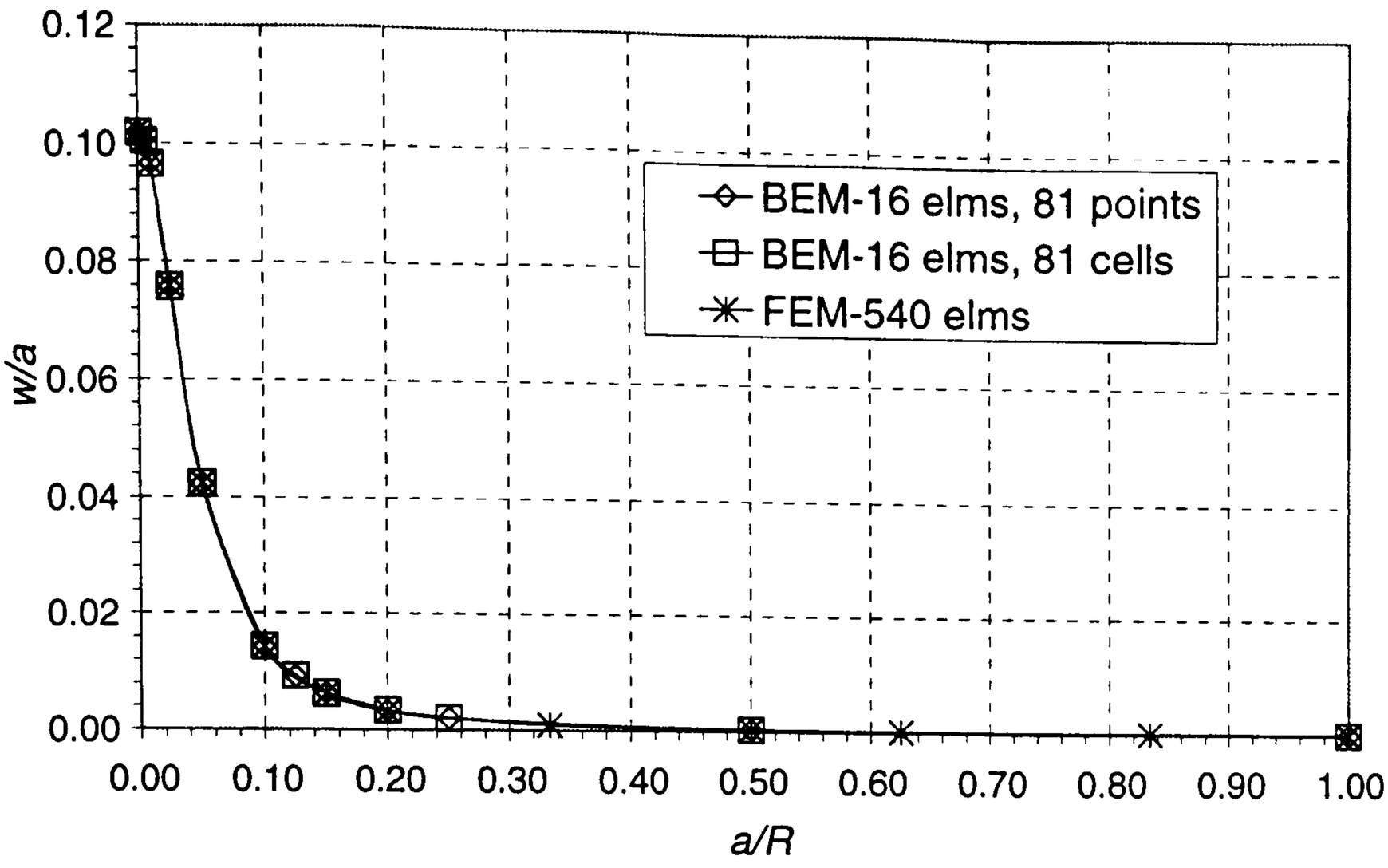

Figure 3-13: Out-of-plane displacement at the centre of clamped spherical shell for different ratio of a/R.

Table 3.2: Boundary results of the simply supported circular shell.

Simply supported	B E M			F E M		
	mesh A	mesh B	mesh C	mesh D	mesh E	mesh F
ϕ_n	0.11142	0.16491	0.16956	0.1618	0.1722	0.1748
$Q_n/(aq_0)$	0.68831	0.68219	0.72014	--	--	--
$N_n/(aq_0)$	14.4539	11.8307	11.2759	10.3358	10.6640	10.6814

reciprocity technique. The clamped spherical shells for different ratios of a/R and loaded with uniform internal pressure are analysed next. The properties of these caps are the same as before, except the curvature of the shells are varied within the range of $ak_{11} = ak_{22} = a/R = 0.0 - 1.0$, where the ratio $a/R = 0.0$ represents a flat circular plate and $a/R = 1.0$ represents half of a sphere. The mesh used for BEM with cells included 16 boundary elements and 81 constant cells, and the mesh for BEM with the dual reciprocity technique included 16 boundary elements and 81 domain points. In the tests carried out, both BEM models were found to be in very good agreement ($< 1\%$) with each other and the FEM mesh F, as can be seen in Figure 3-13.

3.9.2 Circular shallow spherical shell with a hole in the centre

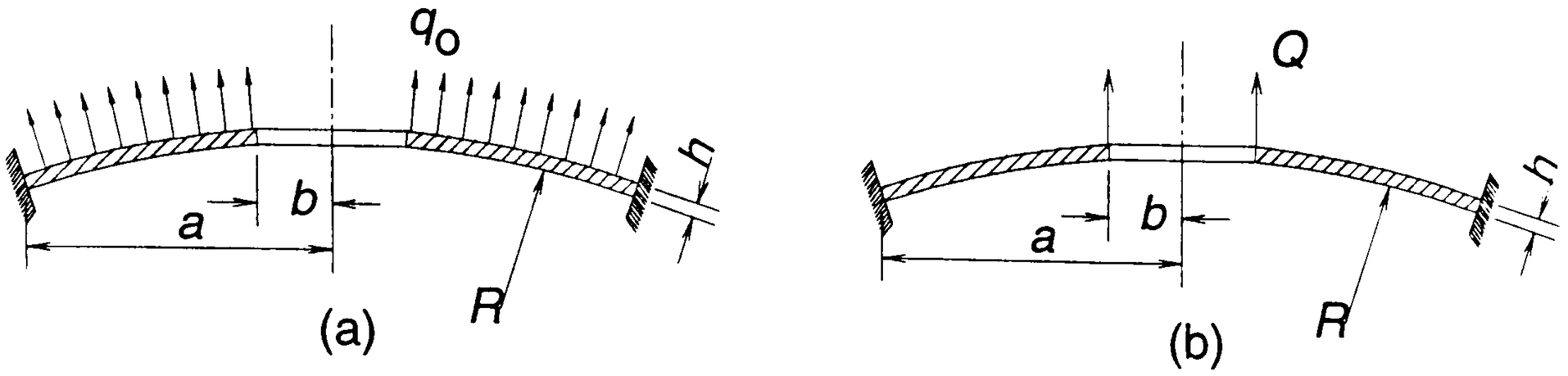

Figure 3-14: Clamped circular shallow spherical shell with a hole in the centre: (a) uniform internal pressure; (b) vertical shear force stress resultant along the hole edge.

In this example, a shallow spherical cap with a hole in the centre as shown in Figure 3-14 is being analysed. The properties of the caps are as follows $a = 5$; $h/a = 0.02$; $b/a = 0.1$; $ak_{11} = ak_{22} = 0.025$; $E/q_0 = 210000$ and $\nu = 0.3$. Two loading conditions are being considered, (a) uniform internal pressure q_0 and (b) vertical shear force stress resultant Q along the hole edge with $Q/(bq_0) = 2$.

Table 3.3: Boundary results of the clamped circular shells with a hole: uniform pressure.

	BEM	*FEM*	Δ
— outer boundary —			
$M_n/\left(a^2 q_0\right)$	−0.096426	−0.096200	0.23 %
$Q_n/\left(aq_0\right)$	−0.405596	—	—
$N_n/\left(aq_0\right)$	3.737920	3.943600	5.22 %
— inner boundary —			
ϕ_n	0.073891	0.076162	2.98 %
w/a	0.079343	0.080566	1.52 %

A BEM mesh with 32 quadratic boundary elements and 80 constant cells are used to model the caps and are compared with a FEM mesh with 240 elements. Tables 3.3 – 3.4 and Figure 3-15 show the result of this example. As it can be seen, the BEM results are in good agreement with FEM results, the maximum difference between those two models are 6.94 % for the membrane stress resultant.

The shallow spherical cap with a hole in the centre loaded by uniform pressure as shown in Figure 3-14(a) is also being analysed using the dual reciprocity technique.

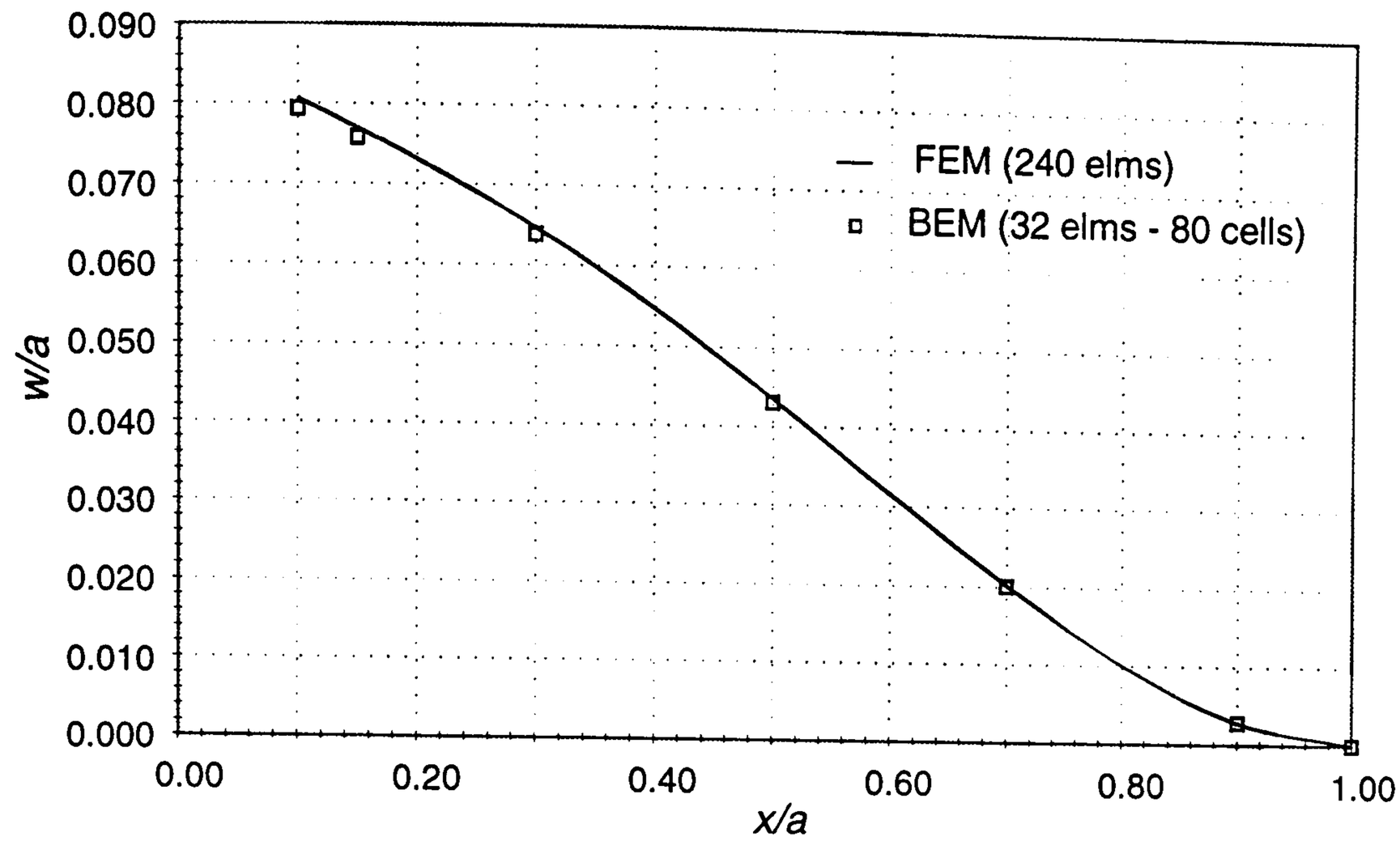

(a) uniform internal pressure

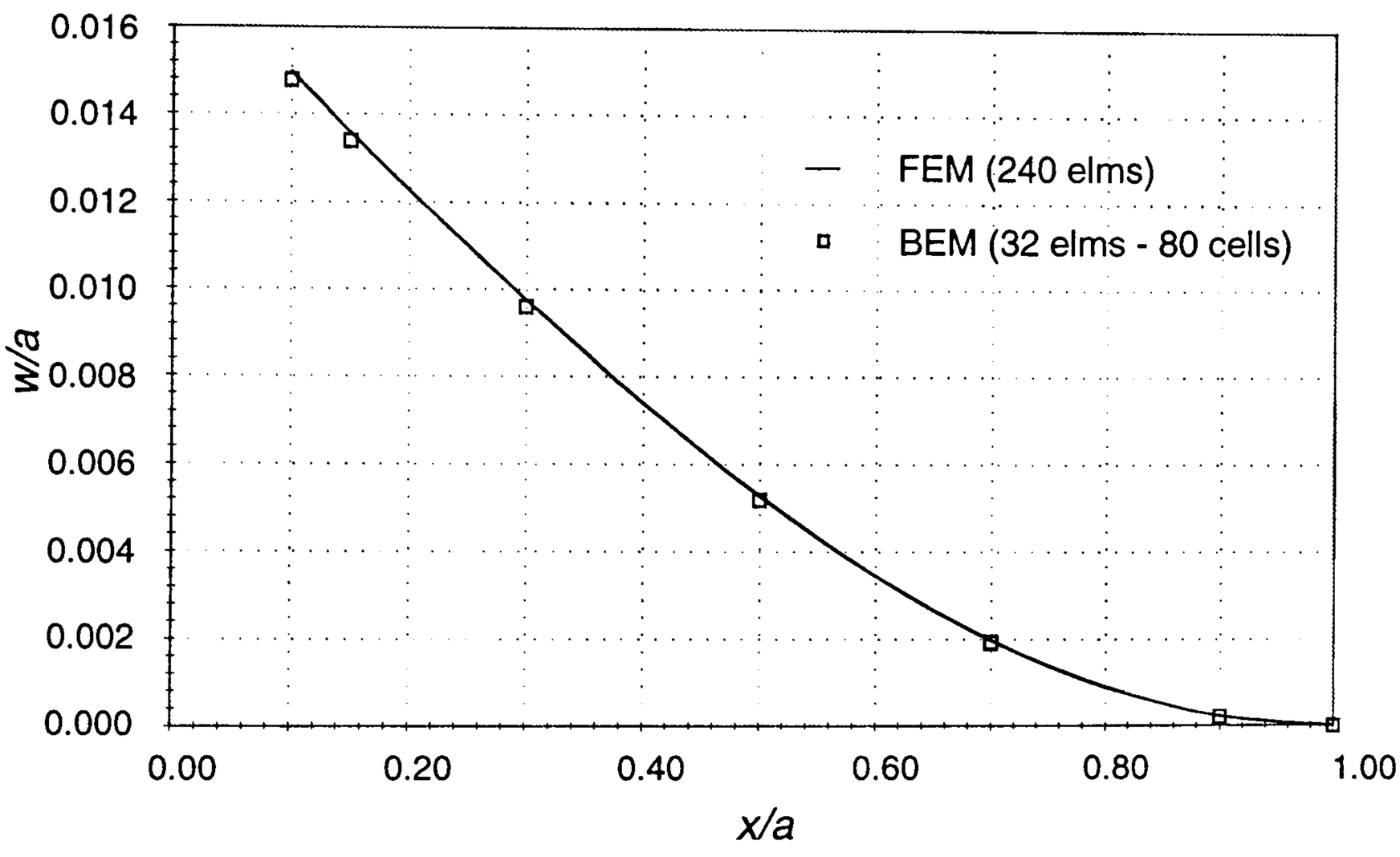

(b) vertical shear stress resultant along the hole edge

Figure 3-15: Out-of-plane displacement along the centre line of the clamped circular shallow spherical shell with a hole in the centre.

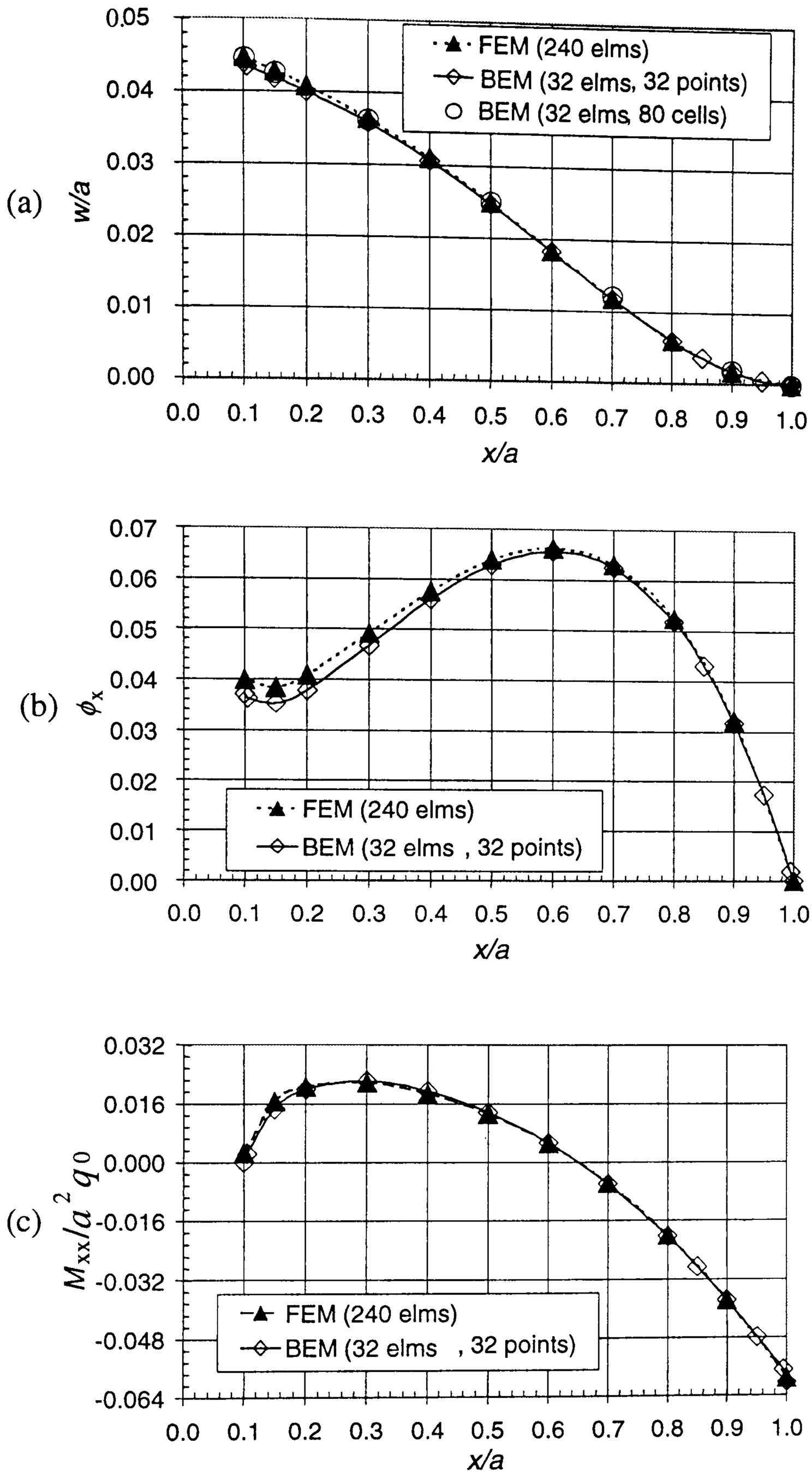

Figure 3-16: Displacements and stress resultants along the x_1- axis of the clamped circular shallow spherical shell with a hole in the centre, uniformly loaded.

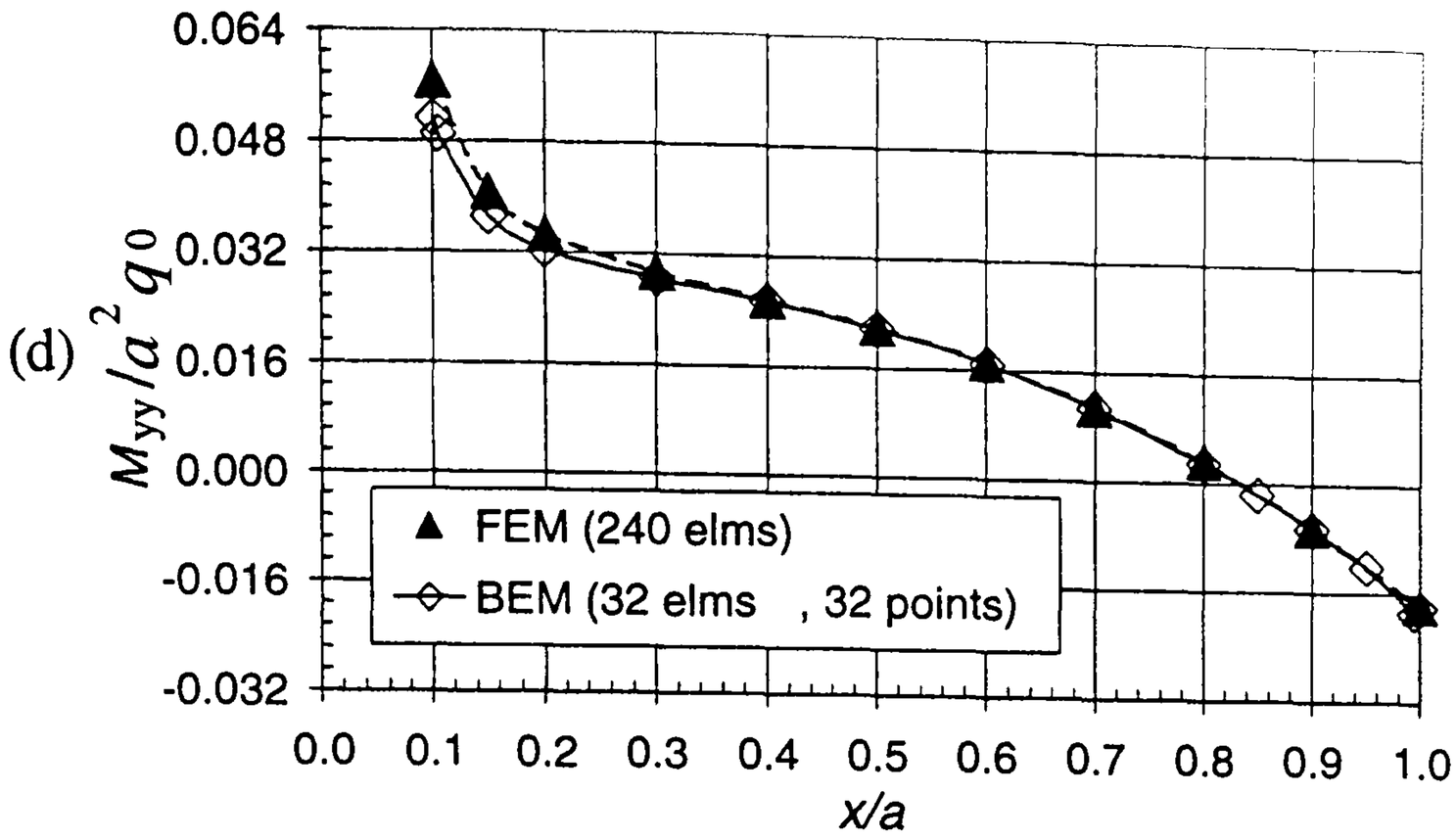

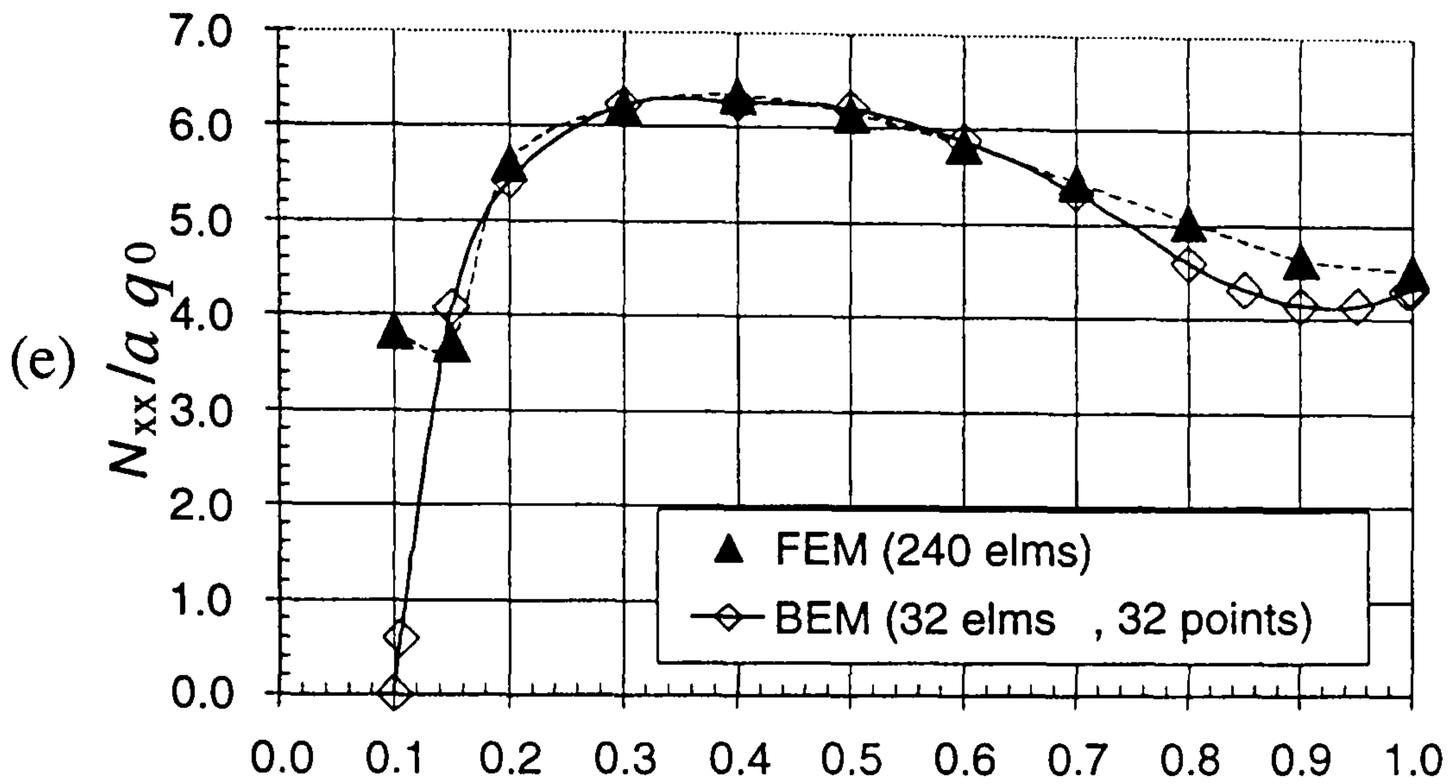

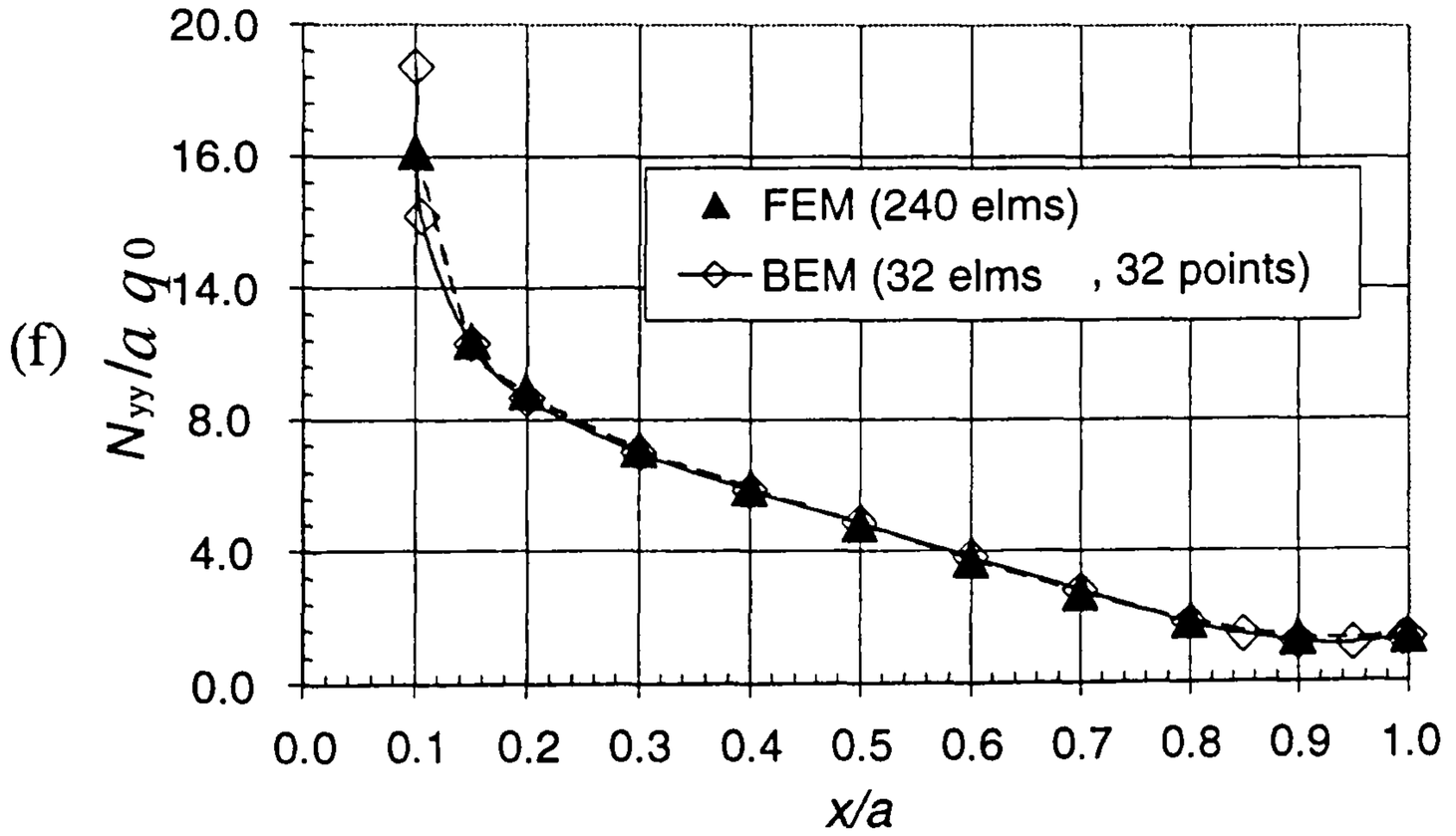

Figure 3-17: Displacements and stress resultants along the x_1- axis of the clamped circular shallow spherical shell with a hole in the centre, uniformly loaded.

Table 3.4: Boundary results of the clamped circular shells with a hole: vertical shear force stress resultant along the hole edge.

	BEM	*FEM*	Δ
— outer boundary —			
$M_n/\left(a^2 q_0\right)$	−0.006892	−0.006921	0.42 %
$Q_n/\left(a q_0\right)$	−0.008632	−−	−−
$N_n/\left(a q_0\right)$	0.474654	0.510060	6.94 %
— inner boundary —			
ϕ_n	0.0289094	0.029175	0.91 %
w/a	0.014777	0.014962	1.23 %

A BEM mesh with 32 quadratic boundary elements and 32 domain points are used to model the caps and are compared with the Domain-BEM mesh with 32 quadratic boundary elements and 80 constant cells and a FEM mesh with 240 elements.

Figures 3-16(a) – 3-17(f) show the results of this example modelled using the dual reciprocity technique. As it can be seen, the BEM results from both of BEM models are in very good agreement with each other and those obtained using FEM. It can also be seen in Figure 3-17(e) that FEM model fails to give zero value for membrane stress resultant at free boundary, because the forces at the element joints are extrapolated from the element forces evaluated at integration points.

3.9.3 Simply supported square shallow spherical shell: uniformly loaded

In this example, a square shallow spherical cap as shown in Figure 3-18 is being analysed. This problem will demonstrate the ability of the proposed method in solving problems which involve the effect of transverse shear deformation. Several shells with different thickness h were analysed. The properties of the caps are as follows: $a = 16$; $h/a = 0.02$, 0.10, 0.20 and 0.40; $ak_{11} = ak_{22} = a/R = 1/6$; $E/q = 10^5$ and $\nu = 0.3$. For the simply supported edge, $M_n = 0, w_3 = 0$, and $u_2 = 0$ along the boundary.

Three different BEM meshes are used. Mesh A has 20 boundary elements and 25 cells, Mesh B has 28 boundary elements and 49 cells, Mesh C has 36 quadratic boundary elements and 81 constant cells.

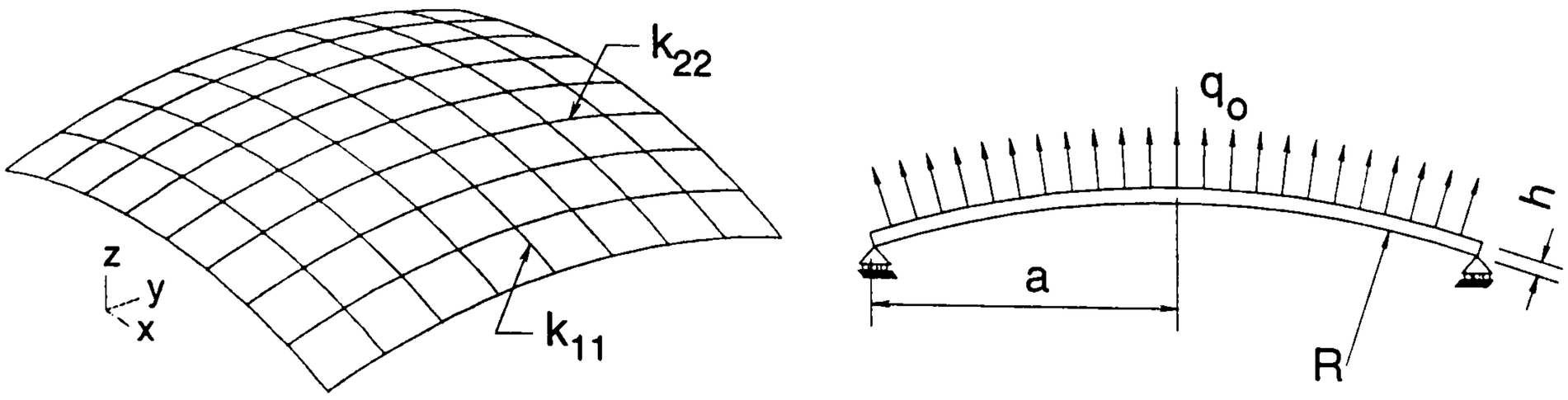

Figure 3-18: Simply supported square shallow shell: uniformly loaded.

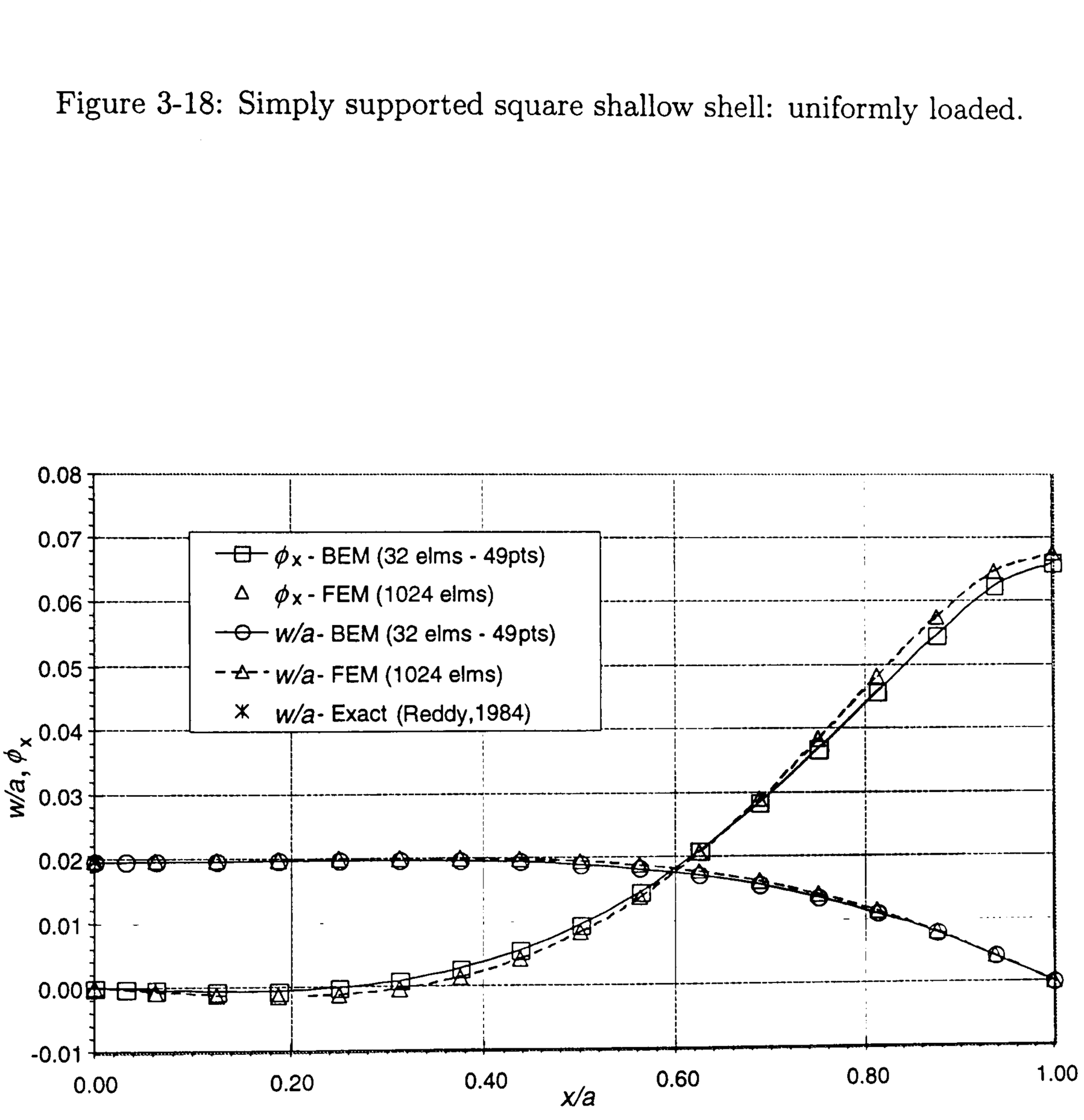

Figure 3-19: Dispacements along x_1- axis for the simply supported shallow spherical shell.

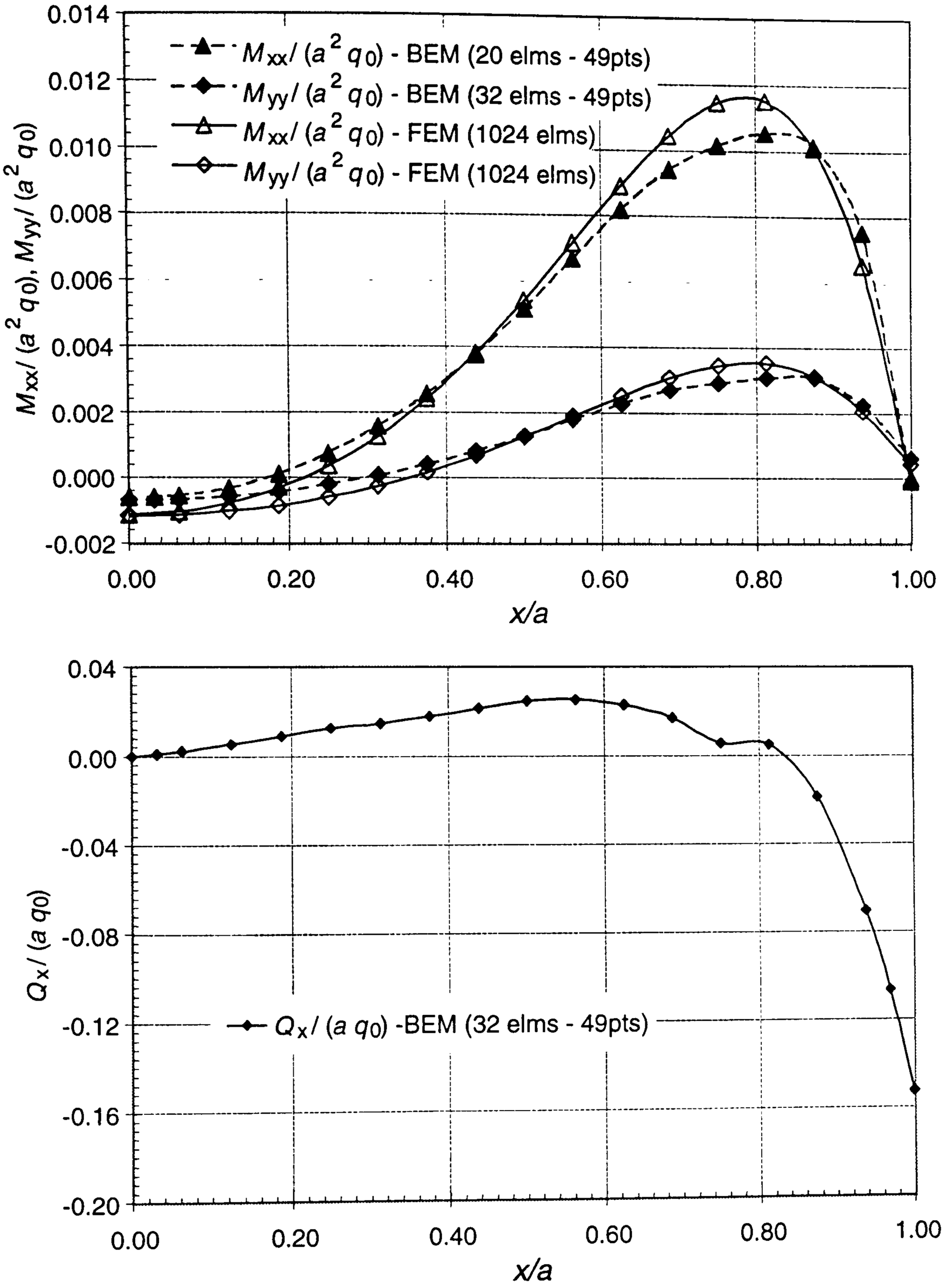

Figure 3-20: Stress resultants along x_1- axis for the simply supported shallow spherical shell.

Table 3.5: Normalised deflection w/a (at $x = 0, y = 0$) of a simply supported square spherical shell: uniformly loaded ($w/a \times 10^3$).

h/a	0.0200	0.1000	0.2000	0.4000
BEM (20 elms-25 cells)	19.1731	2.9896	0.6816	0.1180
BEM (28 elms-49 cells)	19.3988	3.0320	0.6860	0.1183
BEM (36 elms-81 cells)	19.4850	3.0502	0.6879	0.1184
BEM (20 elms-25 points)	19.4331	3.0224	0.6893	0.1213
BEM (20 elms-49 points)	19.4569	3.0491	0.6924	0.1216
BEM (32 elms-49 points)	19.5850	3.0528	0.6926	0.1216
Exact - SDT (Reddy [105])	19.6163	3.1059	0.7041	0.1235
Exact - CT (Reddy [105])	19.6206	3.0952	0.6795	0.1042

SDT= Shear deformable theory; CT= Classical theory

This example is also analysed using the dual reciprocity technique. Three different BEM meshes are used. Mesh D has 20 boundary elements and 25 domain points, Mesh E has 20 boundary elements and 49 domain points and Mesh F has 32 boundary elements and 49 domain points.

Table 3.5 and Figure 3-20 show the results of this example. All the results from the BEM meshes show good agreement with exact solutions [105] and an FEM model with 1024 elements. Comparison of shear deformation theory and classical theory shows that the effect of shear deformation is significant for h/a bigger than 0.2. The differences between classical theory to shear deformation theory are 0.35% for $h/a = 0.1$; 3.6% for $h/a = 0.2$ and 18.6% for $h/a = 0.4$. It can be seen that using the present formulation convergence can be achieved with only small number of elements and cells or domain points.

3.9.4 Simply supported square shallow cylindrical shell: uniformly loaded

In this example, a square shallow cylindrical shell as shown in Figure 3-21 is analysed. The properties of the shell is the same as in the previous example except $h/a = 0.02$ and the curvature $ak_{11} = 1/6$; $ak_{22} = 0$.

Three different BEM meshes are used. Mesh A has 20 boundary elements and 25 cells, Mesh B has 28 boundary elements and 49 cells, Mesh C has 36 quadratic

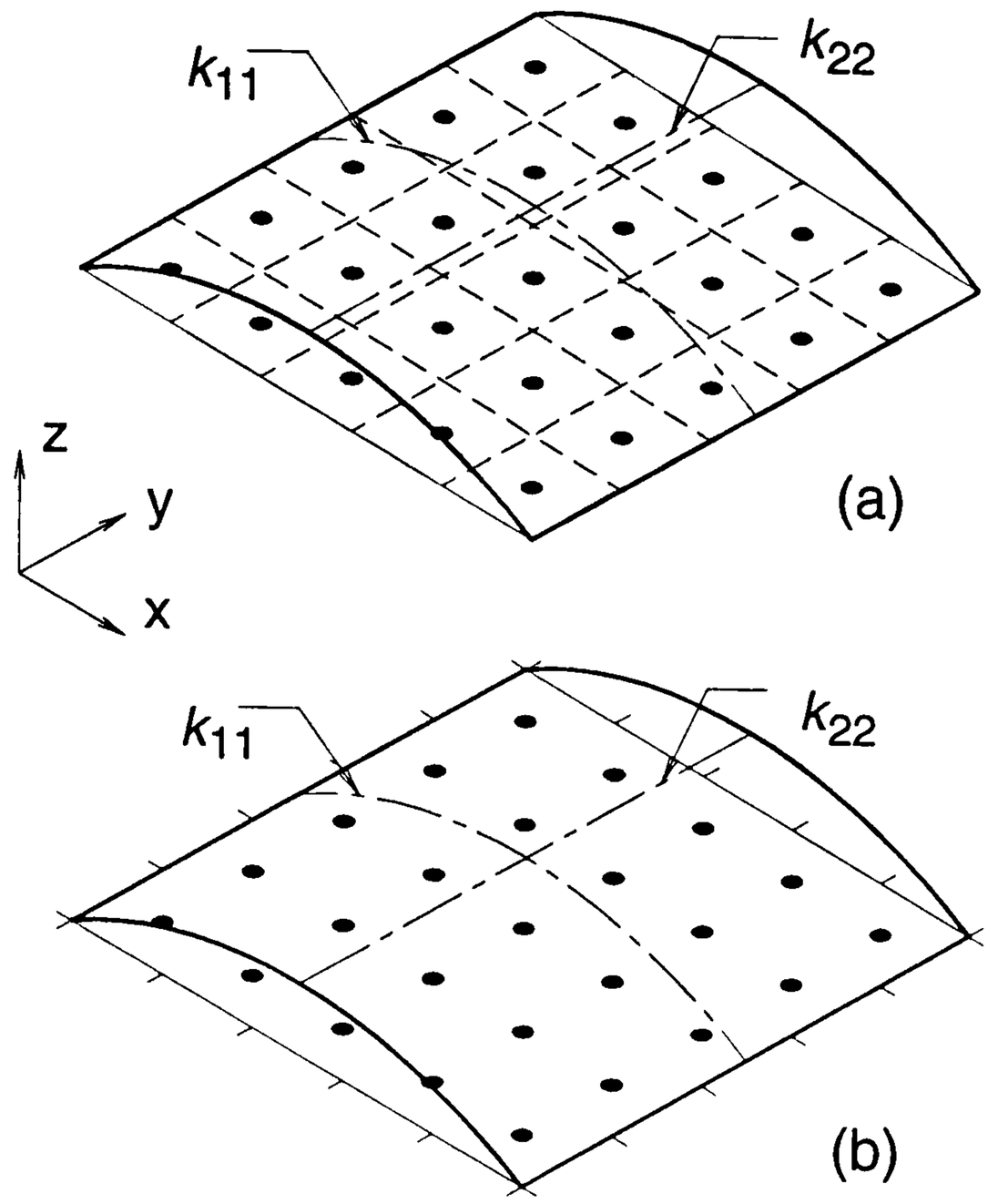

Figure 3-21: BEM model of a square shallow cylindrical shell: (a) cell discretization; (b) dual reciprocity technique.

boundary elements and 81 constant cells. For comparison four FEM meshes are also used, Mesh D has 256 linear shell elements, Mesh E has 576 elements, Mesh F has 1024 elements, Mesh G has 1600 elements.

This example is also analysed using the dual reciprocity technique. Four different meshes are being used. Mesh H has 20 boundary elements and 25 domain points, Mesh J has 20 boundary elements and 49 domain points, Mesh K has 32 boundary elements and 81 domain points and Mesh L has 32 boundary elements and 121 domain points.

Table 3.6 presents the results of this example. As it can be seen, the BEM results are in good agreement with each other and the FEM results.

Generally, computer time taken to solve the problems using the dual reciprocity technique are about three to four times longer compare to the solution time using

Table 3.6: Deflection w/a (at $x = 0, y = 0$) of a simply supported square cylindrical shell: uniformly loaded.

	w
BEM (20 elms - 5×5 cells)	0.176074
BEM (28 elms - 7×7 cells)	0.182253
BEM (36 elms - 9×9 cells)	0.184099
BEM (20 elms - 5×5 points)	0.159019
BEM (20 elms - 7×7 points)	0.170458
BEM (32 elms - 9×9 points)	0.177511
BEM (32 elms - 11×11 points)	0.179903
FEM (16×16 elms)	0.168244
FEM (24×24 elms)	0.173103
FEM (32×32 elms)	0.175734
FEM (40×40 elms)	0.177395

cell discretisation for models with the same number of boundary elements as well as same number of cells and domain points, but with the ability of computer processors today, the solution times for all above examples are less than 2 minutes on Pentium III 650 Mhz, 256 MB RAM, therefore solution time is not an issue any more. The more important issue is the time spent on data preparation.

3.9.5 Rectangular plate with a rectangular opening

An example for a flat plate is presented here. In this example, a rectangular plate with a rectangular opening as shown in Figure 3-22 is considered. The plate is clamped on two sides and hinged on two other sides. The plate thickness is 0.16 m and the material properties are $E = 3 \times 10^7\ kN/m^2$ and $\nu = 0.2$. A uniform load of 10 kN/m^2 is considered as the applied load. A mesh of 46 boundary elements was used for the boundary element analysis, 8 and 5 elements for longer and shorter sides of the outer boundary respectively and 6 and 4 elements for longer and shorter sides of the opening respectively.

Figures 3-23 – 3-26 show the out-of-plane displacement and bending moments along the lines $A - A$ and $B - B$. The results are plotted together with the results of the boundary elements based on the Kirchhoff plate theory and finite element analysis given by Hartmann [59]. The results show, bending moments and deflections

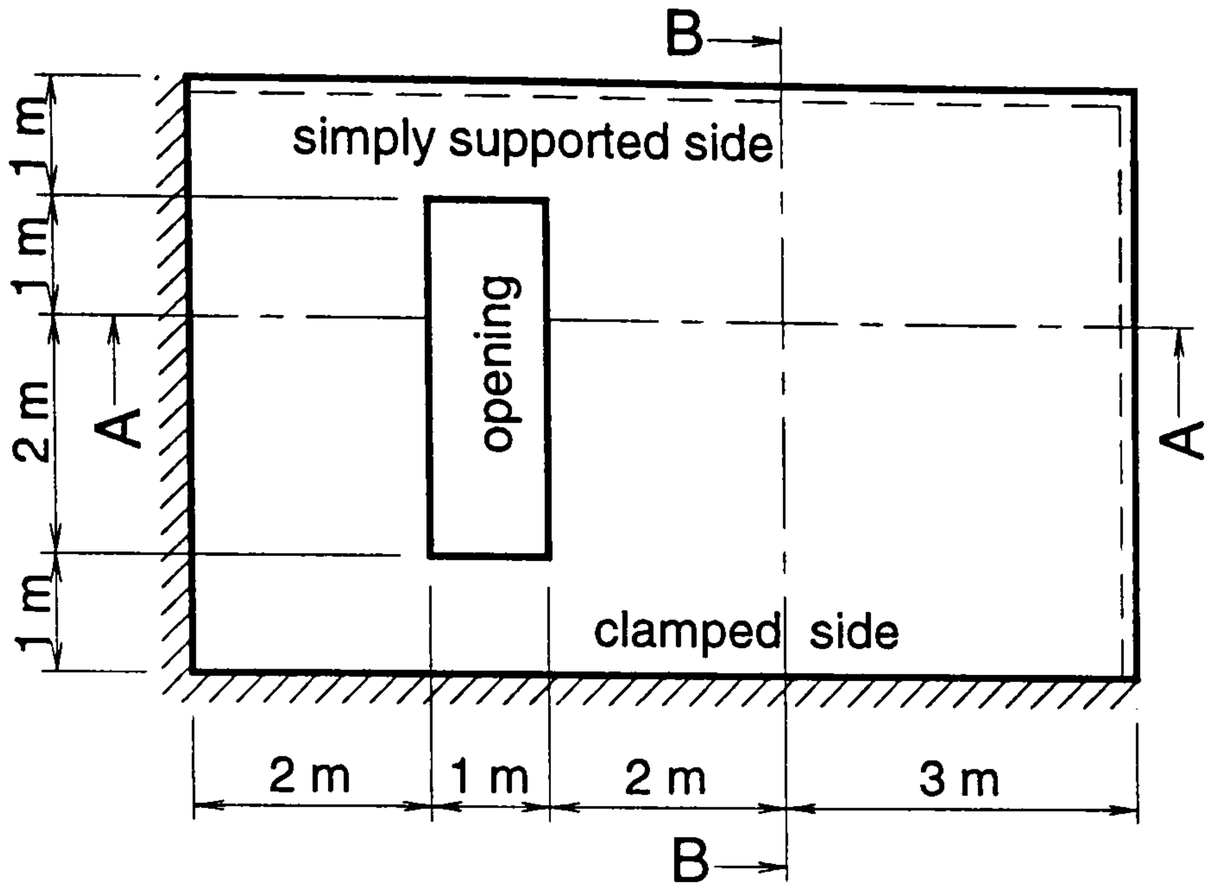

Figure 3-22: Rectangular plate with rectangular opening.

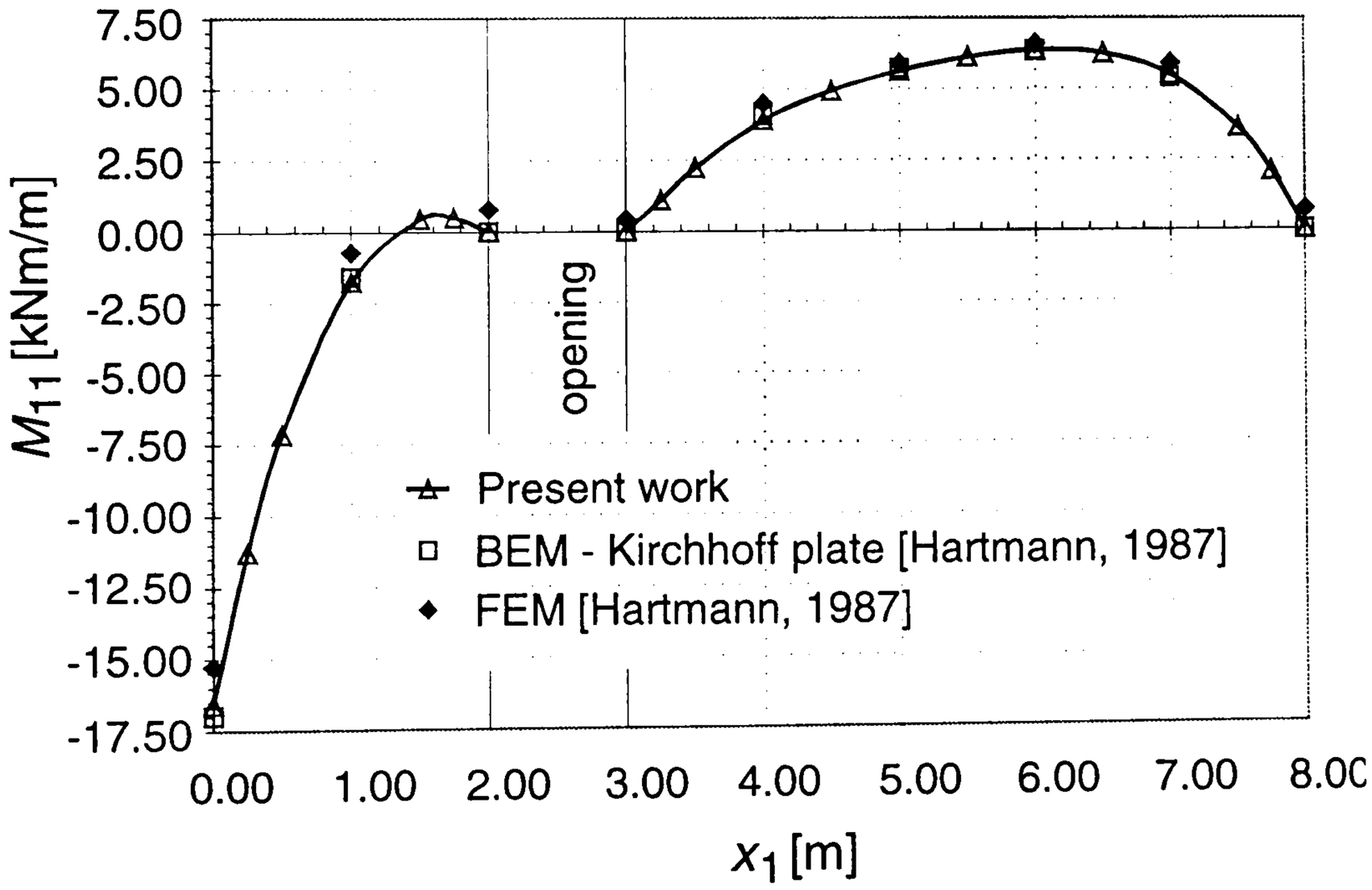

Figure 3-23: Bending stress resultant M_{11} along cross section A−A.

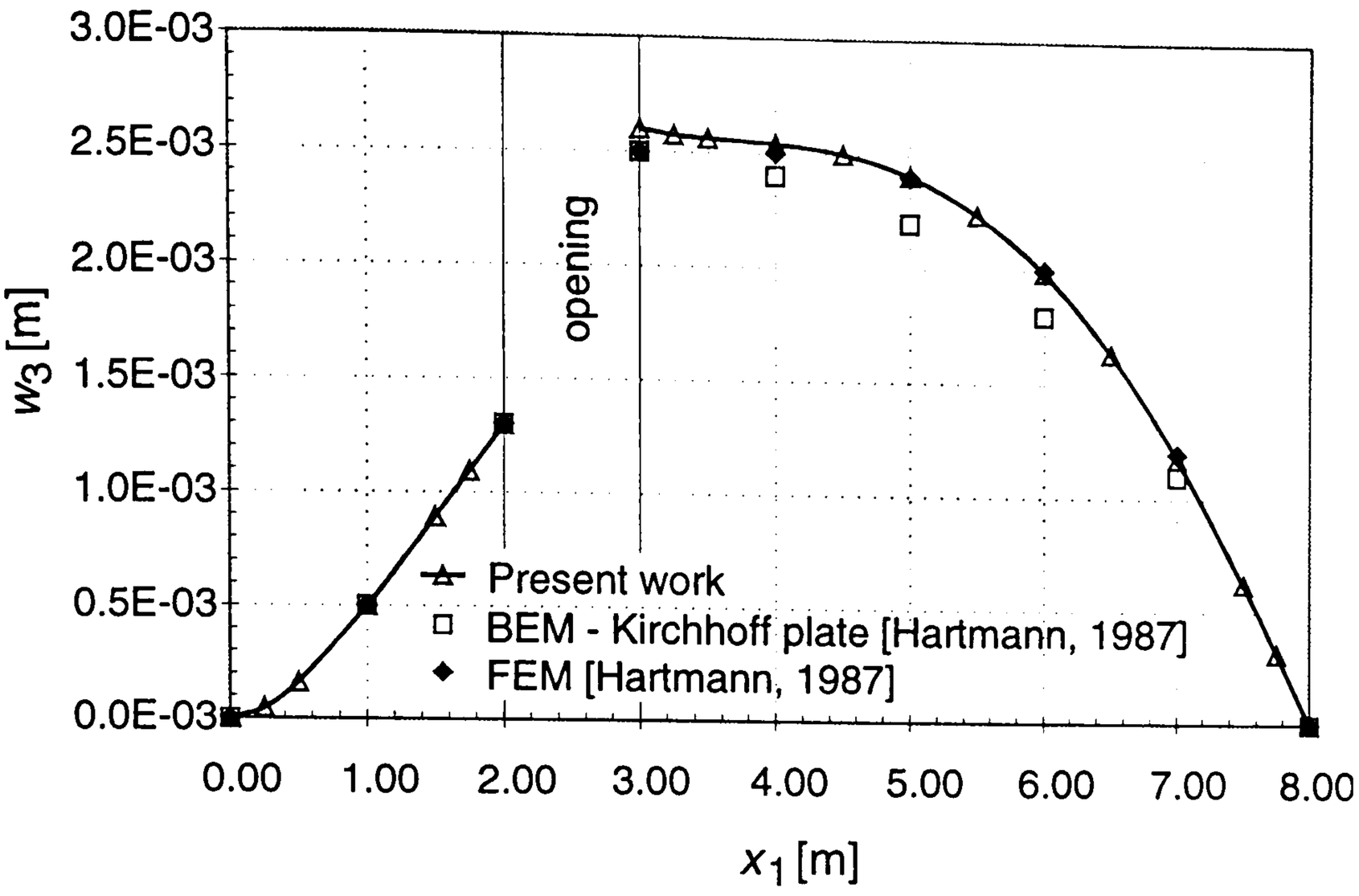

Figure 3-24: Out-of-plane displacement w_3 along cross section A−A.

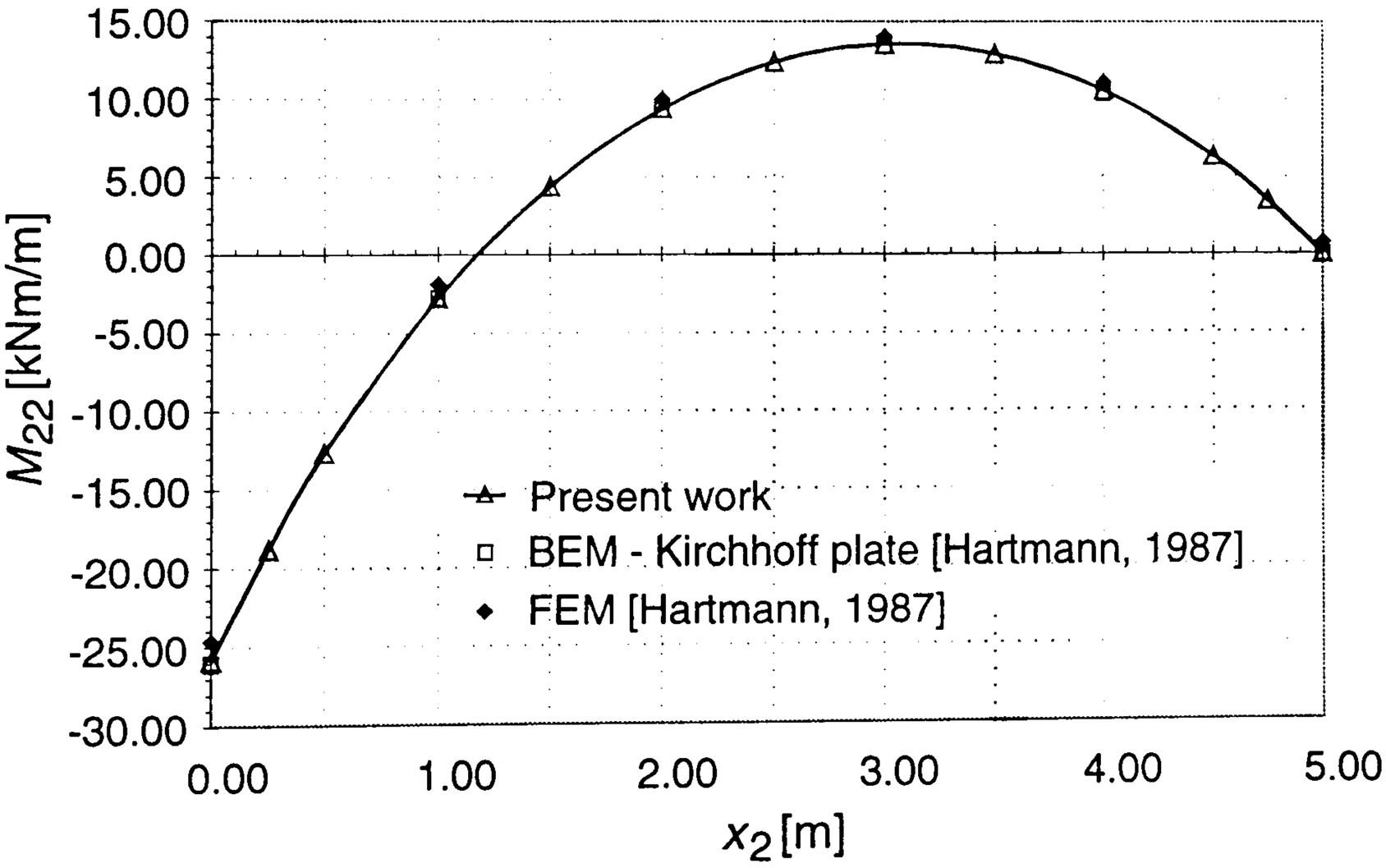

Figure 3-25: Bending stress resultant M_{22} along cross section B−B.

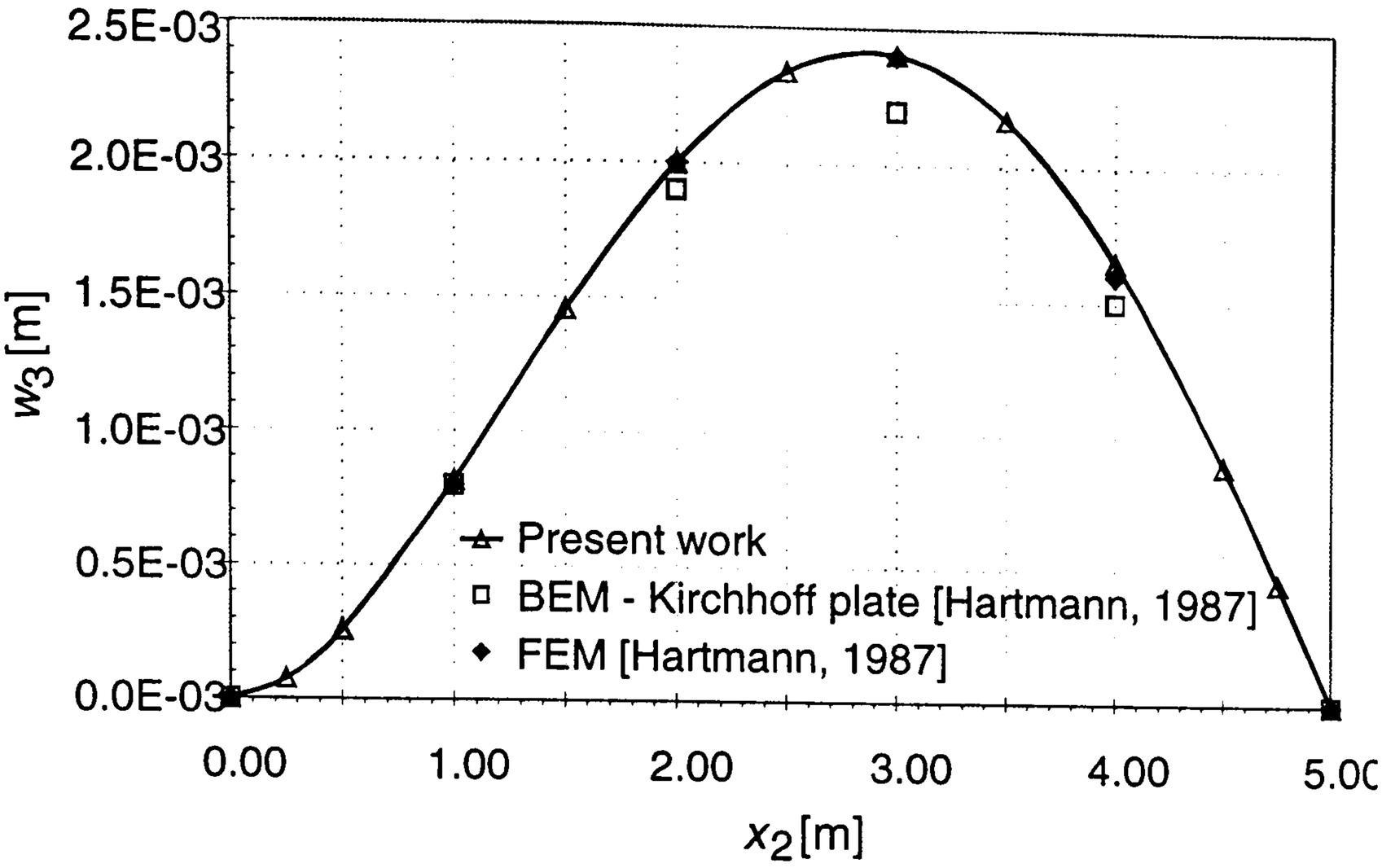

Figure 3-26: Out-of-plane displacement w_3 along cross section B−B.

are nearly the same in the three models.

3.10 Summary

Boundary element formulation for the shear deformable shell was presented in this chapter. The formulation was developed by coupling boundary element formulations of shear deformable plate bending and two dimensional plane stress elasticity. As a result five independent integral equations were obtained, which contained domain integrals as well as boundary integrals. The singular integrals were treated individually based on the order of singularity. The weakly singular boundary integrals were treated using the non-linear coordinate transformation, while the strongly singular integrals were computed indirectly using generalised rigid body movement. The domain integrals were treated in two different ways, firstly they were treated numerically using constant cell elements, and triangle to square transformation was used for the weakly singular domain integrals, then secondly they were transformed to the boundary using the dual reciprocity technique. Also presented in this chapter were boundary element formulations for analyses of shear deformable plate bending and two-dimensional plane stress.

Several numerical examples were presented to test the ability of the proposed method to solve shallow shell problems with various geometry, loading (internal pressure and boundary force) and boundary condition (clamped, simply supported and free edge). It was shown that the proposed method yields accurate results for comparatively few elements.

In the next chapter, derivation of hypersingular boundary integral equations for shear deformable shallow shell will be presented.

Chapter 4

Hypersingular Integral Equations

4.1 Introduction

Since late 1980s, the stress based boundary integral equations, or the hypersingular integral equations have been developed by several researchers. The main applications of these integral equations are in the dual boundary element method for modelling cracks in single domain (see for example, Portela *et al.* [100] for 2-D, and Mi and Aliabadi [83] for 3-D crack problems) and the direct evaluation of the boundary stress tensor (see for example, Huber *et al.* [64], and Wilde and Aliabadi [143]).

Recently, derivation of the hypersingular integral equations for Reissner plates have been reported independently by Rashed, Aliabadi and Brebbia [103] and Ahmadi-Brooghani and Wearing [5]. Rashed *et al.* [103] presented the complete derivation of the hypersingular equations and demonstrated procedures for treating the hypersingular integrals for general boundaries. Ahmadi-Brooghani and Wearing [5] used the hypersingular formulation in the context of the dual boundary element method for the solution of crack problems. Later, the hypersingular integral equations for shear deformable shallow shell have been derived by Dirgantara and Aliabadi [42].

This chapter presents the derivation of traction integral equations (hypersingular integral equations) for shear deformable shallow shells. Strongly singular and hypersingular integrals are treated using a singularity subtraction method based on

the Taylor series expansion. Also presented are traction integral equations of shear deformable plates bending and two-dimensional plane stress. These integral equations together with displacement integral equations are employed in the next chapter to form the dual boundary element formulation for fracture mechanics analyses of shear deformable shell and plate loaded by a combination of bending and tension.

4.2 Hypersingular Integral Equations for Shear Deformable Shallow Shells

The stress resultant boundary integral equations are formed by considering the behaviour of equations (3.92 – 3.94) as $\mathbf{X}'$ approaches $\mathbf{x}'$ on boundary Γ. A semi-circular domain with boundary Γ_ε^* is constructed around the point $\mathbf{x}'$ as shown in Figure 3-4. Taking the limit as $\mathbf{X}' \to \mathbf{x}'$, equations (3.92 – 3.94) can be rewritten as follows:

$$M_{\alpha\beta}\left(\mathbf{x}'\right) + \lim_{\varepsilon\to 0}\int_{\Gamma-\Gamma_\varepsilon+\Gamma_\varepsilon^*} P^*_{\alpha\beta\gamma}(\mathbf{x}',\mathbf{x})w_\gamma(\mathbf{x})d\Gamma(\mathbf{x})$$

$$+\lim_{\varepsilon\to 0}\int_{\Gamma-\Gamma_\varepsilon+\Gamma_\varepsilon^*} P^*_{\alpha\beta 3}(\mathbf{x}',\mathbf{x})w_3(\mathbf{x})d\Gamma(\mathbf{x})$$

$$= \lim_{\varepsilon\to 0}\int_{\Gamma-\Gamma_\varepsilon+\Gamma_\varepsilon^*} W^*_{\alpha\beta\gamma}(\mathbf{x}',\mathbf{x})p_\gamma(\mathbf{x})d\Gamma(\mathbf{x}) + \lim_{\varepsilon\to 0}\int_{\Gamma-\Gamma_\varepsilon+\Gamma_\varepsilon^*} W^*_{\alpha\beta 3}(\mathbf{x}',\mathbf{x})p_3(\mathbf{x})d\Gamma(\mathbf{x})$$

$$+\lim_{\varepsilon\to 0}\int_{\Omega} W^*_{\alpha\beta 3}(\mathbf{X}',\mathbf{X})q^*_3 d\Omega(\mathbf{X})\ ; \tag{4.1}$$

$$Q_\beta\left(\mathbf{x}'\right) + \lim_{\varepsilon\to 0}\int_{\Gamma-\Gamma_\varepsilon+\Gamma_\varepsilon^*} P^*_{3\beta\gamma}(\mathbf{x}',\mathbf{x})w_\gamma(\mathbf{x})d\Gamma(\mathbf{x})$$

$$+\lim_{\varepsilon\to 0}\int_{\Gamma-\Gamma_\varepsilon+\Gamma_\varepsilon^*} P^*_{3\beta 3}(\mathbf{x}',\mathbf{x})w_3(\mathbf{x})d\Gamma(\mathbf{x})$$

$$= \lim_{\varepsilon\to 0}\int_{\Gamma-\Gamma_\varepsilon+\Gamma_\varepsilon^*} W^*_{3\beta\gamma}(\mathbf{x}',\mathbf{x})p_\gamma(\mathbf{x})d\Gamma(\mathbf{x}) + \lim_{\varepsilon\to 0}\int_{\Gamma-\Gamma_\varepsilon+\Gamma_\varepsilon^*} W^*_{3\beta 3}(\mathbf{x}',\mathbf{x})p_3(\mathbf{x})d\Gamma(\mathbf{x})$$

$$+\lim_{\varepsilon\to 0}\int_{\Omega} W^*_{3\beta 3}(\mathbf{X}',\mathbf{X})q^*_3 d\Omega(\mathbf{X}) \tag{4.2}$$

and

$$N_{\alpha\beta}\left(\mathbf{x}'\right) + \lim_{\varepsilon\to 0}\int_{\Gamma-\Gamma_\varepsilon+\Gamma_\varepsilon^*} T^{(i)*}_{\alpha\beta\gamma}(\mathbf{x}',\mathbf{x})u_\gamma(\mathbf{x})d\Gamma(\mathbf{x})$$

$$= \lim_{\varepsilon \to 0} \int_{\Gamma - \Gamma_\varepsilon + \Gamma_\varepsilon^*} U^*_{\alpha\beta\gamma}(\mathbf{x}', \mathbf{x}) t_\gamma(\mathbf{x}) d\Gamma(\mathbf{x})$$

$$- \lim_{\varepsilon \to 0} \int_{\Gamma - \Gamma_\varepsilon + \Gamma_\varepsilon^*} U^*_{\alpha\beta\gamma}(\mathbf{X}', \mathbf{x}) B \left[k_{\alpha\gamma} (1 - \nu) + \nu \delta_{\alpha\gamma} k_{\phi\phi} \right] w_3(\mathbf{x}) n_\gamma(\mathbf{x}) d\Gamma(\mathbf{x})$$

$$+ \lim_{\varepsilon \to 0} \int_\Omega U^*_{\alpha\beta\gamma}(\mathbf{X}', \mathbf{X}) q^*_\gamma d\Omega(\mathbf{X}) + B \left[(1 - \nu) k_{\alpha\beta} + \nu \delta_{\alpha\beta} k_{\phi\phi} \right] w_3 \qquad (4.3)$$

Equations (4.1) and (4.2) represent the bending and shear stress resultant boundary integral equations respectively, while equations (4.3) represent the membrane stress resultant boundary integral equations at the boundary point $\mathbf{x}'$.

In the limits, the kernels exhibit different orders of singularity. The terms $P^*_{\alpha\beta\gamma}$, $P^*_{3\beta3}$ are hypersingular of $O\left(1/r^2 + \ln(r)\right)$ and $T^{(i)*}_{\alpha\beta\gamma}$ are hypersingular of $O\left(1/r^2\right)$, while $P^*_{\alpha\beta3}$, $P^*_{3\beta\gamma}$, $W^*_{\alpha\beta\gamma}$, $W^*_{3\beta3}$, $Q^*_{\alpha\beta}$, and $U^*_{\alpha\beta\gamma}$ are strongly singular of $O\left(1/r\right)$. Other remaining terms, namely $W^*_{\alpha\beta3}, W^*_{3\beta\gamma}$ and $Q^*_{3\beta}$ are weakly singular.

The generalised displacements w_i and u_α are required to be $C^{1,\alpha}$, $(0 < \alpha < 1)$, and the generalised tractions p_i and t_α are required to be $C^{0,\alpha}$, $(0 < \alpha < 1)$, for the principal-value integrals to exist. To satisfy those continuity requirements, the point $\mathbf{x}'$ is assumed to be on a smooth boundary. The evaluation of the integrals in equations (4.1) and (4.3) is reported in the Appendix B. In the limiting processes, some integrals in equations (4.1) and (4.3) lead to a jump on the stress resultants. Taking into account all the limits and the jump terms, as $\varepsilon \to 0$, for a source point on a smooth boundary, stress resultant integral equations are obtained as follows :

$$\frac{1}{2} M_{\alpha\beta}(\mathbf{x}') + \oint_\Gamma P^*_{\alpha\beta\gamma}(\mathbf{x}', \mathbf{x}) w_\gamma(\mathbf{x}) d\Gamma(\mathbf{x}) + \oint_\Gamma P^*_{\alpha\beta3}(\mathbf{x}', \mathbf{x}) w_3(\mathbf{x}) d\Gamma(\mathbf{x})$$

$$= \oint_\Gamma W^*_{\alpha\beta\gamma}(\mathbf{x}', \mathbf{x}) p_\gamma(\mathbf{x}) d\Gamma(\mathbf{x}) + \int_\Gamma W^*_{\alpha\beta3}(\mathbf{x}', \mathbf{x}) p_3(\mathbf{x}) d\Gamma(\mathbf{x})$$

$$+ \int_\Omega W^*_{\alpha\beta3}(\mathbf{x}', \mathbf{X}) q^*_3 d\Omega(\mathbf{X}); \qquad (4.4)$$

$$\frac{1}{2} Q_\beta(\mathbf{x}') + \oint_\Gamma P^*_{3\beta\gamma}(\mathbf{x}', \mathbf{x}) w_\gamma(\mathbf{x}) d\Gamma(\mathbf{x}) + \oint_\Gamma P^*_{3\beta3}(\mathbf{x}', \mathbf{x}) w_3(\mathbf{x}) d\Gamma(\mathbf{x})$$

$$= \int_\Gamma W^*_{3\beta\gamma}(\mathbf{x}', \mathbf{x}) p_\gamma(\mathbf{x}) d\Gamma(\mathbf{x}) + \oint_\Gamma W^*_{3\beta3}(\mathbf{x}', \mathbf{x}) p_3(\mathbf{x}) d\Gamma(\mathbf{x})$$

$$+ \int_\Omega W^*_{3\beta3}(\mathbf{x}', \mathbf{X}) q^*_3 d\Omega(\mathbf{X}) \qquad (4.5)$$

and

$$\frac{1}{2}N_{\alpha\beta}(\mathbf{x}')+ \neq\!\!\!\!\!\!\int_{\Gamma} T^{(i)*}_{\alpha\beta\gamma}(\mathbf{x}',\mathbf{x})u_{\gamma}(\mathbf{x})d\Gamma(\mathbf{x})$$

$$+\int_{\Gamma} U^{*}_{\alpha\beta\gamma}(\mathbf{X}',\mathbf{x})B\left[k_{\alpha\gamma}\left(1-\nu\right)+\nu\delta_{\alpha\gamma}k_{\phi\phi}\right]w_3(\mathbf{x})n_{\gamma}(\mathbf{x})d\Gamma(\mathbf{x})$$

$$=\int_{\Gamma} U^{*}_{\alpha\beta\gamma}(\mathbf{x}',\mathbf{x})t_{\gamma}(\mathbf{x})d\Gamma(\mathbf{x})+\int_{\Omega} U^{*}_{\alpha\beta\gamma}(\mathbf{x}',\mathbf{X})q^{*}_{\gamma}d\Omega(\mathbf{X})$$

$$+\frac{1}{2}B\left[(1-\nu)k_{\alpha\beta}+\nu\delta_{\alpha\beta}k_{\phi\phi}\right]w_3(\mathbf{x}') \tag{4.6}$$

where $\neq\!\!\!\!\int$ denotes the Hadamard principal value integral [57].

Equations (4.4), (4.5) and (4.6) represent five stress resultant integral equations for boundary point $\mathbf{x}'$ on a smooth boundary Γ.

4.3 The Traction Integral Equations

Multiplying equations (4.4), (4.5) and (4.6) by the outward normal n_{β} at the source point $\mathbf{x}'$, and substituting equations (3.6 – 3.8) for q^{*}_{i}, the following integral equations are obtained:

$$\frac{1}{2}p_{\alpha}\left(\mathbf{x}'\right)+n_{\beta}(\mathbf{x}')\neq\!\!\!\!\!\!\int_{\Gamma} P^{*}_{\alpha\beta\gamma}(\mathbf{x}',\mathbf{x})w_{\gamma}(\mathbf{x})d\Gamma(\mathbf{x})+n_{\beta}(\mathbf{x}')\neq\!\!\!\!\!\!\int_{\Gamma} P^{*}_{\alpha\beta3}(\mathbf{x}',\mathbf{x})w_3(\mathbf{x})d\Gamma(\mathbf{x})$$

$$=n_{\beta}(\mathbf{x}')\neq\!\!\!\!\!\!\int_{\Gamma} W^{*}_{\alpha\beta\gamma}(\mathbf{x}',\mathbf{x})p_{\gamma}(\mathbf{x})d\Gamma(\mathbf{x})+n_{\beta}(\mathbf{x}')\int_{\Gamma} W^{*}_{\alpha\beta3}(\mathbf{x}',\mathbf{x})p_3(\mathbf{x})d\Gamma(\mathbf{x})$$

$$-n_{\beta}(\mathbf{x}')\int_{\Omega} k_{\theta\psi}B\frac{1-\nu}{2}\left(u_{\theta,\psi}\left(\mathbf{X}\right)+u_{\psi,\theta}\left(\mathbf{X}\right)+\frac{2\nu}{1-\nu}u_{\phi,\phi}\left(\mathbf{X}\right)\delta_{\theta\psi}\right)W^{*}_{\alpha\beta3}(\mathbf{x}',\mathbf{X})d\Omega(\mathbf{X})$$

$$-n_{\beta}(\mathbf{x}')\int_{\Omega} k_{\theta\psi}B\left((1-\nu)k_{\theta\psi}+\nu\delta_{\theta\psi}k_{\phi\phi}\right)w_3\left(\mathbf{X}\right)W^{*}_{\alpha\beta3}(\mathbf{x}',\mathbf{X})d\Omega(\mathbf{X})$$

$$+n_{\beta}(\mathbf{x}')\int_{\Omega} W^{*}_{\alpha\beta3}(\mathbf{x}',\mathbf{X})q_3d\Omega(\mathbf{X}) \tag{4.7}$$

$$\frac{1}{2}p_3\left(\mathbf{x}'\right)+n_{\beta}(\mathbf{x}')\neq\!\!\!\!\!\!\int_{\Gamma} P^{*}_{3\beta\gamma}(\mathbf{x}',\mathbf{x})w_{\gamma}(\mathbf{x})d\Gamma(\mathbf{x})+n_{\beta}(\mathbf{x}')\neq\!\!\!\!\!\!\int_{\Gamma} P^{*}_{3\beta3}(\mathbf{x}',\mathbf{x})w_3(\mathbf{x})d\Gamma(\mathbf{x})$$

$$=n_{\beta}(\mathbf{x}')\int_{\Gamma} W^{*}_{3\beta\gamma}(\mathbf{x}',\mathbf{x})p_{\gamma}(\mathbf{x})d\Gamma(\mathbf{x})+n_{\beta}(\mathbf{x}')\neq\!\!\!\!\!\!\int_{\Gamma} W^{*}_{3\beta3}(\mathbf{x}',\mathbf{x})p_3(\mathbf{x})d\Gamma(\mathbf{x})$$

$$-n_{\beta}(\mathbf{x}')\int_{\Omega} k_{\theta\psi}B\frac{1-\nu}{2}\left(u_{\theta,\psi}\left(\mathbf{X}\right)+u_{\psi,\theta}\left(\mathbf{X}\right)+\frac{2\nu}{1-\nu}u_{\phi,\phi}\left(\mathbf{X}\right)\delta_{\theta\psi}\right)W^{*}_{3\beta3}(\mathbf{x}',\mathbf{X})d\Omega(\mathbf{X})$$

$$-n_\beta(\mathbf{x}')\int_\Omega k_{\theta\psi}B\left((1-\nu)k_{\theta\psi}+\nu\delta_{\theta\psi}k_{\phi\phi}\right)w_3\left(\mathbf{X}\right)W^*_{3\beta 3}(\mathbf{x}',\mathbf{X})d\Omega(\mathbf{X})$$

$$+n_\beta(\mathbf{x}')\int_\Omega W^*_{3\beta 3}(\mathbf{x}',\mathbf{X})q_3 d\Omega(\mathbf{X}) \tag{4.8}$$

and

$$\frac{1}{2}t_\alpha\left(\mathbf{x}'\right)+n_\beta(\mathbf{x}')\neq\!\!\!\!\!\!\int_\Gamma T^{(i)*}_{\alpha\beta\gamma}(\mathbf{x}',\mathbf{x})u_\gamma(\mathbf{x})d\Gamma(\mathbf{x})+$$

$$n_\beta(\mathbf{x}')\neq\!\!\!\!\!\!\int_\Gamma U^*_{\alpha\beta\gamma}(\mathbf{x}',\mathbf{x})B\left[k_{\theta\psi}\left(1-\nu\right)+\nu\delta_{\theta\psi}k_{\phi\phi}\right]w_3(\mathbf{x})n_\psi(\mathbf{x})d\Gamma(\mathbf{x})$$

$$-n_\beta(\mathbf{x}')\int_\Omega U^*_{\alpha\beta\gamma}(\mathbf{x}',\mathbf{X})B\left[k_{\theta\psi}\left(1-\nu\right)+\nu\delta_{\theta\psi}k_{\phi\phi}\right]w_{3,\beta}(\mathbf{X})d\Omega(\mathbf{X})$$

$$=n_\beta(\mathbf{x}')\neq\!\!\!\!\!\!\int_\Gamma U^*_{\alpha\beta\gamma}(\mathbf{x}',\mathbf{x})t_\gamma(\mathbf{x})d\Gamma(\mathbf{x})+n_\beta(\mathbf{x}')\int_\Omega U^*_{\alpha\beta\gamma}(\mathbf{x}',\mathbf{X})q_\gamma d\Omega(\mathbf{X})$$

$$+\frac{1}{2}n_\beta(\mathbf{x}')B\left[(1-\nu)k_{\theta\psi}+\nu\delta_{\theta\psi}k_{\phi\phi}\right]w_3(\mathbf{x}') \tag{4.9}$$

Equations (4.7 – 4.9) represent five integral equations in terms of boundary tractions, and can be used together with the five displacement integral equations in equations (3.56 – 3.57) to form the dual boundary integral formulation as described in chapter 5.

4.4 Evaluation of Domain Integrals Using the Dual Reciprocity Technique

Domain integrals in the hypersingular integral equations can be transformed to boundary integrals using the dual reciprocity technique results of the displacement boundary integral equations. To evaluate internal stress resultants using integral equations (4.7 – 4.9) there are six domain integrals as follows:

$$n_\beta(\mathbf{x}')I^D_7=n_\beta(\mathbf{x}')\int_\Omega W^*_{i\beta 3}w_3 d\Omega,\qquad n_\beta(\mathbf{x}')I^D_8=n_\beta(\mathbf{x}')\int_\Omega W^*_{i\beta 3}\frac{\partial u_1}{\partial x_1}d\Omega,$$

$$n_\beta(\mathbf{x}')I^D_9=n_\beta(\mathbf{x}')\int_\Omega W^*_{i\beta 3}\frac{\partial u_2}{\partial x_2}d\Omega,\qquad n_\beta(\mathbf{x}')I^D_{10}=n_\beta(\mathbf{x}')\int_\Omega W^*_{i\beta 3}q_3 d\Omega,$$

$$n_\beta(\mathbf{x}')I^D_{11}=n_\beta(\mathbf{x}')\int_\Omega U^*_{\alpha\beta 1}\frac{\partial w_3}{\partial x_1}d\Omega,\qquad n_\beta(\mathbf{x}')I^D_{12}=n_\beta(\mathbf{x}')\int_\Omega U^*_{\alpha\beta 2}\frac{\partial w_3}{\partial x_2}d\Omega \tag{4.10}$$

Using the same particular solutions $\hat{w}^3_{mk}$ and $\hat{p}^3_{mk}$ as in displacement integral

equations, the stress resultant integral equations for plate bending problems can be written as

$$\frac{1}{2}\hat{M}^3_{m\alpha\beta}(\mathbf{x}') + \neq\!\!\!\!\int_\Gamma P^*_{\alpha\beta\gamma}(\mathbf{x}',\mathbf{x})\hat{w}^3_{m\gamma}(\mathbf{x})d\Gamma(\mathbf{x}) + \int_\Gamma P^*_{\alpha\beta 3}(\mathbf{x}',\mathbf{x})\hat{w}^3_{m3}(\mathbf{x})d\Gamma(\mathbf{x})$$

$$= \int_\Gamma W^*_{\alpha\beta\gamma}(\mathbf{x}',\mathbf{x})\hat{p}^3_{m\gamma}(\mathbf{x})d\Gamma(\mathbf{x}) + \int_\Gamma W^*_{\alpha\beta 3}(\mathbf{x}',\mathbf{x})\hat{p}^3_{m3}(\mathbf{x})d\Gamma(\mathbf{x})$$

$$+ \int_\Omega W^*_{\alpha\beta 3}(\mathbf{x}',\mathbf{X})F_m(r)\,d\Omega(\mathbf{X}) \tag{4.11}$$

and

$$\frac{1}{2}\hat{Q}^3_{m\beta}(\mathbf{x}') + \int_\Gamma P^*_{3\beta\gamma}(\mathbf{x}',\mathbf{x})\hat{w}^3_{m\gamma}(\mathbf{x})d\Gamma(\mathbf{x}) + \neq\!\!\!\!\int_\Gamma P^*_{3\beta 3}(\mathbf{x}',\mathbf{x})\hat{w}^3_{m3}(\mathbf{x})d\Gamma(\mathbf{x})$$

$$= \int_\Gamma W^*_{3\beta\gamma}(\mathbf{x}',\mathbf{x})\hat{p}^3_{m\gamma}(\mathbf{x})d\Gamma(\mathbf{x}) + \int_\Gamma W^*_{3\beta 3}(\mathbf{x}',\mathbf{x})\hat{p}^3_{m3}(\mathbf{x})d\Gamma(\mathbf{x})$$

$$+ \int_\Omega W^*_{3\beta 3}(\mathbf{x}',\mathbf{X})F_m(r)\,d\Omega(\mathbf{X}) \tag{4.12}$$

which implies that

$$n_\beta(\mathbf{x}')I^D_7 = n_\beta(\mathbf{x}')\left\{\sum_{m=1}^{M}\left[\frac{1}{2}\hat{M}^3_{m\alpha\beta}(\mathbf{x}') + \neq\!\!\!\!\int_\Gamma P^*_{\alpha\beta\gamma}(\mathbf{x}',\mathbf{x})\hat{w}^3_{m\gamma}(\mathbf{x})d\Gamma(\mathbf{x})\right.\right.$$

$$+ \int_\Gamma P^*_{\alpha\beta 3}(\mathbf{x}',\mathbf{x})\hat{w}^3_{m3}(\mathbf{x})d\Gamma(\mathbf{x}) - \int_\Gamma W^*_{\alpha\beta\gamma}(\mathbf{x}',\mathbf{x})\hat{p}^3_{m\gamma}(\mathbf{x})d\Gamma(\mathbf{x})$$

$$\left.\left. - \int_\Gamma W^*_{\alpha\beta 3}(\mathbf{x}',\mathbf{x})\hat{p}^3_{m3}(\mathbf{x})d\Gamma(\mathbf{x})\right]\mathbf{F}^{-1}w_3\right\} \tag{4.13}$$

and

$$n_\beta(\mathbf{x}')I^D_7 = n_\beta(\mathbf{x}')\left\{\sum_{m=1}^{M}\left[\frac{1}{2}\hat{Q}^3_{m\beta}(\mathbf{x}') + \int_\Gamma P^*_{3\beta\gamma}(\mathbf{x}',\mathbf{x})\hat{w}^3_{m\gamma}(\mathbf{x})d\Gamma(\mathbf{x})\right.\right.$$

$$+ \neq\!\!\!\!\int_\Gamma P^*_{3\beta 3}(\mathbf{x}',\mathbf{x})\hat{w}^3_{m3}(\mathbf{x})d\Gamma(\mathbf{x}) - \int_\Gamma W^*_{3\beta\gamma}(\mathbf{x}',\mathbf{x})\hat{p}^3_{m\gamma}(\mathbf{x})d\Gamma(\mathbf{x})$$

$$\left.\left. - \neq\!\!\!\!\int_\Gamma W^*_{3\beta 3}(\mathbf{x}',\mathbf{x})\hat{p}^3_{m3}(\mathbf{x})d\Gamma(\mathbf{x})\right]\mathbf{F}^{-1}w_3\right\} \tag{4.14}$$

Similar to the previous procedure for the particular solutions $\hat{w}^\alpha_{mk}$ and $\hat{p}^\alpha_{mk}$, the

domain integral I_8^D

$$n_\beta(\mathbf{x}')I_8^D = n_\beta(\mathbf{x}')\left\{\sum_{m=1}^{M}\left[\frac{1}{2}\hat{M}^1_{m\alpha\beta}(\mathbf{x}')+\neq\int_\Gamma P^*_{\alpha\beta\gamma}(\mathbf{x}',\mathbf{x})\hat{w}^1_{m\gamma}(\mathbf{x})d\Gamma(\mathbf{x})\right.\right.$$

$$+\neq\int_\Gamma P^*_{\alpha\beta 3}(\mathbf{x}',\mathbf{x})\hat{w}^1_{m3}(\mathbf{x})d\Gamma(\mathbf{x})-\neq\int_\Gamma W^*_{\alpha\beta\gamma}(\mathbf{x}',\mathbf{x})\hat{p}^1_{m\gamma}(\mathbf{x})d\Gamma(\mathbf{x})$$

$$\left.\left.-\int_\Gamma W^*_{\alpha\beta 3}(\mathbf{x}',\mathbf{x})\hat{p}^1_{m3}(\mathbf{x})d\Gamma(\mathbf{x})\right]\mathbf{F}^{-1}u_1\right\} \tag{4.15}$$

and

$$n_\beta(\mathbf{x}')I_8^D = n_\beta(\mathbf{x}')\left\{\sum_{m=1}^{M}\left[\frac{1}{2}\hat{Q}^1_{m\beta}(\mathbf{x}')+\neq\int_\Gamma P^*_{3\beta\gamma}(\mathbf{x}',\mathbf{x})\hat{w}^1_{m\gamma}(\mathbf{x})d\Gamma(\mathbf{x})\right.\right.$$

$$+\neq\int_\Gamma P^*_{3\beta 3}(\mathbf{x}',\mathbf{x})\hat{w}^1_{m3}(\mathbf{x})d\Gamma(\mathbf{x})-\int_\Gamma W^*_{3\beta\gamma}(\mathbf{x}',\mathbf{x})\hat{p}^1_{m\gamma}(\mathbf{x})d\Gamma(\mathbf{x})$$

$$\left.\left.-\neq\int_\Gamma W^*_{3\beta 3}(\mathbf{x}',\mathbf{x})\hat{p}^1_{m3}(\mathbf{x})d\Gamma(\mathbf{x})\right]\mathbf{F}^{-1}u_1\right\} \tag{4.16}$$

The domain integral I_9^D

$$n_\beta(\mathbf{x}')I_9^D = n_\beta(\mathbf{x}')\left\{\sum_{m=1}^{M}\left[\frac{1}{2}\hat{M}^2_{m\alpha\beta}(\mathbf{x}')+\neq\int_\Gamma P^*_{\alpha\beta\gamma}(\mathbf{x}',\mathbf{x})\hat{w}^2_{m\gamma}(\mathbf{x})d\Gamma(\mathbf{x})\right.\right.$$

$$+\neq\int_\Gamma P^*_{\alpha\beta 3}(\mathbf{x}',\mathbf{x})\hat{w}^2_{m3}(\mathbf{x})d\Gamma(\mathbf{x})-n_\beta(\mathbf{x}')\neq\int_\Gamma W^*_{\alpha\beta\gamma}(\mathbf{x}',\mathbf{x})\hat{p}^2_{m\gamma}(\mathbf{x})d\Gamma(\mathbf{x})$$

$$\left.\left.-\int_\Gamma W^*_{\alpha\beta 3}(\mathbf{x}',\mathbf{x})\hat{p}^2_{m3}(\mathbf{x})d\Gamma(\mathbf{x})\right]\mathbf{F}^{-1}u_2\right\} \tag{4.17}$$

and

$$n_\beta(\mathbf{x}')I_9^D = n_\beta(\mathbf{x}')\left\{\sum_{m=1}^{M}\left[\frac{1}{2}\hat{Q}^2_{m\beta}(\mathbf{x}')+\neq\int_\Gamma P^*_{3\beta\gamma}(\mathbf{x}',\mathbf{x})\hat{w}^2_{m\gamma}(\mathbf{x})d\Gamma(\mathbf{x})\right.\right.$$

$$+\neq\int_\Gamma P^*_{3\beta 3}(\mathbf{x}',\mathbf{x})\hat{w}^2_{m3}(\mathbf{x})d\Gamma(\mathbf{x})-n_\beta(\mathbf{x}')\int_\Gamma W^*_{3\beta\gamma}(\mathbf{x}',\mathbf{x})\hat{p}^2_{m\gamma}(\mathbf{x})d\Gamma(\mathbf{x})$$

$$\left.\left.-\neq\int_\Gamma W^*_{3\beta 3}(\mathbf{x}',\mathbf{x})\hat{p}^2_{m3}(\mathbf{x})d\Gamma(\mathbf{x})\right]\mathbf{F}^{-1}u_2\right\} \tag{4.18}$$

Domain integral I_{10}^D can be obtained from equations (4.13 – 4.14) by replacing w_3 with q_3 to give

$$n_\beta(\mathbf{x}')I_{10}^D = n_\beta(\mathbf{x}')\left\{\sum_{m=1}^{M}\left[\frac{1}{2}\hat{M}^3_{m\alpha\beta}(\mathbf{x}')+\neq\int_\Gamma P^*_{\alpha\beta\gamma}(\mathbf{x}',\mathbf{x})\hat{w}^3_{m\gamma}(\mathbf{x})d\Gamma(\mathbf{x})\right.\right.$$

$$+ \oint_{\Gamma} P^*_{\alpha\beta 3}(\mathbf{x}', \mathbf{x}) \hat{w}^3_{m3}(\mathbf{x}) d\Gamma(\mathbf{x}) - \oint_{\Gamma} W^*_{\alpha\beta\gamma}(\mathbf{x}', \mathbf{x}) \hat{p}^3_{m\gamma}(\mathbf{x}) d\Gamma(\mathbf{x})$$

$$- \int_{\Gamma} W^*_{\alpha\beta 3}(\mathbf{x}', \mathbf{x}) \hat{p}^3_{m3}(\mathbf{x}) d\Gamma(\mathbf{x}) \Big] \mathbf{F}^{-1} q_3 \Bigg\} \tag{4.19}$$

and

$$n_\beta(\mathbf{x}') I^D_{10} = n_\beta(\mathbf{x}') \Bigg\{ \sum_{m=1}^{M} \Big[\frac{1}{2} \hat{Q}^3_{m\beta}(\mathbf{x}') + \oint_{\Gamma} P^*_{3\beta\gamma}(\mathbf{x}', \mathbf{x}) \hat{w}^3_{m\gamma}(\mathbf{x}) d\Gamma(\mathbf{x})$$

$$+ \oint_{\Gamma} P^*_{3\beta 3}(\mathbf{x}', \mathbf{x}) \hat{w}^3_{m3}(\mathbf{x}) d\Gamma(\mathbf{x}) - \int_{\Gamma} W^*_{3\beta\gamma}(\mathbf{x}', \mathbf{x}) \hat{p}^3_{m\gamma}(\mathbf{x}) d\Gamma(\mathbf{x})$$

$$- \oint_{\Gamma} W^*_{3\beta 3}(\mathbf{x}', \mathbf{x}) \hat{p}^3_{m3}(\mathbf{x}) d\Gamma(\mathbf{x}) \Big] \mathbf{F}^{-1} q_3 \Bigg\} \tag{4.20}$$

I^D_{11} can be evaluated from the particular solutions $\hat{u}^1_{m\alpha}$ and $\hat{t}^1_{m\alpha}$ for two-dimensional plane stress elasticity problem, to give

$$n_\beta(\mathbf{x}') I^D_{11} = n_\beta(\mathbf{x}') \Bigg\{ \sum_{m=1}^{M} \Big[\frac{1}{2} \hat{N}^1_{m\alpha\beta}(\mathbf{x}') - \oint_{\Gamma} U^*_{\alpha\beta\gamma}(\mathbf{x}', \mathbf{x}) \hat{t}^1_{m\gamma}(\mathbf{x}) \, d\Gamma(\mathbf{x})$$

$$+ \oint_{\Gamma} T^{(i)*}_{\alpha\beta\gamma}(\mathbf{x}', \mathbf{x}) \hat{u}^1_{m\gamma}(\mathbf{x}) \, d\Gamma(\mathbf{x}) \Big] \mathbf{F}^{-1} w_3 \Bigg\} \tag{4.21}$$

The last domain integral I^D_{12} can be obtained from the particular solution $\hat{u}^2_{m\alpha}$ and $\tilde{t}^2_{m\alpha}$, to give

$$n_\beta(\mathbf{x}') I^D_{12} = n_\beta(\mathbf{x}') \Bigg\{ \sum_{m=1}^{M} \Big[\frac{1}{2} \hat{N}^2_{m\alpha\beta}(\mathbf{x}') - \oint_{\Gamma} U^*_{\alpha\beta\gamma}(\mathbf{x}', \mathbf{x}) \tilde{t}^2_{m\gamma}(\mathbf{x}) \, d\Gamma(\mathbf{x})$$

$$+ \oint_{\Gamma} T^{(i)*}_{\alpha\beta\gamma}(\mathbf{x}', \mathbf{x}) \hat{u}^2_{m\gamma}(\mathbf{x}) \, d\Gamma(\mathbf{x}) \Big] \mathbf{F}^{-1} w_3 \Bigg\} \tag{4.22}$$

4.5 Numerical Implementation

The geometry is approximated by continuous quadratic boundary elements. However for the unknown function, discontinuous elements are employed to satisfy the assumed continuity requirements for the boundary variables.

The quadratic shape function Φ^m_D for a discontinuous quadratic element, with

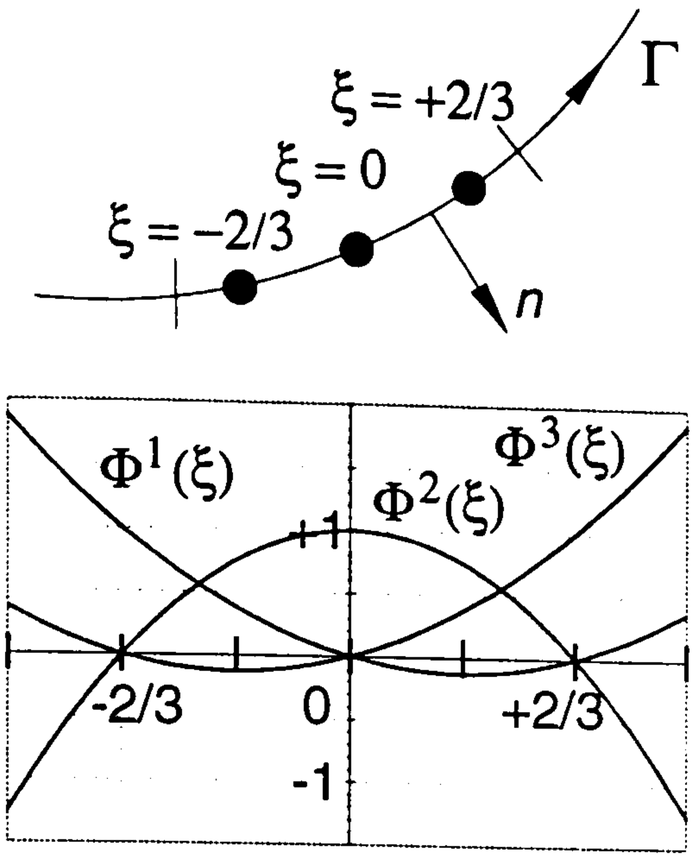

Figure 4-1: Quadratic shape functions for discontinous elements

nodes are placed at $\xi = -\frac{2}{3}, 0, +\frac{2}{3}$ are given as:

$$\begin{aligned} \Phi_D^1(\xi) &= \frac{3}{4}\xi(\frac{3}{2}\xi - 1) \\ \Phi_D^2(\xi) &= (1 - \frac{3}{2}\xi)(1 + \frac{3}{2}\xi) \\ \Phi_D^3(\xi) &= \frac{3}{4}\xi(\frac{3}{2}\xi + 1) \end{aligned} \tag{4.23}$$

As in semi-discontinuous element, the position of the internal node in discontinuous element is chosen arbitrarily but equally spaced at $-\frac{2}{3}, 0, +\frac{2}{3}$, not very close to the element end point to avoid near singularity problems.

After this discretisation, equations (4.7 – 4.9) can be written in the following form:

$$\begin{aligned} & [H]_{5(Nbn+Nin)\times 5(Nbn+Nin)}\{w\}_{5(Nbn+Nin)\times 1} \\ = \; & [G]_{5(Nbn+Nin)\times 15Nbe}\{p\}_{15Nbe\times 1} + \{Q\}_{5(Nbn+Nin)\times 1} \end{aligned} \tag{4.24}$$

where $[H]$ and $[G]$ are the well-known boundary element influence matrices [28], $\{w\}$ and $\{p\}$ are the boundary displacement and traction vectors respectively, and $\{Q\}$ is the domain load vector. By imposing the boundary conditions (see Section 3.5),

equation (4.24) can be written as:

$$[A]_{5(Nbn+Nin)\times 5(Nbn+Nin)}\{x\}_{5(Nbn+Nin)\times 1} = \{b\}_{5(Nbn+Nin)\times 1} \tag{4.25}$$

where $[A]$ is the system matrix, $\{x\}$ is the vector of unknowns and $\{b\}$ is the vector of prescribed boundary values. The system of algebraic equations can be solved for the boundary unknowns.

It has to be noted that the determinant of the matrix $[A]$ is large, due to the higher order of singularity in the kernels. To avoid numerical inaccuracies, the $[H]$ matrix is scaled by the modulus of elasticity. This scaling process is useful when both of the displacement and the traction boundary integral equations are used together.

4.5.1 Treatment of singularities

In the traction integral equations, the singularity order is higher than the displacement integral equations. In the $[H]$ matrix, the kernels $P^*_{\alpha\beta 3}$ and $P^*_{3\beta\gamma}$ are strongly singular, whereas, the kernels $P^*_{\alpha\beta\gamma}$, $P^*_{3\beta 3}$ and $T^{(i)*}_{\alpha\beta\gamma}$ are hypersingular. In the off-diagonal sub-matrices, the shape functions will reduce the order of singularity by one. This means that, element entries in $[H]$ matrix corresponding to the kernels $P^*_{\alpha\beta 3}$ and $P^*_{3\beta\gamma}$ become smooth, whereas, elements of the kernels $P^*_{\alpha\beta\gamma}$, $P^*_{3\beta 3}$ and $T^{(i)*}_{\alpha\beta\gamma}$ still remain strongly singular.

In $[G]$ matrix, the off-diagonal sub-matrices are smooth again due to the shape functions reducing the order of singularity. The diagonal matrices, on the other hand, contain the kernels $W^*_{\alpha\beta 3}$ and $W^*_{3\beta\gamma}$ which are weakly singular and the $W^*_{\alpha\beta\gamma}$, $W^*_{3\beta 3}$ and $U^*_{\alpha\beta\gamma}$ which are strongly singular.

The singular integrals mentioned above are treated individually based on their order of singularity. The weak singularity is treated using a nonlinear coordinate transformation as in Telles [128]. The strong-singular and the hypersingular integrals are evaluated using a singularity subtraction method based on the Taylor series expansion around the singular point, as in Portela, Aliabadi and Rooke [100], and the singular terms are integrated analytically.

As an example, the integral which contains strongly singular kernel of $O(1/r)$

can be regularised as follows:

$$\oint_{\Gamma_e} P^*_{ij}(\mathbf{x}', \mathbf{x}) w_j(\mathbf{x}) d\Gamma(\mathbf{x}) = w^n_j \int_{-1}^{+1} \frac{f^n_{ij}(\xi)}{\xi - \xi'} d\xi \tag{4.26}$$

where $f^n_{ij}(\xi) = P^*_{ij}(\xi', \xi)\Phi^n(\xi)J(\xi)(\xi - \xi')$; Γ_e denotes the boundary of the singular element, Φ^n is the element shape function corresponding to the node n in the element under consideration and J is the Jacobian of the transformation from x_α coordinate system to the local coordinate system ξ (i.e., $d\Gamma = J(\xi)d\xi$). The term $f^n_{ij}(\xi)$ is now a regular function. The integral in the right hand side of equation (4.26) can be regularised with the aid of a Taylor series expansion of the function $f^n_{ij}(\xi)$ about the singular point ξ' in the local coordinate system, as follows:

$$f^n_{ij}(\xi) = f^n_{ij}(\xi') + f^{n\prime}_{ij}(\xi')(\xi - \xi') + \frac{1}{2} f^{n\prime\prime}_{ij}(\xi')(\xi - \xi')^2 + ... \tag{4.27}$$

By substracting the first term of the Taylor expansion of the function $f^n_{ij}(\xi)$ and then adding it again, equation (4.26) can be written as

$$\int_{-1}^{+1} \frac{f^n_{ij}(\xi)}{\xi - \xi'} d\xi = \int_{-1}^{+1} \frac{f^n_{ij}(\xi) - f^n_{ij}(\xi')}{\xi - \xi'} d\xi + f^n_{ij}(\xi') \int_{-1}^{+1} \frac{d\xi}{\xi - \xi'} \tag{4.28}$$

The first integral in the right hand side is now regular and the second integral which is strongly singular can be integrated analytically to give,

$$\int_{-1}^{+1} \frac{d\xi}{\xi - \xi'} = \ln \left| \frac{1 - \xi'}{1 + \xi'} \right| \tag{4.29}$$

The hypersingular integrals of $O(1/r^2)$ can be treated in a similar way,

$$\oint_{\Gamma_e} T^{(i)*}_{\alpha\beta\gamma}(\mathbf{x}', \mathbf{x}) u_\gamma(\mathbf{x}) d\Gamma(\mathbf{x}) = u^n_\gamma \oint_{-1}^{+1} \frac{g^n_{\alpha\beta\gamma}(\xi)}{(\xi - \xi')^2} d\xi \tag{4.30}$$

where $g^n_{\alpha\beta\gamma}(\xi) = T^{(i)*}_{\alpha\beta\gamma}(\xi', \xi)\Phi^n(\xi)J(\xi)(\xi - \xi')^2$ is a regular function. The integral on the right hand side of equation can be regularised with the aid of the first and second term of a Taylor series expansion of the function $g^n_{\alpha\beta\gamma}(\xi)$ about the singular

point ξ' in the local coordinate system, as follows:

$$g^n_{\alpha\beta\gamma}(\xi) = g^n_{\alpha\beta\gamma}(\xi') + g^n_{\alpha\beta\gamma}{}'(\xi')\,(\xi-\xi') + \frac{1}{2}g^n_{\alpha\beta\gamma}{}''(\xi')\,(\xi-\xi')^2 + ... \tag{4.31}$$

By substracting the first and the second terms of the Taylor expansion of the function $g^n_{\alpha\beta\gamma}(\xi)$ and then adding it again, equation (4.30) can be written as

$$\neq\!\!\!\!\!\!\int_{-1}^{+1} \frac{g^n_{\alpha\beta\gamma}(\xi)}{(\xi-\xi')^2}d\xi = \int_{-1}^{+1} \frac{g^n_{\alpha\beta\gamma}(\xi) - g^n_{\alpha\beta\gamma}(\xi') - g^n_{\alpha\beta\gamma}{}'(\xi')\,(\xi-\xi')}{(\xi-\xi')^2}d\xi +$$

$$g^n_{\alpha\beta\gamma}(\xi') \neq\!\!\!\!\!\!\int_{-1}^{+1} \frac{d\xi}{(\xi-\xi')^2} + g^n_{\alpha\beta\gamma}{}'(\xi') \int_{-1}^{+1} \frac{d\xi}{\xi-\xi'} \tag{4.32}$$

where $g^n_{\alpha\beta\gamma}{}'$ denotes the first derivatives of $g^n_{\alpha\beta\gamma}$. At the collocation point the function $g^n_{\alpha\beta\gamma}$ is required to have continuity of its second derivatives, or at least have a Hölder-continuous first derivatives, for the finite part integrals to exist. The requirement is automatically satisfied by the use of discontinuous elements, since the nodes are internal to the element. In equation (4.32) the first integral on the right hand side is now regular, and the third integral is identical with the one given in equation (4.28). The second integral on the right hand side is hypersingular and can be integrated analytically to give,

$$\neq\!\!\!\!\!\!\int_{-1}^{+1} \frac{d\xi}{(\xi-\xi')^2} = -\frac{1}{(1+\xi')} - \frac{1}{(1-\xi')} \tag{4.33}$$

The last type of singularity observed is hypersingular of $O\left(\frac{1}{r^2} + \ln(r)\right)$. This type of singularity can be treated in a similar way to the hypersingular integral of $O\left(1/r^2\right)$ except there is an additional weakly singular term to be treated. The integral is given as

$$\neq\!\!\!\!\!\!\int_{\Gamma_e} P^*_{\alpha\beta\gamma}(\mathbf{x}',\mathbf{x}) w_\gamma(\mathbf{x}) d\Gamma(\mathbf{x}) = w^n_\gamma \neq\!\!\!\!\!\!\int_{-1}^{+1} P^*_{\alpha\beta\gamma}(\xi',\xi)\Phi^n(\xi)J(\xi)d\xi \tag{4.34}$$

The hypersingular integrals can be solved as follows

$$\neq\!\!\!\!\!\!\int_{\Gamma_e} P^*_{\alpha\beta\gamma}(\xi',\xi)\Phi^n(\xi)J(\xi)d\xi =$$

$$\int_{-1}^{+1}\left[P^{*}_{\alpha\beta\gamma}(\xi',\xi)\Phi^{n}(\xi)J(\xi)-\frac{g^{n}_{\alpha\beta\gamma}\left(\xi'\right)+g^{n}_{\alpha\beta\gamma}{}'(\xi')\left(\xi-\xi'\right)}{\left(\xi-\xi'\right)^{2}}-h^{n}_{\alpha\beta\gamma}\left(\xi'\right)\ln\left|\xi-\xi'\right|\right]d\xi$$

$$+g^{n}_{\alpha\beta\gamma}\left(\xi'\right)\oint_{-1}^{+1}\frac{d\xi}{\left(\xi-\xi'\right)^{2}}+g^{n}_{\alpha\beta\gamma}{}'\left(\xi'\right)\oint_{-1}^{+1}\frac{d\xi}{\xi-\xi'}+h^{n}_{\alpha\beta\gamma}\left(\xi'\right)\int_{-1}^{+1}\ln\left|\xi-\xi'\right|d\xi \quad (4.35)$$

where $g^{n}_{\alpha\beta\gamma}\left(\xi\right)=P^{*1}_{\alpha\beta\gamma}(\xi',\xi)\Phi^{n}(\xi)J(\xi)\left(\xi-\xi'\right)^{2}$ on which $P^{*1}_{\alpha\beta\gamma}(\xi',\xi)$ are part of the kernels which contain $1/r^{2}$. The term $h^{n}_{\alpha\beta\gamma}\left(\xi\right)=P^{*2}_{\alpha\beta\gamma}(\xi',\xi)\Phi^{n}(\xi)J(\xi)/\ln\left|\xi-\xi'\right|$, and $P^{*2}_{\alpha\beta\gamma}(\xi',\xi)$ are part of the kernels which contain $\ln\left|\xi-\xi'\right|$. The functions $g^{n}_{\alpha\beta\gamma}(\xi)$ and $h^{n}_{\alpha\beta\gamma}\left(\xi\right)$ are regular and can be expanded in terms of a Taylor series expansion about the singular point ξ' as before.

The first integral on the right hand side of equation (4.35) is now regular, the second integral on the right hand side which is hypersingular can be solved analytically using (4.33), the third integral is identical with the one given in equation (4.28). The last integral on the right hand side which is weakly singular can be integrated analytically to give,

$$\int_{-1}^{+1}\ln\left|\xi-\xi'\right|d\xi=\ln\left|\left(1-\xi'\right)\left(1+\xi'\right)\right|-\xi'\ln\left|\frac{1-\xi'}{1+\xi'}\right|-2 \quad (4.36)$$

Detailed derivation of $f^{n}_{ij}(\xi')$, $g^{n}_{\alpha\beta\gamma}\left(\xi'\right)$ and $h^{n}_{\alpha\beta\gamma}\left(\xi'\right)$ can be found in Appendix C.

4.6 Traction Integral Equations of Shear Deformable Plate Bending and Two-Dimensional Plane Stress

If the shell under consideration is flat, the values of $k_{11}=k_{22}=0$, therefore all integrals which contain $k_{\alpha\beta}$ in equations $(4.4-4.6)$ will be vanished and the integral equations are reduced to the uncoupled plate bending and the plane stress formulations. The integrals in $(4.4-4.5)$ become hypersingular integral representations of the shear deformable plate bending problems, and can be written as follows

$$\frac{1}{2}M_{\alpha\beta}(\mathbf{x}') = \int_{\Gamma}W^{*}_{\alpha\beta k}(\mathbf{x}',\mathbf{x})p_{k}(\mathbf{x})d\Gamma(\mathbf{x})-\int_{\Gamma}P^{*}_{\alpha\beta k}(\mathbf{x}',\mathbf{x})w_{k}(\mathbf{x})d\Gamma(\mathbf{x})$$

$$+\int_{\Omega} W^*_{\alpha\beta 3}(\mathbf{X}',\mathbf{X})q^*_3 d\Omega(\mathbf{X}) \tag{4.37}$$

$$\begin{aligned}\frac{1}{2}Q_\beta(\mathbf{x}') &= \int_\Gamma W^*_{3\beta k}(\mathbf{x}',\mathbf{x})p_k(\mathbf{x})d\Gamma(\mathbf{x}) - \int_\Gamma P^*_{3\beta k}(\mathbf{x}',\mathbf{x})w_k(\mathbf{x})d\Gamma(\mathbf{x}) + \\ &+ \int_\Omega W^*_{3\beta 3}(\mathbf{X}',\mathbf{X})q^*_3 d\Omega(\mathbf{X})\end{aligned} \tag{4.38}$$

and the integrals in equation (4.6) become hypersingular integral representations of the two-dimensional plane stress elasticity problems,

$$\frac{1}{2}N_{\alpha\beta}(\mathbf{x}') + \int_\Gamma T^*_{\alpha\beta\gamma}(\mathbf{x}',\mathbf{x})u_\gamma(\mathbf{x})d\Gamma(\mathbf{x}) = \int_\Gamma U^*_{\alpha\beta\gamma}(\mathbf{x}',\mathbf{x})t_\gamma(\mathbf{x})d\Gamma(\mathbf{x}) \tag{4.39}$$

The corresponding traction integral equations for the integral equations in (4.37 – 4.39) are

$$\frac{1}{2}p_\alpha(\mathbf{x}') + n_\beta(\mathbf{x}') \neq_\Gamma P^*_{\alpha\beta\gamma}(\mathbf{x}',\mathbf{x})w_\gamma(\mathbf{x})d\Gamma(\mathbf{x}) + n_\beta(\mathbf{x}') \neq_\Gamma P^*_{\alpha\beta 3}(\mathbf{x}',\mathbf{x})w_3(\mathbf{x})d\Gamma(\mathbf{x})$$

$$= n_\beta(\mathbf{x}') \neq_\Gamma W^*_{\alpha\beta\gamma}(\mathbf{x}',\mathbf{x})p_\gamma(\mathbf{x})d\Gamma(\mathbf{x}) + n_\beta(\mathbf{x}') \int_\Gamma W^*_{\alpha\beta 3}(\mathbf{x}',\mathbf{x})p_3(\mathbf{x})d\Gamma(\mathbf{x})$$

$$+n_\beta(\mathbf{x}') \int_\Omega W^*_{\alpha\beta 3}(\mathbf{x}',\mathbf{X})q_3 d\Omega(\mathbf{X}); \tag{4.40}$$

$$\frac{1}{2}p_3(\mathbf{x}') + n_\beta(\mathbf{x}') \neq_\Gamma P^*_{3\beta\gamma}(\mathbf{x}',\mathbf{x})u_\gamma(\mathbf{x})d\Gamma(\mathbf{x}) + n_\beta(\mathbf{x}') \neq_\Gamma P^*_{3\beta 3}(\mathbf{x}',\mathbf{x})u_3(\mathbf{x})d\Gamma(\mathbf{x})$$

$$= n_\beta(\mathbf{x}') \int_\Gamma W^*_{3\beta\gamma}(\mathbf{x}',\mathbf{x})p_\gamma(\mathbf{x})d\Gamma(\mathbf{x}) + n_\beta(\mathbf{x}') \neq_\Gamma W^*_{3\beta 3}(\mathbf{x}',\mathbf{x})p_3(\mathbf{x})d\Gamma(\mathbf{x})$$

$$+n_\beta(\mathbf{x}') \int_\Omega W^*_{3\beta 3}(\mathbf{x}',\mathbf{X})q_3 d\Omega(\mathbf{X}) \tag{4.41}$$

and

$$\frac{1}{2}t_\alpha(\mathbf{x}') + n_\beta(\mathbf{x}') \neq_\Gamma T^*_{\alpha\beta\gamma}(\mathbf{x}',\mathbf{x})u_\gamma(\mathbf{x})d\Gamma(\mathbf{x}) +$$

$$= n_\beta(\mathbf{x}') \neq_\Gamma U^*_{\alpha\beta\gamma}(\mathbf{x}',\mathbf{x})t_\gamma(\mathbf{x})d\Gamma(\mathbf{x}) + n_\beta(\mathbf{x}') \int_\Omega U^*_{\alpha\beta\gamma}(\mathbf{x}',\mathbf{X})q_\gamma d\Omega(\mathbf{X}) \tag{4.42}$$

Equations (4.40 – 4.42) represent five integral equations in terms of boundary tractions, and can be used together with the five displacement integral equations in equations (3.112 – 3.113) to form the dual boundary integral formulation.

In the case of a uniform domain load, the domain integrals in (4.37 – 4.38) and (4.40 – 4.41) can be transferred to boundary integral using equation (3.95). For other distribution cases of q_3, the transformation of domain integrals can be carried out by using the dual reciprocity techniques.

4.7 Summary

In this chapter, the hypersingular boundary element formulation for shear deformable shell was presented. The formulation was derived by considering the behaviour of internal stress resultant integral equations as the source point is taken to the boundary. As a result five independent integral equations in terms of tractions were obtained, which contain domain integrals as well as boundary integrals. The strong-singular and the hypersingular integrals were evaluated using a singularity subtraction method based on the Taylor series expansion about the singular point. The domain integrals were transformed to the boundary using the dual reciprocity technique. Also presented in this chapter are hypersingular boundary element formulations for shear deformable plate bending and two-dimensional plane stress. In the next two chapters, these traction integral equations are used together with the five displacement integral equations to form the dual boundary integral formulations.

Chapter 5

The Dual Boundary Element Method

5.1 Introduction

The BEM is an efficient numerical tool for general stress analysis. However, its application to solve general mixed mode crack problems is not straight forward. The coincidence of the crack surfaces makes point collocations on two crack surfaces generate identical equations and results in an ill-conditioned system of linear equations. To overcome this difficulty, several special techniques have been developed to model cracked structures. Among these the most general are the sub-region method [25] and the dual boundary element method [61].

During the last decade, the Dual Boundary Element Method (DBEM) has emerged as a robust numerical method for fracture mechanics problems. This method, which is based on displacement and traction integral equations, has been developed to solve many applications of fracture mechanics e.g. elastostatics, thermoelastic, concrete cracking, elastoplastic, stiffened panel, composite materials and dynamics, as reviewed by Aliabadi [10][11]. Recently, Dirgantara and Aliabadi [42] presented the derivation of the traction integral formulations for shallow shells, on which the DBEM is formed, and also the application of the dual boundary element method for crack analysis of shells. The application of the dual boundary element method to analysis of Reissner plate bending problems was reported by Ahmadi-Brooghani

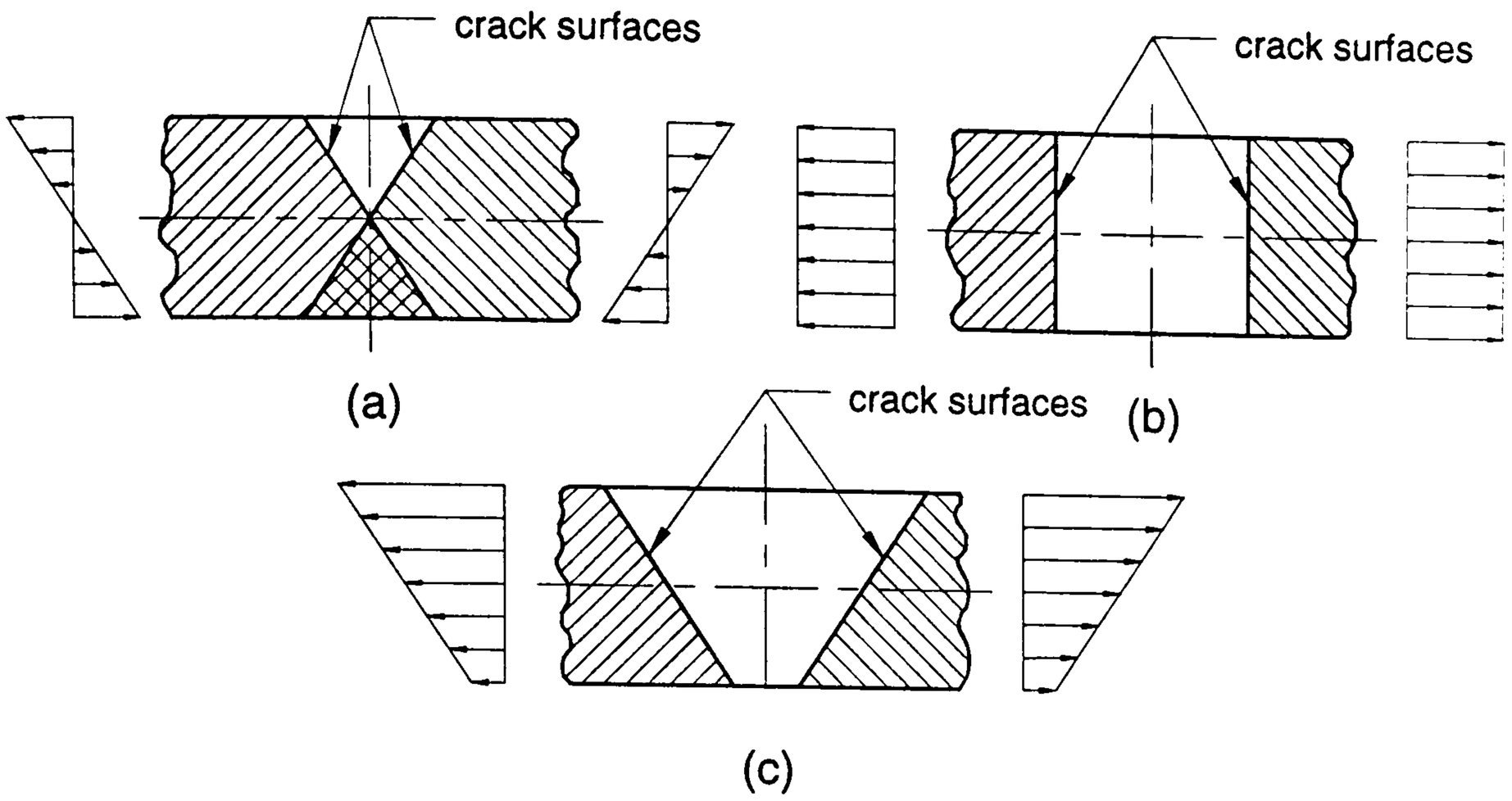

Figure 5-1: Numerical model of cracked plate: (a) pure bending load; (b) pure tension load; (c) bending and tension load.

and Wearing [5].

In this chapter, dual boundary element formulation for the analyses of shear deformable shells and plates loaded by bending and tension is presented. Special crack tip shape functions is developed to allow accurate modelling of the displacement fields near the crack-tip. The crack modelling strategy and the stress intensity factors evaluation using the crack surface displacements extrapolation (CSDE) and the $J-$ integral technique are also presented. Several numerical examples are solved to demonstrate the accuracy of the proposed method.

5.2 The Dual Boundary Integral Equations

If a plate or a shell is loaded by pure bending moment, then half of the plate or the shell will experience tension stress and the other half will experience compression. If the plate or shell contains a crack, then the compressive stress will cause the crack to close. This physical phenomenon creates difficulties when the plate is modelled numerically. As shown in Figure 5-1(a), the compressive stress causes the bottom part of the crack surfaces to overlap with each other, which is not physically correct. Therefore, in this work the basic assumption is that the in-plane loads are large enough to prevent crack closure due to bending loads, as shown in Figure 5-1(c).

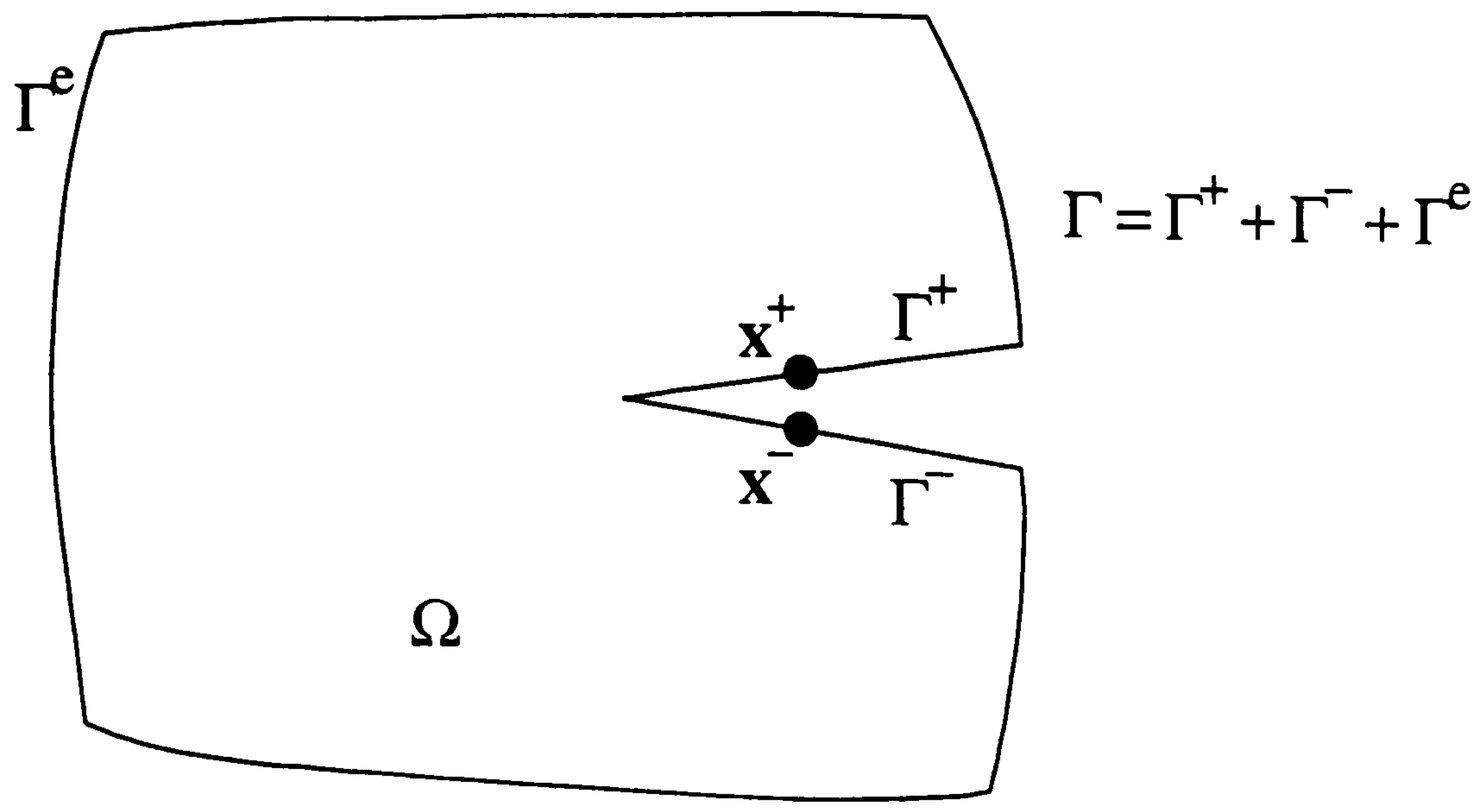

Figure 5-2: A body contains a crack.

5.2.1 Shallow shell problems

The dual equations, on which the dual boundary element method is based, are the displacement and the traction boundary integral equations. The method employs the displacement boundary integral equation for the source points on one crack surface and the traction integral equation on the other crack surface.

Consider a cracked body shown in Figure 5-2, with Γ^+, Γ^- referring to the upper and lower crack surfaces respectively, and Γ^e denotes the rest of the boundary. Recalling the boundary integral representation of the displacement components w_i and u_α for collocation points on the upper crack surface, that is $\mathbf{x}^+ \in \Gamma^+$, then equations $(3.78 - 3.79)$ can be written as:

$$
\begin{aligned}
&\frac{1}{2}w_j(\mathbf{x}^+) + \frac{1}{2}w_j(\mathbf{x}^-) + \oint_\Gamma P^*_{ij}(\mathbf{x}^+, \mathbf{x}) w_j(\mathbf{x})\, d\Gamma(\mathbf{x}) \\
= &\int_\Gamma W^*_{ij}(\mathbf{x}^+, \mathbf{x}) p_j(\mathbf{x})\, d\Gamma(\mathbf{x}) \\
&- \int_\Omega W^*_{i3}(\mathbf{x}^+, \mathbf{X})\, k_{\alpha\beta} B \frac{1-\nu}{2} \left[u_{\alpha,\beta}(\mathbf{X}) + u_{\beta,\alpha}(\mathbf{X}) + \frac{2\nu}{1-\nu} u_{\phi,\phi}(\mathbf{X})\, \delta_{\alpha\beta} \right] d\Omega(\mathbf{X}) \\
&- \int_\Omega W^*_{i3}(\mathbf{x}^+, \mathbf{X})\, k_{\alpha\beta} B \left((1-\nu) k_{\alpha\beta} + \nu \delta_{\alpha\beta} k_{\phi\phi} \right) w_3(\mathbf{X})\, d\Omega(\mathbf{X}) \\
&+ \int_\Omega W^*_{i3}(\mathbf{x}^+, \mathbf{X}) q_3(\mathbf{X}) d\Omega(\mathbf{X})
\end{aligned}
\tag{5.1}
$$

and

$$\begin{aligned}
&\frac{1}{2}u_\alpha(\mathbf{x}^+) + \frac{1}{2}u_\alpha(\mathbf{x}^-) + \oint_\Gamma T^*_{\theta\alpha}(\mathbf{x}^+,\mathbf{x})u_\alpha(\mathbf{x})d\Gamma(\mathbf{x}) \\
&+ \int_\Gamma U^*_{\theta\alpha}(\mathbf{x}^+,\mathbf{x})B\left[k_{\alpha\beta}\left(1-\nu\right)+\nu\delta_{\alpha\beta}k_{\phi\phi}\right]w_3(\mathbf{x})n_\beta(\mathbf{x})d\Gamma(\mathbf{x}) \\
&- \int_\Omega U^*_{\theta\alpha}(\mathbf{x}^+,\mathbf{X})B\left[k_{\alpha\beta}\left(1-\nu\right)+\nu\delta_{\alpha\beta}k_{\phi\phi}\right]w_{3,\beta}(\mathbf{X})d\Omega(\mathbf{X}) \\
= &\int_\Gamma U^*_{\theta\alpha}(\mathbf{x}^+,\mathbf{x})t_\alpha(\mathbf{x})d\Gamma(\mathbf{x}) + \int_\Omega U^*_{\theta\alpha}(\mathbf{x}^+,\mathbf{X})q_\alpha(\mathbf{X})d\Omega(\mathbf{X}) \qquad (5.2)
\end{aligned}$$

As the source point $\mathbf{x}^+$ is coincident with $\mathbf{x}^- \in \Gamma^-$, extra free terms $\frac{1}{2}w_j(\mathbf{x}^-)$ and $\frac{1}{2}u_\alpha(\mathbf{x}^-)$ appear in equations (5.1 – 5.2). It is apparent that collocation at $\mathbf{x}^-$ will give the same integral equations as equations (5.1 – 5.2). This will result in an ill-conditioned system of linear equations.

In order to overcome the above difficulty, the traction integral equations is used for collocations at $\mathbf{x}^- \in \Gamma^-$. Recalling the stress resultants boundary integral equations in (4.4 – 4.6), for collocations on $\mathbf{x}^- \in \Gamma^-$, it gives

$$\begin{aligned}
&\frac{1}{2}M_{\alpha\beta}(\mathbf{x}^-) + \frac{1}{2}M_{\alpha\beta}(\mathbf{x}^+) + \oint_\Gamma P^*_{\alpha\beta\gamma}(\mathbf{x}^-,\mathbf{x})w_\gamma(\mathbf{x})d\Gamma(\mathbf{x}) \\
&+ \oint_\Gamma P^*_{\alpha\beta3}(\mathbf{x}^-,\mathbf{x})w_3(\mathbf{x})d\Gamma(\mathbf{x}) \\
= &\oint_\Gamma W^*_{\alpha\beta\gamma}(\mathbf{x}^-,\mathbf{x})p_\gamma(\mathbf{x})d\Gamma(\mathbf{x}) + \int_\Gamma W^*_{\alpha\beta3}(\mathbf{x}^-,\mathbf{x})p_3(\mathbf{x})d\Gamma(\mathbf{x}) \\
&+ \int_\Omega W^*_{\alpha\beta3}(\mathbf{x}^-,\mathbf{X})q^*_3 d\Omega(\mathbf{X}) \qquad (5.3)
\end{aligned}$$

$$\begin{aligned}
&\frac{1}{2}Q_\beta(\mathbf{x}^-) + \frac{1}{2}Q_\beta(\mathbf{x}^+) + \oint_\Gamma P^*_{3\beta\gamma}(\mathbf{x}^-,\mathbf{x})w_\gamma(\mathbf{x})d\Gamma(\mathbf{x}) \\
&+ \oint_\Gamma P^*_{3\beta3}(\mathbf{x}^-,\mathbf{x})w_3(\mathbf{x})d\Gamma(\mathbf{x}) \\
= &\int_\Gamma W^*_{3\beta\gamma}(\mathbf{x}^-,\mathbf{x})p_\gamma(\mathbf{x})d\Gamma(\mathbf{x}) + \oint_\Gamma W^*_{3\beta3}(\mathbf{x}^-,\mathbf{x})p_3(\mathbf{x})d\Gamma(\mathbf{x}) \\
&+ \int_\Omega W^*_{3\beta3}(\mathbf{x}^-,\mathbf{X})q^*_3 d\Omega(\mathbf{X}) \qquad (5.4)
\end{aligned}$$

and

$$\frac{1}{2}N_{\alpha\beta}(\mathbf{x}^-) + \frac{1}{2}N(\mathbf{x}^+) + \oint_\Gamma T^*_{\alpha\beta\gamma}(\mathbf{x}^-,\mathbf{x})u_\gamma(\mathbf{x})d\Gamma(\mathbf{x})$$

$$= \oint_\Gamma U^*_{\alpha\beta\gamma}(\mathbf{x}^-,\mathbf{x})t_\gamma(\mathbf{x})d\Gamma(\mathbf{x}) + \int_\Omega U^*_{\alpha\beta\gamma}(\mathbf{x}^-,\mathbf{X})q^*_\gamma d\Omega(\mathbf{X})$$
$$+\frac{1}{2}B\left[(1-\nu)k_{\alpha\beta}+\nu\delta_{\alpha\beta}k_{\phi\phi}\right]w_3(\mathbf{x}^-) \tag{5.5}$$

Multiplying equations (5.3 – 5.5) by the outward normal $n_\beta(\mathbf{x}^-)$ and noticing that $n_\beta(\mathbf{x}^+) = -n_\beta(\mathbf{x}^-)$, the traction integral equations for a boundary source point at lower crack surface $\mathbf{x}^-$ are as follows:

$$\frac{1}{2}p_\alpha(\mathbf{x}^-) - \frac{1}{2}p_\alpha(\mathbf{x}^+) + n_\beta(\mathbf{x}^-)\oint_\Gamma P^*_{\alpha\beta\gamma}(\mathbf{x}^-,\mathbf{x})w_\gamma(\mathbf{x})d\Gamma(\mathbf{x})$$
$$+n_\beta(\mathbf{x}^-)\oint_\Gamma P^*_{\alpha\beta3}(\mathbf{x}^-,\mathbf{x})w_3(\mathbf{x})d\Gamma(\mathbf{x})$$
$$= n_\beta(\mathbf{x}^-)\oint_\Gamma W^*_{\alpha\beta\gamma}(\mathbf{x}^-,\mathbf{x})p_\gamma(\mathbf{x})d\Gamma(\mathbf{x}) + n_\beta(\mathbf{x}')\int_\Gamma W^*_{\alpha\beta3}(\mathbf{x}^-,\mathbf{x})p_3(\mathbf{x})d\Gamma(\mathbf{x})$$
$$-n_\beta(\mathbf{x}^-)\int_\Omega k_{\theta\psi}B\frac{1-\nu}{2}\left(u_{\theta,\psi}(\mathbf{X}) + u_{\psi,\theta}(\mathbf{X}) + \frac{2\nu}{1-\nu}u_{\phi,\phi}(\mathbf{X})\,\delta_{\theta\psi}\right)$$
$$\times W^*_{\alpha\beta3}(\mathbf{x}^-,\mathbf{X})d\Omega(\mathbf{X})$$
$$-n_\beta(\mathbf{x}^-)\int_\Omega k_{\theta\psi}B\left((1-\nu)k_{\theta\psi}+\nu\delta_{\theta\psi}k_{\phi\phi}\right)w_3(\mathbf{X})\,W^*_{\alpha\beta3}(\mathbf{x}^-,\mathbf{X})d\Omega(\mathbf{X})$$
$$+n_\beta(\mathbf{x}^-)\int_\Omega W^*_{\alpha\beta3}(\mathbf{x}^-,\mathbf{X})q_3 d\Omega(\mathbf{X}) \tag{5.6}$$

$$\frac{1}{2}p_3(\mathbf{x}^-) - \frac{1}{2}p_3(\mathbf{x}^+) + n_\beta(\mathbf{x}^-)\oint_\Gamma P^*_{3\beta\gamma}(\mathbf{x}^-,\mathbf{x})w_\gamma(\mathbf{x})d\Gamma(\mathbf{x})$$
$$+n_\beta(\mathbf{x}^-)\oint_\Gamma P^*_{3\beta3}(\mathbf{x}^-,\mathbf{x})w_3(\mathbf{x})d\Gamma(\mathbf{x})$$
$$= n_\beta(\mathbf{x}^-)\int_\Gamma W^*_{3\beta\gamma}(\mathbf{x}^-,\mathbf{x})p_\gamma(\mathbf{x})d\Gamma(\mathbf{x}) + n_\beta(\mathbf{x}^-)\oint_\Gamma W^*_{3\beta3}(\mathbf{x}^-,\mathbf{x})p_3(\mathbf{x})d\Gamma(\mathbf{x})$$
$$-n_\beta(\mathbf{x}^-)\int_\Omega k_{\theta\psi}B\frac{1-\nu}{2}\left(u_{\theta,\psi}(\mathbf{X}) + u_{\psi,\theta}(\mathbf{X}) + \frac{2\nu}{1-\nu}u_{\phi,\phi}(\mathbf{X})\,\delta_{\theta\psi}\right)$$
$$\times W^*_{3\beta3}(\mathbf{x}^-,\mathbf{X})d\Omega(\mathbf{X})$$
$$-n_\beta(\mathbf{x}^-)\int_\Omega k_{\theta\psi}B\left((1-\nu)k_{\theta\psi}+\nu\delta_{\theta\psi}k_{\phi\phi}\right)w_3(\mathbf{X})\,W^*_{3\beta3}(\mathbf{x}^-,\mathbf{X})d\Omega(\mathbf{X})$$
$$+n_\beta(\mathbf{x}^-)\int_\Omega W^*_{3\beta3}(\mathbf{x}^-,\mathbf{X})q_3 d\Omega(\mathbf{X}) \tag{5.7}$$

and

$$\frac{1}{2}t_\alpha(\mathbf{x}^-) - \frac{1}{2}t_\alpha(\mathbf{x}^+) + n_\beta(\mathbf{x}^-)\oint_\Gamma T^*_{\alpha\beta\gamma}(\mathbf{x}^-,\mathbf{x})u_\gamma(\mathbf{x})d\Gamma(\mathbf{x})$$

$$
\begin{aligned}
&+n_\beta(\mathbf{x}^-)\oint_\Gamma U^*_{\alpha\beta\gamma}(\mathbf{x}^-,\mathbf{x})B\left[k_{\theta\psi}\left(1-\nu\right)+\nu\delta_{\theta\psi}k_{\phi\phi}\right]w_3(\mathbf{x})n_\psi(\mathbf{x})d\Gamma(\mathbf{x})\\
&-n_\beta(\mathbf{x}^-)\int_\Omega U^*_{\alpha\beta\gamma}(\mathbf{x}^-,\mathbf{X})B\left[k_{\theta\psi}\left(1-\nu\right)+\nu\delta_{\theta\psi}k_{\phi\phi}\right]w_{3,\beta}(\mathbf{X})d\Omega(\mathbf{X})\\
=\;& n_\beta(\mathbf{x}^-)\oint_\Gamma U^*_{\alpha\beta\gamma}(\mathbf{x}^-,\mathbf{x})t_\gamma(\mathbf{x})d\Gamma(\mathbf{x})+n_\beta(\mathbf{x}^-)\int_\Omega U^*_{\alpha\beta\gamma}(\mathbf{x}^-,\mathbf{X})q_\gamma d\Omega(\mathbf{X})\\
&+\frac{1}{2}n_\beta(\mathbf{x}^-)B\left[(1-\nu)k_{\theta\psi}+\nu\delta_{\theta\psi}k_{\phi\phi}\right]w_3(\mathbf{x}^-)
\end{aligned}
\tag{5.8}
$$

Equations (5.1 – 5.2) and (5.6 – 5.8) represent displacement and traction integral equations respectively – on the crack surfaces, and together with the use of the displacement integral equations in (3.78 – 3.79), that is

$$
\begin{aligned}
&c_{ij}(\mathbf{x}')w_j(\mathbf{x}')+\oint_\Gamma P^*_{ij}(\mathbf{x}',\mathbf{x})w_j\left(\mathbf{x}\right)d\Gamma\left(\mathbf{x}\right)=\int_\Gamma W^*_{ij}(\mathbf{x}',\mathbf{x})p_j\left(\mathbf{x}\right)d\Gamma\left(\mathbf{x}\right)\\
&-\int_\Omega W^*_{i3}\left(\mathbf{x}',\mathbf{X}\right)k_{\alpha\beta}B\frac{1-\nu}{2}\left[u_{\alpha,\beta}\left(\mathbf{X}\right)+u_{\beta,\alpha}\left(\mathbf{X}\right)+\frac{2\nu}{1-\nu}u_{\phi,\phi}\left(\mathbf{X}\right)\delta_{\alpha\beta}\right]d\Omega\left(\mathbf{X}\right)\\
&-\int_\Omega W^*_{i3}\left(\mathbf{x}',\mathbf{X}\right)k_{\alpha\beta}B\left(\left(1-\nu\right)k_{\alpha\beta}+\nu\delta_{\alpha\beta}k_{\phi\phi}\right)w_3\left(\mathbf{X}\right)d\Omega\left(\mathbf{X}\right)\\
&+\int_\Omega W^*_{i3}(\mathbf{x}',\mathbf{X})q_3(\mathbf{X})d\Omega(\mathbf{X})
\end{aligned}
\tag{3.78}
$$

and

$$
\begin{aligned}
&c_{\theta\alpha}\left(\mathbf{x}'\right)u_\alpha(\mathbf{x}')+\oint_\Gamma T^{*(i)}_{\theta\alpha}(\mathbf{x}',\mathbf{x})u_\alpha(\mathbf{x})d\Gamma(\mathbf{x})\\
&+\int_\Gamma U^*_{\theta\alpha}(\mathbf{x}',\mathbf{x})B\left[k_{\alpha\beta}\left(1-\nu\right)+\nu\delta_{\alpha\beta}k_{\phi\phi}\right]w_3(\mathbf{x})n_\beta(\mathbf{x})d\Gamma(\mathbf{x})\\
&-\int_\Omega U^*_{\theta\alpha}(\mathbf{x}',\mathbf{X})B\left[k_{\alpha\beta}\left(1-\nu\right)+\nu\delta_{\alpha\beta}k_{\phi\phi}\right]w_{3,\beta}(\mathbf{X})d\Omega(\mathbf{X})\\
&=\int_\Gamma U^*_{\theta\alpha}(\mathbf{x}',\mathbf{x})t_\alpha(\mathbf{x})d\Gamma(\mathbf{x})+\int_\Omega U^*_{\theta\alpha}(\mathbf{x}',\mathbf{X})q_\alpha(\mathbf{X})d\Omega(\mathbf{X})
\end{aligned}
\tag{3.79}
$$

for collocation points on the rest of the boundary Γ^e, form the dual boundary integral formulation for shell problems.

Domain integrals appear in equations (5.1 – 5.2), (5.6 – 5.8) and (3.78 – 3.79) are transferred to the boundary by employing the dual reciprocity technique described in section 3.5 and section 4.4. It is important to note that if the dual reciprocity technique is applied to a structure containing cracks, as the source point $\mathbf{x}^+ \in \Gamma^+$ is coincident with $\mathbf{x}^- \in \Gamma^-$, domain integrals $I^D_1 - I^D_{12}$ will contain extra

free terms as in equations (5.1 – 5.2) and (5.6 – 5.8). The integrals $I_1^D - I_{12}^D$ can be written as follows:

The domain integral I_1^D :

$$I_1^D = \sum_{m=1}^{M} \left[\frac{1}{2} \hat{w}_{mk}^3(\mathbf{x}^+) + \frac{1}{2} \hat{w}_{mk}^3(\mathbf{x}^-) - \int_\Gamma W_{ik}^*(\mathbf{x}^+, \mathbf{x}) \hat{p}_{mk}^3(\mathbf{x})\, d\Gamma(\mathbf{x}) \right.$$

$$\left. + \oint_\Gamma P_{ik}^*(\mathbf{x}^+, \mathbf{x}) \hat{w}_{mk}^3(\mathbf{x})\, d\Gamma(\mathbf{x}) \right] \mathbf{F}^{-1} w_3 \tag{5.9}$$

The domain integral I_2^D :

$$I_2^D = \sum_{m=1}^{M} \left[\frac{1}{2} \hat{w}_{mk}^1(\mathbf{x}^+) + \frac{1}{2} \hat{w}_{mk}^1(\mathbf{x}^-) - \int_\Gamma W_{ik}^*(\mathbf{x}^+, \mathbf{x}) \hat{p}_{mk}^1(\mathbf{x})\, d\Gamma(\mathbf{x}) \right.$$

$$\left. + \oint_\Gamma P_{ik}^*(\mathbf{x}^+, \mathbf{x}) \hat{w}_{mk}^1(\mathbf{x})\, d\Gamma(\mathbf{x}) \right] \mathbf{F}^{-1} u_1 \tag{5.10}$$

The domain integral I_3^D :

$$I_3^D = \sum_{m=1}^{M} \left[\frac{1}{2} \hat{w}_{mk}^2(\mathbf{x}^+) + \frac{1}{2} \hat{w}_{mk}^2(\mathbf{x}^-) - \int_\Gamma W_{ik}^*(\mathbf{x}^+, \mathbf{x}) \hat{p}_{mk}^2(\mathbf{x})\, d\Gamma(\mathbf{x}) \right.$$

$$\left. + \oint_\Gamma P_{ik}^*(\mathbf{x}^+, \mathbf{x}) \hat{w}_{mk}^2(\mathbf{x})\, d\Gamma(\mathbf{x}) \right] \mathbf{F}^{-1} u_2 \tag{5.11}$$

The domain integral I_4^D :

$$I_4^D = \sum_{m=1}^{M} \left[\frac{1}{2} \hat{w}_{mk}^3(\mathbf{x}^+) + \frac{1}{2} \hat{w}_{mk}^3(\mathbf{x}^-) - \int_\Gamma W_{ik}^*(\mathbf{x}^+, \mathbf{x}) \hat{p}_{mk}^3(\mathbf{x})\, d\Gamma(\mathbf{x}) \right.$$

$$\left. + \oint_\Gamma P_{ik}^*(\mathbf{x}^+, \mathbf{x}) \hat{w}_{mk}^3(\mathbf{x})\, d\Gamma(\mathbf{x}) \right] \mathbf{F}^{-1} q_3 \tag{5.12}$$

The domain integral I_5^D :

$$I_5^D = \sum_{m=1}^{M} \left[\frac{1}{2} \hat{u}_{m\beta}^1(\mathbf{x}^+) + \frac{1}{2} \hat{u}_{m\beta}^1(\mathbf{x}^-) - \int_\Gamma U_{\alpha\beta}^*(\mathbf{x}^+, \mathbf{x}) \hat{t}_{m\beta}^1(\mathbf{x})\, d\Gamma(\mathbf{x}) \right.$$

$$\left. + \oint_\Gamma T_{\alpha\beta}^*(\mathbf{x}^+, \mathbf{x}) \hat{u}_{m\beta}^1(\mathbf{x})\, d\Gamma(\mathbf{x}) \right] \mathbf{F}^{-1} w_3 \tag{5.13}$$

The domain integral I_6^D :

$$I_6^D = \sum_{m=1}^{M} \left[\frac{1}{2} \hat{u}_{m\beta}^2(\mathbf{x}^+) + \frac{1}{2} \hat{u}_{m\beta}^2(\mathbf{x}^-) - \int_\Gamma U_{\alpha\beta}^*(\mathbf{x}^+, \mathbf{x}) \hat{t}_{m\beta}^2(\mathbf{x}) \, d\Gamma(\mathbf{x}) \right.$$

$$\left. + \oint_\Gamma T_{\alpha\beta}^*(\mathbf{x}^+, \mathbf{x}) \hat{u}_{m\beta}^2(\mathbf{x}) \, d\Gamma(\mathbf{x}) \right] \mathbf{F}^{-1} w_3 \tag{5.14}$$

The domain integral I_7^D :

$$n_\beta(\mathbf{x}^-) I_7^D = n_\beta(\mathbf{x}^-) \left\{ \sum_{m=1}^{M} \left[\frac{1}{2} \hat{M}_{m\alpha\beta}^3(\mathbf{x}^-) + \frac{1}{2} \hat{M}_{m\alpha\beta}^3(\mathbf{x}^+) + \oint_\Gamma P_{\alpha\beta\gamma}^*(\mathbf{x}^-, \mathbf{x}) \hat{w}_{m\gamma}^3(\mathbf{x}) d\Gamma(\mathbf{x}) \right.\right.$$

$$+ \oint_\Gamma P_{\alpha\beta 3}^*(\mathbf{x}^-, \mathbf{x}) \hat{w}_{m3}^3(\mathbf{x}) d\Gamma(\mathbf{x}) - \oint_\Gamma W_{\alpha\beta\gamma}^*(\mathbf{x}^-, \mathbf{x}) \hat{p}_{m\gamma}^3(\mathbf{x}) d\Gamma(\mathbf{x})$$

$$\left.\left. - \int_\Gamma W_{\alpha\beta 3}^*(\mathbf{x}^-, \mathbf{x}) \hat{p}_{m3}^3(\mathbf{x}) d\Gamma(\mathbf{x}) \right] \mathbf{F}^{-1} w_3 \right\} \tag{5.15}$$

and

$$n_\beta(\mathbf{x}^-) I_7^D = n_\beta(\mathbf{x}^-) \left\{ \sum_{m=1}^{M} \left[\frac{1}{2} \hat{Q}_{m\beta}^3(\mathbf{x}^-) + \frac{1}{2} \hat{Q}_{m\beta}^3(\mathbf{x}^+) + \oint_\Gamma P_{3\beta\gamma}^*(\mathbf{x}^-, \mathbf{x}) \hat{w}_{m\gamma}^3(\mathbf{x}) d\Gamma(\mathbf{x}) \right.\right.$$

$$+ \oint_\Gamma P_{3\beta 3}^*(\mathbf{x}^-, \mathbf{x}) \hat{w}_{m3}^3(\mathbf{x}) d\Gamma(\mathbf{x}) - \int_\Gamma W_{3\beta\gamma}^*(\mathbf{x}^-, \mathbf{x}) \hat{p}_{m\gamma}^3(\mathbf{x}) d\Gamma(\mathbf{x})$$

$$\left.\left. - \oint_\Gamma W_{3\beta 3}^*(\mathbf{x}^-, \mathbf{x}) \hat{p}_{m3}^3(\mathbf{x}) d\Gamma(\mathbf{x}) \right] \mathbf{F}^{-1} w_3 \right\} \tag{5.16}$$

The domain integral I_8^D :

$$n_\beta(\mathbf{x}^-) I_8^D = n_\beta(\mathbf{x}^-) \left\{ \sum_{m=1}^{M} \left[\frac{1}{2} \hat{M}_{m\alpha\beta}^1(\mathbf{x}^-) + \frac{1}{2} \hat{M}_{m\alpha\beta}^1(\mathbf{x}^+) + \oint_\Gamma P_{\alpha\beta\gamma}^*(\mathbf{x}^-, \mathbf{x}) \hat{w}_{m\gamma}^1(\mathbf{x}) d\Gamma(\mathbf{x}) \right.\right.$$

$$+ \oint_\Gamma P_{\alpha\beta 3}^*(\mathbf{x}^-, \mathbf{x}) \hat{w}_{m3}^1(\mathbf{x}) d\Gamma(\mathbf{x}) - \oint_\Gamma W_{\alpha\beta\gamma}^*(\mathbf{x}^-, \mathbf{x}) \hat{p}_{m\gamma}^1(\mathbf{x}) d\Gamma(\mathbf{x})$$

$$\left.\left. - \int_\Gamma W_{\alpha\beta 3}^*(\mathbf{x}^-, \mathbf{x}) \hat{p}_{m3}^1(\mathbf{x}) d\Gamma(\mathbf{x}) \right] \mathbf{F}^{-1} u_1 \right\} \tag{5.17}$$

and

$$n_\beta(\mathbf{x}^-) I_8^D = n_\beta(\mathbf{x}^-) \left\{ \sum_{m=1}^{M} \left[\frac{1}{2} \hat{Q}_{m\beta}^1(\mathbf{x}^-) + \frac{1}{2} \hat{Q}_{m\beta}^1(\mathbf{x}^+) + \oint_\Gamma P_{3\beta\gamma}^*(\mathbf{x}^-, \mathbf{x}) \hat{w}_{m\gamma}^1(\mathbf{x}) d\Gamma(\mathbf{x}) \right.\right.$$

$$+ \neq_{\Gamma} P^*_{3\beta 3}(\mathbf{x}^-, \mathbf{x}) \hat{w}^1_{m3}(\mathbf{x}) d\Gamma(\mathbf{x}) - \int_{\Gamma} W^*_{3\beta\gamma}(\mathbf{x}^-, \mathbf{x}) \hat{p}^1_{m\gamma}(\mathbf{x}) d\Gamma(\mathbf{x})$$

$$- \neq_{\Gamma} W^*_{3\beta 3}(\mathbf{x}^-, \mathbf{x}) \hat{p}^1_{m3}(\mathbf{x}) d\Gamma(\mathbf{x}) \Big] \mathbf{F}^{-1} u_1 \Big\} \tag{5.18}$$

The domain integral I_9^D :

$$n_\beta(\mathbf{x}^-) I_9^D = n_\beta(\mathbf{x}^-) \Big\{ \sum_{m=1}^{M} \Big[\frac{1}{2} \hat{M}^2_{m\alpha\beta}(\mathbf{x}^-) + \frac{1}{2} \hat{M}^2_{m\alpha\beta}(\mathbf{x}^+) + \neq_{\Gamma} P^*_{\alpha\beta\gamma}(\mathbf{x}^-, \mathbf{x}) \hat{w}^2_{m\gamma}(\mathbf{x}) d\Gamma(\mathbf{x})$$

$$+ \neq_{\Gamma} P^*_{\alpha\beta 3}(\mathbf{x}^-, \mathbf{x}) \hat{w}^2_{m3}(\mathbf{x}) d\Gamma(\mathbf{x}) - \neq_{\Gamma} W^*_{\alpha\beta\gamma}(\mathbf{x}^-, \mathbf{x}) \hat{p}^2_{m\gamma}(\mathbf{x}) d\Gamma(\mathbf{x})$$

$$- \int_{\Gamma} W^*_{\alpha\beta 3}(\mathbf{x}^-, \mathbf{x}) \hat{p}^2_{m3}(\mathbf{x}) d\Gamma(\mathbf{x}) \Big] \mathbf{F}^{-1} u_2 \Big\} \tag{5.19}$$

and

$$n_\beta(\mathbf{x}^-) I_9^D = n_\beta(\mathbf{x}^-) \Big\{ \sum_{m=1}^{M} \Big[\frac{1}{2} \hat{Q}^2_{m\beta}(\mathbf{x}^-) + \frac{1}{2} \hat{Q}^2_{m\beta}(\mathbf{x}^+) + \neq_{\Gamma} P^*_{3\beta\gamma}(\mathbf{x}^-, \mathbf{x}) \hat{w}^2_{m\gamma}(\mathbf{x}) d\Gamma(\mathbf{x})$$

$$+ \neq_{\Gamma} P^*_{3\beta 3}(\mathbf{x}^-, \mathbf{x}) \hat{w}^2_{m3}(\mathbf{x}) d\Gamma(\mathbf{x}) - \int_{\Gamma} W^*_{3\beta\gamma}(\mathbf{x}^-, \mathbf{x}) \hat{p}^2_{m\gamma}(\mathbf{x}) d\Gamma(\mathbf{x})$$

$$- \neq_{\Gamma} W^*_{3\beta 3}(\mathbf{x}^-, \mathbf{x}) \hat{p}^2_{m3}(\mathbf{x}) d\Gamma(\mathbf{x}) \Big] \mathbf{F}^{-1} u_2 \Big\} \tag{5.20}$$

The domain integral I_{10}^D :

$$n_\beta(\mathbf{x}^-) I_{10}^D = n_\beta(\mathbf{x}^-) \Big\{ \sum_{m=1}^{M} \Big[\frac{1}{2} \hat{M}^3_{m\alpha\beta}(\mathbf{x}^-) + \frac{1}{2} \hat{M}^3_{m\alpha\beta}(\mathbf{x}^+) + \neq_{\Gamma} P^*_{\alpha\beta\gamma}(\mathbf{x}^-, \mathbf{x}) \hat{w}^3_{m\gamma}(\mathbf{x}) d\Gamma(\mathbf{x})$$

$$+ \int_{\Gamma} P^*_{\alpha\beta 3}(\mathbf{x}^-, \mathbf{x}) \hat{w}^3_{m3}(\mathbf{x}) d\Gamma(\mathbf{x}) - \neq_{\Gamma} W^*_{\alpha\beta\gamma}(\mathbf{x}^-, \mathbf{x}) \hat{p}^3_{m\gamma}(\mathbf{x}) d\Gamma(\mathbf{x})$$

$$- \int_{\Gamma} W^*_{\alpha\beta 3}(\mathbf{x}^-, \mathbf{x}) \hat{p}^3_{m3}(\mathbf{x}) d\Gamma(\mathbf{x}) \Big] \mathbf{F}^{-1} q_3 \Big\} \tag{5.21}$$

and

$$n_\beta(\mathbf{x}^-) I_{10}^D = n_\beta(\mathbf{x}^-) \Big\{ \sum_{m=1}^{M} \Big[\frac{1}{2} \hat{Q}^3_{m\beta}(\mathbf{x}^-) + \frac{1}{2} \hat{Q}^3_{m\beta}(\mathbf{x}^+) + \neq_{\Gamma} P^*_{3\beta\gamma}(\mathbf{x}^-, \mathbf{x}) \hat{w}^3_{m\gamma}(\mathbf{x}) d\Gamma(\mathbf{x})$$

$$+ \neq_{\Gamma} P^*_{3\beta 3}(\mathbf{x}^-, \mathbf{x}) \hat{w}^3_{m3}(\mathbf{x}) d\Gamma(\mathbf{x}) - \int_{\Gamma} W^*_{3\beta\gamma}(\mathbf{x}^-, \mathbf{x}) \hat{p}^3_{m\gamma}(\mathbf{x}) d\Gamma(\mathbf{x})$$

$$- \oint_{\Gamma} W^*_{3\beta 3}(\mathbf{x}^-, \mathbf{x}) \hat{p}^3_{m3}(\mathbf{x}) d\Gamma(\mathbf{x}) \Big] \mathbf{F}^{-1} q_3 \Big\} \tag{5.22}$$

The domain integral I^D_{11} :

$$n_\beta(\mathbf{x}^-) I^D_{11} = n_\beta(\mathbf{x}^-) \Big\{ \sum_{m=1}^{M} \Big[\frac{1}{2} \hat{N}^1_{m\alpha\beta}(\mathbf{x}^-) + \frac{1}{2} \hat{N}^1_{m\alpha\beta}(\mathbf{x}^+) - \oint_{\Gamma} U^*_{\alpha\beta\gamma}(\mathbf{x}^-, \mathbf{x}) \hat{t}^1_{m\gamma}(\mathbf{x}) \, d\Gamma(\mathbf{x})$$

$$+ \oint_{\Gamma} T^{(i)*}_{\alpha\beta\gamma}(\mathbf{x}^-, \mathbf{x}) \hat{u}^1_{m\gamma}(\mathbf{x}) \, d\Gamma(\mathbf{x}) \Big] \mathbf{F}^{-1} w_3 \Big\} \tag{5.23}$$

The domain integral I^D_{12} :

$$n_\beta(\mathbf{x}^-) I^D_{12} = n_\beta(\mathbf{x}^-) \Big\{ \sum_{m=1}^{M} \Big[\frac{1}{2} \hat{N}^2_{m\alpha\beta}(\mathbf{x}^-) + \frac{1}{2} \hat{N}^2_{m\alpha\beta}(\mathbf{x}^+) - \oint_{\Gamma} U^*_{\alpha\beta\gamma}(\mathbf{x}^-, \mathbf{x}) \hat{t}^2_{m\gamma}(\mathbf{x}) \, d\Gamma(\mathbf{x})$$

$$+ \oint_{\Gamma} T^{(i)*}_{\alpha\beta\gamma}(\mathbf{x}^-, \mathbf{x}) \hat{u}^2_{m\gamma}(\mathbf{x}) \, d\Gamma(\mathbf{x}) \Big] \mathbf{F}^{-1} w_3 \Big\} \tag{5.24}$$

5.2.2 Plate bending and tension problems

If the panel is flat, that is $k_{11} = k_{22} = 0$, then equations (5.1 – 5.2) and (5.6 – 5.8) become uncoupled equations for shear deformable plate bending and two-dimensional plane stress problems. Hence the displacement boundary integral equations (5.1 – 5.2), for collocation points on the upper crack surface $\mathbf{x}^+ \in \Gamma^+$, will become:

$$\begin{aligned} &\frac{1}{2} w_j(\mathbf{x}^+) + \frac{1}{2} w_j(\mathbf{x}^-) + \oint_{\Gamma} P^*_{ij}(\mathbf{x}^+, \mathbf{x}) w_j(\mathbf{x}) \, d\Gamma(\mathbf{x}) \\ = &\int_{\Gamma} W^*_{ij}(\mathbf{x}^+, \mathbf{x}) p_j(\mathbf{x}) \, d\Gamma(\mathbf{x}) + \int_{\Omega} W^*_{i3}(\mathbf{x}^+, \mathbf{X}) q_3(\mathbf{X}) d\Omega(\mathbf{X}) \end{aligned} \tag{5.25}$$

and

$$\frac{1}{2} u_\alpha(\mathbf{x}^+) + \frac{1}{2} u_\alpha(\mathbf{x}^-) + \oint_{\Gamma} T^*_{\theta\alpha}(\mathbf{x}^+, \mathbf{x}) u_\alpha(\mathbf{x}) d\Gamma(\mathbf{x}) = \int_{\Gamma} U^*_{\theta\alpha}(\mathbf{x}^+, \mathbf{x}) t_\alpha(\mathbf{x}) d\Gamma(\mathbf{x}) \tag{5.26}$$

and the traction integral equations (5.6 – 5.8) at lower crack surface Γ^- are become:

$$\begin{aligned} &\frac{1}{2} p_\alpha(\mathbf{x}^-) - \frac{1}{2} p_\alpha(\mathbf{x}^+) + n_\beta(\mathbf{x}^-) \oint_{\Gamma} P^*_{\alpha\beta\gamma}(\mathbf{x}^-, \mathbf{x}) w_\gamma(\mathbf{x}) d\Gamma(\mathbf{x}) \\ &+ n_\beta(\mathbf{x}^-) \oint_{\Gamma} P^*_{\alpha\beta 3}(\mathbf{x}^-, \mathbf{x}) w_3(\mathbf{x}) d\Gamma(\mathbf{x}) \end{aligned}$$

$$
\begin{aligned}
= \quad & n_\beta(\mathbf{x}^-) \oint_\Gamma W^*_{\alpha\beta\gamma}(\mathbf{x}^-, \mathbf{x}) p_\gamma(\mathbf{x}) d\Gamma(\mathbf{x}) + n_\beta(\mathbf{x}^-) \int_\Gamma W^*_{\alpha\beta 3}(\mathbf{x}^-, \mathbf{x}) p_3(\mathbf{x}) d\Gamma(\mathbf{x}) \\
& + n_\beta(\mathbf{x}^-) \int_\Omega W^*_{\alpha\beta 3}(\mathbf{x}^-, \mathbf{X}) q_3 d\Omega(\mathbf{X})
\end{aligned} \tag{5.27}
$$

$$
\begin{aligned}
& \frac{1}{2} p_3(\mathbf{x}^-) - \frac{1}{2} p_3(\mathbf{x}^+) + n_\beta(\mathbf{x}^-) \oint_\Gamma P^*_{3\beta\gamma}(\mathbf{x}^-, \mathbf{x}) w_\gamma(\mathbf{x}) d\Gamma(\mathbf{x}) \\
& + n_\beta(\mathbf{x}^-) \oint_\Gamma P^*_{3\beta 3}(\mathbf{x}^-, \mathbf{x}) w_3(\mathbf{x}) d\Gamma(\mathbf{x}) \\
= \quad & n_\beta(\mathbf{x}^-) \int_\Gamma W^*_{3\beta\gamma}(\mathbf{x}^-, \mathbf{x}) p_\gamma(\mathbf{x}) d\Gamma(\mathbf{x}) + n_\beta(\mathbf{x}^-) \oint_\Gamma W^*_{3\beta 3}(\mathbf{x}^-, \mathbf{x}) p_3(\mathbf{x}) d\Gamma(\mathbf{x}) \\
& + n_\beta(\mathbf{x}^-) \int_\Omega W^*_{3\beta 3}(\mathbf{x}^-, \mathbf{X}) q_3 d\Omega(\mathbf{X})
\end{aligned} \tag{5.28}
$$

and

$$
\begin{aligned}
& \frac{1}{2} t_\alpha(\mathbf{x}^-) - \frac{1}{2} t_\alpha(\mathbf{x}^+) + n_\beta(\mathbf{x}^-) \oint_\Gamma T^*_{\alpha\beta\gamma}(\mathbf{x}^-, \mathbf{x}) u_\gamma(\mathbf{x}) d\Gamma(\mathbf{x}) \\
= \quad & n_\beta(\mathbf{x}^-) \oint_\Gamma U^*_{\alpha\beta\gamma}(\mathbf{x}^-, \mathbf{x}) t_\gamma(\mathbf{x}) d\Gamma(\mathbf{x})
\end{aligned} \tag{5.29}
$$

Equations (5.25 – 5.26) and (5.27 – 5.29) represent displacement and traction integral equations respectively – on the crack surfaces, and together with the use of the displacement integral equations in (3.112 – 3.113), that is

$$
\begin{aligned}
c_{ij}(\mathbf{x}') w_j(\mathbf{x}') + \oint_\Gamma P^*_{ij}(\mathbf{x}', \mathbf{x}) w_j(\mathbf{x}) \, d\Gamma(\mathbf{x}) &= \int_\Gamma W^*_{ij}(\mathbf{x}', \mathbf{x}) p_j(\mathbf{x}) \, d\Gamma(\mathbf{x}) \\
& + \int_\Omega W^*_{i3}(\mathbf{x}', \mathbf{X}) q_3(\mathbf{X}) d\Omega(\mathbf{X})
\end{aligned} \tag{3.112}
$$

$$
c_{\theta\alpha}(\mathbf{x}') \, u_\alpha(\mathbf{x}') + \oint_\Gamma T^*_{\theta\alpha}(\mathbf{x}', \mathbf{x}) u_\alpha(\mathbf{x}) d\Gamma(\mathbf{x}) = \int_\Gamma U^*_{\theta\alpha}(\mathbf{x}', \mathbf{x}) t_\alpha(\mathbf{x}) d\Gamma(\mathbf{x}) \tag{3.113}
$$

for collocation points on the rest of the boundary Γ^e, form the dual boundary integral formulation for plate loaded by bending and tension.

In the case of a uniform domain load (q_3 = constant), the domain integrals in (5.25) and (3.112) can be transferred to boundary integral using equation (3.58), and equation (3.95) for transformation of domain integrals in (5.27 – 5.28). For any other load distribution case, then the dual reciprocity technique described in section 3.5 and 4.4 can be used.

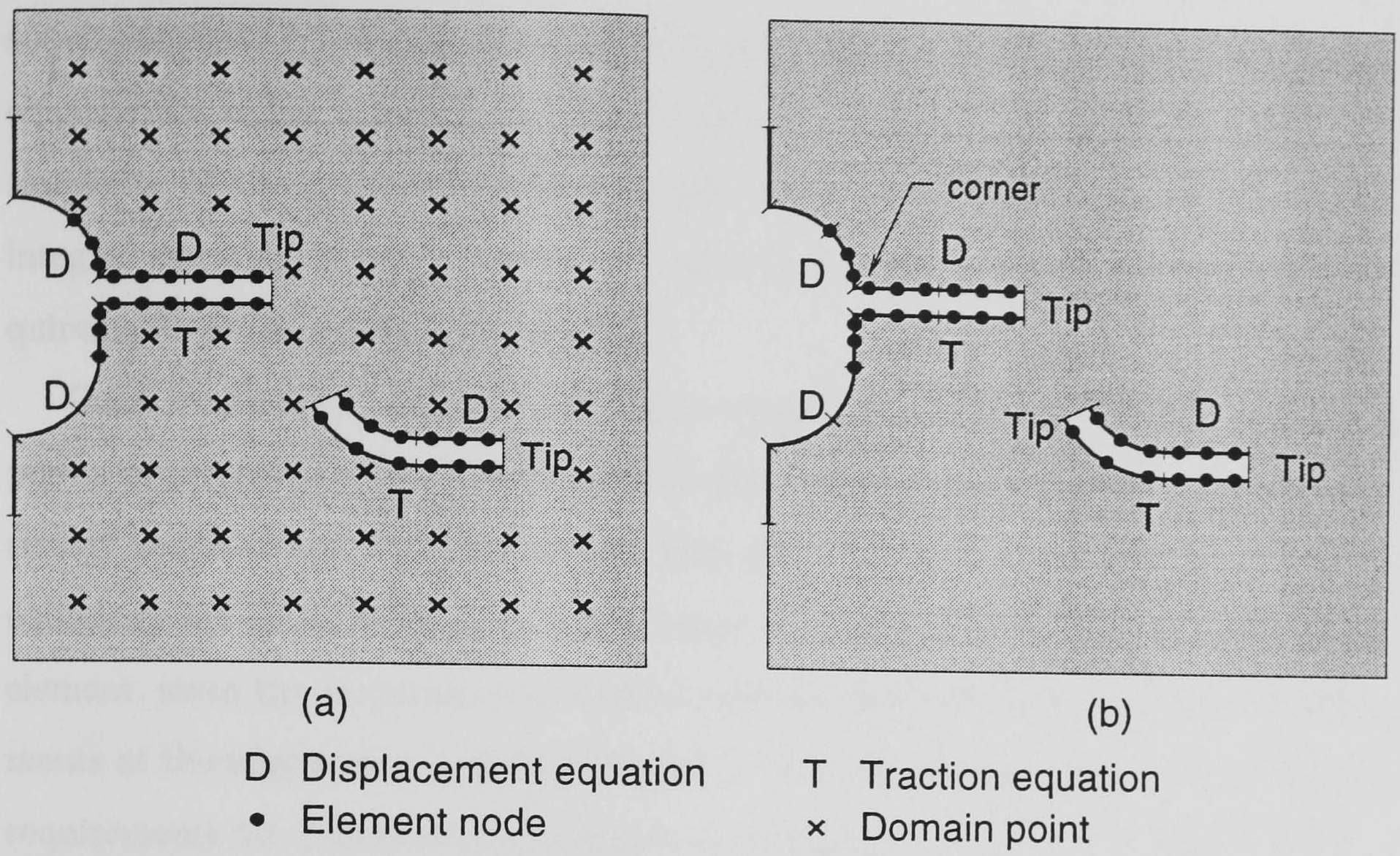

Figure 5-3: Modelling strategy for the dual boundary element method: (a) shells; (b) plates.

5.3 Numerical Implementation

5.3.1 Crack modelling strategy

In order to implement the dual boundary element method, the boundary including crack surfaces are discretised into elements. As described in chapters 3 and 4, isoparametric quadratic elements are used in this work. A modelling strategy has to be derived, taking into account the continuity requirements of displacements and tractions at collocation points for displacement and traction integral equations.

For displacement integral equation, at boundary collocation points $\mathbf{x}'$, the continuity requirement for displacements w_i and u_α are $C^{0,\alpha}$, $(0 < \alpha < 1)$ for Cauchy principal-value integrals to exist. On the other hand, for traction integral equation, at boundary collocation points $\mathbf{x}'$, the continuity requirement for the displacements w_i and u_α is $C^{1,\alpha}$, $(0 < \alpha < 1)$ for the existence of Hadamard principal-value integral, and p_i and t_α are required to be at least $C^{0,\alpha}$, $(0 < \alpha < 1)$, for Cauchy principal-value integrals to exist.

The continuity requirement of displacement integral equation can be fulfilled when the collocation point is either on a smooth or a non-smooth boundary. Using

super-elements, Wilde and Aliabadi [143] presented treatments of traction integral equation for either a smooth or non-smooth boundaries. However, to maintain the simplicity of the proposed method in this thesis the collocation point of traction integral equation is only located at a smooth boundary where the continuity requirements are automatically satisfied.

Consider that the boundary is approximated by elements, and the collocation points are restricted to the nodes of elements. Under these consideration, the continuity requirements for Cauchy principal-value integrals in displacement integral equations can be satisfied by any Lagrangian continuous or discontinuous boundary element, since the isoparametric shape functions imply Hölder continuous displacements at the edge nodes, and they imply C^{∞} at internal nodes. However, continuity requirements for Hadamard principal-value integrals in traction integral equations are satisfied only by discontinuous elements, since all nodes are located at internal points of the element where continuously differentiable interpolation functions are defined.

Taking into consideration the above requirements, and to maintain efficiency and simplicity of the boundary element, in the present method, discontinuous elements are used for the crack modelling. The general modelling strategies used in this work are similar to those used in [100] and can be summarised as follows:

- crack boundaries are modelled with discontinuous quadratic elements, as shown in Figure 5-3, in such a way that each node of one of the crack surfaces is coincident with the node on the opposite surfaces;

- the traction equations (5.6 – 5.8) are applied for collocation on one of the crack surfaces;

- the displacement equations (5.1 – 5.2) are applied for collocation on the opposite crack surface and for the other non-crack boundaries the displacement equations (3.112 – 3.113) are employed;

- continuous quadratic elements are applied along the remaining boundary of the body, except at the intersection between a crack and an edge, where discontinuous or semi-discontinuous elements are required on the edge in order

to avoid a common node at intersection, and also at boundary corners, where semi-discontinuous are preferred.

- for shell problems, several dual reciprocity collocation points are placed in the domain.

This simple strategy is robust and allows the DBEM to effectively model general edge or embedded crack problems; crack tips, crack-edge corners and crack kinks do not require special treatment, since they are not located at nodal points where the collocation is carried out.

5.3.2 Special crack-tip elements

To be able to model the displacement field $\sqrt{r}$ behaviour near crack tip, a set of special shape function has been used for crack tip element similar to those reported by Mi and Aliabadi [84] for three dimensional elasticity problems. In this work, a discontinuous quadratic element with $\xi = -\frac{2}{3}, 0, +\frac{2}{3}$ is used. The variation of the displacements along the element is required to have the form of $u(\xi) = u^{\alpha} N^{\alpha}(\xi) = a_1^{\alpha} + a_2^{\alpha}\sqrt{r} + a_3^{\alpha}(r)$. If the crack tip is located at $\xi = -1$, then the shape function in the form $N^{\alpha}(\xi) = a_1^{\alpha} + a_2^{\alpha}\sqrt{1+\xi} + a_3^{\alpha}(1+\xi)$ is used. On the other hand, if the crack tip is located at $\xi = +1$, then the shape function in the form $N^{\alpha}(\xi) = b_1^{\alpha} + b_2^{\alpha}\sqrt{1-\xi} + b_3^{\alpha}(1-\xi)$ is used. If $N^{\alpha}(\xi)$ is set to equal 1 at the collocation node α, and 0 at the other nodes, a set of linear system of equations are established and the unknown constants can be obtained.

Finally, the shape functions for crack tip elements with the crack tip located at $\xi = -1$ are

$$N_1^{(-1)}(\xi) = \frac{3}{2}\frac{\left(3-\sqrt{15}\right)\xi + 2\sqrt{1+\xi} - 2}{\sqrt{15}+\sqrt{3}-6} \tag{5.30}$$

$$N_2^{(-1)}(\xi) = \frac{3\left(\sqrt{15}-\sqrt{3}\right)\xi - 12\sqrt{1+\xi} + 2\left(\sqrt{15}+\sqrt{3}\right)}{2\left(\sqrt{15}+\sqrt{3}-6\right)} \tag{5.31}$$

$$N_3^{(-1)}(\xi) = \frac{3}{2}\frac{\left(\sqrt{3}-3\right)\xi + 2\sqrt{1+\xi} - 2}{\sqrt{15}+\sqrt{3}-6} \tag{5.32}$$

and for crack tip element with the crack tip located at $\xi = +1$ are

$$N_1^{(+1)}(\xi) = \frac{3}{2}\frac{\left(3-\sqrt{3}\right)\xi + 2\sqrt{1-\xi} - 2}{\sqrt{15}+\sqrt{3}-6} \tag{5.33}$$

$$N_2^{(+1)}(\xi) = \frac{3\left(\sqrt{3}-\sqrt{15}\right)\xi - 12\sqrt{1-\xi} + 2\left(\sqrt{15}+\sqrt{3}\right)}{2\left(\sqrt{15}+\sqrt{3}-6\right)} \tag{5.34}$$

$$N_3^{(+1)}(\xi) = \frac{3}{2}\frac{\left(\sqrt{15}-3\right)\xi + 2\sqrt{1-\xi} - 2}{\sqrt{15}+\sqrt{3}-6} \tag{5.35}$$

5.3.3 Discretisation strategy

Following the procedure describe in chapter 3, after the discretisation process and as the collocation point passes through all collocation nodes, a linear system of equations is obtained which can be written in matrix form as

$$\begin{bmatrix} \mathbf{H}^p + \mathbf{H}^{mod} & \mathbf{H}^u \\ \mathbf{H}^w & \mathbf{H}^e \end{bmatrix} \begin{Bmatrix} \mathbf{w} \\ \mathbf{u} \end{Bmatrix} = \begin{bmatrix} \mathbf{G}^p & 0 \\ 0 & \mathbf{G}^e \end{bmatrix} \begin{Bmatrix} \mathbf{p} \\ \mathbf{t} \end{Bmatrix} + \begin{Bmatrix} \mathbf{b} \\ 0 \end{Bmatrix} \tag{5.36}$$

where $\mathbf{H}^p, \mathbf{G}^p, \mathbf{H}^e$,and $\mathbf{G}^e$ are the boundary element influence matrices for plate bending and plane stress elasticity respectively, $\mathbf{H}^u$ and $\mathbf{H}^w$ are coupling matrices of shallow shell, $\mathbf{H}^{mod}$ is an additional matrix caused by the shell curvature. Vectors $\mathbf{w} = \{w_1, w_2, w_3\}^{\mathrm{T}}$ and $\mathbf{u} = \{u_1, u_2\}^{\mathrm{T}}$ are the boundary displacement vectors, $\mathbf{p} = \{p_1, p_2, p_3\}^{\mathrm{T}}$, $\mathbf{t} = \{t_1, t_2\}^{\mathrm{T}}$ are the boundary traction vectors, and $\mathbf{b}$ is the domain load vector.

In the case of plate loaded by bending and tension, the system of equations becomes uncoupled and can be written as follows

$$\begin{bmatrix} \mathbf{H}^p & 0 \\ 0 & \mathbf{H}^e \end{bmatrix} \begin{Bmatrix} \mathbf{w} \\ \mathbf{u} \end{Bmatrix} = \begin{bmatrix} \mathbf{G}^p & 0 \\ 0 & \mathbf{G}^e \end{bmatrix} \begin{Bmatrix} \mathbf{p} \\ \mathbf{t} \end{Bmatrix} + \begin{Bmatrix} \mathbf{b} \\ 0 \end{Bmatrix} \tag{5.37}$$

and after imposing boundary condition, equations (5.36 – 5.37) can be written as:

$$[A]_{5Nbn\times 5Nbn}\{x\}_{5Nbn\times 1} = \{b\}_{5Nbn\times 1} \tag{5.38}$$

where $[A]$ is the system matrix, $\{x\}$ is the unknown vector and $\{b\}$ is the vector

of prescribed boundary values. Nn are number of boundary nodes. Using $LU-$ decomposition, the system of algebraic equations can be solved for the boundary unknowns.

5.3.4 Modelling consideration of the dual reciprocity technique

There are some difficulties in implementing the dual reciprocity technique for the dual boundary element analysis, due to the coincidence nodes along crack surfaces. These difficulties are summarized as follows:

1. The dual reciprocity collocation points at crack boundaries. The existence of two coincident collocation points would make the coefficient matrix $\mathbf{F}$ singular and requires a special treatment.

2. Integrating over crack boundaries. In an incremental crack growth analysis, the inclusion of crack boundary implies that the boundary Γ is continuously changing from one incremental analysis to the next, and consequently the coefficient matrix has to be updated after each increment.

Similar to the argument reported in Salgado and Aliabadi [115], the contribution of the integration over crack boundaries can be calculated by considering a collocation point $\mathbf{x}'$ and two coincidence nodes $\mathbf{x}^-$ and $\mathbf{x}^+$ on opposite crack surfaces. The integrals can be written in matrix form as

$$\begin{aligned} \Psi \;=\; & \left[\begin{array}{cc} \mathbf{H}(\mathbf{x}',\mathbf{x}^+) & \mathbf{H}(\mathbf{x}',\mathbf{x}^-) \end{array}\right] \left\{\begin{array}{c} \hat{\mathbf{w}}_k(\mathbf{x}',\mathbf{x}^+) \\ \hat{\mathbf{w}}_k(\mathbf{x}',\mathbf{x}^-) \end{array}\right\} \\ & - \left[\begin{array}{cc} \mathbf{G}(\mathbf{x}',\mathbf{x}^+) & \mathbf{G}(\mathbf{x}',\mathbf{x}^-) \end{array}\right] \left\{\begin{array}{c} \hat{\mathbf{p}}_k(\mathbf{x}',\mathbf{x}^+) \\ \hat{\mathbf{p}}_k(\mathbf{x}',\mathbf{x}^-) \end{array}\right\} \end{aligned} \tag{5.39}$$

It can be observed that particular solutions and fundamental solutions have properties as follows:

$$
\begin{array}{lll}
\hat{p}_k(\mathbf{x}', \mathbf{x}^+) = -\hat{p}_k(\mathbf{x}', \mathbf{x}^-); & \text{and} & \hat{t}_\beta(\mathbf{x}', \mathbf{x}^+) = -\hat{t}_\beta(\mathbf{x}', \mathbf{x}^-) \\
\hat{w}_k(\mathbf{x}', \mathbf{x}^+) = \hat{w}_k(\mathbf{x}', \mathbf{x}^-); & \text{and} & \hat{u}_\beta(\mathbf{x}', \mathbf{x}^+) = \hat{u}_\beta(\mathbf{x}', \mathbf{x}^-) \\
P^*_{ik}(\mathbf{x}', \mathbf{x}^+) = -P^*_{ik}(\mathbf{x}', \mathbf{x}^-); & \text{and} & T^*_{\alpha\beta}(\mathbf{x}', \mathbf{x}^+) = -T^*_{\alpha\beta}(\mathbf{x}', \mathbf{x}^-) \\
P^*_{i\beta k}(\mathbf{x}', \mathbf{x}^+) = -P^*_{i\beta k}(\mathbf{x}', \mathbf{x}^-); & \text{and} & T^*_{\alpha\beta\gamma}(\mathbf{x}', \mathbf{x}^+) = -T^*_{\alpha\beta\gamma}(\mathbf{x}', \mathbf{x}^-) \\
W^*_{ik}(\mathbf{x}', \mathbf{x}^+) = W^*_{ik}(\mathbf{x}', \mathbf{x}^-); & \text{and} & U^*_{\alpha\beta}(\mathbf{x}', \mathbf{x}^+) = U^*_{\alpha\beta}(\mathbf{x}', \mathbf{x}^-) \\
W^*_{i\beta k}(\mathbf{x}', \mathbf{x}^+) = W^*_{i\beta k}(\mathbf{x}', \mathbf{x}^-); & \text{and} & U^*_{\alpha\beta\gamma}(\mathbf{x}', \mathbf{x}^+) = U^*_{\alpha\beta\gamma}(\mathbf{x}', \mathbf{x}^-)
\end{array}
\tag{5.40}
$$

Substituting properties in equation (5.40) into the matrix in equation (5.39), it can be seen that the contribution of the integration over crack boundaries to the coefficient matrix is equal to zero. Therefore, it is not necessary to include the crack boundaries in the integration process of $I_1^D - I_{12}^D$. In that case, the difficulties mentioned above are eliminated since the exclusion of crack boundary also means that there will be no dual reciprocity collocation points along the crack boundaries.

5.3.5 Treatment of the singularities

Three different order of singularities occur in the dual boundary integral equations, i.e. weakly singular, strongly singular and hypersingular integrals. The weakly singular integrals are cancelled using a bi-cubic nonlinear coordinate transformation as described in Appendix C. Strongly singular integrals at non-crack boundaries are evaluated indirectly using the generalised rigid body movements as described in Chapter 3.

On the crack surfaces, the strongly singular and the hypersingular integrals are evaluated using a singularity subtraction method based on the Taylor series expansion around the singular point for bending and shear integrals, and subsequently, the singular terms are integrated analytically. For straight elements along the crack, the evaluation of the strongly singular and the hypersingular integrals in membrane integral equations are most effectively carried out using direct analytic integrations. Details of singularity subtraction method and direct analytic integrations are described in Chapter 4 and Appendix C.

5.4 Stress Intensity Factors Evaluation

Five stress intensity factors (SIFs), two SIFs due to membrane loads and three due to bending moments and shear loads have to be computed. The stress intensity factor can be carried out in several ways. In this work, the crack surface displacements extrapolation and the $J-$ integral technique are employed to calculate the stress intensity factors.

5.4.1 The crack surface displacements extrapolation technique (CSDE)

As discussed in chapter 2, the displacements on the crack surfaces near the crack tip can be obtained as:

$$\left\{\begin{array}{c}\Delta\phi_2\\ \Delta\phi_1\\ \Delta w_3\\ \Delta u_2\\ \Delta u_1\end{array}\right\} = \left\{\begin{array}{c}\phi_2\\ \phi_1\\ w_3\\ u_2\\ u_1\end{array}\right\}_{\theta=180^0} - \left\{\begin{array}{c}\phi_2\\ \phi_1\\ w_3\\ u_2\\ u_1\end{array}\right\}_{\theta=-180^0} \tag{2.96}$$

$$= \left[\begin{array}{ccccc} \frac{48}{Eh^3}\sqrt{\frac{2r}{\pi}} & 0 & 0 & 0 & 0 \\ 0 & \frac{48}{Eh^3}\sqrt{\frac{2r}{\pi}} & 0 & 0 & 0 \\ 0 & 0 & \frac{24\,(1+\nu)}{5Eh}\sqrt{\frac{2r}{\pi}} & 0 & 0 \\ 0 & 0 & 0 & \frac{8}{Eh}\sqrt{\frac{r}{2\pi}} & 0 \\ 0 & 0 & 0 & 0 & \frac{8}{Eh}\sqrt{\frac{r}{2\pi}} \end{array}\right] \left\{\begin{array}{c}K_{1b}\\ K_{2b}\\ K_{3b}\\ K_{1m}\\ K_{2m}\end{array}\right\}$$

The stress intensity factors can then be written in terms of displacements on the crack surfaces, as

$$\{K\} = \frac{1}{\sqrt{r}}\,[\mathbf{C}]\,\{\Delta w\} \tag{2.97}$$

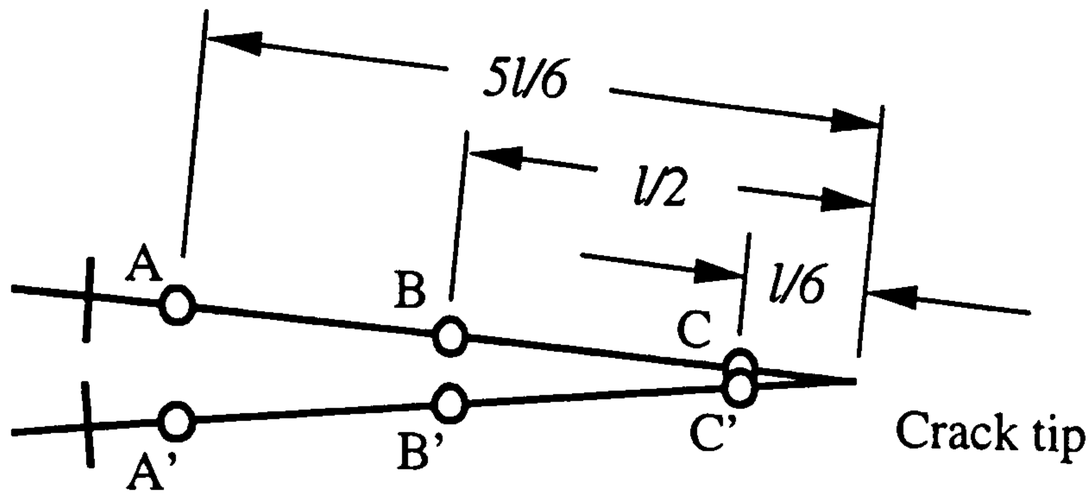

Figure 5-4: Crack tip element.

where

$$\{K\} = \begin{Bmatrix} K_{1b} \\ K_{2b} \\ K_{3b} \\ K_{1m} \\ K_{2m} \end{Bmatrix}, \qquad \{\Delta w\} = \begin{Bmatrix} \Delta\phi_2 \\ \Delta\phi_1 \\ \Delta w_3 \\ \Delta u_2 \\ \Delta u_1 \end{Bmatrix} \tag{2.98}$$

and

$$[\mathbf{C}] = \begin{bmatrix} \frac{Eh^3}{48}\sqrt{\frac{\pi}{2}} & 0 & 0 & 0 & 0 \\ 0 & \frac{Eh^3}{48}\sqrt{\frac{\pi}{2}} & 0 & 0 & 0 \\ 0 & 0 & \frac{5Eh}{24\,(1+\nu)}\sqrt{\frac{\pi}{2}} & 0 & 0 \\ 0 & 0 & 0 & \frac{Eh}{8}\sqrt{2\pi} & 0 \\ 0 & 0 & 0 & 0 & \frac{Eh}{8}\sqrt{2\pi} \end{bmatrix} \tag{2.99}$$

When discontinuous elements with nodes located at $\xi = -\frac{2}{3}, 0, +\frac{2}{3}$ are used for modelling crack surfaces, then at crack tip elements the distance of every node to the crack tip is given in Figure 5-4. The value of SIFs can then be obtained at any point in crack tip elements by substituting into equation (5.41) relevant value of generalised displacements and distance of the point from crack tip.

Hence,

$$\{K\}^{AA'} = \sqrt{\frac{6}{5l}}\,[\mathbf{C}]\left(\{w\}^{A} - \{w\}^{A'}\right) \tag{5.41}$$

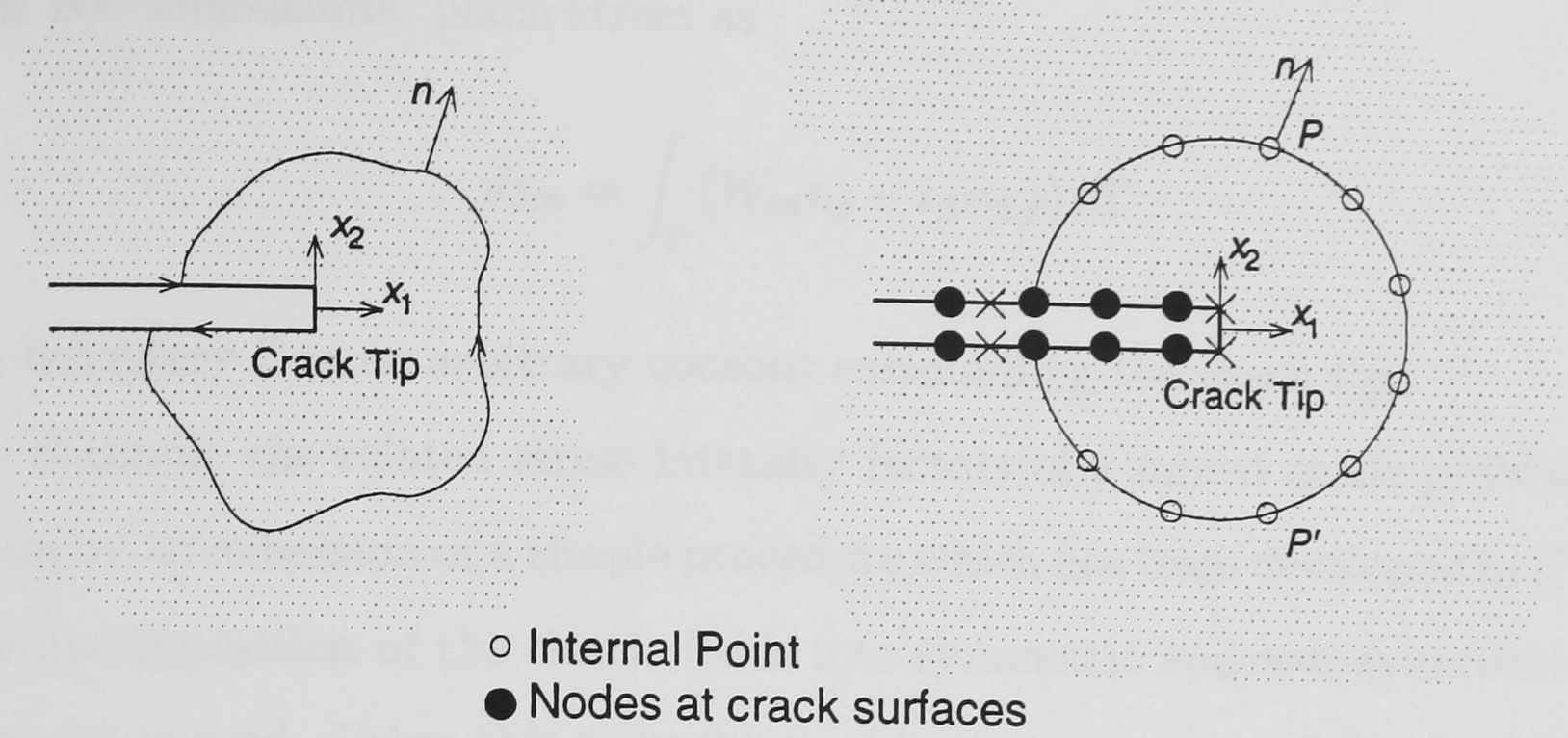

Figure 5-5: Local crack tip coordinate reference system and contour path for $J-$ integral.

and

$$\{K\}^{BB'} = \sqrt{\frac{2}{l}}\,[\mathbf{C}]\left(\{w\}^{B} - \{w\}^{B'}\right) \tag{5.42}$$

Then, SIF values are extrapolated to the crack tip using relationship

$$\{K\}^{tip} = \frac{r_{AA'}}{r_{AA'} - r_{BB'}}\left(\{K\}^{BB'} - \frac{r_{BB'}}{r_{AA'}}\{K\}^{AA'}\right) \tag{5.43}$$

where $r_{AA'} = \frac{5}{6}l$ and $r_{BB'} = \frac{1}{2}l$.

Using the above technique, the SIFs can be evaluated simply by using the value of generalised displacements at crack tip elements obtained from the dual boundary element analysis.

5.4.2 The J-integral technique

For plates loaded by a combination of bending and tension, the evaluation of the SIFs can also be done numerically by the $J-$ integral technique. The path independent $J-$ integral, presented in chapter 2, is defined for plate bending as

$$J_{\delta b} = \int_{\Gamma}\left(W_b - qw_3\right)n_\delta d\Gamma - \int_{\Gamma} p_i w_{i,\delta} d\Gamma + \int_{\Omega} q_{,\delta} w_3 d\Omega \tag{2.100}$$

and for two-dimensional plane stress as

$$J_{\delta m} = \int_{\Gamma} \left(W_m n_\delta - t_\beta u_{\beta,\delta} \right) d\Gamma \tag{2.101}$$

where boundary Γ is an arbitrary contour surrounding the crack tip.

To decouple the related stress intensity factors of a mixed mode problem from $J-$ integral an extension of a simple procedure which has been developed in [7] based on the decomposition of the elastic fields into symmetric and anti-symmetric mode component is used. Using this procedure only one component of the $J-$ integral is required, and in this work the x_1- component of the $J-$ integral is used.

The relationship between the component of $J-$ integral in x_1- direction and the bending and shear stress resultant intensity factors is given as

$$J_{1b} = \frac{12}{Eh^3} \left[{K_{1b}}^2 + {K_{2b}}^2 + \frac{h^2}{10} \left(1+\nu\right) {K_{3b}}^2 \right] \tag{2.104}$$

and the relationship between the component of $J-$ integral and the membrane stress resultant intensity factors is given as

$$J_{1m} = \frac{{K_{1m}}^2 + {K_{2m}}^2}{E'} \tag{2.105}$$

where the constants E' is the elasticity modulus; E' is equal to E for plane stress conditions and $E' = E/\left(1-\nu^2\right)$ for plane strain conditions.

Applying the decomposition procedure given in the Appendix E, the integral J_1 can be represented by the sum of two integral as follows :

$$J_1 = J_1^S + J_1^{AS} \tag{5.44}$$

where the superscript indicate the pertinent deformation mode.

When the decomposed stress resultants and displacements are introduced to equations (5.44) and (5.44), equation (5.44) will be obtained, with the $J-$ integral components given by

$$J_{1b}^N = \int_\Gamma \left(W_1^N - q w_3^N\right) n_1 d\Gamma - \int_\Gamma \left[M_{\alpha\beta}^N w_{\alpha,1}^N + Q_\beta^N w_{3,1}^N\right] n_\beta d\Gamma + \int_\Omega q_{,1}^N w_3^N d\Omega \quad (5.45)$$

and

$$J_{1m}^N = \int_\Gamma \frac{1}{h}\left(W^N n_1 - t_\alpha^N u_{\alpha,1}^N\right) d\Gamma \quad (5.46)$$

for $N = S$ or $N = AS$. Finally the stress intensity factor are obtained through the following relationship

$$J_{1b}^S = J_{1b}^I = \frac{12\, {K_{1b}}^2}{Eh^3} \quad (5.47)$$

$$J_{1b}^{AS} = J_{1b}^{II} + J_{1b}^{III} = \frac{12}{Eh^3}\left[{K_{2b}}^2 + \frac{h^2}{10}\left(1+\nu\right){K_{3b}}^2\right] \quad (5.48)$$

$$J_{1m}^S = J_{1m}^I = \frac{{K_{1m}}^2}{E'} \quad (5.49)$$

and

$$J_{1m}^{AS} = J_{1m}^{II} = \frac{{K_{2m}}^2}{E'} \quad (5.50)$$

To split mode II and mode III component from J_{1b}^{AS}, the displacement ratio as proposed by Rigby and Aliabadi [112] for three dimensional problem will be used.

$$\Delta w_1 = w_{1(+180^0)} - w_{1(-180^0)} = \frac{48}{Eh^3}\sqrt{2r}K_{2b} \quad (5.51)$$

$$\Delta w_3 = w_{3(+180^0)} - w_{3(-180^0)} = \frac{24\left(1+\nu\right)}{5Eh}\sqrt{2r}K_{3b} \quad (5.52)$$

$$\frac{\Delta w_1}{\Delta w_3} = \frac{10}{\left(1+\nu\right)h^2}\frac{K_{2b}}{K_{3b}} \quad (5.53)$$

Substituting equation (5.53) into equation (5.48) the following relations hold:

$$J_{1b}^{AS} = \frac{12\left(1+\nu\right)}{10Eh}\,{K_{3b}}^2\left[\frac{h^2\left(1+\nu\right)}{10}\left(\frac{\Delta w_1}{\Delta w_3}\right)^2 + 1\right] \quad (5.54)$$

or

$$J_{1b}^{AS} = \frac{12}{Eh^3}\,{K_{2b}}^2\left[1 + \frac{10}{h^2\left(1+\nu\right)}\left(\frac{\Delta w_3}{\Delta w_1}\right)^2\right] \quad (5.55)$$

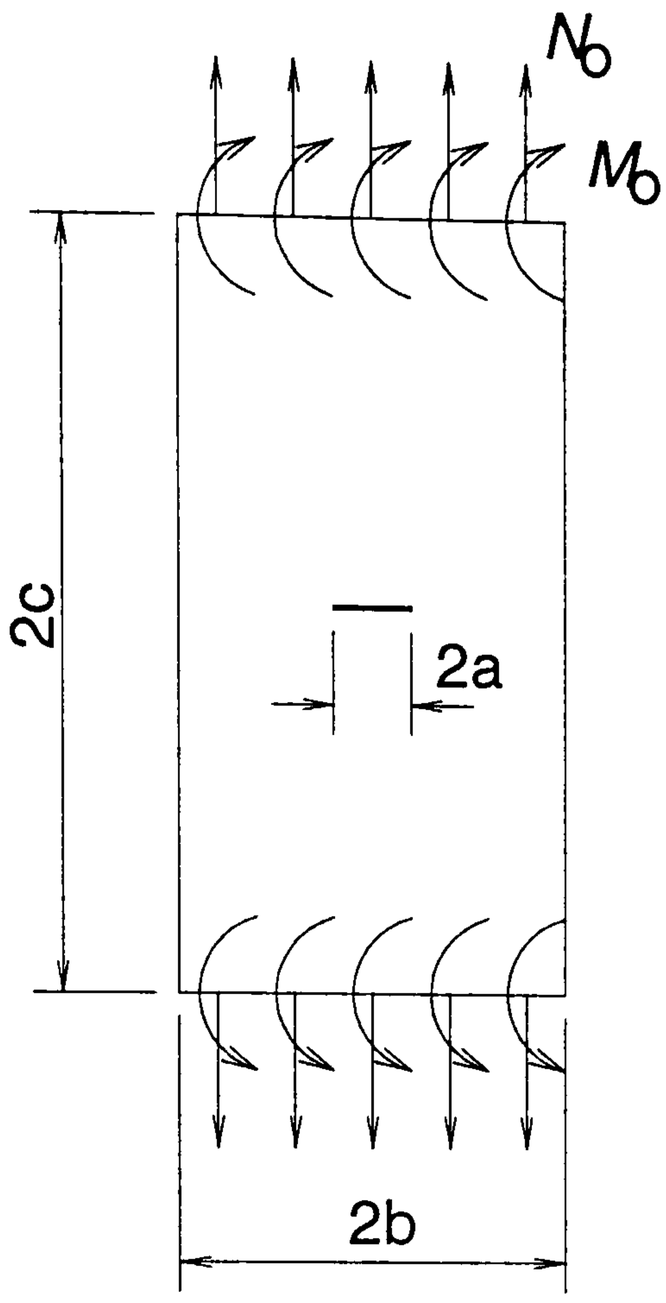

Figure 5-6: Rectangular plate with a centre crack loaded by bending moment and tension, and deformed shape of DBEM model.

To implement this procedure into the boundary element analysis, a circular contour path around the crack tip is defined as a set of internal points located at symmetrical positions relative to the crack plane, as shown in Figure 5-5. The numerical integration along the contour path is accomplished with the trapezoidal rule. Using this technique, regular discontinuous elements can be used for crack tip elements.

5.5 Numerical Examples

Several numerical examples are presented to demonstrate the ability of this proposed method for crack analyses of plates subjected to bending and tension, and shells, with different loadings and boundary conditions.

5.5.1 Rectangular plate with a centre crack loaded by bending and tension

As the first example, a rectangular plate with central crack loaded by edge bend-

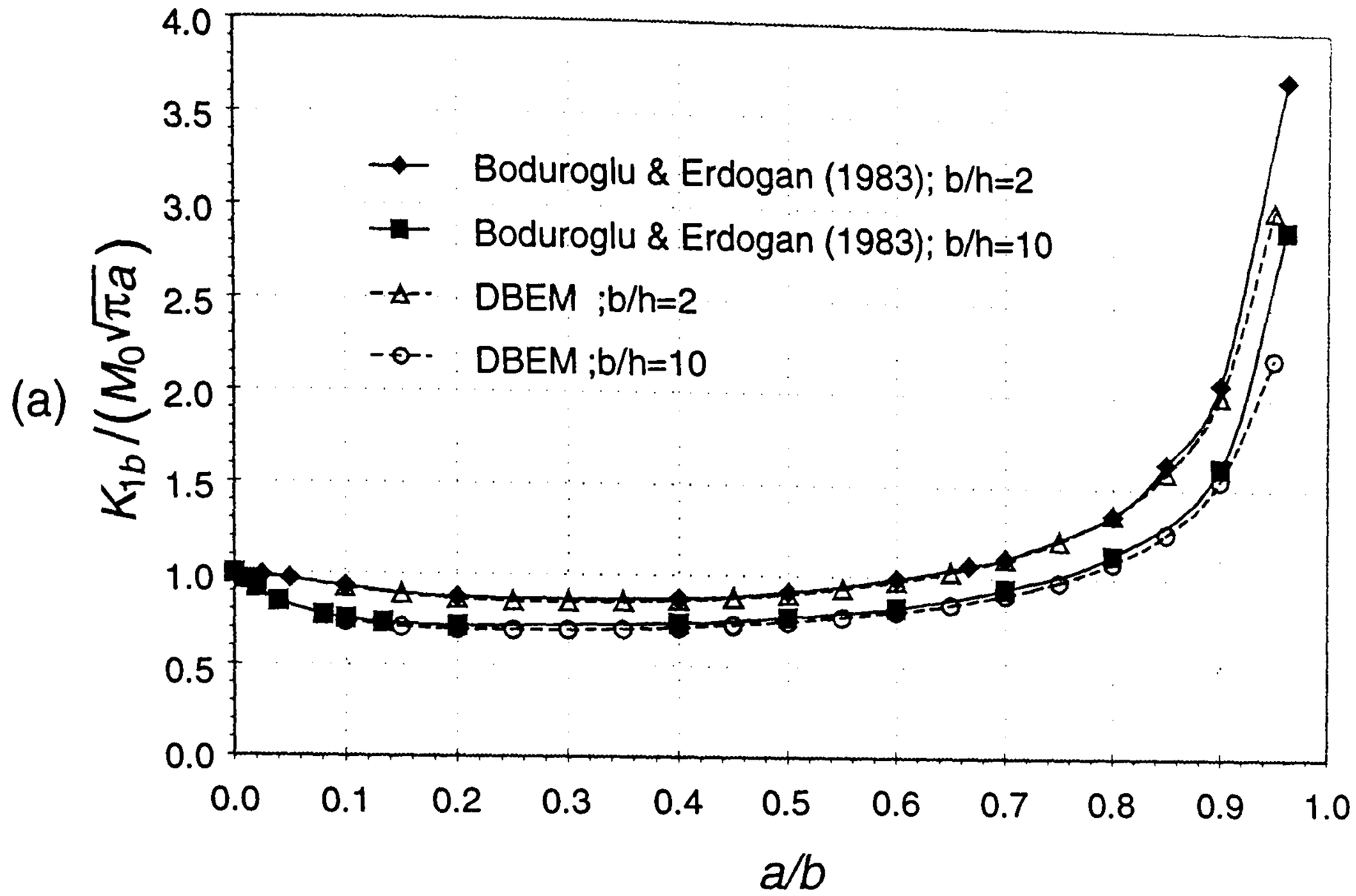

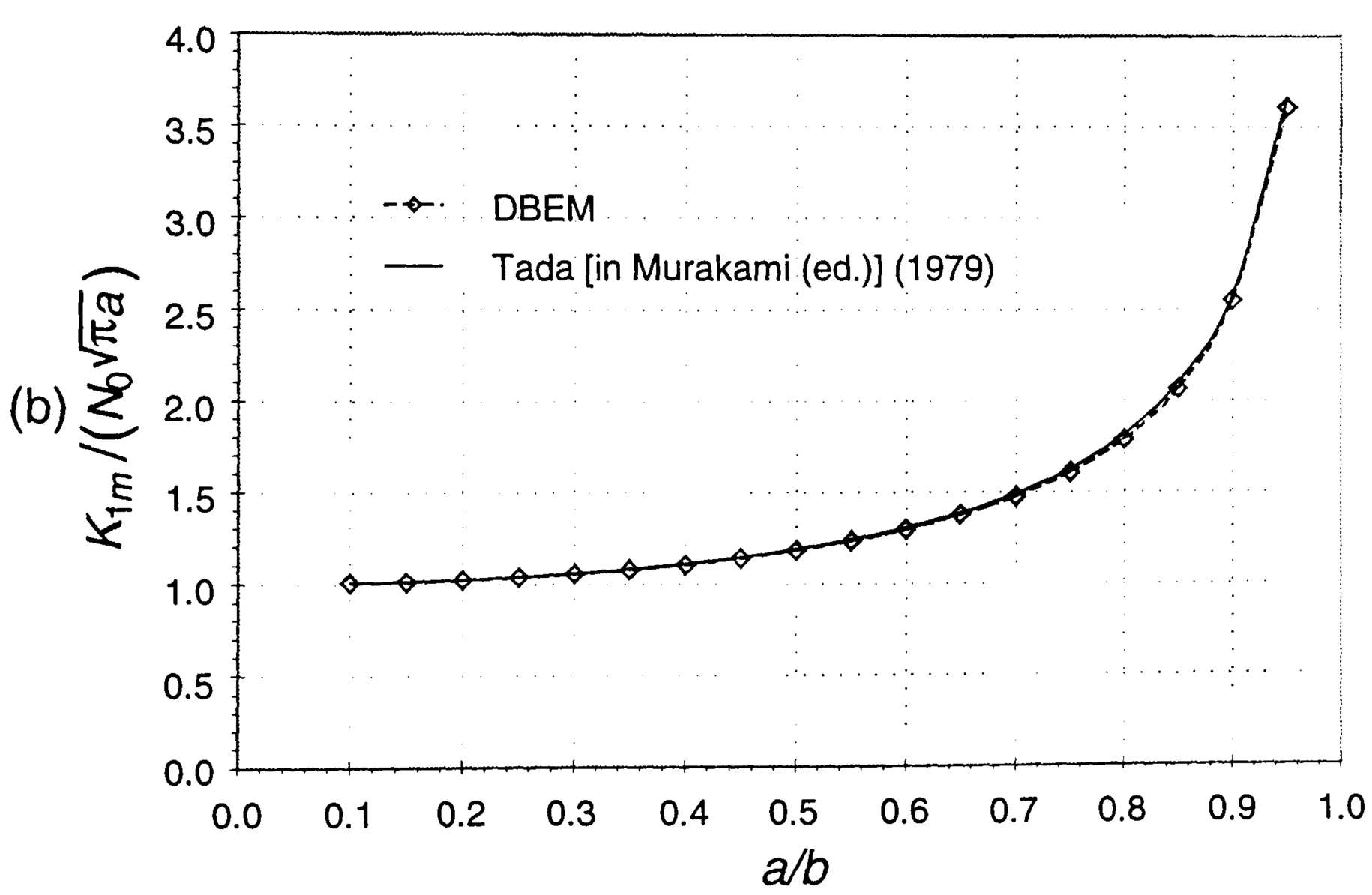

Figure 5-7: Normalised bending stress resultant intensity factors and membrane stress intensity factors results for rectangular plate with a centre crack subjected to bending and tension.

Table 5.1: Normalised SIFs for the plate with a centre crack loaded by bending and tension.

	$\frac{K_{1b}}{M_0\sqrt{\pi a}}$		$\frac{K_{1m}}{N_0\sqrt{\pi a}}$	
	$CSDE$	$J-$ integral	$CSDE$	$J-$ integral
8 elements	0.870628	0.872950	1.157324	1.194918
12 elements	0.906885	0.909564	1.187012	1.189913
16 elements	0.909715	0.910614	1.187478	1.188630
References	0.9094[33]		1.186234[86]	

Table 5.2: Effect of mesh sizes on SIFs of the plate with a centre crack loaded by bending and tension.

$l/2a$	$\frac{K_{1b}}{M_0\sqrt{\pi a}}$		$\frac{K_{1m}}{N_0\sqrt{\pi a}}$	
		Δ		Δ
0.125	0.858659	-5.580%	1.147946	-3.228%
0.100	0.870628	-4.263%	1.157324	-2.437%
0.050	0.895219	-1.559%	1.177714	-0.718%
0.025	0.906885	-0.277%	1.187012	$+0.066\%$
0.015	0.909715	$+0.035\%$	1.187478	$+0.105\%$
References	0.9094[33]		1.186234[86]	

ing and tension (as shown in Figure 5-6) is analysed. The stress intensity factors for this problem have been calculated by Boduroglu and Erdogan [33] for edge bending load and Tada [86] for tension. The properties of the plate are: $b/h = 2$ and 10; $c/b = 2$; $M_0 = N_0 b$; $Eb/N_0 = 210000$ and $\nu = 0.3$.

For BEM analysis, 8 quadratic elements per side of the plate and three different meshes using 8, 12 and 16 elements for each crack surface are used. SIFs are evaluated using both crack surface displacements extrapolation (CSDE) and $J-$ integral techniques. Table 5.1 and Figure 5-7 show the results of this example. In Table 5.1, normalised K_1 evaluated using both CSDE and $J-$ integral techniques for $a/b = 0.5$ is presented for different meshes. The results show that both CSDE and $J-$ integral techniques can achieve accurate results ($< 1\%$ difference) compare to the references

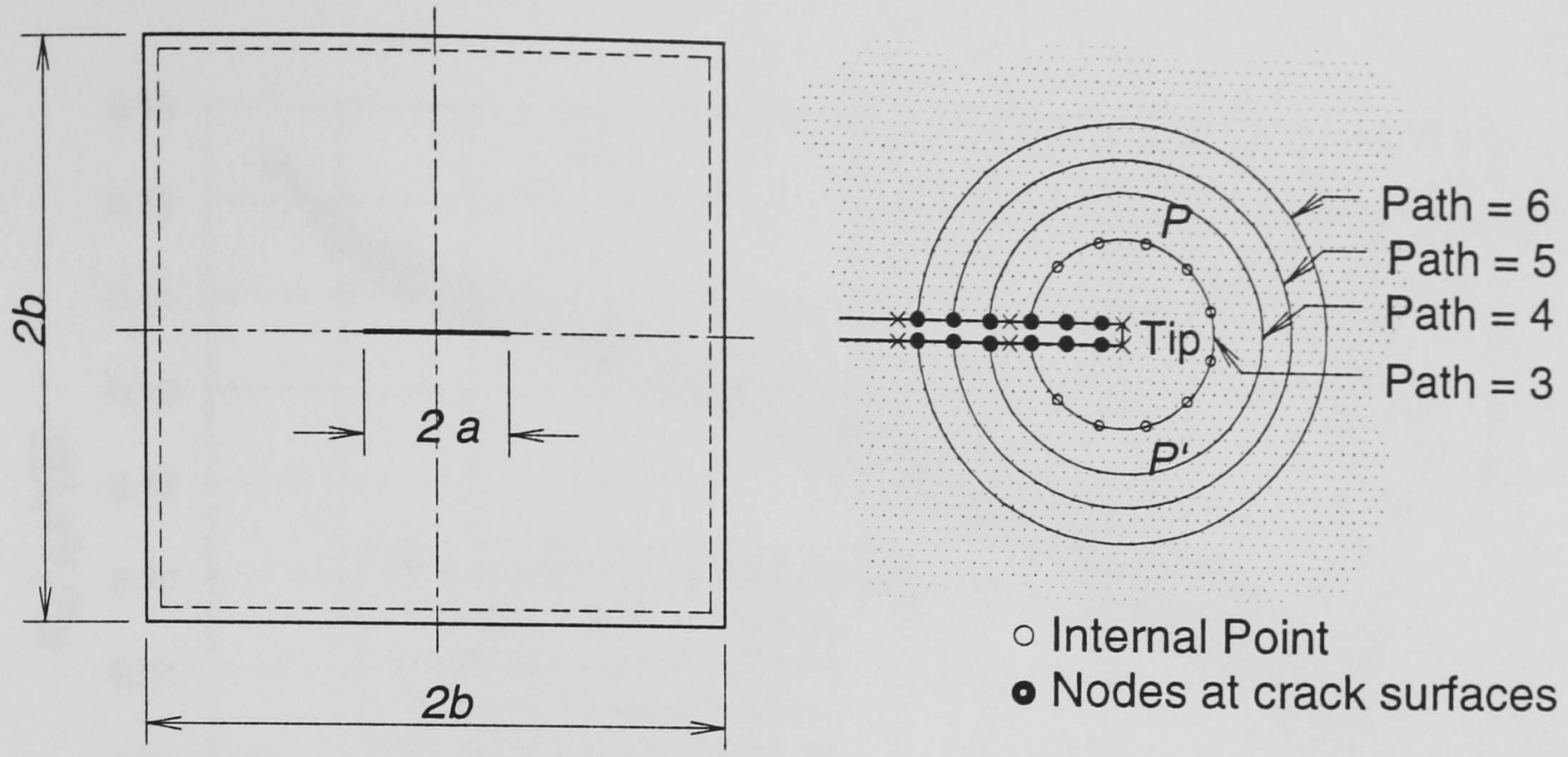

Figure 5-8: Square simply supported plate with a centre crack: uniform pressure.

[86] and [33][1]. Figure 5-7 shows normalised K_1 for different values of a/b. The DBEM results show excellent agreement with references [86] and [33] for the whole range of a/b.

The effect of different mesh sizes to the accuracy of CSDE technique is also studied. Five different meshes using 6, 8, 10, 12 and 16 elements for each crack surface are used, with ratios between crack tip element length and crack length are taken as 0.125, 0.10, 0.050, 0.025 and 0.15. All models are discretised with 8 boundary elements per side of the plate. Table 5.2 shows that 0.3% accuracy can be achieved on model with $l/2a = 0.025$ and 0.015.

5.5.2 Simply supported square plate with a centre crack: uniform pressure

In this example, a simply supported square plate with a centre crack loaded by uniform pressure (as shown in Figure 5-8) is analysed. This configuration is important for aircraft structures, as it represents a simplified fuselage or wing panel. The bending and shear stress intensity factors for this problem have been calculated by Sosa

[1]It is worth mentioning that Boduroglu and Erdogan [33] used normalisation factor $M_0\sqrt{a}$ instead of $M_0\sqrt{\pi a}$ in their formulation, and Tada [86] solution is for two-dimensional problem, therefore the normalisation factor used is $\sigma_0\sqrt{\pi a}$. However, normalised K obtained in [33] and [86] can be compared to the present results.

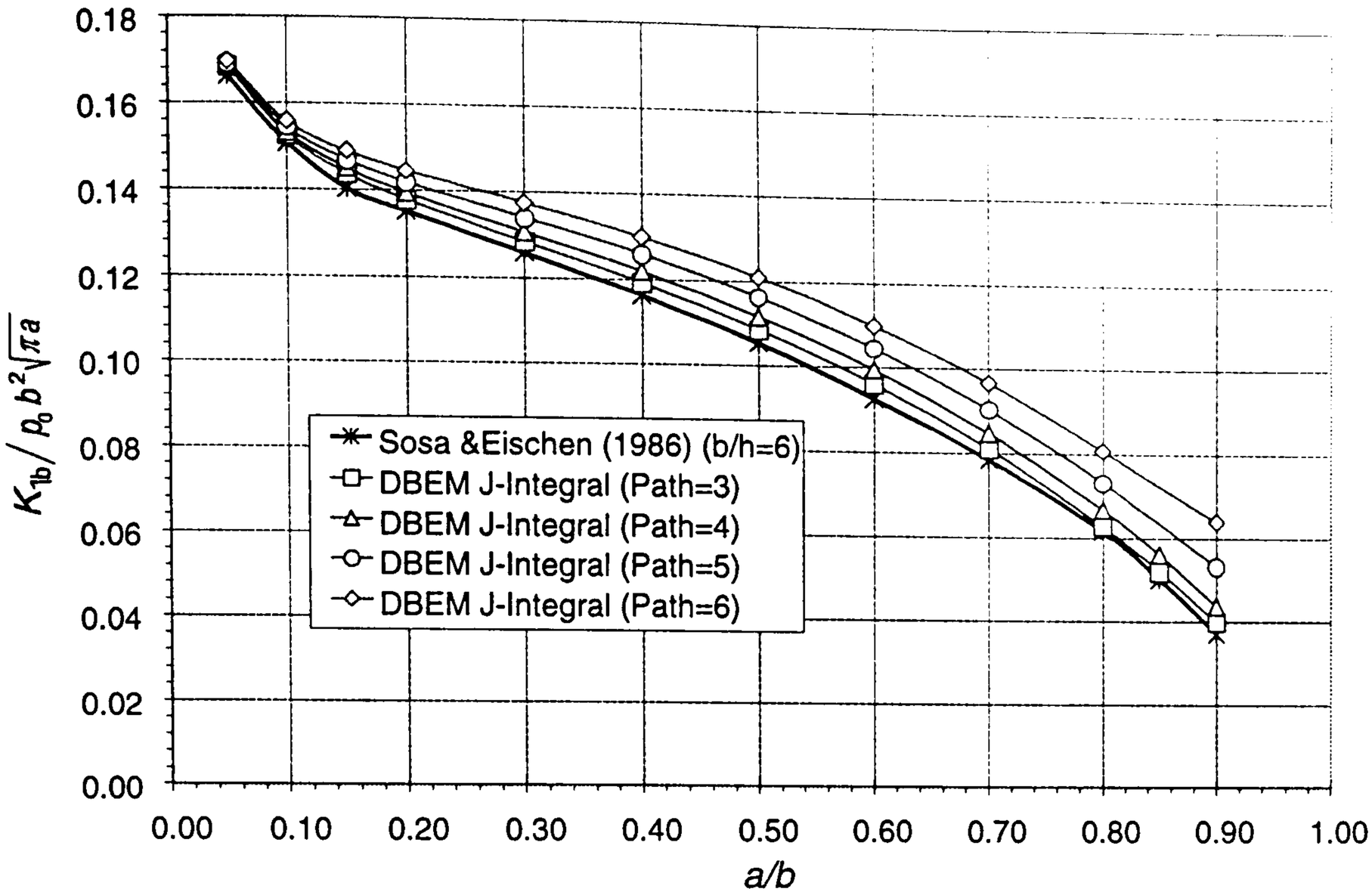

(a) 4 elements per side; 8 elements for each crack surface

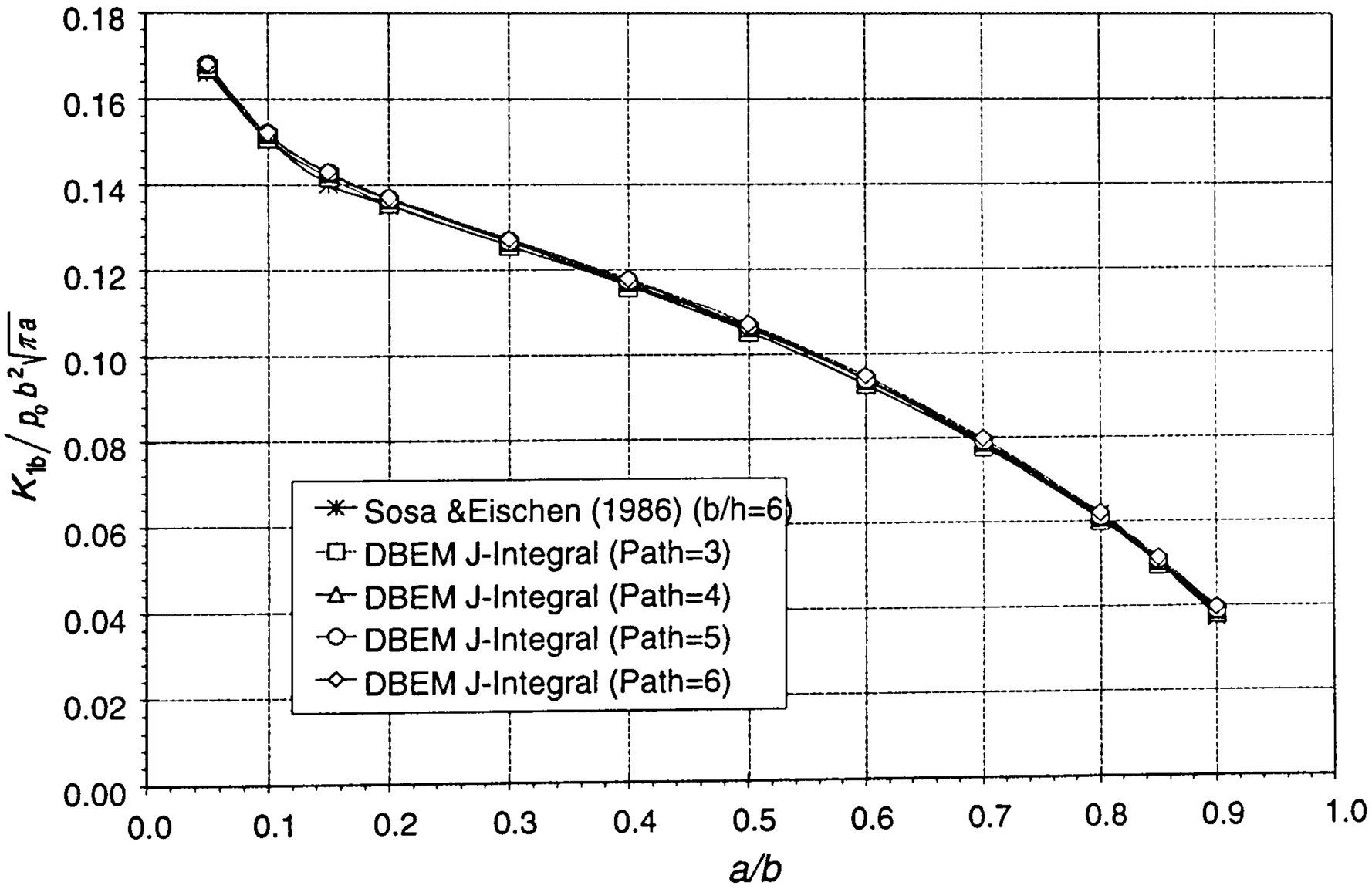

(b) 8 elements per side; 16 elements for each crack surface

Figure 5-9: Effect of different path of $J-$ integral to the normalised bending stress resultant intensity factors.

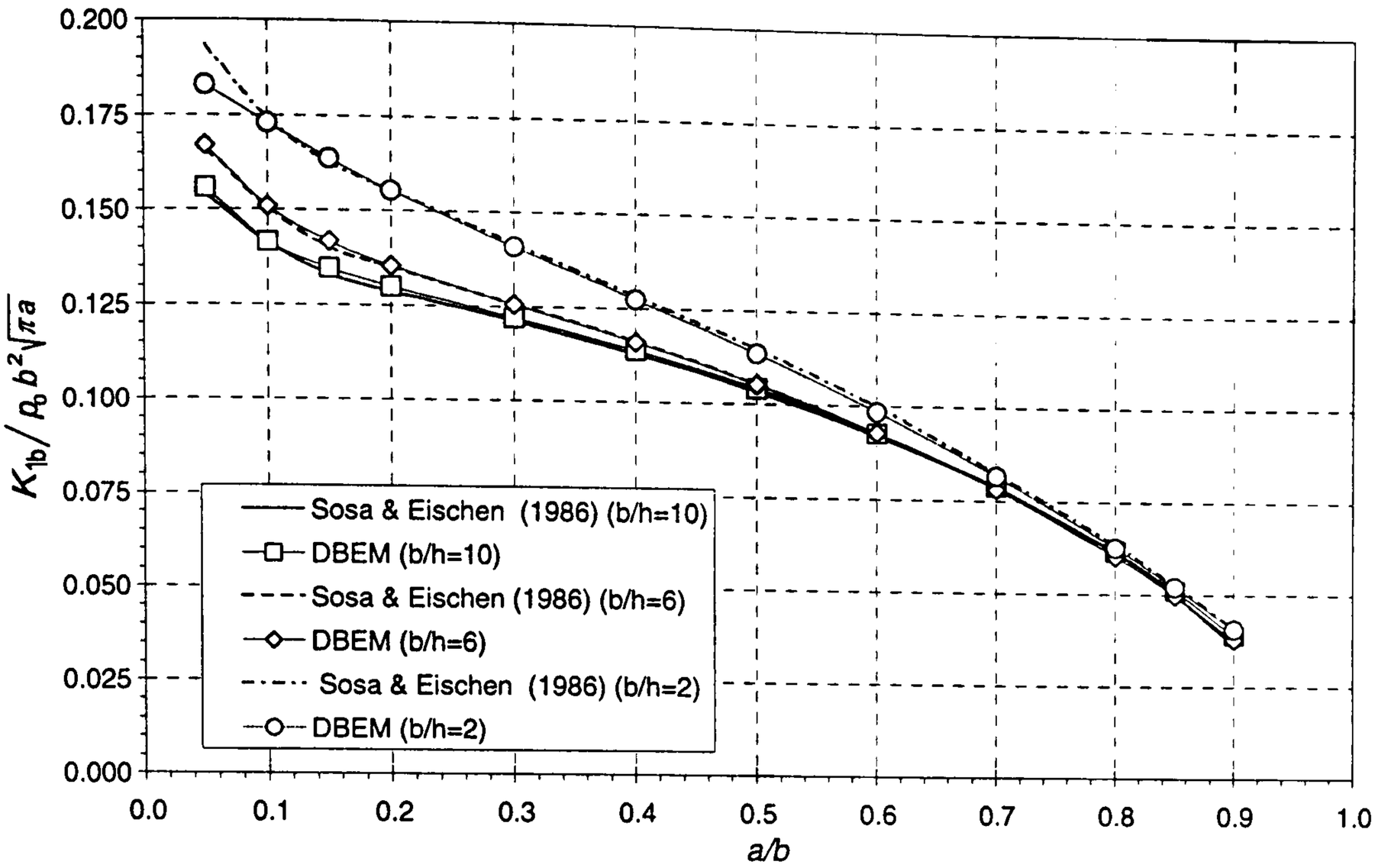

Figure 5-10: Normalised bending stress resultant intensity factors for a plate with a centre crack subjected to uniform pressure.

and Eischen [121]. The properties of this plate are: $b = 1$; $E = 1000$ and $\nu = 0.3$. Three different ratios between width and thickness modelled are $b/h = 2$, 6 and 10.

For analysis, 2 different meshes are used. The first model is meshed by 4 elements per side of the plate and 8 elements for each crack surface, while for the second model 8 elements per side of the plate and 16 elements for each crack surface are used.

To study the effect of different paths of $J-$ integral technique, the stress intensity factors are evaluated using several different integration paths as shown in Figure 5-8. Figures 5-9 – 5-10 show the results of this example. It can be seen in Figure 5-9(a) that for the model with a very coarse mesh, different path of the $J-$ integral tend to give divergence result for the bending stress resultant intensity factor, but using more elements on the second model with different path of the $J-$ integral does not have much effect on the results. As shown in Figure 5-9(b), results obtained from all paths are within 1.5% of the reference solutions.

Figure 5-10 shows the normalised bending stress resultant intensity factors for different plate thickness. The bending stress intensity factor is evaluated using 32 internal points on a circular path starting and ending at the third node from the

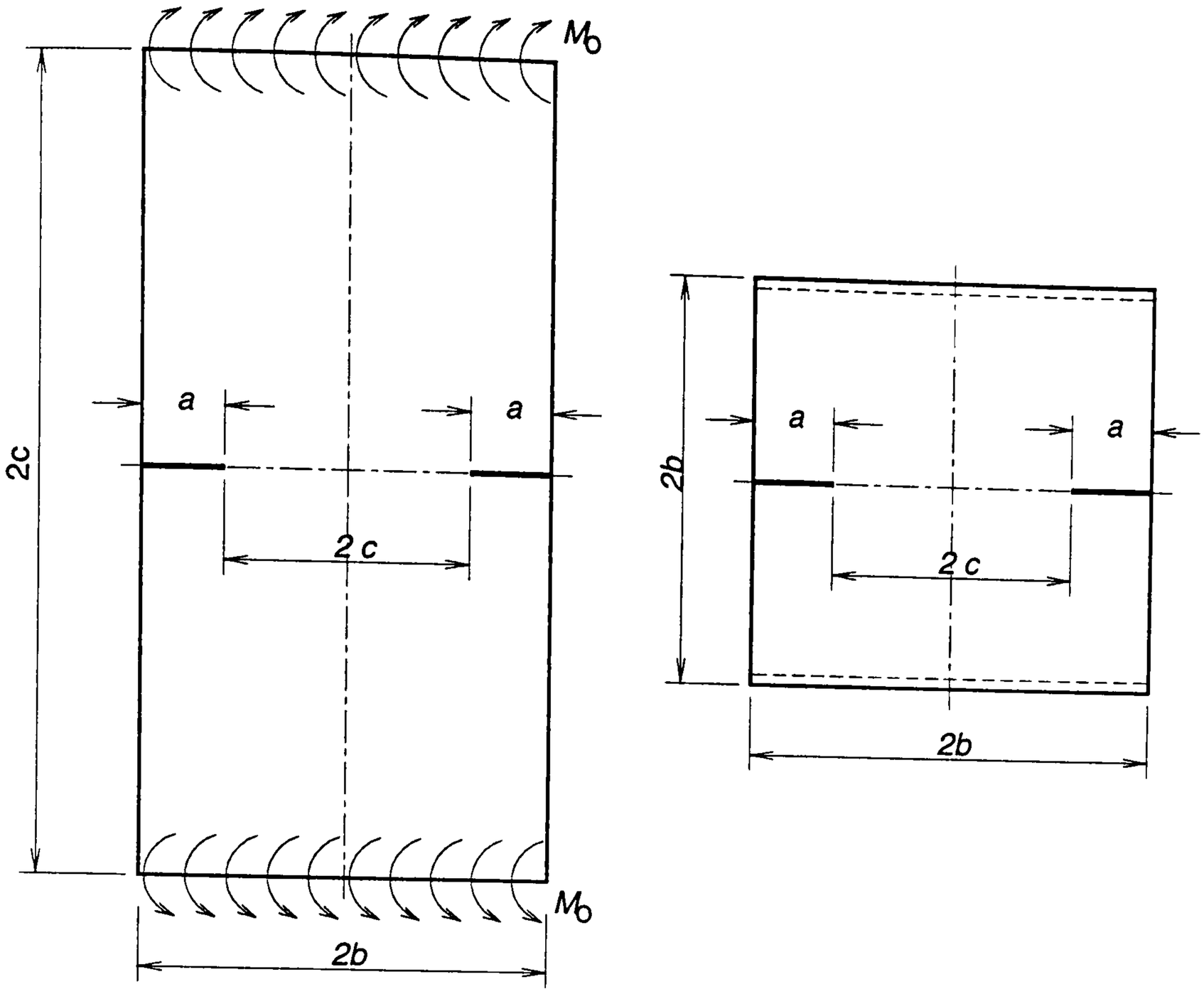

(a) bending load

(b) simply supported on two side, uniform pressure

Figure 5-11: Symmetric double edge cracks in a plate

crack tip (path=3 in Figure 5-8). As it can be seen, the results are in good agreement with those presented by Sosa and Eischen [121].

5.5.3 A plate with symmetric double edge cracks

In this example, a plate with symmetric double edge cracks as shown in Figure 5-11 is analysed. Two configuration are considered here: (a) rectangular plate loaded by bending with $b = 1$; $c/b = 2$; $Eb^2/M_0 = 1000$ and $\nu = 0.3$; and (b) square plate simply supported on two side and subjected to uniform pressure with $b = 1$; $E/p_0 = 1000$ and $\nu = 0.3$. The first case was solved by Boduroglu and Erdogan [33] while the second case has been analysed by Sosa and Eischen [121]. Three different ratios of width to thickness are analysed, that are $b/h = 2$, 6 and 10. For analysis, 8 elements per side of the plate and 16 elements for each crack surface are used.

Figures 5-12 – 5-13 show the results of this example. It can be seen from the

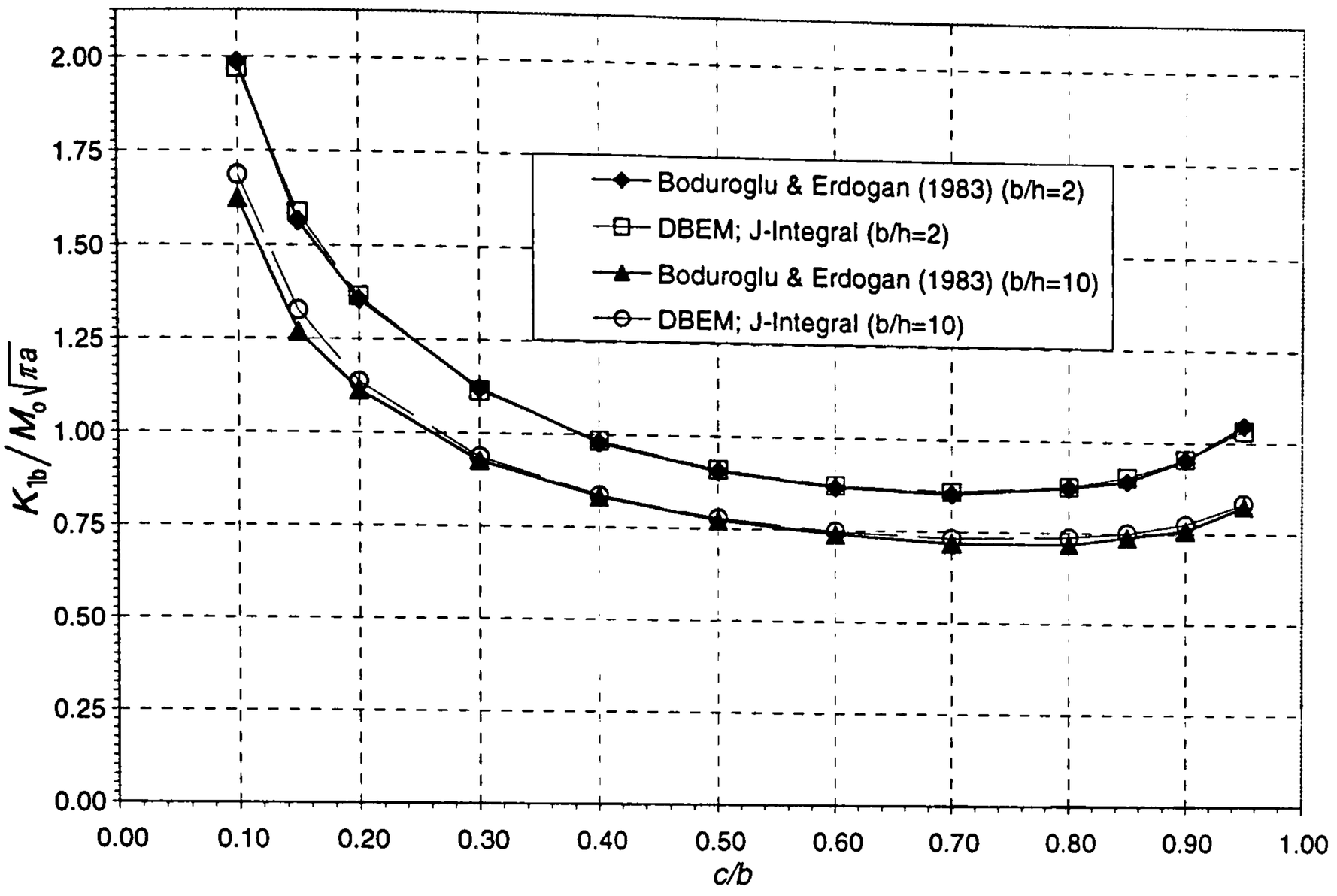

Figure 5-12: Normalised bending stress resultant intensity factors for a plate with symmetric double edge cracks subjected to bending load.

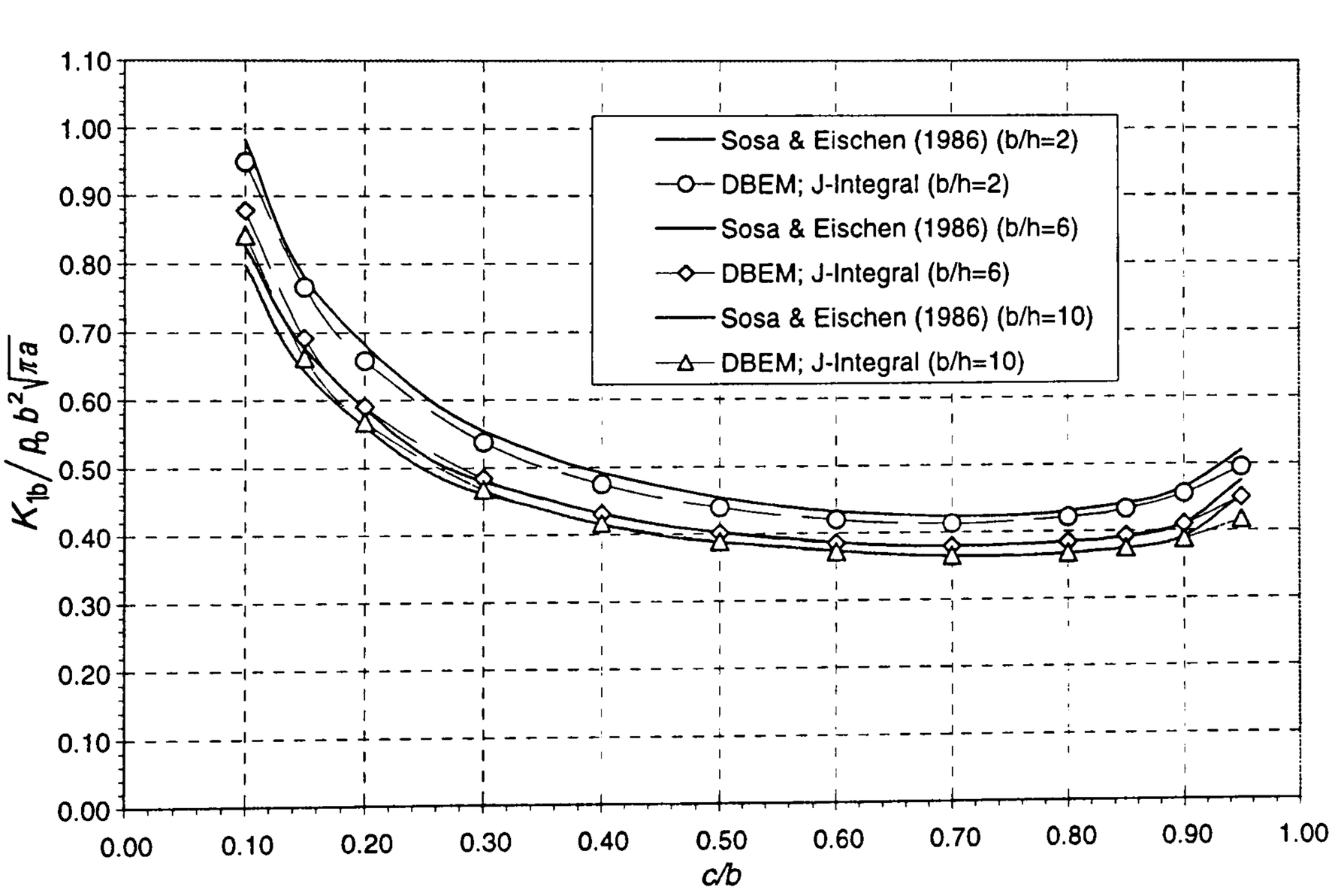

Figure 5-13: Normalised bending stress resultant intensity factors for a plate with symmetric double edge cracks subjected to uniform pressure.

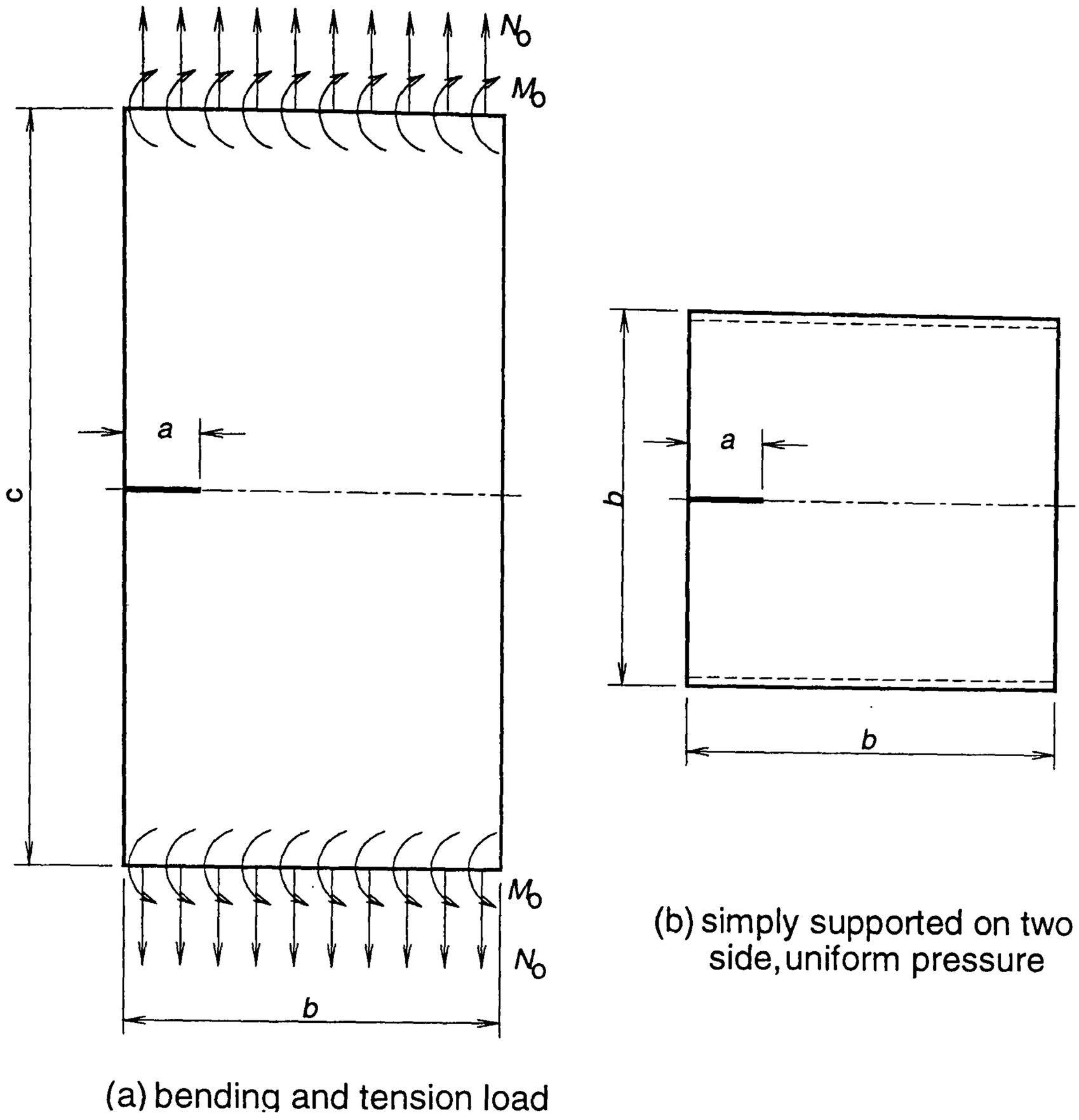

(a) bending and tension load

(b) simply supported on two side, uniform pressure

Figure 5-14: Single edge crack in a plate.

Figures that the present results are in good agreements with those presented in Boduroglu and Erdogan [33], and Sosa and Eischen [121] for the first and second configuration respectively.

5.5.4 A plate with an edge crack

In this example, a plate with an edge crack as shown in Figure 5-14 are analysed. Two configuration are considered here: (a) loaded by tension and bending $b = 1$; $c/b = 2$; $Eb/N_0 = 210000$; $M_0 = bN_0$ and $\nu = 0.3$; and (b) simply supported on two side and subjected to uniform pressure. The properties of this plate are: $b = 1$; $E/p_0 = 21000$ and $\nu = 0.3$. Two different ratios between width and thickness are modelled, that are $b/h = 2$ and 10. This model is discretised into 8 elements per

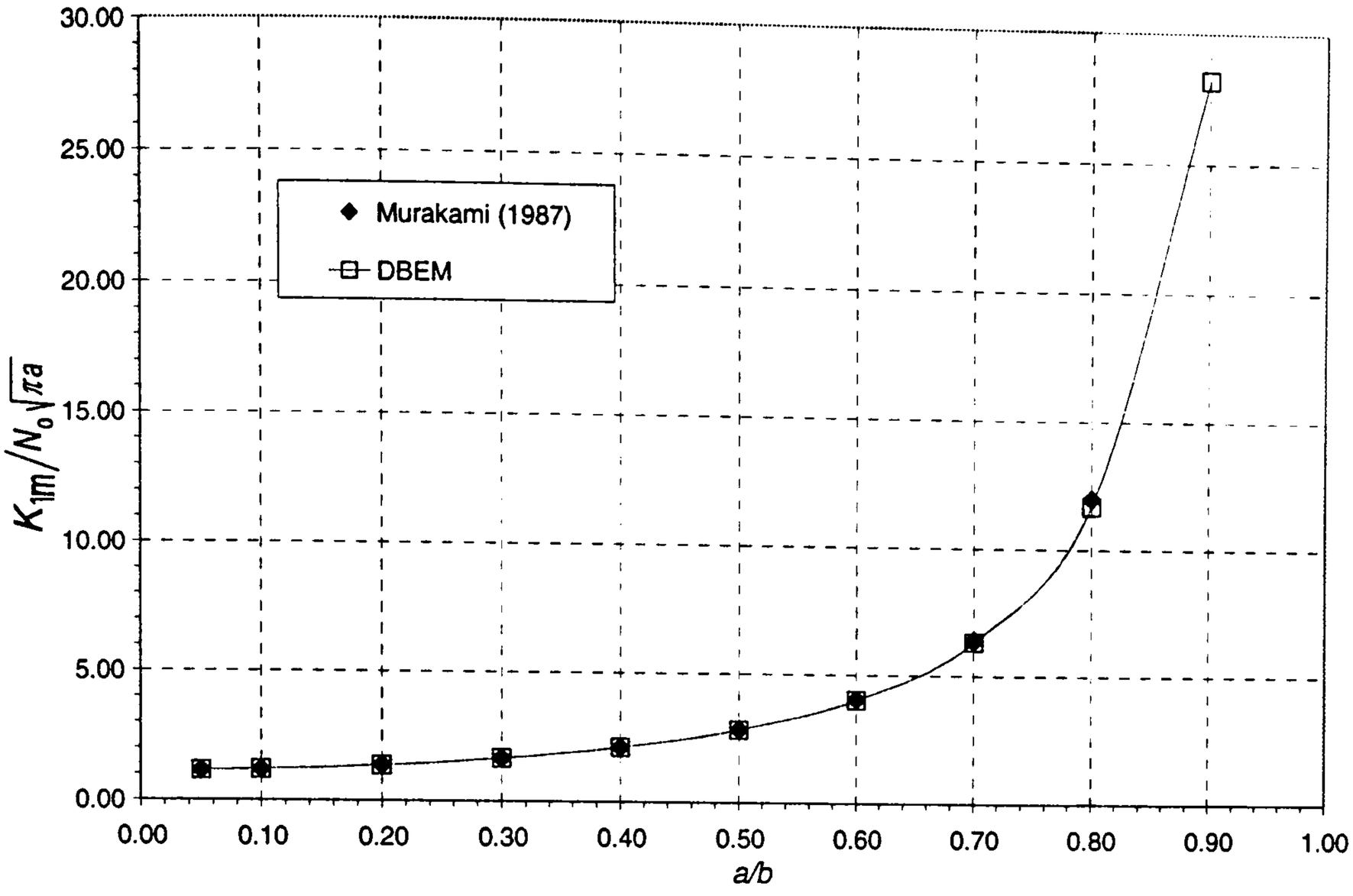

Figure 5-15: Normalised membrane stress resultant intensity factors for a plate with a single edge crack subjected to bending and tension load.

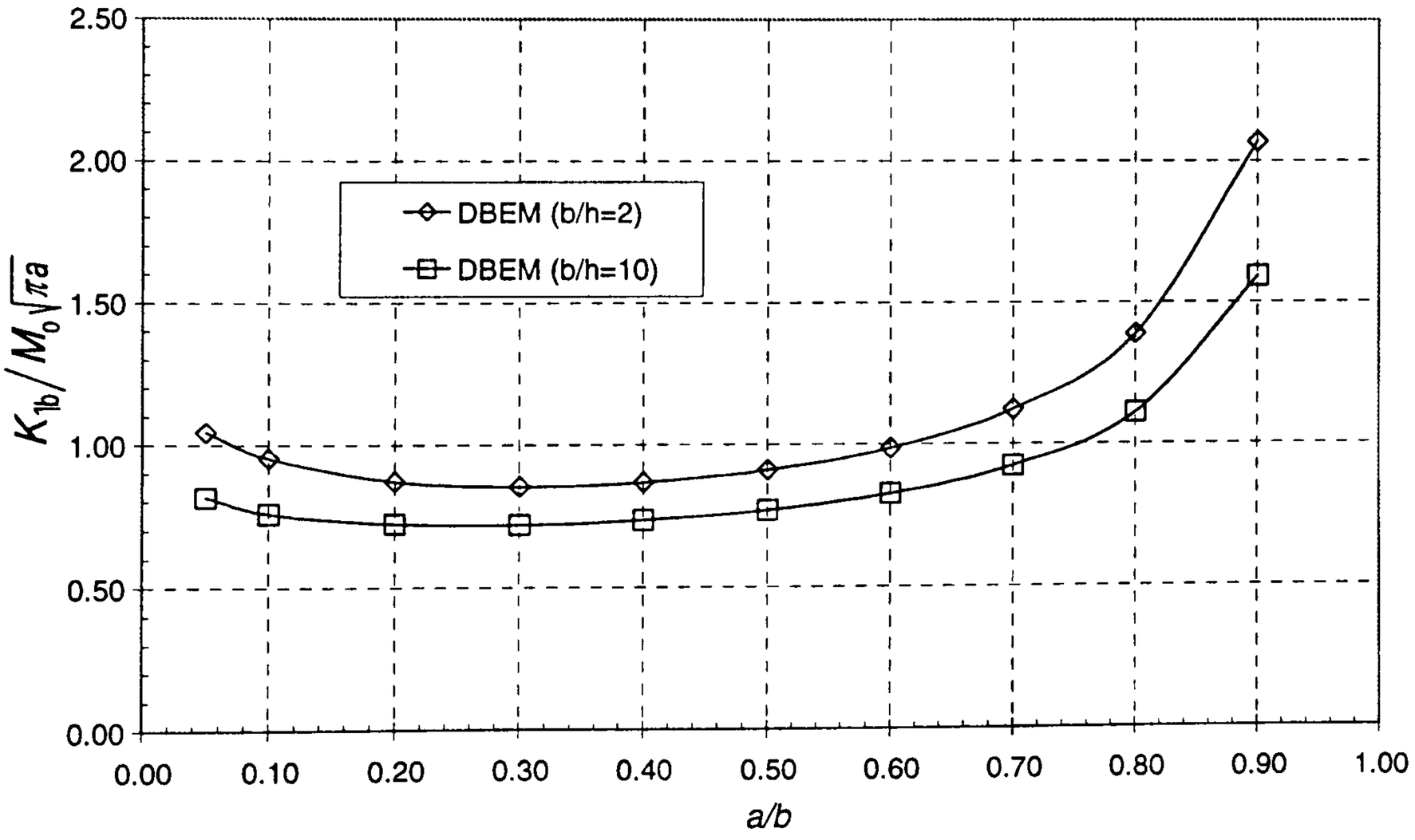

Figure 5-16: Normalised bending stress resultant intensity factors for a plate with a single edge crack subjected to bending load.

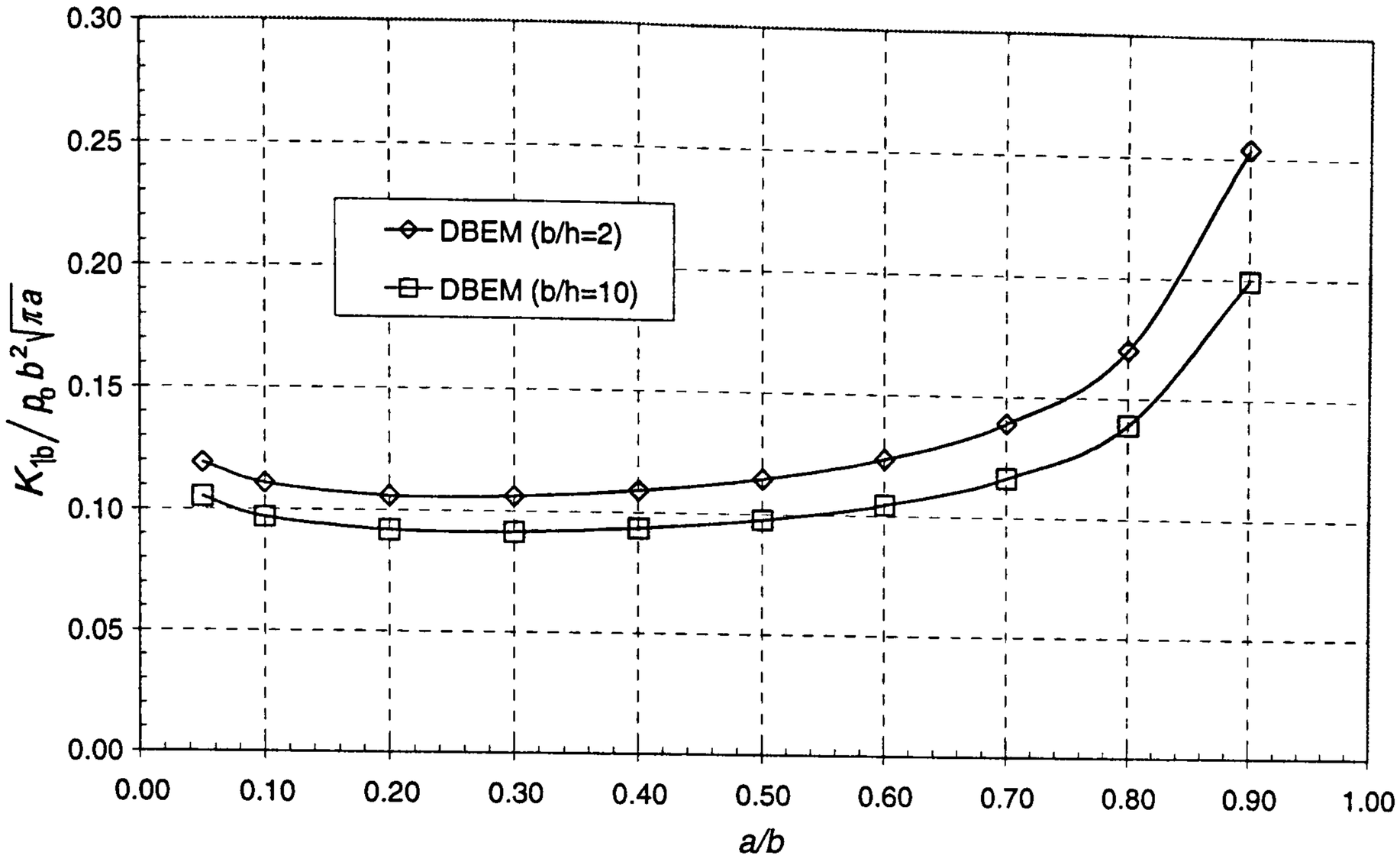

Figure 5-17: Normalised bending stress resultant intensity factors for a plate with a single edge crack subjected to uniform pressure.

side of the plate and 16 elements for each crack surface.

Figures 5-15 – 5-17 show the results of this example. It can be seen in Figures that the present results are in good agreement with results presented by Murakami [86] for the membrane stress resultant intensity factors. Bending stress resultant intensity factors are not available in the literature. Comparing the results with symmetric edge cracks, the bending stress resultant intensity factors do not differ much on both configurations.

5.5.5 A single crack emanating from a hole in a finite width plate

In this example, a single crack emanating from a hole in a finite width plate as shown in Figure 5-18 is analysed. Two configurations are considered here: (a) rectangular plate loaded by tension and bending with $b = 1$; $c/b = 2$; $Eb/N_0 = 210000$ and $\nu = 0.3$; and (b) square plate simply supported on two side and subjected to uniform pressure with $b = 1$; $E/p_0 = 210000$ and $\nu = 0.3$. Three different hole sizes are analysed, those are $r/b = 0.1$, 0.25, and 0.5, with four different width to thickness ratios $b/h = 2$, 4, 10 and 50.

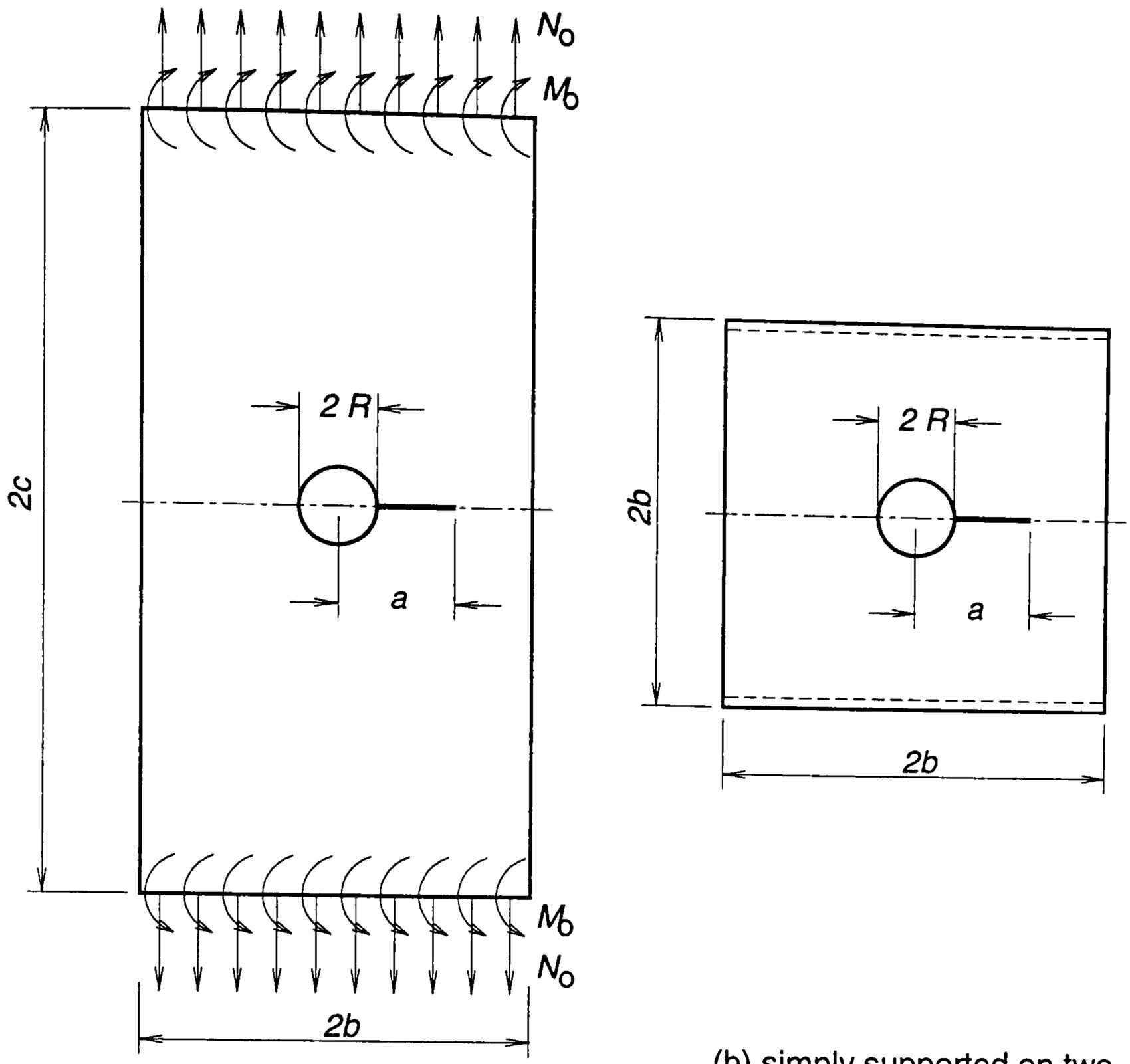

(a) bending and tension load

(b) simply supported on two side, uniform pressure

Figure 5-18: A crack emanating form a hole in a finite width plate.

All models are discretised into 8 elements per side of the plate. To study the convergence of the results, a case with $r/W = 0.25$ and $a/W = 0.4$ is analysed using several different meshes on the crack surfaces. The convergence test results are shown in Figure 5-19. As it can be seen, convergence within $< 1\%$ accuracy for K_{1b} can be achieved after the crack surfaces are modelled using 20 elements for each crack surface, while convergence for K_{1m} is obtained with less elements. Other configurations are modelled using 20 element for each crack surfaces. The hole is modelled using 10 elements except for the case with $r/W = 0.5$ and $a/W \leqslant 0.55$, the hole is modelled with 16 elements. Figures 5-20 – 5-22 show the results of this example. In the case of short cracks in a very thick plate ($b/h = 2$ and $a/r \leqslant 1.5$), the results are not satisfactory and the problem should be modelled as a three-

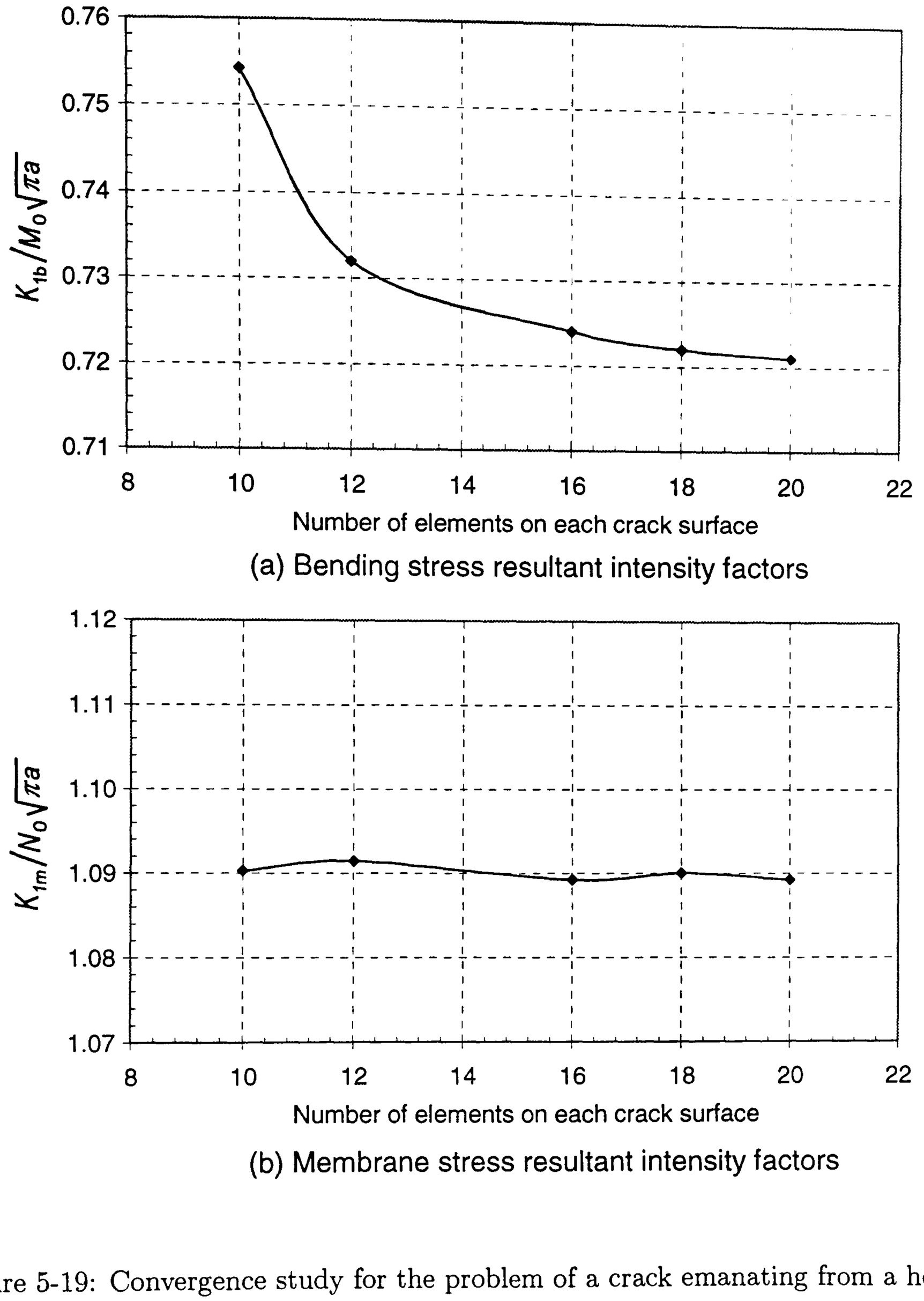

Figure 5-19: Convergence study for the problem of a crack emanating from a hole.

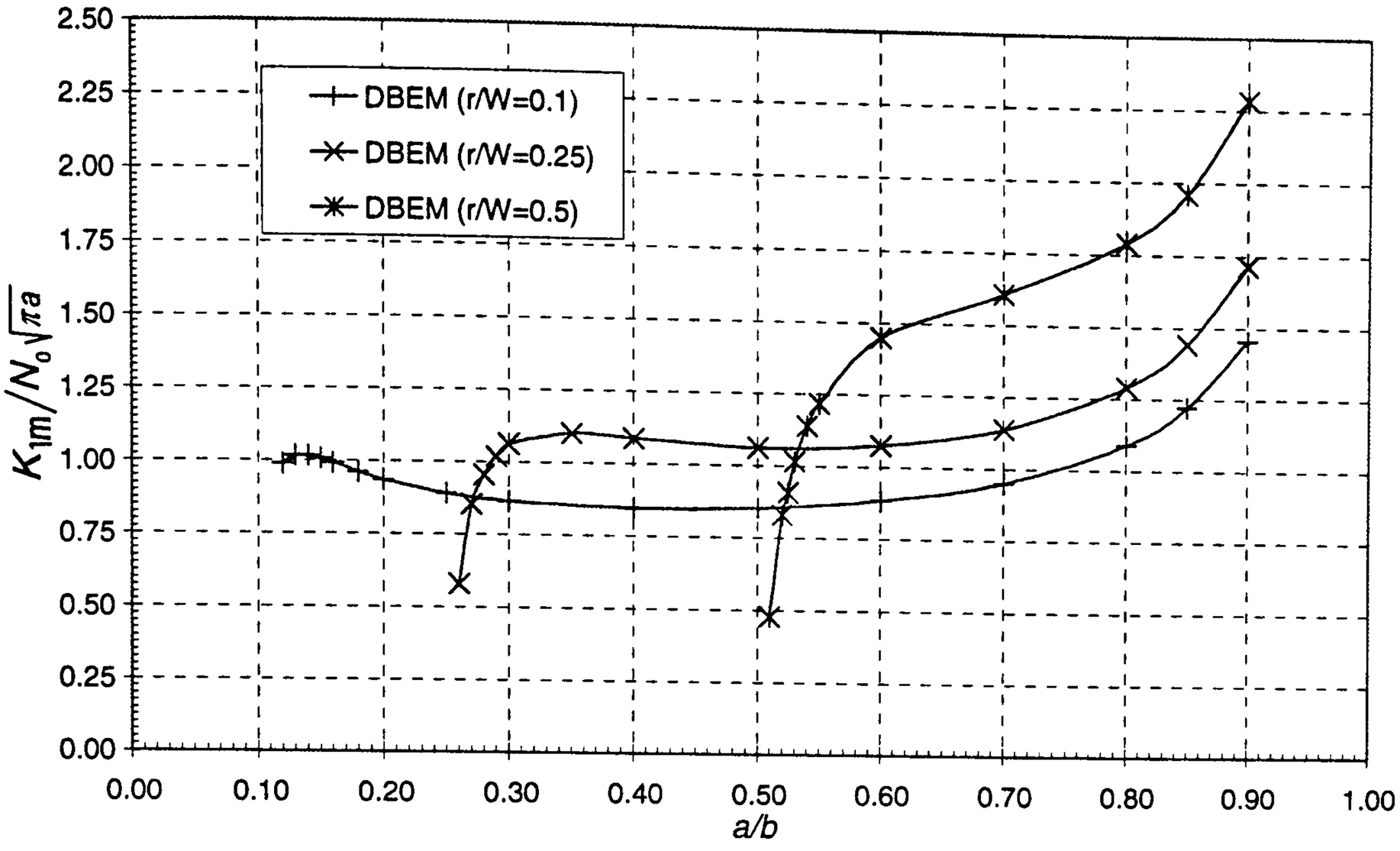

Figure 5-20: Normalised membrane stress resultant intensity factors for a crack emanating from a hole in a finite width plate subjected to bending and tension load.

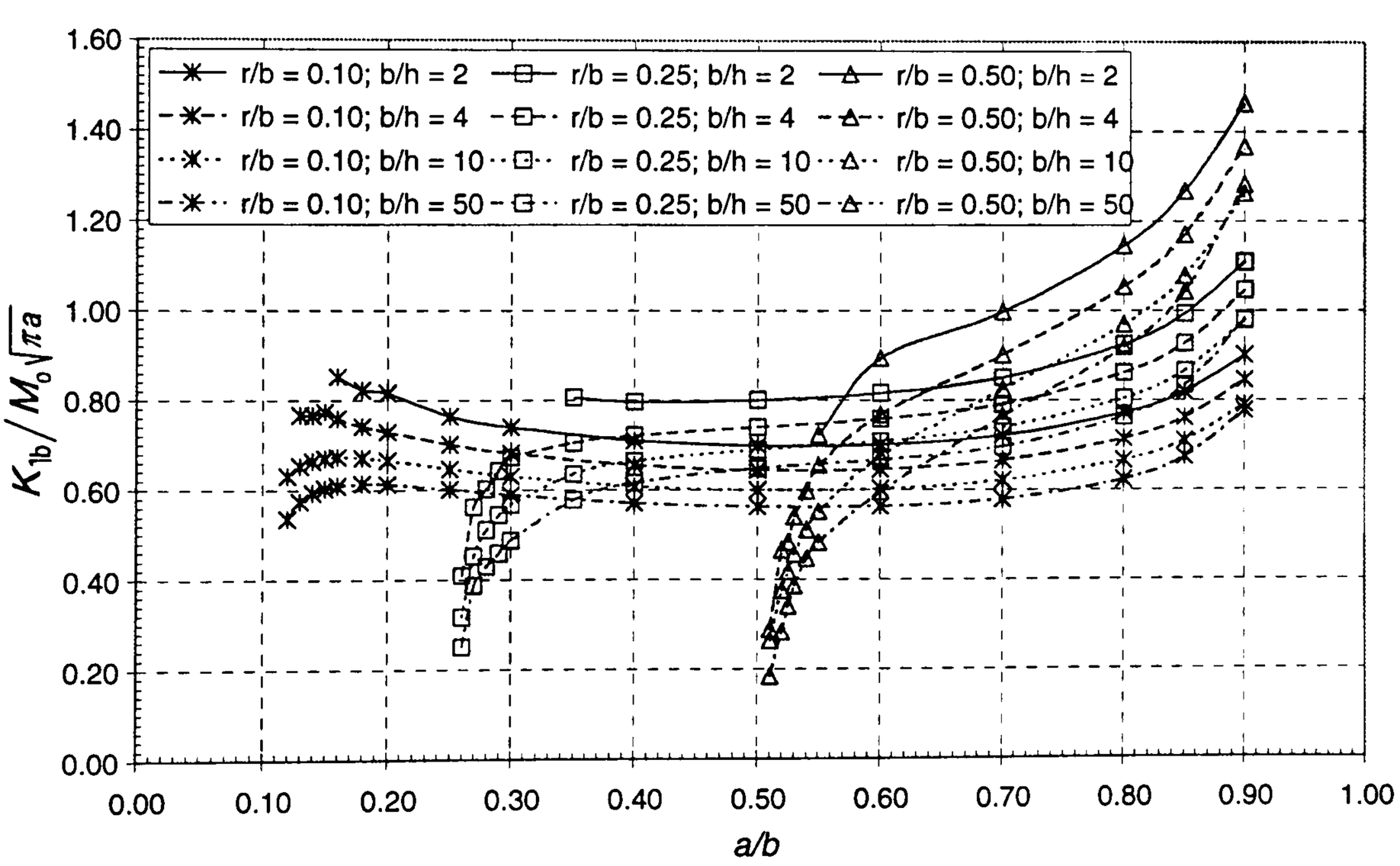

Figure 5-21: Normalised bending stress resultant intensity factors for a crack emanating from a hole in a finite width plate subjected to bending and tension load.

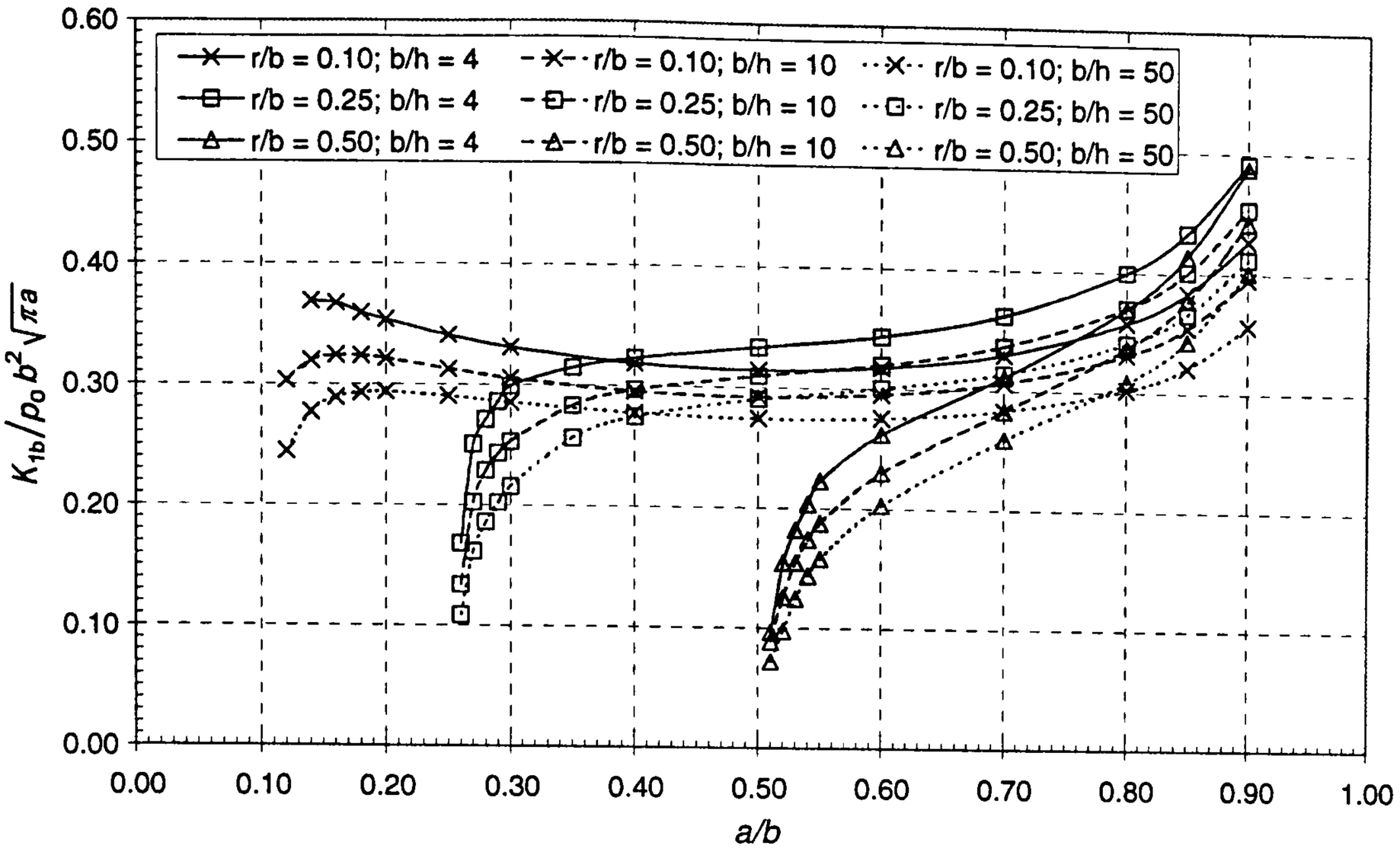

Figure 5-22: Normalised bending stress resultant intensity factors for a crack emanating from a hole in a finite width plate subjected to uniform pressure.

dimensional model.

5.5.6 Two symmetric cracks emanating from a hole in a finite width plate

In this example, two symmetric cracks emanating from a hole in a finite width plate as shown in Figure 5-23 is analysed. Two configuration are considered here: (a) rectangular plate loaded by tension and bending with $b = 1$; $c/b = 2$; $Eb/N_0 = 210000$ and $\nu = 0.3$; and (b) square plate simply supported on two side and subjected to uniform pressure with $b = 1$; $E/p_0 = 210000$ and $\nu = 0.3$. Three different hole sizes $r/b = 0.1$, $r/b = 0.25$, and $r/b = 0.5$, with four different width to thickness ratios $b/h = 2$, $b/h = 4$, $b/h = 10$ and $b/h = 50$ are analysed. Normalised stress intensity factors for a plate loaded by tension is available in Murakami [86].

Figures 5-24 – 5-26 show the results of this example. In the case of short cracks in a very thick plate ($b/h = 2$ and $a/r \leqslant 1.5$), the results are not satisfactory and the problem should be modelled as a three-dimensional model.

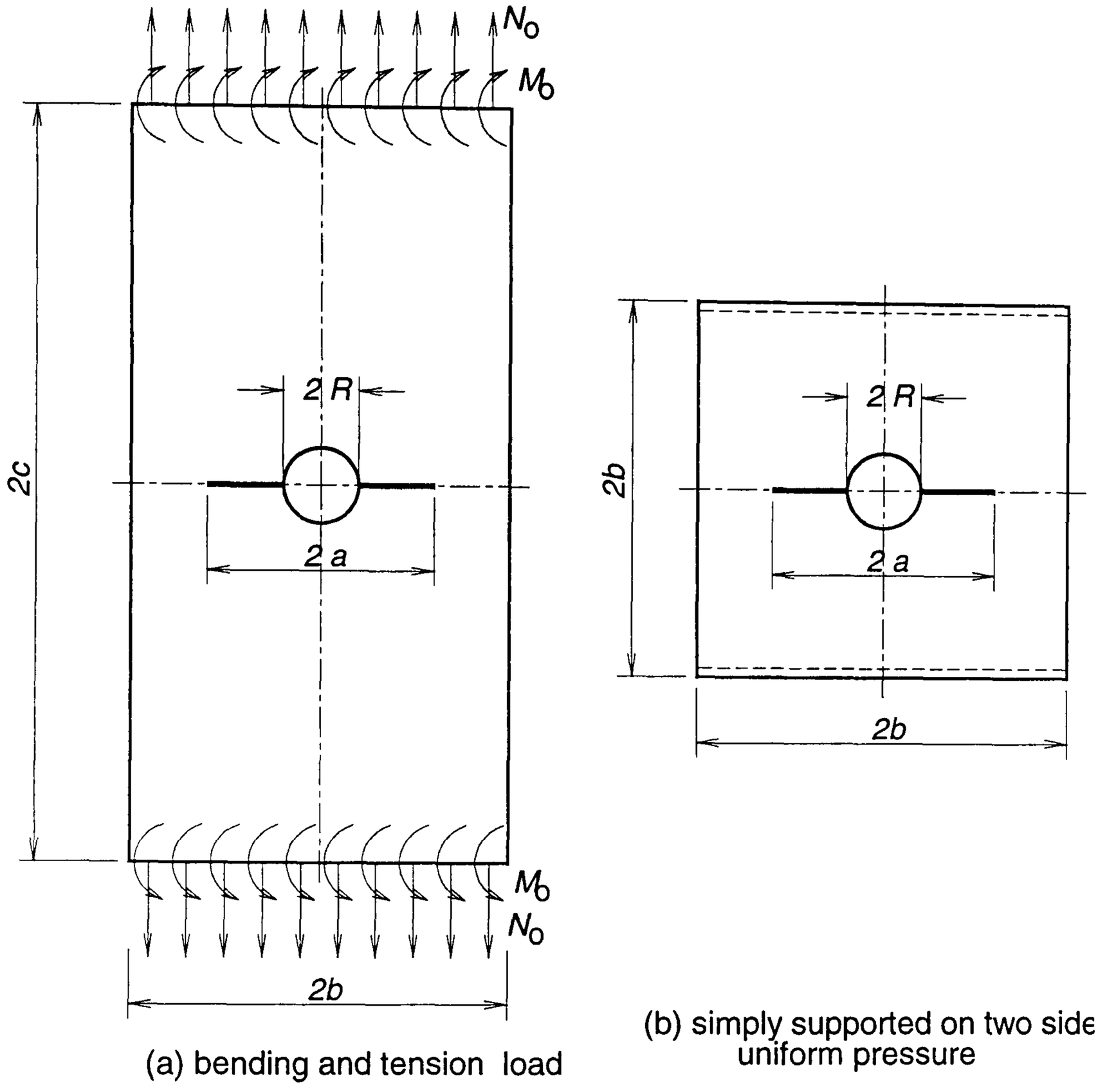

(a) bending and tension load

(b) simply supported on two side uniform pressure

Figure 5-23: Two symmetric cracks emanating form a hole in a finite width plate

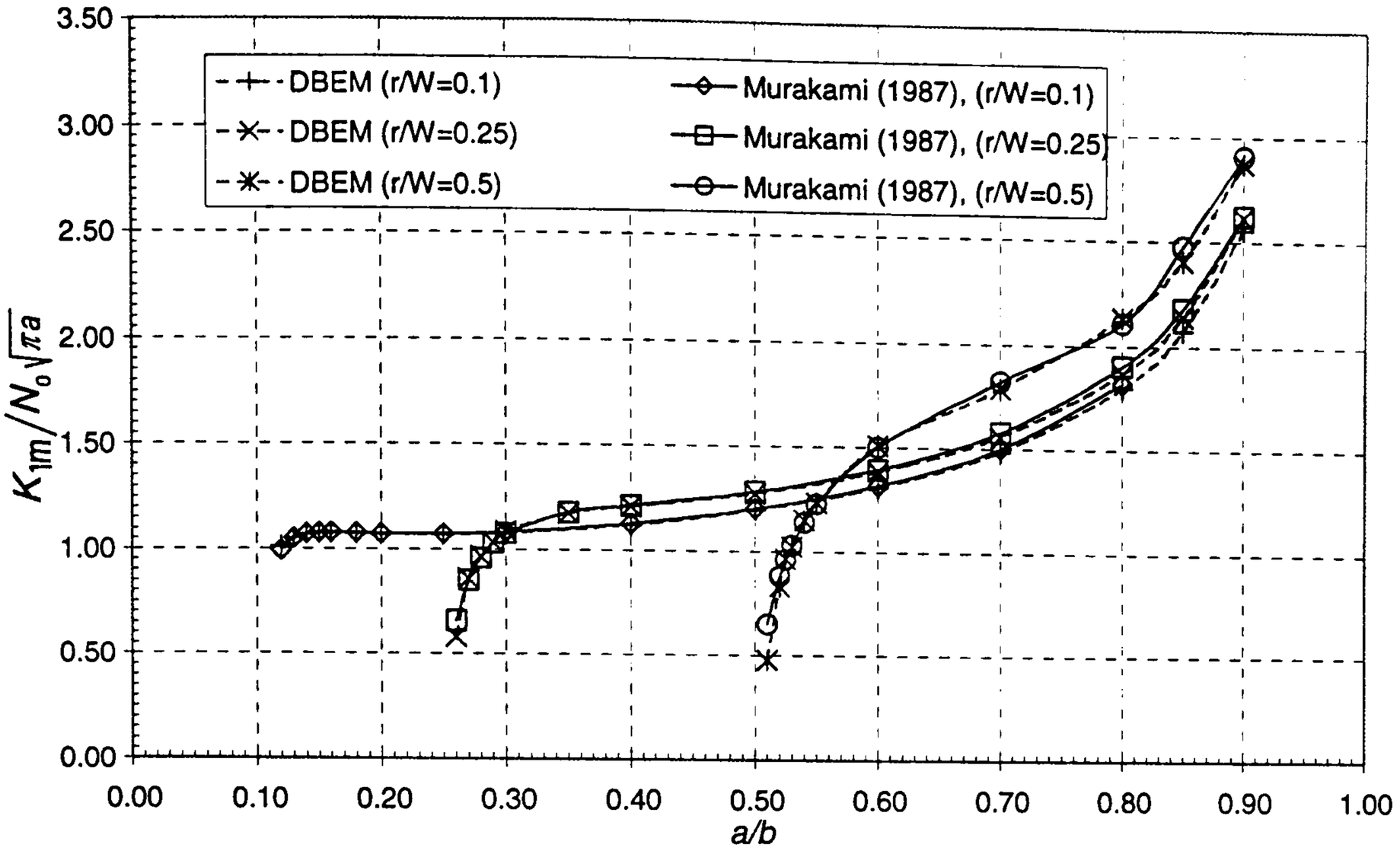

Figure 5-24: Normalised membrane stress resultant intensity factors for two symmetric cracks emanating from a hole in finite width plate subjected to bending and tension load.

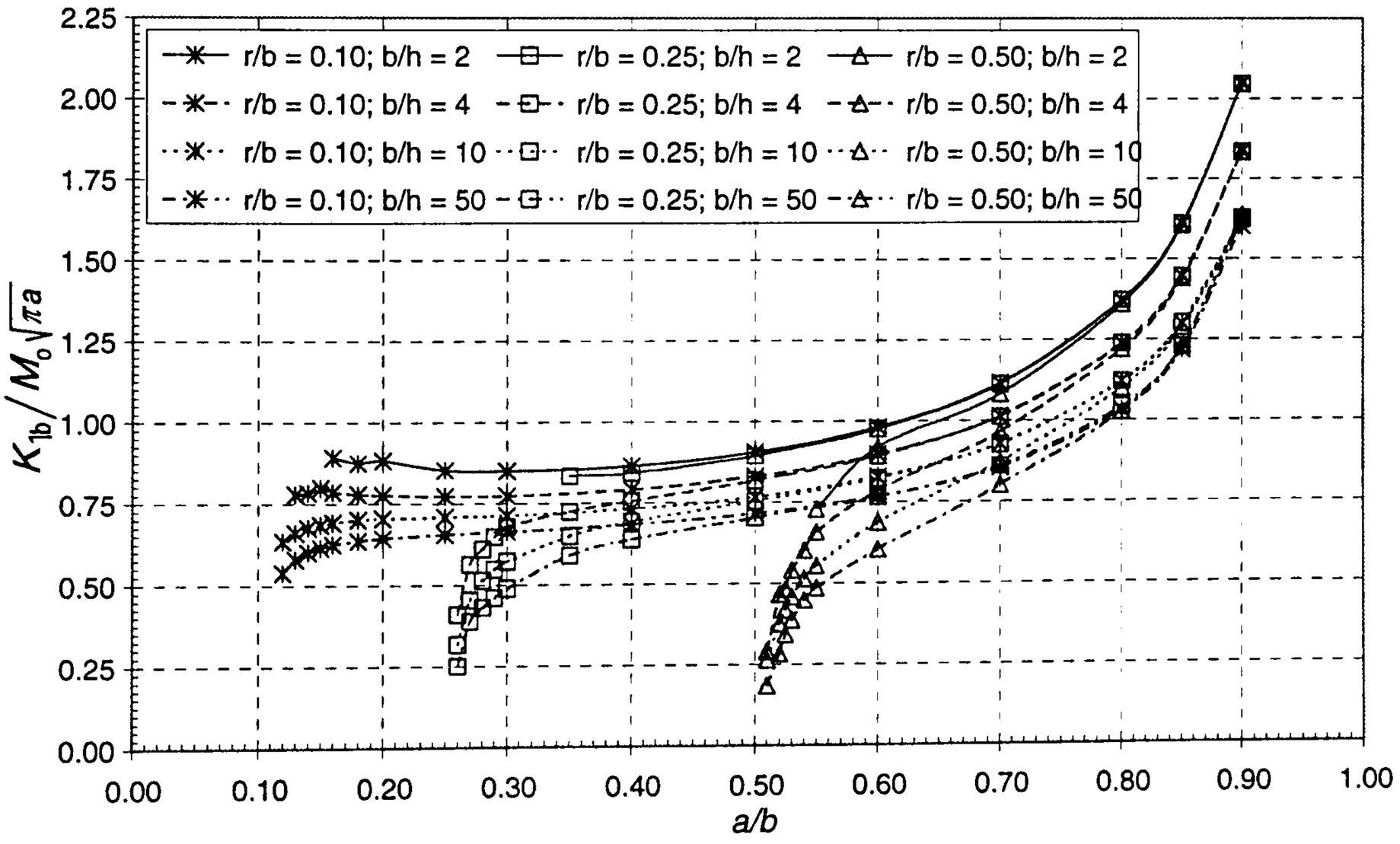

Figure 5-25: Normalised bending stress resultant intensity factors for two symmetric cracks emanating from a hole in finite width plate subjected to bending and tension load.

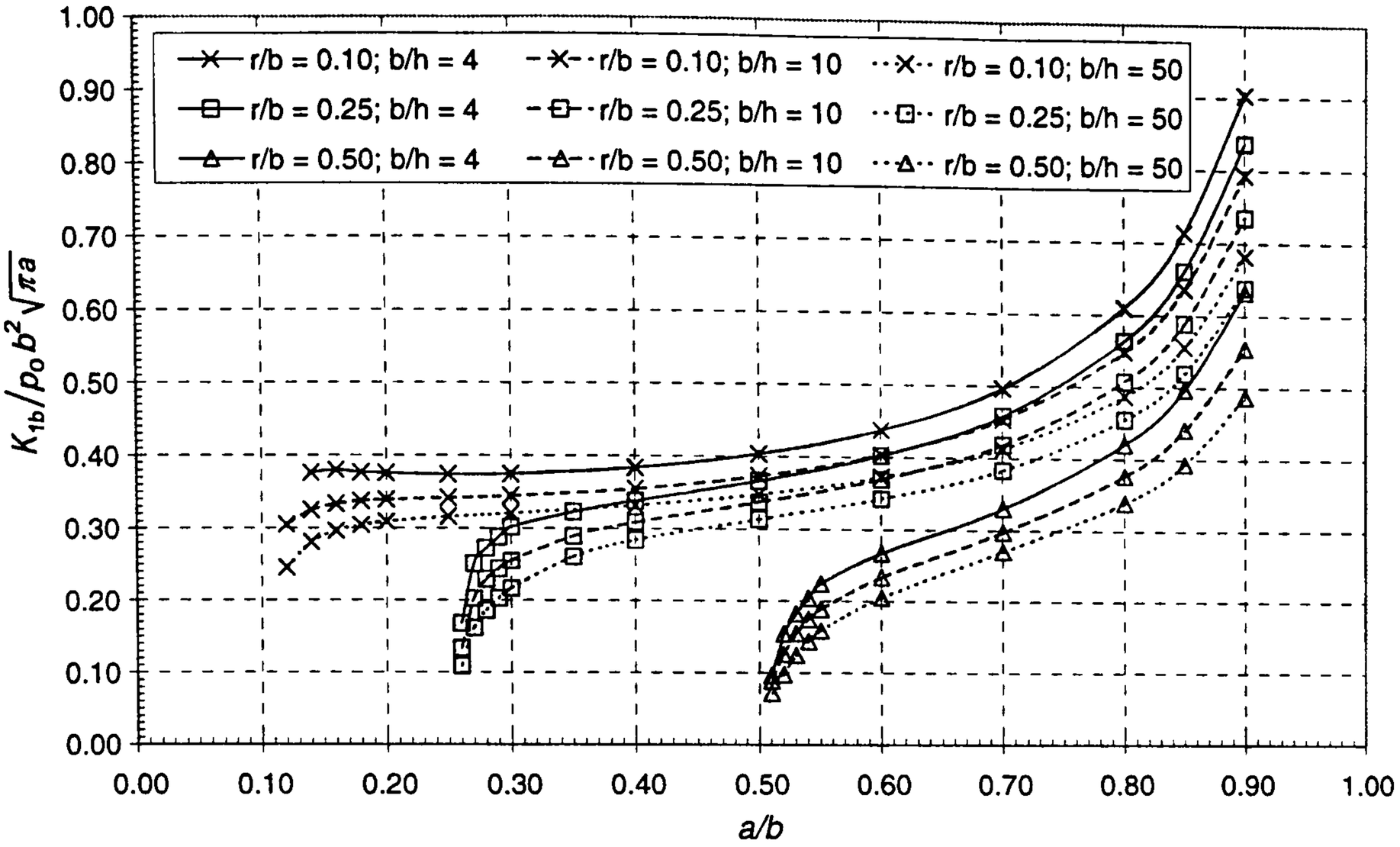

Figure 5-26: Normalised bending stress resultant intensity factors for two symmetric cracks emanating from a hole in a finite width plate subjected to uniform pressure.

5.5.7 An infinite plate with a slant centre crack loaded by bending and bi-axial tension

In this example, a mixed mode crack problem is presented. An infinite plate with a slant centre crack loaded by edge bending and bi-axial tension (as shown in Figure 5-27) is analysed. The bending and shear stress intensity factors for this problem have been calculated by Sih [118]. To model this problem, a plate with very large b/h ratio , i.e. $2b/h = 100/\sqrt{10}$ is used; $Eb^2/M_0 = 210000$ and $\nu = 0.25$.

For analysis, 8 elements per side of the plate and 12 elements for each crack surface are used. Figures 5-28 – 5-30 shows the bending stress resultant intensity factors of this example. It is shown that the numerical results using the proposed method are in good agreement with the reference solutions. Normalised membrane stress resultant intensity factor for this case is equal to 1.

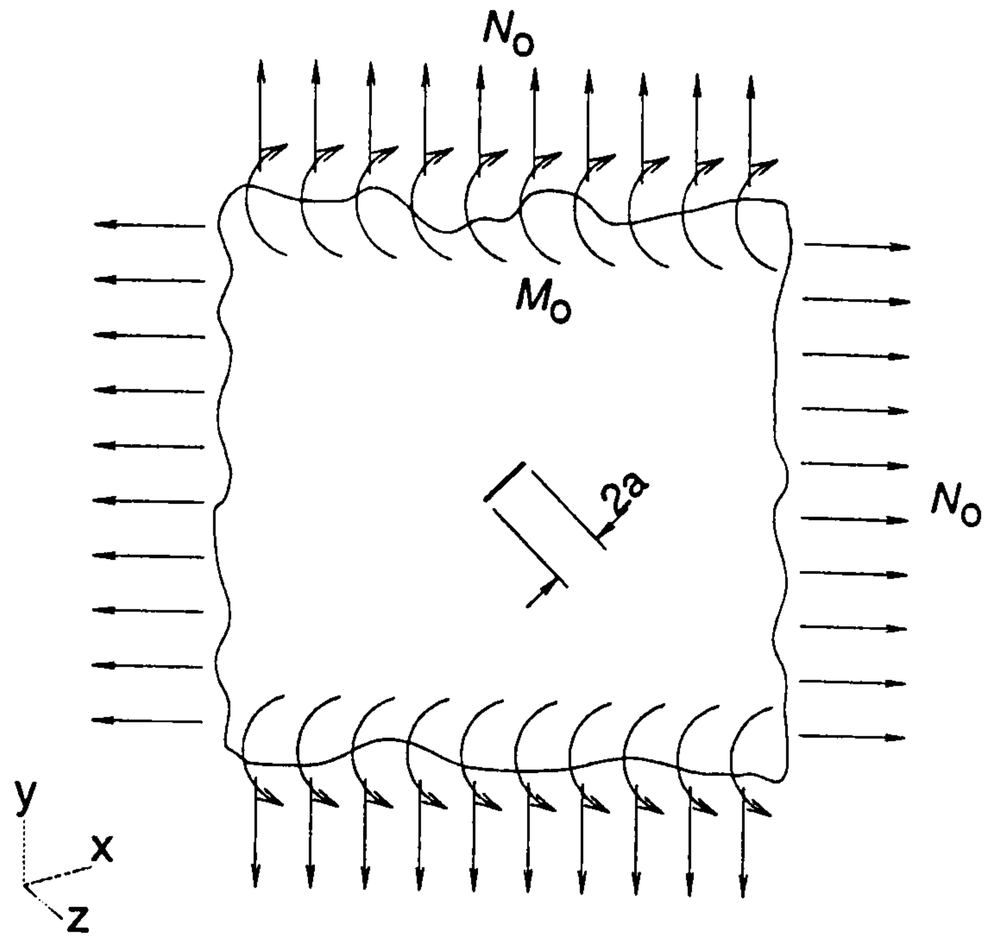

Figure 5-27: Infinite plate with slant centre crack loaded by bending and bi-axial tension, and deformed result of DBEM model.

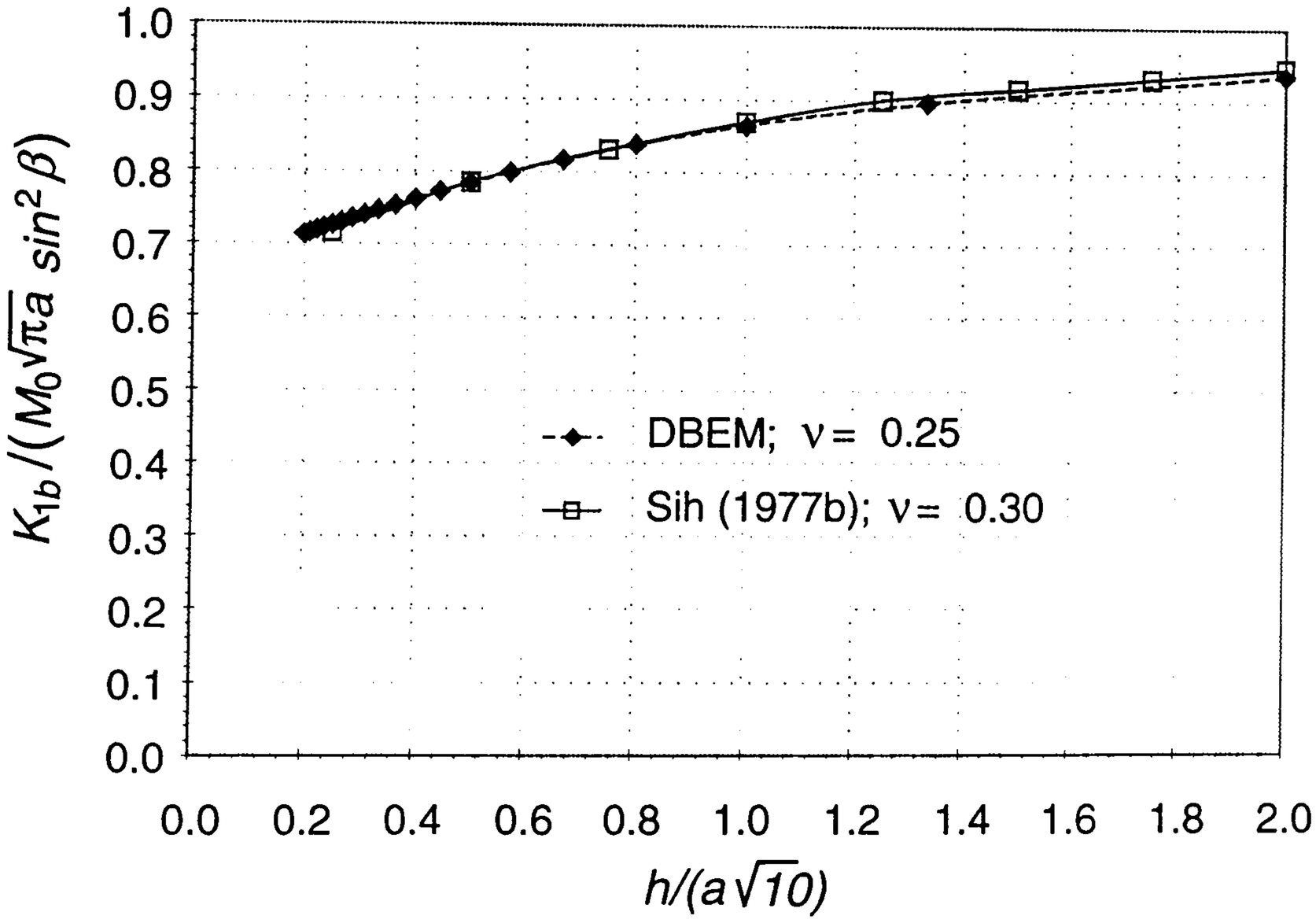

Figure 5-28: Normalised mode I bending stress resultant intensity factors for the slant crack in an infinite plate.

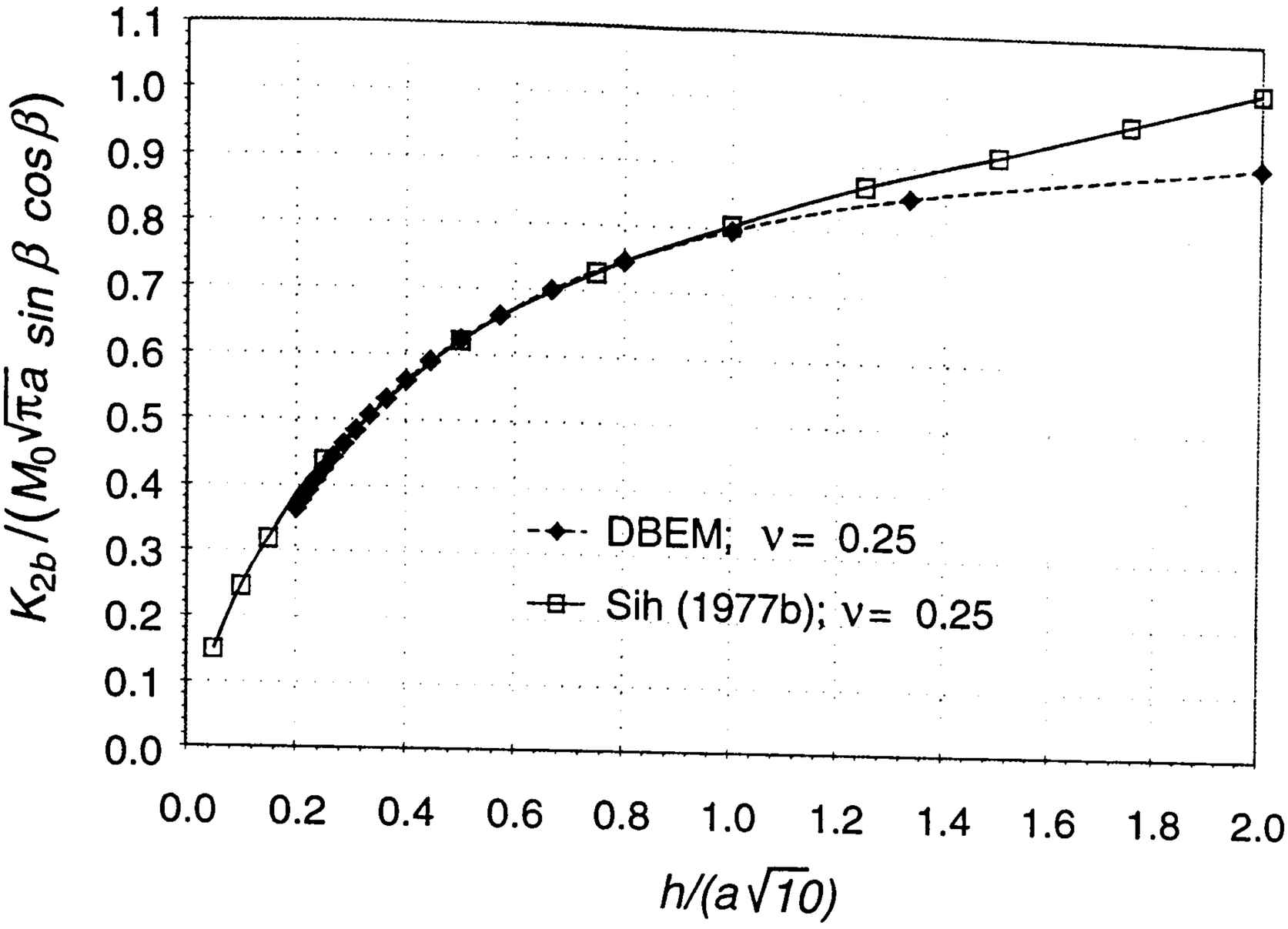

Figure 5-29: Normalised mode II bending stress resultant intensity factor for the slant crack in an infinite plate.

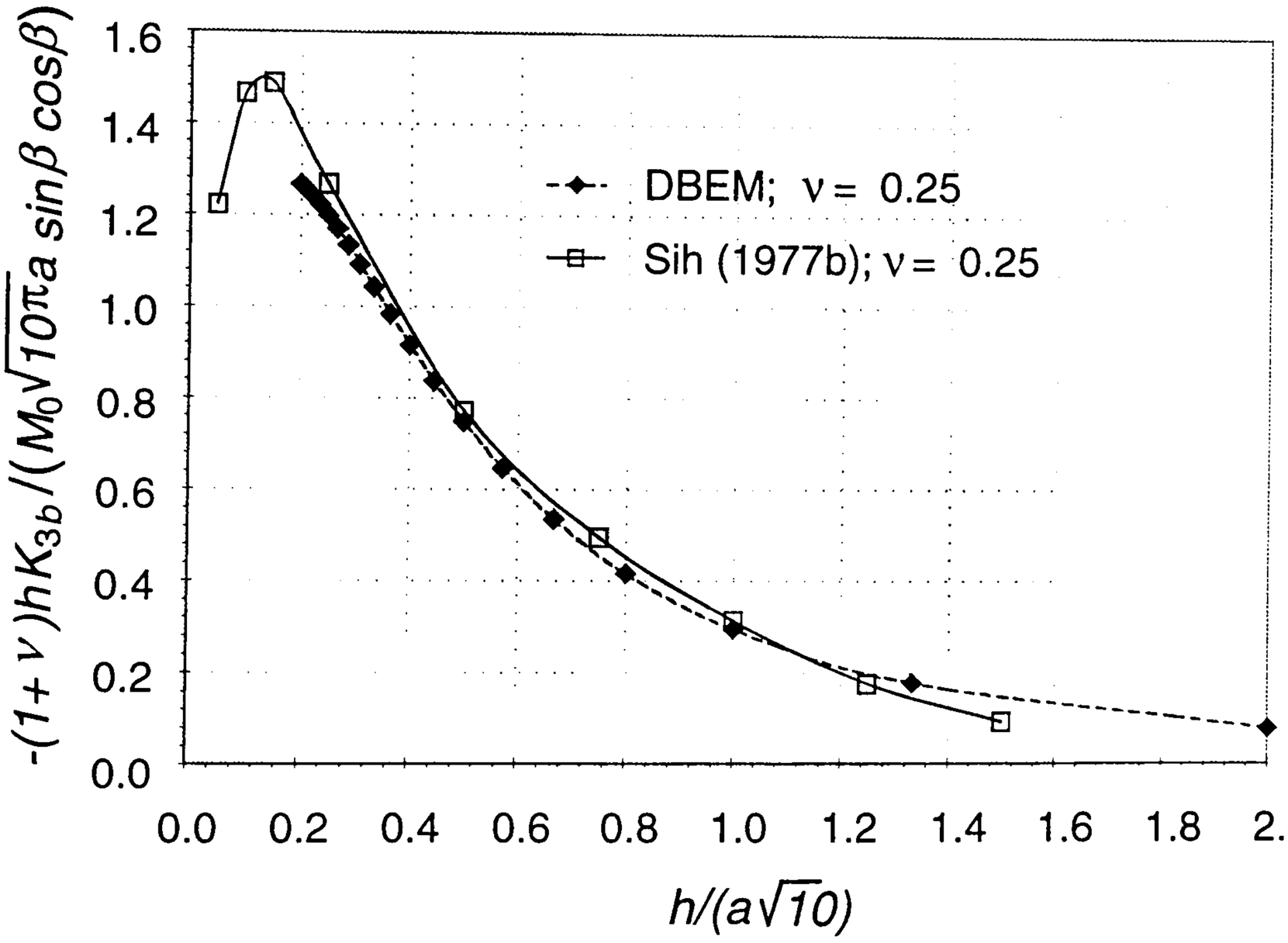

Figure 5-30: Normalised mode III bending stress resultant intensity factors for the slant crack in an infinite plate.

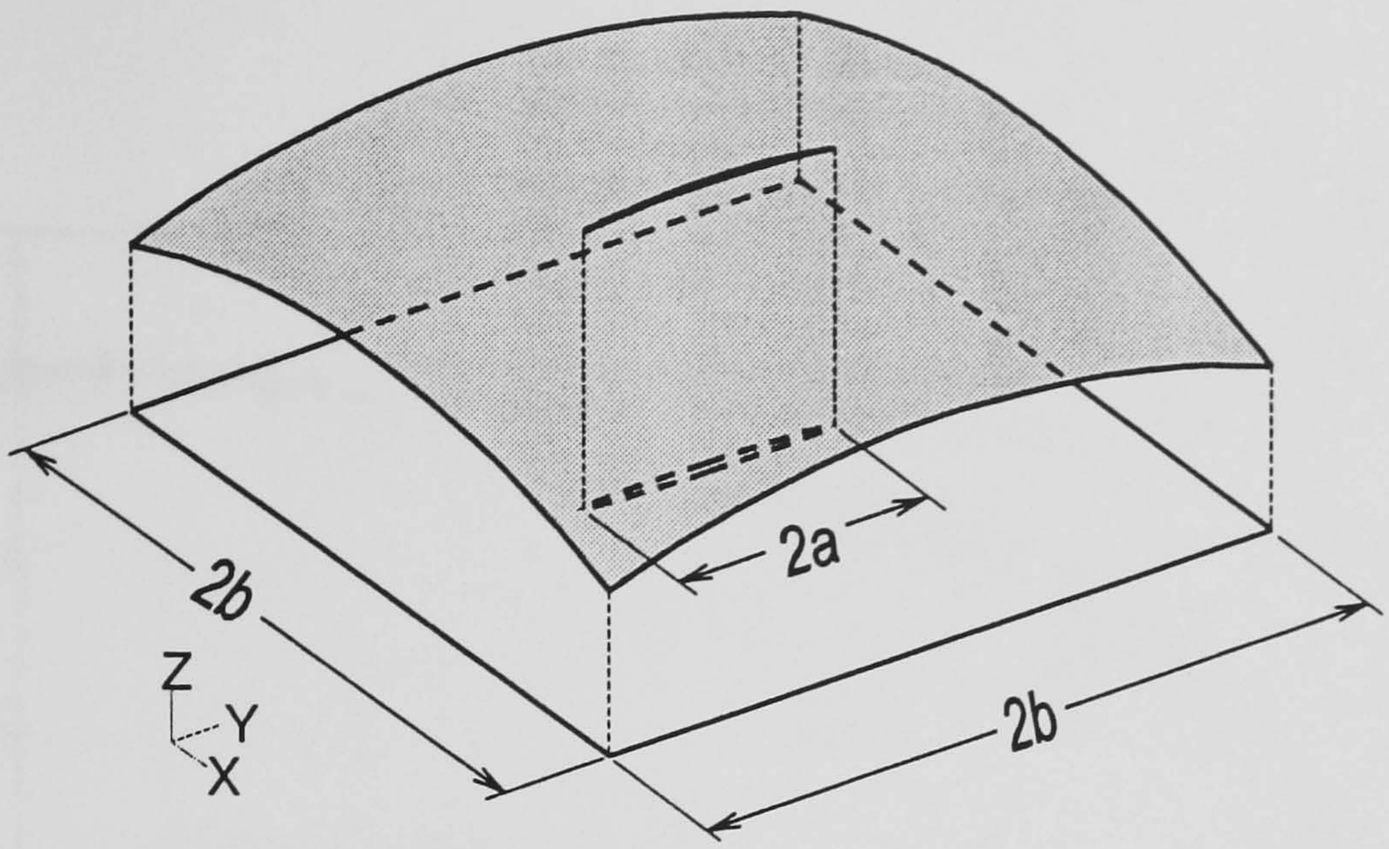

Figure 5-31: Square spherical shell with a centre crack.

5.5.8 Clamped and simply supported square spherical shells with a centre crack: uniformly loaded

Consider a square spherical shell with a centre crack shown in Figure 5-31 with $b = 1$; $a/b = 0.2, 0.4$ and 0.6. Two cases of boundary conditions are considered in this example: clamped and simply supported on all sides. A uniform pressure is applied over the shell domain. Modulus of elasticity $E/p_0 = 210000$, Poisson's ratio $\nu = 0.3$ and ratio between the width and the shell thickness $b/h = 10$. The value of b/R is varied between $0.0 - 0.2$, where $b/R = 0.0$ represent a flat plate.

For the analysis, 8 elements per side of the shell, 12 elements for each crack surface are used, and 7×7 DRM domain points are used. SIFs are evaluated using crack surface displacements extrapolation (CSDE) technique.

Figures 5-32 – 5-34 show the displacements on the crack surface and along symmetry line for shell having $b/R = 0.01$. They are compared to half model using only displacement equations of BEM. As it can be seen, the results show good agreement between the two models.

At the top and bottom surfaces of the shell, that is $x_3 = \pm h/2$, stress intensity factors for this problem can be obtained from equations (2.85 – 2.87) as follows

$$\left(1 \pm \frac{h}{2R}\right) K_I = \frac{1}{h} K_{1m} \pm \frac{6}{h^2} K_{1b}; \tag{5.56}$$

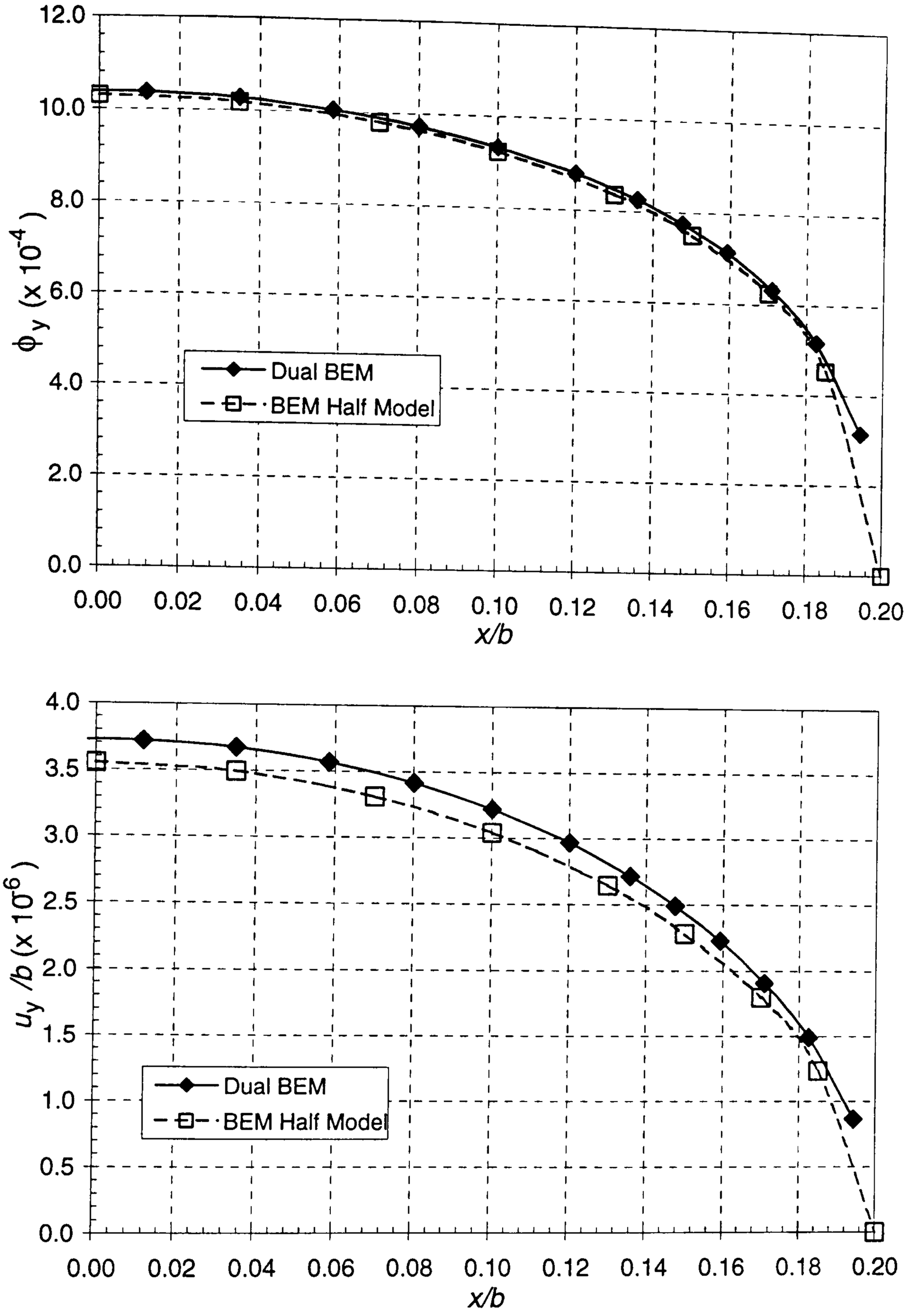

Figure 5-32: Displacements on the crack surface and along the line of symmetry, ($b/R = 0.01$, $a/b = 0.2$ and $b/h = 10$).

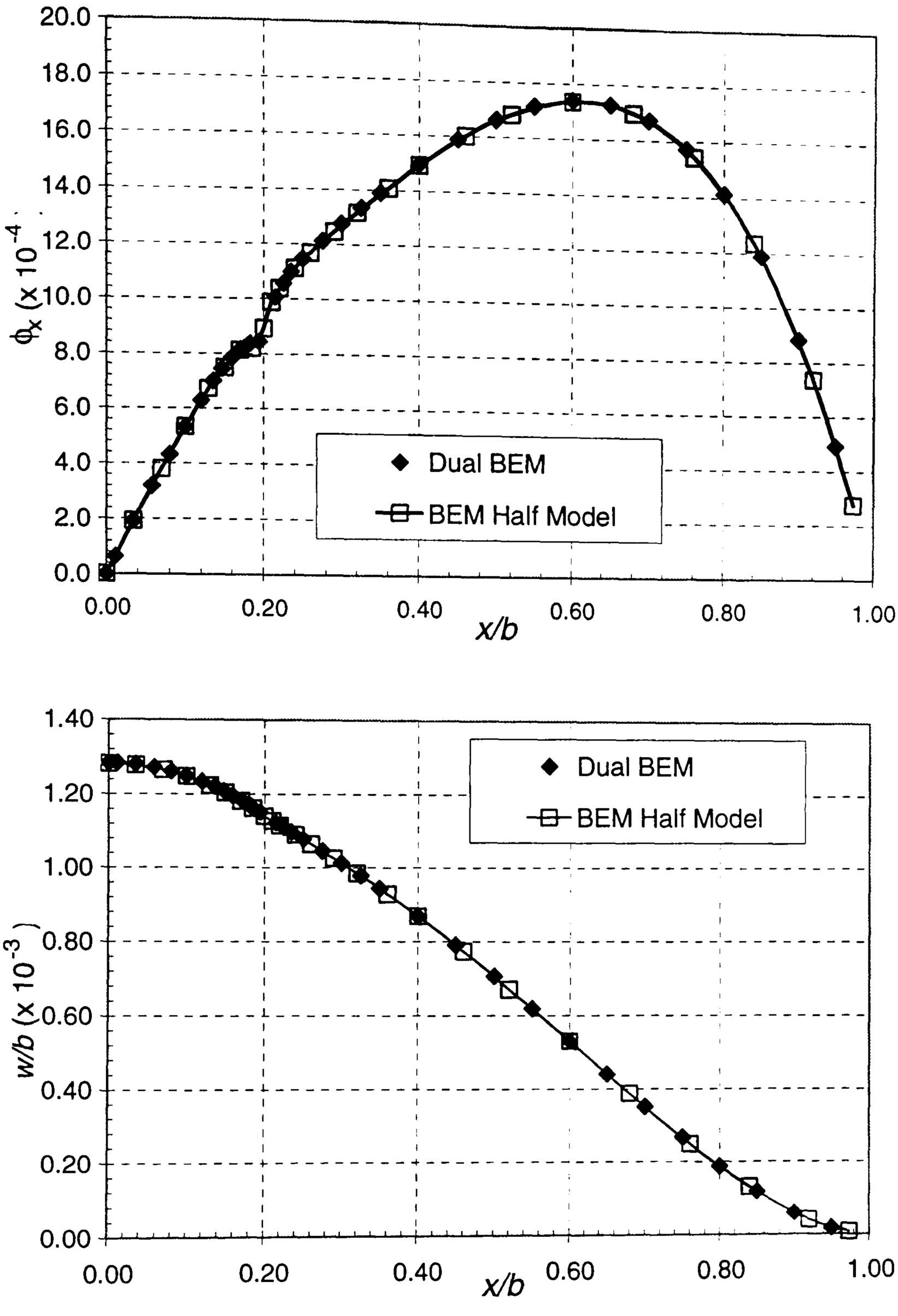

Figure 5-33: Displacements on the crack surface and along the line of symmetry, ($b/R = 0.01$, $a/b = 0.2$ and $b/h = 10$).

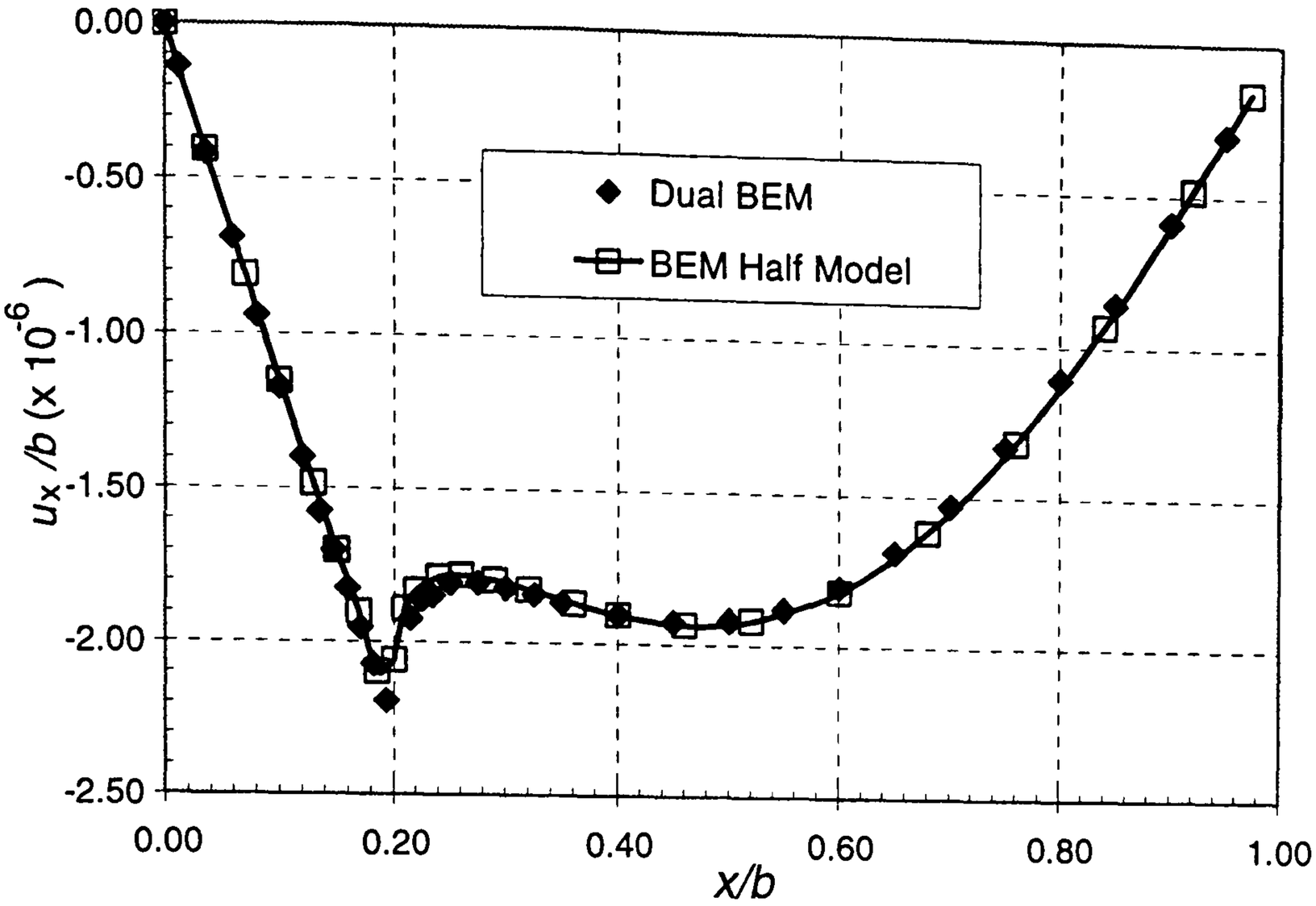

Figure 5-34: Displacements on the crack surface and along the line of symmetry, ($b/R = 0.01$, $a/b = 0.2$ and $b/h = 10$).

$$\left(1 \pm \frac{h}{2R}\right) K_{II} = \frac{1}{h} K_{2m} \pm \frac{6}{h^2} K_{2b} \tag{5.57}$$

and

$$K_{III} = 0 \tag{5.58}$$

On the other hand along the middle surface, that is $x_3 = 0$, the stress intensity factors are given by

$$K_I = \frac{1}{h} K_{1m}; \tag{5.59}$$

$$K_{II} = \frac{1}{h} K_{2m}; \tag{5.60}$$

and

$$K_{III} = \frac{3}{2h} K_{3b} \tag{5.61}$$

In this example, values of normalised K_{II} and K_{III} are very small (of order 10^{-7}), therefore this case can be considered as pure mode I. The normalised stress intensity factors for mode I, K_I due to bending and membrane are shown in Tables

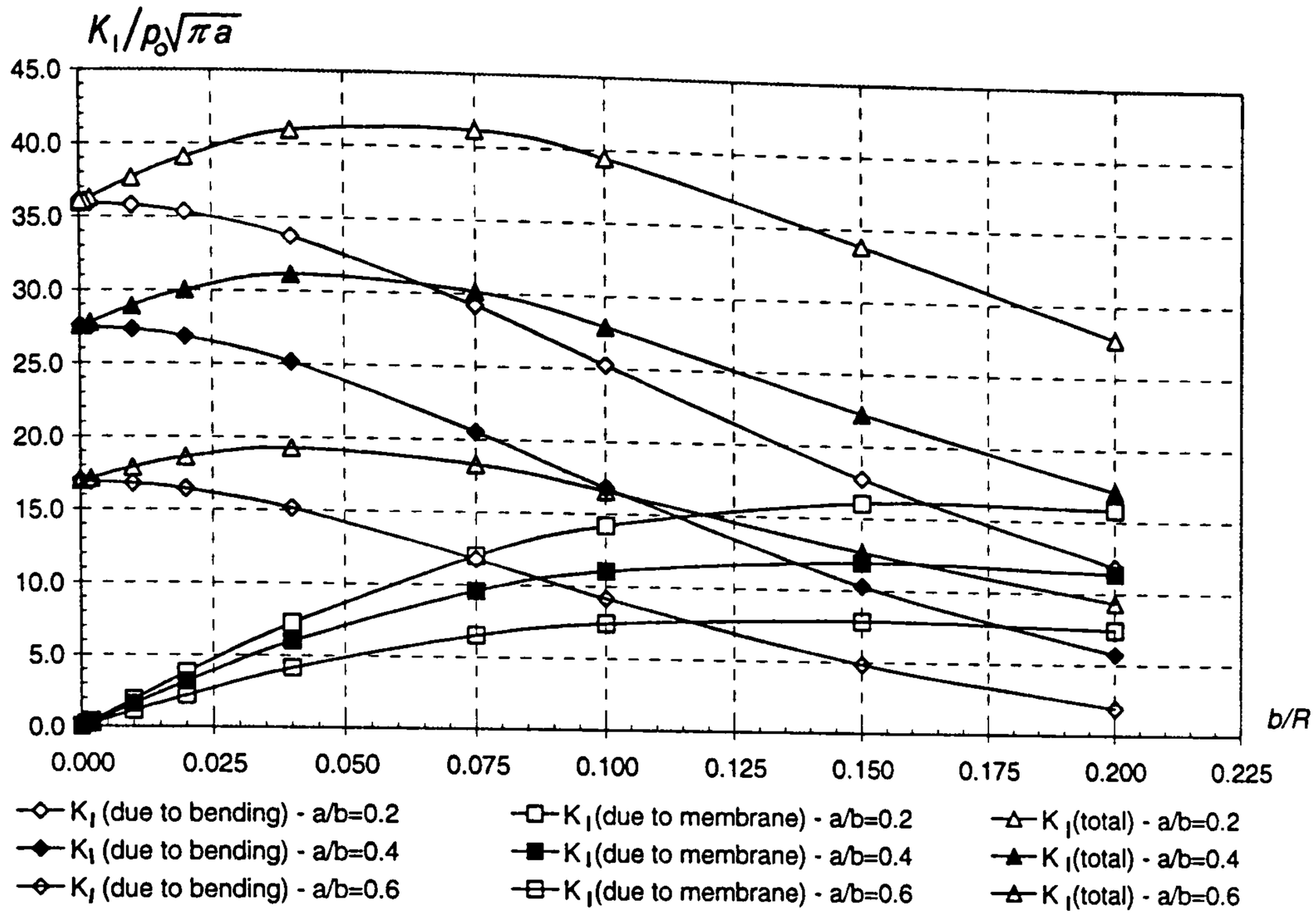

Figure 5-35: Normalised K_I on the top surface of a clamped square spherical shell: uniform pressure.

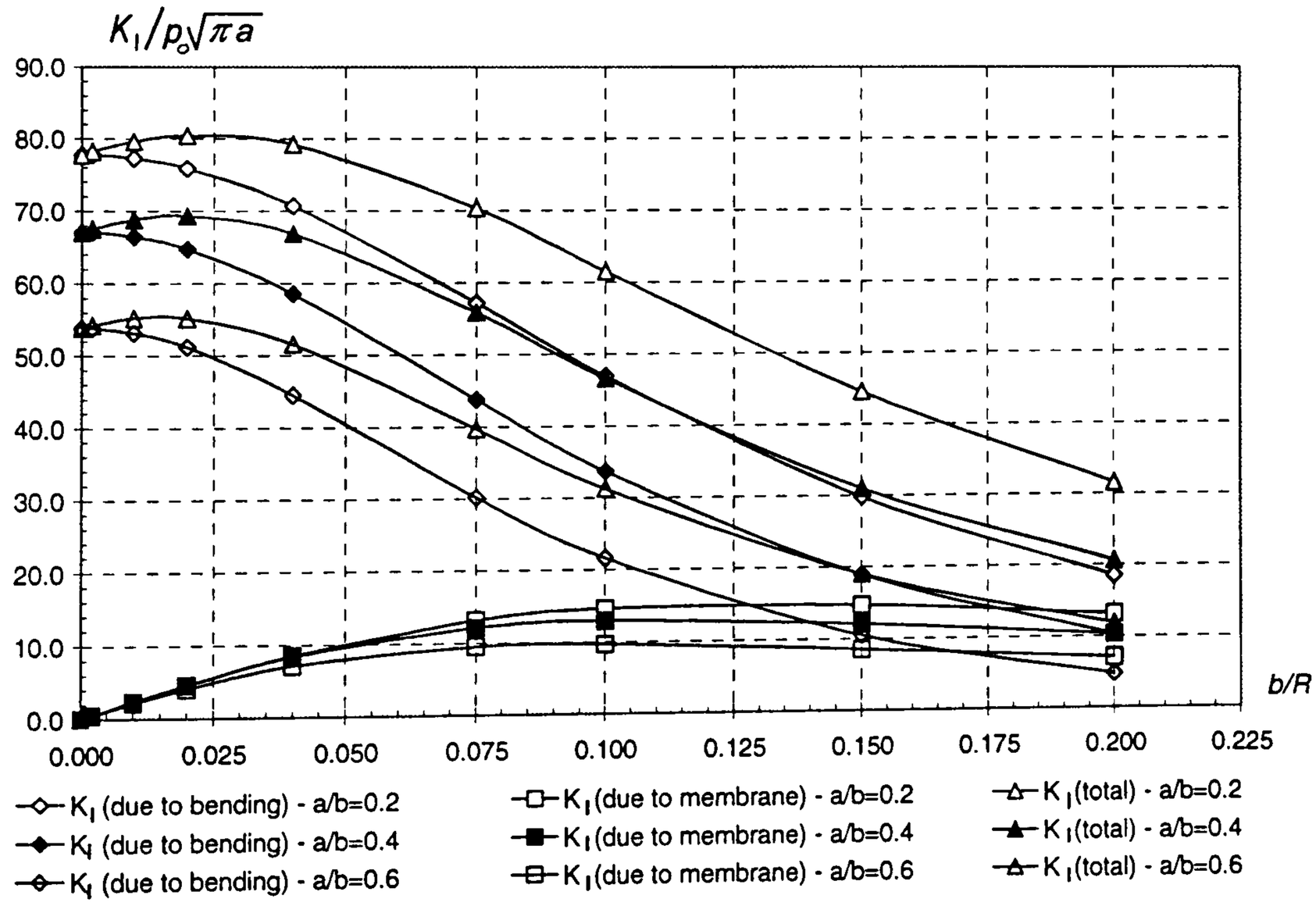

Figure 5-36: Normalised K_I on the top surface of a simply supported square spherical shell: uniform pressure.

Table 5.3: Normalised K_I of the clamped square shallow spherical shell: uniform pressure.

R	b/R	*top surface* $\frac{K_{1b}}{\left[1+\frac{h}{2R}\right]\frac{h^2}{6}p_0\sqrt{\pi a}}$			$\frac{K_{1m}}{\left[1+\frac{h}{2R}\right]hp_0\sqrt{\pi a}}$		
	a/b	0.2	0.4	0.6	0.2	0.4	0.6
5.000	0.200	11.8576	5.72645	1.91637	15.8543	11.3816	7.43347
6.667	0.150	17.7677	10.3154	4.82156	16.0752	11.9336	7.84673
10.00	0.100	25.2679	16.8270	9.18507	14.2049	11.0655	7.41104
13.33	0.075	29.1626	20.5239	11.7853	12.0033	9.60461	6.51529
25.00	0.040	33.7220	25.1443	15.1630	7.24219	5.98741	4.13289
50.00	0.020	35.3319	26.8519	16.4472	3.76942	3.15322	2.19123
100.0	0.010	35.7634	27.3142	16.7974	1.90464	1.59826	1.11268
500.0	0.002	35.9119	27.4714	16.9158	0.38231	0.32114	0.22370
1000.	0.001	35.9179	− − −	− − −	0.19118	− − −	− − −
∞	0.000	36.0607	27.5433	16.9794	0.00000	0.00000	0.00000
R	b/R	*bottom surface* $\frac{K_{1b}}{\left[1-\frac{h}{2R}\right]\frac{h^2}{6}p_0\sqrt{\pi a}}$			$\frac{K_{1m}}{\left[1-\frac{h}{2R}\right]hp_0\sqrt{\pi a}}$		
	a/b	0.2	0.4	0.6	0.2	0.4	0.6
5.000	0.200	12.0971	5.84213	1.95508	16.1746	11.6116	7.58364
6.667	0.150	18.0363	10.4713	4.89443	16.3181	12.1139	7.96532
10.00	0.100	25.5218	16.9961	9.27739	14.3477	11.1767	7.48553
13.33	0.075	29.3822	20.6784	11.8741	12.0937	9.67692	6.56434
25.00	0.040	33.8572	25.2451	15.2238	7.27121	6.01141	4.14946
50.00	0.020	35.4026	26.9057	16.4801	3.77696	3.15954	2.19561
100.0	0.010	35.7992	27.3415	16.8142	1.90654	1.59986	1.11379
500.0	0.002	35.9191	27.4769	16.9192	0.38239	0.32120	0.22375
1000.	0.001	35.9215	− − −	− − −	0.19120	− − −	− − −
∞	0.000	36.0607	27.5433	16.9794	0.00000	0.00000	0.00000

Table 5.4: Normalised K_I of the simply supported square shallow spherical shell: uniform pressure.

R	b/R	$\frac{K_{1b}}{\left[1+\frac{h}{2R}\right]\frac{h^2}{6}p_0\sqrt{\pi a}}$			$\frac{K_{1m}}{\left[1+\frac{h}{2R}\right]hp_0\sqrt{\pi a}}$		
		top surface					
	a/b	0.2	0.4	0.6	0.2	0.4	0.6
5.000	0.200	18.4175	10.2902	4.74536	13.1019	10.3086	7.04886
6.667	0.150	29.8239	18.8904	10.4661	14.6926	12.0718	8.49493
10.00	0.100	46.9306	33.6801	21.5906	14.5928	12.8754	9.64351
13.33	0.075	57.2093	43.7522	30.1648	13.0940	12.0922	9.49534
25.00	0.040	70.7003	58.5302	44.4647	8.48423	8.34518	7.06299
50.00	0.020	75.8776	64.7219	51.1552	4.52980	4.56886	3.99769
100.0	0.010	77.2961	66.4670	53.1197	2.30433	2.34028	2.06728
500.0	0.002	77.7784	67.0589	53.7892	0.46356	0.47185	0.41813
∞	0.000	77.7295	67.0338	53.7851	0.00000	0.00000	0.00000
		bottom surface					
R	b/R	$\frac{K_{1b}}{\left[1-\frac{h}{2R}\right]\frac{h^2}{6}p_0\sqrt{\pi a}}$			$\frac{K_{1m}}{\left[1-\frac{h}{2R}\right]hp_0\sqrt{\pi a}}$		
	a/b	0.2	0.4	0.6	0.2	0.4	0.6
5.000	0.200	18.7896	10.4980	4.84122	13.3666	10.5169	7.19126
6.667	0.150	30.2747	19.1759	10.6243	14.9146	12.2542	8.62332
10.00	0.100	47.4022	34.0185	21.8076	14.7395	13.0048	9.74043
13.33	0.075	57.6400	44.0816	30.3919	13.1925	12.1833	9.56682
25.00	0.040	70.9837	58.7648	44.6429	8.51824	8.37863	7.09130
50.00	0.020	76.0295	64.8515	51.2576	4.53887	4.57800	4.00569
100.0	0.010	77.3734	66.5335	53.1728	2.30664	2.34262	2.06935
500.0	0.002	77.7940	67.0723	53.7999	0.46365	0.47195	0.41821
∞	0.000	77.7295	67.0338	53.7851	0.00000	0.00000	0.00000

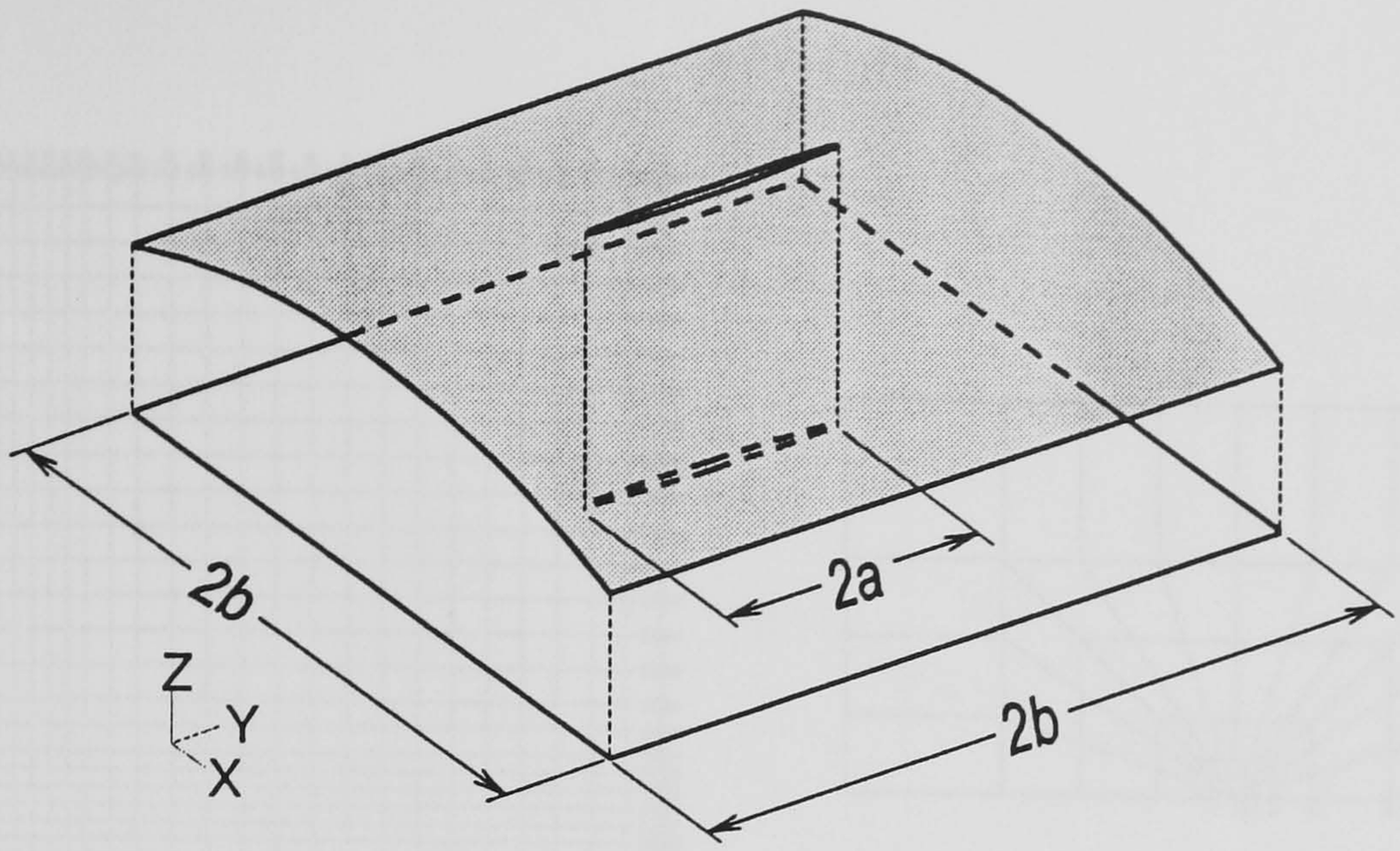

Figure 5-37: Square cylindrical shell with a centre crack.

5.3 – 5.4 and Figures 5-35 – 5-36. It can be seen from the results that as the radius of curvature R become smaller, the K_I due to membrane increases while the K_I due to bending decreases. This is because as the shell becomes deeper, more part of the pressure is transferred to membrane load. The results also show that as the $R \rightarrow \infty$, that is when the panel is flat, only K_I due to bending exist.

5.5.9 Clamped and simply supported square cylindrical shells with a centre crack: uniformly loaded

The second shell example considered here is a square cylindrical shell with a centre crack shown in Figure 5-37 with $b = 1$; $a/b = 0.2$. A uniform pressure is applied over the shell domain. Modulus of elasticity of the material is chosen $E/p_0 = 210000$, Poisson's ratio $\nu = 0.3$ and shell thickness $b/h = 20$.

For the DBEM analysis, 8 elements per side of the shell and 12 elements for each crack surface are used, together with 7×7 DRM domain points. For comparison, half model of the shell is also analysed using 48 elements and 28 domain points (i.e. Displacement BEM only), as well as FEM analysis using a quarter model of the shell with 3092 nodes and 1646 elements.

Figures 5-40 – 5-42 present the displacements on the crack surface and along the line of symmetry. Also presented are the BEM results obtained using the half model using only displacement equations and FEM results. As it can be seen, the

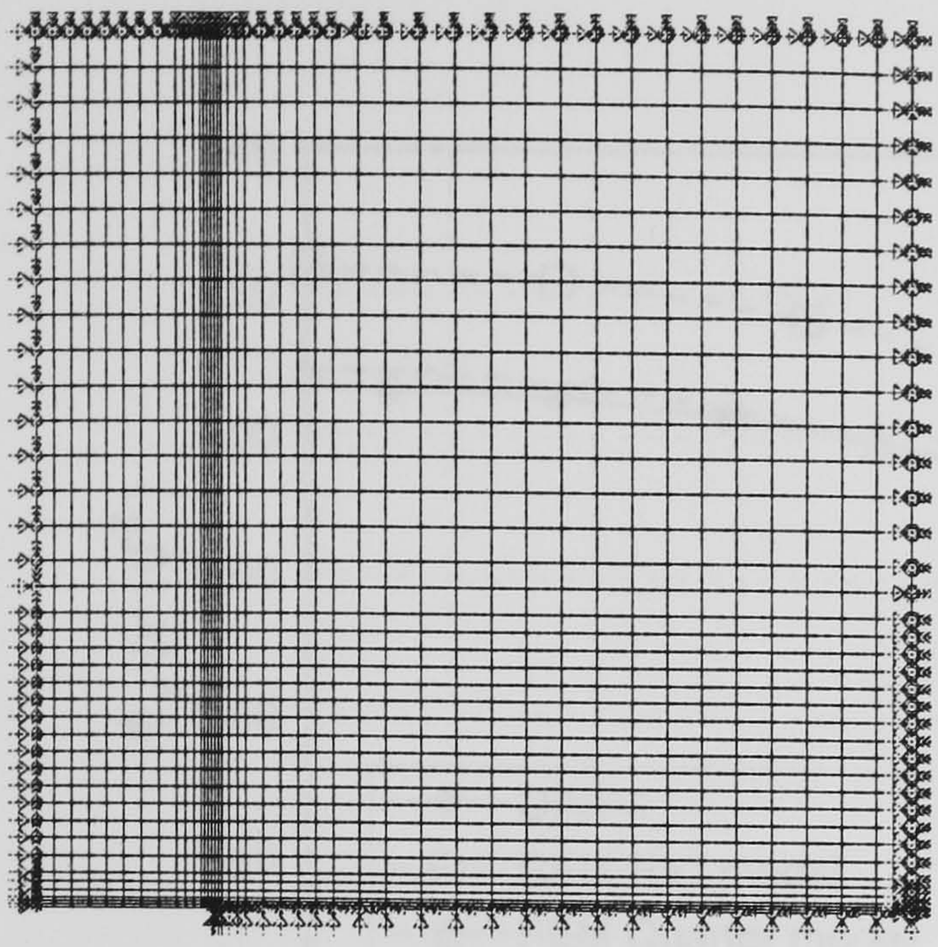

Figure 5-38: FEM - quarter model of centre crack in cylindrical shell: 3092 nodes, 1646 elements.

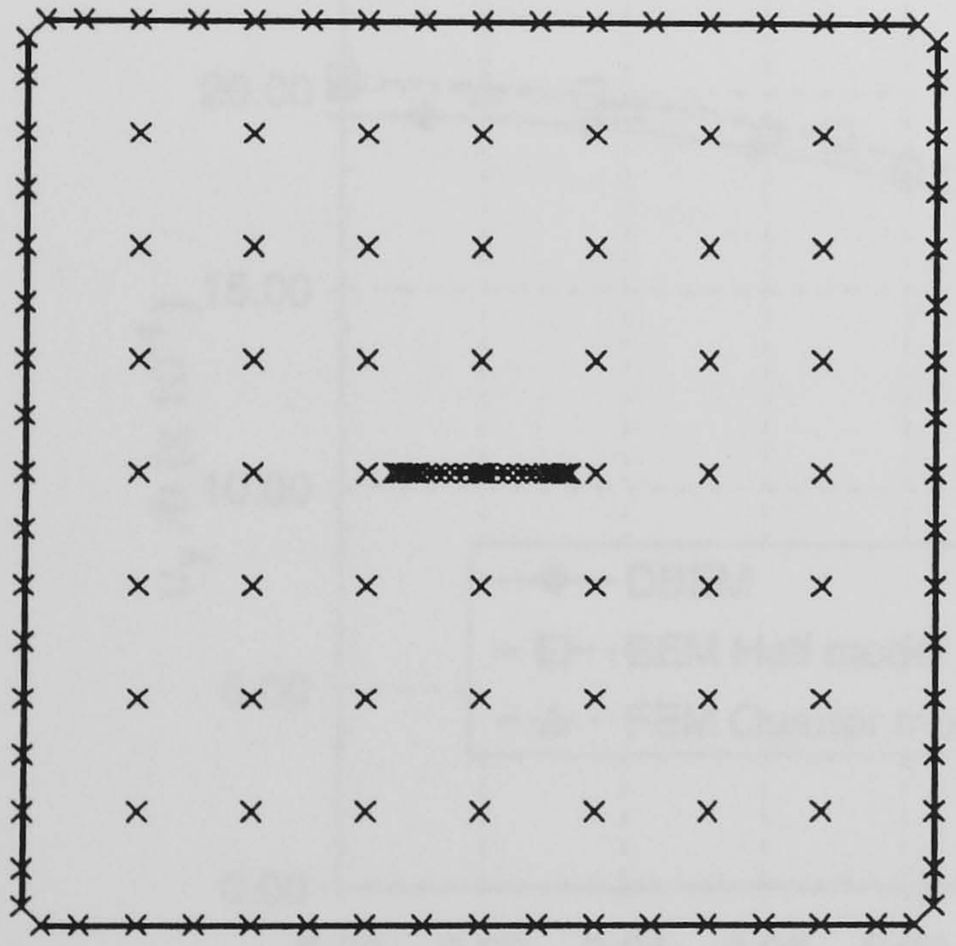

(a) Dual Boundary Element Model
56 elements, 49domain points

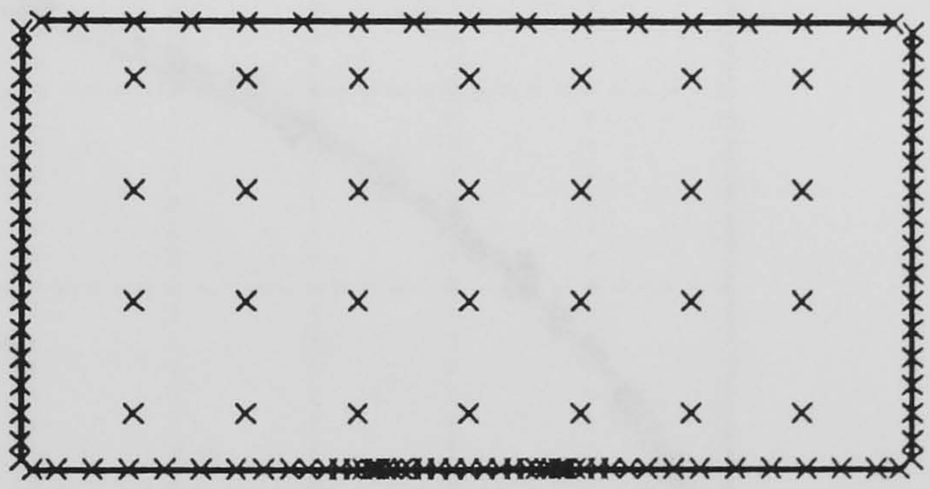

(b) Boundary Element Method – half model
48 elements, 28 domain points

Figure 5-39: Boundary element models for a centre crack in cylindrical shell: (a) Dual BEM; (b) BEM – half model.

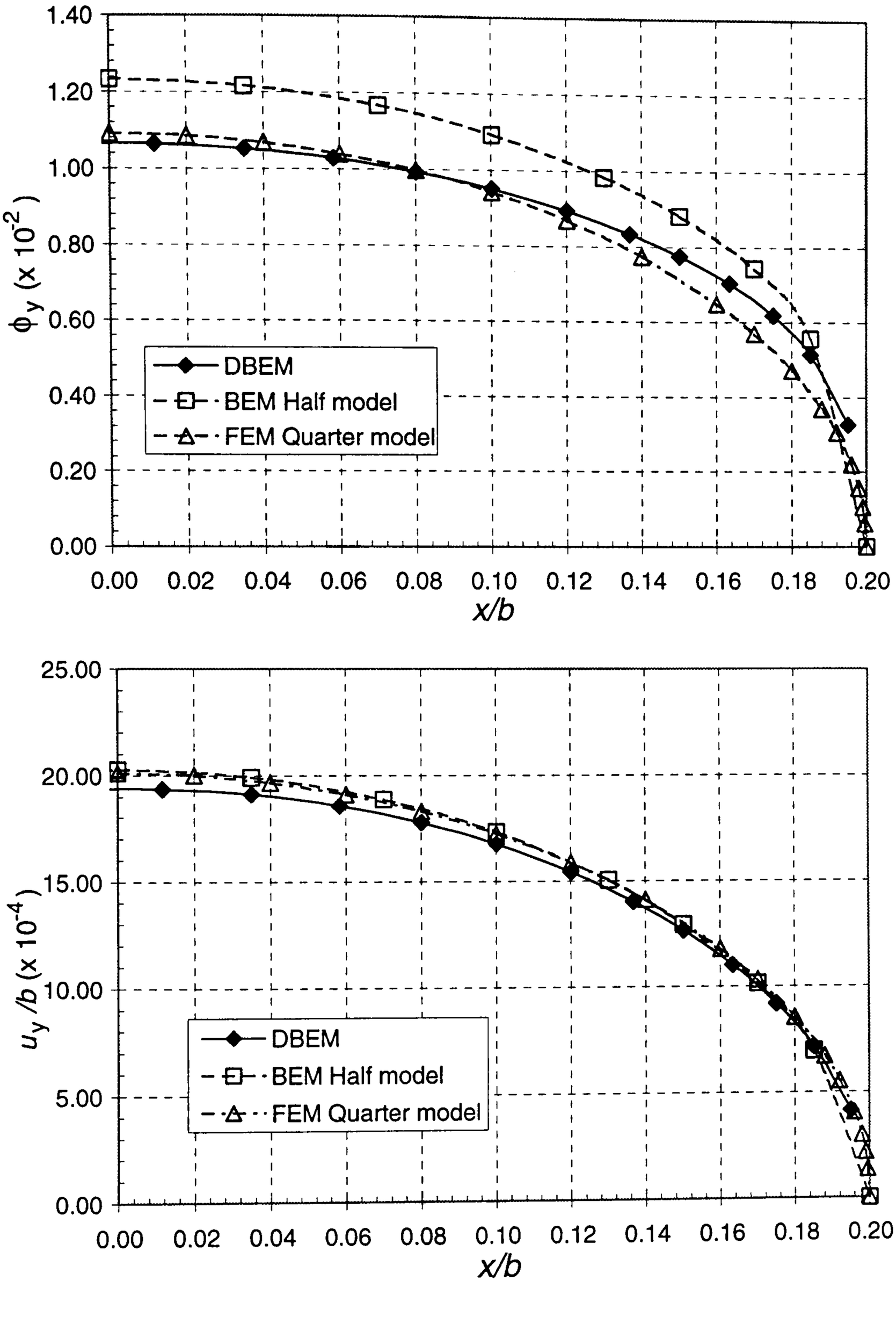

Figure 5-40: Displacements on the crack surface and along the line of symmetry, ($b/R = 0.01$, $a/b = 0.2$ and $b/h = 20$).

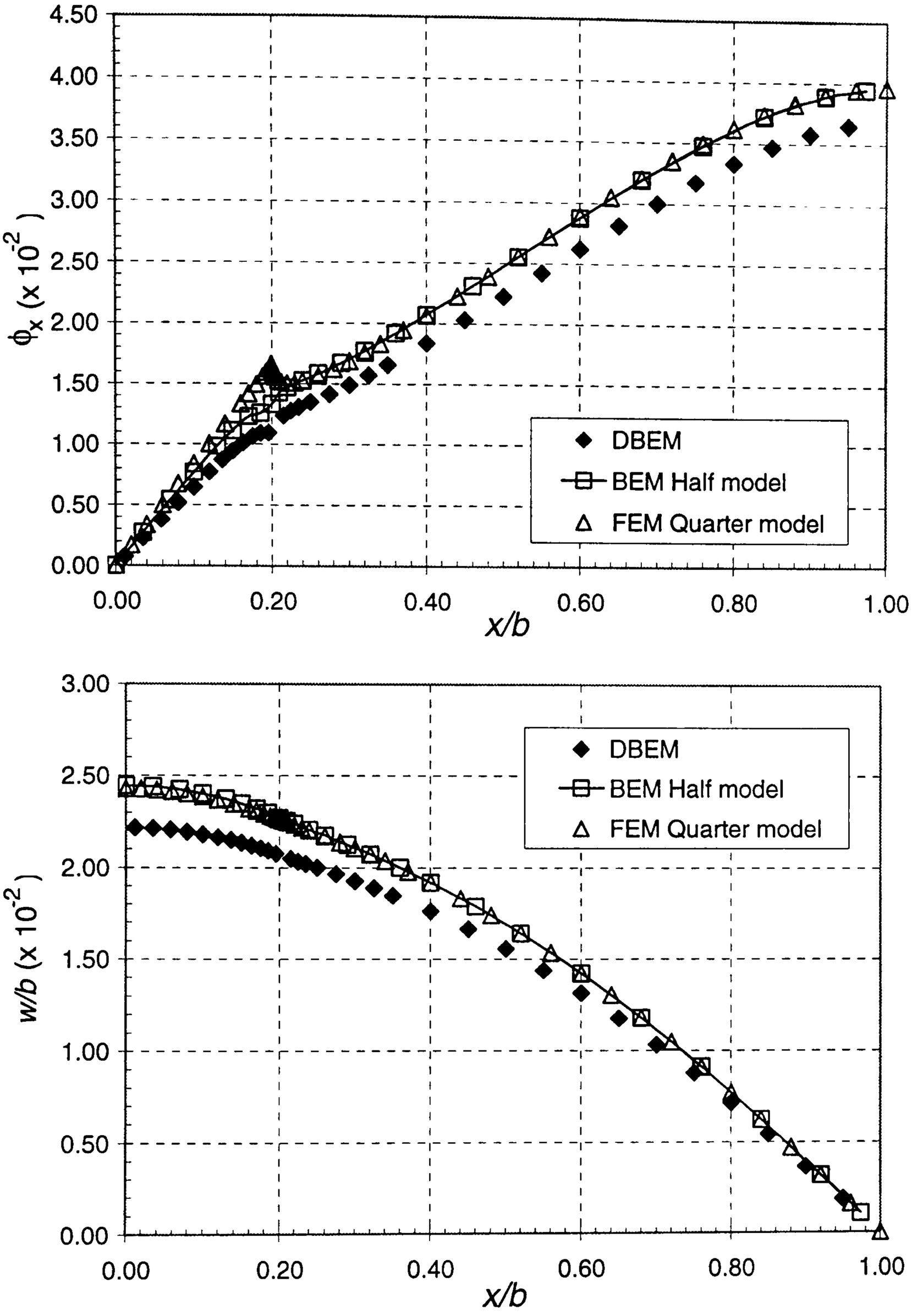

Figure 5-41: Displacements on the crack surface and along the line of symmetry, ($b/R = 0.01$, $a/b = 0.2$ and $b/h = 20$).

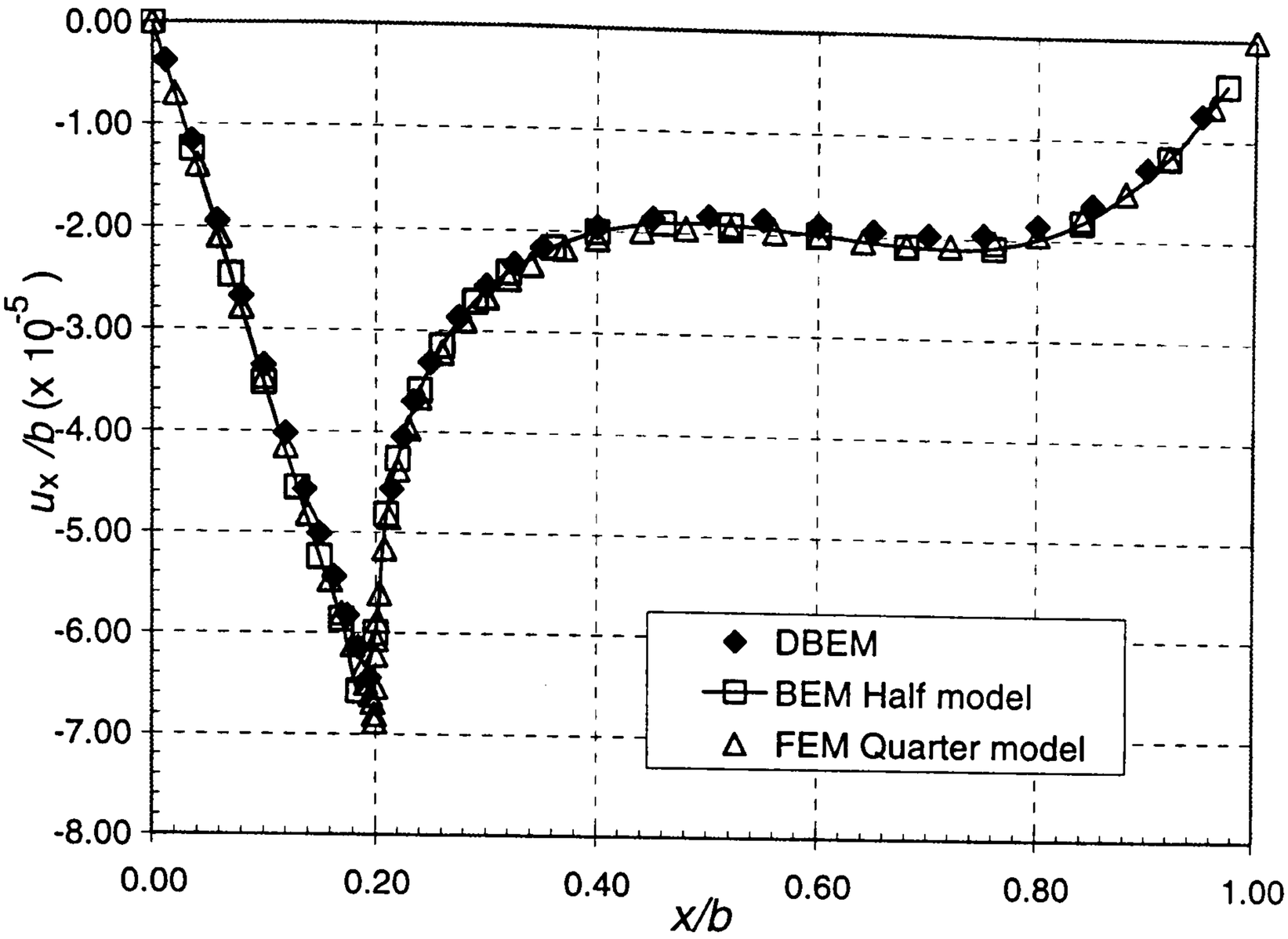

Figure 5-42: Displacements on the crack surface and along the line of symmetry, ($b/R = 0.01$, $a/b = 0.2$ and $b/h = 20$).

results presented are in good agreements.

To study the effect of different type of shell on the stress intensity factors, in this example clamped and simply supported square cylindrical shells are considered. A uniform load is applied over the shell domain. Modulus of elasticity of the material is chosen $E/p_0 = 210000$, Poisson's ratio $\nu = 0.3$ and shell thickness $b/h = 0.1$. Three different crack length, $a/b = 0.2$, 0.4 and 0.6 are analysed. Ratios between the width and the radius of curvature $b/R_1 = 0$ and b/R_2 is varied between $0.0 - 0.2$.

The SIF values of normalised K_{II} and K_{III} obtained are very small (of order 10^{-7}), therefore this case can be considered as pure mode I. The normalised stress intensity factors for mode I, K_I due to bending and membrane are shown in Table 5.4 and Figures 5-43 – 5-44. Similar to the previous example, the results show that as the radius of curvature R become smaller, the K_I due to membrane increases while the K_I due to bending decreases. The result also shows that as the $R \to \infty$, that is when the panel is flat, only K_I due to bending exist.

By comparing the results from spherical shell and cylindrical shells, it can be

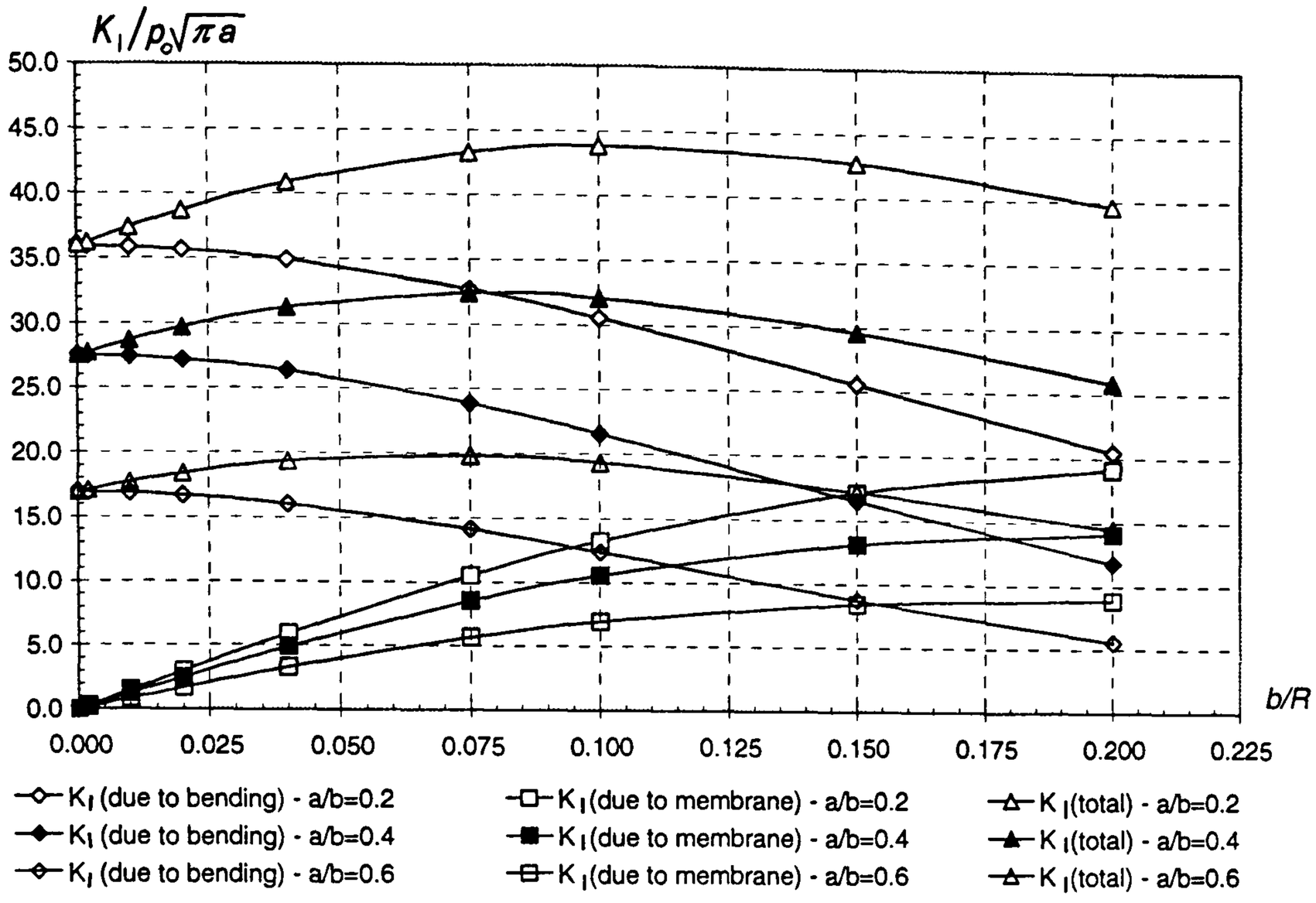

Figure 5-43: Normalised K_I on the top surface of a clamped square cylindrical shell: uniform pressure.

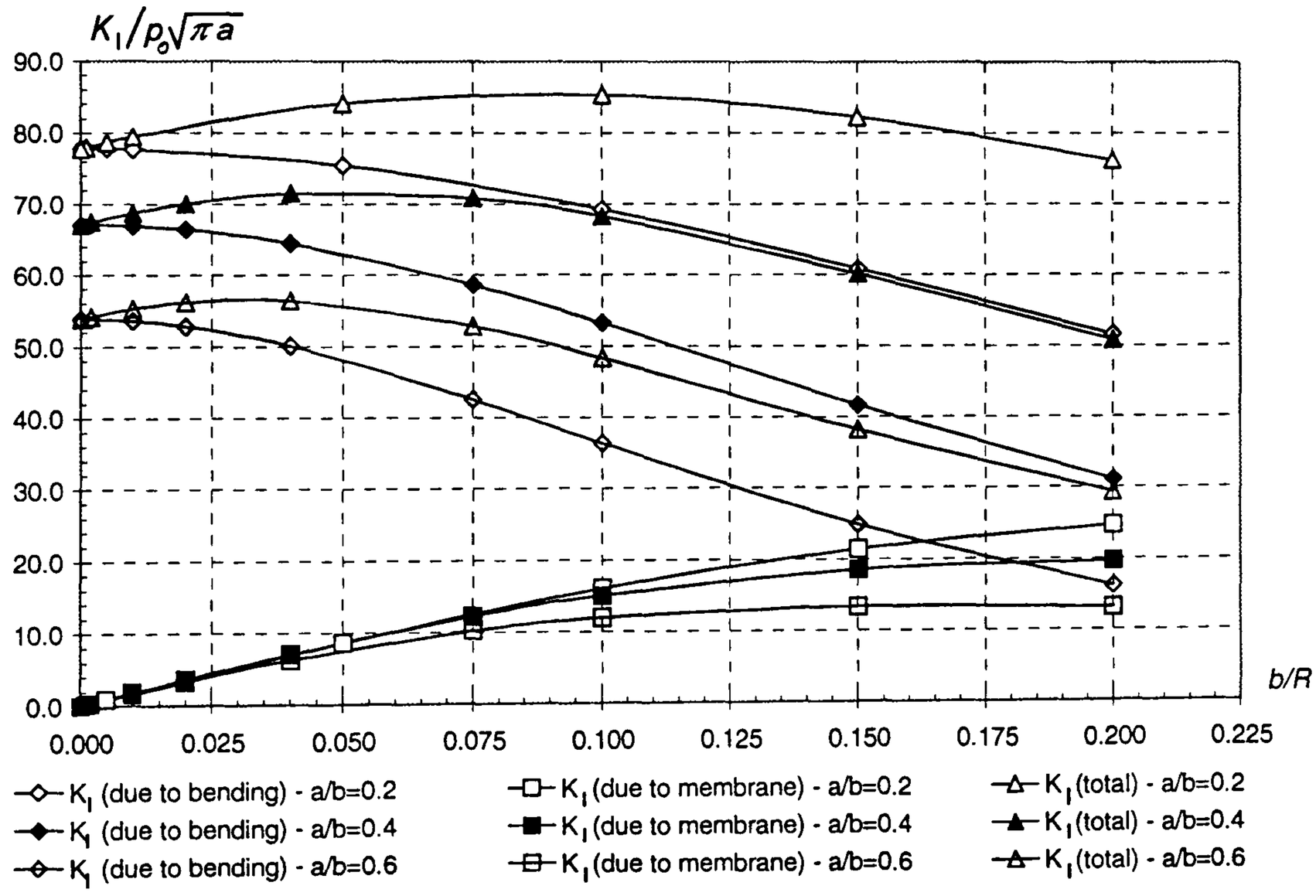

Figure 5-44: Normalised K_I on the top surface of a simply supported square cylindrical shell: uniform pressure.

Table 5.5: Normalised K_I of the clamped square shallow cylindrical shell: uniform pressure.

top surface

R	b/R	$\frac{K_{1b}}{\left[1+\frac{h}{4R}\right]\frac{h^2}{6}p_0\sqrt{\pi a}}$			$\frac{K_{1m}}{\left[1+\frac{h}{4R}\right]hp_0\sqrt{\pi a}}$		
	a/b	0.2	0.4	0.6	0.2	0.4	0.6
5.000	0.200	20.4852	11.7872	5.58714	19.1303	14.0838	8.89070
6.667	0.150	25.5740	16.4996	8.75632	17.1440	13.1080	8.43203
10.00	0.100	30.5692	21.5596	12.3788	13.2518	10.5446	6.95206
13.33	0.075	32.7101	23.8696	14.1129	10.5238	8.52456	5.68983
25.00	0.040	34.9251	26.3499	16.0324	5.93555	4.89903	3.31526
50.00	0.020	35.6501	27.1774	16.6849	3.02077	2.50851	1.70548
100.0	0.010	35.8441	27.3972	16.8582	1.51752	1.26216	0.85915
500.0	0.002	35.9151	27.4747	16.9182	0.30404	0.25300	0.17228
∞	0.000	36.0607	27.5433	16.9794	0.00000	0.00000	0.00000

bottom surface

R	b/R	$\frac{K_{1b}}{\left[1-\frac{h}{4R}\right]\frac{h^2}{6}p_0\sqrt{\pi a}}$			$\frac{K_{1m}}{\left[1-\frac{h}{4R}\right]hp_0\sqrt{\pi a}}$		
	a/b	0.2	0.4	0.6	0.2	0.4	0.6
5.000	0.200	20.8990	12.0253	5.70001	19.5168	14.3683	9.07031
6.667	0.150	25.9605	16.7490	8.88866	17.4030	13.3061	8.55947
10.00	0.100	30.8764	21.7762	12.5032	13.3850	10.6506	7.02193
13.33	0.075	32.9564	24.0493	14.2191	10.6031	8.58873	5.73266
25.00	0.040	35.0651	26.4555	16.0967	5.95934	4.91866	3.32855
50.00	0.020	35.7215	27.2318	16.7183	3.02682	2.51354	1.70889
100.0	0.010	35.8799	27.4246	16.8751	1.51904	1.26342	0.86001
500.0	0.002	35.9223	27.4802	16.9216	0.30410	0.25305	0.17232
∞	0.000	36.0607	27.5433	16.9794	0.00000	0.00000	0.00000

Table 5.6: Normalised K_I of the simply supported square shallow cylindrical shell: uniform pressure.

top surface

R	b/R	$\frac{K_{1b}}{\left[1+\frac{h}{4R}\right]\frac{h^2}{6}p_0\sqrt{\pi a}}$			$\frac{K_{1m}}{\left[1+\frac{h}{4R}\right]hp_0\sqrt{\pi a}}$		
	a/b	0.2	0.4	0.6	0.2	0.4	0.6
5.000	0.200	51.5532	31.0765	16.1747	24.6702	19.6380	13.1412
6.667	0.150	60.8026	41.6170	24.8250	21.4142	18.4776	13.3529
10.00	0.100	69.2715	53.1856	36.3114	16.0492	15.0478	11.9805
13.33	0.075	72.7372	58.5610	42.5414	12.5806	12.2350	10.2349
20.00	0.050	75.4208	− − −	− − −	8.66785	− − −	− − −
25.00	0.040	− − −	64.4017	50.0627	− − −	7.07517	6.26217
50.00	0.020	− − −	66.3670	52.8184	− − −	3.63025	3.27870
100.0	0.010	77.6764	66.8908	53.5546	1.78090	1.82753	1.65909
200.0	0.005	77.7632	− − −	− − −	0.89138	− − −	− − −
500.0	0.002	− − −	67.0760	53.8068	− − −	0.36640	0.33318
1000.	0.001	77.8003	− − −	− − −	0.17836	− − −	− − −
∞	0.000	77.7295	67.0338	53.7851	0.00000	0.00000	0.00000

bottom surface

R	b/R	$\frac{K_{1b}}{\left[1-\frac{h}{4R}\right]\frac{h^2}{6}p_0\sqrt{\pi a}}$			$\frac{K_{1m}}{\left[1-\frac{h}{4R}\right]hp_0\sqrt{\pi a}}$		
	a/b	0.2	0.4	0.6	0.2	0.4	0.6
5.000	0.200	52.5947	31.7043	16.5014	25.1686	20.0348	13.4067
6.667	0.150	61.7215	42.2459	25.2002	21.7378	18.7569	13.5547
10.00	0.100	69.9677	53.7201	36.6763	16.2105	15.1990	12.1009
13.33	0.075	73.2848	59.0019	42.8617	12.6753	12.3271	10.3119
20.00	0.050	75.7989	− − −	− − −	8.71130	− − −	− − −
25.00	0.040	− − −	64.6598	50.2884	− − −	7.10352	6.29040
50.00	0.020	− − −	66.4999	52.9241	− − −	3.63752	3.28526
100.0	0.010	77.7541	66.9577	53.6082	1.78268	1.82936	1.66075
200.0	0.005	77.8021	− − −	− − −	0.89182	− − −	− − −
500.0	0.002	− − −	67.0894	53.8176	− − −	0.36647	0.33325
1000.	0.001	77.8081	− − −	− − −	0.17837	− − −	− − −
∞	0.000	77.7295	67.0338	53.7851	0.00000	0.00000	0.00000

seen that as the R become smaller, the total stress intensity factor decreases faster in spherical shell. Also shown in the results that as the $R \rightarrow \infty$, both examples approaching the same value of K_I which is K_I of a flat plate due to bending.

As has been mentioned in chapter 3, with the capability of computer today, it takes only a few minute computer time for solving computational model of structures (in this case, using Pentium III 650 Mhz with 256 MB RAM, this example was solved in less than two minutes). Therefore the main issue of computer modelling of structure is the time spent for data preparation. For example, the graph shown in Figures 5-43 is obtained from 30 models of different combinations of crack length and radius of curvature. As it can be seen in Figures 5-38 – 5-39, crack modelling using FEM is quite tedious. It took several hours to prepare data for a model shown in Figure 5-38. To obtain an accurate results, the area around the crack tip has to be modelled with a very fine mesh. Moreover it is not easy to modify the model for different crack length and different radius of curvature. Each different configuration has to be modelled individually from scratch. On the other hand, crack modelling using BEM is relatively easy compare to FEM. Using simple mesh generator developed in this work, the model can be easily modified for different crack length and different curvature. It took only about one hour to make all 30 different models.

5.5.10 Symmetric cracks emanating from a hole in a square cylindrical shells

As the last example, consider a symmetric cracks emanating from a hole in a square cylindrical shell $b = 1$; $a/b = 0.2$ and 0.5 as shown in Figure 5-45. The shell is simply supported on two sides. A uniform load is applied over the shell domain. Modulus of elasticity $E/p_0 = 210000$ and Poisson's ratio $\nu = 0.3$. Ratio between hole size and shell width is $r/b = 0.1$, and the shell width to thickness ratio is $b/h = 10$. The value of b/R is varied between $0.0 - 0.2$, where $b/R = 0.0$ represent a flat plate.

For the analysis, a total of 132 elements, that is 8 boundary elements per side of the shell, 20 elements for the hole and 20 elements for each crack surface, and 7×7 DRM domain points are used.

The normalised stress intensity factors for mode I, K_I due to bending and mem-

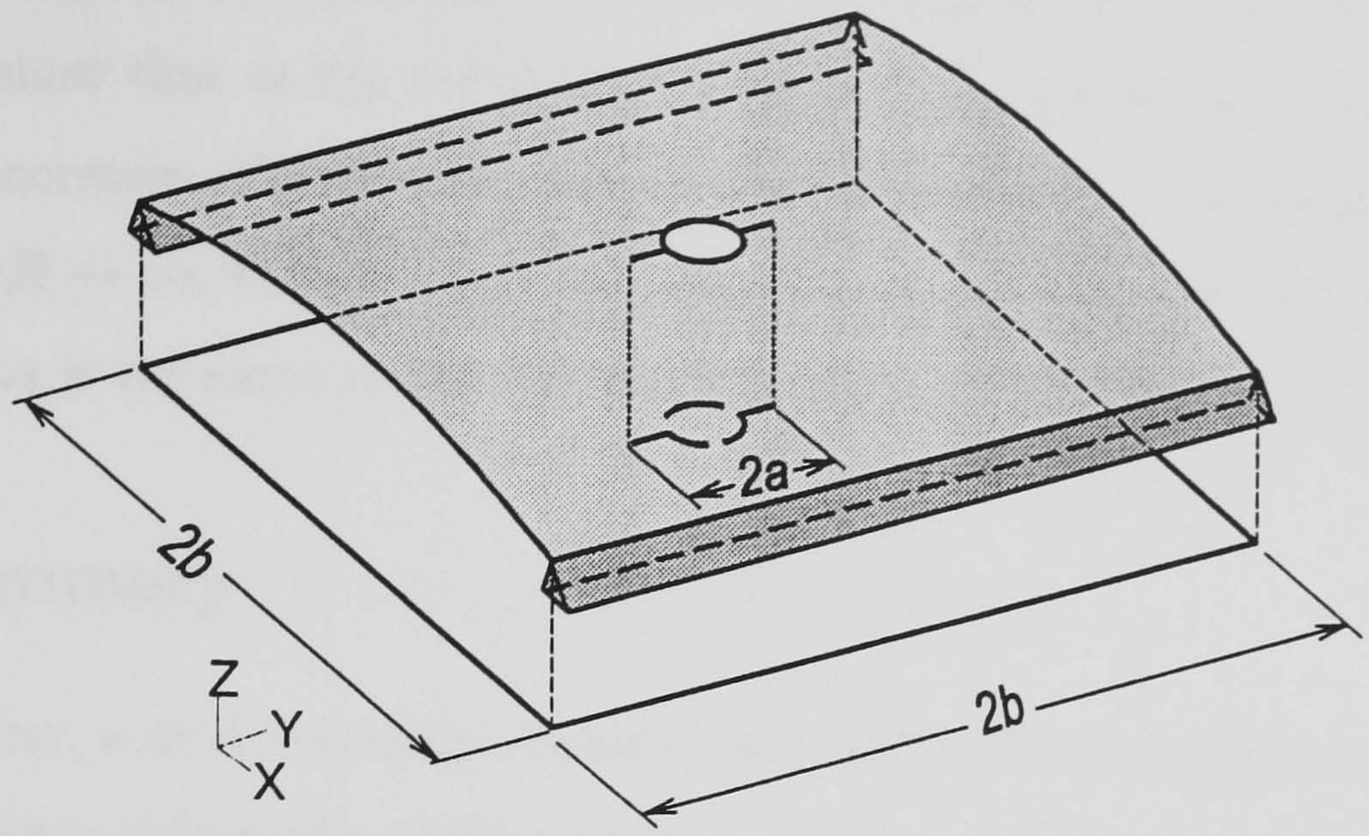

Figure 5-45: Symmetric cracks emanating from a hole in a square cylindrical shell, simply supported on two sides, subjected to uniform pressure.

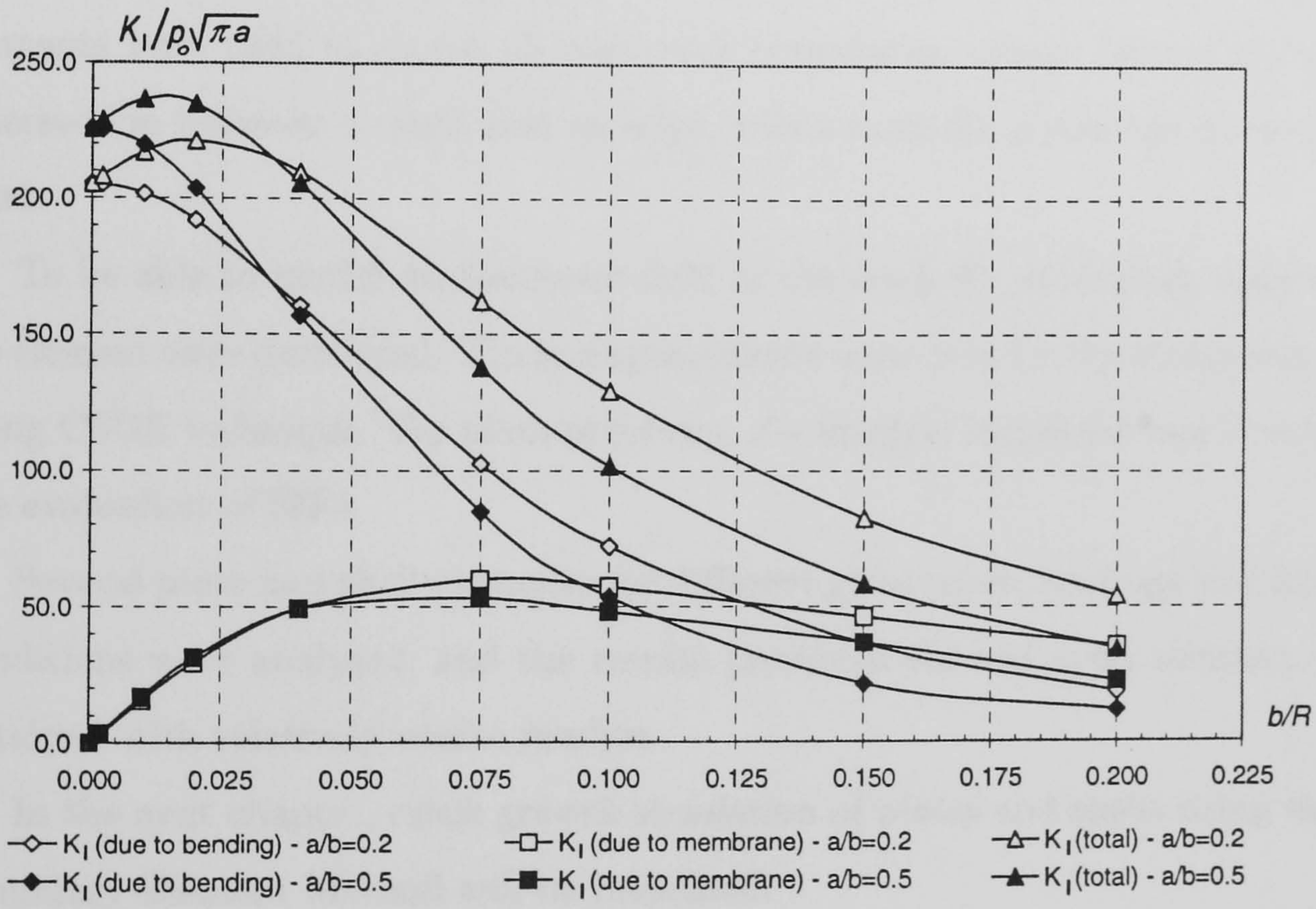

Figure 5-46: Normalised K_I on the top surface of symmetric cracks emanating from a hole in a square cylindrical shell, simply supported on two sides, subjected to uniform pressure.

brane are shown in Figures 5-46. The normalisation factors used here are the same as the ones used in the cylindrical shell example. Similar to the previous example, the results show that as the radius of curvature R become smaller, the K_I due to membrane increases while the K_I due to bending decreases. The results also show that as the $R \rightarrow \infty$, that is when the panel is flat, only K_I due to bending exist, and the value is the same as the one which is obtained for plate bending example.

5.6 Summary

In this chapter, a dual boundary element method formulation of fracture mechanics analysis of shear deformable shallow shells and plates loaded by bending and tension was presented. The traction integral equations were applied on one of the crack surface and the usual displacement integral equations on the other crack surface and on all non-crack boundaries. By this technique, the problems were solved in a single region formulation.

Crack surfaces were discretised using discontinuous elements, while continuous elements were used to model all non-crack boundaries, except for corners and the intersection between a crack and an edge, where semi-discontinuous elements were used.

To be able to model displacement field at the crack tip accurately, special crack tip element were developed. These displacements were used for the evaluation of SIFs using CSDE technique. For plate problems, $J-$ integral technique was developed in the evaluation of SIFs.

Several plate and shell examples for different geometries, loadings and boundary conditions were analysed, and the results presented showed good accuracy can be obtained with relatively coarse meshes.

In the next chapter, crack growth simulation of plates and shells using the Dual Boundary Element Method will be presented.

Chapter 6

Crack Growth Simulation

6.1 Introduction

Damage tolerance design of engineering structures are based on analysis of crack propagation and its effect on the structural strength. In general numerical methods such as the Boundary Element Method (BEM) and the Finite Element Method (FEM) must be used for the evaluation of crack growth parameters, as their complex shape and the continuously changing path of growing cracks. The simulation of general crack propagation using numerical techniques requires the ability to predict the direction and magnitude of the crack growth for a given load cycle as well as the ability to update the numerical model to account for the changing geometry.

Reports on the application of the finite element method to crack growth simulation can be found in Valliapan, S. and Murti, V. [133], Remzi and Blackburn [110], O'Donoghue *et al.* [92], Potyondy *et al.* [102], Bittencourt *et al.* [24]. Crack analysis using finite element method can be quite tedious, due to intrinsic features of the method. Very fine mesh is needed in order to obtain accurate solutions. Furthermore, it is very difficult to simulate crack growth using FEM, because the model has to be remeshed for each step of the crack extension.

The Dual Boundary Element Method (DBEM) has in recent years become an established numerical tool for solving crack problems. This is due to the inherent efficiencies within the method which include accurate representation of stresses (essential in accurate life prediction methods) and reduced modelling requirements

compared to other methods (i.e. only the surface of the problem needs to be modelled). Using the DBEM, cracked structure can be modelled using a single region, and crack extension process is simulated by introducing new boundary elements in each crack growth increment. Hence, remeshing of the non-cracked boundary is not necessary, and this has resulted in the development of techniques for automatic simulation of crack growth with substantially simplified modelling and improved accuracy of the computation.

DBEM has been applied to two- and three-dimensional analysis of elastic, fully non-linear elastoplastic, elastodynamics (rapid crack growth and impact loading), thermo-mechanical fatigue, fretting, concrete cracking, composite materials, stiffened panel and crack growth in cold-expanded specimens, as has been reviewed by Aliabadi [10]. Recently, Dirgantara and Aliabadi presented application of dual boundary element method to crack growth analysis of plates [41] and shallow shells [44].

In this chapter, the dual boundary element formulation for the analysis of crack growth in plates and shells subjected to bending and tension is presented. Crack extension processes are simulated by introducing new boundary elements in each crack growth increment. For each increment of the crack extension analysis, five stress intensity factors, two for membrane behaviour and three for bending and shear are computed. Crack-growth direction is defined based on the maximum principal stress criterion, and crack-growth life calculations for single crack or multiple cracks are obtained using the Paris empirical formula. All procedures are computed automatically for each cycle of crack increment.

6.2 Crack Growth Simulation

In general, cracking processes can extend the cracks along curved paths. However, in practice, curved paths are usually modelled with flat increments which lead to piece-wise flat cracks. Crack growth incremental analysis, regardless of the numerical method being used, requires remeshing at the end of each iteration. The remeshing process can be quite cumbersome with domain type methods such as the FEM. On the application of conventional BEM formulation to crack growth analysis,

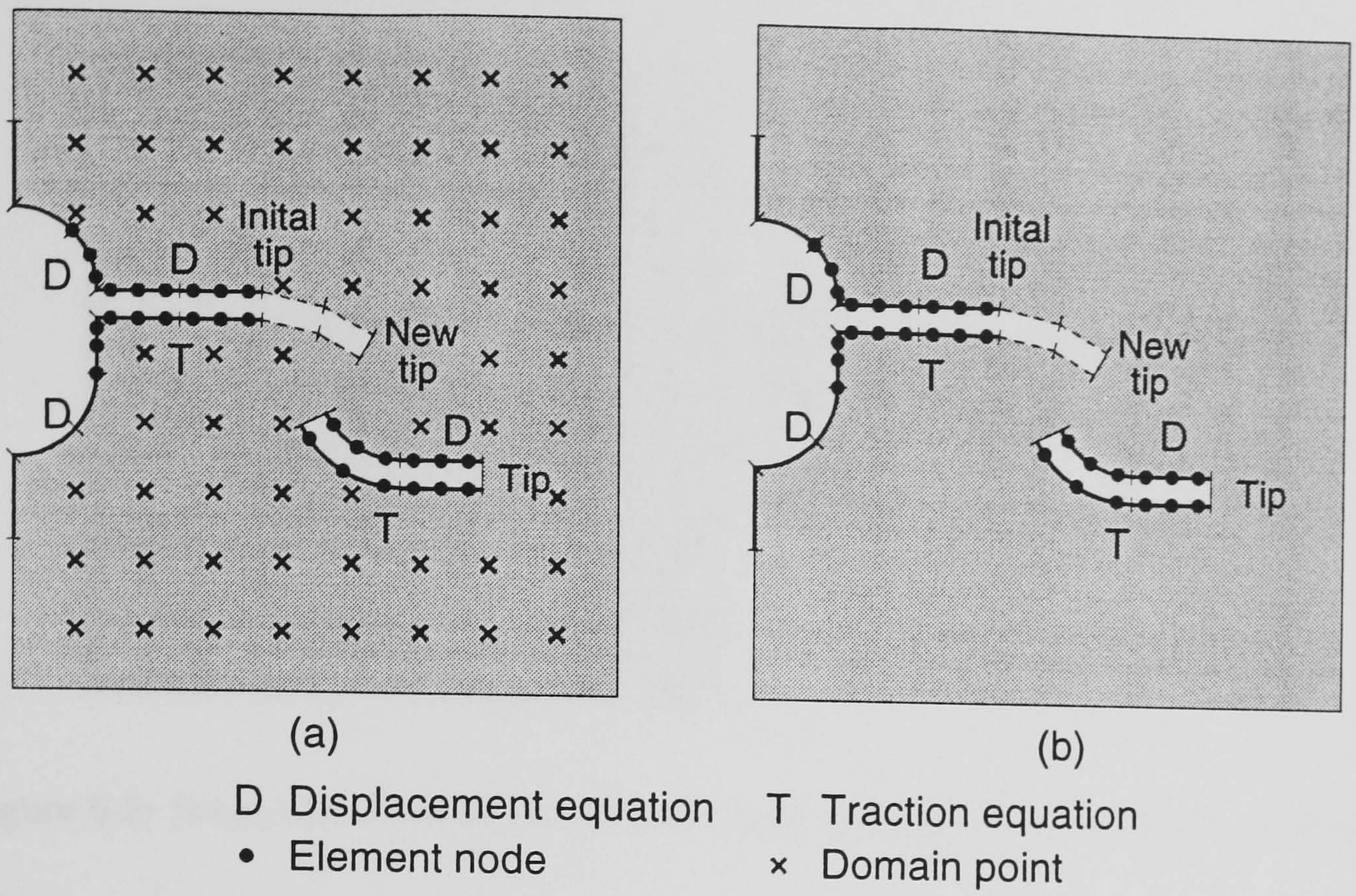

Figure 6-1: Modelling strategies for dual boundary element method: (a) shells; (b) plates.

using sub-regions technique, artificial boundaries which are required by sub-region have to be generated at each iteration [25]. As such, the method cannot be easily automated.

The use of only single region, an intrinsic feature of the DBEM, eliminates the above mentioned remeshing difficulties. At the end of each iteration, new crack extension increments are modelled with new discontinuous elements, as shown in Figure 6-1. The new discontinuous boundary elements of the crack-extension increment will generate new equations and update the ones already existing with new unknowns. In other words, new boundary elements will generate new rows and columns in the system matrix. This procedure is illustrated schematically in Figure 6-2.

If the $LU-$ decomposition method is adopted for the solution of the system of equations, a very efficient incremental analysis can be carried out. For each increment of the analysis, only the new rows and new columns need to be $LU-$ decomposed. The existing rows and columns, already decomposed, are brought from the previous iteration into the current one. In this work, this procedure is implemented to crack growth simulation of plate loaded in combine bending and

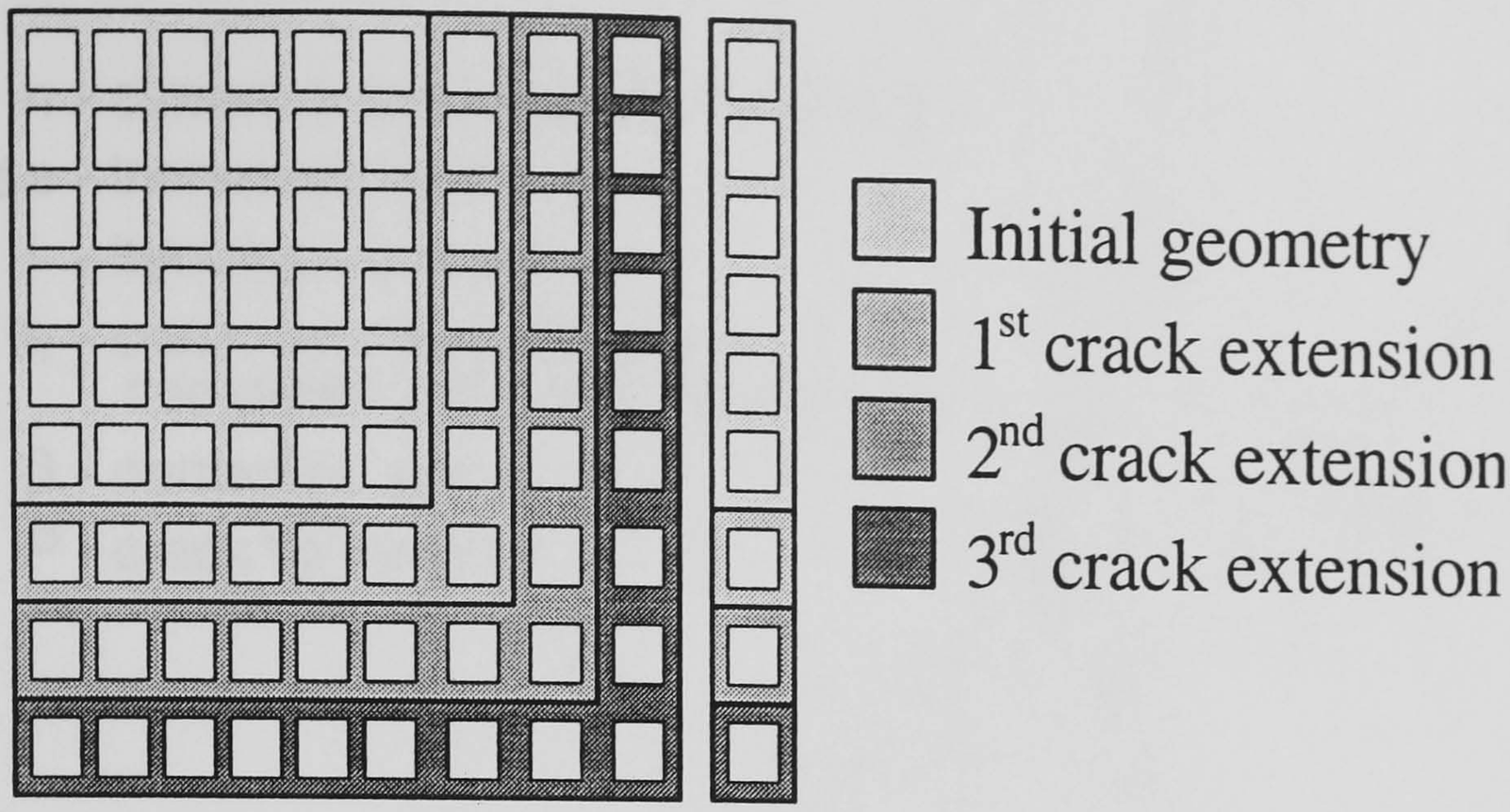

Figure 6-2: Schematic illustration of incremental generation of the system matrices.

tension.

The procedure for crack growth simulation of shell is slightly different. In this work, the bending and membrane stress intensity factors are evaluated using the crack surface displacements extrapolation technique (CSDE) , in which special crack tip elements are used (see section 5.4). In every increment, new crack extension increments are modelled with new discontinuous elements. Those new additional discontinuous elements become new crack tip elements, and the old crack tip elements are modified to regular element. This feature changes some rows of the system of equation from preceding increment. Therefore, in this procedure, for each increment of the analysis the complete system of equation needs to be $LU-$ decomposed.

6.2.1 Crack propagation direction

As discussed in chapter 2, the bending and shear stress intensity factors do not affect the direction of the crack propagation, since only mid-surface of the plate or shell is considered in the numerical model. The maximum principal stress criterion correlated only to the two membrane stress intensity factors, is used to evaluate the direction of crack extension. The crack will grow from the tip in the direction θ_t along which the shear stress is zero, that is

$$K_{I(m)} \sin\theta_t + K_{II(m)} (3\cos\theta_t - 1) = 0 \tag{2.108}$$

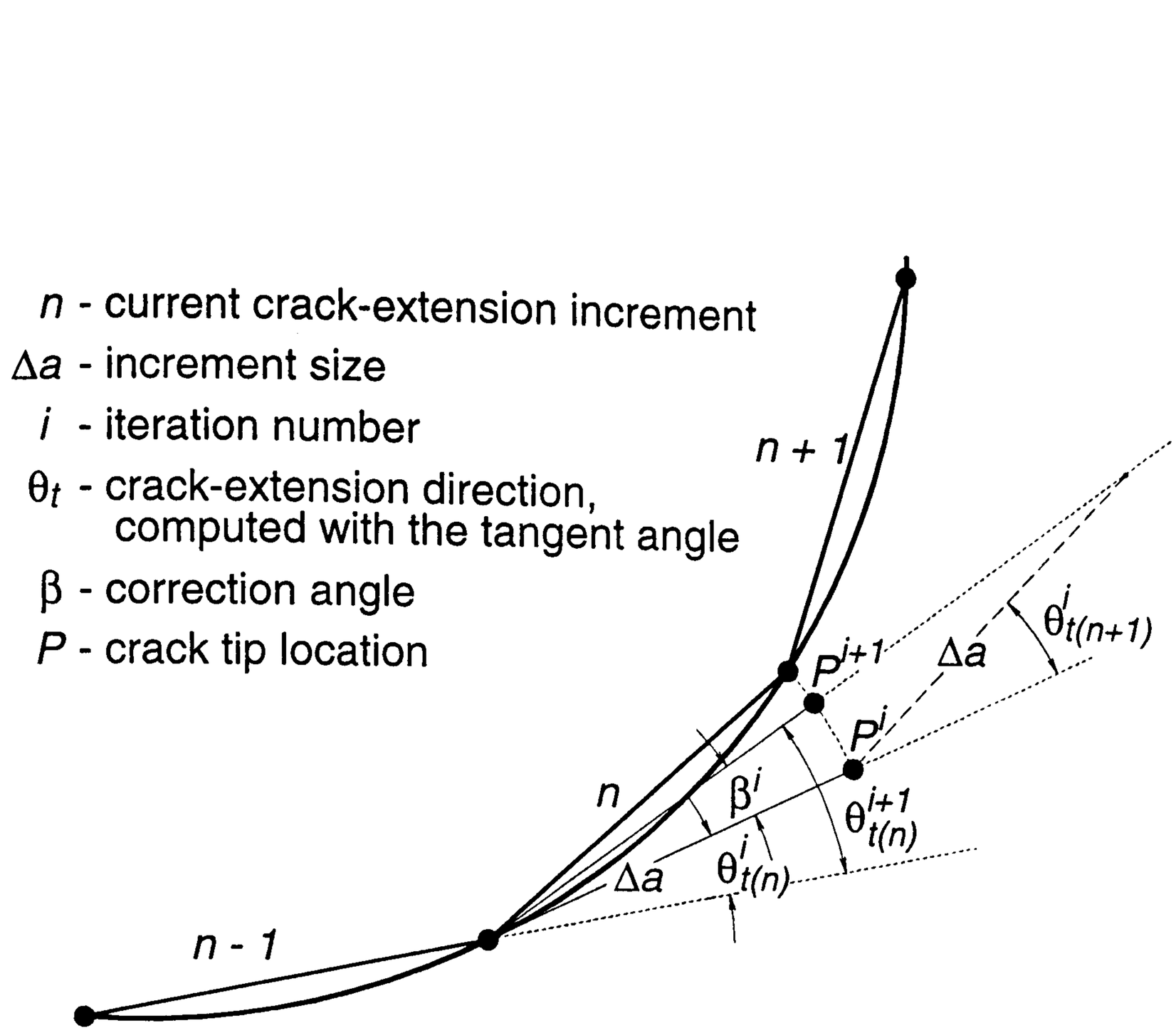

Figure 6-3: Incremental crack-extension direction.

where θ_t is an angular coordinate centered at the crack tip and measured from the crack axis ahead of the crack tip.

According to maximum principal stress criterion, the crack path is defined continuously by the trajectory of the maximum principal stress at the crack tip. The criterion does not take account of the discreteness of the crack-extension modelling approach. Hence, the crack extension direction in a general mixed-mode deformation field, indicates by local tangent angle θ_t shown in Figure 6-3, is always defined by the local stress field in the same direction, whatever length of crack extension is considered. As a consequence, the uniqueness of the continuous crack path cannot be guaranteed for different increment size of the crack-extension. Thus, the tangent direction of the crack path predicted by equation (6.1) must be corrected to give the direction of the actual crack-extension increment, taking into account the increment size, such that the requirement of uniqueness is satisfied.

In this work, a procedure developed by Portela *et al.* [101] for two-dimensional crack growth analysis is adopted to overcome that difficulty. Procedure for an n-th crack-extension increment is schematically shown in Figure 6-3. A correction angle β is introduced in this procedure to the tangent direction $\theta_{t(n)}$. The correction angle is

$\beta = \theta_{t(n+1)}/2$, in which $\theta_{t(n+1)}$ is the direction of the next crack-extension increment. This prediction-correction procedure can be applied iteratively until convergence is obtained for θ_t. For the current n-th crack-extension increment, the i-th iteration of this process can be summarized as follows:

- the crack path tangent direction $\theta^i_{t(n)}$ is predicted by equation (6.1), for the first iteration only;
- the crack is extended one increment, Δa, to P^i and the new stress intensity factors are evaluated;
- the new crack path tangent direction $\theta^i_{t(n+1)}$ is evaluated by equation (6.1) using the new stress intensity factors;
- the correction angle $\beta^i = \theta^i_{t(n+1)}/2$ is defined;
- the direction of the crack extension increment defined in previously is corrected to a new direction, given by $\theta^{i+1}_{t(n)} = \theta^i_{t(n)} + \beta^i$
- the above steps are repeated sequentially, starting with the second step, while $|\beta^{i+1}| < |\beta^i|$

It can be seen that as $\Delta a \rightarrow 0$, so does the correction angle β and hence, the crack path extension direction tends to follow the continuous crack path.

6.2.2 Fatigue life prediction

There are not many numerical studies reported for fatigue lives prediction of plates subjected to bending and tension and shells. Potyondy *et al.* [102] proposed an empirical procedure for incorporating the effect of the bending stress intensity factors on the crack growth rate. It is assumed that a fraction of energy from bending stress intensity factors also give contribution to fatigue crack growth, through the following relationship:

$$K_{eff} = \sqrt{EG_{eff}} \tag{6.1}$$

where the effective energy release rate G_{eff} is defined empirically as

$$G_{eff} = G_1 + \alpha \left(G_2 + G_3 + G_4 + G_5 \right), 0 \leqslant \alpha \leqslant 1.0 \tag{6.2}$$

In their examples, $\alpha = 0.4$ is chosen arbitrarily. Knops [72] also used the above empirical relationship with $\alpha = 1.0$, also chosen arbitrarily. The energy release rate components G_1 and G_2 are related to stress intensity factors due to membrane loads, via relationships

$$G_1 = \frac{{K_{I(m)}}^2}{E} \tag{6.3}$$

$$G_2 = \frac{{K_{II(m)}}^2}{E} \tag{6.4}$$

and G_3, G_4 and G_5 are components of energy release rate related to maximum value of stress intensity factors due to bending and shear loads,

$$G_3 = \frac{\pi \, {K_{I(b)}}^2}{3E} \tag{6.5}$$

$$G_4 = \frac{\pi \, {K_{II(b)}}^2}{E} \tag{6.6}$$

$$G_5 = \frac{8\pi \left(1 + \nu\right) {K_{III(b)}}^2}{5E} \tag{6.7}$$

where $K_{I(m)}, K_{II(m)}$ are stress intensity factors due to membrane loads, and $K_{I(b)}$, $K_{II(b)}$, $K_{III(b)}$ are stress intensity factors due to bending and shear loads. The relationships between stress intensity factors and membrane, bending and shear stress resultant intensity factors K_{1m}, K_{2m}, K_{1b}, K_{2b}, and K_{3b} are presented in equations (2.85 – 2.90). Since the thickness of the plate is relatively small compared to the other geometries, only the maximum values of $K_{I(b)}, K_{II(b)}, K_{III(b)}$ is considered for fatigue life calculation using the numerical model based on plate and shell theories, where in physical reality $K_{I(b)}, K_{II(b)}$ varied linearly across the thickness and the maximum value of $K_{I(b)}$ and $K_{II(b)}$ occur at the top or bottom surface, while $K_{III(b)}$ varied quadratically across the thickness and the maximum value of $K_{III(b)}$ occur at the middle surface. Based on the above considerations it is reasonable that the value

of α is expected to vary between 0 and 1. In this work the value of α is proposed as equal to $\sqrt{\frac{|\Delta K_{I(b)}|}{|\Delta K_{I(b)}|+|\Delta K_{I(m)}|}}$.

Knowing the effective stress intensity factor K_{eff}, the fatigue crack growth properties of the structural material (da/dN) can be calculated using the Paris law presented in chapter 2, i.e.

$$\frac{da}{dN} = C_p \left(\Delta K_{eff}\right)^{m_p} \tag{2.107}$$

In the present analysis, an arbitrary crack-extension increment size (Δa_0) is defined before starting the simulation. The size may be defined as the result of a compromise between accuracy and computational cost. The smaller the size of the crack-extension increment, the more accurate and time consuming is the analysis.

6.2.3 Multiple cracks growth simulation

The present method can also be applied for simulating the growth of multiple cracks. In this case, for the same number of cycles, the cracks may grow at different rates, therefore the crack-extension increment size for each crack tip (Δa_i) for every increment has to be determined. A prediction-correction procedure for two dimensional problem developed by Salgado and Aliabadi [114] is adopted in the present analysis.

At the end of each incremental analysis, the effective stress intensity factors are calculated for each crack tip, and equation (6.8) is integrated to determine, for each crack tip (i) the number of cycles (ΔN_i) necessary to grow an arbitrary crack-extension increment size (Δa_0), that is

$$\Delta N_i = \frac{1}{C_p} \int_{a_i}^{a_i+\Delta a_0} \frac{1}{\left(\Delta K_{eff}\right)^{m_p}} da \tag{6.8}$$

The size of Δa_0 is constant for the whole iterations, and is defined arbitrarily before starting the simulation. For the first iteration, the integration of equation (6.8) is performed assuming that the stress intensity factors remain constant as the crack grows from the initial size a_i to $a_i + \Delta a_0$.

It is then assumed that the fastest growing crack tip will grow until the chosen increment size Δa_0, and the number of cycles needed $[\Delta NC = \min\left(\Delta N_i\right)]$ by that

crack tip is selected as the reference number of cycles. Then the crack-extension increment sizes of the other cracks are calculated by integrating

$$\Delta a_i = C_p \int_{NC}^{NC+\Delta NC} (\Delta K_{eff})^{m_p} \, dN \tag{6.9}$$

Again, the stress intensity factors are assumed to remain constant.

However, as the cracks grow, the stress intensity factors generally change. More importantly, due to the crack interaction, their relative value may change as well. Therefore, as in the prediction of crack growth direction, the uniqueness of the crack extensions cannot be guaranteed for different increment size of the crack-extension.

To overcome the problem, an iterative procedure is applied here. After the first iteration, the boundary element mesh is then updated to include the new increments, and a structural analysis is carried out, at the end of which, the new stress intensity factors are calculated. The increment size is then recalculated, now taking into account the variation of the stress intensity factors range when integrating equations (6.8) and (6.9). The increments of crack extension are remeshed and another analysis is performed. This procedure is repeated until convergence of the increment size is achieved.

Actually, the prediction-correction procedure for direction and increment size are done simultaneously.

6.2.4 Computational procedure

Finally, by applying the procedures explained above, the computational procedure the DBEM for each increment of the crack extension can be summarized as follows:

1. Carry out a DBEM analysis of the cracked plate subjected to bending and tension;
2. For each crack tip compute the five stress intensity factors with the CSDE or $J-$ integral technique, and calculate the effective stress intensity factors range (ΔK_{eff});
3. For each crack tip compute the direction of the crack-extension increment using the maximum principal stress criterion;

4. For each crack tip calculate crack-extension increment size assuming that, as the crack grows, the effective stress intensity factors remain constant;
5. Extend each crack tip one increment along the direction and by the size computed in the previous step;
6. Perform a new DBEM analysis;
7. Calculate a new effective stress intensity factors range;
8. Recalculate the direction and the size using the prediction-correction procedure explained above, taking into account the variation of the stress intensity factors range;
9. Verify convergence for the crack-extension increment direction and size. If not achieved, return to step (5);
10. Repeat all the above steps sequentially until a specified number of crack increments is reached.

6.3 Numerical examples

To present the capability of the proposed method, several numerical examples are analysed.

6.3.1 Rectangular plate with a centre crack loaded by bending and tension

In this example, a rectangular plate with central crack loaded by edge bending and tension (as shown in Figure 6-4) is analysed. The stress intensity factors for this problem have been calculated by Boduroglu and Erdogan [33] for edge bending load and Tada [86] for tension. The properties of the plate are: $h = 0.1$ and 0.5 m; $2a_0 = 0.2$ m; $2b = 2$ m; $E = 210000$ MPa and $\nu = 0.3$.

For the analysis, 8 elements per side of the plate and 8 elements for each initial crack surface are being used. The crack grows to both direction, with two elements for each crack surface are added on each increment.

Figure 6-5 shows the result of this example. This example is a symmetric case, therefore - as expected - the crack grows straightly along the symmetric line. The

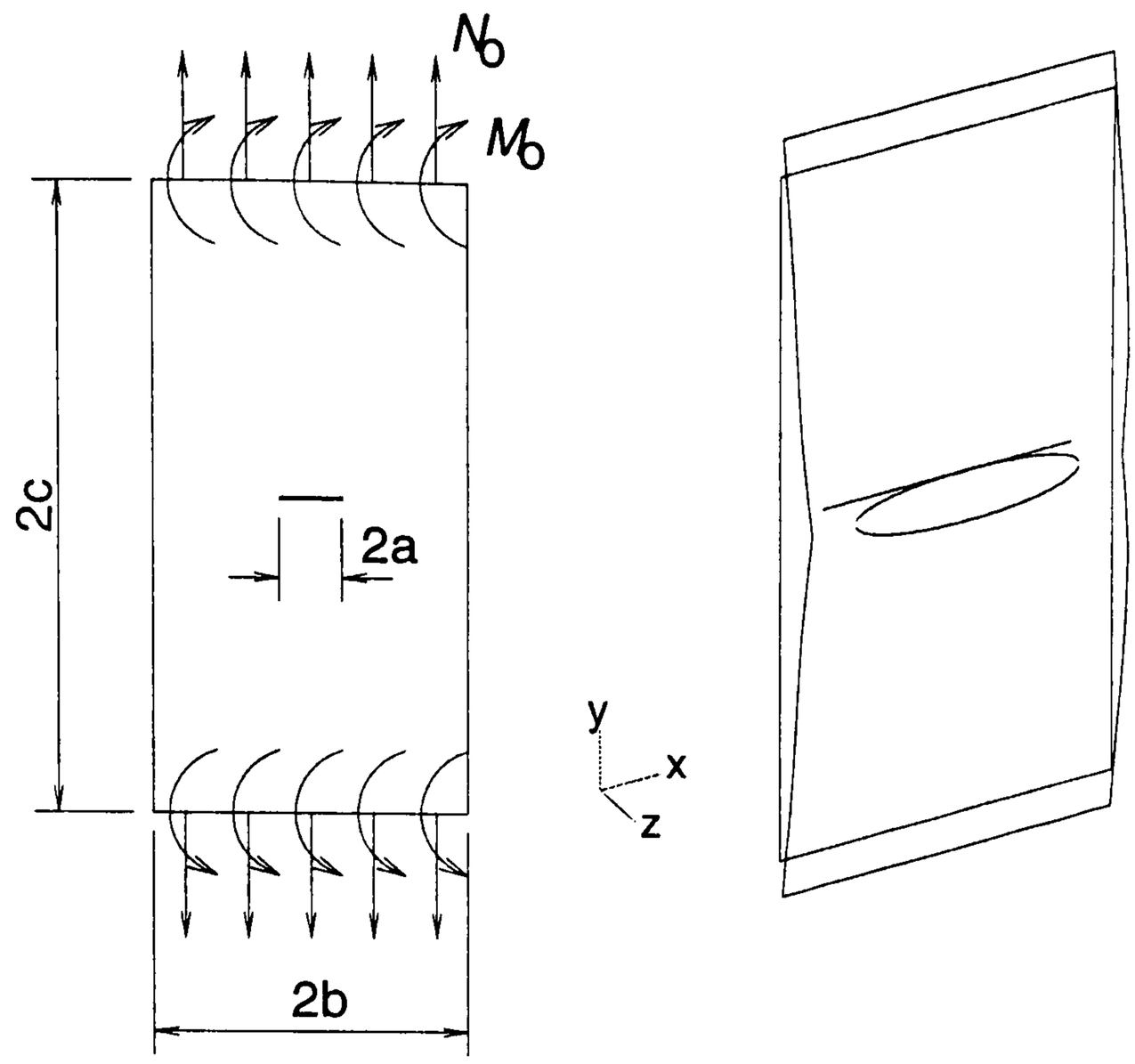

Figure 6-4: Rectangular plate with a centre crack loaded by bending moment and tension, and deformed shape of DBEM model.

DBEM results show excellent agreement with References [86] and [33].

6.3.2 Infinite plate with a slant centre crack loaded by bending and bi-axial tension

In this example, an infinite plate with a slant centre crack loaded by edge bending and bi-axial tension (as shown in Figure 6-6), similar to the example presented in chapter 5 is analysed. To demonstrate the effect of different loading to the direction of crack propagation, four cases with $N_1/N_2 = 0.0$, 0.5, 1.0 and 10.0 are considered. For all cases the initial crack angle β is set to be 45^0. The properties of this plate are: $h = \sqrt{10}$ m; $2a_0 = 1$ m; $2b = 100$ m; $E = 210000$ MPa and $\nu = 0.25$. Experimental results of this example with $N_1/N_2 = 0.0$ were reported by Erdogan and Sih [50].

For the analysis, 8 elements per side of the plate and 8 elements for each initial crack surface are being used. Figure 6-8 shows the crack growth path for this example. It is shown that the crack grows in different direction for different ratios of N_1/N_2. For the case with $N_1/N_2 = 0.0$, fracture angle θ (see Figure 6-7)obtained from the DBEM analysis is 51.76^0, while the experimental result, extracted from

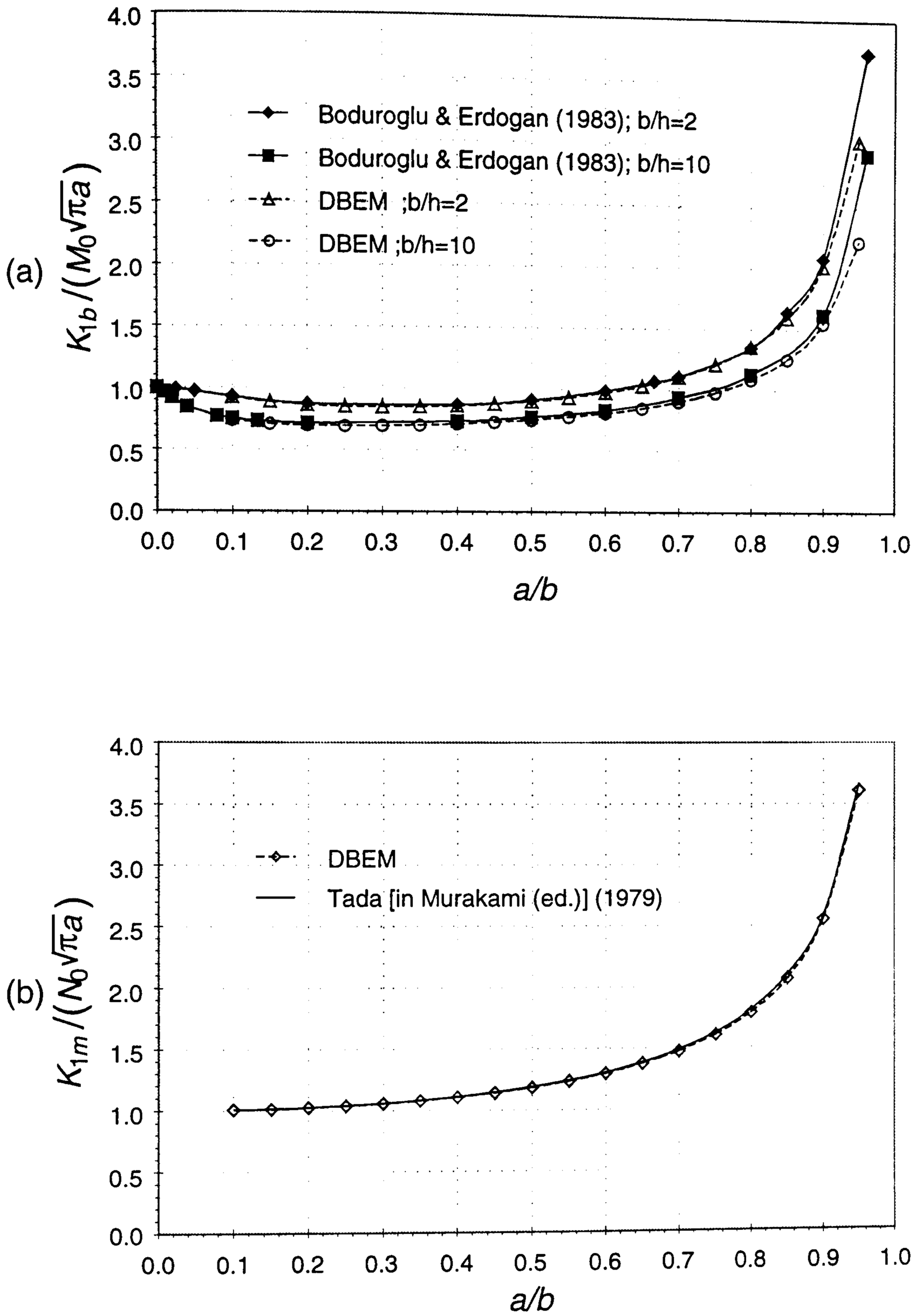

Figure 6-5: Normalised bending stress resultant intensity factors and membrane stress intensity factors results for the rectangular plate with a centre crack.

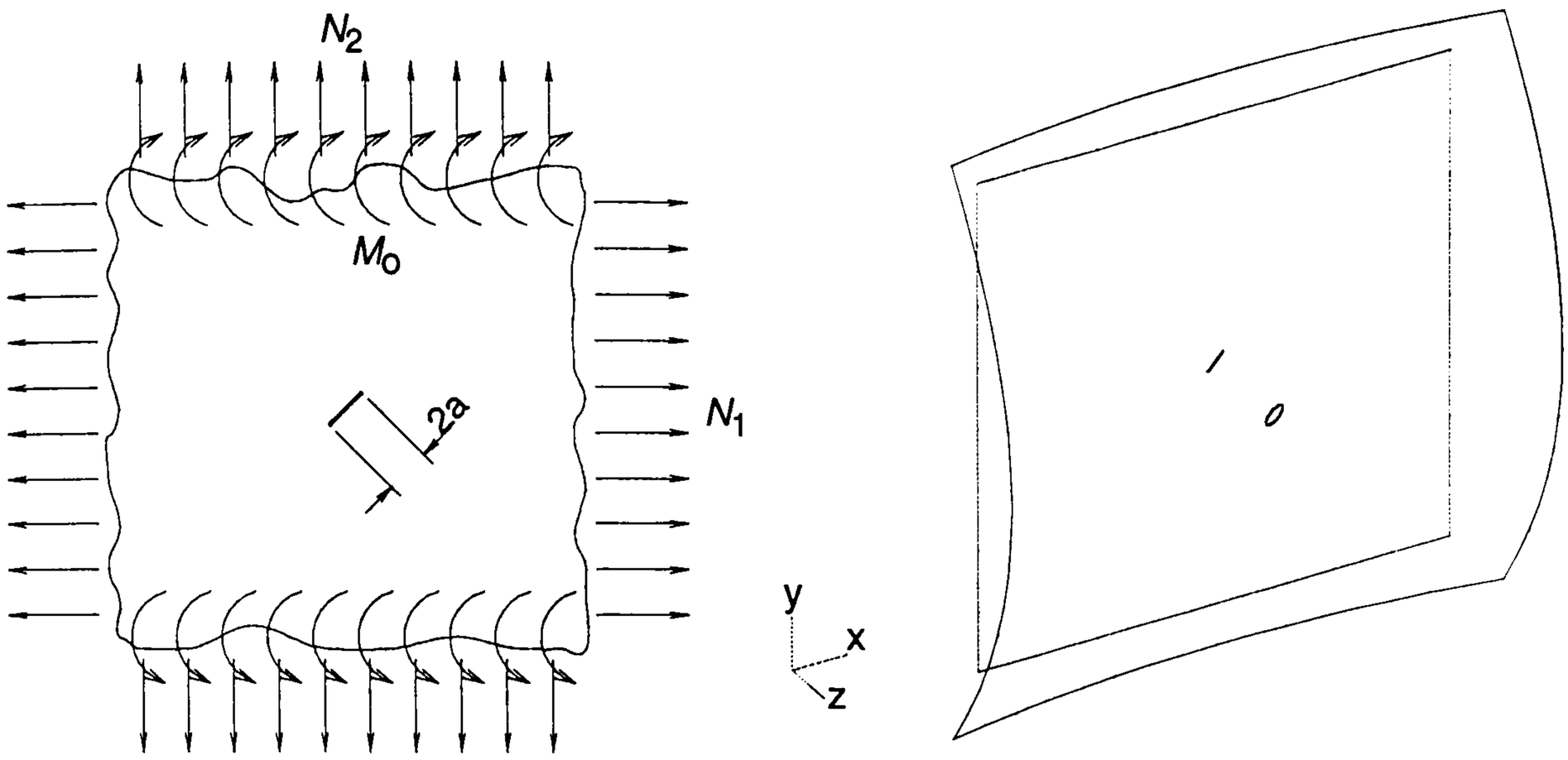

Figure 6-6: Infinite plate with a slant centre crack loaded by bending and bi-axial tension, and deformed result of DBEM model.

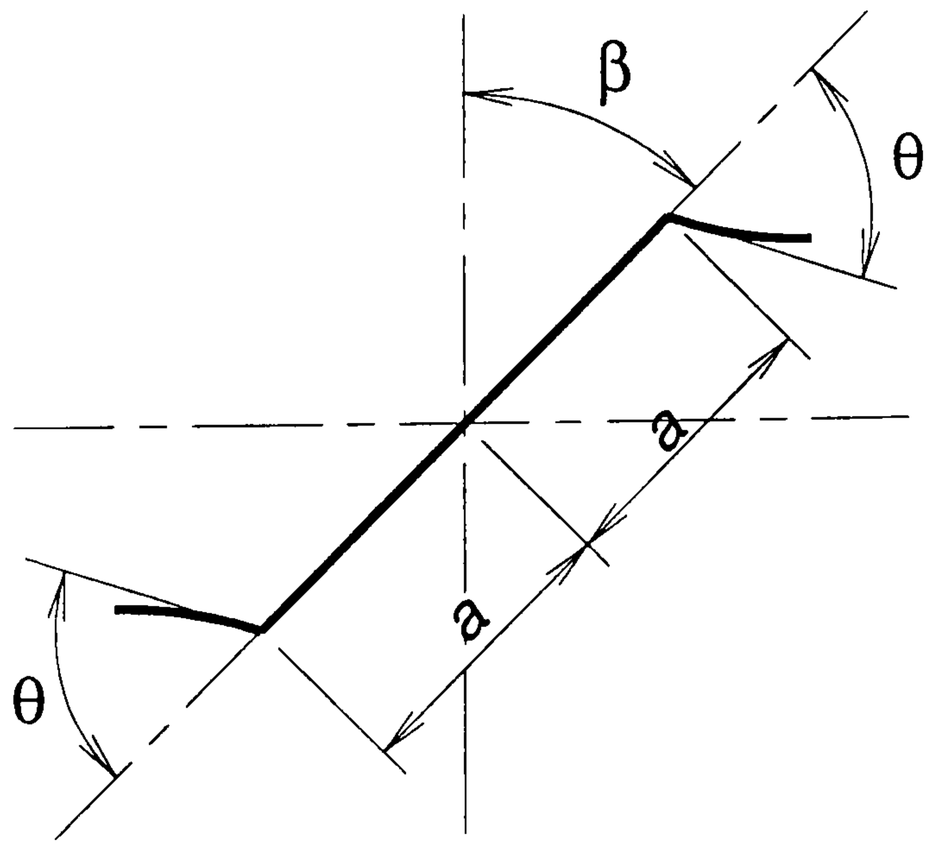

Figure 6-7: Fracture angle for a slant crack.

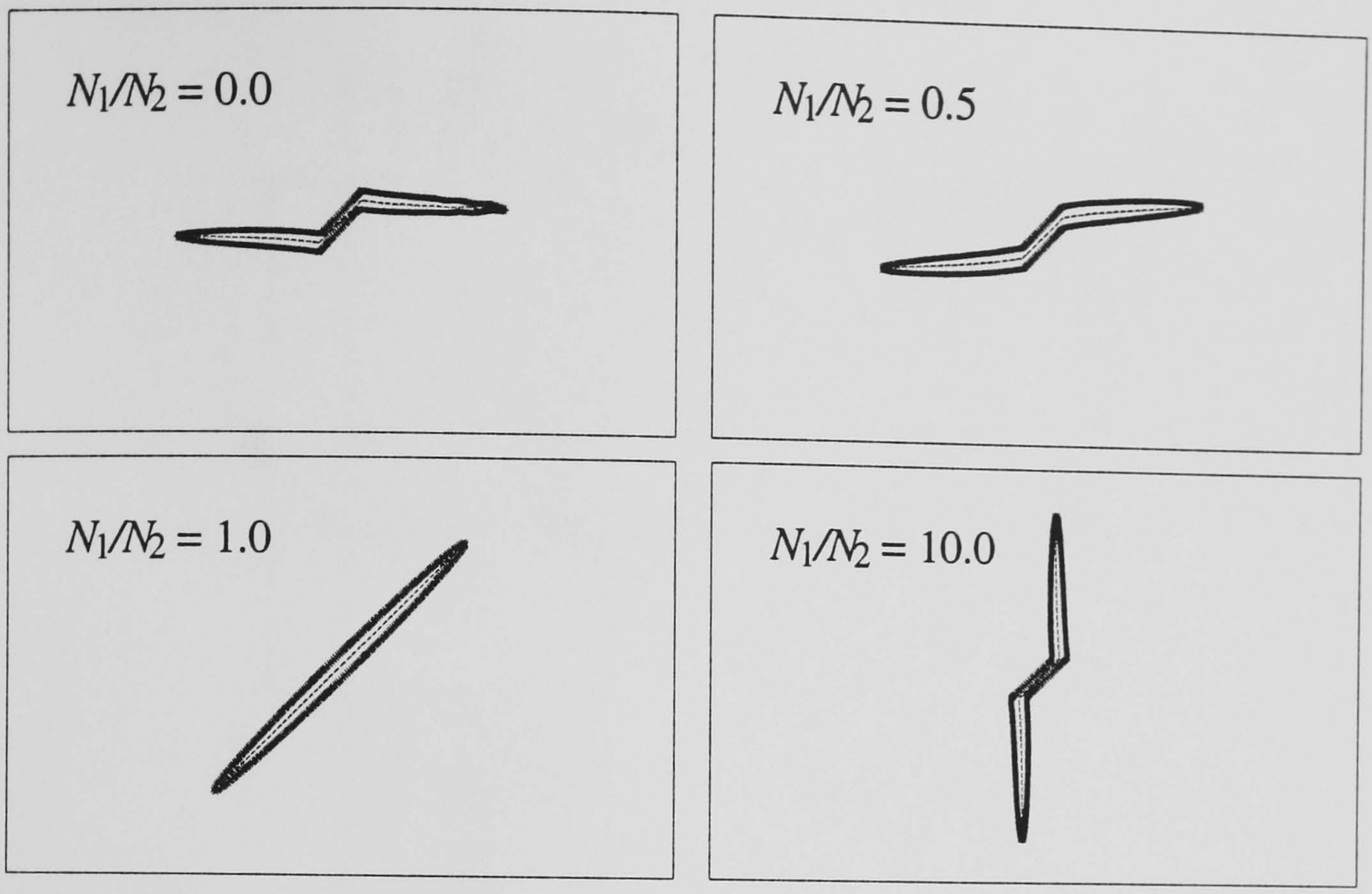

Figure 6-8: Crack growth path of a slant crack in an infinite plate subjected to different ratios of N_1 and N_2.

the graph plotted in [50], is 53.25^0. In the case where $N_1/N_2 = 1.0$, the same amount of load is transferred in horizontal and vertical directions. The resulting maximum principal stresses is in directions perpendicular to the initial crack line. Consequently, the crack grows on a straight path in the same direction as the initial crack.

For the case with $N_1/N_2 = 0.5$, the crack tends to grow in the direction closer to a horizontal line and for the case with $N_1/N_2 = 10.0$, the crack tends to grow in the direction closer to a vertical line.

6.3.3 Rectangular plate with symmetric edge cracks loaded by torsion and tension

In this example, a rectangular plate with symmetric edge cracks loaded by edge bending and tension (as shown in Figure 6-9) is analysed. Experimental measurements for this geometry and loading were reported by Viz, Zehnder and Bamford [137] using Aluminium alloy 2024-T3. The properties of the plate are: $h = 2.29$ mm; $a_0 = 6.86$ mm; $2b = 152$ mm; $2c = 313$ mm; $E = 72397.5$ MPa and $\nu = 0.33$.

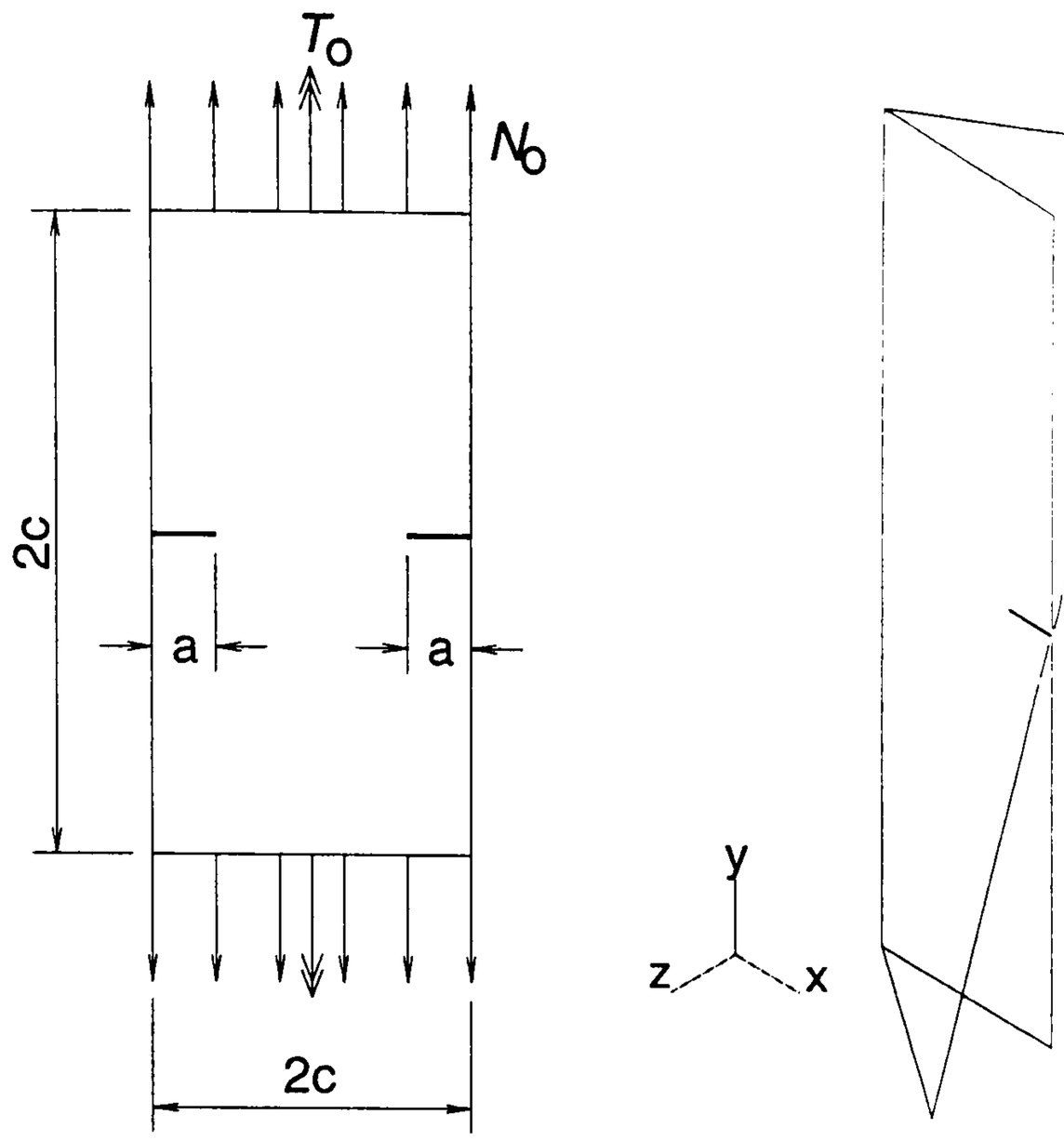

Figure 6-9: Rectangular plate with symmetric edge cracks loaded by torsion and tension, and deformed result of DBEM model.

Two loading combinations are presented here. In the first case, $T_0 = 112.0$ Nm and $N_0 = 44.5$ kN and in the second case $T_0 = 112.0$ Nm and $N_0 = 4.5$ kN. In all loading cases, the stress ratios $R = 0.7$ is applied to the specimen.

Since it is a symmetric case, only half of the plate is modelled. A total of 30 elements for plate boundary and 8 elements for each initial crack surface are used. Two boundary elements for each crack surface are added in each increment.

To obtain the fatigue diagram, constants of material data for Paris equation $\frac{da}{dN}\left[\frac{mm}{cycle}\right] = C_p\left(\Delta K_{eff}\left[Nmm^{-3/2}\right]\right)^{m_p}$ from Hudson [65] are used. For $R = 0.7$, $C_p = 1.24 \times 10^{-14}$; $m_p = 4$. To investigate the effect of bending stress intensity factors, three values of α are used in this work, i.e. 1.0, 0.0 and $\alpha = \sqrt{\frac{|\Delta K_{I(b)}|}{|\Delta K_{I(b)}| + |\Delta K_{I(m)}|}}$.

Figure 6-10 shows numerical crack growth diagram of the specimen using the proposed method compared to the average crack lengths taken from the experiment [137].

As it can be seen, the numerical results using $\alpha = 0.0$ underestimate the experi-

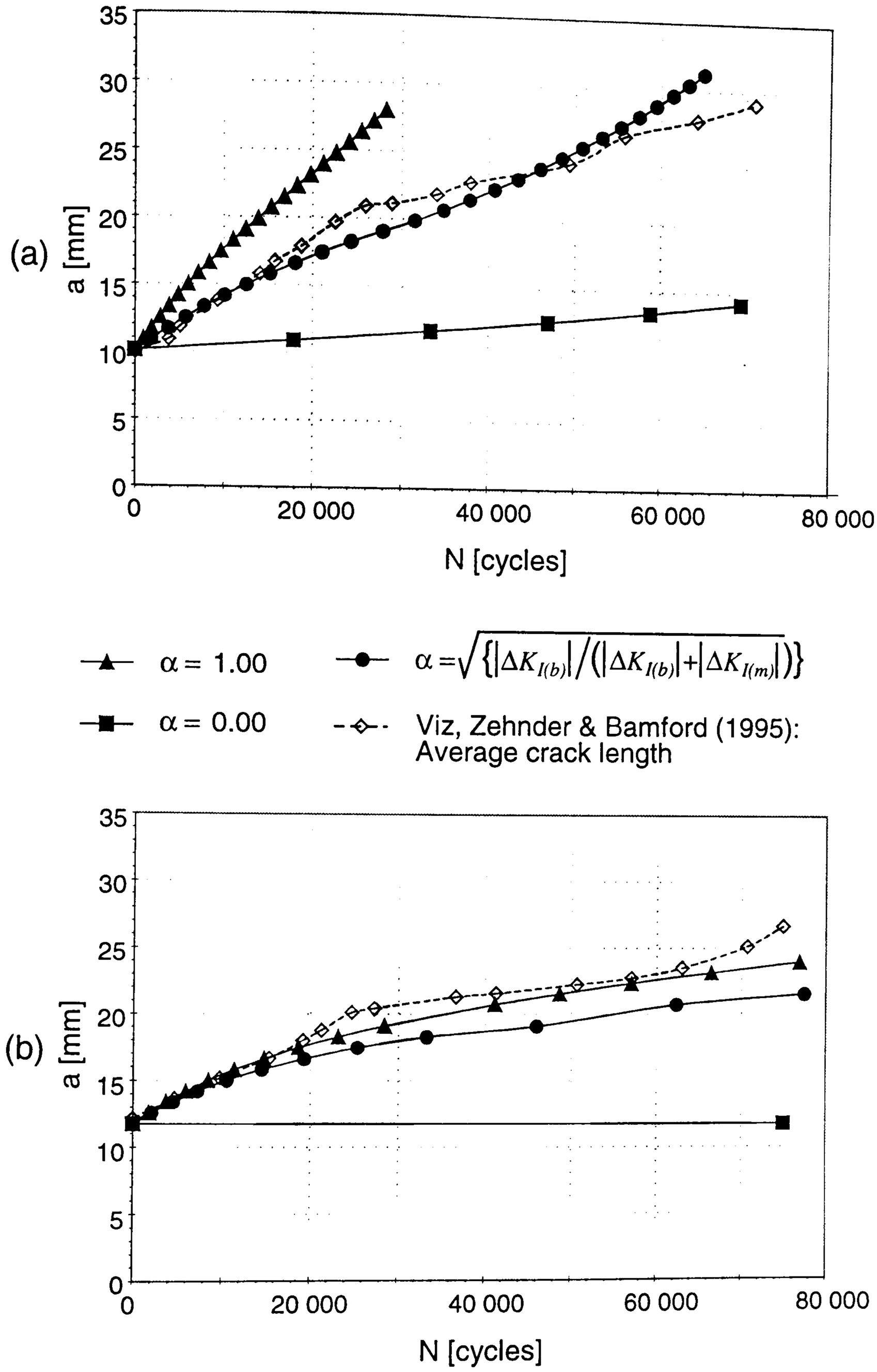

Figure 6-10: Crack growth curve for two loading cases of example 3; (a) first loading case (b) second loading case.

mental results. They show that stress intensity factor due to torsion moment have significant contribution to the crack growth rate of plate loaded in combine moment and tension. It can also be seen that the results using $\alpha = \sqrt{\frac{|\Delta K_{I(b)}|}{|\Delta K_{I(b)}| + |\Delta K_{I(m)}|}}$ give relatively good agreement with the experimental results.

It is worth noting that in the experiment the left and right crack tips grow at different rates and hence the configuration is not symmetrical anymore, while in the numerical study, if the initial conditions are symmetrical then the cracks will grow symmetrically.

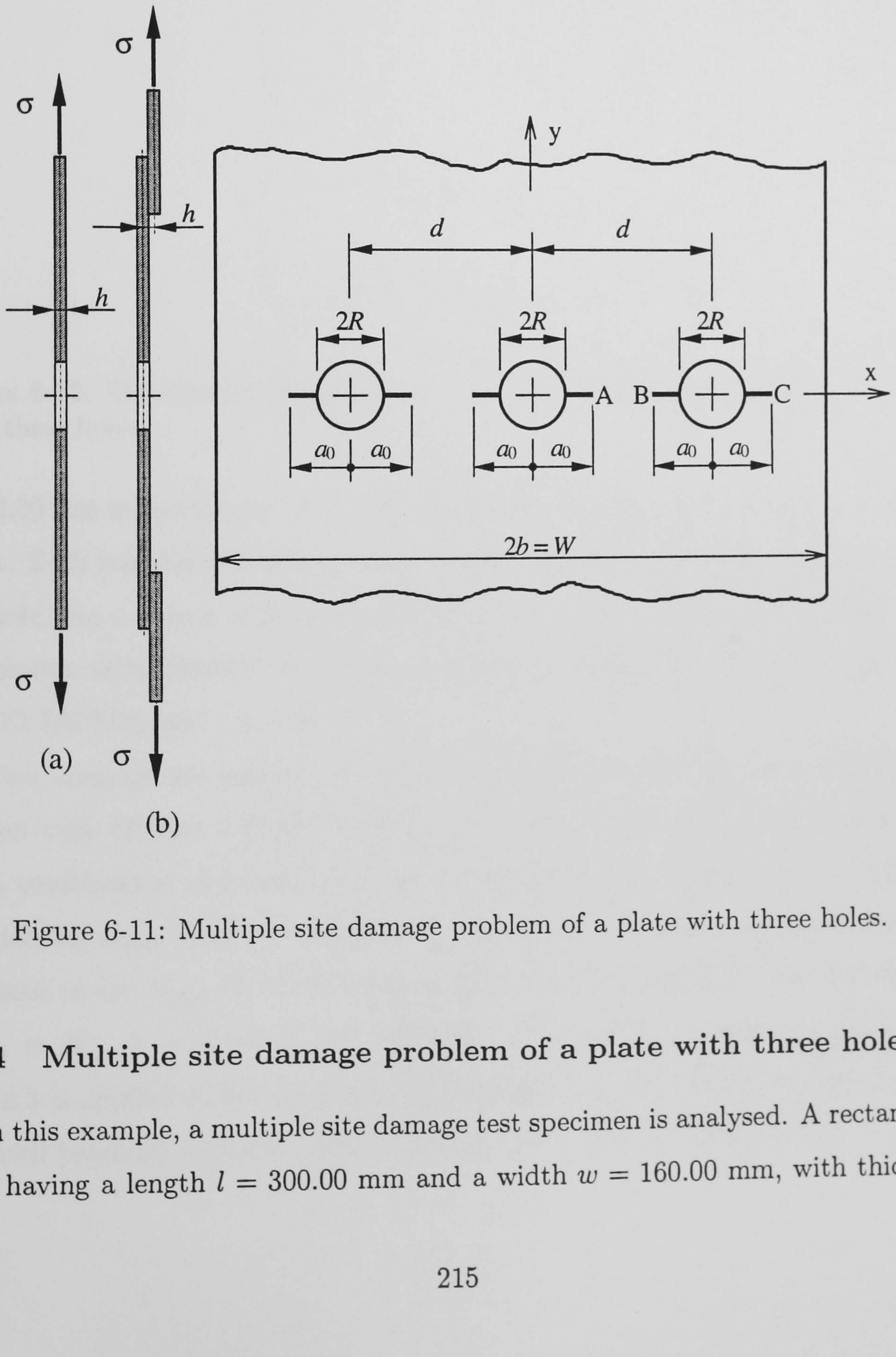

Figure 6-11: Multiple site damage problem of a plate with three holes.

6.3.4 Multiple site damage problem of a plate with three holes

In this example, a multiple site damage test specimen is analysed. A rectangular plate having a length $l = 300.00$ mm and a width $w = 160.00$ mm, with thickness

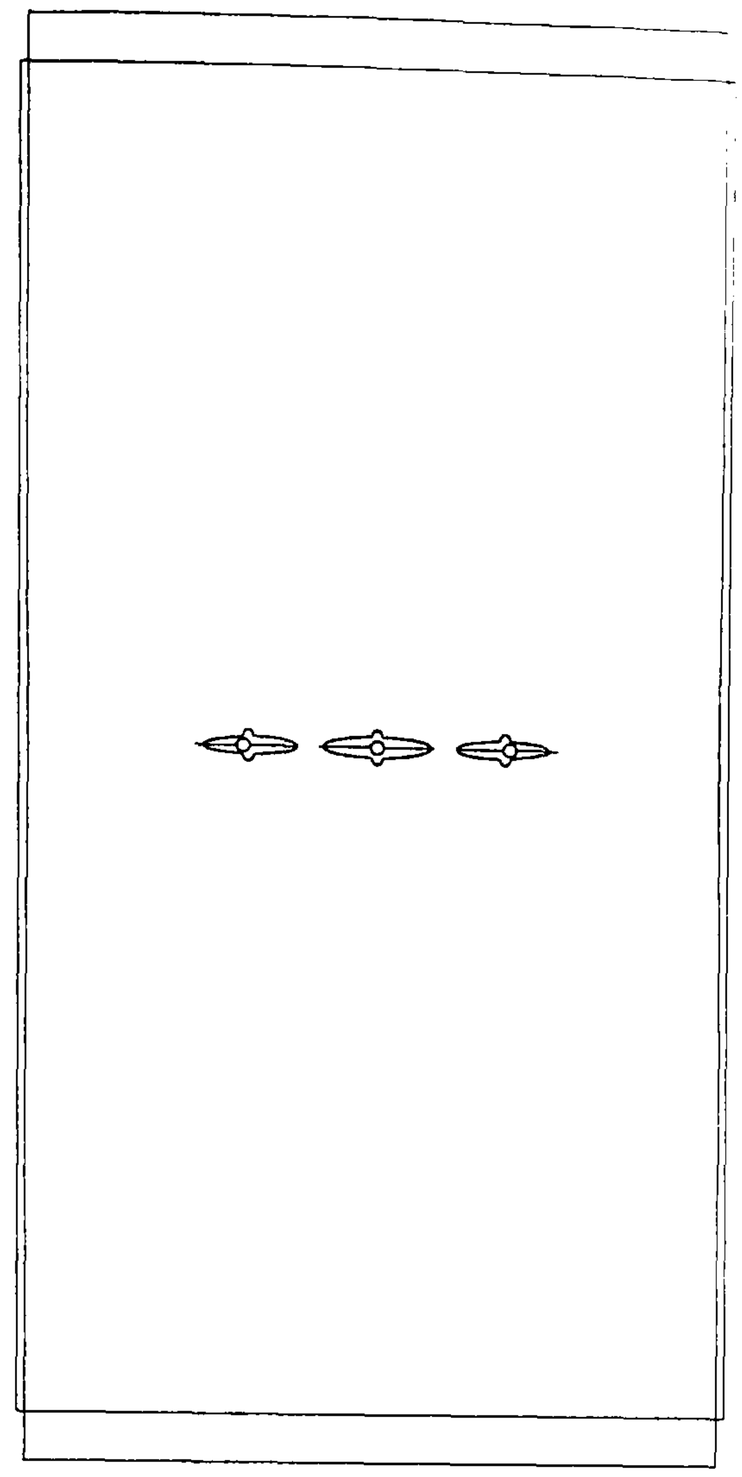

Figure 6-12: Deformed DBEM model of multiple site damage problem of a plate with three holes.

$h = 2.00$ mm is considered. The plate has three holes of 3.0 mm in diameter, 30 mm apart. Each hole has two initial cracks length of 3.5 mm measured from the edge of the hole, ($a_0 = 5$ mm as shown in Figure 6-11). The material used for this test is Aluminium alloy 2024-T3, with yield strength $\sigma_y = 331$ MPa, modulus of elasticity $E = 73\ 780$ MPa and $\nu = 0.33$.

Two analyses are carried out in this example. Firstly the plate is loaded by tension only (Figure 6-11(a)) with $\sigma_{\max} = 20\%$ of σ_y and for the second loading a combination of tension and secondary bending is applied (Figure 6-11(b)). Multiplying $\sigma_{\max}$ with the thickness h, maximum membrane stress resultant is obtained to be $N_{\max} = 0.1324$ MN/m and secondary bending stress resultant is $M_{\max} = N_{\max} h = 2.648 \times 10^{-4}$ MNm/m. In all loading cases, the stress ratio $R = 0.3$ is applied to the specimen. Experimental results for the first loading case (without bending) described above have been reported by Widagdo [142].

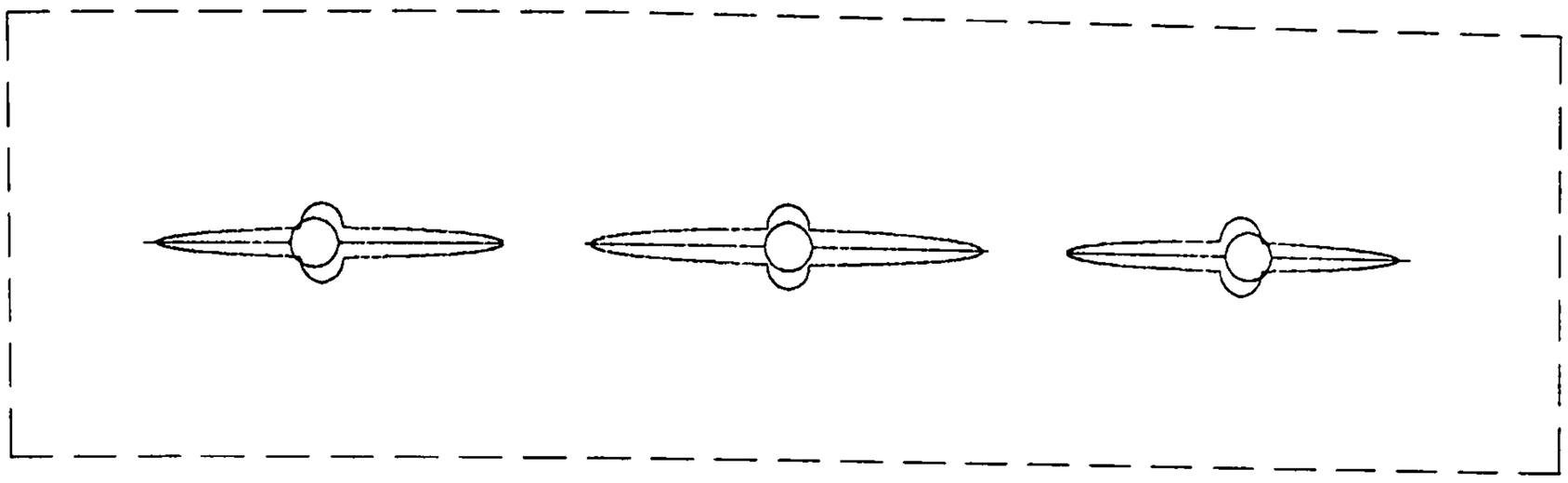

Figure 6-13: Deformed DBEM model around the holes of multiple site damage problem of a plate with three holes.

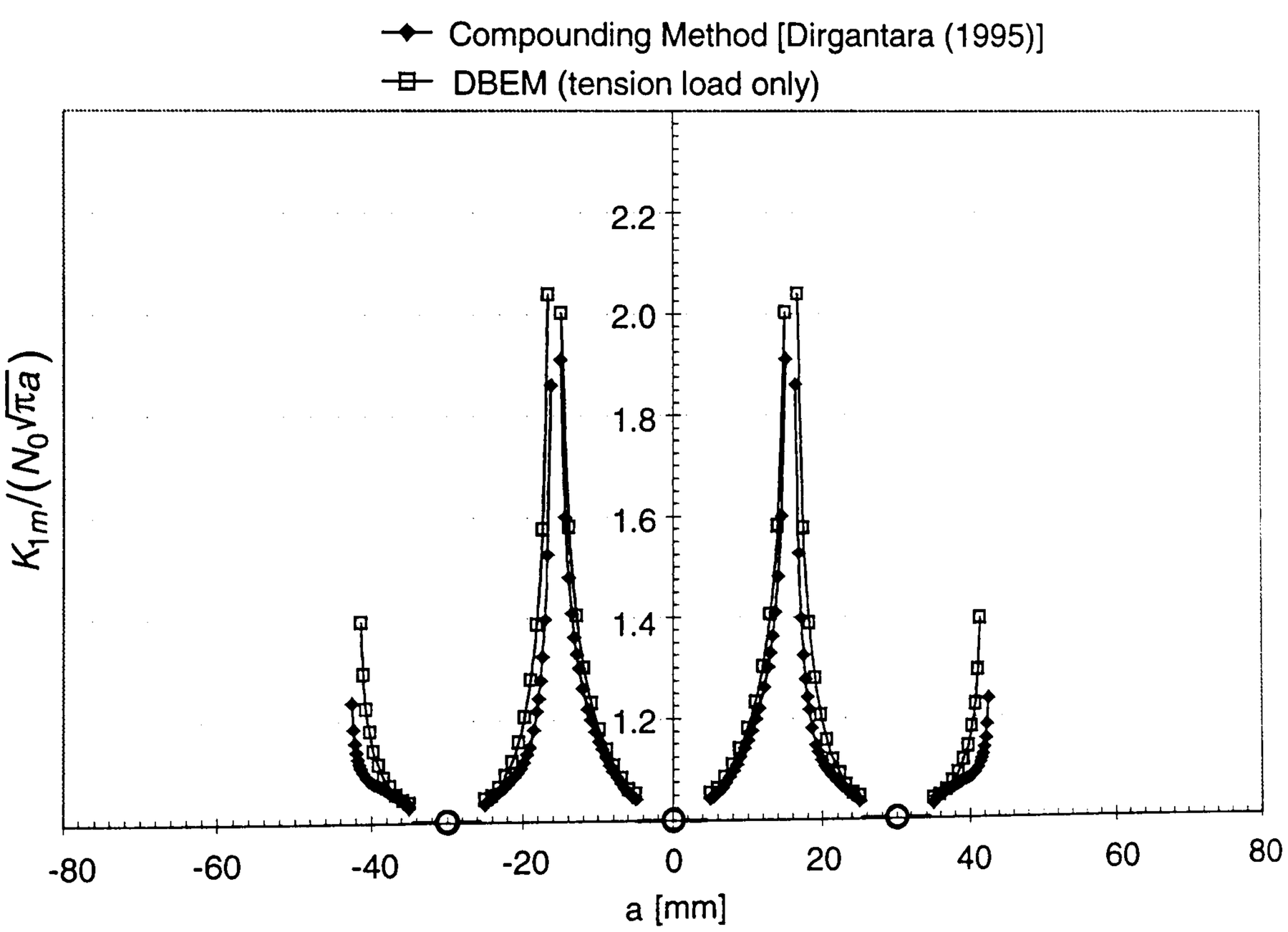

Figure 6-14: Normalised K_I for multiple site damage problems of a plate with three holes.

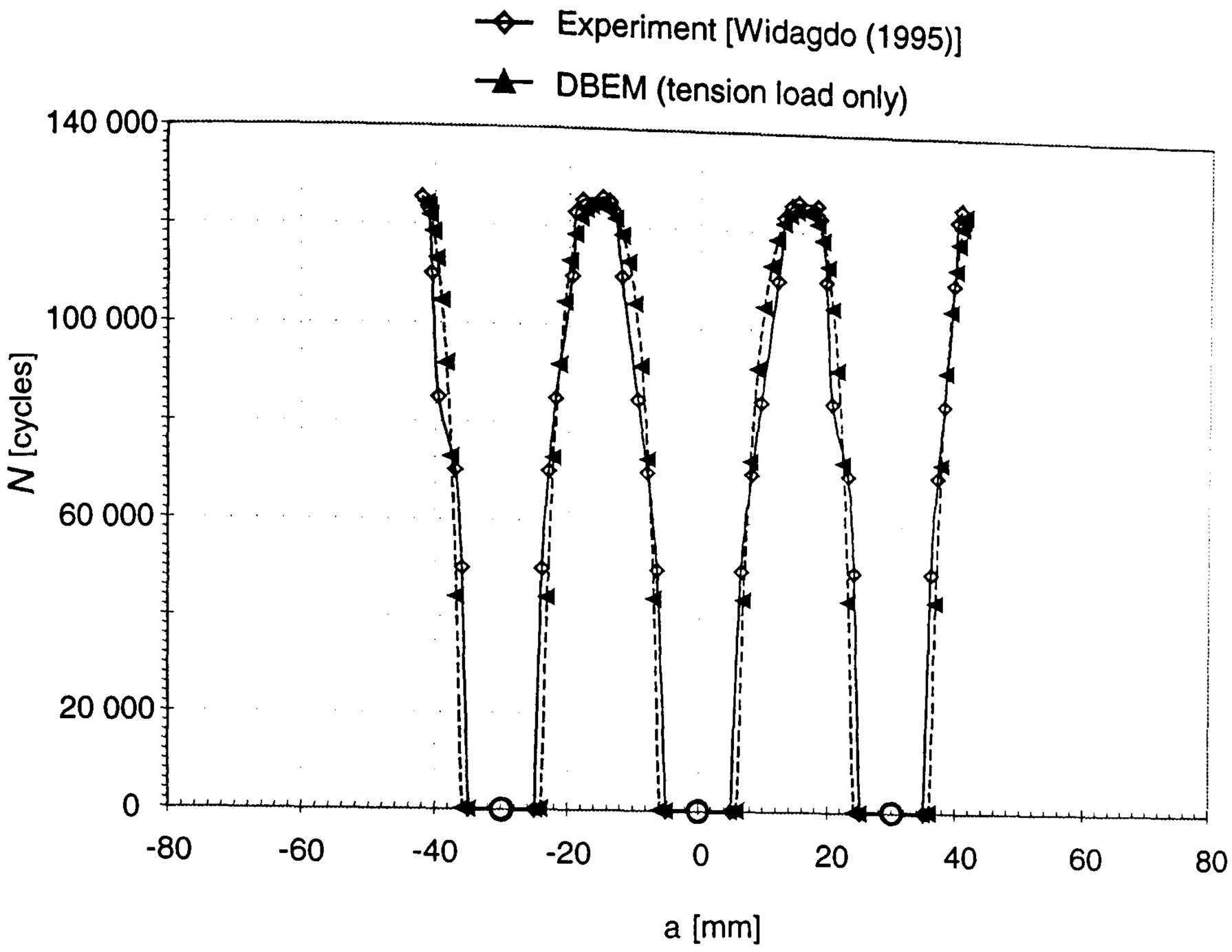

Figure 6-15: Crack growth diagram for multiple site damage problems of a plate with three holes.

Constants of material data for Paris equation $\frac{da}{dN}\left[\frac{\text{m}}{\text{cycle}}\right] = C_p\,(\Delta K_{eff}\,[\text{MPa}\sqrt{\text{m}}])^{m_p}$ is taken from the experimental data [142]. For $R = 0.3$, the constants are as follows:

Zone II ($\Delta K \leqslant 46$ MPa$\sqrt{\text{m}}$)	$C_p = 2.838573 \times 10^{-12}$	$m_p = 4.6$
Zone III ($\Delta K > 46$ MPa$\sqrt{\text{m}}$)	$C_p = 1.92750 \times 10^{-32}$	$m_p = 16.758$

As described in chapter 2, Zone II is stable crack growth region, and Zone III is unstable/ rapid crack growth region.

A total of 30 elements for plate boundary and 8 elements for each initial crack surface are used. Two boundary elements for each crack surface are added in each increment.

Figure 6-12 shows deformed BEM model and 6-13 shows crack growth path diagram of the specimen. As the geometry and loadings of this case are symmetric, the cracks grow along the symmetric line.

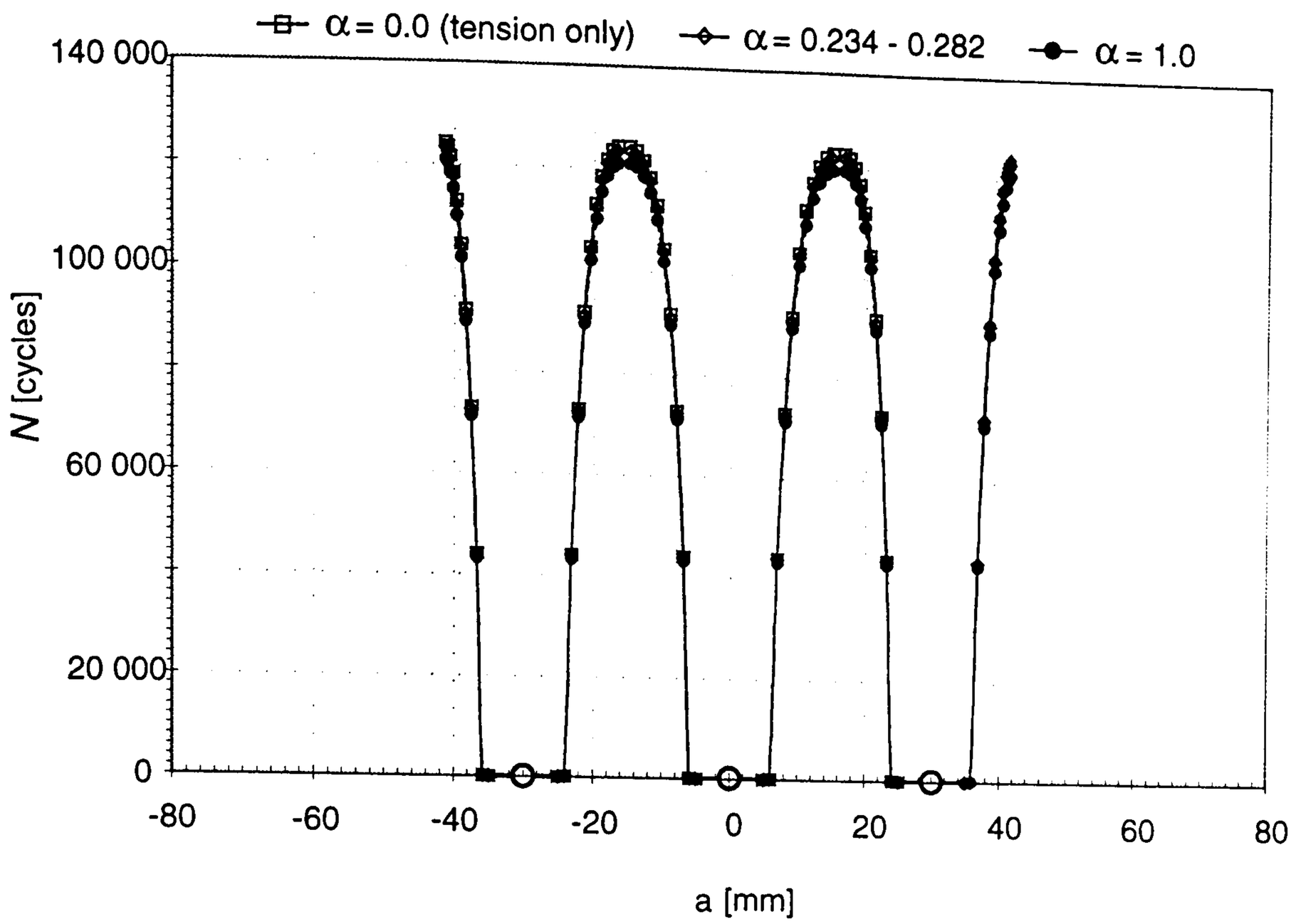

Figure 6-16: Comparison of crack growth diagram for multiple site damage problems of a plate with three holes: (a) tension load only ($\alpha = 0.0$); (b) tension and bending loads ($\alpha = 0.234 - 0.282$ and $\alpha = 1.0$).

The normalised stress intensity factor results are shown in Figure 6-14. The results are compared to the results reported by Dirgantara [35], obtained using compounding method. As it can be seen, interaction between cracks increase the stress intensity factors significantly.

Figure 6-15 shows numerical crack growth diagram for this problem loaded by tension only compared to the experimental results. As shown in the Figure, the crack growth life results obtained using the proposed method are in good agreement with the ones reported in [142].

Figure 6-16 and Table 6.1 show comparison of numerical crack growth diagram for this problems for $\alpha = 0.0$ (tension only), 1.0, and the α values computed using the proposed formula. The α values obtained for this example are not the same for each increment, and are found between $0.234 - 0.282$. As shown in the figure, in this case the secondary bending does not give much effect on the crack growth life results.

Table 6.1: Fatigue crack growth life of multiple site damage problem of a plate with three holes.

	N (cycles)
Experiment (tension only) (Widagdo, 1995)	125976
$\alpha = 0.0$(tension only)	124245
$\alpha = 0.234 - 0.282$	123361
$\alpha = 1.0$	121001

6.3.5 Crack propagation in a cylindrical shell

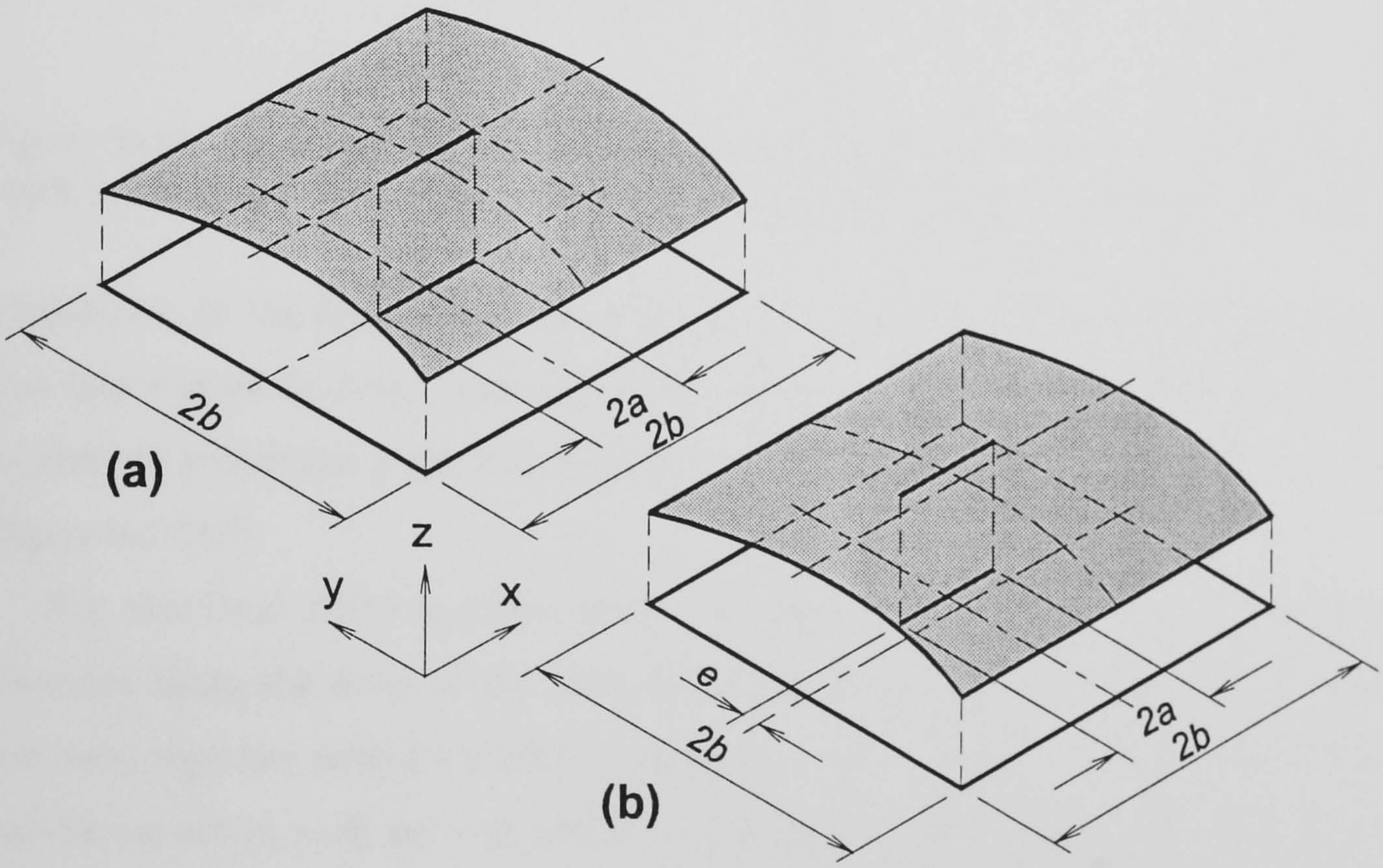

Figure 6-17: A cylindrical shell with a crack, simply supported and subjected to internal pressure. (a) the crack is along symmetric line; (b) the crack is at distance e from symmteric line.

The first shell example analysed here is a simply supported square cylindrical shell of length $b = 1$ with a centre crack of initial length $a/b = 0.2$ as shown in Figure 6-17. A uniform pressure is applied over the shell domain. Modulus of elasticity of the material is chosen $E/p_0 = 210000$, Poisson's ratio $\nu = 0.3$ and shell thickness $b/h = 10$. The curvature $k_{11} = 0.0$ and $k_{22} = 0.1$. Ratio between the shell width and radius of curvature $b/R = 0.1$. To study the effect of curvature and crack position to the direction of crack propagation, two different initial crack positions are

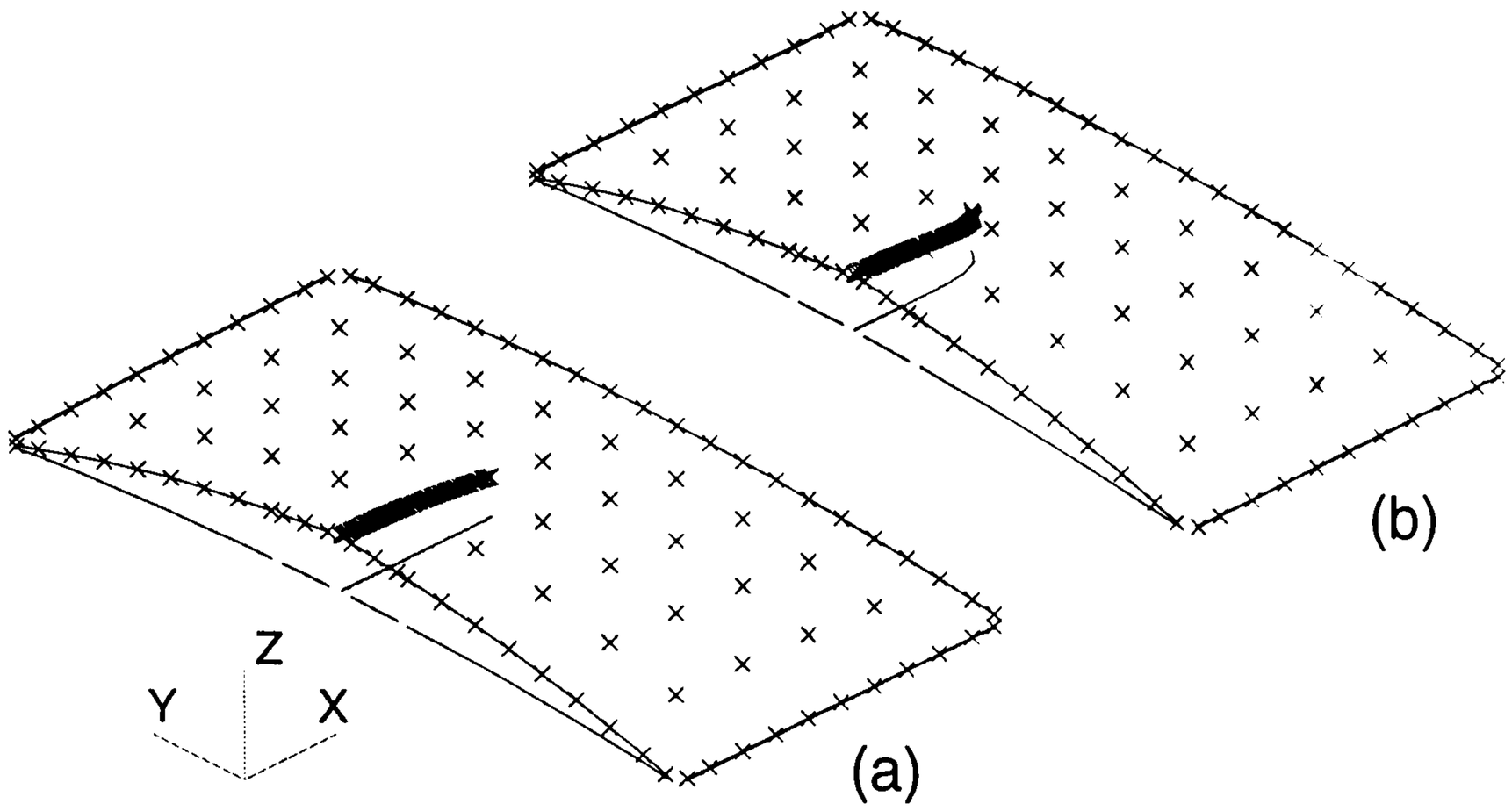

Figure 6-18: Deformed DBEM model of a cylindrical shell with a crack: (a) the crack is along symmetric line; (b) the crack is at distance e from symmteric line.

considered. In the first configuration an initial crack is located along the symmetric line (see Figure 6-17(a)), whereas in the second configuration the initial crack is located at a distance e (in this example $e = 0.025b$) from the symmetric line (see Figure 6-17(b)).

For the Dual BEM analysis, half of the shell is modelled with a total of 30 elements along the sides of the shell and 10 elements for each initial crack surface are used, together with 4×9 DRM domain points. The simply supported boundary conditions are $\phi_t = 0$; $w_3 = 0$; and $u_1 = 0$ along the sides of the shell, and $\phi_n = 0$ and $u_1 = 0$ along the symmetric line. Two elements for each crack surface are added in each increment of crack propagation.

Figures 6-18 – 6-21 present deformed shape and crack trajectories of analyses. As it can be seen, the crack which is located along the line of symmetry grows along a straight path, while the crack which is located at a distance e from the symmetric line (in this example $e = 0.025b$) initially grows in a direction parallel to the symmetric line before changing direction. This type of crack growth is referred to as flapping effect of cracked cylinder. This effect is also observed during experiments, reported by Peters and Khun [98], as can be seen in Figure 6-22.

Stress intensity factor results are presented in Figure 6-23. As it can be seen K_{II}

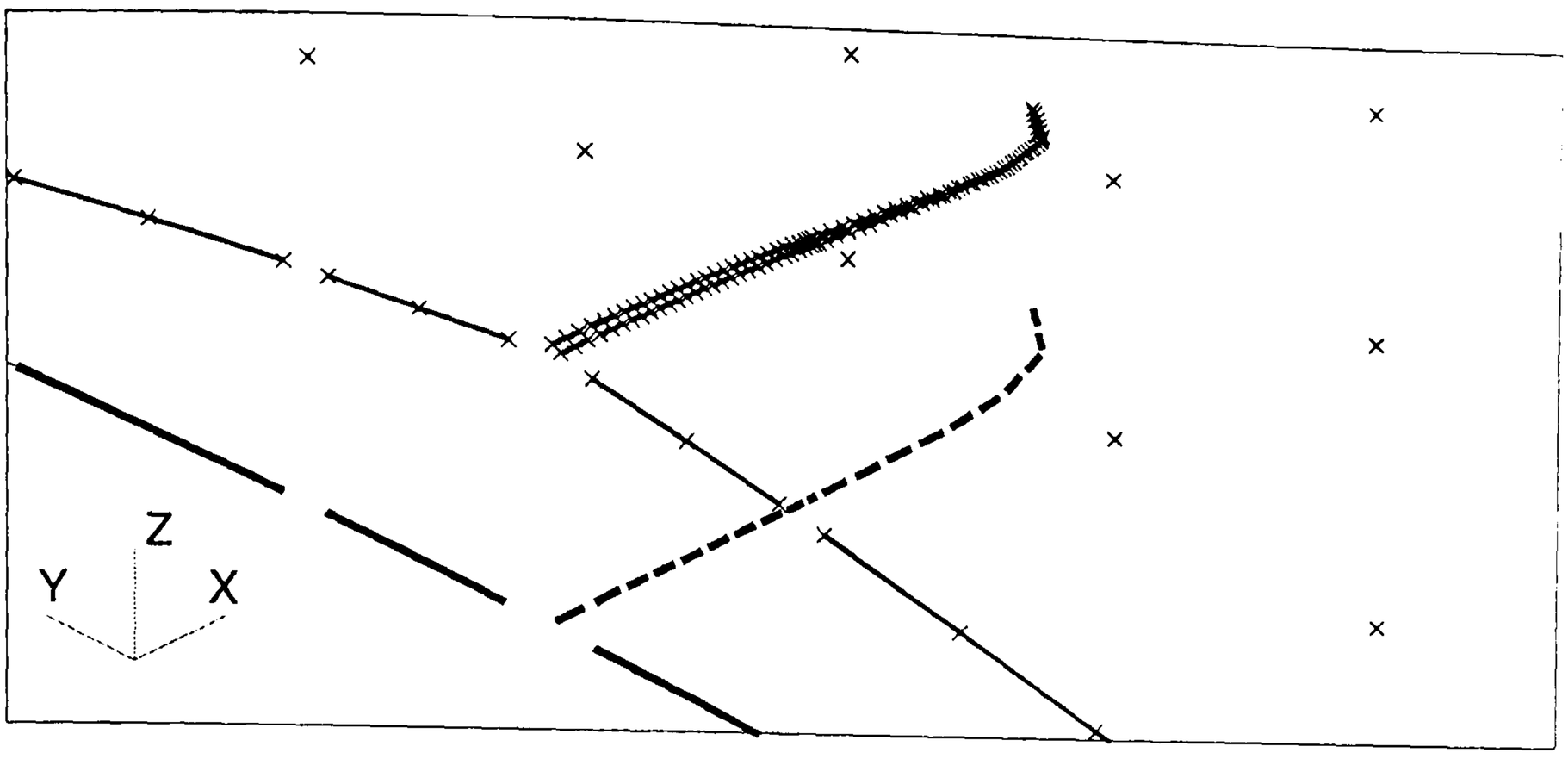

Figure 6-19: Crack trajectory of a cylindrical shell with the initial crack is located at distance e from symmteric line.

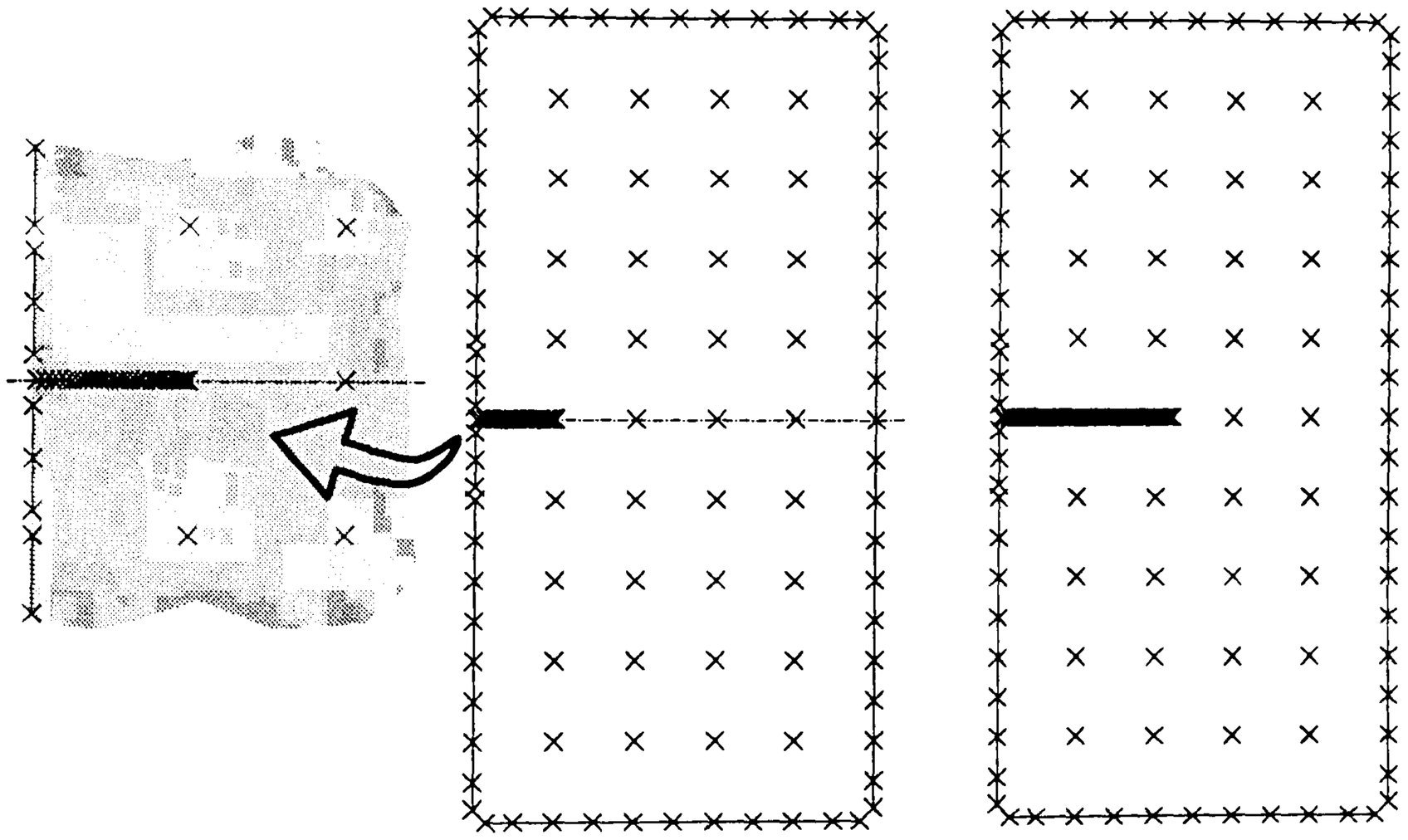

Figure 6-20: Top view of DBEM model of a cylindrical shell with the crack is along symmetric line: (a) initial geometry; (b) after the crack has grown.

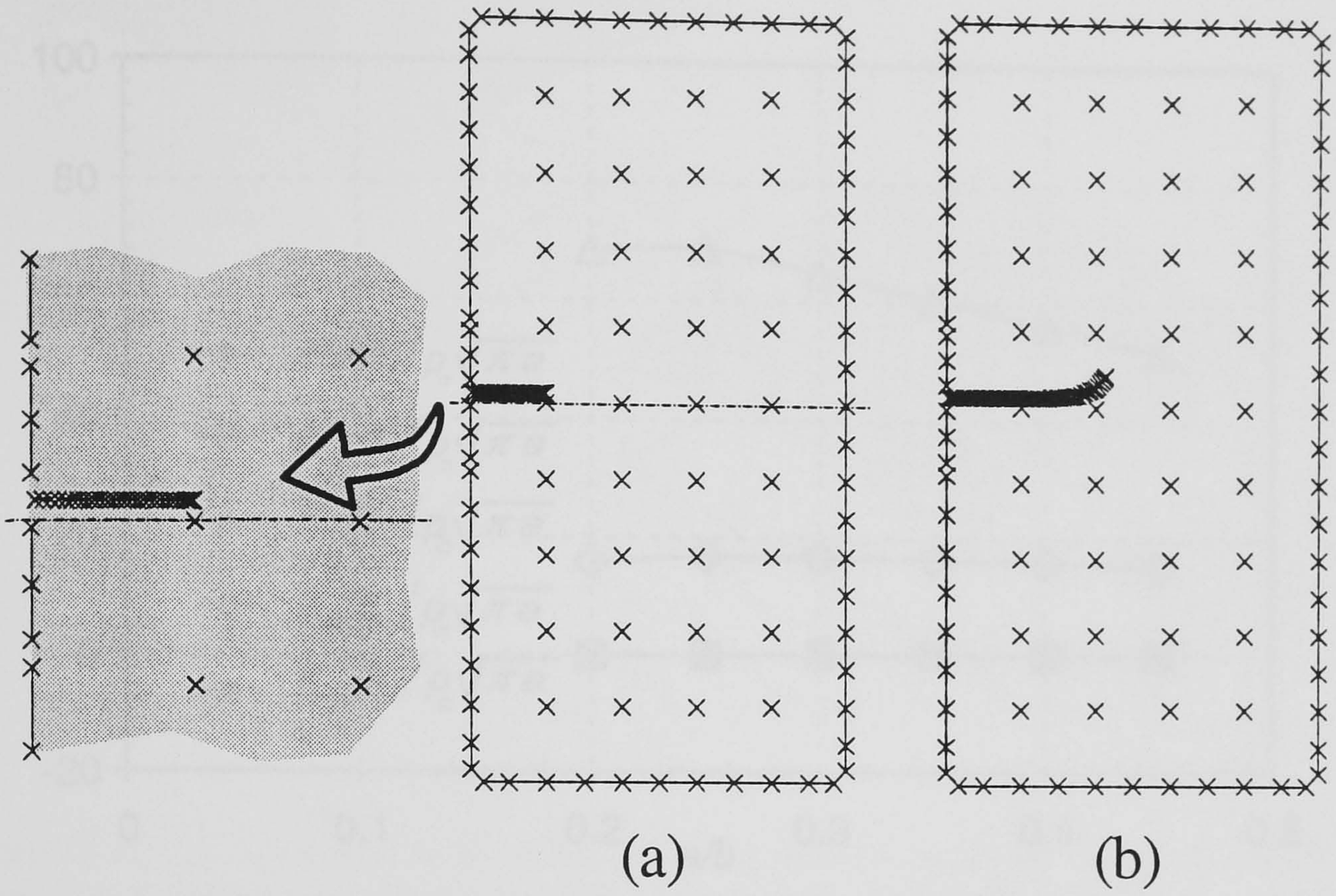

Figure 6-21: Top view of DBEM model of a cylindrical shell with the crack is at distance e from symmetric line: (a) initial geometry; (b) after the crack has grown.

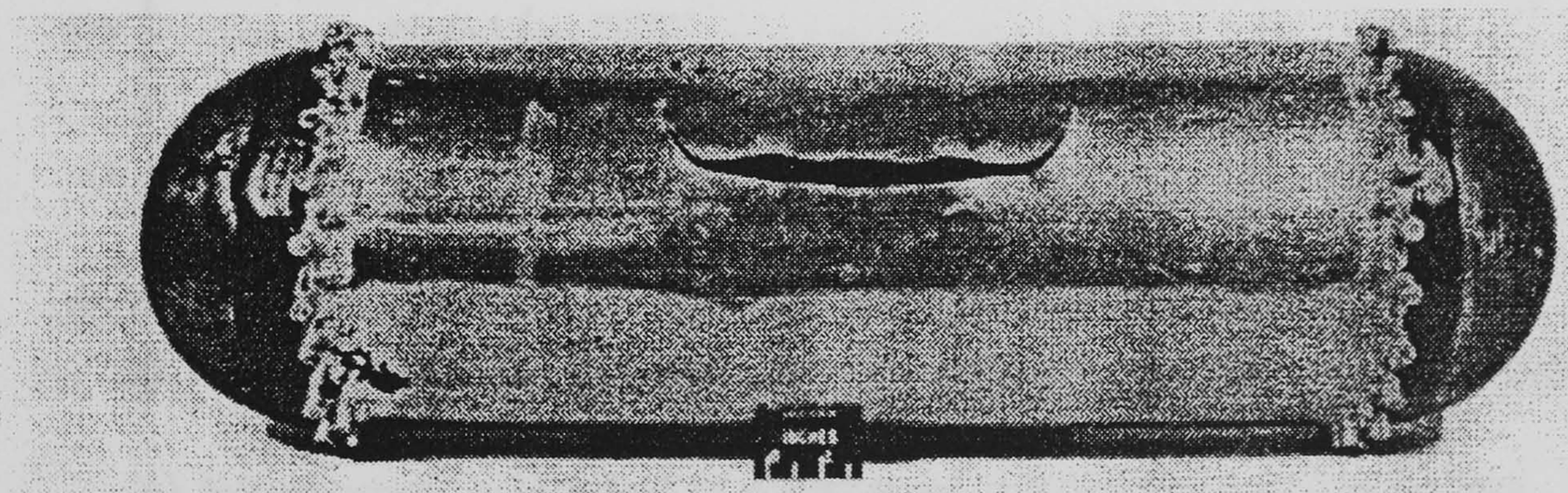

Figure 6-22: Experimental results of an unstiffened pressurized cylinder (Peters and Kuhn [98]).

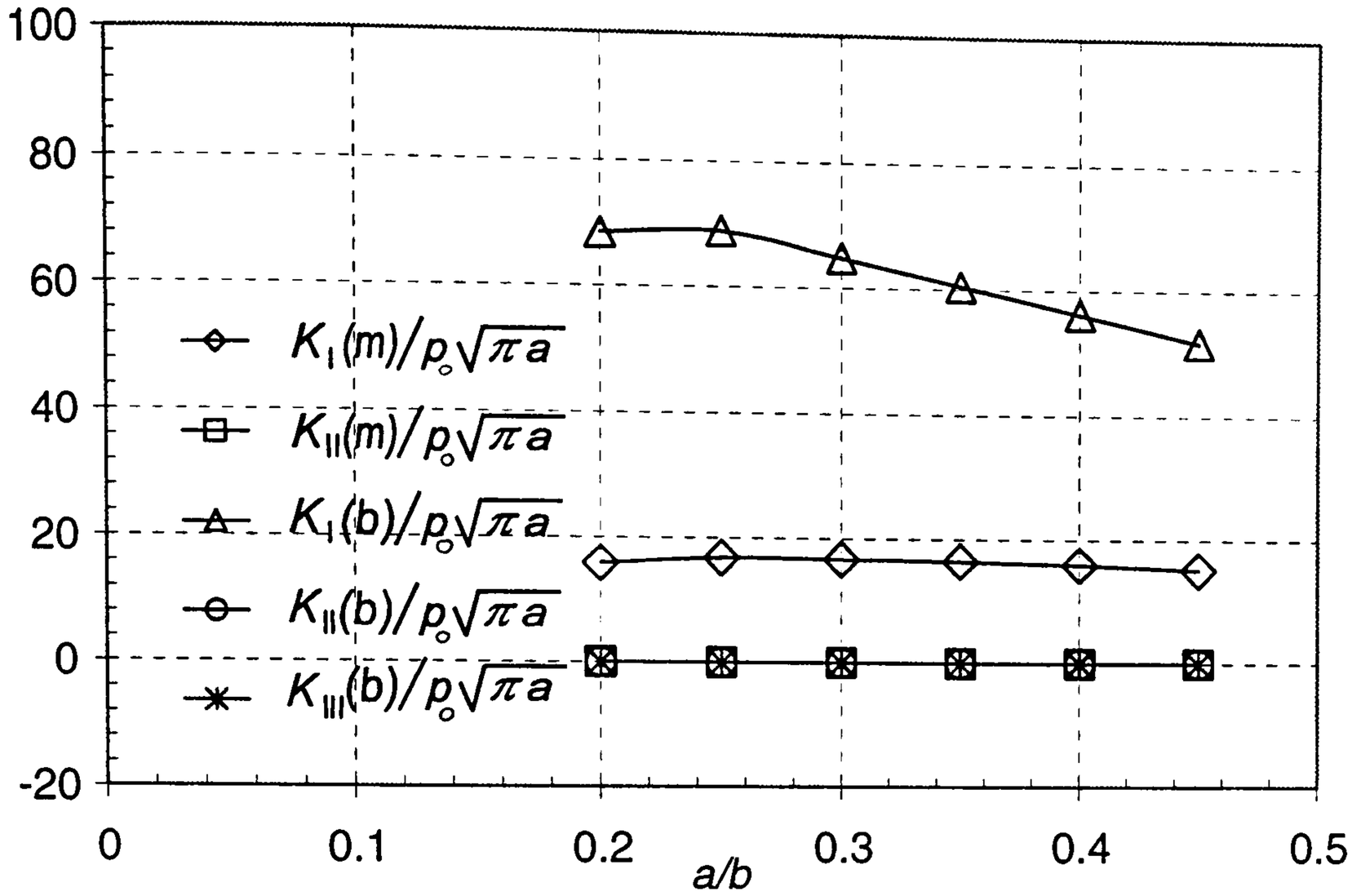

(a) Initial crack is located along the symmetric line

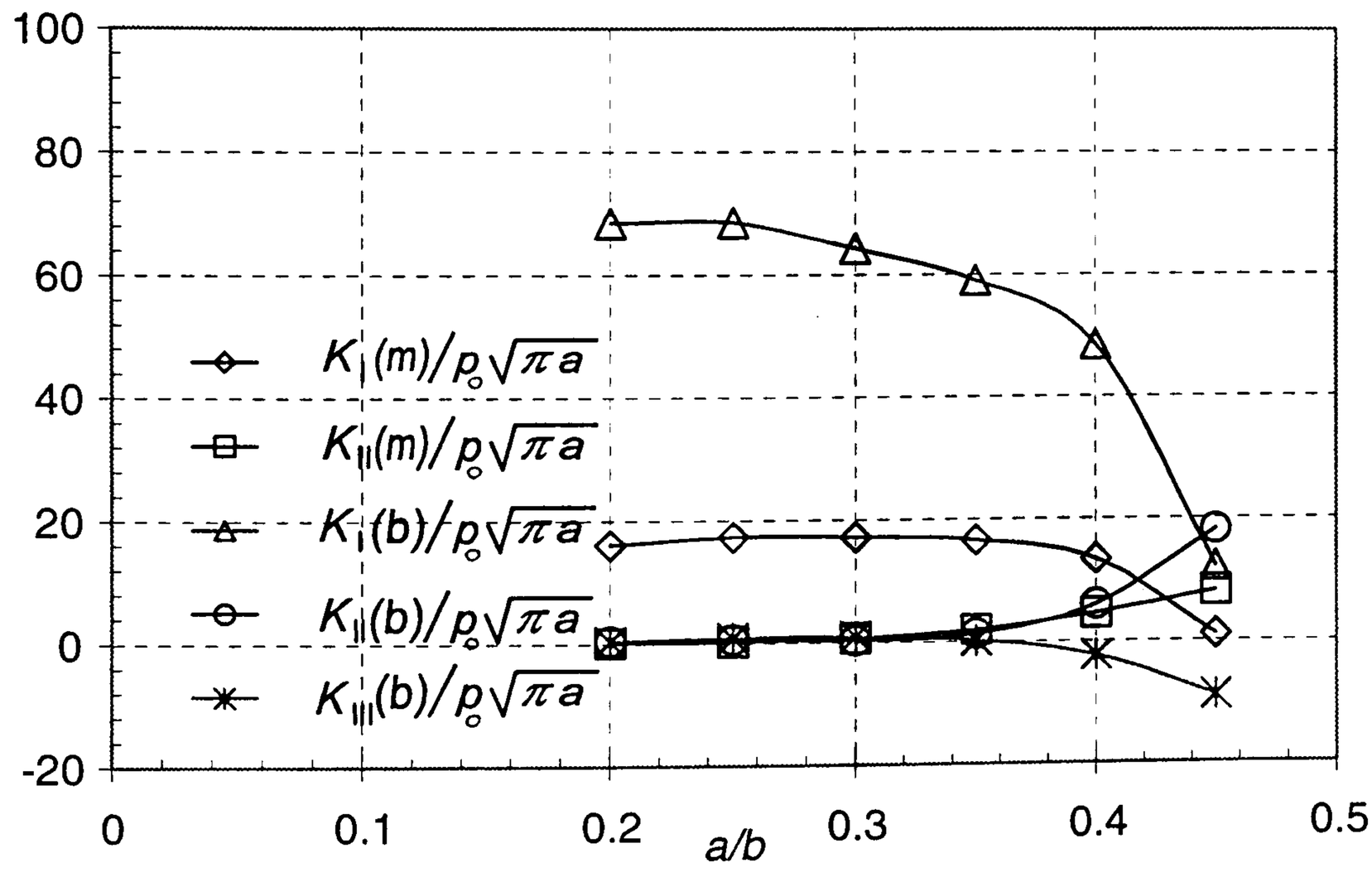

(b) Initial crack is located at a distance e from the symmetric line

Figure 6-23: Normalised stress intensity factors of simply supported cylindrical shell subjected to uniform pressure.

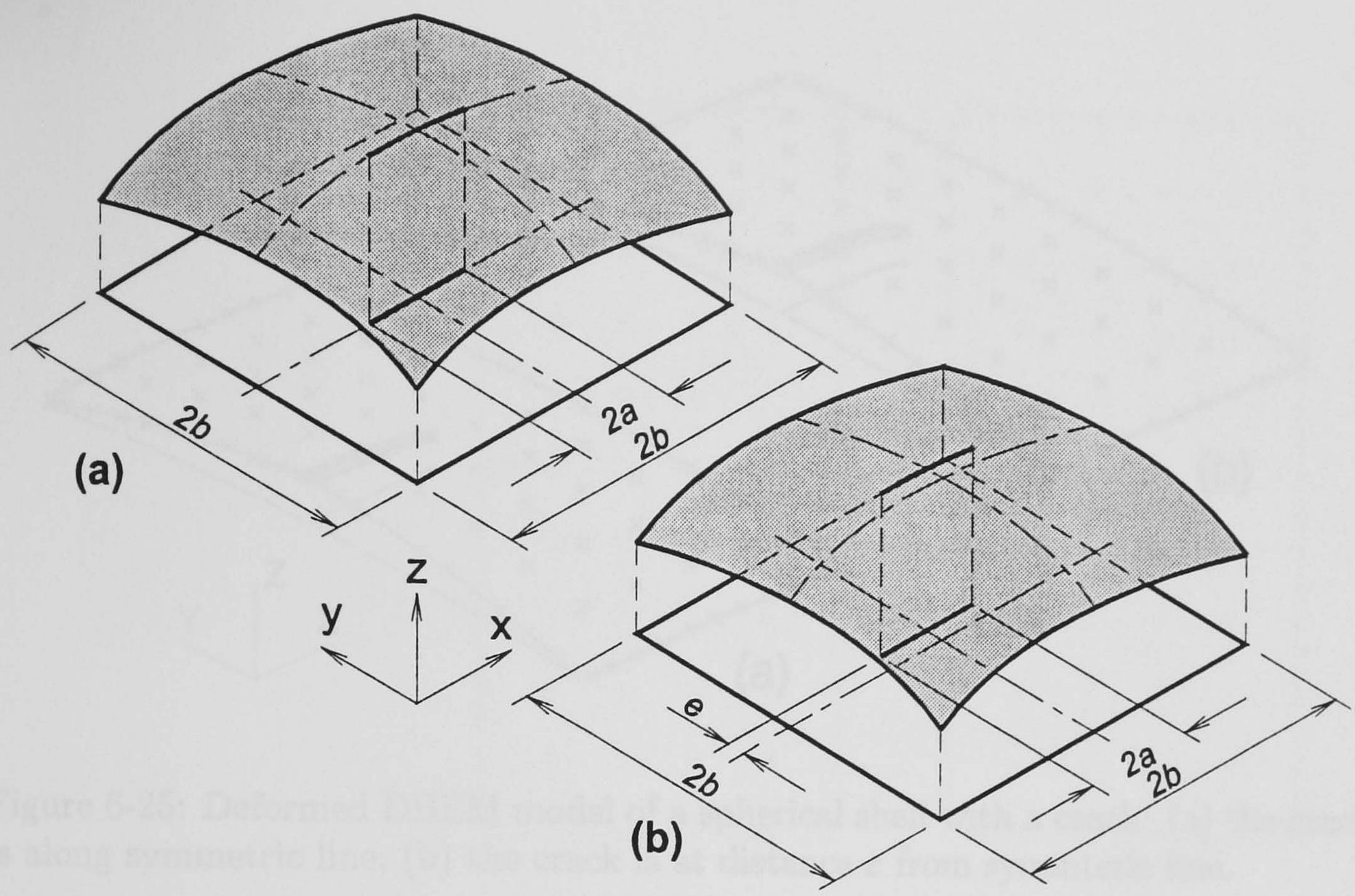

Figure 6-24: A spherical shell with a crack, simply supported and subjected to internal pressure: (a) the crack is along symmetric line; (b) the crack is at distance e from symmteric line.

and K_{III} of the crack which is located along the line of symmetry are very small and this case can be considered as pure mode I case. On the contrary, the case with the crack located at a distance e from the symmetric line is a mixed mode crack problem. K_{II} and K_{III} initially are very small, however as the crack grows and start to flap, $K_{I(m)}$ and $K_{I(b)}$ decrease while K_{II} and K_{III} increase rapidly.

6.3.6 Crack propagation in a spherical shell

As the second shell example, a simply supported square spherical shell of length $b = 1$ with a centre crack of initial length $a/b = 0.2$ as shown in Figure 6-24 is analysed. A uniform pressure is applied over the shell domain. Modulus of elasticity of the material is chosen $E/p_0 = 210000$, Poisson's ratio $\nu = 0.3$ and shell thickness $b/h = 10$. The curvature $k_{11} = k_{22} = 0.1$. Ratio between the shell width and radius of curvature $b/R = 0.1$. As in the previous example, two different initial crack positions are considered. In the first configuration the crack is located along the symmetric line (see Figure 6-24(a)) whereas in the second configuration, the crack is located at a distance e from the symmetric line (in this example $e = 0.025b$) (see

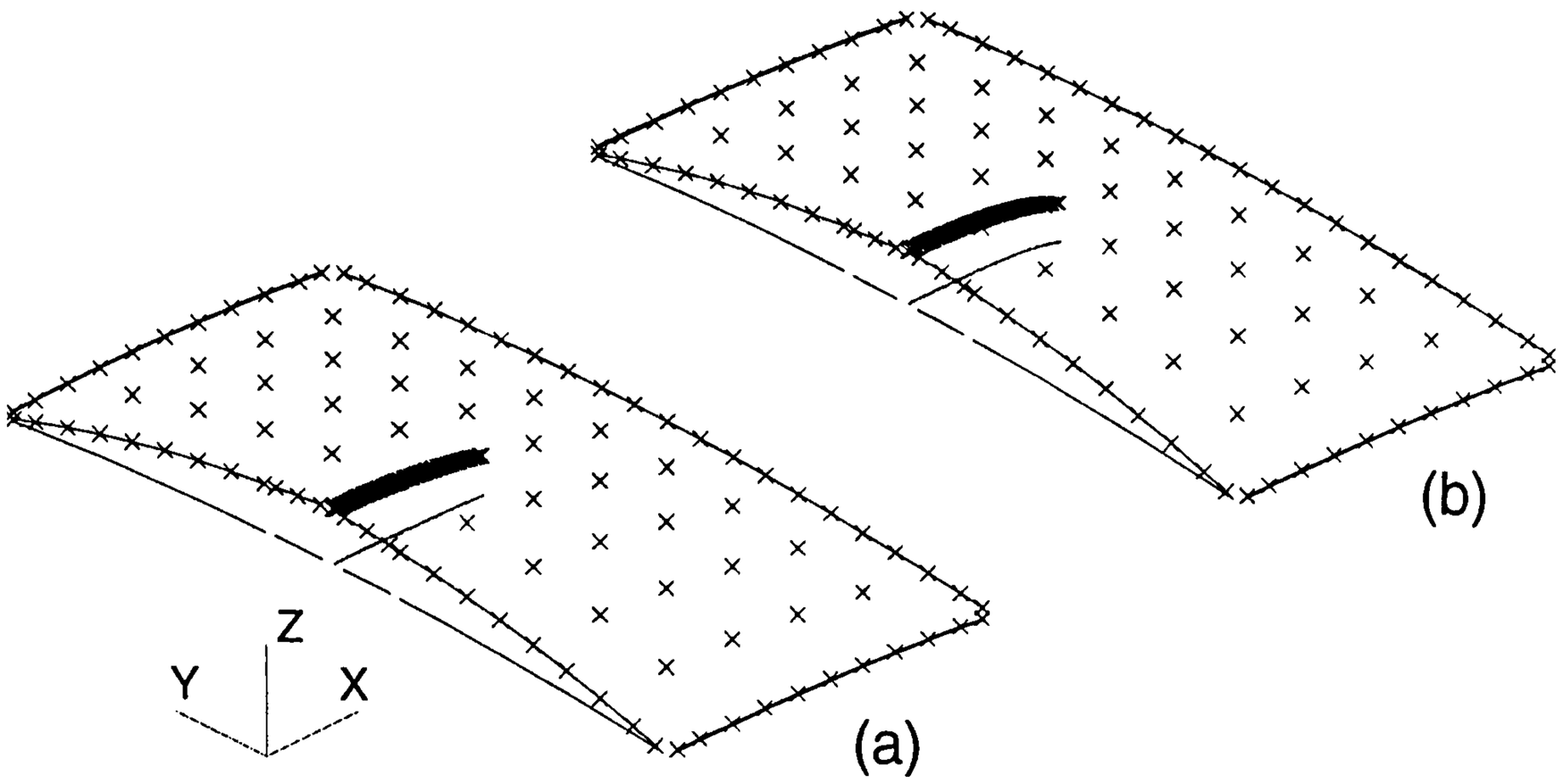

Figure 6-25: Deformed DBEM model of a spherical shell with a crack: (a) the crack is along symmetric line; (b) the crack is at distance e from symmteric line.

Figure 6-24(b)).

As in the previous example, half of the shell is modelled with a total of 30 elements along the sides of the shell and 10 elements for each initial crack surface are used, together with 4×9 DRM domain points. The simply supported boundary conditions are $\phi_t = 0$; $w_3 = 0$; and $u_1 = 0$ along the sides of the shell, and $\phi_n = 0$ and $u_1 = 0$ along the symmetric line. In this DBEM simulation, two boundary elements for each crack surface are added in each increment of crack propagation.

Figures 6-25 – 6-27 present deformed shape and crack trajectories of analyses. As it can be seen, same as in cylindrical shell, the crack which is located along the line of symmetry grows in a straight path. In the second case where the crack which is located at a distance e from the symmetric line (in this example $e = 0.025b$), the crack trajectory is different compare to the one in cylindrical shell. Here, the crack tends to grow in a direction approaching the symmetric line.

Figure 6-28 presents stress intensity factor results of this example. Same as the one in cylindrical shell, the case with the crack located along the line of symmetry can be considered as pure mode I case, and the case with the crack located at a distance e from the symmetric line is a mixed mode crack problem. However, the growth behaviour of the crack is different to cylindrical shell. In this example, K_I decreases, and, K_{II} and K_{III} increase in a relatively constant rate.

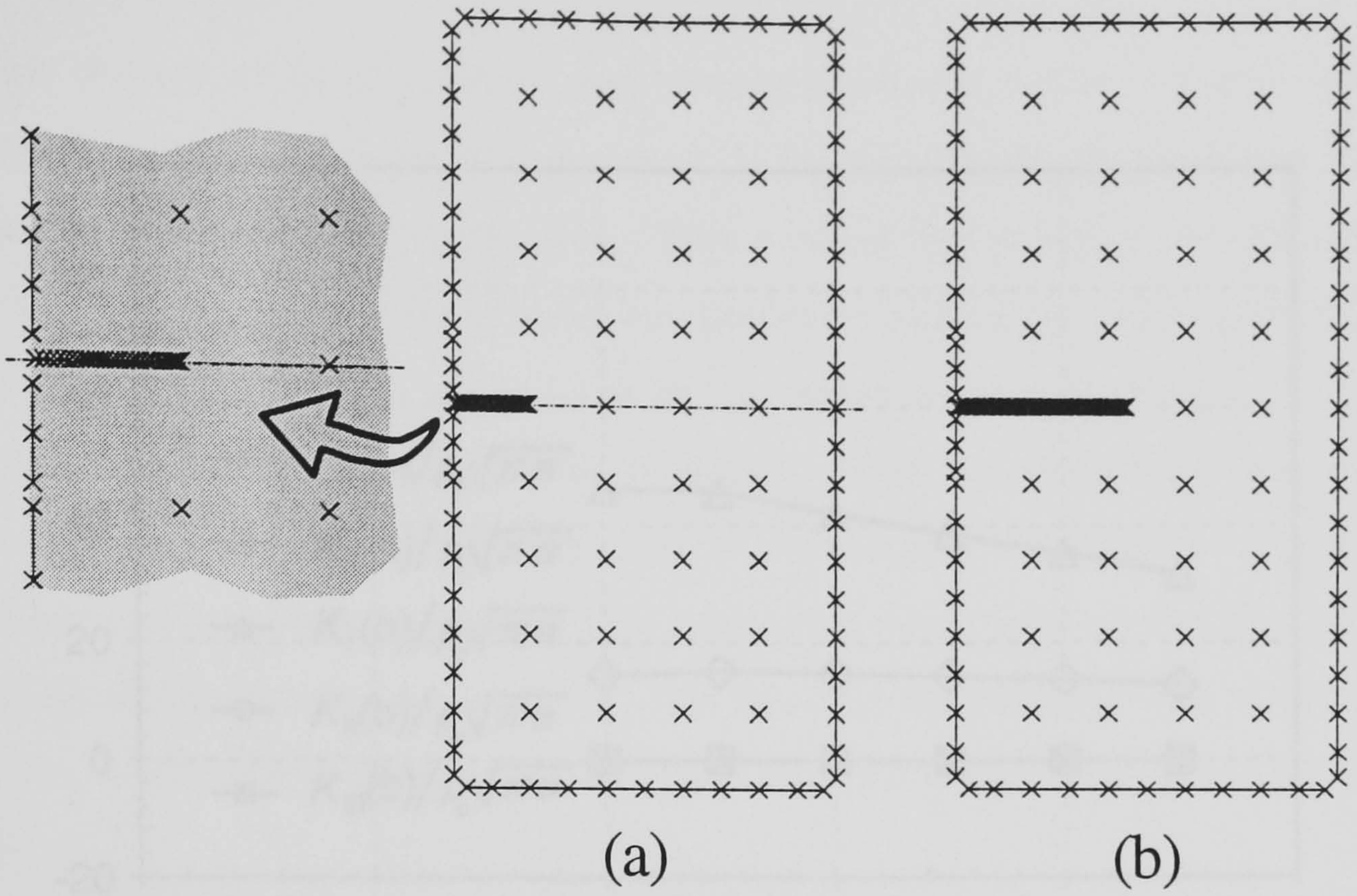

Figure 6-26: Top view of DBEM model of a spherical shell with the crack is along symmetric line: (a) initial geometry; (b) after the crack has grown.

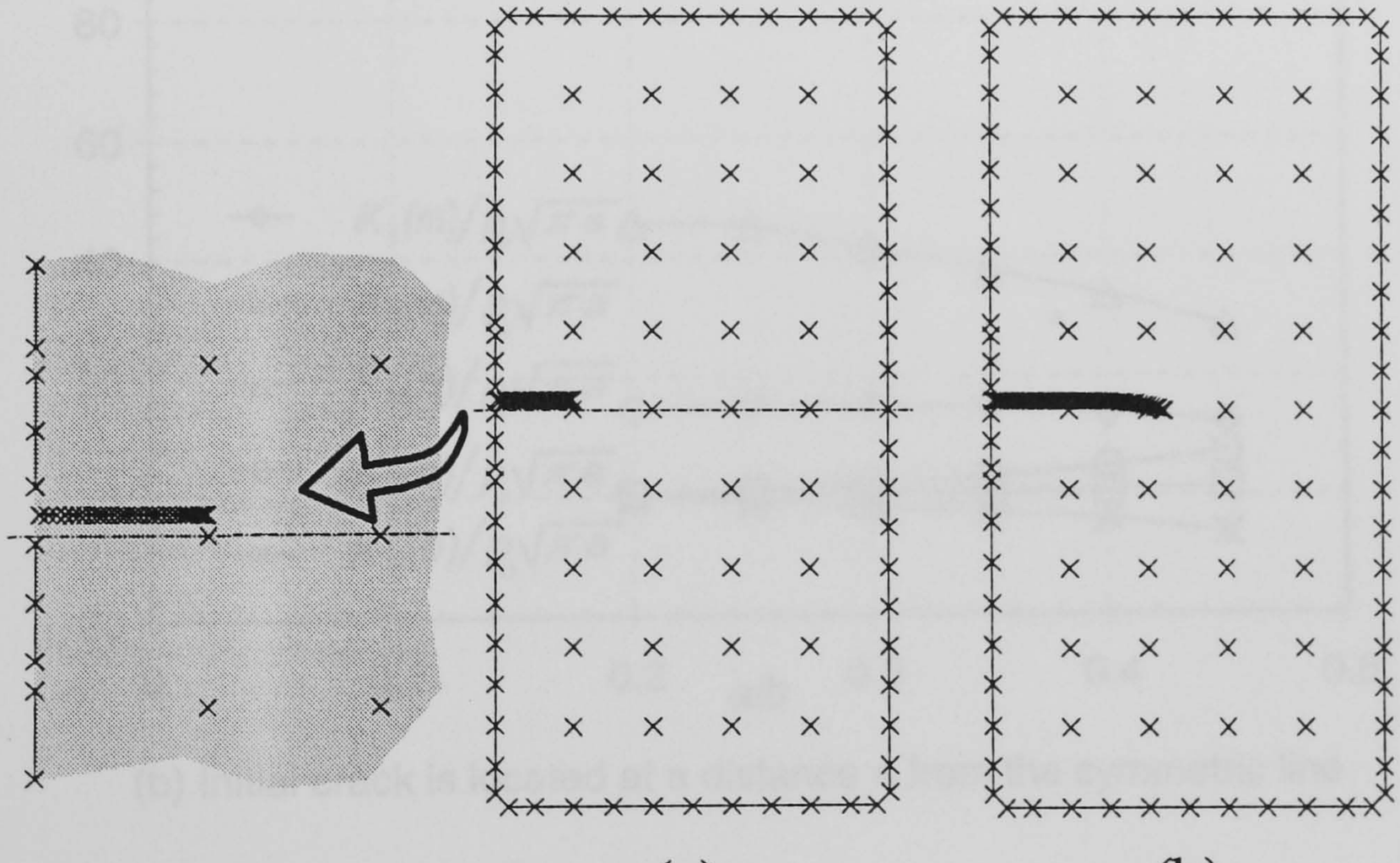

Figure 6-27: Top view of DBEM model of a spherical shell with the crack is at distance e from symmteric line: (a) initial geometry; (b) after the crack has grown.

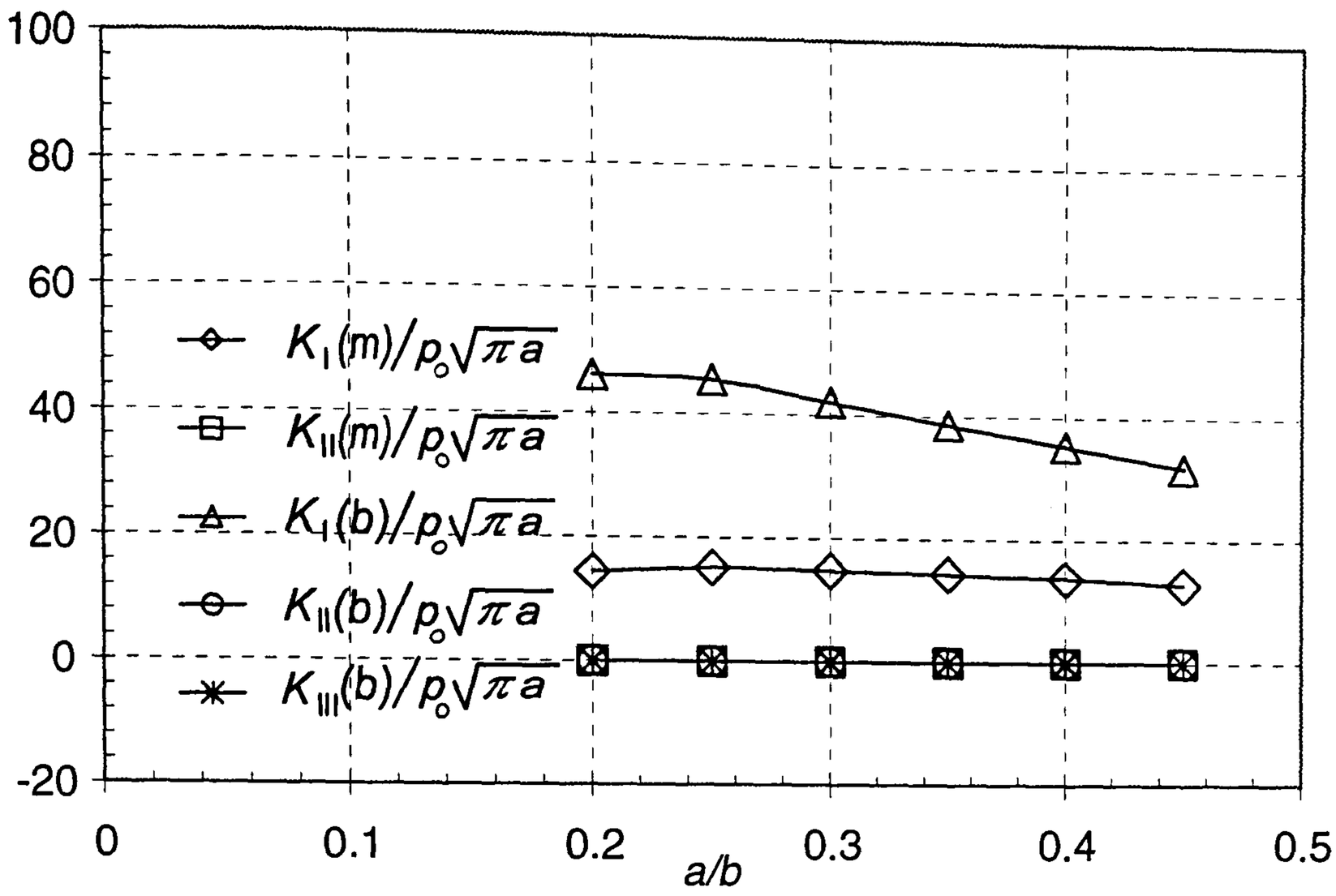

(a) Initial crack is located along the symmetric line

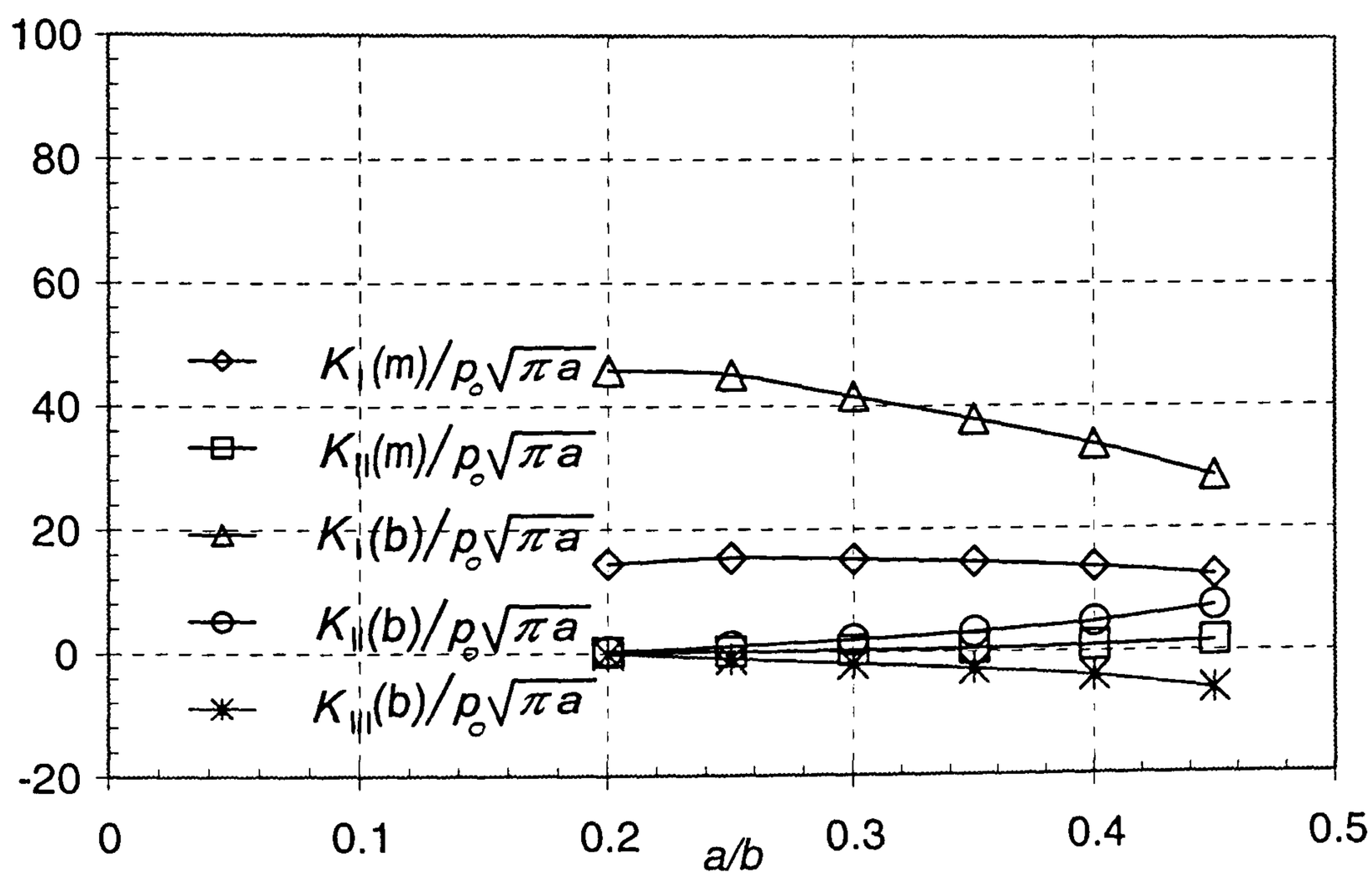

(b) Initial crack is located at a distance e from the symmetric line

Figure 6-28: Normalised stress intensity factors of simply supported spherical shell subjected to uniform pressure.

6.4 Summary

In this chapter, an application of dual boundary element method to crack growth analysis of plates and shells was presented. Using the DBEM, the problems can be solved in a single region formulation. This method was shown to be efficient for crack propagation, as no remeshing was needed in simulating crack growth since new elements were simply added for every increment of crack extension.

Several examples of crack growth analyses in plates and shells for a single crack as well as multiple cracks, including mixed mode example with different geometries, loadings and boundary conditions were presented. Crack growth direction and fatigue life of some examples presented in this chapter were validated with experiments and the results obtained were shown to be in good agreement with experimental results.

The following chapter will presents the application of multi region formulation of boundary element method for analysis of assembled plate-structures.

Chapter 7

A Multi-Domain BEM Formulation for Assembled Plate-Structures

7.1 Introduction

Thin walled structures loaded by in-plane and out-of-plane loading are widely used engineering, therefore it is important to develop tools for the analysis of such structures. Tanaka and Miyazaki [126] presented the direct BEM for elastic plate-structure based on boundary element formulations of Kirchhoff plate and plane stress elasticity theory. The above paper appears to be the only BEM work reported for assembled plate-structures.

In the present work the boundary element method is applied to the analysis of assembled plate-structure subjected to arbitrary loadings. The structure is divided into several regions, and equilibrium and compatibility equations along the interface edges are imposed. In each region, formulation is formed by coupling the boundary element formulation of shear deformable plate bending and the two dimensional plane stress elasticity. The boundaries are discretised into quadratic isoparametric elements. Several examples with different geometries and loading conditions are presented to demonstrate the efficiency of the proposed formulation. The results obtained show good agreements with exact solutions and the finite elements results.

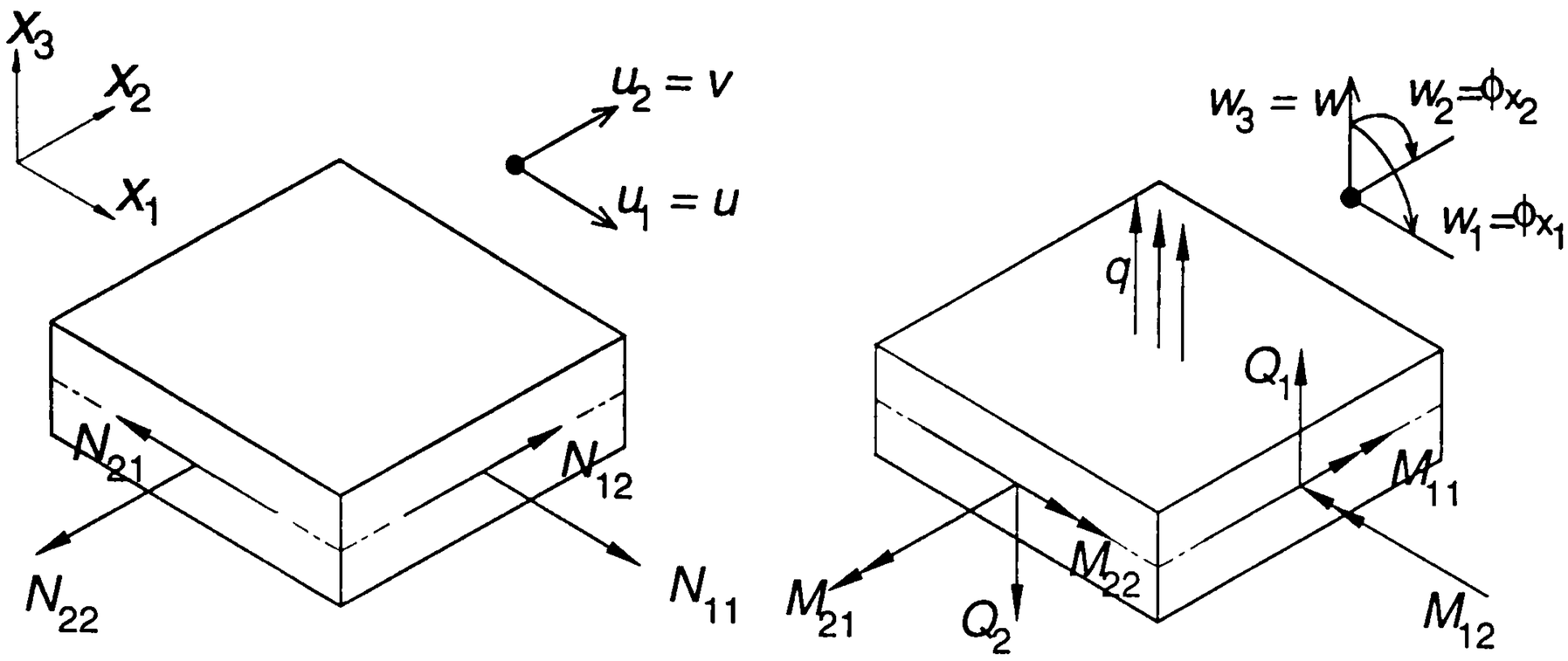

Figure 7-1: A flat plate subjected to bending and membrane loads.

7.2 Multi-Region Formulation of Plate Structure

Consider a flat plate subjected to bending and membrane loads as shown in Figure 7-1. The boundary integral equations for the problem were presented in chapter 3 (see equations (3.112 – 3.113)) as,

$$c_{ij}(\mathbf{x}')w_j(\mathbf{x}') + \oint_\Gamma P^*_{ij}(\mathbf{x}', \mathbf{x})w_j(\mathbf{x})\, d\Gamma(\mathbf{x}) = \int_\Gamma W^*_{ij}(\mathbf{x}', \mathbf{x})p_j(\mathbf{x})\, d\Gamma(\mathbf{x})$$
$$+ \int_\Omega W^*_{i3}(\mathbf{x}', \mathbf{X})q_3(\mathbf{X})d\Omega(\mathbf{X}) \qquad (3.112)$$

$$c_{\theta\alpha}(\mathbf{x}')\, u_\alpha(\mathbf{x}') + \oint_\Gamma T^*_{\theta\alpha}(\mathbf{x}', \mathbf{x})u_\alpha(\mathbf{x})d\Gamma(\mathbf{x}) = \int_\Gamma U^*_{\theta\alpha}(\mathbf{x}', \mathbf{x})t_\alpha(\mathbf{x})d\Gamma(\mathbf{x}) \qquad (3.113)$$

represent five displacement integral equations for this problem.

Now, consider the assembled plate structure as shown in Figure 7-2(i). The global coordinate system is denoted by $O - x_1 - x_2 - x_3$, and the local coordinate system by $O' - x'_1 - x'_2 - x'_3$. By observation of Figure 2-3 for the local coordinate system and Figure 7-3 for global coordinate system, the boundary element method parameters in local coordinate system $\mathbf{w}' = \{w'_1, w'_2, w'_3\}^\intercal$, $\mathbf{u}' = \{u'_1, u'_2\}^\intercal$, $\mathbf{p}' = \{p'_1, p'_2, p'_3\}^\intercal$, and $\mathbf{t}' = \{t'_1, t'_2\}^\intercal$ can be transformed to global coordinate system using the coordinate

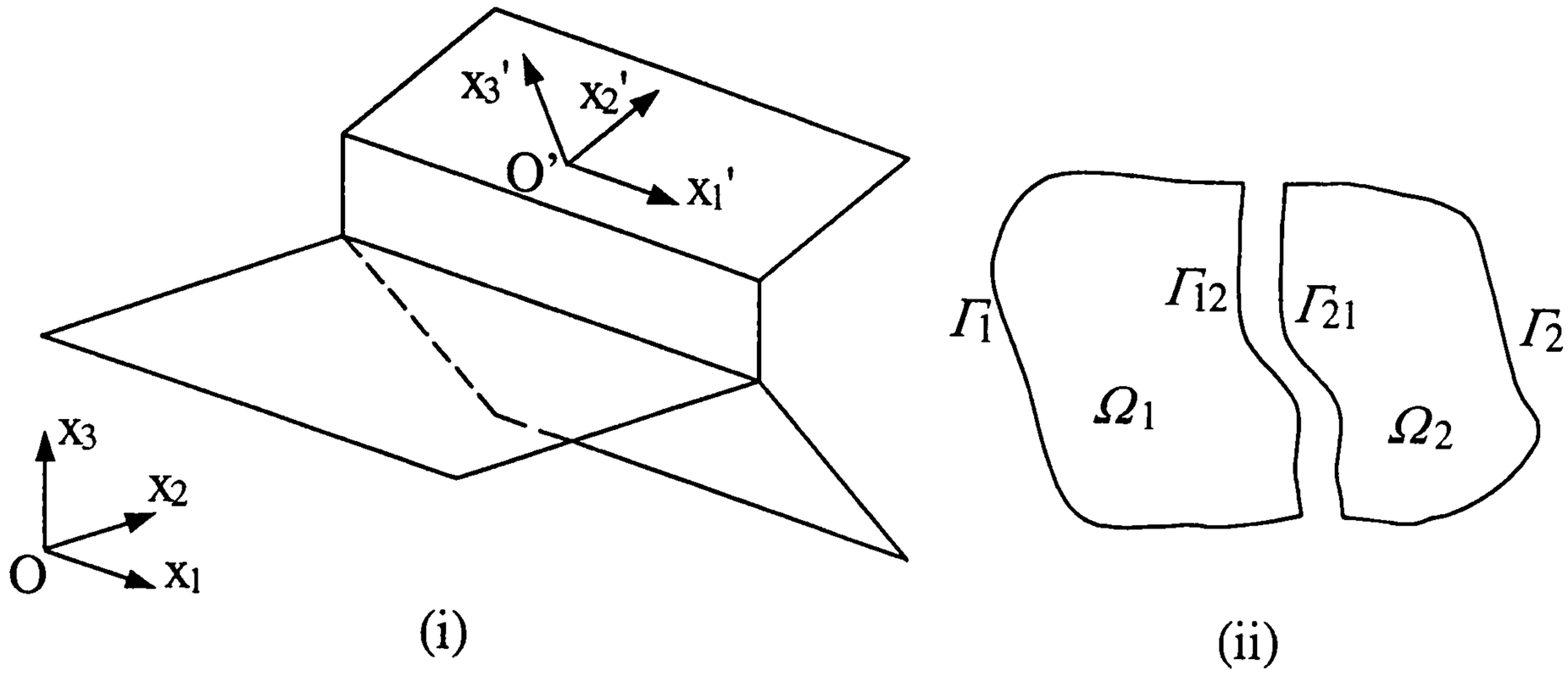

Figure 7-2: (i) Assembled plate structure; (ii) Multi region model.

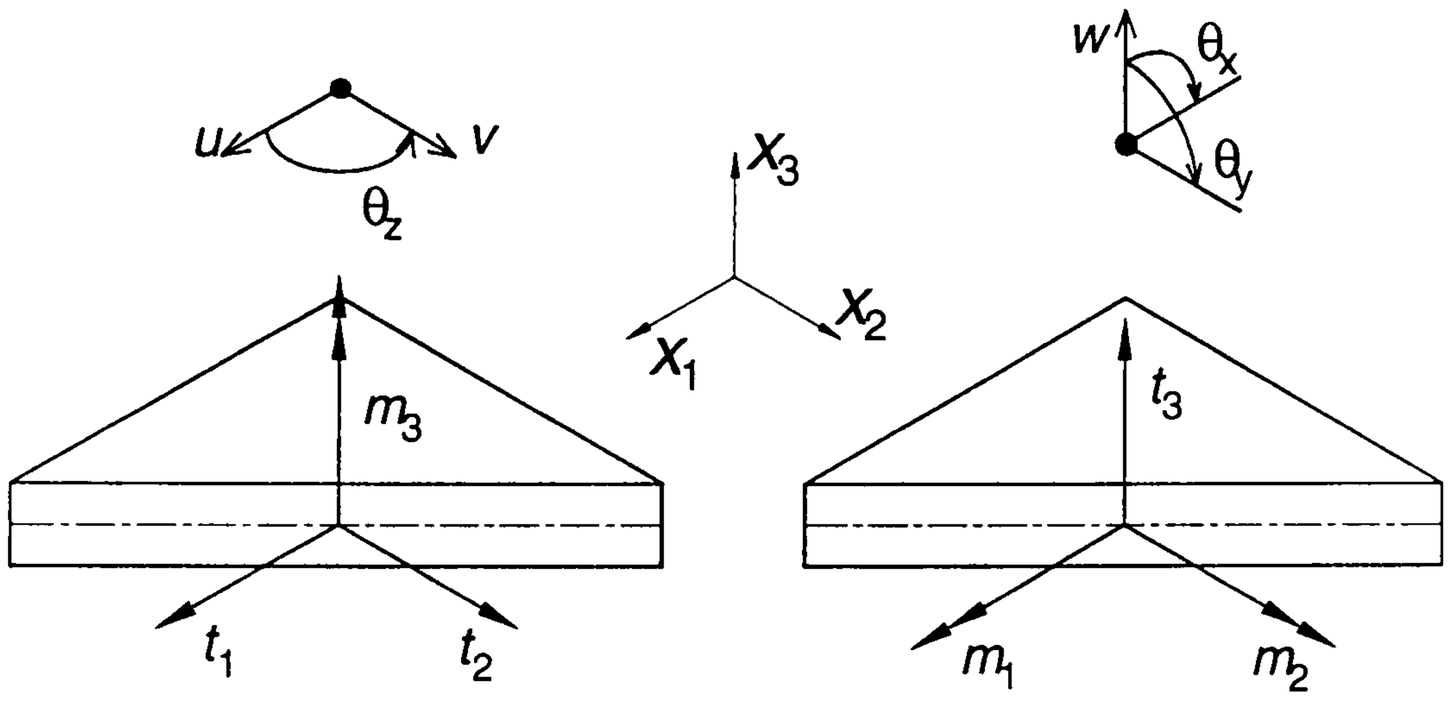

Figure 7-3: Sign convension for displacements and tractions in global coordinate system.

transformation matrix to obtain

$$[\mathbf{T}]\begin{Bmatrix} u_1' \\ u_2' \\ w_3' \end{Bmatrix} = \begin{Bmatrix} u_1 \\ u_2 \\ u_3 \end{Bmatrix}; \qquad [\mathbf{T}]\begin{Bmatrix} w_2' \\ w_1' \\ 0 \end{Bmatrix} = \begin{Bmatrix} \theta_1 \\ \theta_2 \\ \theta_3 \end{Bmatrix} \tag{7.1}$$

$$[\mathbf{T}]\begin{Bmatrix} t_1' \\ t_2' \\ p_3' \end{Bmatrix} = \begin{Bmatrix} t_1 \\ t_2 \\ t_3 \end{Bmatrix}; \qquad [\mathbf{T}]\begin{Bmatrix} -p_2' \\ p_1' \\ 0 \end{Bmatrix} = \begin{Bmatrix} m_1 \\ m_2 \\ m_3 \end{Bmatrix} \tag{7.2}$$

where $\mathbf{u} = \{u_1, u_2, u_3\}^{\mathrm{T}}$ are displacements in x_1-, x_2-, and x_3- directions respectively and $\boldsymbol{\theta} = \{\theta_1, \theta_2, \theta_3\}^{\mathrm{T}}$ are rotations about x_1-, x_2-, and x_3- axes respectively. The vector $\mathbf{t} = \{t_1, t_2, t_3\}^{\mathrm{T}}$ are tractions due to membrane and shear stress resultants in x_1-, x_2-, and x_3- directions respectively and $\mathbf{m} = \{m_1, m_2, m_3\}^{\mathrm{T}}$ are tractions due to bending stress resultants about x_1-, x_2-, and x_3- axes respectively and $[\mathbf{T}]$ is the coordinate transformation matrix.

To solve the problem using boundary elements, the structure is divided into several region, as shown in Figure 7-2(ii) with at least one region for each plate component. For each region, boundary element influence matrices in their local coordinate system are assembled. The overall system matrices are formed by enforcing along the interface boundary of the plates, compatibility equations of displacements and equilibrium equations of tractions are satisfied, that is

$$u_1^{(1)} = u_1^{(2)};\ u_2^{(1)} = u_2^{(2)};\ \text{and}\ u_3^{(1)} = u_3^{(2)} \tag{7.3}$$

$$\theta_1^{(1)} = \theta_1^{(2)};\ \theta_2^{(1)} = \theta_2^{(2)};\ \text{and}\ \theta_3^{(1)} = \theta_3^{(2)} \tag{7.4}$$

and

$$t_1^{(1)} = -t_1^{(2)};\ t_2^{(1)} = -t_2^{(2)};\ \text{and}\ t_3^{(1)} = -t_3^{(2)} \tag{7.5}$$

$$m_1^{(1)} = -m_1^{(2)};\ m_2^{(1)} = -m_2^{(2)};\ \text{and}\ m_3^{(1)} = -m_3^{(2)} \tag{7.6}$$

Arranging all equations into linear system of equations, the final matrix for assembled plate-structure can be obtained as follows :

$$\begin{bmatrix} \mathbf{H}_1' & \mathbf{H}_{12}' & \mathbf{0} & \mathbf{0} & -\mathbf{G}_{12}' & \mathbf{0} \\ \mathbf{0} & \mathbf{0} & \mathbf{H}_2'' & \mathbf{H}_{21}'' & \mathbf{0} & -\mathbf{G}_{21}'' \\ \mathbf{0} & \mathbf{0} & \mathbf{0} & \mathbf{0} & \mathbf{E}_{12} & \mathbf{E}_{21} \\ \mathbf{0} & \mathbf{C}_{12} & \mathbf{0} & \mathbf{C}_{21} & \mathbf{0} & \mathbf{0} \end{bmatrix} \begin{Bmatrix} u_1' \\ u_{12}' \\ u_2'' \\ u_{21}'' \\ t_{12}' \\ t_{21}'' \end{Bmatrix}$$

$$= \begin{bmatrix} \mathbf{G}_1' & \mathbf{0} \\ \mathbf{0} & \mathbf{G}_2'' \end{bmatrix} \begin{Bmatrix} t_1' \\ t_2'' \end{Bmatrix} + \begin{Bmatrix} b_1' \\ b_{12}' \\ b_2'' \\ b_{21}'' \\ 0 \\ 0 \end{Bmatrix} \tag{7.7}$$

where $\mathbf{E}_{12}$, $\mathbf{E}_{21}$ are the matrices for equilibrium equations and $\mathbf{C}_{12}, \mathbf{C}_{21}$ are the matrices for compatibility equations. After imposing the boundary conditions, the system of algebraic equations can be solved for the boundary unknowns using standard Gauss elimination procedure.

This simple strategy is robust and allows the BEM to effectively model general assembled plate structures subjected to arbitrary loadings.

7.3 Numerical Examples

Several numerical examples are presented to demonstrate the ability of the proposed method for analyses of assembled plate structures subjected to general loadings with different boundary conditions.

7.3.1 Cantilever plate with variable thickness and modulus of elasticity

In this example, a cantilever beam with variable thickness loaded by uniformly distributed vertical load per unit area q (as shown in Figure 7-4) is analysed. The properties of the plate are: $L_1 = 1.0$; $L_2/L_1 = 1.0$; $L_3/L_1 = 2.0$; $t_1/L_1 = 0.10$;

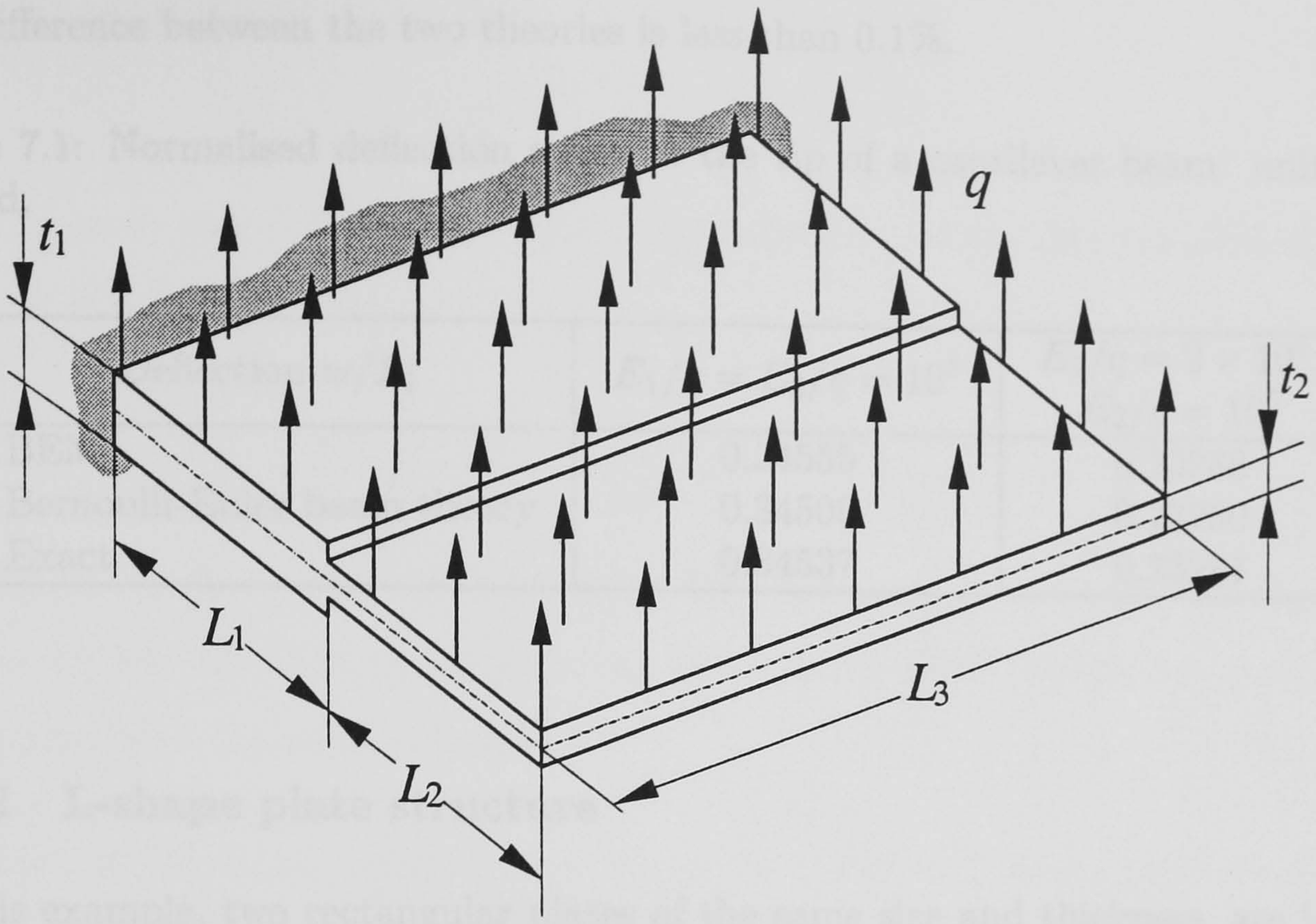

Figure 7-4: Cantilever plate with a variable thickness: uniformly loaded.

$t_2/L_1 = 0.05$. The Poisson's ratio is chosen to be $\nu = 0.0$ to allow comparison with exact beam solution. In this example, two analyses are carried out, that is $E_1/q = E_2/q = 100000$, and, $E_1/q = 200000$ and $E_2/q = 100000$.

The configuration is divided into two sub-regions, where 12 elements for each region are used. Analytical solution for this example can be derived using the Bernoulli-Euler beam theory to give

$$w = \frac{15qL_3\ {L_1}^4}{8E_1I_1} + \frac{qL_3\ {L_2}^4}{8E_2I_2} \quad \text{where} \quad I_1 = \frac{L_3\ {t_1}^3}{12} \text{ and } I_2 = \frac{L_3\ {t_2}^3}{12} \tag{7.8}$$

and the exact solution for the vertical tip deflection taking into consideration the effect of shear deformation can be derived using solutions presented in [129] to give

$$w = \frac{15qL_3\ {L_1}^4}{8E_1I_1} + \frac{qL_3\ {L_2}^4}{8E_2I_2} + \frac{33qL_3\ {t_1}^2\ {L_1}^2}{40E_1I_1} + \frac{3qL_3\ {t_2}^2\ {L_2}^2}{20E_2I_2} \tag{7.9}$$

Table 7.1 shows the result of this example. As it can be seen, with a relatively coarse mesh, the BEM results are in excellent agreement with the exact solution. It can also be seen that the difference between exact solution and the analytical solution using Bernoulli-Euler beam theory for thin plate structure is not significant,

the difference between the two theories is less than 0.1%.

Table 7.1: Normalised deflection w/L_1 at the tip of a cantilever beam: uniformly loaded.

Deflection w/L_1	$E_1/q = E_2/q = 10^5$	$E_1/q = 2 \times 10^5$; $E_2/q = 10^5$
BEM	0.34555	0.23288
Bernoulli-Euler beam theory	0.34500	0.23250
Exact	0.34537	0.23287

7.3.2 L-shape plate structure

In this example, two rectangular plates of the same size and thickness, are jointed together to form an L-shape plate structure (as shown in Figure 7-5). The properties of the plates are: $L_1 = 1.0$; $L_2/L_1 = 1.0$; $L_3/L_1 = 2.0$; $t_1/L_1 = t_2/L_1 = 0.1$; $EL_1/q = 100000$ and $\nu = 0.0$. Angle between the two plates is 90^0. The L-shape plate structure is loaded by a distributed loading per unit length q along the tip edge of horizontal plate.

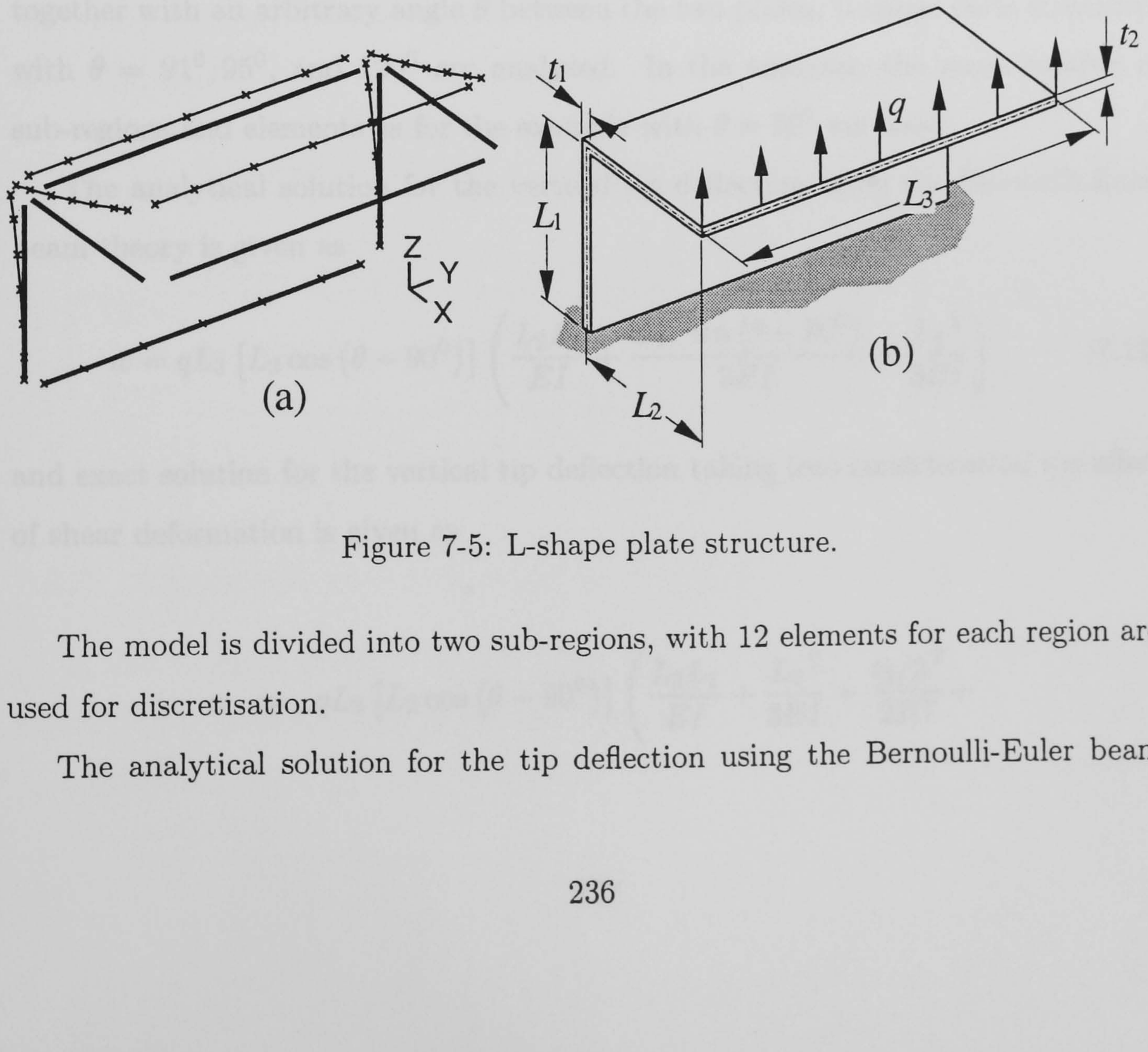

Figure 7-5: L-shape plate structure.

The model is divided into two sub-regions, with 12 elements for each region are used for discretisation.

The analytical solution for the tip deflection using the Bernoulli-Euler beam

theory is given as

$$w = \frac{qL_3\ {L_2}^3}{3EI} + \frac{qL_3\ {L_2}^2\ L_1}{EI} \tag{7.10}$$

and the exact solution for the vertical tip deflection taking into consideration the effect of shear deformation is given as

$$w = \frac{qL_3\ {L_2}^2\ L_1}{EI} + \frac{qL_3\ {L_2}^3}{3EI} + \frac{qL_3\ t_2/2^2\ L_2}{2IG} + \frac{qL_1}{t_1 E} \tag{7.11}$$

Figure 7-5 shows the deformed shape for this example and table 7.2 shows the results for the tip deflection. As it can be seen the BEM results are in excellent agreement with the exact solution.

Table 7.2: Normalised deflection w/L_1 at the tip of an L-shape plate structure.

	Deflection w/L_1
BEM	0.16033
Bernoulli-Euler beam theory	0.16000
Exact	0.16040

To demonstrate that this method is capable of modelling plate structures jointed together with an arbitrary angle θ between the two plates, L-shape plate structures with $\theta = 91^0, 95^0$, and 120^0 are analysed. In the analyses, the same number of sub-regions and elements as for the example with $\theta = 90^0$ are used.

The analytical solution for the vertical tip deflection using the Bernoulli-Euler beam theory is given as

$$w = qL_3\left[L_2\cos\left(\theta - 90^0\right)\right]\left(\frac{L_2L_1}{EI} + \frac{{L_1}^2\sin\left(\theta - 90^0\right)}{2EI} + \frac{{L_2}^2}{3EI}\right) \tag{7.12}$$

and exact solution for the vertical tip deflection taking into consideration the effect of shear deformation is given as

$$w = qL_3\left[L_2\cos\left(\theta - 90^0\right)\right]\left(\frac{L_2L_1}{EI} + \frac{{L_2}^2}{3EI} + \frac{{t_2/2}^2}{2IG} +\right.$$

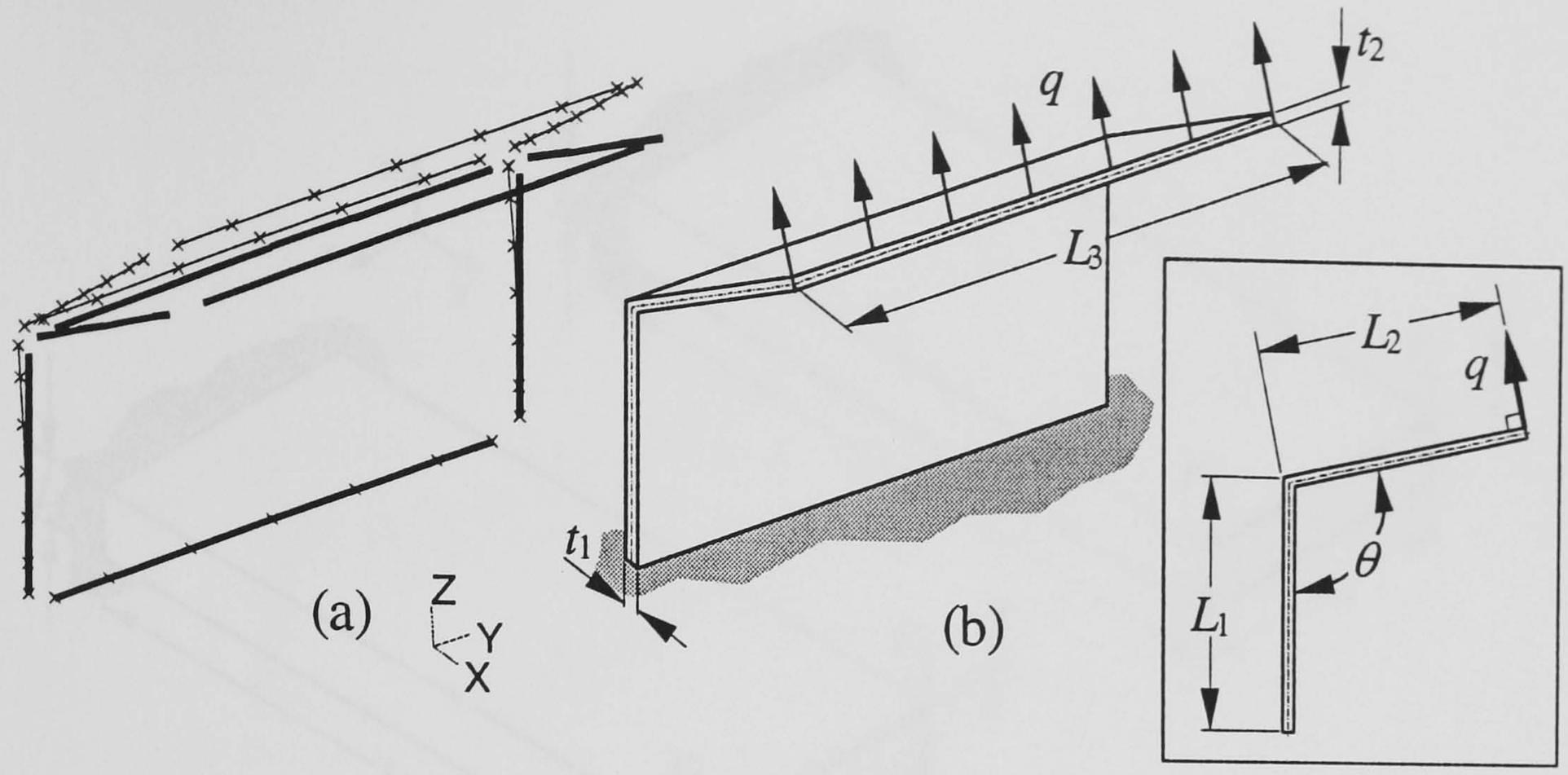

Figure 7-6: L-shape plate structure jointed with an arbitrary angle θ.

$$\frac{{L_1}^2 \sin\left(\theta - 90^0\right)}{2EI} - \frac{{t_1/2}^2 \sin\left(\theta - 90^0\right)}{2IG}\Bigg) + \frac{qL_1 \cos\left(\theta - 90^0\right)}{t_1 E} \tag{7.13}$$

Figure 7-6 shows the deformed shape of this example and table 7.3 shows the results for the tip deflection. The BEM results are in excellent agreement with the exact solution.

Table 7.3: Normalised deflection w/L_1 at the tip of an L-shape plate structure.

Deflection w/L_1	$\theta = 91^0$	$\theta = 95^0$	$\theta = 120^0$
BEM	0.16136	0.16493	0.16483
Bernoulli-Euler beam theory	0.16102	0.16460	0.16455
Exact	0.16142	0.16497	0.16476

7.3.3 Cantilever box subjected to bending and torsion

In this example, a cantilever box subjected to bending and torsion (as shown in Figure 7-4) is analysed. The properties of the plate are: $t = 2.0$ mm; $L_1 = 800$ mm; $L_2 = 2000$ mm; $L_3 = 100$ mm; $E = 70000$ MPa and $\nu = 0.3$. The load is simulated

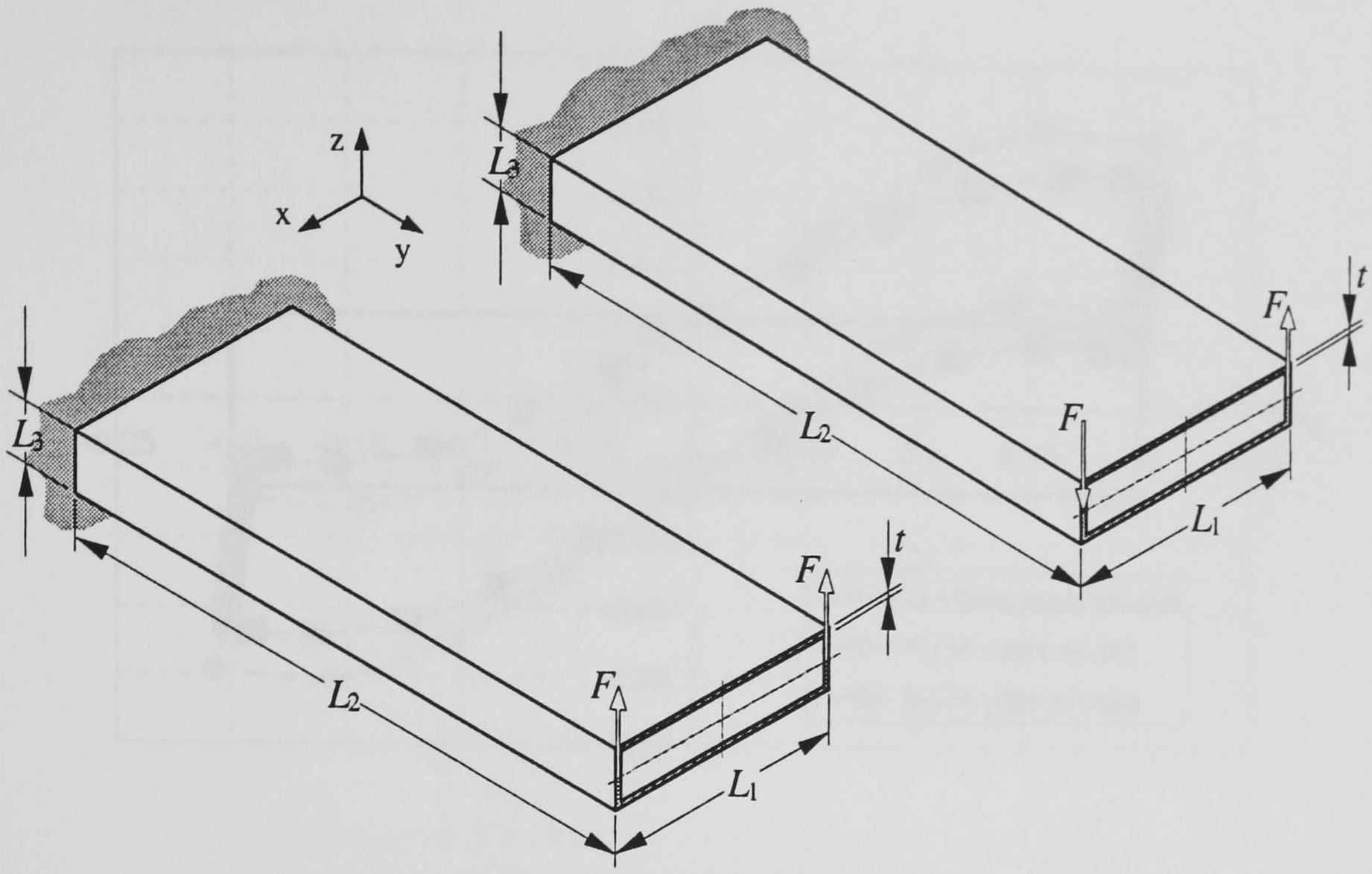

Figure 7-7: Cantilever box subject to (a) bending and (b) torsion.

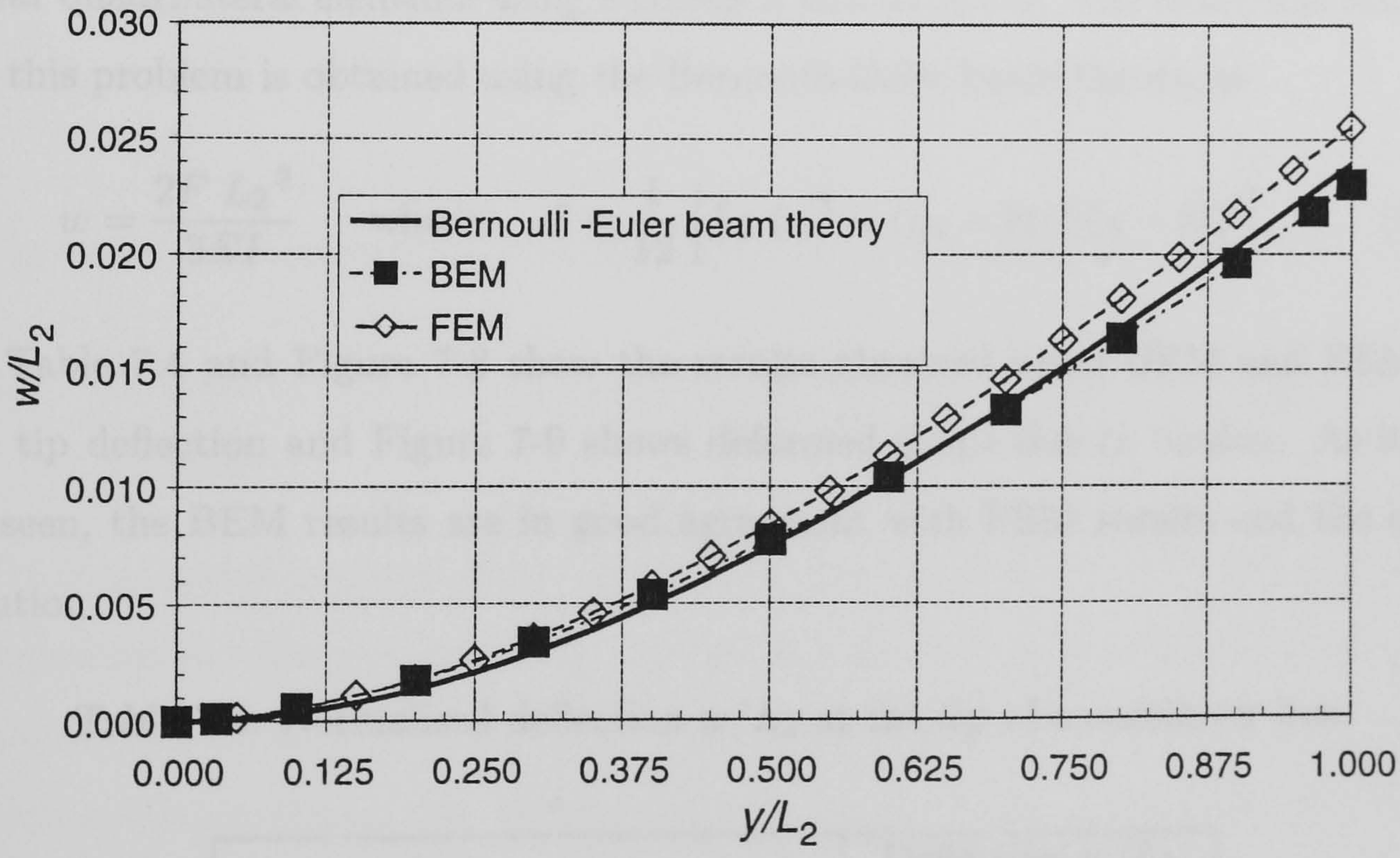

Figure 7-8: Deflection of the box due to bending.

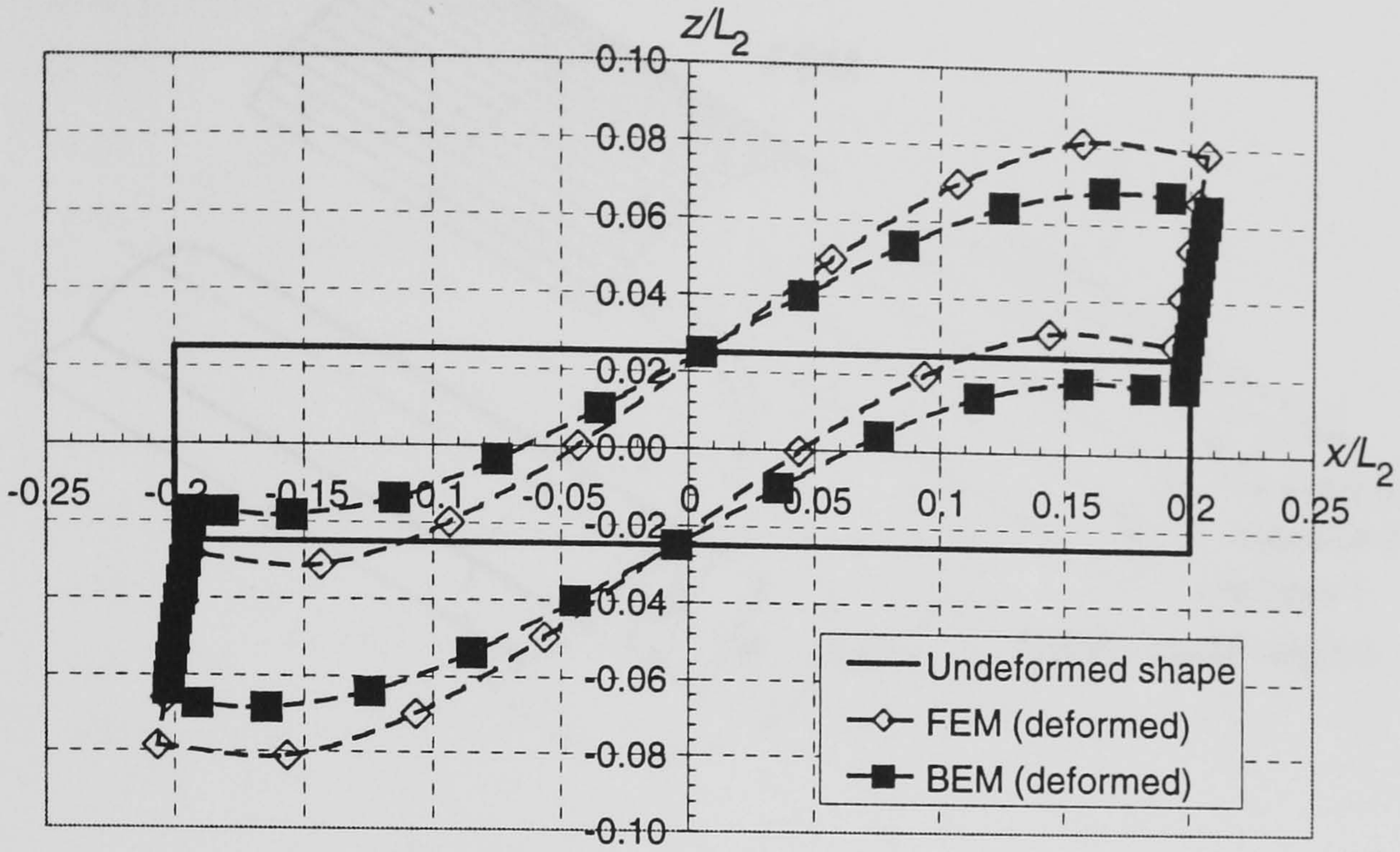

Figure 7-9: Deformed shape of the box due to torsion.

by placing a force couple $F = 5000$ N at the tip.

The boundary element model is divided into four sub-regions, where 16 elements for each region are used. For comparison, a finite element model with 400, four-node linear quadrilateral elements using I-DEAS is also analysed. The analytical solution for this problem is obtained using the Bernoulli-Euler beam theory, as

$$w = \frac{2F\ {L_2}^3}{3EI} \qquad \text{where} \qquad I = \frac{1}{12}\left[L_1\ {L_3}^3 - (L_1 - 2t)\,(L_3 - 2t)^3\right] \tag{7.14}$$

Table 7.4 and Figure 7-8 show the results obtained using BEM and FEM for the tip deflection and Figure 7-9 shows deformed shape due to torsion. As it can be seen, the BEM results are in good agreement with FEM results and the exact solution.

Table 7.4: Normalised deflection w/L_2 at the tip of a cantilever box.

	Deflection w/L_2
BEM (64 elms)	0.023009
FEM (400 elms)	0.025559
Bernoulli-Euler beam theory	0.023872

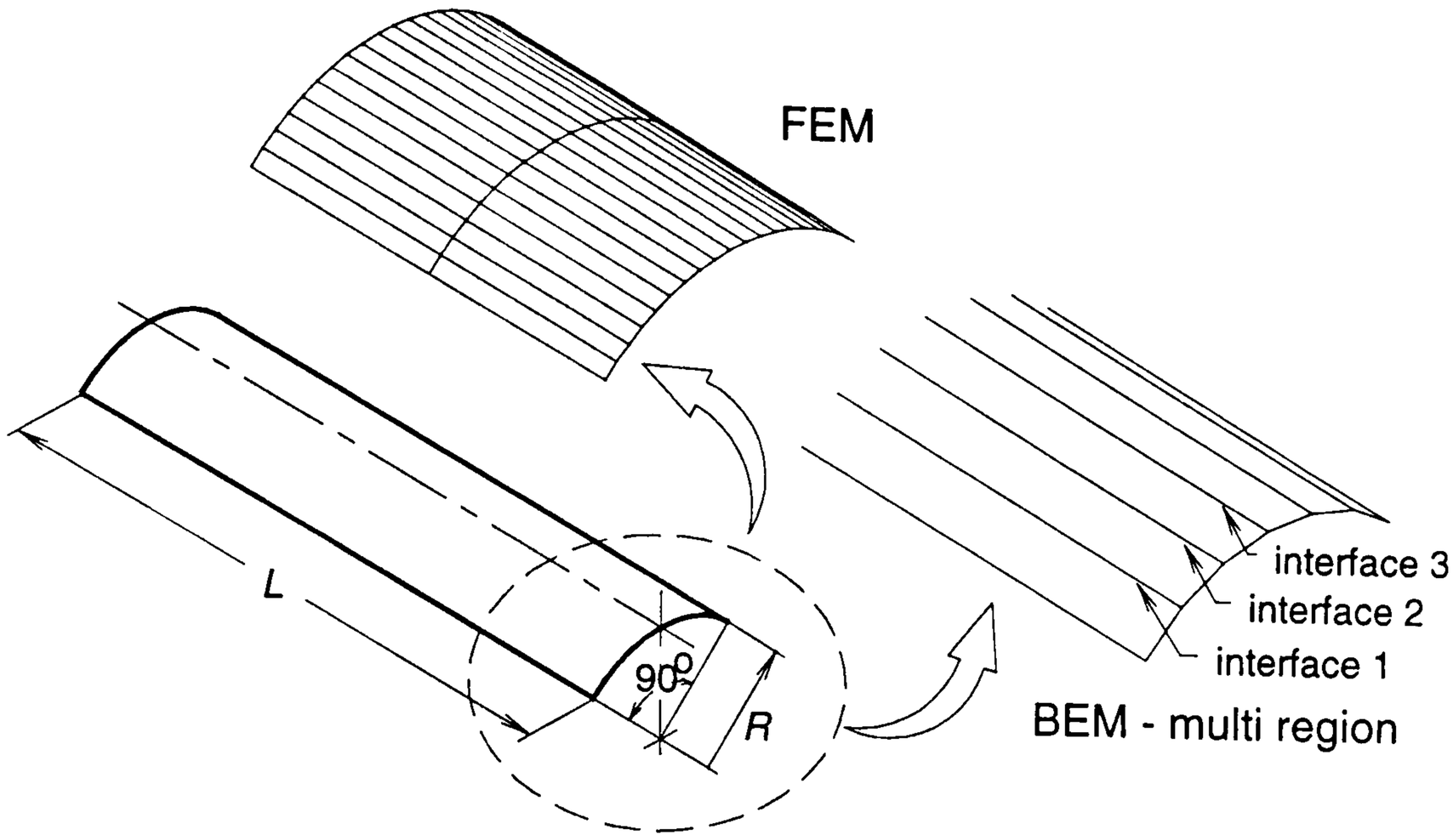

Figure 7-10: Quarter of a pressurized cylinder.

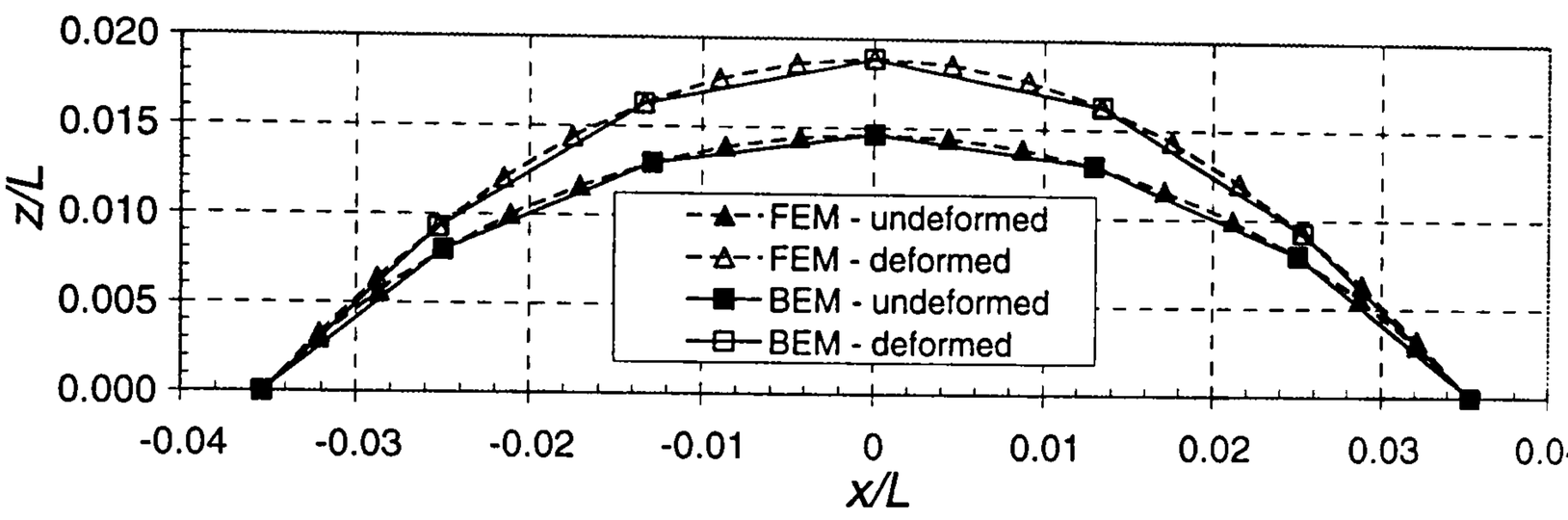

Figure 7-11: Deformed shape of clamped quarter cylinder (50× magnification).

7.3.4 A quarter of a long cylinder, clamped and loaded by internal pressure

In this example, a quarter of a cylinder having a radius R and length $L/R = 20$, clamped on all sides and loaded by internal pressure p is analysed, see Figure 7-10. Ratio of the modulus of elasticity and internal pressure $E/p = 100000$ and Poisson's ratio $\nu = 0.3$ are chosen. Six BEM regions are used to model the structure with 24 elements for each region (4 elements on the short side and 8 elements on the long side). A total number of elements used are 144. For comparison, the structure is also modelled using FEM with 396 (18×20) elements. Figure 7-11 shows deformed

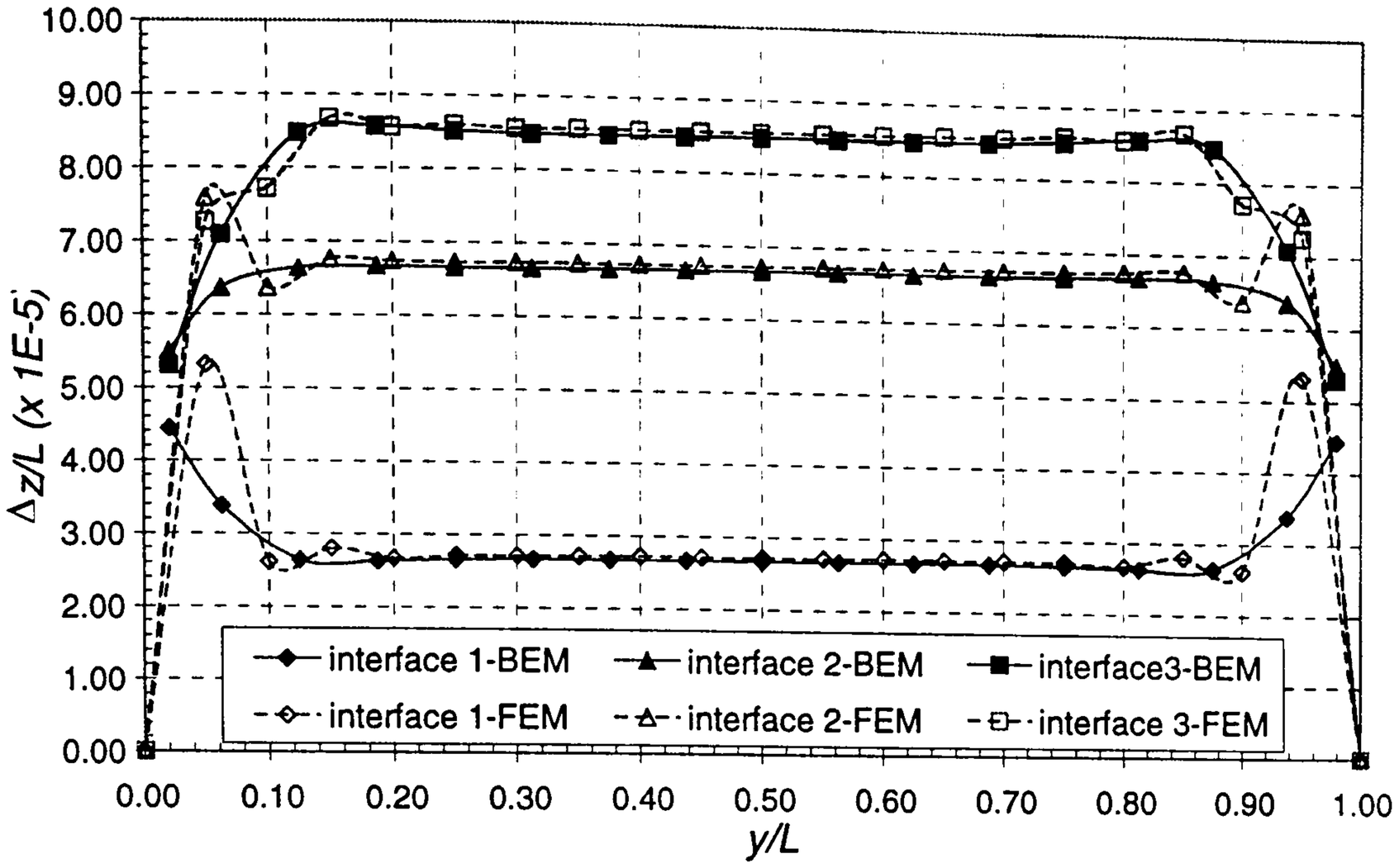

Figure 7-12: Displacement in global $z-$ direction along the interface between regions.

shape of the structure at $y/L = 1/2$. Figure 7-12 shows the displacement in global $z-$ direction along the interface between regions. As it can be seen from the figure, the FEM results show an oscillation near the edges, which is not occurring in the BEM results. For the points away from the edges, BEM results are in good agreement with FEM results.

7.3.5 A cantilever box with a centre crack on the upper skin, subjected to bending

To demonstrate the application of the dual boundary element method in multi-region formulation, a cantilever box with a centre crack on the upper skin subjected to bending (as shown in Figure 7-13) is analysed. The properties of the plate are the same as in the previous example, i.e. $t = 2.0$ mm; $L_1 = 800$ mm; $L_2 = 2000$ mm; $L_3 = 100$ mm; $E = 70000$ MPa and $\nu = 0.3$. The load is simulated by placing a force couple $F = 5000$ N at the tip. The crack is modelled with 12 elements for each surface.

Along the wall, the maximum stress occurred at the top of the box, and is given as

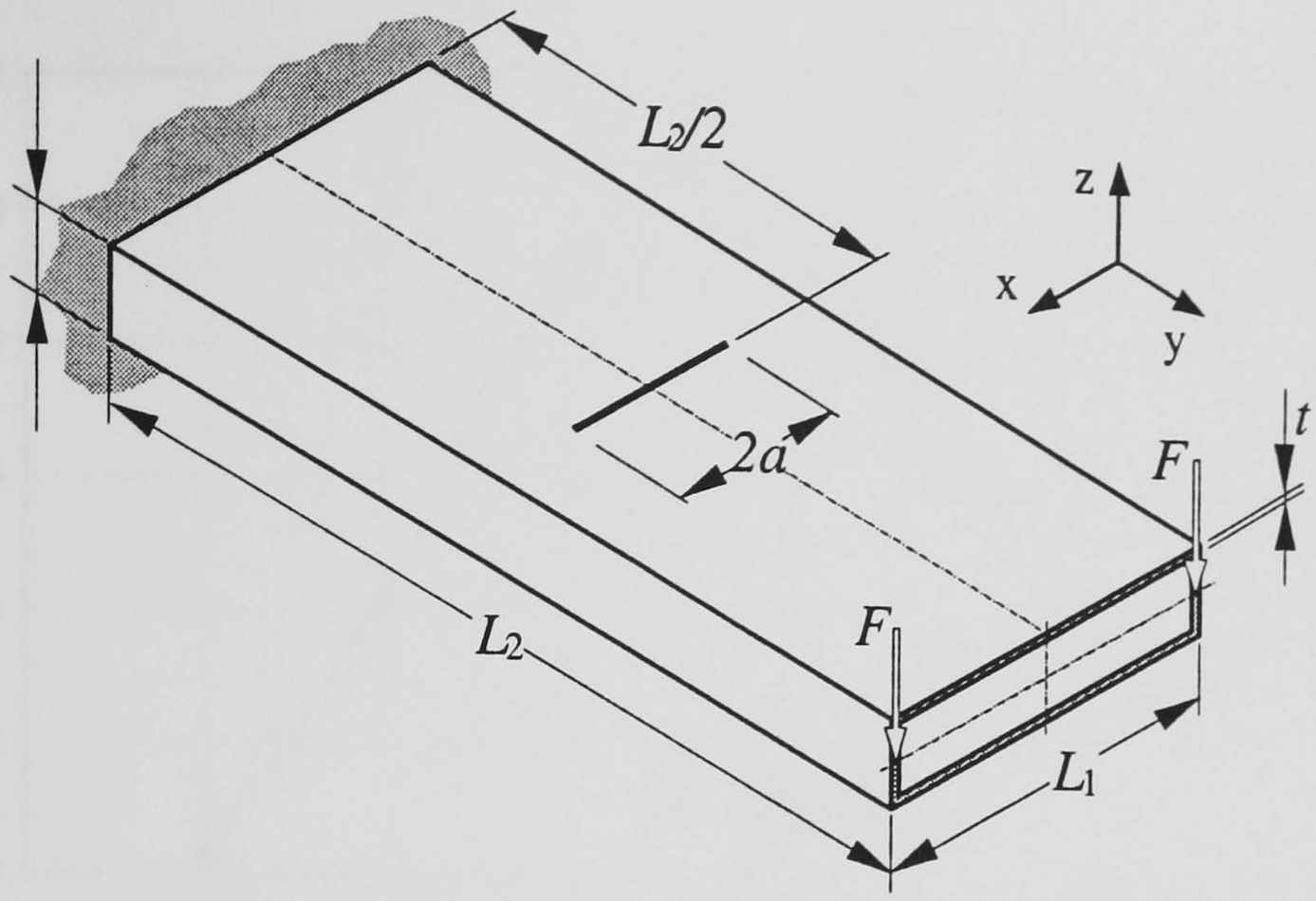

Figure 7-13: A cantilever box with a centre crack on the upper skin, subjected to bending.

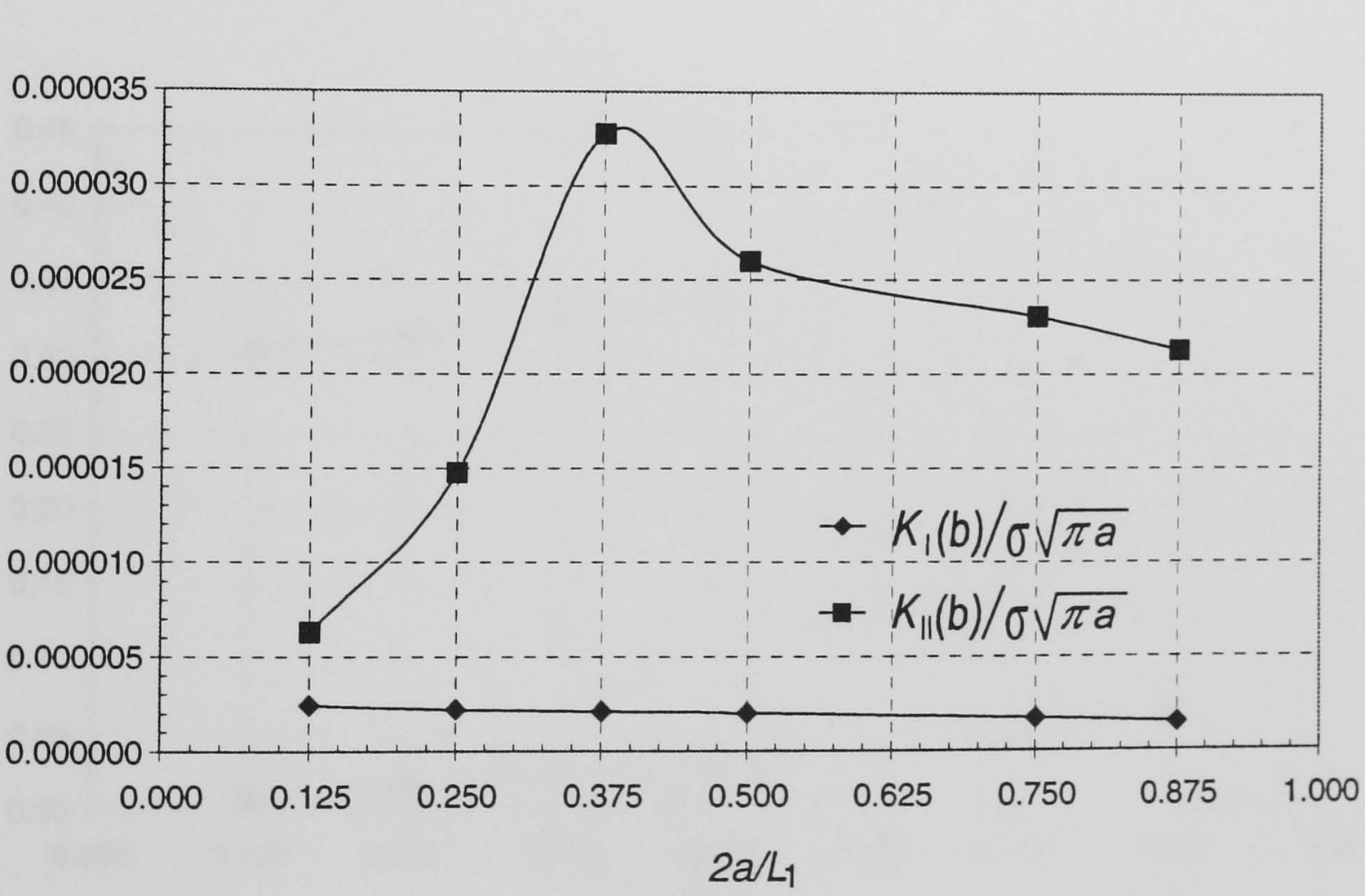

Figure 7-14: Normalised mode I and II stress intensity factors due to bending load for a cantilever box with a centre crack on the upper skin.

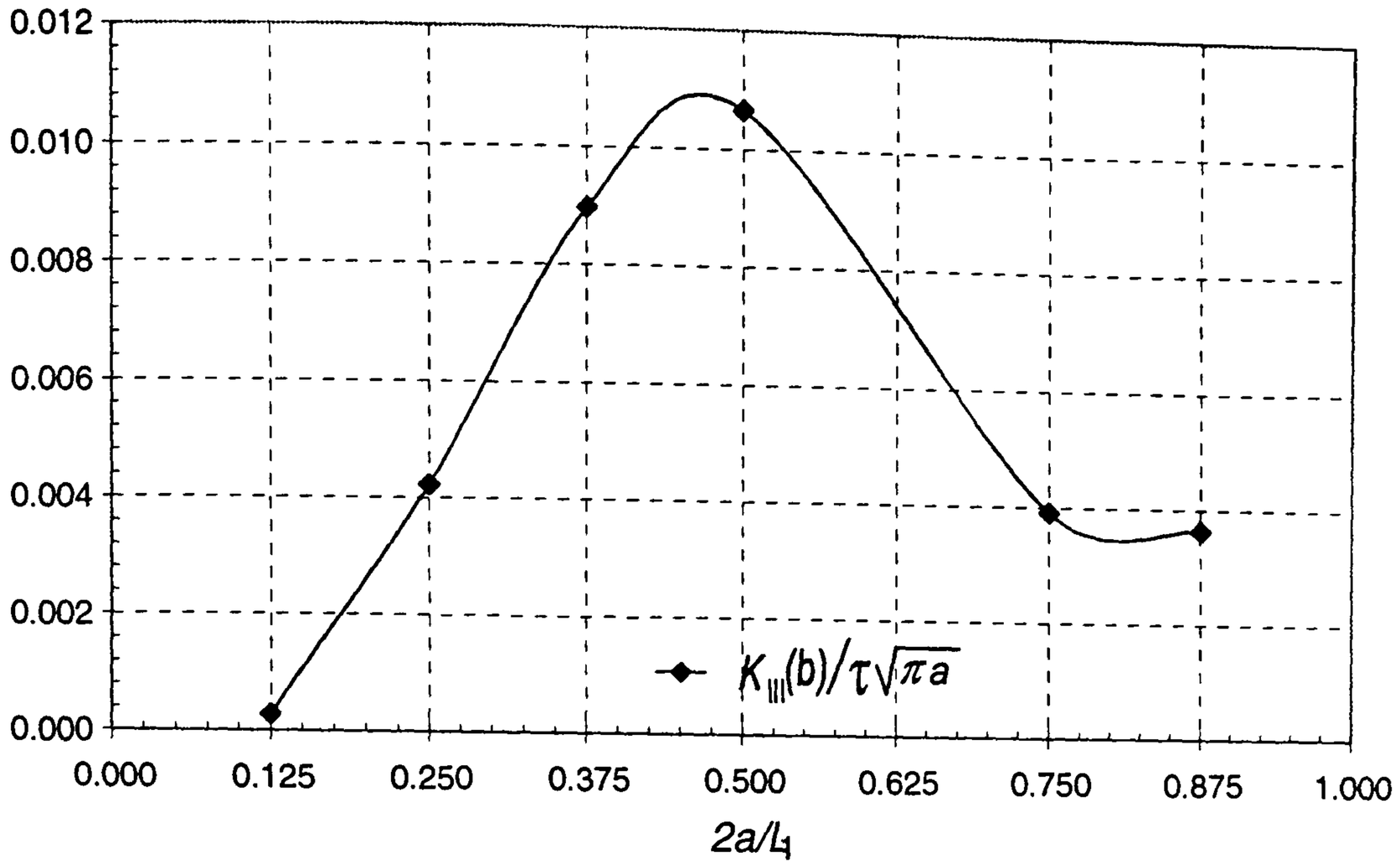

Figure 7-15: Normalised mode III stress intensity factors due to shear load for a cantilever box with a centre crack on the upper skin.

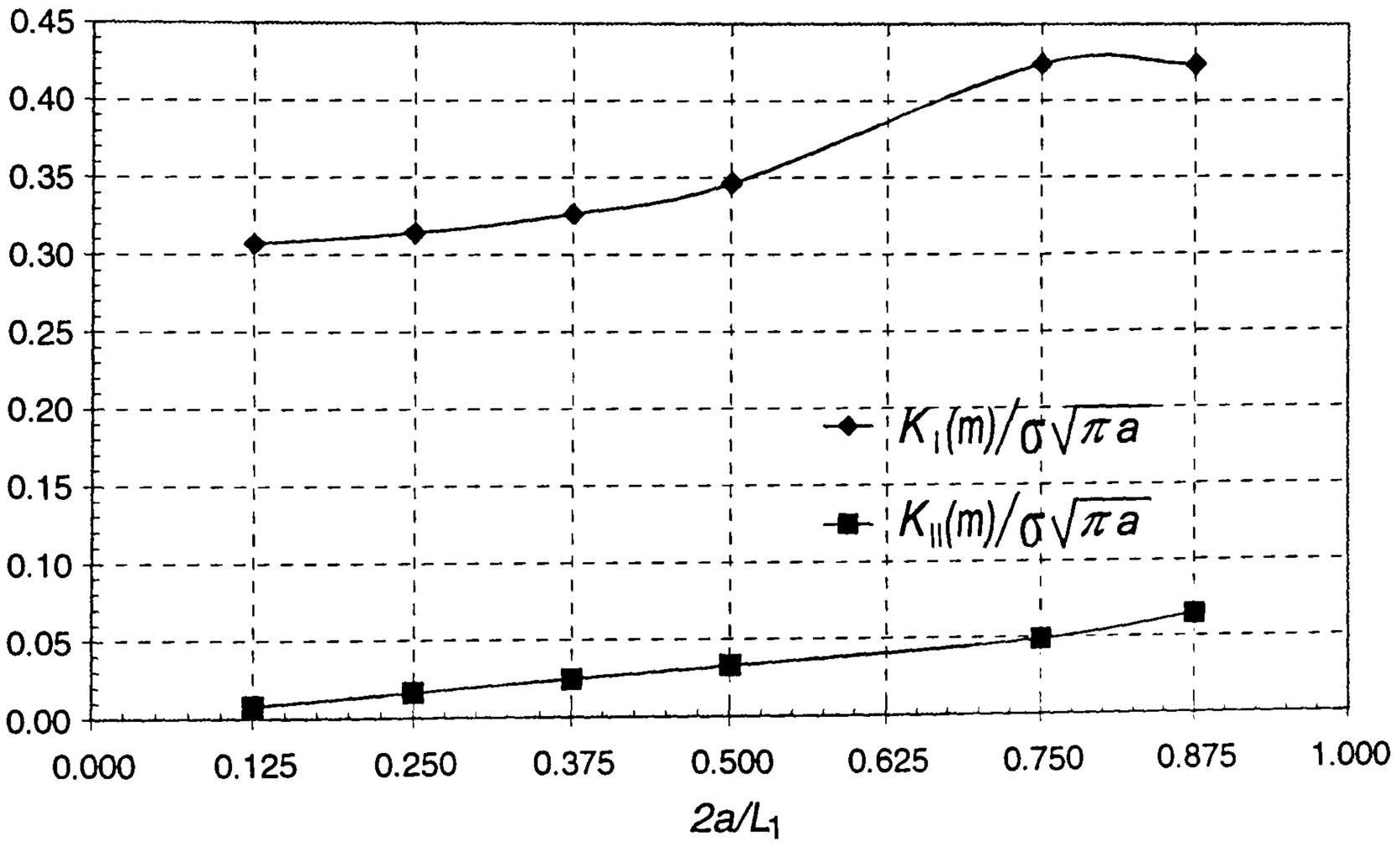

Figure 7-16: Normalised mode I and II stress intensity factors due to membrane load for a cantilever box with a centre crack on the upper skin.

$$\sigma_{\max} = \frac{2F\,(L_2)\,(L_3/2)}{I} \quad \text{where} \quad I = \frac{1}{12}\left[L_1\,{L_3}^3 - (L_1 - 2t)\,(L_3 - 2t)^3\right]$$

and the maximum shear stress occurred along at the middle of the box, and is given as

$$\tau_{\max} = \frac{2F}{I}\left[\frac{L_3 - 2t}{4} + \frac{L_1}{2}\,(L_3 - t)\right]$$

The above normal and shear stresses are chosen as far field stresses in the normalisation factor for the stress intensity factors.

Figures 7-14 – 7-16 show the stress intensity factors obtained here. As it can be seen, this case is dominated by membrane stress intensity factors.

7.4 Summary

In this chapter, an application of boundary element method to analyses of assembled plate-structures subjected to arbitrary loading was presented. Multi-region technique was used to model the structure. Additional equations needed to solve the problem were obtained by imposing compatibility and equilibrium equations along the interface boundaries.

Several examples with variable material properties, variable thickness and variable positions as well as plate structure containing crack with different loadings and boundary conditions were analysed. It is shown that good accuracy can be obtained with relatively coarse meshes.

Chapter 8

Conclusions and Future Work

This chapter contains the final conclusions and recommendations for future research. These conclusions are based on methods developed in the previous chapters, by which the main objectives outlined in Chapter 1 were achieved. The possible extensions of the present work are also discussed.

8.1 Conclusions

The work presented in this thesis can be divided into two main categories: the boundary element formulation including hypersingular formulation for shear deformable plates and shells and the application of dual boundary element method for fracture mechanics analysis of shear deformable plates and shells.

The main conclusion of the work are that the proposed boundary element methods are efficient for solving plate and shell structures subjected to bending, membrane and pressure loads. The method can also be applied efficiently to fracture mechanics analysis of plates and shells.

In chapter 3, the basic displacement boundary integral equations were derived. The formulation was implemented in a computer code using quadratic boundary elements. The domain integrals are evaluated using cell integration and the dual reciprocity technique. The boundary stress resultants were computed using the derivatives of the shape functions. Several examples were solved. The results were compared to results of the classical and shear deformable plate and shell theories. The following conclusions can be made based on the results presented in chapter 3:

1. The shear deformable plate and shell theories can be used to model both thin as well as thick plates and shells. The range of thickness to width ratios h/b tested in this work were $0.01 - 0.2$. It was shown that the method was capable to accurately analyse shells having $h/b = 0.2$, while for the same case the classical theory resulted in 18.6% error. The theory used, hence, overcome the difficulties that arise from the modelling via the classical plate and shell theory.

2. The evaluation of domain boundary integrals using the dual reciprocity technique were found to be more accurate than domain integration using constant cell discretisation. The computing time needed for the dual reciprocity technique is about four times longer than the corresponding domain integration using constant cell.

3. The present formulation has the same singular behaviour as that in two-dimensional elasticity problems, therefore modelling strategy, and the evaluation of singular integrals which has been developed for two-dimensional problems can be applied directly to the present formulation.

The hypersingular boundary integral equations were derived in Chapter 4. Both the bending moment and the shear force integral equations were considered and finally the traction integral equations for plates and shells were formed. The domain integrals are evaluated using the dual reciprocity technique. The traction equations were used together with displacement equations to form the dual boundary element method (DBEM).

Applications of the DBEM to fracture mechanics analysis of plates and shells are the second main category of the work in this thesis. Chapter 5 presented the DBEM and methods for evaluation of the stress intensity factors, that is a special crack tip elements, crack surface displacements extrapolation (CSDE) and $J-$ integral techniques. In Chapter 6, incremental crack growth analysis using DBEM was presented. Modelling strategies, determination of crack growth direction, fatigue life calculations and multiple crack growth analysis were explained in this chapter. The conclusions made from the work related to this subject are:

1. In evaluation of the stress intensity factors, the CSDE techniques using special

crack tip elements gives the same level of accuracy compare to the $J-$ integral techniques for the same number of elements, and both techniques were shown to give accurate results. It was shown that $< 1\%$ accuracy can be achieved using both techniques. Using both techniques, this level of accuracy were achieved with crack tip element length to crack length ratio $l/2a < 0.025$.

2. If the crack is modelled with enough number of elements, different integral path does not give significant effect to the stress intensity factors. Number of internal points used for $J-$ integral technique in this work is 32.

3. The shell curvature has significant effect on the stress intensity factors. It was shown that for shell subjected to internal pressure, as the radius of curvature R become smaller, i.e. the shell become deeper, the stress intensity factors due to bending decrease while the stress intensity factors due to membrane increase. This phenomena happened because shell structure is capable of transferring the pressure loads into membrane stresses.

4. Several fatigue life calculation examples were shown to be in good agreement with experimental results. It was also demonstrated that the proposed method was capable of modelling crack flapping effect which has been observed in the experimental study of pressurized cylindrical shells.

5. The present formulation is a robust and efficient alternative to domain type methods. Moreover, it is reliable in the prediction of the stress resultant intensity factors and very efficient for crack growth simulation, since remeshing is not needed during simulation.

6. The formulation was shown to be accurate and requiring small number of elements compared to domain type methods.

Chapter 7 presented a multi-region boundary element formulation for assembled plate-structures. In this chapter, compatibility and equilibrium equations needed to solve the problem were explained. Several conclusions drawn from the work related to this subject are:

1. The proposed method was shown to be able to analysed assembled plate-structures with variable material properties, thickness and positions including fracture mechanics analysis of plate-structure.

2. Using a coarse mesh, example results were shown to be in a good agreement with exact solutions and other numerical techniques.

8.2 Future Research

The application of the boundary element method for plates and shells presented in this work can be extended further to several area of researches, and are described as follows:

1. More accurate calculation of bending and shear stress intensity factor by taking into consideration crack closure due to bending.

2. Elastoplastic analysis of plates and shells including fracture mechanics analysis. Here, non-linear $J-$ integral can be utilised as a fracture parameter.

3. DBEM for thin shells can also be extended for modelling large cracks, to include the effect of bulging which will involve geometric non-linearity.

4. The coupling of plates and shell model to three-dimensional analysis will provide extensive area of research, such as study of surface cracks, through thickness plasticity.

Bibliography

[1] – , *Aircraft Accident Report : Aloha Airlines, Flight 243, Boeing 737-200, N 73711, near Maui, Hawaii, April, 28, 1988*, US National Transportation Safety Board, Washington, 1989.

[2] Abdel-Akher, A. and Hartley, G. A., Evaluation of boundary integrals for plate bending, *International Journal for Numerical Methods in Engineering*, **28**, 75-93, 1989.

[3] Abdel-Akher, A. and Hartley, G. A., Boundary integration and interpolation procedures for plate bending, *International Journal for Numerical Methods in Engineering*, **28**, 1389-1408, 1989.

[4] Abramowitz, M. and Stegun, I. A. (Eds.), *Handbook of mathematical functions*, Dover, New York, 1965.

[5] Ahmadi-Brooghani, S. Y. and Wearing, J. L., The application of the dual boundary element method in linear elastic crack problem in plate bending. in *Boundary Element Methods XVIII*, C. A. Brebbia, J. B. Martins, M. H. Aliabadi and N. Haie (Eds.), Portugal, 429-438, Computational Mechanics Publications, 1996.

[6] Aliabadi, M. H., Hall, W. S., and Phemister, T. G., Taylor expansion for singular kernels in the boundary element method, *International Journal for Numerical Methods in Engineering*, 21, 2221-2236, 1985.

[7] Aliabadi, M. H., Evaluation of mixed mode stress intensity factors using the path independent $J-$ integral, in *Proceeding of Boundary Elements in*

Engineering XII, Hokaido, Japan, Computational Mechanics Publications, Southampton, UK, 1990.

[8] Aliabadi, M. H. and Rooke, D. P., *Numerical Fracture Mechanics*, Kluwer Academic Publisher, AA Dordrecht, The Netherlands, 1991.

[9] Aliabadi, M. H., *Database of Stress Intensity Factors*, Computational Mechanics Publications, Southampton, 1996.

[10] Aliabadi, M. H., Boundary element formulations in fracture mechanics, *Applied Mechanics Review*, **50**(2), 83-96, 1997.

[11] Aliabadi, M. H., A new generation of boundary element methods in fracture mechanics, *International Journal of Fracture*, **86**, 91-125, 1997.

[12] Aliabadi, M. H. (Ed.), *Plate Bending Analysis with Boundary Elements, Advanced in Boundary Element Series*, Computational Mechanics Publications, Southampton, 1998.

[13] Anderson, T. L., *Fracture Mechanics, Fundamentals and Applications*, CRC Press, Boca Raton, Florida, 1991.

[14] Antes, H., On boundary integral equations for circular cylindrical shells, in *Boundary Elements*, C. A. Brebbia (Ed.), Springer Verlag, Berlin, 224-238, 1981.

[15] Antes, H., An indirectly derived integral equations system for simply supported Reissner plates, *Mech. Res. Comm.*, **13**, 63-69, 1986.

[16] Antes, H., The stress functions of point loading in Reissner's plate theory, *Mech. Res. Comm.*, **11**, 115-120, 1984.

[17] Antes, H., Basic geometrical singularities in Reissner's plate theory, *Mech. Res. Comm.*, **12**, 295-302, 1985.

[18] Barcellos, C. A. and Silva, L. H. M., A boundary element formulation for the Mindlin's plate model, in *Boundary Element Technology*, C. A. Brebbia and W. S. Venturini (Eds.), Computational Mechanics Publications, 123-130, 1989.

[19] Barsoum, R. S., A degenerate solid element for linear fracture analysis of plate bending and general shells, *International Journal for Numerical Methods in Engineering*, **10**, 551-564, 1976.

[20] Barsoum, R. S., Loomis, R. W., and Stewart, B. D., Analysis of through crack in cylindrical shells by quarter point elements, *International Journal of Fracture*, **15**(3), 259-280, 1979.

[21] Batoz, J. L. and Tahar, M. B., Evaluation of a new quadrilateral thin plate bending element, *International Journal for Numerical Methods in Engineering*, **18**, 1655-1677, 1982.

[22] Beskos, D. E., Static and dynamic analysis of shells, in *Boundary Element Analysis of Plate and Shells*, D.E. Beskos (Ed.), Spinger Verlag, Berlin, 93-140, 1991.

[23] Bézine, G., Boundary integral formulation for plate flexure with arbitrary boundary conditions, *Mech. Res. Comm.*, **5**(4), 197-206, 1978.

[24] Bittencourt, T. N., Wawrzynek, P. A., Ingraffea, A. R. and Sousa, J. L., Quasi-automatic simulation of crack propagation for 2D LEFM problems, *Engineering Fracture Mechanics*, **55**(2), 321-334, 1996.

[25] Blandford, G. E., Ingraffea, A. R. and Liggett, J. A., Two-dimensional stress intensity factor computations using the boundary element method, *International Journal for Numerical Methods in Engineering*, **17**, 387-406, 1981.

[26] Boduroglu, H. and Erdogan, F., Internal and edge cracks in a plate of finite width under bending, *Transactions of the ASME, Journal of Applied Mechanics*, **50**, 621-629, 1983.

[27] Brebbia, C. A., Telles, J. C. F. and Wrobel, L. C., *Boundary Element Techniques: Theory and Applications in Engineering*, Springer-Verlag, Berlin-Heidelberg, 1984.

[28] Brebbia, C. A. and Dominguez, J., *Boundary Elements, an Introductory Course*, 2nd edition, Computational Mechanics Publication, Southampton, McGraw-Hill Book Company, New York, 1992.

[29] Broek, D., *Elementary Engineering Fracture Mechanics*, 4th edition, Martinus Nijhoff Publishers, Dordrecht, 1987.

[30] Broek, D., *The Practical Use of Fracture Mechanics*, Kluwer Academic Publishers, Dordrecht, 1988.

[31] Budiman, H. T. and Lagace, P. A., Non dimensional parameters for geometric nonlinear effects in pressurized cylinders with axial cracks, *Journal of Applied Mechanics*, **64**, 401-406, 1997.

[32] Cohen L., Farren W. S., Duncan J. W. and Wheeler A. H., *'Report of the Court of Inquiry into the Accidents to Comet G-ALYP on 10 January 1954 and Comet G-ALYY on 8 April 1954'*, HMSO London, 1955.

[33] Delale, F. and Erdogan, F., Effect of transverse shear and material orthotrophy in a cracked spherical cap, *International Journal of Solids and Structures* , **15**, 907-926, 1979.

[34] Delale, F. and Erdogan, F., Transverse shear effect in a circumferentially cracked cylindrical shell, *Quarterly of Applied Mechanics,* **37**, 239-258, 1979.

[35] Dirgantara, T., *Computation of stress intensity factors for plate with holes* (in bahasa Indonesia), Master thesis (unpublished), Mechanical Engineering Study Programme, Faculty of Post Graduate Programme, Institut Teknologi Bandung, Indonesia, 1995.

[36] Dirgantara, T. and Aliabadi, M. H., A new boundary element formulation for shear deformable shells analysis, *International Journal for Numerical Methods in Engineering,* **45**, 1257-1275, 1999.

[37] Dirgantara, T., Aliabadi, M. H., Boundary element method for analysis of shallow shells, in *Association for Computational Mechanics in Engineering, The 7th. Annual Conference*, P. Bettess, (Ed.), University of Durham, UK, Spring 1999.

[38] Dirgantara, T., Aliabadi, M. H., Dual boundary element analysis of the crack propagation of plate bending and tension, in *Boundary Element Techniques*,

M. H. Aliabadi (Ed.), Queen Mary and Westfield College, University Of London, UK, 87-96, July 1999.

[39] Dirgantara, T., Aliabadi, M. H., Fatigue crack growth simulation of plate bending and tension, in *Fracture and Damage Mechanics*, M. H. Aliabadi (Ed.), Queen Mary and Westfield College, University Of London, UK, 91-100, July 1999.

[40] Dirgantara, T., Aliabadi, M. H., Shear deformable shallow shells analysis using boundary element method, in *Second UK Conference on Boundary Integral Methods*, L. C. Wrobel and S. N. Chandler-Wilde (Eds.), Brunell University, UK, 62-72, September 1999.

[41] Dirgantara, T. and Aliabadi, M. H., Crack growth analysis of plates loaded by bending and tension using dual boundary element method, *International Journal of Fracture* (accepted for publication and due to appear), 2000.

[42] Dirgantara, T. and Aliabadi, M. H., Dual boundary element formulation for fracture mechanics analysis of shear deformable shells, (submitted for publication), 2000

[43] Dirgantara, T. and Aliabadi, M. H., Boundary element method analysis of assembled plate-structure, (submitted for publication), 2000.

[44] Dirgantara, T. and Aliabadi, M. H., Incremental crack growth simulation of shallow shells using dual boundary element method, *(*submitted for publication), 2000.

[45] Ehlers, R., Stress intensity factors and crack opening areas for axial through cracks in hollow cylinders under internal pressure loading, *Engineering Fracture Mechanics*, **25**, 1, 63-77, 1986.

[46] El-Zafrany, A., Debbih, M. and Fadhil, S., Boundary element analysis of thick Reissner plates in bending. *Engineering Analysis with Boundary Elements*, **14**, 159-169, 1994.

[47] El-Zafrany, A., Debbih, M. and Fadhil, S., An efficient approach for boundary element bending analysis of thin and thick plates, *Computer and Structures*, **56**, 565-576, 1995.

[48] El-Zafrany, A., Stress analysis of thick Reissner plates in bending under generalized loading, in *Boundary Element Techniques*, Aliabadi M. H. (Ed.), Department of Engineering, Queen Mary and Westfield College, University of London, 1-11, 1999.

[49] Erdogan, F. and Kibler, J. J., Cylindrical and spherical shells with crack, *International Journal of Fracture Mechanics*, **5**(3), 229-237, 1968.

[50] Erdogan, F. and Sih, G. C., On the crack extension of plates under plane loading and transverse shear, *Journal of Basic Engineering*, **85**, Series D, No.4, 519-527, 1963.

[51] Flügge, W., *Stresses in Shells*, 2nd edition, Springer-Verlag, Berlin, 1973.

[52] Folias, E., A finite line crack in a pressurized spherical shell, *International Journal of Fracture Mechanics*, **1**, 20-46, 1965.

[53] Folias, E., An axial crack in a pressurized cylindrical shell, *International Journal of Fracture Mechanics*, **1**, 104-113, 1965.

[54] Forbes, D. J. and Robinson, A. R., *Numerical Analysis of Elastic Plates and Shallow Shells by an Integral Equation Method*, Structural research series report no. 345. University of Illinois, Urbana, 1969.

[55] Griffith, A. A., The phenomena of rupture and flow in solids, *Philosophical Transactions of the Royal Society of London*, A221,163-197, 1920.

[56] Greenberg, M. D., *Application of Green's Functions in Science and Engineering*, Prentice-Hall Inc., 1971.

[57] Hadamard, J., *Lectures on Cauchy's Problem in Linear Partial Diferential Equations*, Yale University Press, New Haven, 1923.

[58] Hartmann, F. and Zormantel, R., The direct boundary element method in plate bending, *International Journal for Numerical Methods in Engineering*, **23**, 2049-2069, 1986.

[59] Hartmann, F., Boundary elements on personal computers, *Microsoftware for Engineers*, **3**(4), 213-215, 1987.

[60] Henwood, D. J., Whiteman, J. R. and Yettram, A. L., Finite difference solution of a system of first-order partial differential equations, *International Journal for Numerical Methods in Engineering*, **17**, 1385-1395, 1981.

[61] Hong, H. and Chen, J., Derivations of integral equations of elasticity, *Journal of Engineering Mechanics*, **114**(6), 1028-1044, 1988.

[62] Huang, N. C., Li, Y. C. and Russell, S. G., Fracture mechanics of plates and shells applied to fail safe analysis of fuselage. Part I: theory, *Theoretical and Applied Fracture Mechanics*, **27**, 221-236, 1997.

[63] Huang, N. C., Li, Y. C. and Russell, S. G., Fracture mechanics of plates and shells applied to fail safe analysis of fuselage. Part II: computational results, *Theoretical and Applied Fracture Mechanics*, **27**, 237-253, 1997.

[64] Huber, O., Dallner, R., Partheymuller, P., and Kuhn, G., Evaluation of the stress tensor in 3-D elastoplasticity by direct solving of hypersingular integrals, *International Journal for Numerical Methods in Engineering*, **39**, 2555-2573, 1996.

[65] Hudson, C. M., *Effect of stress ratio on fatigue-crack growth in 7075-T6 and 2024-T3 aluminium alloy specimens*, NASA TN D5390, NASA Langley Research Center, 1969.

[66] Hussain, M. A., Pu, S. U. and Underwood, J., Strain energy release rate for a crack under combined mode I and II, *ASTM STP 560*, 2-28, 1974.

[67] Irwin, G. R., Fracture dynamics, *Fracturing of Metals*, American Society of Metals, Cleveland, 147-166, 1948.

[68] Jaswon, M. A., Maiti, M. and Symm, G. T., Numerical biharmonic analysis and some applications, *International Journal of Solids and Structures*, **3**, 309-332, 1967.

[69] Karam, V. J. and Telles, J. C. F., On boundary elements for Reissner's plate theory, *Engineering Analysis*, **5**, 21-27, 1988.

[70] Karam, V. J. and Telles, J. C. F., The BEM applied to plate bending elasto-plastic analysis using Reissner's theory, *Engineering Analysis with Boundary Elements*, **9**, 351-357, 1992.

[71] Karami, G., Zarrinchang, J. and Foroughi, B., Analytical treatment of boundary integrals in direct boundary element analysis of plate bending problems, *International Journal for Numerical Methods in Engineering*, **37**, 2409-2427, 1994.

[72] Knops, B., *Numerical simulation of crack growth in pressurized fuselages*, Ph.D Thesis, Faculty of Aerospace Engineering, Delft University of Technology, The Netherlands, 1994.

[73] Krenk, S., Influence of transverse shear on an axial crack in a cylindrical shell, *International Journal of Fracture*, **14**(2), 123-143, 1978.

[74] Lei, X. Y., Huang M. K., Wang, X., Analysis of the explicit fundamental solution of a shallow spherical shell involving shear deformation, *Applied Mathematical Modelling*, **19**, 194-200, 1995.

[75] Lin Jinmu and Long Shuyao, Geometrically nonlinear analysis of the shallow shell by the displacement-based boundary element formulation, *Engineering Analysis with Boundary Elements*, **18**, 63-70, 1996.

[76] Kirchhoff, G., Uber das gleichgewicht und die bewegung einer elastischen scheibe, *J. Reine Angew. Math.*, **40**, 51-88, 1850.

[77] Knöpke, B., The hypersingular integral equation for the bending moments m_{xx}, m_{xy} and m_{yy} of the Kirchhoff plate, *Computational Mechanics*, **15**, 19-30, 1994.

'8] Love, A. E. H., *A Treatise on the Mathematical Theory of Elasticity*, Dover Publications, 4^{th} edition, New York, 1944.

9] Lu, P. and Huang, M., Computation of the fundamental solution for shallow shells involving shear deformation, *International Journal of Solids and Structures*, **28**(5), 631-645, 1991.

0] Lu, P. and Huang, M., Boundary element analysis of shallow shells involving shear deformation, *International Journal of Solids and Structures*, **29**(10), 1273-1282, 1992.

1] Matsui ,T. and Matsuoka, O., The fundamental solution in the theory of shallow shells, *International Journal of Solids and Structures*, **14**, 971-986, 1978.

2] Mi, Y., *Three Dimensional Analysis of Crack Growth*, Topics in Engineering Vol. 28, Computational Mechanics Publications, Southampton, 1996.

3] Mi, Y. and Aliabadi, M. H., Dual boundary element method for three-dimensional fracture mechanics analysis, *Engineering Analysis with Boundary Elements*, **10**, 161-171, 1992.

4] Mi, Y. and Aliabadi, M. H., Discontinuous crack-tip elements: application to 3-D boundary element method, *International Journal of Fracture*, **67**, R67-R71, 1994.

5] Mindlin, R. D., Influence of rotatory inertia and shear on flexural motions of isotropic, elastic plates, *Journal of Applied Mechanics*, **18**, 31-38, 1951.

6] Murakami, Y., *et al.*, *Stress Intensity Factors Handbook*, Pergamon Press, England, 1990.

7] Naghdi, P. M., Note on the equations of shallow elastic shells, *Quarterly of Applied Mathematics*, **14**, 331-333, 1956.

8] Naghdi, P. M., On the theory of thin elastic shells, *Quarterly of Applied Mathematics*, **14**, 369-380, 1956.

9] Niu, M. C., *Airframe Structural Design*, Hong Kong Conmilit Press Ltd., Hong Kong, 1988.

10] Novozhilov, V. V., *The Theory of Thin Shells,* translated by P. G. Lowe, P. Noordhoff Ltd., Gronigen, The Netherland, 1959.

1] Newton D. A. and Tottenham, H., Boundary value problems in thin shallow shells of arbitrary plan form, *Journal of Engineering Mathematics*, **2**, 211-223, 1968.

2] O'Donoghue, P. E., Atluri, S. N. and Pipkins, D. S., Computational strategies for fatigue crack growth in three dimensions with application to aircraft components, *Engineering Fracture Mechanics*, **52**(1), 51-64, 1995.

3] Okada, H., Rakiyah, H. and Atluri, S. N., A novel displacement gradient boundary element for elastic stress analysis with high accuracy, *Trans ASME Journal of Applied Mechanics*, **55**, 786-794, 1988.

4] Providakis, C. P. and Beskos, D. E., Free and forced vibration of shallow shells by boundary and interior elements, *Computer Methods in Applied Mechanics and Engineering*, **92**(1), 55-74, 1991.

5] Paris, P. C. and Erdogan, F. A., A critical analysis of crack propagation laws, Transaction ASME, *Journal of Basic Engineering*, **85**, 528-534, 1963.

6] Paris, P. C., Gomez, R. E. and Anderson, W. E., A rational analytic theory of fatigue, *The Trend in Engineering*, **13**, 9-14, 1961.

7] Partridge, P. W., Brebbia, C. A. and Wrobel, L. C., *The Dual Reciprocity Boundary Element Method*, Computational Mechanics Publication, Southampton, 1992.

8] Peters, R. W. and Kuhn, P., Bursting strength of unstiffened pressure cylinders with slits, *NACA Technical Note* 3993, April 1957.

9] Portela, A., *Dual Boundary Element Analysis of Crack Growth*, Topics in Engineering Vol. 14, Computational Mechanics Publications, Southampton, 1993.

[100] Portela, A., Aliabadi, M. H. and Rooke, D. P. , The dual boundary element method: effective implementation for crack problems, *International Journal for Numerical Methods in Engineering*, **33**, 1269-1287, 1992.

[101] Portela, A., Aliabadi, M. H. and Rooke, D. P., Dual boundary incremental analysis of crack propagation, *Computer and Structures*, **46**(2), 237-247, 1993.

[102] Potyondy, D. O. ,Wawrzynek, P. A. and Ingraffea A. R., Discrete crack growth analysis methodology for through cracks in pressurized fuselage structure, *International Journal for Numerical Methods in Engineering*, **38**, 1611-1633, 1995.

[103] Rashed, Y. F., Aliabadi, M. H., Brebbia, C. A., Hyper-singular boundary element formulation for Reissner plates, *International Journal of Solids and Structures*, **35**(18), 2229-2249, 1998.

[104] Rashed, Y. F., Aliabadi, M. H., Brebbia, C. A., Stress and displacement boundary integral formulations for shear deformable plate bending analysis, in *Boundary Element Methods XVIII*, C. A. Brebbia, J. B. Martins, M. H. Aliabadi and N. Haie (Eds.), Portugal, 493-502, Computational Mechanics Publication, 1996.

[105] Reddy, J. N., Exact solutions of moderately thick laminated shells, *Journal of Engineering Mechanics*. ASCE, **110**, 794-809, 1984.

[106] Reddy, J. N., Two-dimensional theories of plates. In *Finite Element Analysis for Engineering Design*, J. N. Reddy, C. S. Krishnamoorthy and K. N. Seetharaunu (Eds.), Lecture Notes in Engineering, **37**, C. A. Brebbia and S. A. Orszag, (Eds.) Springer-Verlag, 249-273, 1988.

[107] Reissner, E., On bending of elastic plates, *Quarterly of Applied Mathematics*, **5**, 55-68, 1947.

[108] Reissner, E., On a variational theorem in elasticity, *Journal of Mathematics and Physics*, **29**, 90-95, 1950.

[109] Reissner, E., Stress strain relations in the theory of thin elastic shells, *Journal of Mathematics and Physics*, **31**, 109-119, 1952.

[110] Remzi, E. M., Blackburn, W. S., Automatic crack propagation studies in T-junctions and cross bars, *Engineering Computational,* **7**, 116-124, 1990.

[111] Rice, J. R., A path independent integral and the approximate analysis of strain concentration by notches and cracks, *Journal of Applied Mechanics, Transaction of ASME*, **35**, 379-386, 1968.

[112] Rigby, R. H., Aliabadi, M. H., Mixed mode J-integral method for analysis of 3D fracture problems using BEM, *Engineering Analysis with Boundary Elements,* **11**, 239-256, 1993.

[113] Rigby, R. H., Aliabadi, M. H., Decomposition of the mixed mode $J-$ integral - revisited, *International Journal of Solids and Structures,* **35**(17), 2073-2099, 1998.

[114] Salgado, N. K. and Aliabadi, M. H., The application of the dual boundary element method to the analysis of cracked stiffened panels, *Engineering Fracture Mechanics*, **54**(1), 91-105, 1996.

[115] Salgado, N. K. and Aliabadi, M. H., Boundary element analysis of cracked stiffened sheets, reinforced by adhesively bonded patches, *International Journal for Numerical Methods in Engineering*, **42**(2), 195-217, 1998.

[116] Sih, G. C., A review of three-dimensional stress problem for a cracked plate, *International Journal of Fracture Mechanics*, **7**, 39-61, 1971.

[117] Sih, G. C., Strain energy density factor applied to mixed mode crack problems, *International Journal of Fracture Mechanics*, **10**, 305-321, 1974.

[118] Sih, G. C. (Ed.) *Mechanics of Fracture Volume 3: Plate and Shells with Cracks*, Noordhoff International Publishing, Leyden, 1977a.

[119] Sih, G. C., Strain energy density theory applied to plate bending problems, in *Mechanics of Fracture Volume 3: Plates and Shells with Cracks*, , G. C. Sih (Ed.), Noordhoff International Publishing, Leyden, The Netherland, XVII-XLVIII, 1977b.

[120] Sih, G. C. and Hagendorf, H. C. , On cracks in shells with shear deformation, in *Mechanics of Fracture*, Vol. 3, *Plates and Shells with Cracks*, , G. C. Sih (Ed.), Noordhoff International Publishing, Leyden, 201-229, 1977c.

[121] Sosa, H. A. and Eischen, J. W., Computation of stress intensity factors for plate bending via a path-independent integral, *Engineering Fracture Mechanics*, **25**, 451-462, 1986.

[122] Sosa, H. A. and Herrmann, G., On invariant integrals in the analysis of cracked plates, *International Journal of Fracture*, **40**, 111-126, 1989.

[123] Stern, M., A General boundary integral formulation for plate bending problems, *International Journal of Solids and Structures*, **15**, 769-782, 1979.

[124] Stern, M., Boundary integral equations for bending of thin plates, in *Progress in Boundary Element Methods*, Prentech Press, London, 158-181, 1983.

[125] Stern, M. and Lin, T.-L., Thin elastic plates in bending, in *Development in Boundary Element Methods - 4*, Banarjee, P. K. and Watson, J. O. (Eds.), Elsevier Applied Science Publishers, London, 91-119, 1986.

[126] Tanaka, M. and Miyazaki, K., A direct BEM for elastic plate-structures subjected to arbitrary loadings, in *Boundary Elements VII* , C. A. Brebbia (Ed.), Springer-Verlag, Berlin, 4-3–4-16, 1985.

[127] Taylor, R. L. and Simo, J. C., Bending and membrane elements for analysis of thick and thin shells, *Proceeding of the NUMEETA 1985 Conference*, Swansea, January 7-11, 1985.

[128] Telles, J. C. F., A self-adaptive coordinate transformation for efficient numerical evaluation of general boundary element integrals, *International Journal for Numerical Methods in Engineering*, **24**, 959-973, 1987.

[129] Timoshenko, S. and Goodier, J. N., *Theory of Elasticity*, 3rd edition, McGraw-Hill International Editions, Singapore, 1970.

[130] Timoshenko, S. P. and Woinowsky-Krieger, S., *Theory of Plates and Shells*, 2nd edition, McGraw-Hill International Editions, Singapore, 1959.

[131] Tosaka, N. and Miyake, S., A boundary integral equation formulation for elastic shallow shell bending problems, in *Boundary Elements*, C. A. Brebbia, T. Futagami and M. Tanaka (Eds.), Springer Verlag, Berlin, 527-538, 1983.

[132] Tottenham, H., The boundary element method for plates and shells, in *Developments in Boundary Element Methods - 1*, P. K. Banarjee and R. Butterfield (Eds.) , Applied Science, London, 173-205, 1979.

[133] Valliapan, S. and Murti, V., Automatic remeshing technique in quasi static and dynamic crack propagation, in *Proceeding of NUMETA'85 Conference*, Swansea, 107-116, 1985.

[134] Vander Weeën, F., Application of the boundary integral equation method to Reissner's plate model, *International Journal for Numerical Methods in Engineering*, **18**, 1-10, 1982.

[135] Vander Weeën, F., Application of the direct boundary element method to Reissner's plate model, in *Boundary Element Methods in Engineering*, C. A. Brebbia, (Ed.), Springer-Verlag, Berlin, 1982.

[136] Viz, M. J. *et al.*, Computation of membrane and bending stress intensity factors for thin, cracked plates, *International Journal of Fracture*, **72**, 21-38, 1995.

[137] Viz, M. J., Zehnder, A. T., and Bamford, J. D., Fatigue fracture of thin plates under tensile and transverse shear stress, *Fracture Mechanics: 26th Volume, ASTM STP 1256*, Reuter, W. G., Underwood, J. H., and Newman Jr, J. C., (Eds.), American Society for Testing and Materials, Philadelphia, 631-651, 1995.

[138] Vlasov, V. Z., *General Theory of Shells and Its Applications in Engineering*, National Technical Information Services, U.S. Department of Commerce, 1964.

[139] Wearing, J. L. and Ahmadi-Brooghani, S. Y., Fracture analysis of plate bending problems using boundary element method, in *Plate Bending Analysis with Boundary Elements*, *Advanced in Boundary Element Series*, M. H. Aliabadi (Ed.), Computational Mechanics Publications, Southampton, 1998.

[140] Wen, P. H., Aliabadi, M. H. and Young, A., Plane stress and plate bending coupling in BEM analysis of shallow shells, *International Journal for Numerical Methods in Engineering*, **48**, 1107-1125, 2000.

[141] Westphal, T. Jr. and Barcellos, C. A., Application of the boundary element method to Reissner's and Mindlin's plate model, in *Boundary Elements XII*, M. Tanaka, C. A. Brebbia and T. Honna (Eds.), Computational Mechanics Publication, **1**, 467-477, 1990.

[142] Widagdo, D., *Crack Growth Prediction of Multiple Site Damage Problems using Compounding Method* (in bahasa Indonesia), Undergraduate final project (unpublished), Aeronautical Engineering Study Programme, Mechanical Engineering Department, Institut Teknologi Bandung, Indonesia, 1995.

[143] Wilde, A. J. and Aliabadi, M. H., Direct evaluation of boundary stresses in the 3-D BEM of elastostatics, *Communication in Numerical Methods in Engineering*, **14**, 505-517, 1998.

[144] Zhang, J. D. and Atluri, S. N., A boundary/ interior element method for quasi static and transient response analysis of shallow shells, *Computer and Structures*, **24**, 213-223, 1986.

[145] Zhang, J. D. and Atluri, S. N., Nonlinear quasi-static and transient response analysis of shallow shells: formulation and interior/ boundary element algorithms, in *Boundary Elements*, Du Qinghua (Ed.), Pergamon Press, Oxford, 87-109, 1986.

[146] Zienkiewicz, O. C. and Taylor, R., *The Finite Element Method, Vol 1: Basic Formulation and Linear Problems,* 4^{th} edition, McGraw-Hill Publishing Company, London, 1994.

[147] Zienkiewicz, O. C. and Taylor, R., *The Finite Element Method, Vol 2: Non Linear Problems,* 4^{th} edition, McGraw-Hill Publishing Company, London, 1991.

[148] Zingoni, A., *Shell Structures in Civil and Mechanical Engineering,* Thomas Telford Publishing, London, 1997.

Appendix A

Evaluation of Modified Bessel Functions

$I_{\pm v}(z)$, the v^{th} order modified Bessel function of the first kind, and $K_v(z)$ the v^{th} order modified Bessel function of the second kind, are the solution of differential equation:

$$z^2\frac{d^2w}{dz^2} + z\frac{dw}{dz} - \left(z^2 + v^2\right)w = 0$$

$I_v(z)$ is bounded as $z \to 0$ in any range of arg z. The function $K_v(z)$ tends to zero as $|z| \to \infty$ in the sector $|\arg z| < \frac{\pi}{2}$. The functions $I_v(z)$ and $K_v(z)$ are real and positive when $v > -1$ and $z > 0$. Polynomial approximations of the functions $I_0(z)$, $I_1(z)$, and $K_0(z)$ and $K_1(z)$ can be found in Abramowitz & Stengun [4], and are given in the following sections.

A.1 Polynomial Approximations of $I_0(x)$

The polynomial approximations of the zeroth order modified Bessel function of the first kind $I_0(x)$ are:

for $-3.75 \leqslant x \leqslant 3.75$

$$I_0(x) = 1 + 3.5156229\left(\frac{x}{3.75}\right)^2 + 3.0899424\left(\frac{x}{3.75}\right)^4$$

$$+1.2067492\left(\frac{x}{3.75}\right)^6+0.2659732\left(\frac{x}{3.75}\right)^8+0.0360768\left(\frac{x}{3.75}\right)^{10}$$
$$+0.0045813\left(\frac{x}{3.75}\right)^{12}+\epsilon_1 \tag{A.1}$$

where

$$|\epsilon_1|<1.6\times10^{-7} \tag{A.2}$$

and for $3.75\leqslant x\leqslant\infty$

$$\begin{aligned} e^{-x}\sqrt{x}I_0(x) &= 0.39894228+0.01328592\left(\frac{3.75}{x}\right)+0.00225319\left(\frac{3.75}{x}\right)^2 \\ &\quad -0.00157565\left(\frac{3.75}{x}\right)^3+0.00916281\left(\frac{3.75}{x}\right)^4 \\ &\quad -0.02057706\left(\frac{3.75}{x}\right)^5+0.02635537\left(\frac{3.75}{x}\right)^6 \\ &\quad -0.01647633\left(\frac{3.75}{x}\right)^7+0.00392377\left(\frac{3.75}{x}\right)^8+\epsilon_2 \end{aligned} \tag{A.3}$$

where

$$|\epsilon_2|<1.9\times10^{-7} \tag{A.4}$$

A.2 Polynomial Approximations of $I_1(x)$

The polynomial approximations of the first order modified Bessel function of the first kind $I_1(x)$ are:

for $-3.75\leqslant x\leqslant3.75$

$$\begin{aligned} x^{-1}I_1(x) &= 0.5+0.87890594\left(\frac{x}{3.75}\right)^2+0.51498869\left(\frac{x}{3.75}\right)^4 \\ &\quad +15084934\left(\frac{x}{3.75}\right)^6+02658733\left(\frac{x}{3.75}\right)^8+0.00301532\left(\frac{x}{3.75}\right)^{10} \\ &\quad +0.00032411\left(\frac{x}{3.75}\right)^{12}+\epsilon_3 \end{aligned} \tag{A.5}$$

where

$$|\epsilon_3| < 8 \times 10^{-9} \tag{A.6}$$

and for $3.75 \leqslant x \leqslant \infty$

$$\begin{aligned} e^{-x}\sqrt{x}I_1(x) &= 0.39894228 - 0.03988024\left(\frac{3.75}{x}\right) - 0.00362018\left(\frac{3.75}{x}\right)^2 \\ &+0.00163801\left(\frac{3.75}{x}\right)^3 - 0.01031555\left(\frac{3.75}{x}\right)^4 \\ &+0.02282967\left(\frac{3.75}{x}\right)^5 - 0.02895312\left(\frac{3.75}{x}\right)^6 \\ &+0.01787654\left(\frac{3.75}{x}\right)^7 - 0.00420059\left(\frac{3.75}{x}\right)^8 + \epsilon_4 \end{aligned} \tag{A.7}$$

where

$$|\epsilon_4| < 2.2 \times 10^{-7} \tag{A.8}$$

A.3 Polynomial Approximations of $K_0(x)$

The polynomial approximations of the zeroth order modified Bessel function of the second kind $K_0(x)$ are:

for $0 < x \leqslant 2$

$$\begin{aligned} K_0(x) &= -\ln\left(\frac{x}{2}\right) I_0(x) - 0.57721566 + 0.42278420\left(\frac{x}{2}\right)^2 \\ &+0.23069756\left(\frac{x}{2}\right)^4 + 0.03488590\left(\frac{x}{2}\right)^6 + 0.00262698\left(\frac{x}{2}\right)^8 \\ &+0.00010750\left(\frac{x}{2}\right)^{10} + 0.00000740\left(\frac{x}{2}\right)^{12} + \epsilon_5 \end{aligned} \tag{A.9}$$

where

$$|\epsilon_5| < 1 \times 10^{-8} \tag{A.10}$$

and for $2 \leqslant x \leqslant \infty$

$$e^x\sqrt{x}K_0(x) = 1.25331414 - 0.07832358\left(\frac{2}{x}\right) + 0.02189568\left(\frac{2}{x}\right)^2 - 0.01062446\left(\frac{2}{x}\right)^3 + 0.00587872\left(\frac{2}{x}\right)^4 - 0.00251540\left(\frac{2}{x}\right)^5 + 0.00053208\left(\frac{2}{x}\right)^6 + \epsilon_6 \quad \text{(A.11)}$$

where

$$|\epsilon_6| < 1.9 \times 10^{-7} \quad \text{(A.12)}$$

A.4 Polynomial Approximations of $K_1(x)$

The polynomial approximations of the first order modified Bessel function of the second kind $K_1(x)$ are:

for $0 < x \leqslant 2$

$$xK_1(x) = x\ln\left(\frac{x}{2}\right)I_1(x) + 1 + 0.15443144\left(\frac{x}{2}\right)^2 - 0.67278579\left(\frac{x}{2}\right)^4 - 0.18156897\left(\frac{x}{2}\right)^6 - 0.01919402\left(\frac{x}{2}\right)^8 - 0.00110404\left(\frac{x}{2}\right)^{10} - 0.00004686\left(\frac{x}{2}\right)^{12} + \epsilon_7 \quad \text{(A.13)}$$

where

$$|\epsilon_7| < 8 \times 10^{-9} \quad \text{(A.14)}$$

and for $2 \leqslant x \leqslant \infty$

$$e^x\sqrt{x}K_1(x) = 1.25331414 + 0.23498619\left(\frac{2}{x}\right) - 0.03655620\left(\frac{2}{x}\right)^2 + 0.01504268\left(\frac{2}{x}\right)^3 - 0.00780353\left(\frac{2}{x}\right)^4 + 0.00325614\left(\frac{2}{x}\right)^5$$

$$-0.00068245\left(\frac{2}{x}\right)^6 + \epsilon_8 \tag{A.15}$$

where

$$|\epsilon_8| < 2.2 \times 10^{-7} \tag{A.16}$$

Appendix B

The Limits and Jump Terms of the Integral Equations for Shallow Shells

From Figure 3-4 shown in chapter 3, the following relationships can be obtained:

$$r = \varepsilon; \qquad r_{,n} = 1; \qquad d\Gamma = \varepsilon d\varphi; \tag{B.1}$$

$$r_{,1} = n_1 = \cos\varphi; \qquad r_{,2} = n_2 = \sin\varphi; \tag{B.2}$$

$$\int_{\Gamma_\varepsilon^*} \cdots d\Gamma = \int_0^\pi \cdots \varepsilon d\varphi \tag{B.3}$$

and

$$\begin{aligned} &\lim_{\varepsilon\to 0} A(\lambda\varepsilon) = \frac{-1}{2}; \\ &\lim_{\varepsilon\to 0} \lambda^2\varepsilon^2 K_0(\lambda\varepsilon) = 0; \\ &\lim_{\varepsilon\to 0} \lambda\varepsilon K_1(\lambda\varepsilon) = 1; \\ &\lim_{\varepsilon\to 0} \lambda^2\varepsilon^2 B(\lambda\varepsilon) = 0 \end{aligned} \tag{B.4}$$

B.1 The Displacement Integral Equations

Equation (3.54) can be written in the following form:

$$w_i\left(\mathbf{x}'\right) + I_1^* = I_2^* - I_3^* + I_4^* - I_5^* + I_6^* \tag{B.5}$$

The boundary values of w_i are assumed to satisfy Hölder continuity. The boundary integrals I_2^* and I_3^* contain weakly singular kernels and the integrals I_4^*, I_5^* and I_6^* are domain integrals which also contain weakly singular kernels, and these integrals will lead to no jump terms and they exist in the limit in normal sense.

The integral I_1^* contains P_{ij}^* which has a strong singularity of $O(1/r)$, therefore one term of the Taylor series expansion for the integrand is appropriate. Hence, the integral I_1^* can be written as follows:

$$\begin{aligned} I_1^* &= \lim_{\varepsilon\to 0}\int_{\Gamma-\Gamma_\varepsilon+\Gamma_\varepsilon^*} P_{ij}^*(\mathbf{x}',\mathbf{x}) w_j\left(\mathbf{x}\right) d\Gamma\left(\mathbf{x}\right) \\ &= \lim_{\varepsilon\to 0}\int_{\Gamma-\Gamma_\varepsilon} P_{ij}^*(\mathbf{x}',\mathbf{x}) w_j(\mathbf{x}) d\Gamma(\mathbf{x}) + \lim_{\varepsilon\to 0}\int_{\Gamma_\varepsilon^*} P_{ij}^*(\mathbf{x}',\mathbf{x})[w_j(\mathbf{x}) - w_j(\mathbf{x}')] d\Gamma(\mathbf{x}) \\ &\quad + w_j(\mathbf{x}')\lim_{\varepsilon\to 0}\int_{\Gamma_\varepsilon^*} P_{ij}^*(\mathbf{x}',\mathbf{x}) d\Gamma(\mathbf{x}) \end{aligned} \tag{B.6}$$

where Γ_ε^* is the boundary a semi-circular domain around the point $\mathbf{x}'$, Γ_ε is the original boundary which is replaced by Γ_ε^*, and Γ is the rest of the boundary, as shown in Figure 3-4.

In the above integrals, the second term on the right hand side (RHS) is zero in the limit as $\varepsilon \to 0$. The first term on the RHS forms a Cauchy principal value integral. By considering the relationships in equations (B.1 – B.3) and the limits in equation (B.4), the last term on the RHS leads to the following jump term:

$$w_j(\mathbf{x}')\lim_{\varepsilon\to 0}\int_{\Gamma_\varepsilon^*} P_{ij}^*(\mathbf{x}',\mathbf{x}) d\Gamma(\mathbf{x}) = -\frac{1}{2}\delta_{ij} w_j(\mathbf{x}') \tag{B.7}$$

Equation (3.55) can be written in the following form:

$$u_\theta\left(\mathbf{x}'\right) + I_7^* + I_8^* = I_9^* + I_{10}^* \tag{B.8}$$

The boundary values of u_θ are assumed to satisfy Hölder continuity. The integral

I_9^* contains weakly singular kernels and the integrals I_8^* and I_{10}^* are domain integrals which also contain weakly singular kernels. These integrals will lead to no jump term and they exist in the limit in normal sense.

The integral I_7^* contains $T_{\theta\alpha}^{(i)*}$ which has a strong singularity of $O(1/r)$, therefore one term of the Taylor series expansion for the integrand is appropriate. Hence, the integral I_1^* can be written as follows:

$$\begin{aligned} I_7^* &= \lim_{\varepsilon\to 0}\int_{\Gamma-\Gamma_\varepsilon+\Gamma_\varepsilon^*} T_{\theta\alpha}^{(i)*}\left(\mathbf{x}',\mathbf{x}\right) u_\alpha\left(\mathbf{x}\right) d\Gamma\left(\mathbf{x}\right) \\ &= \lim_{\varepsilon\to 0}\int_{\Gamma-\Gamma_\varepsilon} T_{\theta\alpha}^{(i)*}\left(\mathbf{x}',\mathbf{x}\right) u_\alpha\left(\mathbf{x}\right) d\Gamma(\mathbf{x}) \\ &\quad + \lim_{\varepsilon\to 0}\int_{\Gamma_\varepsilon^*} T_{\theta\alpha}^{(i)*}\left(\mathbf{x}',\mathbf{x}\right)\left[u_\alpha(\mathbf{x})-u_\alpha(\mathbf{x}')\right] d\Gamma(\mathbf{x}) \\ &\quad + u_\alpha(\mathbf{x}')\lim_{\varepsilon\to 0}\int_{\Gamma_\varepsilon^*} T_{\theta\alpha}^{(i)*}\left(\mathbf{x}',\mathbf{x}\right) d\Gamma(\mathbf{x}) \end{aligned} \tag{B.9}$$

The second term on the RHS in equation (B.9) is zero in the limit as $\varepsilon \to 0$. The first term on the RHS forms a Cauchy principal value integral. Again, by considering the relationships in equations (B.1 – B.3), the jump term appear from the last term on the RHS as follows:

$$u_\alpha(\mathbf{x}')\lim_{\varepsilon\to 0}\int_{\Gamma_\varepsilon^*} T_{\theta\alpha}^{(i)*}(\mathbf{x}',\mathbf{x})d\Gamma(\mathbf{x}) = -\frac{1}{2}\delta_{\theta\alpha}u_\alpha(\mathbf{x}') \tag{B.10}$$

B.2 The Bending Stress Resultant Integral Equations

Equation (4.1) can be written in the following form:

$$M_{\alpha\beta}\left(\mathbf{x}'\right) + I_{11}^* + I_{12}^* = I_{13}^* + I_{14}^* + I_{15}^* \tag{B.11}$$

The boundary values of w_i are assumed to be $C^{1,\alpha}$, $(0 < \alpha < 1)$ to allow for the Taylor series expansion for the integrands up to two terms. In the following, each of the integrals in equation (B.11) will be expanded and considered individually.

The integral I_{11}^*

The integral I_{11}^* can be written as:

$$\begin{aligned} I_{11}^* &= \lim_{\varepsilon\to 0}\int_{\Gamma-\Gamma_\varepsilon+\Gamma_\varepsilon^*} P^*_{\alpha\beta\gamma}(\mathbf{x}',\mathbf{x})w_\gamma(\mathbf{x})d\Gamma(\mathbf{x}) = \lim_{\varepsilon\to 0}\int_{\Gamma-\Gamma_\varepsilon} P^*_{\alpha\beta\gamma}(\mathbf{x}',\mathbf{x})w_\gamma(\mathbf{x})d\Gamma(\mathbf{x}) \\ &+ \lim_{\varepsilon\to 0}\int_{\Gamma_\varepsilon^*} P^*_{\alpha\beta\gamma}(\mathbf{x}',\mathbf{x})[w_\gamma(\mathbf{x}) - w_\gamma(\mathbf{x}') - w_{\gamma,\theta}(\mathbf{x}')(x_\theta(\mathbf{x}) - x_\theta(\mathbf{x}'))]d\Gamma(\mathbf{x}) \\ &+ w_\gamma(\mathbf{x}')\lim_{\varepsilon\to 0}\int_{\Gamma_\varepsilon^*} P^*_{\alpha\beta\gamma}(\mathbf{x}',\mathbf{x})d\Gamma(\mathbf{x}) \\ &+ w_{\gamma,\theta}(\mathbf{x}')\lim_{\varepsilon\to 0}\int_{\Gamma_\varepsilon^*} P^*_{\alpha\beta\gamma}(\mathbf{x}',\mathbf{x})(x_\theta(\mathbf{x}) - x_\theta(\mathbf{x}'))d\Gamma(\mathbf{x}) \end{aligned} \tag{B.12}$$

It has to be noted that the integral I_{11}^* contains the kernel $P^*_{\alpha\beta\gamma}$ which is hyper-singular of $O\left(\frac{1}{r^2} + \ln r\right)$, therefore two terms of the Taylor series expansion for the integrand are appropriate.

In the above integrals, the second term of the RHS is zero in the limit as $\varepsilon \to 0$. The first and third RHS terms together form a Hadamard principal value integral [57]. Detail explanation of limiting processes for Hadamard principal value integral and its application to BEM can be found in Portela [99] and Mi [82]. By considering the relationships in equations (B.1 – B.3) and the limits in equation (B.4), the last term on the RHS leads to the following jump terms:

$$\begin{aligned} & w_{\gamma,\theta}(\mathbf{x}')\lim_{\varepsilon\to 0}\int_{\Gamma_\varepsilon^*} P^*_{\alpha\beta\gamma}(\mathbf{x}',\mathbf{x})(x_\theta(\mathbf{x}) - x_\theta(\mathbf{x}'))d\Gamma(\mathbf{x}) \\ = \; & -\frac{D(1+\nu)(1-\nu)}{16}(w_{\beta,\alpha}(\mathbf{x}') + w_{\alpha,\beta}(\mathbf{x}') + w_{\gamma,\gamma}(\mathbf{x}')\delta_{\alpha\beta}) \end{aligned} \tag{B.13}$$

Now, the integral I_{11}^* can be written as follow:

$$\begin{aligned} I_{11}^* &= \; \fint_\Gamma P^*_{\alpha\beta\gamma}(\mathbf{x}',\mathbf{x})w_\gamma(\mathbf{x})d\Gamma(\mathbf{x}) \\ &- \; \frac{D(1+\nu)(1-\nu)}{16}(w_{\beta,\alpha}(\mathbf{x}') + w_{\alpha,\beta}(\mathbf{x}') + w_{\gamma,\gamma}(\mathbf{x}')\delta_{\alpha\beta}) \end{aligned} \tag{B.14}$$

where $\fint$ denotes the Hadamard principal value integral.

The integral I_{12}^*

The integral I_{12}^* can be treated in a similar way as that of the integral I_{11}^*, but as the kernel $P_{\alpha\beta 3}^*$ contains a strong singularity of $O(1/r)$ then only one term of the Taylor series expansion is needed for I_{12}^*. So that the integral I_{12}^* can be written as follows:

$$\begin{aligned} I_{12}^* &= \lim_{\varepsilon\to 0}\int_{\Gamma-\Gamma_\varepsilon+\Gamma_\varepsilon^*} P_{\alpha\beta 3}^*(\mathbf{x}',\mathbf{x})w_3(\mathbf{x})d\Gamma(\mathbf{x}) \\ &= \lim_{\varepsilon\to 0}\int_{\Gamma-\Gamma_\varepsilon} P_{\alpha\beta 3}^*(\mathbf{x}',\mathbf{x})w_3(\mathbf{x})d\Gamma(\mathbf{x}) + \lim_{\varepsilon\to 0}\int_{\Gamma_\varepsilon^*} P_{\alpha\beta 3}^*(\mathbf{x}',\mathbf{x})[w_3(\mathbf{x})-w_3(\mathbf{x}')]d\Gamma(\mathbf{x}) \\ &+ w_3(\mathbf{x}')\lim_{\varepsilon\to 0}\int_{\Gamma_\varepsilon^*} P_{\alpha\beta 3}^*(\mathbf{x}',\mathbf{x})d\Gamma(\mathbf{x}) \end{aligned} \tag{B.15}$$

In the above integrals, the second term on the RHS is zero in the limit as $\varepsilon \to 0$. The first term on the RHS forms a Cauchy principal value integral. By considering the relationships in equations (B.1 – B.3) and the limits in (B.4), the jump terms that appear from the last term on the RHS vanish. So that the integral I_{12}^* can be written as follows:

$$I_{12}^* = \oint_\Gamma P_{\alpha\beta 3}^*(\mathbf{x}',\mathbf{x})w_3(\mathbf{x})d\Gamma(\mathbf{x}) \tag{B.16}$$

The integral I_{13}^*

The integral I_{13}^* contains $W_{\alpha\beta\gamma}^*$ which is strongly singular of $O(1/r)$. Using the first term of the Taylor series expansion of $M_{\gamma\theta}$ the following form can be written:

$$\begin{aligned} I_{13}^* &= \lim_{\varepsilon\to 0}\int_{\Gamma-\Gamma_\varepsilon+\Gamma_\varepsilon^*} W_{\alpha\beta\gamma}^*(\mathbf{x}',\mathbf{x})p_\gamma(\mathbf{x})d\Gamma(\mathbf{x}) = \lim_{\varepsilon\to 0}\int_{\Gamma-\Gamma_\varepsilon} W_{\alpha\beta\gamma}^*(\mathbf{x}',\mathbf{x})p_\gamma(\mathbf{x})d\Gamma(\mathbf{x}) + \\ &+ \lim_{\varepsilon\to 0}\int_{\Gamma_\varepsilon^*} W_{\alpha\beta\gamma}^*(\mathbf{x}',\mathbf{x})n_\theta(\mathbf{x})[M_{\gamma\theta}(\mathbf{x})-M_{\gamma\theta}(\mathbf{x}')]d\Gamma(\mathbf{x}) + \\ &+ M_{\gamma\theta}(\mathbf{x}')\lim_{\varepsilon\to 0}\int_{\Gamma_\varepsilon^*} W_{\alpha\beta\gamma}^*(\mathbf{x}',\mathbf{x})n_\theta(\mathbf{x})d\Gamma(\mathbf{x}) \end{aligned} \tag{B.17}$$

In the above integrals, the second term on the RHS is zero in the limit as $\varepsilon \to 0$. The first term on the RHS forms a Cauchy principal value integral. Considering the relationships in equations (B.1 – B.3) and the limits in (B.4), the last term on the

RHS leads to the following jump terms:

$$M_{\gamma\theta}(\mathbf{x}')\lim_{\varepsilon\to 0}\int_{\Gamma_\varepsilon^*} W^*_{\alpha\beta\gamma}(\mathbf{x}',\mathbf{x})n_\theta(\mathbf{x})d\Gamma(\mathbf{x})$$
$$= \left(\frac{(3\nu-1)}{16}M_{\gamma\gamma}(\mathbf{x}')\delta_{\alpha\beta} - \frac{2(\nu-3)}{16}M_{\alpha\beta}(\mathbf{x}')\right) \tag{B.18}$$

Now, the integral I^*_{13} can be written as follows:

$$\begin{aligned} I^*_{13} &= \oint_\Gamma W^*_{\alpha\beta\gamma}(\mathbf{x}',\mathbf{x})p_\gamma(\mathbf{x})d\Gamma(\mathbf{x}) \\ &+ \left(\frac{(3\nu-1)}{16}M_{\gamma\gamma}(\mathbf{x}')\delta_{\alpha\beta} - \frac{2(\nu-3)}{16}M_{\alpha\beta}(\mathbf{x}')\right) \end{aligned} \tag{B.19}$$

The integral I^*_{14}

This integral contains $W^*_{\alpha\beta 3}$ which is a weakly singular kernel. This integral will lead to no jump term and it exists in the limit in normal sense, so that the integral I^*_{14} can be directly written as follows:

$$I^*_{14} = \int_\Gamma W^*_{\alpha\beta 3}(\mathbf{x}',\mathbf{x})p_3(\mathbf{x})d\Gamma(\mathbf{x}) \tag{B.20}$$

The integral I^*_{15}

This integral is domain integral which contains a weakly singular kernel, therefore this integral will lead to no jump term and it exists in the limit in normal sense, so that the integral I^*_{15} can be directly written as follows:

$$I^*_{15} = \int_\Omega W^*_{\alpha\beta 3}(\mathbf{X}',\mathbf{X})q^*_3 d\Omega(\mathbf{X}) \tag{B.21}$$

Substituting from equations (B.14), (B.16), (B.19), (B.20), and (B.21) into equation (B.11), and using equation (2.44), gives:

$$\frac{1}{2}M_{\alpha\beta}(\mathbf{x}') + \oint_\Gamma P^*_{\alpha\beta\gamma}(\mathbf{x}',\mathbf{x})u_\gamma(\mathbf{x})d\Gamma(\mathbf{x}) + \oint_\Gamma P^*_{\alpha\beta 3}(\mathbf{x}',\mathbf{x})u_3(\mathbf{x})d\Gamma(\mathbf{x})$$
$$= \oint_\Gamma W^*_{\alpha\beta\gamma}(\mathbf{x}',\mathbf{x})p_\gamma(\mathbf{x})d\Gamma(\mathbf{x}) + \int_\Gamma W^*_{\alpha\beta 3}(\mathbf{x}',\mathbf{x})p_3(\mathbf{x})d\Gamma(\mathbf{x})$$

$$+\int_{\Omega} W^*_{\alpha\beta 3}(\mathbf{x}',\mathbf{X})q^*_3 d\Omega(\mathbf{X}) \tag{4.4}$$

which is the bending stress resultant boundary integral equation.

B.3 The Shear Stress Resultant Integral Equation

Equation (4.2) can be written in the following form:

$$Q_\beta(\mathbf{x}') + I^*_{16} + I^*_{17} = I^*_{18} + I^*_{19} + I^*_{20} \tag{B.22}$$

In the following, each of the integrals I^*_{16} to I^*_{20} will be considered individually.

The integral I^*_{16}

This integral contains $P^*_{3\beta\gamma}$ which is strongly singular. Using the first term of the Taylor series expansion of w_γ the following form can be written:

$$\begin{aligned} I^*_{16} &= \lim_{\varepsilon\to 0}\int_{\Gamma-\Gamma_\varepsilon+\Gamma^*_\varepsilon} P^*_{3\beta\gamma}(\mathbf{x}',\mathbf{x})w_\gamma(\mathbf{x})d\Gamma(\mathbf{x}) = \lim_{\varepsilon\to 0}\int_{\Gamma-\Gamma_\varepsilon} P^*_{3\beta\gamma}(\mathbf{x}',\mathbf{x})w_\gamma(\mathbf{x})d\Gamma(\mathbf{x}) \\ &+ \lim_{\varepsilon\to 0}\int_{\Gamma^*_\varepsilon} P^*_{3\beta\gamma}(\mathbf{x}',\mathbf{x})[w_\gamma(\mathbf{x}) - w_\gamma(\mathbf{x}')]d\Gamma(\mathbf{x}) \\ &+ w_\gamma(\mathbf{x}')\lim_{\varepsilon\to 0}\int_{\Gamma^*_\varepsilon} P^*_{3\beta\gamma}(\mathbf{x}',\mathbf{x})d\Gamma(\mathbf{x}) \end{aligned} \tag{B.23}$$

In the above integrals, the second term on the RHS is zero in the limit $\varepsilon \to 0$. The first term forms a Cauchy principal value integral. Considering the relationships in equations (B.1 – B.3) and the limits in (B.4), the jump terms that appear from the last term on the RHS can be written in the following form:

$$w_\gamma(\mathbf{x}')\lim_{\varepsilon\to 0}\int_{\Gamma^*_\varepsilon} P^*_{3\beta\gamma}(\mathbf{x}',\mathbf{x})d\Gamma(\mathbf{x}) = -\frac{D(1-\nu)\lambda^2}{8}w_\beta(\mathbf{x}') \tag{B.24}$$

Then the integral I^*_{16} can be written in the following form:

$$I^*_{16} = \oint_{\Gamma} P^*_{3\beta\gamma}(\mathbf{x}',\mathbf{x})w_\gamma(\mathbf{x})d\Gamma(\mathbf{x}) - \frac{D(1-\nu)\lambda^2}{8}w_\beta(\mathbf{x}') \tag{B.25}$$

The integral I_{17}^*

This integral contains $P_{3\beta 3}^*$ which is a hypersingular kernel of order $O\left(\frac{1}{r^2} \div \ln r\right)$. Using the first two terms of the Taylor series expansion of w_3 the following form can be written:

$$\begin{aligned} I_{17}^* &= \lim_{\varepsilon \to 0} \int_{\Gamma - \Gamma_\varepsilon + \Gamma_\varepsilon^*} P_{3\beta 3}^*(\mathbf{x}', \mathbf{x}) w_3(\mathbf{x}) d\Gamma(\mathbf{x}) = \lim_{\varepsilon \to 0} \int_{\Gamma - \Gamma_\varepsilon} P_{3\beta 3}^*(\mathbf{x}', \mathbf{x}) w_3(\mathbf{x}) d\Gamma(\mathbf{x}) \\ &+ \lim_{\varepsilon \to 0} \int_{\Gamma_\varepsilon^*} P_{3\beta 3}^*(\mathbf{x}', \mathbf{x}) [w_3(\mathbf{x}) - w_3(\mathbf{x}') - w_{3,\alpha}(\mathbf{x}')(x_\alpha(\mathbf{x}) - x_\alpha(\mathbf{x}'))] d\Gamma(\mathbf{x}) \\ &+ w_3(\mathbf{x}') \lim_{\varepsilon \to 0} \int_{\Gamma_\varepsilon^*} P_{3\beta 3}^*(\mathbf{x}', \mathbf{x}) d\Gamma(\mathbf{x}) \\ &+ w_{3,\alpha}(\mathbf{x}') \lim_{\varepsilon \to 0} \int_{\Gamma_\varepsilon^*} P_{3\beta 3}^*(\mathbf{x}', \mathbf{x})(x_\alpha(\mathbf{x}) - x_\alpha(\mathbf{x}')) d\Gamma(\mathbf{x}) \end{aligned} \tag{B.26}$$

In the above integrals, the second term on the RHS is zero in the limit $\varepsilon \to 0$. The first and third terms together form a Hadamard principal value integral. Considering the relationships in equations (B.1 – B.3) and the limits in (B.4), the last term on the RHS leads to the following jump terms:

$$\begin{aligned} & w_{3,\alpha}(\mathbf{x}') \lim_{\varepsilon \to 0} \int_{\Gamma_\varepsilon^*} P_{3\beta 3}^*(\mathbf{x}', \mathbf{x})(x_\alpha(\mathbf{x}) - x_\alpha(\mathbf{x}')) d\Gamma(\mathbf{x}) \\ = & -\frac{D(1-\nu)\lambda^2}{8} u_{3,\beta}(\mathbf{x}') \end{aligned} \tag{B.27}$$

Now, the integral I_{17}^* can be written as follows:

$$I_{17}^* = \neq \int_\Gamma P_{3\beta 3}^*(\mathbf{x}', \mathbf{x}) w_3(\mathbf{x}) d\Gamma(\mathbf{x}) - \frac{D(1-\nu)\lambda^2}{8} w_{3,\beta}(\mathbf{x}') \tag{B.28}$$

The integral I_{18}^*

Similarly to the integral I_{14}^*, the integral I_{18}^* contains $W_{3\beta\gamma}^*$ which is weakly singular. This integral will lead to no jump term and it exists in the limit. The integral I_{18}^* can be written directly as follows:

$$I_{18}^* = \int_\Gamma W_{3\beta\gamma}^*(\mathbf{x}', \mathbf{x}) p_\gamma(\mathbf{x}) d\Gamma(\mathbf{x}) \tag{B.29}$$

The integral I_{19}^*

This integral contains $W_{3\beta 3}^*$ which is a strongly singular kernel. Using the first term of the Taylor series expansion of Q_θ the following form can be written:

$$\begin{aligned} I_{19}^* &= \lim_{\varepsilon\to 0}\int_{\Gamma-\Gamma_\varepsilon+\Gamma_\varepsilon^*} W_{3\beta 3}^*(\mathbf{x}',\mathbf{x})p_3(\mathbf{x})d\Gamma(\mathbf{x}) = \lim_{\varepsilon\to 0}\int_{\Gamma-\Gamma_\varepsilon} W_{3\beta 3}^*(\mathbf{x}',\mathbf{x})p_3(\mathbf{x})d\Gamma(\mathbf{x}) \\ &+ \lim_{\varepsilon\to 0}\int_{\Gamma_\varepsilon^*} W_{3\beta 3}^*(\mathbf{x}',\mathbf{x})n_\theta(\mathbf{x})[Q_\theta(\mathbf{x})-Q_\theta(\mathbf{x}')]d\Gamma(\mathbf{x}) \\ &+ Q_\theta(\mathbf{x}')\lim_{\varepsilon\to 0}\int_{\Gamma_\varepsilon^*} W_{3\beta 3}^*(\mathbf{x}',\mathbf{x})n_\theta(\mathbf{x})d\Gamma(\mathbf{x}) \end{aligned} \tag{B.30}$$

In the above integrals, the second term on the RHS is zero in the limit $\varepsilon \to 0$. The first term on the RHS forms a Cauchy principal value integral. By considering the relationships in equations (B.1 – B.3) and the limits in (B.4), the jump terms that appear from the last term on the RHS can be written in the following form:

$$Q_\theta(\mathbf{x}')\lim_{\varepsilon\to 0}\int_{\Gamma_\varepsilon^*} W_{3\beta 3}^*(\mathbf{x}',\mathbf{x})n_\theta(\mathbf{x})d\Gamma(\mathbf{x}) = \frac{Q_\beta(\mathbf{x}')}{4} \tag{B.31}$$

Then the integral I_{19}^* can be written in the following form:

$$I_{19}^* = \oint_\Gamma W_{3\beta 3}^*(\mathbf{x}',\mathbf{x})p_3(\mathbf{x})d\Gamma(\mathbf{x}) + \frac{Q_\beta(\mathbf{x}')}{4} \tag{B.32}$$

The integral I_{20}^*

Same as I_{15}^*, this integral is domain integral which contains weakly singular kernel, therefore this integral will lead to no jump term and it exists in the limit in normal sense, so that the integral I_{20}^* can be written as:

$$I_{20}^* = \int_\Omega W_{3\beta 3}^*(\mathbf{X}',\mathbf{X})q_3^* d\Omega(\mathbf{X}) \tag{B.33}$$

Substituting from equations (B.25), (B.28), (B.29), (B.32), and (B.33) into equation (B.22), and using equation (2.45) gives:

$$\frac{1}{2}Q_\beta(\mathbf{x}') + \oint_\Gamma P_{3\beta\gamma}^*(\mathbf{x}',\mathbf{x})w_\gamma(\mathbf{x})d\Gamma(\mathbf{x}) + \oint_\Gamma P_{3\beta 3}^*(\mathbf{x}',\mathbf{x})w_3(\mathbf{x})d\Gamma(\mathbf{x})$$

$$= \int_\Gamma W^*_{3\beta\gamma}(\mathbf{x}', \mathbf{x}) p_\gamma(\mathbf{x}) d\Gamma(\mathbf{x}) + \oint_\Gamma W^*_{3\beta 3}(\mathbf{x}', \mathbf{x}) p_3(\mathbf{x}) d\Gamma(\mathbf{x})$$

$$+ \int_\Omega W^*_{3\beta 3}(\mathbf{x}', \mathbf{X}) q^*_3 d\Omega(\mathbf{X}) \tag{4.5}$$

which is the shear stress resultant boundary integral equation.

B.4 The Membrane Stress Resultant Integral Equations

Equation (4.3) can be written in the following form:

$$N_{\alpha\beta}(\mathbf{x}') + I^*_{21} = I^*_{22} - I^*_{23} + I^*_{24} + B\left[(1-\nu)k_{\alpha\beta} + \nu\delta_{\alpha\beta}k_{\phi\phi}\right] w_3(\mathbf{x}') \tag{B.34}$$

The boundary values of u_i are assumed to be $C^{1,\alpha}$, $(0 < \alpha < 1)$ to allow for the Taylor series expansion for the integrands up to two terms. In the following, each of the integrals in equation (B.34) will be expanded and considered individually.

The integral I^*_{21}

This integral contains $T^*_{\alpha\beta\gamma}$ which is a hypersingular kernel of order $O(1/r^2)$. Using the first two terms of the Taylor series expansion of u_γ the following form can be written:

$$\begin{aligned}
I^*_{21} &= \lim_{\varepsilon\to 0} \int_{\Gamma-\Gamma_\varepsilon+\Gamma^*_\varepsilon} T^*_{\alpha\beta\gamma}(\mathbf{x}', \mathbf{x}) u_\gamma(\mathbf{x}) d\Gamma(\mathbf{x}) = \lim_{\varepsilon\to 0} \int_{\Gamma-\Gamma_\varepsilon} T^*_{\alpha\beta\gamma}(\mathbf{x}', \mathbf{x}) u_\gamma(\mathbf{x}) d\Gamma(\mathbf{x}) \\
&+ \lim_{\varepsilon\to 0} \int_{\Gamma^*_\varepsilon} T^*_{\alpha\beta\gamma}(\mathbf{x}', \mathbf{x}) [u_\gamma(\mathbf{x}) - u_\gamma(\mathbf{x}') - u_{\gamma,\theta}(\mathbf{x}')(x_\theta(\mathbf{x}) - x_\theta(\mathbf{x}'))] d\Gamma(\mathbf{x}) \\
&+ u_\gamma(\mathbf{x}') \lim_{\varepsilon\to 0} \int_{\Gamma^*_\varepsilon} T^*_{\alpha\beta\gamma}(\mathbf{x}', \mathbf{x}) d\Gamma(\mathbf{x}) \\
&+ u_{\gamma,\theta}(\mathbf{x}') \lim_{\varepsilon\to 0} \int_{\Gamma^*_\varepsilon} T^*_{\alpha\beta\gamma}(\mathbf{x}', \mathbf{x}) (x_\theta(\mathbf{x}) - x_\theta(\mathbf{x}')) d\Gamma(\mathbf{x})
\end{aligned} \tag{B.35}$$

In the above integrals, the second term on the RHS is zero in the limit $\varepsilon \to 0$. The first and third terms together form a Hadamard principal value integral. Considering the relationships in equations (B.1 – B.3), the last term on the RHS leads to the following jump terms:

$$u_{\gamma,\theta}(\mathbf{x}') \lim_{\varepsilon\to 0} \int_{\Gamma^*_\varepsilon} T^*_{\alpha\beta\gamma}(\mathbf{x}', \mathbf{x}) (x_\theta(\mathbf{x}) - x_\theta(\mathbf{x}')) d\Gamma(\mathbf{x})$$

$$= \frac{B(1+\nu)(1-\nu)}{16}(u_{\beta,\alpha}(\mathbf{x}') + u_{\alpha,\beta}(\mathbf{x}') + u_{\gamma,\gamma}(\mathbf{x}')\delta_{\alpha\beta}) \qquad \text{(B.36)}$$

Now, the integral I_{21}^* can be written as follow:

$$\begin{aligned} I_{21}^* &= \oint_\Gamma T_{\alpha\beta\gamma}^*(\mathbf{x}', \mathbf{x}) u_\gamma(\mathbf{x}) d\Gamma(\mathbf{x}) \\ &- \frac{B(1+\nu)(1-\nu)}{16}(u_{\beta,\alpha}(\mathbf{x}') + u_{\alpha,\beta}(\mathbf{x}') + u_{\gamma,\gamma}(\mathbf{x}')\delta_{\alpha\beta}) \end{aligned} \qquad \text{(B.37)}$$

The integral I_{22}^*

The integral I_{22}^* contains $U_{\alpha\beta\gamma}^*$ which is strongly singular. Using the first term of the Taylor series expansion of $N_{\gamma\theta}$ the following form can be written:

$$\begin{aligned} I_{22}^* &= \lim_{\varepsilon\to 0} \int_{\Gamma-\Gamma_\varepsilon+\Gamma_\varepsilon^*} U_{\alpha\beta\gamma}^*(\mathbf{x}', \mathbf{x}) t_\gamma(\mathbf{x}) d\Gamma(\mathbf{x}) = \lim_{\varepsilon\to 0} \int_{\Gamma-\Gamma_\varepsilon} U_{\alpha\beta\gamma}^*(\mathbf{x}', \mathbf{x}) t_\gamma(\mathbf{x}) d\Gamma(\mathbf{x}) + \\ &+ \lim_{\varepsilon\to 0} \int_{\Gamma_\varepsilon^*} U_{\alpha\beta\gamma}^*(\mathbf{x}', \mathbf{x}) n_\theta(\mathbf{x}) [N_{\gamma\theta}(\mathbf{x}) - N_{\gamma\theta}(\mathbf{x}')] d\Gamma(\mathbf{x}) + \\ &+ N_{\gamma\theta}(\mathbf{x}') \lim_{\varepsilon\to 0} \int_{\Gamma_\varepsilon^*} U_{\alpha\beta\gamma}^*(\mathbf{x}', \mathbf{x}) n_\theta(\mathbf{x}) d\Gamma(\mathbf{x}) \end{aligned} \qquad \text{(B.38)}$$

In the above integrals, the second term on the RHS is zero in the limit as $\varepsilon \to 0$. The first term on the RHS forms a Cauchy principal value integral. Considering the relationships in equations (B.1 – B.3), the last term on the RHS leads to the following jump terms:

$$\begin{aligned} &N_{\gamma\theta}(\mathbf{x}') \lim_{\varepsilon\to 0} \int_{\Gamma_\varepsilon^*} U_{\alpha\beta\gamma}^*(\mathbf{x}', \mathbf{x}) n_\theta(\mathbf{x}) d\Gamma(\mathbf{x}) \\ &= \left(\frac{(3-\nu)}{16} \left[N_{\alpha\beta}(\mathbf{x}') + N_{\beta\alpha}(\mathbf{x}') \right] + \frac{(3\nu-1)}{16} N_{\gamma\gamma}(\mathbf{x}') \delta_{\alpha\beta} \right) \end{aligned} \qquad \text{(B.39)}$$

Now, the integral I_{22}^* can be written as follows:

$$\begin{aligned} I_{22}^* &= \oint_\Gamma U_{\alpha\beta\gamma}^*(\mathbf{x}', \mathbf{x}) t_\gamma(\mathbf{x}) d\Gamma(\mathbf{x}) \\ &+ \left(\frac{(3-\nu)}{16} \left[N_{\alpha\beta}(\mathbf{x}') + N_{\beta\alpha}(\mathbf{x}') \right] + \frac{(3\nu-1)}{16} N_{\gamma\gamma}(\mathbf{x}') \delta_{\alpha\beta} \right) \end{aligned} \qquad \text{(B.40)}$$

The integral I_{23}^*

The integral I_{23}^* contains $U_{\alpha\beta\gamma}^*$ which is strongly singular. Using the first term of the Taylor series expansion of $N_{\gamma\theta}$ the following form can be written:

$$\begin{aligned} I_{23}^* &= \lim_{\varepsilon\to 0}\int_{\Gamma-\Gamma_\varepsilon+\Gamma_\varepsilon^*} U_{\alpha\beta\gamma}^*(\mathbf{x}',\mathbf{x})B\left[k_{\alpha\gamma}\left(1-\nu\right)+\nu\delta_{\alpha\gamma}k_{\phi\phi}\right]w_3(\mathbf{x})n_\gamma(\mathbf{x})d\Gamma(\mathbf{x}) \\ &= \lim_{\varepsilon\to 0}\int_{\Gamma-\Gamma_\varepsilon} U_{\alpha\beta\gamma}^*(\mathbf{x}',\mathbf{x})B\left[k_{\alpha\gamma}\left(1-\nu\right)+\nu\delta_{\alpha\gamma}k_{\phi\phi}\right]w_3(\mathbf{x})n_\gamma(\mathbf{x})d\Gamma(\mathbf{x}) + \\ &+ \lim_{\varepsilon\to 0}\int_{\Gamma_\varepsilon^*} U_{\alpha\beta\gamma}^*(\mathbf{x}',\mathbf{x})B\left[k_{\alpha\gamma}\left(1-\nu\right)+\nu\delta_{\alpha\gamma}k_{\phi\phi}\right]n_\gamma(\mathbf{x})[w_3(\mathbf{x})-w_3(\mathbf{x}')]d\Gamma(\mathbf{x}) + \\ &+ w_3(\mathbf{x}')\lim_{\varepsilon\to 0}\int_{\Gamma_\varepsilon^*} U_{\alpha\beta\gamma}^*(\mathbf{x}',\mathbf{x})B\left[k_{\alpha\gamma}\left(1-\nu\right)+\nu\delta_{\alpha\gamma}k_{\phi\phi}\right]n_\gamma(\mathbf{x})d\Gamma(\mathbf{x}) \qquad \text{(B.41)} \end{aligned}$$

In the above integrals, the second term on the RHS is zero in the limit as $\varepsilon \to 0$. The first term on the RHS forms a Cauchy principal value integral. Considering the relationships in equations (B.1 – B.3), the last term on the RHS leads to the following jump terms:

$$\begin{aligned} & w_3(\mathbf{x}')\lim_{\varepsilon\to 0}\int_{\Gamma_\varepsilon^*} U_{\alpha\beta\gamma}^*(\mathbf{x}',\mathbf{x})B\left[k_{\alpha\gamma}\left(1-\nu\right)+\nu\delta_{\alpha\gamma}k_{\phi\phi}\right]n_\gamma(\mathbf{x})d\Gamma(\mathbf{x}) \qquad \text{(B.42)} \\ &= \left(\frac{(3-\nu)}{16}B\left[2k_{\alpha\beta}\left(1-\nu\right)+2\nu\delta_{\alpha\beta}k_{\phi\phi}\right]+\frac{(3\nu-1)}{16}B\delta_{\alpha\beta}\left(1+\nu\right)k_{\phi\phi}\right)w_3(\mathbf{x}') \end{aligned}$$

Now, the integral I_{23}^* can be written as follows:

$$\begin{aligned} I_{23}^* &= \int_\Gamma U_{\alpha\beta\gamma}^*(\mathbf{x}',\mathbf{x})B\left[k_{\alpha\gamma}\left(1-\nu\right)+\nu\delta_{\alpha\gamma}k_{\phi\phi}\right]w_3(\mathbf{x})n_\gamma(\mathbf{x})d\Gamma(\mathbf{x}) \qquad \text{(B.43)} \\ &+ \left(\frac{(3-\nu)}{16}B\left[2k_{\alpha\beta}\left(1-\nu\right)+2\nu\delta_{\alpha\beta}k_{\phi\phi}\right]+\frac{(3\nu-1)}{16}B\delta_{\alpha\beta}\left(1+\nu\right)k_{\phi\phi}\right)w_3(\mathbf{x}') \end{aligned}$$

The integral I_{24}^*

The integral I_{24}^* is domain integral which contain weakly singular kernel, therefore it will lead to no jump term and it exists in the limit in normal sense, so that the integral I_{24}^* can be directly written as follows:

$$I_{24}^* = \int_\Omega U_{\alpha\beta\gamma}^*(\mathbf{X}',\mathbf{X})q_\gamma^* d\Omega(\mathbf{X}) \qquad \text{(B.44)}$$

Substituting from equations (B.37), (B.40), (B.43), and (B.44) into equation (B.34), and using equation (2.46), gives:

$$\frac{1}{2}N_{\alpha\beta}(\mathbf{x}')+ \neq\!\!\!\!\!\!\int_{\Gamma} T^{*}_{\alpha\beta\gamma}(\mathbf{x}',\mathbf{x})u_{\gamma}(\mathbf{x})d\Gamma(\mathbf{x})$$

$$+\int_{\Gamma} U^{*}_{\alpha\beta\gamma}(\mathbf{X}',\mathbf{x})B\left[k_{\alpha\gamma}\left(1-\nu\right)+\nu\delta_{\alpha\gamma}k_{\phi\phi}\right]w_{3}(\mathbf{x})n_{\gamma}(\mathbf{x})d\Gamma(\mathbf{x})$$

$$=\neq\!\!\!\!\!\!\int_{\Gamma} U^{*}_{\alpha\beta\gamma}(\mathbf{x}',\mathbf{x})t_{\gamma}(\mathbf{x})d\Gamma(\mathbf{x})+\int_{\Omega} U^{*}_{\alpha\beta\gamma}(\mathbf{x}',\mathbf{X})q^{*}_{\gamma}d\Omega(\mathbf{X})$$

$$+\frac{1}{2}B\left[(1-\nu)k_{\alpha\beta}+\nu\delta_{\alpha\beta}k_{\phi\phi}\right]w_{3} \tag{4.6}$$

which is the membrane stress resultant boundary integral equation.

Appendix C

Treatment of Singularities

C.1 Bi-cubic Nonlinear Coordinate Transformation

This coordinate transformation was developed by Telles[128]. Consider the integral

$$I = \int_{-1}^{+1} f(\eta)\, d\eta \tag{C.1}$$

in which $f(\eta)$ is singular at a point η'. Using a third-degree non-linear transformation

$$\eta(\gamma) = a\gamma^3 + b\gamma^2 + c\gamma + d \tag{C.2}$$

such that the following requirement are met:

$$\begin{aligned} \frac{d\eta}{d\gamma}|_{\eta'} &= 0 \\ \frac{d^2\eta}{d\gamma^2}|_{\eta'} &= 0 \\ \eta(1) &= 1 \\ \eta(-1) &= -1 \end{aligned} \tag{C.3}$$

Then the following solution is obtained

$$\begin{aligned} a &= \frac{1}{Q} \\ b &= -\frac{3\gamma'}{Q} \end{aligned}$$

$$
\begin{aligned}
c &= \frac{3(\gamma')^2}{Q} \\
d &= -b \\
Q &= 1+3(\gamma')^2
\end{aligned}
\tag{C.4}
$$

where γ' is the value of γ which satisfies $\eta\left(\gamma'\right) = \eta'$; this parameter can be calculated by

$$
\gamma' = \left(\eta'\eta^* + |\eta^*|\right)^{\frac{1}{3}} + \left(\eta'\eta^* - |\eta^*|\right)^{\frac{1}{3}} + \eta' \tag{C.5}
$$

where $\eta^* = (\eta')^2 - 1$. Therefore, equation (C.1) becomes

$$
I = \int_{-1}^{+1} f\left\{\frac{(\gamma-\gamma')^3 + \gamma'\left[(\gamma')^2+3\right]}{1+3(\gamma')^2}\right\}\frac{3(\gamma-\gamma')^2}{1+3(\gamma')^2}d\gamma \tag{C.6}
$$

The above transformation can be used to calculate integral with a logaritmic singularity for any position of the singularity. Its main advantage is that since the Jacobian cancels the singularity, standard Gaussian quadrature can be employed without the need to separate the regular part from the singular term in the numerical evaluation of the integrals.

C.2 Singularity Substraction Method

C.2.1 Strongly singular integrals

In the displacement boundary integral equations, P^*_{ij} and $T^*_{\theta\alpha}$ are strongly singular of $O(1/r)$ and in the traction boundary integral equations, $P^*_{\alpha\beta 3}$, $P^*_{3\beta\gamma}$, $W^*_{\alpha\beta\gamma}$, $W^*_{3\beta 3}$ and $U^*_{\alpha\beta\gamma}$ are strongly singular. In order to solve equation (4.28), the value of $f^n_{ij}\left(\xi'\right)$ has to be expressed.

To find the value of $f^n_{ij}\left(\xi'\right)$, then consider the Taylor series expansion about the singular point ξ' in the local coordinate system, as follows:

$$
\begin{aligned}
\Phi^i(\xi) &= \Phi^i(\xi') + \Phi^{i\prime}(\xi')\delta\xi + \frac{1}{2}\Phi^{i\prime\prime}(\xi')\delta\xi^2 + \cdots \\
J(\xi) &= J(\xi') + J'(\xi')\delta\xi + \frac{1}{2}J''(\xi')\delta\xi^2 + \cdots \\
x_\alpha(\xi) &= x_\alpha(\xi') + x^{'}_\alpha(\xi')\delta\xi + \frac{1}{2}x^{''}_\alpha(\xi')\delta\xi^2 + \cdots
\end{aligned}
\tag{C.7}
$$

in which

$$x_\alpha(\xi) = \sum_{i=1}^{3} M^i(\xi) x_\alpha^i \tag{C.8}$$

where, x_α^i is the coordinate x_α at the nodal point i, M^i are the geometric shape functions. For isoparametric element used in this work, formulation for M^i is the same as the shape function for continuous element. The term $(...)'$ denotes the partial derivatives of $(...)$ with respect to ξ, i.e. $\frac{\partial}{\partial \xi}(...)$ and $\delta\xi = \xi - \xi'$. Using equation (C.7), the following expressions for quadratic elements can be written (Aliabadi *et al.* [6]):

$$\begin{aligned} r_\alpha &= x_\alpha^{'}(\xi')\delta\xi + \frac{1}{2}x_\alpha^{''}(\xi')\delta\xi^2 \\ r &= |\delta\xi| \sqrt{d_0 + d_1\delta\xi + d_2\delta\xi^2} \end{aligned} \tag{C.9}$$

where

$$\begin{aligned} d_0 &= x_\alpha^{'}(\xi')x_\alpha^{'}(\xi') \\ d_1 &= x_\alpha^{'}(\xi')x_\alpha^{''}(\xi') \\ d_2 &= \frac{1}{4}x_\alpha^{''}(\xi')x_\alpha^{''}(\xi') \end{aligned} \tag{C.10}$$

The Jacobian $J(\xi)$ can be expressed as

$$\begin{aligned} J(\xi) &= \sqrt{x_\alpha'(\xi)\, x_\alpha'(\xi)} \\ &= \sqrt{d_0 + 2d_1\delta\xi + 4d_2\delta\xi^2} \end{aligned} \tag{C.11}$$

The kernel $P^*_{\gamma\alpha}$

Substituting the kernels $P^*_{\gamma\alpha}$ in equation (3.33), then $f^{np}_{\gamma\alpha}(\xi)$ can be written as follows:

$$\begin{aligned} f^{np}_{\gamma\alpha}(\xi) &= P^*_{\gamma\alpha}(\xi', \xi)\Phi^n(\xi)J(\xi)\left(\xi - \xi'\right) \\ &= \frac{-\Phi^n(\xi)J(\xi)\left(\xi - \xi'\right)}{4\pi\,|\delta\xi|\sqrt{d_0 + d_1\delta\xi + d_2\delta\xi^2}}[(4A(z) + 2zK_1(z) + 1 - \nu)(\delta_{\alpha\gamma}r_{,n} + r_{,\alpha}n_\gamma) \\ &+ (4A(z) + 1 + \nu)r_{,\gamma}n_\alpha - 2(8A(z) + 2zK_1(z) + 1 - \nu)r_{,\alpha}r_{,\gamma}r_{,n}] \end{aligned} \tag{C.12}$$

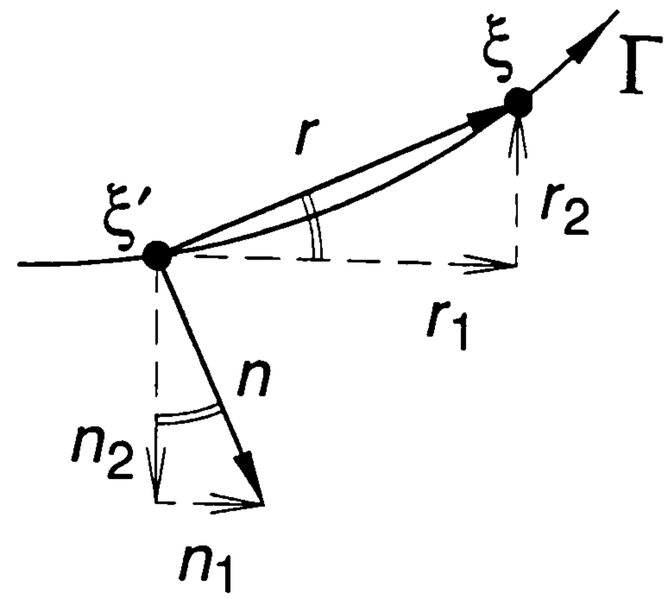

Figure C-1: Vectors r and n in a boundary element.

In the limit, as ξ approaching ξ', that is when $r \rightarrow 0$, then

$$\begin{aligned} \lim_{r\to 0} r_{,1} &= -n_2 \\ \lim_{r\to 0} r_{,2} &= n_1 \end{aligned} \tag{C.13}$$

as shown in Figure (C-1), and hence

$$\lim_{r\to 0} r_{,n} = \lim_{r\to 0} \left(r_{,1}n_1 + r_{,2}n_2\right) = 0 \tag{C.14}$$

Considering the limits in equations (B.4) and (C.14), substituting equations (C.7) and (C.11), then the value $f^{np}_{\gamma\alpha}(\xi)$ at singular point ξ' can be obtained as

$$f^{np}_{\gamma\alpha}(\xi') = -\frac{\Phi^n(\xi')}{4\pi}\left(1-\nu\right)\left(r_{,\alpha}n_\gamma - r_{,\gamma}n_\alpha\right) \tag{C.15}$$

The kernel P^*_{33}

Substituting the kernel P^*_{33} in equation (3.33), then $f^{np}_{\gamma\alpha}(\xi)$ can be written as follows:

$$\begin{aligned} f^{np}_{33}(\xi) &= P^*_{33}(\xi',\xi)\Phi^n(\xi)J(\xi)\left(\xi-\xi'\right) \\ &= \frac{-\Phi^n(\xi)J(\xi)\left(\xi-\xi'\right)}{2\pi\left|\delta\xi\right|\sqrt{d_0+d_1\delta\xi+d_2\delta\xi^2}} r_{,n} \end{aligned} \tag{C.16}$$

Considering the limit in equation (C.14) and substituting equations (C.7) and

(C.11), the value $f_{33}^{np}(\xi)$ at singular point ξ' can be obtained as

$$f_{33}^{np}(\xi') = 0 \tag{C.17}$$

The kernel $T_{\theta\alpha}^{(i)*}$

Substituting the kernels $T_{\theta\alpha}^{(i)*}$ in equation (3.52), then $f_{\theta\alpha}^{nt}(\xi)$ can be written as follows:

$$\begin{aligned} f_{\theta\alpha}^{nt}(\xi) &= T_{\theta\alpha}^{(i)*}(\xi',\xi)\Phi^n(\xi)J(\xi)\left(\xi-\xi'\right) \\ &= \frac{-\Phi^n(\xi)J(\xi)\left(\xi-\xi'\right)}{4\pi\left|\delta\xi\right|\sqrt{d_0+d_1\delta\xi+d_2\delta\xi^2}}\left\{r_{,n}\left[\left(1-\nu\right)\delta_{\theta\alpha}+2\left(1+\nu\right)r_{,\theta}r_{,\alpha}\right]\right. \\ &\quad \left.+\left(1-\nu\right)\left[n_\theta r_{,\alpha}-n_\alpha r_{,\theta}\right]\right\} \end{aligned} \tag{C.18}$$

Again, by considering the limit in equation (C.14) and substituting equations (C.7) and (C.11), the value $f_{\theta\alpha}^{nt}(\xi)$ at singular point ξ' can be obtained as

$$f_{\theta\alpha}^{nt}(\xi') = -\frac{\Phi^n(\xi')}{4\pi}\left(1-\nu\right)\left(n_\theta r_{,\alpha}-n_\alpha r_{,\theta}\right) \tag{C.19}$$

The kernel $P_{\alpha\beta3}^{*}$

Substituting the kernels $P_{\alpha\beta3}^{*}$ in equation (3.97), then $f_{\alpha\beta3}^{np}(\xi)$ can be written as follows:

$$\begin{aligned} f_{\alpha\beta3}^{np}(\xi) &= P_{\alpha\beta3}^{*}(\xi',\xi)\Phi^n(\xi)J(\xi)\left(\xi-\xi'\right) \\ &= \frac{D(1-\nu)\lambda^2\Phi^n(\xi)J(\xi)\left(\xi-\xi'\right)}{4\pi\left|\delta\xi\right|\sqrt{d_0+d_1\delta\xi+d_2\delta\xi^2}}[(2A(z)+zK_1(z))(r_{,\beta}n_\alpha+r_{,\alpha}n_\beta) \\ &\quad -2(4A(z)+zK_1(z))r_{,\alpha}r_{,\beta}r_{,n}+2A(z)\delta_{\alpha\beta}r_{,n}] \end{aligned} \tag{C.20}$$

Considering the limits in equations (B.4) and (C.14), then substituting equations (C.7) and (C.11), the value $f_{\alpha\beta3}^{np}(\xi)$ at singular point ξ' can be obtained as

$$f_{\alpha\beta3}^{np}(\xi') = 0 \tag{C.21}$$

The kernel $P^*_{3\beta\gamma}$

Substituting the kernels $P^*_{3\beta\gamma}$ in equation (3.97), then $f^{np}_{3\beta\gamma}(\xi)$ can be written as follows:

$$\begin{aligned} f^{np}_{3\beta\gamma}(\xi) &= P^*_{3\beta\gamma}(\xi',\xi)\Phi^n(\xi)J(\xi)\left(\xi-\xi'\right) \\ &= \frac{-D(1-\nu)\lambda^2\Phi^n(\xi)J(\xi)\left(\xi-\xi'\right)}{4\pi\left|\delta\xi\right|\sqrt{d_0+d_1\delta\xi+d_2\delta\xi^2}}[(2A(z)+zK_1(z))(\delta_{\gamma\beta}r_{,n}+r_{,\gamma}n_\beta) \\ &\quad +2A(z)n_\gamma r_{,\beta}-2(4A(z)+zK_1(z))r_{,\gamma}r_{,\beta}r_{,n}] \end{aligned} \tag{C.22}$$

Considering the limits in equations (B.4) and (C.14), then substituting equations (C.7) and (C.11), the value $f^{np}_{3\beta\gamma}(\xi)$ at singular point ξ' can be obtained as

$$f^{np}_{3\beta\gamma}(\xi') = \frac{D(1-\nu)\lambda^2\Phi^n(\xi')}{4\pi}n_\gamma r_{,\beta} \tag{C.23}$$

The kernel $W^*_{\alpha\beta\gamma}$

Substituting the kernels $W^*_{\alpha\beta\gamma}$ in equation (3.96), then $f^{nw}_{\alpha\beta\gamma}(\xi)$ can be written as follows:

$$\begin{aligned} f^{nw}_{\alpha\beta\gamma}(\xi) &= W^*_{\alpha\beta\gamma}(\xi',\xi)\Phi^n(\xi)J(\xi)\left(\xi-\xi'\right) \\ &= \frac{\Phi^n(\xi)J(\xi)\left(\xi-\xi'\right)}{4\pi\left|\delta\xi\right|\sqrt{d_0+d_1\delta\xi+d_2\delta\xi^2}}\times \\ &\quad [(4A(z)+2zK_1(z)+1-\nu)\left(\delta_{\beta\gamma}r_{,\alpha}+\delta_{\alpha\gamma}r_{,\beta}\right) \\ &\quad -2\left(8A(z)+2zK_1(z)+1-\nu\right)r_{,\alpha}r_{,\beta}r_{,\gamma} \\ &\quad +\left(4A(z)+1+\nu\right)\delta_{\alpha\beta}r_{,\gamma}] \end{aligned} \tag{C.24}$$

Considering the limits in equations (B.4) and (C.14), then substituting equations (C.7) and (C.11), the value $f^{nw}_{\alpha\beta\gamma}(\xi)$ at singular point ξ' can be obtained as

$$f^{nw}_{\alpha\beta\gamma}(\xi') = \frac{\Phi^n(\xi')}{4\pi}\left[(1-\nu)\left(\delta_{\beta\gamma}r_{,\alpha}+\delta_{\alpha\gamma}r_{,\beta}-\delta_{\alpha\beta}r_{,\gamma}\right)+2\left(1+\nu\right)r_{,\alpha}r_{,\beta}r_{,\gamma}\right] \tag{C.25}$$

The kernel $W^*_{3\beta 3}$

Substituting the kernels $W^*_{\alpha\beta\gamma}$ in equation (3.96), then $f^{nw}_{\alpha\beta\gamma}(\xi)$ can be written as follows:

$$\begin{aligned} f^{nw}_{3\beta 3}(\xi) &= W^*_{3\beta 3}(\xi',\xi)\Phi^n(\xi)J(\xi)\left(\xi-\xi'\right) \\ &= \frac{\Phi^n(\xi)J(\xi)\left(\xi-\xi'\right)}{2\pi\left|\delta\xi\right|\sqrt{d_0+d_1\delta\xi+d_2\delta\xi^2}}r_{,\beta} \end{aligned} \tag{C.26}$$

and by substituting equations (C.7) and (C.11), the value $f^{nw}_{\alpha\beta\gamma}(\xi)$ at singular point ξ' can be obtained as

$$f^{nw}_{3\beta 3}(\xi') = \frac{\Phi^n(\xi')}{2\pi}r_{,\beta} \tag{C.27}$$

The kernel $U^*_{\alpha\beta\gamma}$

Substituting the kernels $U^*_{\alpha\beta\gamma}$ in equation (3.99), then $f^{nu}_{\alpha\beta\gamma}(\xi)$ can be written as follows:

$$\begin{aligned} f^{nu}_{\alpha\beta\gamma}(\xi) &= U^*_{\alpha\beta\gamma}(\xi',\xi)\Phi^n(\xi)J(\xi)\left(\xi-\xi'\right) \\ &= \frac{\Phi^n(\xi)J(\xi)\left(\xi-\xi'\right)}{4\pi\left|\delta\xi\right|\sqrt{d_0+d_1\delta\xi+d_2\delta\xi^2}}\left[\left(1-\nu\right)\left(\delta_{\gamma\alpha}r_{,\beta}+\delta_{\gamma\beta}r_{,\alpha}-\delta_{\alpha\beta}r_{,\gamma}\right)\right. \\ &\quad \left.+2\left(1+\nu\right)r_{,\alpha}r_{,\beta}r_{,\gamma}\right] \end{aligned} \tag{C.28}$$

and by substituting equations (C.7) and (C.11), the value $f^{nt}_{\theta\alpha}(\xi)$ at singular point ξ' can be obtained as

$$f^{nu}_{\alpha\beta\gamma}(\xi') = \frac{\Phi^n(\xi')}{4\pi}\left[\left(1-\nu\right)\left(\delta_{\gamma\alpha}r_{,\beta}+\delta_{\gamma\beta}r_{,\alpha}-\delta_{\alpha\beta}r_{,\gamma}\right)+2\left(1+\nu\right)r_{,\alpha}r_{,\beta}r_{,\gamma}\right] \tag{C.29}$$

C.2.2 Hypersingular integrals

In traction boundary integral equations, $P^*_{\alpha\beta\gamma}$, $P^*_{3\beta 3}$, and $T^{(i)*}_{\alpha\beta\gamma}$ are hypersingular. The $T^{(i)*}_{\alpha\beta\gamma}$ is hypersingular integrals of order $O\left(\frac{1}{r^2}\right)$ and the $P^*_{\alpha\beta\gamma}$ and $P^*_{3\beta 3}$ are hypersingular integrals of order $O\left(\frac{1}{r^2}+\ln\left(r\right)\right)$.

To be able to solve equation (4.32), the value of $g^n_{\alpha\beta\gamma}(\xi)$ and $g^n_{\alpha\beta\gamma}{}'(\xi)$ have to be expressed, and to solve equation (4.35), the value of $g^n_{\alpha\beta\gamma}(\xi)$, $g^n_{\alpha\beta\gamma}{}'(\xi)$ and $h^n_{\alpha\beta\gamma}(\xi)$ also have to be expressed.

The kernel $T^{(i)*}_{\alpha\beta\gamma}$

Using Taylor series expansion about the singular point ξ' in the local coordinate system, as defined in equations (C.7 – C.9), and substituting the kernels $T^{(i)*}_{\alpha\beta\gamma}$ in equation (3.100), then $g^{nt}_{\alpha\beta\gamma}(\xi)$ can be written as follows:

$$\begin{aligned} g^{nt}_{\alpha\beta\gamma}(\xi) &= T^{(i)*}_{\alpha\beta\gamma}(\xi',\xi)\Phi^n(\xi)J(\xi)\left(\xi-\xi'\right)^2 \\ &= \frac{B\left(1-\nu\right)\Phi^n(\xi)J(\xi)\left(\xi-\xi'\right)^2}{4\pi\left|\delta\xi\right|^2\left(d_0+d_1\delta\xi+d_2\delta\xi^2\right)}\times \\ &\quad \{2r_{,n}\left[\left(1-\nu\right)\delta_{\alpha\beta}r_{,\gamma}+\nu\left(\delta_{\gamma\alpha}r_{,\beta}+\delta_{\gamma\beta}r_{,\alpha}\right)-4\left(1+\nu\right)r_{,\alpha}r_{,\beta}r_{,\gamma}\right] \\ &\quad +2\nu\left(n_\alpha r_{,\beta}r_{,\gamma}+n_\beta r_{,\alpha}r_{,\gamma}\right)+\left(1-\nu\right)\left(2n_\gamma r_{,\alpha}r_{,\beta}+n_\beta\delta_{\alpha\gamma}+n_\alpha\delta_{\beta\gamma}\right) \\ &\quad -\left(1-3\nu\right)n_\gamma\delta_{\alpha\beta}\} \end{aligned} \tag{C.30}$$

By considering the limit in equation (C.14) and substituting equations (C.7) and (C.11), the value $g^{nt}_{\alpha\beta\gamma}(\xi)$ at singular point ξ' can be obtained as

$$\begin{aligned} g^{nt}_{\alpha\beta\gamma}(\xi') &= \frac{B\left(1-\nu\right)\Phi^n(\xi')}{4\pi J(\xi')}\{2\nu\left(n_\alpha r_{,\beta}r_{,\gamma}+n_\beta r_{,\alpha}r_{,\gamma}\right) \\ &\quad +\left(1-\nu\right)\left(2n_\gamma r_{,\alpha}r_{,\beta}+n_\beta\delta_{\alpha\gamma}+n_\alpha\delta_{\beta\gamma}\right) \\ &\quad -\left(1-3\nu\right)n_\gamma\delta_{\alpha\beta}\} \end{aligned} \tag{C.31}$$

and the derivatives of $g^{nt}_{\alpha\beta\gamma}(\xi')$can be obtained as

$$\begin{aligned} g^{nt}_{\alpha\beta\gamma}{}'(\xi') &= \frac{d\left[g^{nt}_{\alpha\beta\gamma}(\xi')\right]}{d\xi} \\ &= \frac{d\left[\Phi^n(\xi')\right]}{d\xi}\frac{B\left(1-\nu\right)}{4\pi J(\xi')}\{2\nu\left(n_\alpha r_{,\beta}r_{,\gamma}+n_\beta r_{,\alpha}r_{,\gamma}\right) \\ &\quad +\left(1-\nu\right)\left(2n_\gamma r_{,\alpha}r_{,\beta}+n_\beta\delta_{\alpha\gamma}+n_\alpha\delta_{\beta\gamma}\right) \\ &\quad -\left(1-3\nu\right)n_\gamma\delta_{\alpha\beta}\} \end{aligned} \tag{C.32}$$

The hypersingular of order $O\left(\frac{1}{r^2}+\ln(r)\right)$ can be treated by separating the term of the kernel which contain $1/r^2$ and $\ln(\xi-\xi')$.

Substituting the expansion of modified Bessel functions for small arguments in equations (3.35 − 3.36), functions $A(z)$, $B(z)$, $zK_1(z)$,and $z^2K_0(z)$ can be expanded as follows:

$$\begin{aligned}
A(z) &= K_0(z)+\frac{2}{z}\left\{K_1(z)-\frac{1}{z}\right\} \\
&= \left[-\gamma-\ln(\frac{z}{2})\right]+\left[-\gamma+1-\ln(\frac{z}{2})\right]\frac{(z^2/4)}{(1!)^2}+O\left(z^4\right)+.... \\
&\quad +\frac{2}{z}\left\{\frac{1}{z}-\left[-\gamma+\frac{1}{2}-\ln(\frac{z}{2})\right]\frac{(z^2/4)^{1/2}}{0!1!}\right. \\
&\quad \left.-\left[-\gamma+1+\frac{1}{4}-\ln(\frac{z}{2})\right]\frac{(z^2/4)^{3/2}}{1!2!}+O\left(z^5\right)+...-\frac{1}{z}\right\} \\
&= \left[-\frac{1}{2}\right]+\frac{z^2}{4}\left[-\frac{\gamma}{2}+\frac{1}{2}-\frac{1}{8}-\frac{1}{2}\ln(\frac{z}{2})\right]+O\left(z^4\right)+... \qquad \text{(C.33)}
\end{aligned}$$

$$\begin{aligned}
B(z) &= K_0(z)+\frac{1}{z}\left[K_1(z)-\frac{1}{z}\right] \\
&= \left[-\gamma-\ln(\frac{z}{2})\right]+\left[-\gamma+1-\ln(\frac{z}{2})\right]\frac{(z^2/4)}{(1!)^2}+O\left(z^4\right)+.... \\
&\quad +\frac{1}{z}\left\{\frac{1}{z}-\left[-\gamma+\frac{1}{2}-\ln(\frac{z}{2})\right]\frac{(z^2/4)^{1/2}}{0!1!}\right. \qquad \text{(C.34)} \\
&\quad \left.-\left[-\gamma+1+\frac{1}{4}-\ln(\frac{z}{2})\right]\frac{(z^2/4)^{3/2}}{1!2!}+O\left(z^5\right)+...-\frac{1}{z}\right\} \\
&= \left[-\frac{\gamma}{2}-\frac{1}{4}-\frac{1}{2}\ln(\frac{z}{2})\right]+\frac{z^2}{4}\left[-\frac{3\gamma}{4}+\frac{3}{4}-\frac{1}{16}-\frac{3}{4}\ln(\frac{z}{2})\right]+O\left(z^4\right)+...
\end{aligned}$$

$$\begin{aligned}
zK_1(z) &= z\left\{\frac{1}{z}-\left[-\gamma+\frac{1}{2}-\ln(\frac{z}{2})\right]\frac{(z^2/4)^{1/2}}{0!1!}+O\left(z^3\right)+...\right\} \\
&= 1-\frac{z^2}{2}\left[-\gamma+\frac{1}{2}-\ln(\frac{z}{2})\right]+O\left(z^4\right)+... \qquad \text{(C.35)}
\end{aligned}$$

$$\begin{aligned}
z^2K_0(z) &= z^2\left\{\left[-\gamma-\ln(\frac{z}{2})\right]+O\left(z^2\right)+....\right\} \\
&= z^2\left[-\gamma-\ln(\frac{z}{2})\right]+O\left(z^4\right)+... \qquad \text{(C.36)}
\end{aligned}$$

Using relationship for $z = \lambda r$ and substituting equation (C.9), the term $\ln(z/2)$ can be expanded as

$$\ln(\frac{z}{2}) = \ln(\lambda) + \ln|\delta\xi| + \ln\left(\sqrt{d_0 + d_1\delta\xi + d_2\delta\xi^2}\right) - \ln(2) \tag{C.37}$$

The kernel $P^*_{\alpha\beta\gamma}$

Substituting equations (C.33 – C.37) into the kernel $P^*_{\alpha\beta\gamma}$ in equation (3.97), and separating singular and regular terms, then $P^*_{\alpha\beta\gamma}$ can be rewritten as

$$\begin{aligned}
P^*_{\alpha\beta\gamma}(\xi',\xi) &= \left[P^*_{\alpha\beta\gamma}(\xi',\xi)\right]_{\text{singular}} + \left[P^*_{\alpha\beta\gamma}(\xi',\xi)\right]_{\text{regular}} \\
&= \frac{D(1-\nu)}{4\pi r^2}\left\{\left(\frac{1}{2}z^2\ln|\delta\xi| + 1 - \nu\right)(\delta_{\gamma\alpha}n_\beta + \delta_{\gamma\beta}n_\alpha)\right. \\
&\quad + \left(-\frac{1}{2}z^2\ln|\delta\xi| - 1 + 3\nu\right)\delta_{\alpha\beta}n_\gamma \\
&\quad + 2\nu\left[(n_\alpha r_{,\beta} + n_\beta r_{,\alpha})\, r_{,\gamma} + (\delta_{\gamma\alpha}r_{,\beta} + \delta_{\gamma\beta}r_{,\alpha})\, r_{,n}\right] \\
&\quad + 2(1-\nu)(\delta_{\alpha\beta}r_{,\gamma}r_{,n} + n_\gamma r_{,\alpha}r_{,\beta}) \\
&\quad \left. - 4(2+2\nu)\, r_{,\alpha}r_{,\beta}r_{,\gamma}r_{,n}\right\} + \left[P^*_{\alpha\beta\gamma}(\xi',\xi)\right]_{\text{regular}}
\end{aligned} \tag{C.38}$$

Separating the part of the kernels $P^*_{\alpha\beta\gamma}(\xi',\xi)$ which contain $1/r^2$, and multiplied it with $\Phi^n(\xi)J(\xi)\left(\xi - \xi'\right)^2$, gives

$$\begin{aligned}
g^{np}_{\alpha\beta\gamma}(\xi) &= P^{*1}_{\alpha\beta\gamma}(\xi',\xi)\Phi^n(\xi)J(\xi)\left(\xi - \xi'\right)^2 \\
&= \frac{D(1-\nu)\Phi^n(\xi)J(\xi)\left(\xi - \xi'\right)^2}{4\pi|\delta\xi|^2\left(d_0 + d_1\delta\xi + d_2\delta\xi^2\right)} \times \\
&\quad \{(1-\nu)(\delta_{\gamma\alpha}n_\beta + \delta_{\gamma\beta}n_\alpha) + (-1+3\nu)\delta_{\alpha\beta}n_\gamma \\
&\quad + 2\nu\left[(n_\alpha r_{,\beta} + n_\beta r_{,\alpha})\, r_{,\gamma} + (\delta_{\gamma\alpha}r_{,\beta} + \delta_{\gamma\beta}r_{,\alpha})\, r_{,n}\right] \\
&\quad + 2(1-\nu)(\delta_{\alpha\beta}r_{,\gamma}r_{,n} + n_\gamma r_{,\alpha}r_{,\beta}) - 4(2+2\nu)\, r_{,\alpha}r_{,\beta}r_{,\gamma}r_{,n}\} \\
&\quad + \Phi^n(\xi)J(\xi)\left(\xi - \xi'\right)^2\left[P^*_{\alpha\beta\gamma}(\xi',\xi)\right]_{\text{regular}}
\end{aligned} \tag{C.39}$$

By considering the limit in equation (C.14) and substituting equations (C.7) and (C.11), the value $g^{np}_{\alpha\beta\gamma}(\xi)$at singular point ξ' can be obtained as

$$g^{np}_{\alpha\beta\gamma}(\xi') = \frac{D(1-\nu)\Phi^n(\xi')}{4\pi J(\xi')}\{(1-\nu)(\delta_{\gamma\alpha}n_\beta + \delta_{\gamma\beta}n_\alpha) + (-1+3\nu)\,\delta_{\alpha\beta}n_\gamma$$

$$+2\nu\left(n_\alpha r_{,\beta}+n_\beta r_{,\alpha}\right)r_{,\gamma}+2\left(1-\nu\right)n_\gamma r_{,\alpha}r_{,\beta}\} \tag{C.40}$$

and the derivatives of $g^{np}_{\alpha\beta\gamma}\left(\xi'\right)$can be obtained as

$$\begin{aligned} g^{np}_{\alpha\beta\gamma}{}'\left(\xi'\right) &= \frac{d\left[g^{np}_{\alpha\beta\gamma}\left(\xi'\right)\right]}{d\xi} \\ &= \frac{d\left[\Phi^n(\xi')\right]}{d\xi}\frac{D(1-\nu)}{4\pi J(\xi')}\{(1-\nu)\left(\delta_{\gamma\alpha}n_\beta+\delta_{\gamma\beta}n_\alpha\right)+\left(-1+3\nu\right)\delta_{\alpha\beta}n_\gamma \\ &\quad +2\nu\left(n_\alpha r_{,\beta}+n_\beta r_{,\alpha}\right)r_{,\gamma}+2\left(1-\nu\right)n_\gamma r_{,\alpha}r_{,\beta}\} \end{aligned} \tag{C.41}$$

Now, separating the part of the kernels $P^*_{\alpha\beta\gamma}(\xi',\xi)$ which contain $\ln|\delta\xi|$, and multiplied it with $\Phi^n(\xi)J(\xi)/\ln\left|\xi-\xi'\right|$, gives

$$\begin{aligned} h^{np}_{\alpha\beta\gamma}\left(\xi\right) &= \frac{P^{*2}_{\alpha\beta\gamma}(\xi',\xi)\Phi^n(\xi)J(\xi)}{\ln\left|\xi-\xi'\right|} \\ &= \frac{D(1-\nu)\lambda^2\Phi^n(\xi)J(\xi)}{4\pi z^2\ln\left|\xi-\xi'\right|}\times\left(\frac{1}{2}z^2\ln|\delta\xi|\right)\left(\delta_{\gamma\alpha}n_\beta+\delta_{\gamma\beta}n_\alpha-\delta_{\alpha\beta}n_\gamma\right) \end{aligned} \tag{C.42}$$

and the value $h^{np}_{\alpha\beta\gamma}\left(\xi\right)$at singular point ξ' can be obtained as

$$h^{np}_{\alpha\beta\gamma}\left(\xi'\right)=\frac{D(1-\nu)\lambda^2\Phi^n(\xi')J(\xi')}{8\pi}\left(\delta_{\gamma\alpha}n_\beta+\delta_{\gamma\beta}n_\alpha-\delta_{\alpha\beta}n_\gamma\right) \tag{C.43}$$

The kernel $P^*_{3\beta3}$

Substituting equations (C.33 – C.37) into the kernel $P^*_{3\beta3}$ in equation (3.97), and separating singular and regular terms, then $P^*_{3\beta3}$ can be rewritten as

$$\begin{aligned} P^*_{3\beta3}(\xi',\xi) &= \left[P^*_{3\beta3}(\xi',\xi)\right]_{\text{singular}}+\left[P^*_{3\beta3}(\xi',\xi)\right]_{\text{regular}} \\ &= \frac{D(1-\nu)\lambda^2}{4\pi r^2}\left[\left(-\frac{1}{2}z^2\ln|\delta\xi|+1\right)n_\beta-2r_{,\beta}r_{,n}\right] \\ &\quad +\left[P^*_{3\beta3}(\xi',\xi)\right]_{\text{regular}} \end{aligned} \tag{C.44}$$

Separating the part of the kernels $P^*_{\alpha\beta\gamma}(\xi',\xi)$ which contain $1/r^2$, and multiplied it with $\Phi^n(\xi)J(\xi)\left(\xi-\xi'\right)^2$, gives

$$g^{np}_{3\beta3}\left(\xi\right) = P^{*1}_{3\beta3}(\xi',\xi)\Phi^n(\xi)J(\xi)\left(\xi-\xi'\right)^2$$

$$= \frac{D(1-\nu)\lambda^2\Phi^n(\xi)J(\xi)\left(\xi-\xi'\right)^2}{4\pi\left|\delta\xi\right|^2\left(d_0+d_1\delta\xi+d_2\delta\xi^2\right)}\left[n_\beta-2r_{,\beta}r_{,n}\right]$$
$$+\Phi^n(\xi)J(\xi)\left(\xi-\xi'\right)^2\left[P^*_{3\beta3}(\xi',\xi)\right]_{\text{regular}} \tag{C.45}$$

By considering the limit in equation (C.14) and substituting equations (C.7) and (C.11), the value $g^{np}_{3\beta3}(\xi)$ at singular point ξ' can be obtained as

$$g^{np}_{3\beta3}(\xi') = \frac{D(1-\nu)\lambda^2\Phi^n(\xi')}{4\pi J(\xi')}n_\beta \tag{C.46}$$

and the derivatives of $g^{np}_{3\beta3}(\xi')$can be obtained as

$$\begin{aligned} g^{np}{}'_{3\beta3}(\xi') &= \frac{d\left[g^{np}_{\alpha\beta\gamma}(\xi')\right]}{d\xi} \\ &= \frac{d\left[\Phi^n(\xi')\right]}{d\xi}\frac{D(1-\nu)}{4\pi J(\xi')}n_\beta \end{aligned} \tag{C.47}$$

Now, separating the part of the kernels $P^*_{3\beta3}(\xi',\xi)$ which contain $\ln|\delta\xi|$, and multiplied it with $\Phi^n(\xi)J(\xi)/\ln\left|\xi-\xi'\right|$, gives

$$\begin{aligned} h^{np}_{3\beta3}(\xi) &= \frac{P^{*2}_{3\beta3}(\xi',\xi)\Phi^n(\xi)J(\xi)}{\ln\left|\xi-\xi'\right|} \\ &= \frac{D(1-\nu)\lambda^4\Phi^n(\xi)J(\xi)}{4\pi z^2\ln\left|\xi-\xi'\right|}\left(-\frac{1}{2}z^2\ln|\delta\xi|\right)n_\beta \end{aligned} \tag{C.48}$$

and the value $h^{np}_{\alpha\beta\gamma}(\xi)$at singular point ξ' can be obtained as

$$h^{np}_{3\beta3}(\xi') = -\frac{D(1-\nu)\lambda^4\Phi^n(\xi')J(\xi')}{8\pi}n_\beta \tag{C.49}$$

In the case of the off-diagonal sub-matrices the shape function $\Phi^i(\xi^{node}) = 0$ for $\xi^{node} \neq \xi'$, and the order of singularity decreases by one. The strongly singular integrals become smooth whereas the hypersingular integrals become strongly singular integrals.

C.3 Analytical Integration of Membrane Fundamental Solutions

In a flat element, coordinate of middle node in the element can be defined from coordinates of the other nodes in the element, that is

$$x_\alpha^2 = \frac{1}{2}\left(x_\alpha^1 + x_\alpha^3\right) \tag{C.50}$$

By using equations (C.10 – C.11), the Jacobian of the coordinate transformation is found to be constant, i.e.

$$J\left(\xi\right) = \frac{l}{2} \tag{C.51}$$

where l is the element length. For such element, the singular integrals contain $T_{\theta\alpha}^*, U_{\alpha\beta\gamma}^*, T_{\alpha\beta\gamma}^{(i)*}$ kernels can be integrated analytically.

The integral in equation (3.57) is represented by

$$\oint_{\Gamma e} T_{\theta\alpha}^{*(i)}(\mathbf{x}', \mathbf{x}) u_\alpha(\mathbf{x}) d\Gamma(\mathbf{x}) = u_\alpha^m \int_{-1}^{+1} T_{\theta\alpha}^{*(i)}\left(\xi', \mathbf{x}(\xi)\right) \Phi^m(\xi) J_n(\xi) d\xi \tag{C.52}$$

Substituting equation (C.51)and $T_{\theta\alpha}^{*(i)}$ in equation (3.52), and considering the limits in equation (C.13), gives

$$\frac{1-\nu}{4\pi}\begin{bmatrix} 0 & -1 \\ +1 & 0 \end{bmatrix}\begin{Bmatrix} u_1^m \\ u_2^m \end{Bmatrix} \int_{-1}^{+1} \frac{\Phi^m(\xi)}{\xi - \xi'} d\xi \tag{C.53}$$

For discontinuous element with the nodes are located at $\xi = -\frac{2}{3}, 0, +\frac{2}{3}$, the integrals in equation (C.53) are integrated analytically to give

$$\int_{-1}^{+1} \frac{\Phi^1(\xi)}{\xi - \xi'} d\xi = \frac{3}{4}\left[\frac{\xi'\left(3\xi' - 2\right)}{2} \ln\left|\frac{1-\xi'}{1+\xi'}\right| + 3\xi' - 2\right] \tag{C.54}$$

$$\int_{-1}^{+1} \frac{\Phi^2(\xi)}{\xi - \xi'} d\xi = \frac{1}{2}\left[\frac{\left(3\xi' - 2\right)\left(3\xi' + 2\right)}{2} \ln\left|\frac{1+\xi'}{1-\xi'}\right| - 9\xi'\right] \tag{C.55}$$

and

$$\int_{-1}^{+1} \frac{\Phi^3(\xi)}{\xi - \xi'} d\xi = \frac{3}{4}\left[\frac{\xi'\left(3\xi' + 2\right)}{2} \ln\left|\frac{1-\xi'}{1+\xi'}\right| + 3\xi' + 2\right] \tag{C.56}$$

The integral in equation (4.9) is represented by

$$\neq\!\!\!\!\!\!\int_{\Gamma e} T^{(i)*}_{\alpha\beta\gamma}(\mathbf{x}',\mathbf{x})u_\gamma(\mathbf{x})d\Gamma(\mathbf{x}) = u^m_\gamma \neq\!\!\!\!\!\!\int_{-1}^{+1} T^{(i)*}_{\alpha\beta\gamma}\left(\xi',\mathbf{x}(\xi)\right)\Phi^m(\xi)J_n(\xi)d\xi \qquad \text{(C.57)}$$

Substituting equation (C.51) and $T^{(i)*}_{\alpha\beta\gamma}$ in equation (3.100), and considering the limits in equation (C.13), gives

$$\frac{B\left(1-\nu^2\right)}{4\pi}\frac{2}{l}\begin{bmatrix} +n_1\left(2n_2^2+1\right) & -n_2\left(-2n_2^2+1\right) \\ +n_1\left(2n_1^2-1\right) & -n2\left(-2n_1^2-1\right) \\ -n_2\left(2n_1^2-1\right) & +n_1\left(-2n_2^2+1\right) \end{bmatrix}\begin{Bmatrix} u_1^m \\ u_2^m \end{Bmatrix} \neq\!\!\!\!\!\!\int_{-1}^{+1} \frac{\Phi^m(\xi)}{\left(\xi-\xi'\right)^2}d\xi \qquad \text{(C.58)}$$

For discontinuous element with the nodes are located at $\xi = -\frac{2}{3}, 0, +\frac{2}{3}$, the integrals in equation (C.58) are integrated analytically to give

$$\neq\!\!\!\!\!\!\int_{-1}^{+1} \frac{\Phi^1(\xi)}{\left(\xi-\xi'\right)^2}d\xi = \frac{3}{4}\left[\left(3\xi'-1\right)\ln\left|\frac{1-\xi'}{1+\xi'}\right| + \frac{6\left(\xi'\right)^2-2\xi'-3}{\left(\xi'\right)^2-1}\right] \qquad \text{(C.59)}$$

$$\neq\!\!\!\!\!\!\int_{-1}^{+1} \frac{\Phi^2(\xi)}{\left(\xi-\xi'\right)^2}d\xi = \frac{1}{2}\left[9\xi'\ln\left|\frac{1+\xi'}{1-\xi'}\right| - \frac{18\left(\xi'\right)^2-13}{\left(\xi'\right)^2-1}\right] \qquad \text{(C.60)}$$

and

$$\neq\!\!\!\!\!\!\int_{-1}^{+1} \frac{\Phi^3(\xi)}{\left(\xi-\xi'\right)^2}d\xi = \frac{3}{4}\left[\left(3\xi'+1\right)\ln\left|\frac{1-\xi'}{1+\xi'}\right| + \frac{6\left(\xi'\right)^2+2\xi'-3}{\left(\xi'\right)^2-1}\right] \qquad \text{(C.61)}$$

C.4 Triangle to Square Transformation

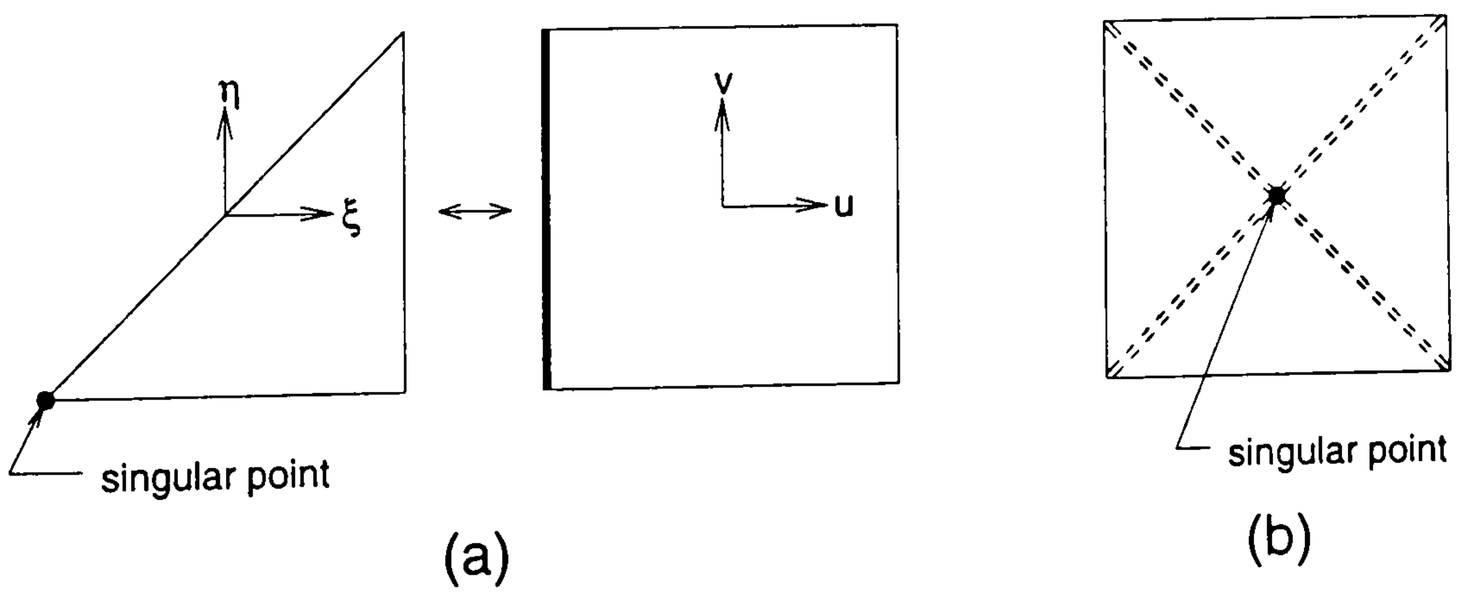

Figure C-2: (a) Transformation of triangle to square ; (b) Subdivision of quadrilateral element into four triangular sub element.

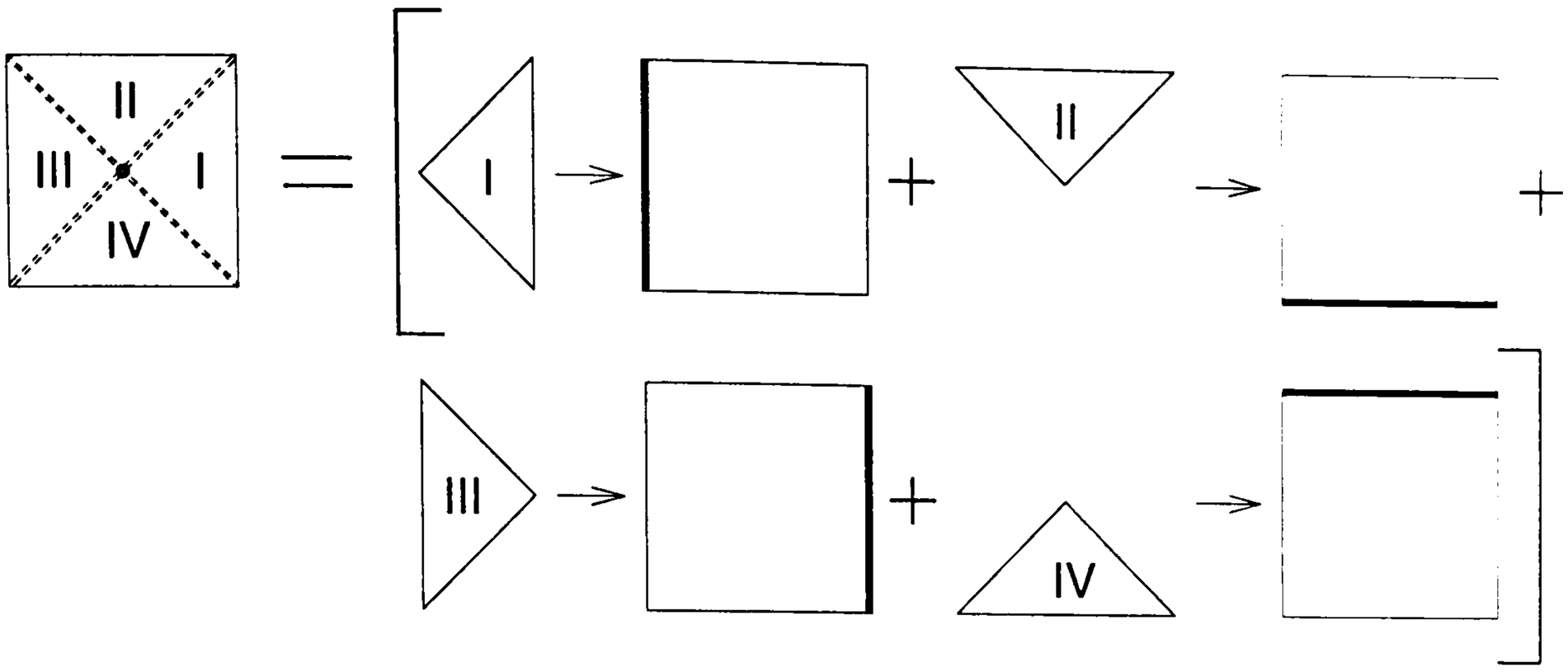

Figure C-3: Systematic use of transformation of variable technique.

The procedure for the triangle to square transformation follows Aliabadi and Rooke [8]. This procedure is used to cancel weak singularity in an integral over the domain. Consider a triangular element, shown in the Figure C-2(a), which has a singularity at $(\xi, \eta) = (-1, -1)$ in the local (ξ, η) plane. The singular integral is transformed in the following manner,

$$\int_{-1}^{1}\int_{-1}^{\xi} \frac{M(\xi,\eta)\,J(\xi,\eta)}{R} d\eta d\xi = \int_{-1}^{1}\int_{-1}^{1} \frac{M(\xi,\eta)\,J(\xi,\eta)\,J^c(\xi,\eta)}{R} du dv \qquad \text{(C.62)}$$

where $\xi = u$ and $\eta = \frac{1}{2}\left[(1+u)\,v - (1-u)\right]$. The Jacobian of this transformation $J^c(\xi,\eta) = \frac{1}{2}(1+\xi)$ exactly cancel out the singularity [8].

For constant cell element, where the singular point is at the centre of the quadrilateral element, as shown in Figure C-2(b), the element is divided into four triangular element and each triangular element is transformed to square, as shown in Figure C-3. The transformation are

triangle I : $\xi = \frac{1}{2}(1+u_1)$ and $\eta = \frac{1}{2}(1+u_1)\,v_1$; $J^c(u_1) = \frac{1}{4}(1+u_1)$

triangle II : $\xi = \frac{1}{2}(1+v_2)\,u_2$ and $\eta = \frac{1}{2}(1+v_2)$; $J^c(v_2) = \frac{1}{4}(1+v_2)$

triangle III : $\xi = \frac{1}{2}(u_3-1)$ and $\eta = \frac{1}{2}(1-u_3)\,v_3$; $J^c(u_3) = \frac{1}{4}(1-u_3)$

triangle IV : $\xi = \frac{1}{2}(1-v_4)\,u_4$ and $\eta = \frac{1}{2}(v_4-1)$; $J^c(v_4) = \frac{1}{4}(1-v_4)$

Thus,

$$\int_{-1}^{1}\int_{-1}^{1}\frac{M(\xi,\eta)\,J(\xi,\eta)}{R}d\eta d\xi = \int_{-1}^{1}\int_{-1}^{1}\frac{M(\xi,\eta)\,J(\xi,\eta)\,J^{c}(u_1)}{R}du_1dv_1 + \int_{-1}^{1}\int_{-1}^{1}\frac{M(\xi,\eta)\,J(\xi,\eta)\,J^{c}(v_2)}{R}du_2dv_2 + \int_{-1}^{1}\int_{-1}^{1}\frac{M(\xi,\eta)\,J(\xi,\eta)\,J^{c}(u_3)}{R}du_3dv_3 + \int_{-1}^{1}\int_{-1}^{1}\frac{M(\xi,\eta)\,J(\xi,\eta)\,J^{c}(v_4)}{R}du_4dv_4 \quad \text{(C.63)}$$

where the Jacobian factors cancel out the $\frac{1}{R}$ singularity.

Appendix D

Particular solutions

Particular solutions needed for dual reciprocity technique in chapter 3 and chapter 4 are derived by Wen, Aliabadi and Young [140] and are given in the following sections.

D.1 Particular solutions for two-dimensional plane stress

An expression displacement particular solution $\hat{u}^{\gamma}_{m\alpha}$ can be found in polar coordinates with the use of the Galerkin vector $G_{\alpha\beta}$ as

$$\hat{u}^{\gamma}_{m\alpha}(r) = G^{\gamma}_{\beta\alpha,\gamma\gamma}(r) - \frac{1+\nu}{2} G^{\gamma}_{\gamma\alpha,\beta\gamma}(r) \tag{D.1}$$

where $G_{\alpha\beta}$ satifies

$$\nabla^4 G^{\gamma}_{\beta\alpha} + \frac{2}{(1-\nu)B} \frac{x_\gamma}{r} \delta_{\gamma\beta} = 0 \tag{D.2}$$

and a solution is determined by

$$G^{\gamma}_{\beta\alpha} = -\frac{r^3 x_\gamma}{45\,(1-v)\,B} \delta_{\alpha\beta} \tag{D.3}$$

Substituting equation (D.3) into equation (D.1), then the displacement particular solutions can be arranged as

$$\hat{u}^{1}_{m1} = -\frac{2}{(1-\nu)B} \left[\frac{r x_1}{3} - \frac{1+\nu}{30} \left(\frac{x_1^3}{r} + 3 x_1 r \right) \right]$$

$$\hat{u}^{1}_{m2} = \frac{(1+\nu)}{15(1-\nu)B} \left(\frac{x_1^2 x_2}{r} + x_2 r \right) \tag{D.4}$$

and using strain displacement relationships in equation (2.60), the strain are obtained as

$$\hat{\varepsilon}^1_{m11} = -\frac{2}{(1-\nu)}\left[\left(\frac{x_1^2}{r}+\frac{r}{3}\right)-\frac{1+\nu}{30}\left(-\frac{x_1^4}{r^3}+\frac{6x_1^2}{r}+3r\right)\right]$$

$$\hat{\varepsilon}^1_{m12} = -\frac{2}{(1-\nu)}\left[\frac{x_1x_2}{6r}-\frac{1+\nu}{30}\left(-\frac{x_1^3x_2}{r^3}+\frac{3x_1x_2}{r}\right)\right]$$

$$\hat{\varepsilon}^1_{m22} = \frac{2}{(1-\nu)}\frac{1+\nu}{30}\left(-\frac{x_1^2x_2^2}{r^3}+2r\right) \tag{D.5}$$

The particular solution for membrane stress resultant can be derived by substituting equation (D.5) into the stress resultant-strain relationships in equation (2.64) to give:

$$\hat{N}^1_{m11} = B\left[(1-\nu)\hat{\varepsilon}^1_{m11}+\nu\hat{\varepsilon}^1_{m\alpha\alpha}\right]$$

$$\hat{N}^1_{m12} = B(1-\nu)\hat{\varepsilon}^1_{m12}$$

$$\hat{N}^1_{m22} = B\left[(1-\nu)\hat{\varepsilon}^1_{m22}+\nu\hat{\varepsilon}^1_{m\alpha\alpha}\right] \tag{D.6}$$

and the traction particular solutions are obtained from

$$\hat{t}^1_{m\alpha} = \hat{N}^1_{m\alpha\beta}n_\beta \tag{D.7}$$

In the same way, displacement particular solutions $\hat{u}^2_{m\alpha}$ can be obtained as follows:

$$\hat{u}^2_{m1} = \frac{(1+\nu)}{15(1-\nu)B}\left(\frac{x_2^2x_1}{r}+x_1r\right)$$

$$\hat{u}^2_{m2} = -\frac{2}{(1-\nu)B}\left[\frac{rx_2}{3}-\frac{1+\nu}{30}\left(\frac{x_2^3}{r}+3x_2r\right)\right] \tag{D.8}$$

and the strains are

$$\hat{\varepsilon}^2_{m11} = \frac{2}{(1-\nu)}\frac{1+\nu}{30}\left(-\frac{x_1^2x_2^2}{r^3}+2r\right)$$

$$\hat{\varepsilon}^2_{m12} = -\frac{2}{(1-\nu)}\left[\frac{x_1x_2}{6r}-\frac{1+\nu}{30}\left(-\frac{x_2^3x_1}{r^3}+\frac{3x_1x_2}{r}\right)\right]$$

$$\hat{\varepsilon}^2_{m22} = -\frac{2}{(1-\nu)}\left[\left(\frac{x_2^2}{r}+\frac{r}{3}\right)-\frac{1+\nu}{30}\left(-\frac{x_2^4}{r^3}+\frac{6x_2^2}{r}+3r\right)\right] \tag{D.9}$$

The particular solution for membrane stress resultant are

$$\hat{N}^2_{m11} = B\left[(1-\nu)\hat{\varepsilon}^2_{m11} + \nu\hat{\varepsilon}^2_{m\alpha\alpha}\right]$$

$$\hat{N}^2_{m12} = B(1-\nu)\hat{\varepsilon}^2_{m12}$$

$$\hat{N}^2_{m22} = B\left[(1-\nu)\hat{\varepsilon}^2_{m22} + \nu\hat{\varepsilon}^2_{m\alpha\alpha}\right] \tag{D.10}$$

and finally the traction particular solutions are obtained from

$$\hat{t}^2_{m\alpha} = \hat{N}^2_{m\alpha\beta} n_\beta \tag{D.11}$$

D.2 Particular solutions for plate bending

Governing equation for shear deformable plate bending problem can be written as

$$\hat{\mathbf{w}} = \mathbf{H}\mathbf{e}\varphi \tag{D.12}$$

where particular solutions of displacement $\hat{\mathbf{w}} = \{\hat{w}_1, \hat{w}_2, \hat{w}_3\}^\top$, $\mathbf{e} = \{e_1, e_2, e_3\}^\top$ is arbitrary constant vector and components of matrix $\mathbf{H}$ are

$$H_{\alpha\beta} = 2\delta_{\alpha\beta}\bigtriangledown^4 - [(1+\nu)\bigtriangledown^2 + (1-\nu)\lambda^2)]\frac{\partial^2}{\partial x_\alpha \partial x_\beta}$$

$$H_{3\alpha} = -H_{\alpha 3} = -(1-\nu)(\bigtriangledown^2 - \lambda^2)\frac{\partial}{\partial x_\alpha}$$

$$H_{33} = (\bigtriangledown^2 - \lambda^2)[2\bigtriangledown^2 - (1-\nu)\lambda^2]/\lambda^2 \tag{D.13}$$

The function φ can be defined from equation (D.12) such that

$$D(1-\nu)(\bigtriangledown^2 - \lambda^2)\bigtriangledown^4\varphi + F(r) = 0 \tag{D.14}$$

If $e_1 = 0, e_2 = 0$ and $e_3 = 1$, the particular solution used in equation (3.83) can be written as

$$\hat{w}_{m\alpha} = -\frac{1}{D}\frac{\partial\psi}{\partial x_\alpha}$$

$$\hat{w}_{m3} = \frac{1}{(1-\nu)D\lambda^2}[2\nabla^2\psi - (1-\nu)\lambda^2\psi] \tag{D.15}$$

where

$$\nabla^4\psi(r) + F(r) = 0 \tag{D.16}$$

The particular solutions of moment and shear force can be determined from equations $(2.44 - 2.45)$. The tractions on the boundary can be obtained by

$$\hat{p}_{m\alpha} = \hat{M}_{\alpha\beta}n_\beta, \;\; \hat{p}_{m3} = \hat{Q}_\alpha n_\alpha \tag{D.17}$$

If radial basis function $F(r) = 1+r$, The function $\psi(r)$ can be solved from equation (D.16)

$$\psi(r) = -\left(\frac{r^4}{64} + \frac{r^5}{225}\right) \tag{D.18}$$

and the rotations and deflection can be deduced

$$\hat{w}^3_{m1} = -\left(\frac{1}{16} + \frac{r}{45}\right)\frac{x_1 r^2}{D}$$

$$\hat{w}^3_{m2} = -\left(\frac{1}{16} + \frac{r}{45}\right)\frac{x_2 r^2}{D} \tag{D.19}$$

$$\hat{w}^3_{m3} = -\left(\frac{1}{2} + \frac{2r}{9}\right)\frac{r^2}{(1-\nu)\lambda^2 D} + \left(\frac{1}{64} + \frac{r}{225}\right)\frac{1}{D}$$

The particular solutions of moments $\hat{M}_{\alpha\beta}$ and shear forces $\hat{Q}_\beta$ can be determined by equations $(2.44 - 2.45)$ to give

$$\hat{M}^3_{m11} = -\left[\left(\frac{1}{8} + \frac{r}{15}\right)(x_1^2 + \nu x_2^2) + (1+\nu)\left(\frac{r^2}{16} + \frac{r^3}{45}\right)\right]$$

$$\hat{M}^3_{m12} = -(1+\nu)\left(\frac{1}{8} + \frac{r}{15}\right)(x_1 x_2)$$

$$\hat{M}^3_{m22} = -\left[\left(\frac{1}{8} + \frac{r}{15}\right)(\nu x_1^2 + x_2^2) + (1+\nu)\left(\frac{r^2}{16} + \frac{r^3}{45}\right)\right] \tag{D.20}$$

$$\hat{Q}^3_{m1} = -\frac{x_1}{2}\left(1 + \frac{2r}{3}\right)$$

$$\hat{Q}^3_{m2} = -\frac{x_2}{2}\left(1 + \frac{2r}{3}\right)$$

and the tractions on the boundary can be obtained from relationships in equation (D.17).

For the derivative of function $F_{,\alpha} = x_\alpha / r$, the solution $\psi^\alpha(r)$ can be found

$$\psi^\alpha(r) = -\frac{r^3 x_\alpha}{45} \tag{D.21}$$

and particular solutions $\hat{w}^\alpha_{mk}$ are

$$\hat{w}^1_{m1} = -(3x_1^2 + r^2)\frac{r}{45D}$$

$$\hat{w}^1_{m2} = -\frac{x_1 x_2 r}{15D} \tag{D.22}$$

$$\hat{w}^1_{m3} = -[30 - (1-\nu)\lambda^2 r^2]\frac{r x_1}{45(1-\nu)\lambda^2 D}$$

and the particular solutions of moments $\hat{M}_{\alpha\beta}$ and shear forces $\hat{Q}_\beta$ are

$$\hat{M}^1_{m11} = -\frac{x_1}{15}\left[\nu\left(\frac{x_1^2}{r} + 3r\right) + \left(\frac{x_2^2}{r} + r\right)\right]$$

$$\hat{M}^1_{m12} = -(1-\nu)\frac{x_2}{15}\left(\frac{x_1^2}{r} + r\right)$$

$$\hat{M}^1_{m22} = -\frac{x_1}{15}\left[\nu\left(\frac{x_1^2}{r} + 3r\right) + \left(\frac{x_2^2}{r} + r\right)\right] \tag{D.23}$$

$$\hat{Q}^1_{m1} = -\frac{1}{3}\left(\frac{x_1^2}{r} + r\right)$$

$$\hat{Q}^1_{m2} = -\frac{1}{3}\frac{x_1 x_2}{r}$$

for $\alpha = 1$, and

$$\hat{w}^2_{m1} = -\frac{x_1 x_2 r}{15D}$$

$$\hat{w}^2_{m1} = -(3x_2^2 + r^2)\frac{r}{45D} \tag{D.24}$$

$$\hat{w}^2_{m3} = -[30 - (1-\nu)\lambda^2 r^2]\frac{r x_2}{45(1-\nu)\lambda^2 D}$$

and the particular solutions of moments $\hat{M}_{\alpha\beta}$ and shear forces $\hat{Q}_\beta$ are

$$\hat{M}^2_{m11} = -\frac{x_2}{15}\left[\nu\left(\frac{x_1^2}{r} + r\right) + \left(\frac{x_2^2}{r} + 3r\right)\right]$$

$$\hat{M}^2_{m12} = -(1-\nu)\frac{x_1}{15}\left(\frac{x_2^2}{r}+r\right)$$

$$\hat{M}^2_{m22} = -\frac{x_2}{15}\left[\nu\left(\frac{x_1^2}{r}+r\right)+\left(\frac{x_2^2}{r}+3r\right)\right] \tag{D.25}$$

$$\hat{Q}^2_{m1} = -\frac{1}{3}\frac{x_1 x_2}{r}$$

$$\hat{Q}^2_{m2} = -\frac{1}{3}\left(\frac{x_2^2}{r}+r\right)$$

for $\alpha = 2$.

Appendix E

Decompositions for the $J-$ Integral Technique

The decomposition of the elastic fields are as follows:

$$\left\{\begin{array}{c} M_{11}^S \\ M_{12}^S \\ M_{22}^S \\ Q_1^S \\ Q_2^S \end{array}\right\} = \frac{1}{2}\left\{\begin{array}{c} M_{11}+M_{11}^{'} \\ M_{12}-M_{12}^{'} \\ M_{22}+M_{22}^{'} \\ Q_1+Q_1^{'} \\ Q_2-Q_2^{'} \end{array}\right\}, \left\{\begin{array}{c} M_{11}^{AS} \\ M_{12}^{AS} \\ M_{22}^{AS} \\ Q_1^{AS} \\ Q_2^{AS} \end{array}\right\} = \frac{1}{2}\left\{\begin{array}{c} M_{11}-M_{11}^{'} \\ M_{12}+M_{12}^{'} \\ M_{22}-M_{22}^{'} \\ Q_1-Q_1^{'} \\ Q_2+Q_2^{'} \end{array}\right\} \tag{E.1}$$

$$\left\{\begin{array}{c} N_{11}^S \\ N_{22}^S \\ N_{12}^S \end{array}\right\} = \frac{1}{2}\left\{\begin{array}{c} N_{11}+N_{11}^{\prime} \\ N_{22}+N_{22}^{\prime} \\ N_{12}-N_{12}^{\prime} \end{array}\right\}, \left\{\begin{array}{c} N_{11}^{AS} \\ N_{22}^{AS} \\ N_{12}^{AS} \end{array}\right\} = \frac{1}{2}\left\{\begin{array}{c} N_{11}-N_{11}^{\prime} \\ N_{22}-N_{22}^{\prime} \\ N_{12}+N_{12}^{\prime} \end{array}\right\} \tag{E.2}$$

and

$$\left\{\begin{array}{c} w_1^S \\ w_2^S \\ w_3^S \end{array}\right\} = \frac{1}{2}\left\{\begin{array}{c} w_1+w_1^{\prime} \\ w_2-w_2^{\prime} \\ w_3+w_3^{\prime} \end{array}\right\}, \left\{\begin{array}{c} w_1^S \\ w_2^S \\ w_3^S \end{array}\right\} = \frac{1}{2}\left\{\begin{array}{c} w_1-w_1^{\prime} \\ w_2+w_2^{\prime} \\ w_3-w_3^{\prime} \end{array}\right\} \tag{E.3}$$

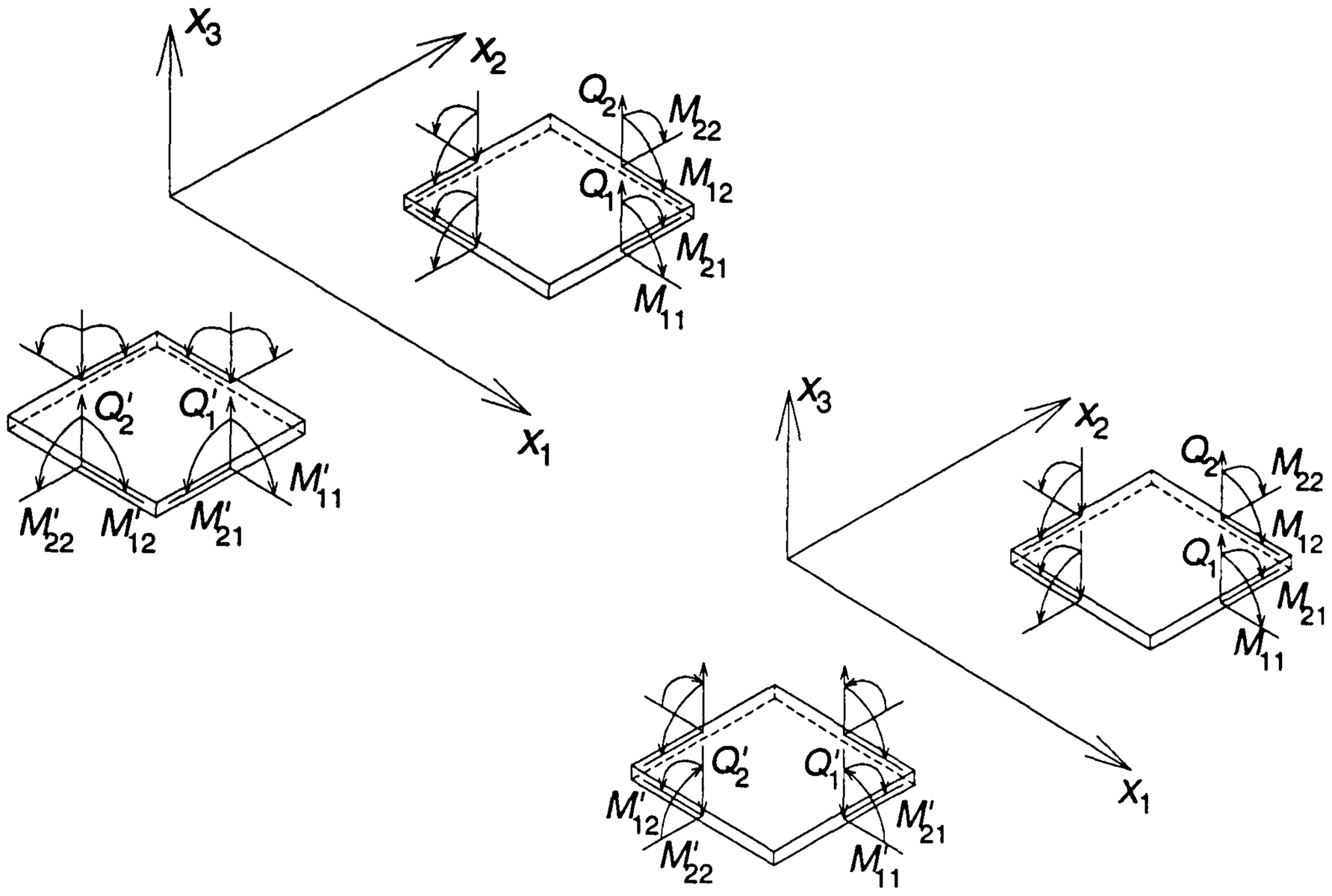

Figure E-1: Symmetric and anti-symmetric moment and shear force stress resultants at two points located symmetrically relative to the crack axis.

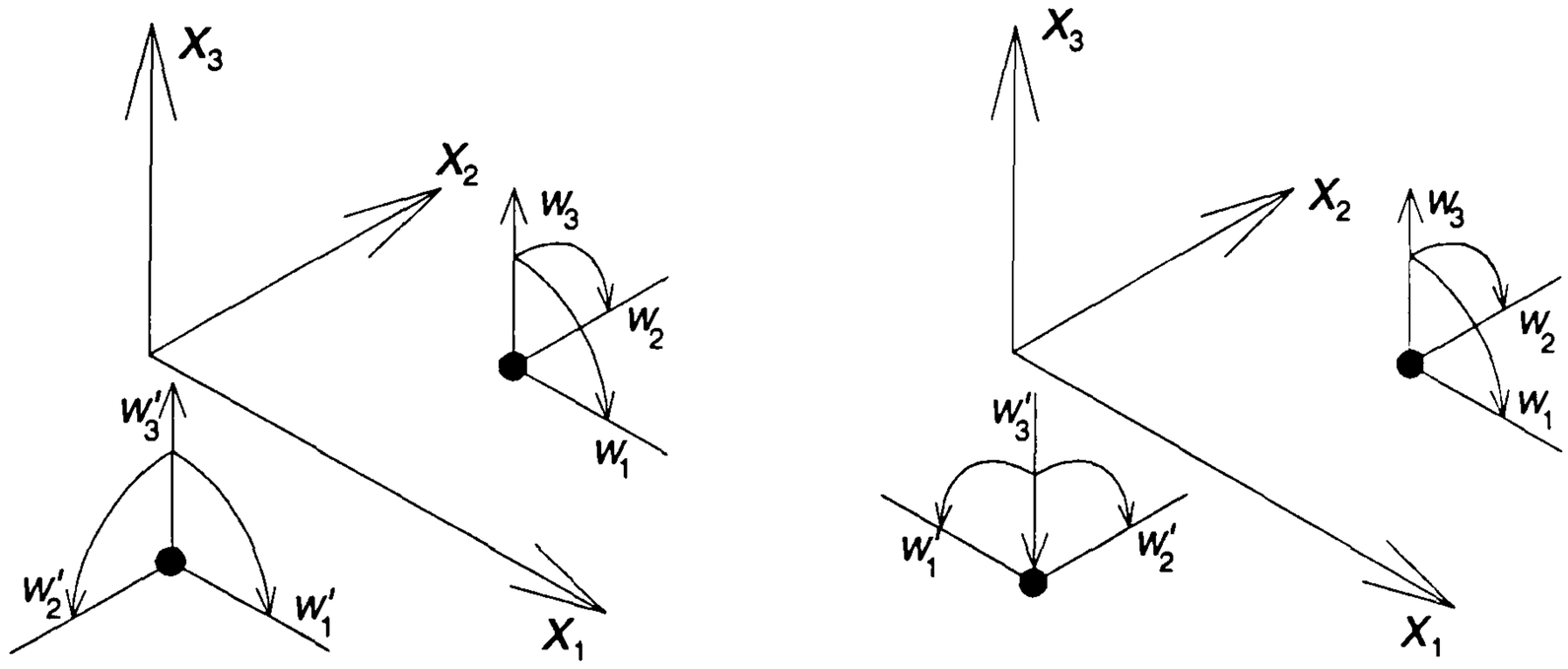

Figure E-2: Symmetric and anti-symmetric rotations and out-of-plane displacement at two points located symmetrically relative to the crack axis.

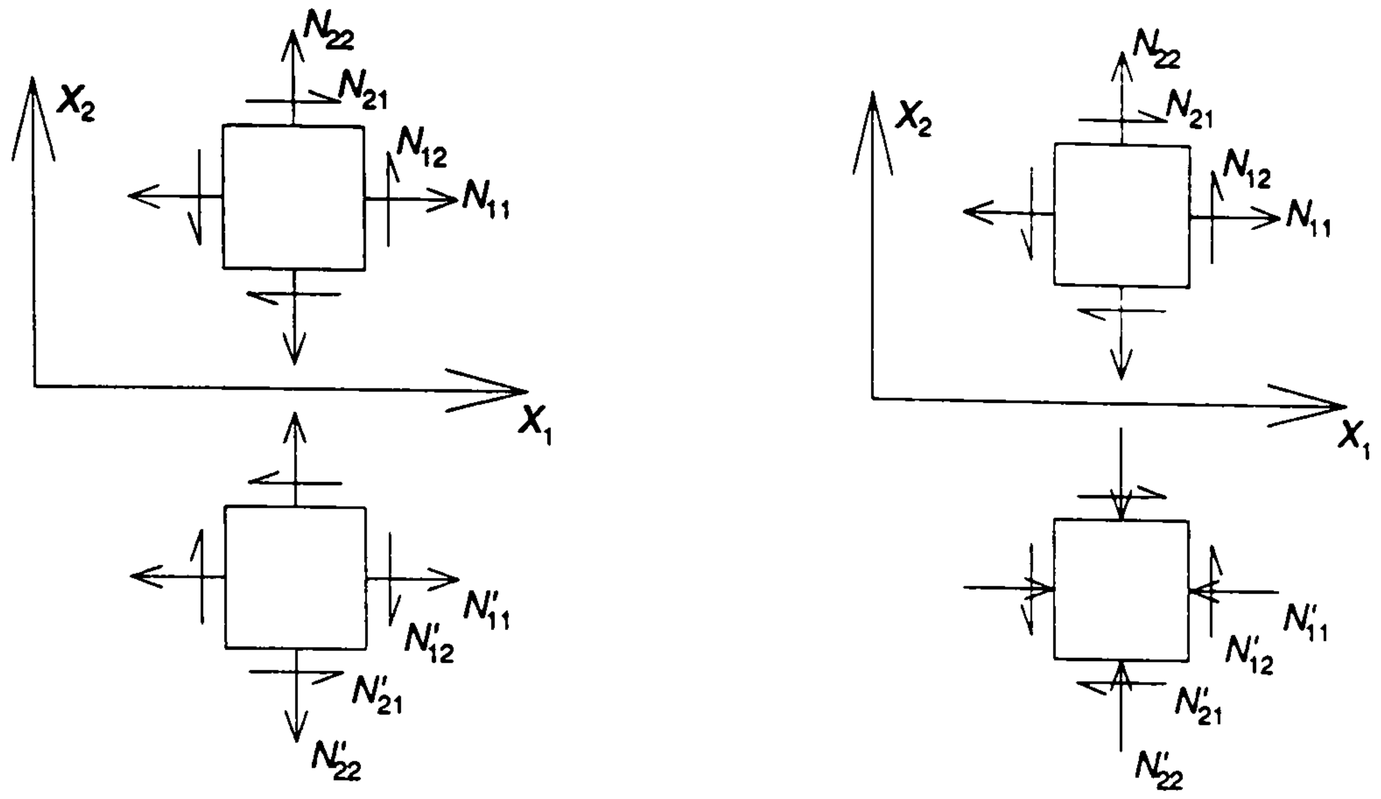

Figure E-3: Symmetric and anti-symmetric in-plane stress resultants at two points located symmetrically relative to the crack axis.

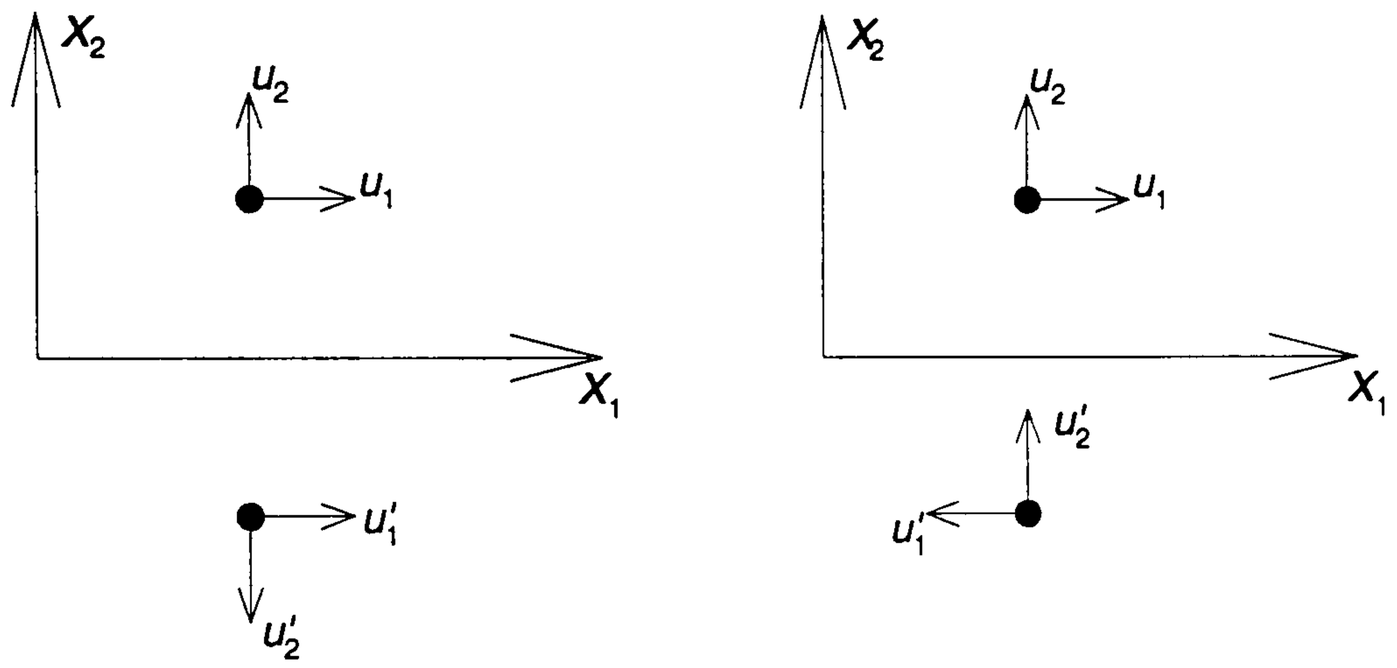

Figure E-4: Symmetric and anti-symmetric in-plane displacements at two points located symmetrically to the crack axis.

$$\left\{ \begin{array}{c} u_1^S \\ u_2^S \end{array} \right\} = \frac{1}{2} \left\{ \begin{array}{c} u_1 + u'_1 \\ u_2 - u'_2 \end{array} \right\} , \left\{ \begin{array}{c} u_1^{AS} \\ u_2^{AS} \end{array} \right\} = \frac{1}{2} \left\{ \begin{array}{c} u_1 - u'_1 \\ u_2 + u'_2 \end{array} \right\} \tag{E.4}$$

as shown in Figure E-1-E-4 where $M'_{\alpha\beta}, Q'_\alpha, N'_{ij}, w'_i,\ u'_i$ and $M_{\alpha\beta}, Q_\alpha, N_{ij},\ w_i, u_i$ represent the elastic field at symmetric points $P'(x_1, -x_2)$ and $P(x_1, x_2)$, as represented in Figure 5-5. Equations (E.1 – E.4) lead to the following decomposition of the elastic field

$$
\begin{aligned}
M_{\alpha\beta} &= M^S_{\alpha\beta} + M^{AS}_{\alpha\beta} \\
Q_\alpha &= Q^S_\alpha + Q^{AS}_\alpha \\
N_{\alpha\beta} &= N^S_{\alpha\beta} + N^{AS}_{\alpha\beta}
\end{aligned}
\tag{E.5}
$$

and

$$
\begin{aligned}
w_i &= w^S_i + w^{AS}_i \\
u_\alpha &= u^S_\alpha + u^{AS}_\alpha
\end{aligned}
\tag{E.6}
$$

Appendix F

Computer Code

This appendix describes a software developed for the dual boundary element analysis of linear elastic fracture mechanics fatigue crack-growth problems for plates and shallow shells. This software is an extension of the software developed for two-dimensional dual boundary element analysis and static analysis of shear deformable plate bending developed previously.

This software can be used in the following type of application problems:

- Boundary element stress analysis of non-cracked structures.
- Dual boundary element fracture mechanics analysis of structures.
- Dual boundary element incremental analysis of fatigue crack growth of structures.

F.1 Software Organisation

F.1.1 Plate Bending

The **plate bending software** contains the following program modules:

BEGENP - This program performs the boundary element mesh generation with quadratic continuous elements.

CRACKERP - This is the main program of the software package. It has the following capabilities:

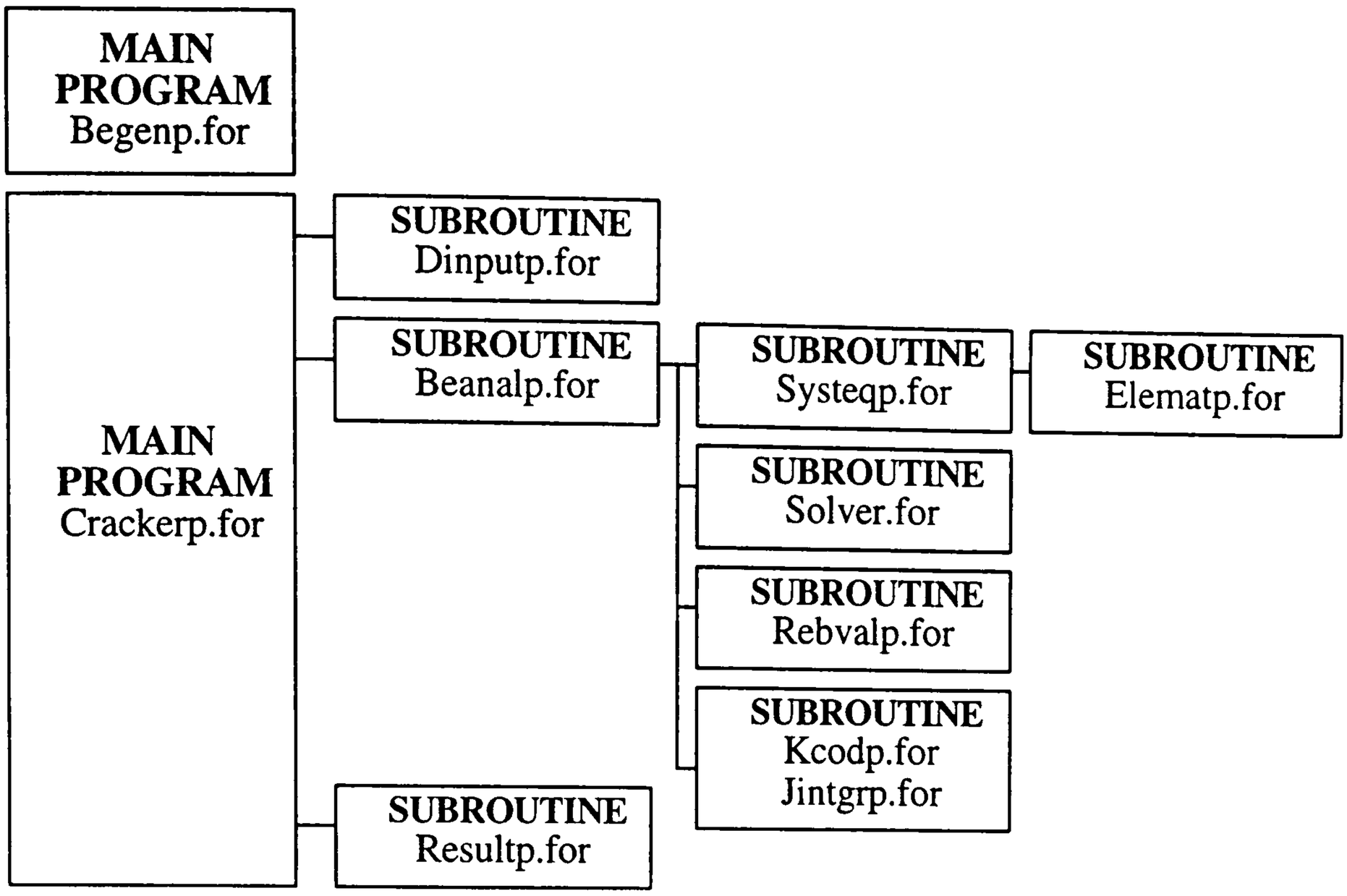

Figure F-1: Organisation of the code for DBEM analysis of plate bending.

- Boundary element analysis of shear deformable plate bending problems with isotropic material properties in arbitrary cracked or non-cracked homogeneous domains with quadratic boundary elements.

- Computation of boundary tractions; computation of displacements, stress resultants at boundary and internal points.

- Analysis of multi-boundary domains with an arbitrary geometry and general loadings.

- Single-region analysis of cracked domains in which the cracks are assumed as traction free.

- Automatic generation of quadratic discontinuous elements along both of the crack boundaries which can be defined by an arbitrary piece-wise straight geometry.

- Computation of the stress intensity factors by the decomposition technique of the J-integral or Crack surface displacements extrapolation.

Organisation of the code for plate bending can be seen in Figure F-1.

F.1.2 Shallow shells

The **shallow shells software** contains the following program modules:

BEGENS - This program performs the boundary element mesh generation with quadratic continuous elements.

CRACKERS - This is the main program of the software package. It has the following capabilities:

- Boundary element analysis of two-dimensional elastostatic plane-stress and plane-strain, shear deformable shallow shells, and plates loaded by combined bending and tension problems with isotropic material properties in arbitrary cracked or non-cracked homogeneous domains with quadratic boundary elements.

- Computation of boundary tractions; computation of displacements, stress resultants at boundary and internal points.

- Computation of boundary tractions; computation of displacements, stresses, principal stresses, octahedral shear stresses and strain energy density at boundary and internal points. (for two-dimensional analysis)

- Analysis of multi-boundary domains with an arbitrary geometry and general loadings.

- Single-region analysis of cracked domains in which the cracks are assumed as traction free.

- Automatic generation of quadratic discontinuous elements along both of the crack boundaries which can be defined by an arbitrary piece-wise straight geometry.

- Computation of the stress intensity factors by the decomposition technique of the J-integral or Crack surface displacements extrapolation.

- Automatic incremental crack-extension analysis with no remeshing.

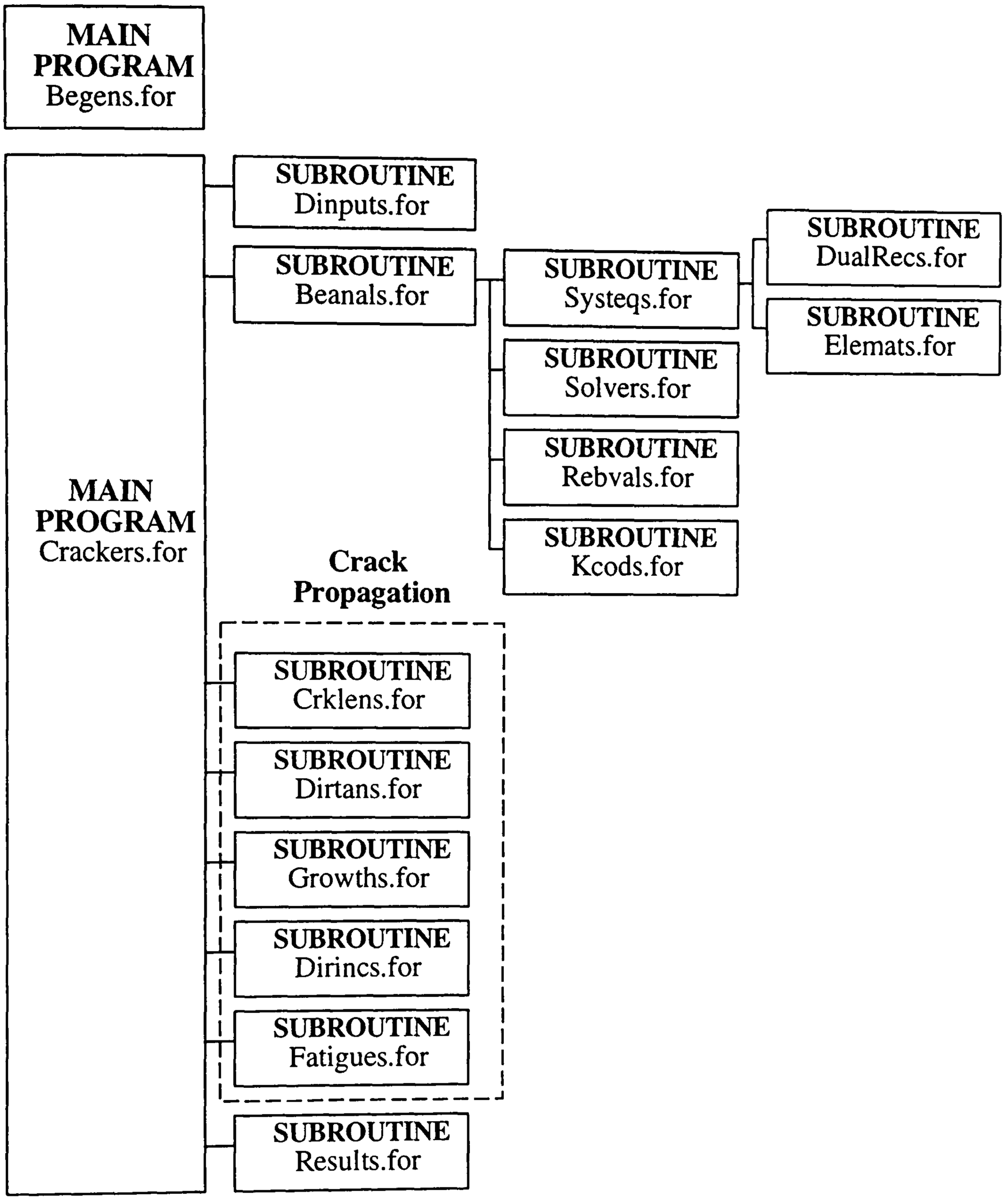

Figure F-2: Organisation of the code for DBEM analysis of shallow shells and plate subjected to combine bending and tension loads.

- Multiple crack growth analysis.

- Incremental evaluation of the fatigue life.

Organisation of the code for shallow shells, and plate bending and tension can be seen in Figure F-2.

The software package is written in FORTRAN and operates without modifications on the IBM/PC or compatible machines, the SUN
workstation and the IBM3090 supercomputer.

F.2 BEGENP and BEGENS

This program performs the generation of the boundary element mesh with continuous quadratic elements. The program assumes the input data organised in six main sets, and proceeds as follows:

1. General Section

It contains the title of the problem under analysis, the elastic case CASE(two-dimensional plane stress, plane strain, plate bending or shell), the elastic constants E and RNU, plate thickness TH (for plate and shell analysis), curvature K_11 and K_22 (for plate bending and tension ($k_{11} = k_{22} = 0.0$), and shallow shell analysis only), the total number of nodes NNOD, the total number of elements NNEL, the total number of domain points NPTD and the order of Gauss quadrature NGAUS used for numerical integration. After reading this set of data and performing some checks on dimensions, the program generates the abscissae and weights for numerical integration through the subroutines NUMINT and GAULEG.

2. Plate/ Shell/ Sheet geometry

It contains the geometric data organized sequentially in the following subsets:

BP - Geometric points referred to by the respective point number N and its cartesian coordinates X and Y.

DP - Domain points required by Dual Reciprocity Technique (for shallow shell analysis only) referred to by the respective point number N and its cartesian coordinates X and Y.

BL and BC - Geometric segments organized by lines BL and circular arcs BC.

The line and arc-segments can be read in any order, after the points BP and before the zones BZ.

BZ - Geometric boundary zones referred to by a boundary zone number IZN, the total number of segments in the zone and the ordered listing of the segment numbers in the zone. The program assumes that each zone is closed.

3. Internal Points and Boundary conditions

It contains the remaining data organized in the following subsets:

IPT - Internal points referred to by the respective point number N and its cartesian coordinates X and Y.

DBC- Displacement boundary conditions sequentially organized in the following subsets:

- NDBCI - Element constraint. Specifies a uniform displacement DISP in the direction IDIR along the element IELEM.
- NDBC2 - Local node constraint. Specifies the displacement DISP in the direction IDIR at the local node NODE of the element IELEM.
- NDBC3 - Global node constraint. Specifies the displacement IDISP in the direction IDIR at the global node NODE.

TBC - Traction boundary conditions sequentially organized in the following subsets:

- NTBCI - Element traction. Specifies a uniform traction TRAC in the direction IDIR along the element IELEM.
- NTBC2 - Local node traction. Specifies the traction TRAC in the direction IDIR at the local node NODE of the element IELEM.
- NTBC3 - Global node traction. Specifies the traction TRAC in the direction IDIR at the global node NODE.

4. Crack propagation data

CRP - Crack propagation data sequentially organized as: the total number of crack-extension increments NCRI; the number of times the crack-extension increment is greater than the crack-tip element ADV; Paris parameters PPC and PPN;

load ratio (min/max) SRAT; contribution factor in K_{eff} calculation (plate bending and tension, and shallow shell only) BFACT, the number of crack-extension increments between each output and logical STRAIGHT and SAMESIZE. If STRAIGHT is .TRUE., then the cracks will grow in a straight line, otherwise the crack growth direction will be determined by the program. If SAMESIZE is .TRUE. then all cracks will grow the same increment size, otherwise the relative growth rates will be determined by the program

5. Uniform Load data (Plates and Shells only)

It contains the value of uniform domain load ALOAD.

6. Termination label

It contains the termination label END.

The output files of this program are formatted to be used as input to the modules CRACKERP or CRACKERS.

F.3 CRACKERP and CRACKERS

The module CRACKERP is constituted by the main program and 62 subroutines, and CRACKERS is constituted by the main program and 95 subroutines from which the most important are described in the subsections presented bellow.

F.3.1 MAIN PROGRAM

The main program of this module controls the overall flow of the analysis.

F.3.2 DINPUTP/ DINPUTS

This subroutine inputs the data.

F.3.3 CRACKSP/ FCMESH

By using the geometric mesh, this subroutine sets up the functional mesh. The crack boundaries are discretised by discontinuous elements in such a way that each node of one of the crack boundaries is coincident with a node on the opposite boundary. Continuous elements are used along the remaining boundaries, except at the corner

and at the intersection between a crack and an edge, where semi-discontinuous elements are used.

F.3.4 BEANALP/ BEANALS

This subroutine performs an incremental boundary element analysis. The system matrices are computed only for the new boundary elements introduced along the current crack-extension increment. This corresponds to add new rows and columns to the system matrices between the orders NEQO and NEQN. For the first boundary element analysis or for stress analysis of non-cracked structures, this subroutine is called with NEQO=1.

F.3.5 ARRAYS

This subroutine extracts the element arrays from the global ones.

F.3.6 SHAPES, SHAPESP, SHAPEST

This subroutine evaluates the shape functions and their derivatives for continuous elements, discontinuous elements with

nodes at H= + 2/3 in which H is the local coordinate, semi-discontinuous elements with nodes at H= - 2/3,0,+1 and H= 1–,0,+ 2/3 and special crack tip element.

F.3.7 JACOBI

This subroutine evaluates the Jacobian of the transformation of coordinates, from the global system to the local one, and the unit

outward normal.

F.3.8 SYSTEQP/ SYSTEQS

This subroutine incrementally forms the system of equations between the orders NEQO and NEQN. The computations are carried out

column-wise with the integration element loop outside of the nodal collocation loop. This procedure minimizes the processing time, since

the element computations that do not depend on the collocation point are performed once and for all by the subroutine FASTER, before

entering the collocation loop. Moreover, the computation of the integrals that contain the displacement fundamental solution are skipped,

for traction-free elements.

F.3.9 DUALREC

This subroutine performs domain integrals evaluation by dual reciprocity technique. It forms the radial basis function $\mathbf{F}$ matrices and its invers $\mathbf{F}^{-1}$, and compute particular solutions.

F.3.10 ELEMATP/ ELEMATS

This subroutine performs the element integrations as follows:

For an element that contains the collocation node (self-point element), the subroutine SCRACKP/ SCRACKS is called to carry out the singular integral using singularity substraction technique or analytic integration of both the H and the G element matrices, whenever the element is on a crack boundary. For a self-point element on a non-crack boundary, the integral of the displacement fundamental solution is weakly singular at the collocation node and therefore, a regularization with the bi-cubic coordinate transformation is carried out. The terms of the H-matrix of non-crack elements are computed indirectly using the rigid body condition.

All the remaining element integrations are carried out in this subroutine by standard Gauss quadrature. Sub-element integration is used whenever the collocation node and the integration element are too close.

F.3.11 SOLVER

This subroutine solves a system of equations. It performs an incremental LU-decomposition, except for multi-region problems, where Gauss elimination procedure is used.

F.3.12 KCODS

This subroutine compute the stress intensity factors using crack surface displacements extrapolation technique.

F.3.13 JINTGR

This subroutine applies the decomposition technique of the J-integral along a circular contour path to compute the stress intensity

factors.

F.3.14 DIRTAN

This subroutine computes the direction of the tangent to the crack-path through the subroutine MXPRST which applies the maximum principal stress criterion. It computes also the mode I equivalent stress intensity factor and the residual strength.

F.3.15 GROWTH

This subroutine advances the crack-tip by one crack-extension increment, along the direction of the tangent to the crack-path. The crack-extension is discretized with NELINC new discontinuous boundary elements that are assumed as traction-free. It calls the subroutine CRKROT to update both the geometry and the functional definitions. The first and the last of the new equations NEQO and NEQN, respectively, are computed in this subroutine.

F.3.16 FATIGUES

This subroutine is used for multiple crack growth analysis. It computes the number of cycles necessary to grow an arbitrary crack-extension increment size (Δa_0) for every crack tip, and then computes the crack-extension increment sizes of the every cracks.